

VOLUME 77 FEBRUARY 15, 1973 NUMBER 4

JPCHAx

---

THE JOURNAL OF

PHYSICAL  
CHEMISTRY

---

PUBLISHED BIWEEKLY BY THE AMERICAN CHEMICAL SOCIETY

# THE JOURNAL OF PHYSICAL CHEMISTRY

---

**BRYCE CRAWFORD, Jr.**, *Editor*  
**STEPHEN PRAGER**, *Associate Editor*  
**ROBERT W. CARR, Jr.**, **FREDERIC A. VAN-CATLEDGE**, *Assistant Editors*

**EDITORIAL BOARD:** A. O. ALLEN (1970-1974), C. A. ANGELL (1973-1977), J. R. BOLTON (1971-1975), F. S. DAINTON (1972-1976), M. FIXMAN (1970-1974), H. S. FRANK (1970-1974), R. R. HENTZ (1972-1976), J. R. HUIZENGA (1969-1973), W. J. KAUZMANN (1969-1973), R. L. KAY (1972-1976), W. R. KRIGBAUM (1969-1973), W. J. MOORE (1969-1973), R. M. NOYES (1973-1977), J. A. POPLE (1971-1975), B. S. RABINOVITCH (1971-1975), H. REISS (1970-1974), S. A. RICE (1969-1975), F. S. ROWLAND (1973-1977), R. L. SCOTT (1973-1977); W. A. ZISMAN (1972-1976)

AMERICAN CHEMICAL SOCIETY, 1155 Sixteenth St., N.W., Washington, D. C. 20036

## Books and Journals Division

**JOHN K CRUM** *Director*  
**RUTH REYNARD** *Assistant to the Director*

**CHARLES R. BERTSCH** *Head, Editorial Processing Department*  
**D. H. MICHAEL BOWEN** *Head, Journals Department*  
**BACIL GUILLEY** *Head, Graphics and Production Department*  
**SELDON W. TERRANT** *Head, Research and Development Department*

©Copyright, 1973, by the American Chemical Society. Published biweekly by the American Chemical Society at 20th and Northampton Sts., Easton, Pa. 18042. Second-class postage paid at Washington, D. C., and at additional mailing offices.

All manuscripts should be sent to *The Journal of Physical Chemistry*, Department of Chemistry, University of Minnesota, Minneapolis, Minn. 55455.

*Additions and Corrections* are published once yearly in the final issue. See Volume 76, Number 26 for the proper form.

*Extensive or unusual alterations in an article after it has been set in type are made at the author's expense*, and it is understood that by requesting such alterations the author agrees to defray the cost thereof.

The American Chemical Society and the Editor of *The Journal of Physical Chemistry* assume no responsibility for the statements and opinions advanced by contributors.

Correspondence regarding accepted copy, proofs, and reprints should be directed to Editorial Processing Department, American Chemical Society, 20th and Northampton Sts., Easton, Pa. 18042. Head: CHARLES R. BERTSCH. Assistant Editor: EDWARD A. BORGER. Editorial Assistant: JOSEPH E. YURVATI.

Advertising Office: Centcom, Ltd., 142 East Avenue, Norwalk, Conn. 06851.

## Business and Subscription Information

Remittances and orders for subscriptions and for single copies,

notices of changes of address and new professional connections, and claims for missing numbers should be sent to the Subscription Service Department, American Chemical Society, 1155 Sixteenth St., N.W., Washington, D. C. 20036. Allow 4 weeks for change of address. Please include an old address label with the notification.

Claims for missing numbers will not be allowed (1) if received more than sixty days from date of issue, (2) if loss was due to failure of notice of change of address to be received before the date specified in the preceding paragraph, or (3) if the reason for the claim is "missing from files."

Subscription rates (1973): members of the American Chemical Society, \$20.00 for 1 year; to nonmembers, \$60.00 for 1 year. Those interested in becoming members should write to the Admissions Department, American Chemical Society, 1155 Sixteenth St., N.W., Washington, D. C. 20036. Postage to Canada and countries in the Pan-American Union, \$5.00; all other countries, \$6.00. Single copies for current year: \$3.00. Rates for back issues from Volume 56 to date are available from the Special Issues Sales Department, 1155 Sixteenth St., N.W., Washington, D. C. 20036.

This publication and the other ACS periodical publications are now available on microfilm. For information write to MICROFILM, Special Issues Sales Department, 1155 Sixteenth St., N.W., Washington, D. C. 20036.

THE JOURNAL OF  
PHYSICAL CHEMISTRY

Volume 77, Number 4 February 15, 1973

JPCA 77(4) 427-568 (1973)

Reaction of Singlet Methylene with Cyclopropane . . . . .	<b>G. B. Kistiakowsky* and B. B. Saunders</b>	427
Heteronuclear Recombination of Chlorine and Iodine Atoms in the Flash Photolysis of Iodine Monochloride . . . . .	<b>H. N. Maier and F. W. Lampe*</b>	430
Primary and Secondary Photolytic Processes in the Photodecomposition of Thietane Vapor . . . . .	<b>D. R. Dice and R. P. Steer*</b>	434
Kinetics of Particle Growth. I. Ammonium Nitrate from the Ammonia-Ozone Reaction . . . . .	<b>R. G. de Pena, Kenneth Olszyna, and Julian Heicklen*</b>	438
Kinetics of Particle Growth. II. Kinetics of the Reaction of Ammonia with Hydrogen Chloride and the Growth of Particulate Ammonium Chloride. <b>Richard J. Countess and Julian Heicklen*</b>		444
Identification of Rate-Controlling Steps for the Water-Gas Shift Reaction over an Iron Oxide Catalyst . . . . .	<b>Shoichi Oki and Reiji Mezaki*</b>	447
<i>g</i> Factor and Hyperfine Coupling Anisotropy in the Electron Spin Resonance Spectra of Methyl-, Ethyl-, and Allyl-Type Radicals Adsorbed on Silica Gel . . . . .	<b>Tetsuo Shiga and Anders Lund*</b>	453
Electron Spin Resonance Spectra of the Radicals Produced in the Radiolysis of Aqueous Solutions of Furan and Its Derivatives . . . . .	<b>Robert H. Schuler,* Gary P. Laroff, and Richard W. Fessenden</b>	456
Infrared Spectra and Geometries of Matrix Isolated Yttrium Tri- and Difluorides . . . . .	<b>R. D. Wesley and C. W. DeKock*</b>	466
Vibrational Spectra and Rotational Isomerism of 1,2-Propanedithiol . . . . .	<b>S. K. Nandy, D. K. Mukherjee, S. B. Roy, and G. S. Kastha*</b>	469
A Spectrophotometric Study of the Palladium(II) Chloride-Aluminum Chloride Vapor Complex . . . . .	<b>G. N. Papatheodorou</b>	472
Dimeric Structure of a Copper Phthalocyanine Polymorph . . . . .	<b>James H. Sharp* and Martin Abkowitz</b>	477
$C\pi \rightarrow \pi^*$ Transition. III. Experimental and Theoretical Verification of the Assignment . . . . .	<b>John C. Nnadi,* Allen W. Peters, and Shih Yi Wang</b>	482
Theory of Simple Electron Transfer Reactions . . . . .	<b>P. P. Schmidt</b>	488
INDO Theoretical Studies. The Geometry of 1-Substituted Vinyl Radicals and 1-Fluorovinyl Cations . . . . .	<b>Charles U. Pittman, Jr.,* Lowell D. Kispert, and Thurman B. Patterson, Jr.</b>	494
The Determination of the Intermolecular Forces of Attraction between Macroscopic Bodies for Separations down to the Contact Point . . . . .	<b>A. I. Bailey* and H. Daniels</b>	501
Nonstoichiometric Interactions of Long-Chain Ammonium Salts in Organic Solvents . . . . .	<b>Y. Marcus</b>	516
Conductance and Ion-Pair Formation of Bis(2,9-dimethyl-1,10-phenanthroline)copper(I) Perchlorate. II. In Nitrobenzene-Carbon Tetrachloride and Methanol-Carbon Tetrachloride Mixtures . . . . .	<b>Katsuhiko Miyoshi* and Toshihiro Tominaga</b>	519



Medium Activity Coefficient of Iodate in Methanol, Acetonitrile, and Dimethyl Sulfoxide with Reference to Water . . . . .	I. M. Kolthoff* and M. K. Chantooni, Jr.	523
Medium Activity Coefficients in Methanol and Some Aprotic Solvents of Substituted Benzoic Acids and Their Anions as Related to Their Hydrogen Bonding Properties . . . . .	M. K. Chantooni, Jr., and I. M. Kolthoff*	527
Solubilities of Alkali Metal Chlorides in Some Amine and Ether Solvents . . . . .	J. Strong and T. R. Tuttle, Jr.*	533
A Comparative Study of the Enthalpy of Ionization of Polycarboxylic Acids in Aqueous Solution . . . . .	V. Crescenzi,* F. Delben, F. Quadrifoglio, and D. Dolar	539
Calorimetric Investigation of the Association of Various Purine Bases in Aqueous Media . . . . .	Michael G. Marenchic and Julian M. Sturtevant*	544
The Association of Heptanol-1 in Carbon Tetrachloride from Static Dielectric Measurements . . . . .	P. Bordewijk,* M. Kunst, and A. Rip	548
Studies on the Properties of Large Ions in Solvents of High Dielectric Constant. III. Refractive Index of Solutions of Some Salts Containing an Ion with a Long Alkyl Chain in Formamide, <i>N</i> -Methylacetamide, <i>N,N'</i> -Dimethylformamide, and <i>N,N'</i> -Dimethylacetamide . . . . .	Ram Gopal* and Jug Raj Singh	554
Charge Transfer of Adsorbed Ozone . . . . .	H. Kiess and T. Freund*	556
Formation Constants and Enthalpies of Some Organomercury-Nitrogen Base Adducts . . . . .	Warren H. Puhl and H. F. Henneike*	558
Empirical Study of Heavy-Atom Collisional Quenching of the Fluorescence State of Aromatic Compounds in Solution . . . . .	Isadore B. Berلمان	562

#### COMMUNICATIONS TO THE EDITOR

Comment on the Paper "Application of Density Matrix Methods to the Study of Spin Exchange," by K.-I. Dahlqvist and S. Forsén . . . . .	D. N. Pinder	567
Comments on the Paper "Ionic Solvation Numbers from Compressibilities and Ionic Vibration Potentials Measurements," by J. O'M. Bockris and P. P. S. Saluja . . . . .	Jacques E. Desnoyers	567

#### AUTHOR INDEX

Abkowitz, M., 477	Freund, T., 556	Marcus, Y., 516	Quadrifoglio, F., 539
Bailey, A. I., 501	Gopal, R., 554	Marenchic, M. G., 544	Rip, A., 548
Berلمان, I. B., 562	Heicklen, J., 438, 444	Mezaki, R., 447	Roy, S. B., 469
Bordewijk, P., 548	Henneike, H. F., 558	Miyoshi, K., 519	Saunders, B. B., 427
Chantooni, M. K., Jr., 523, 527	Kastha, G. S., 469	Mukherjee, D. K., 469	Schmidt, P. P., 488
Countess, R. J., 444	Kiess, H., 556	Nandy, S. K., 469	Schuler, R. H., 456
Crescenzi, V., 539	Kispert, L. D., 494	Nnadi, J. C., 482	Sharp, J. H., 477
Daniels, H., 501	Kistiakowsky, G. B., 427	Okii, S., 447	Shiga, T., 453
DeKock, C. W., 466	Kolthoff, I. M., 523, 527	Olszyna, K., 438	Singh, J. R., 554
Delben, F., 539	Kunst, M., 548	Papatheodorou, G. N., 472	Steer, R. P., 434
de Pena, R. G., 438	Lampe, F. W., 430	Patterson, T. B., Jr., 494	Strong, J., 533
Desnoyers, J. E., 567	Laroff, G. P., 456	Peters, A. W., 482	Sturtevant, J. M., 544
Dice, D. R., 434	Lund, A., 453	Pinder, D. N., 567	Tominaga, T., 519
Dolar, D., 539	Maier, H. N., 430	Pittman, C. U., Jr., 494	Tuttle, T. R., Jr., 533
Fessenden, R. W., 456		Puhl, W. H., 558	Wang, S. Y., 482
			Wesley, R. D., 466

In papers with more than one author the name of the author to whom inquiries about the paper should be addressed is marked with an asterisk in the by-line.



# THE JOURNAL OF PHYSICAL CHEMISTRY

Registered in U. S. Patent Office © Copyright, 1973, by the American Chemical Society

VOLUME 77, NUMBER 4 FEBRUARY 15, 1973

## Reaction of Singlet Methylene with Cyclopropane

G. B. Kistiakowsky\* and B. B. Saunders

The Gibbs Chemical Laboratory, Harvard University, Cambridge, Massachusetts 02138 (Received July 5, 1972)

Publication costs assisted by the National Science Foundation

Ketene in excess of cyclopropane containing enough  $O_2$  to eliminate its reactions with  $CH_2$  ( $^3B_1$ ) was photolyzed, using a monochromator and suitable filters, at four different wavelengths, 214, 277, 313, and 330 nm. The lifetimes of the resultant "hot" methylcyclopropane prior to isomerization into butenes were found to be 2.55, 3.92, 5.40, and  $6.29 \times 10^{-10}$  sec, increasing with decreasing photolyzing energy. The RRKM theory was used to estimate the internal energy of the excited methylcyclopropane and the energies so obtained ranged from 104 kcal/mol at 330 nm to 110 kcal/mol at 214 nm. According to these calculations the fraction of excess photon energy carried into methylcyclopropane rapidly decreases as the photon energy increases.

Methylene has been used extensively in chemical activation studies.<sup>1</sup> Butler and Kistiakowsky (BK) photolyzed both ketene and diazomethane at several wavelengths and reacted the resulting  $CH_2$  with propene or cyclopropane to produce vibrationally excited methylcyclopropane (MCP).<sup>2</sup> The excited MCP either isomerized to form isobutene, 1-butene, and *cis*- and *trans*-2-butene or was deactivated by collision. Their work was done before the importance of  $CH_2$  ( $^3B_1$ ) as a reactant distinct from  $CH_2$  ( $^1A_1$ ), but present along with  $CH_2$  ( $^1A_1$ ) in the methylene systems was recognized; consequently no effort was made to prevent the  $CH_2$  ( $^3B_1$ ) from reacting with the hydrocarbons. BK's main conclusion that the distribution of energy in the MCP produced from cyclopropane does not differ from that produced from propene is unaffected by the knowledge that two distinct electronic states of  $CH_2$  were present in the reaction system. However, one would expect the lifetimes of the MCP to be shorter when there is more vibrational energy brought to it by the methylene, as might be the case when shorter photolyzing wavelengths are used. The results of BK's experiments were not consistent with these expectations since they found that photolyses in their ketene system at 310 nm produced MCP with shorter lifetimes than photolyses at 260 nm did. Now one might suspect that this inconsistency was the result of some complicating reactions of the  $CH_2$  ( $^3B_1$ ), except that the reaction of  $CH_2$  with cyclopropane

is quite slow.<sup>3</sup>  $CH_2$  ( $^3B_1$ ) undoubtedly was significant in their ketene-propene system.

Dorer and Rabinovitch<sup>4</sup> also studied the reaction of  $CH_2$  with propene using both ketene and diazomethane as a source of  $CH_2$ . In some of their experiments, they used the well-known technique of adding  $O_2$  to scavenge the  $CH_2$  ( $^3B_1$ ), but they photolyzed ketene at one wavelength only and consequently could not investigate the lifetime of MCP as a function of the photolyzing wavelength. Strachan and Thornton<sup>3</sup> studied the photolysis of ketene and cyclopropane in the presence of  $O_2$  but used their results only to determine at what cyclopropane/ketene ratio the reactions of  $CH_2$  ( $^3B_1$ ) and  $CH_2$  ( $^1A_1$ ) with ketene become negligible compared to their reactions with cyclopropane.

We repeated BK's experiments and photolyzed ketene and cyclopropane at four different wavelengths. Although  $CH_2$  ( $^3B_1$ ) is not expected to react extensively with cyclopropane,<sup>3</sup> we added a small amount of  $O_2$  (5% of the total

- (1) See, for example, the reviews by H. M. Frey, *Prog. React. Kinet.*, **2**, 131 (1964); B. S. Rabinovitch and M. C. Flowers, *Quart. Rev. Chem. Soc.*, **122** (1964).
- (2) J. N. Butler and G. B. Kistiakowsky, *J. Amer. Chem. Soc.*, **82**, 759 (1960).
- (3) D. E. Thornton and A. N. Strachan, *J. Phys. Chem.*, **71**, 4583 (1967).
- (4) F. H. Dorer and B. S. Rabinovitch, *J. Phys. Chem.*, **69**, 1952, 1964, 1973 (1965).

mixture) to ensure that the only methylene species reacting with cyclopropane was singlet  $\text{CH}_2$ .

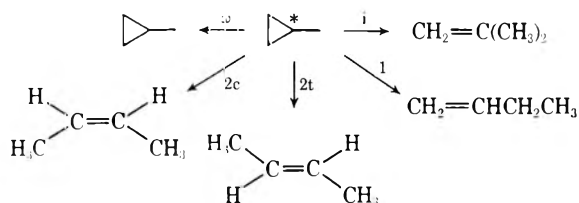
### Experimental Section

Mixtures containing cyclopropane, ketene, and oxygen in the ratio of 20:1:1 were photolyzed at 330, 313, and 277 nm using an Osram HBO 500-W mercury lamp with a Bausch and Lomb monochromator and at 214 nm using a 25-W Phillips zinc lamp with a Baird-Atomic 214-nm standard line filter. The total pressure of the photolysis mixture was varied between 30 and 700 Torr with at least three different pressures within this range being used at each wavelength. In each photolysis, only 2-5% of the ketene was decomposed. The condensable products were transferred using liquid nitrogen to a gas chromatograph equipped with a flame ionization detector. The products were then separated on a 10 ft, 0.25-in. o.d. column filled with two parts of Porapak Q and one part of Porapak Q-S (both 50-80 mesh) operated at 80° with a carrier (helium) flow rate of 100 cc/min. Isobutene and 1-butene were not resolved from each other on this column, but the separation of these two products was not necessary to determine the lifetimes of MCP. Ketene was prepared by the pyrolysis of acetic anhydride.<sup>5</sup> The cyclopropane used was Matheson's CP grade which contained 0.3% propene as its major impurity. Air Reduction Co. research grade  $\text{O}_2$  was used. Further details are discussed in ref 6 and 7.

### Results and Discussion

$\text{CH}_2$  ( $^1\text{A}_1$ ) inserts into the C-H bonds of cyclopropane to form excited MCP whose fate is decided according to the reaction shown in Scheme I.<sup>2,3,8,9</sup> The overall rate

#### Scheme I



constant for the isomerization of MCP,  $k_a = k_i + k_{2c} + k_{2t}$ , is equal to the collision frequency,  $\omega$ , multiplied by the ratio of the sum of concentrations of olefin products,  $D$ , to the concentration of the stabilized MCP,  $S$

$$k_a = \omega(D/S) = \omega[\text{butenes}]/[\text{MCP}]$$

The  $k_a$  values were determined from plots of [butenes]/[MCP] vs.  $1/\omega$  or  $1/\text{total pressure}$  at each wavelength, and these plots are shown in Figure 1. The dashed line in Figure 1 represents BK's average of both the 260- and 310-nm experiments. The scatter of individual points in BK's experiments is much larger than in ours. In direct contrast to BK,<sup>2</sup> the lifetimes of the MCP,  $1/k_a$ , became shorter as the photolyzing energy was increased.

The ratios of *trans*-2-butene to *cis*-2-butene and that of the 2-butenes to isobutene and 1-butene were about 1.0 and varied somewhat with pressure,<sup>6</sup> in agreement with other workers.<sup>2,8</sup> Dorer and Rabinovitch<sup>4</sup> studied further reactions of 1-butene resulting from the isomerization of "hot" methylcyclopropane and found that in the pressure range employed in the present work butene was over-

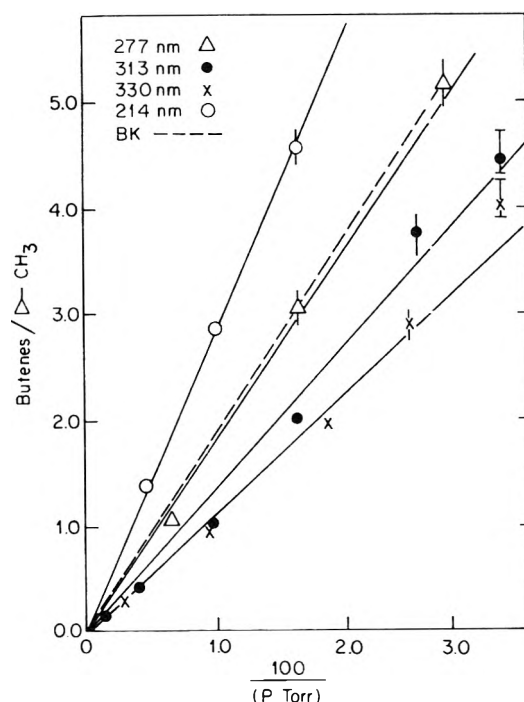


Figure 1. Plot of butene/MCP vs.  $100/P$  (Torr).

whelmingly stabilized by collisions. We felt justified therefore in using the plots of Figure 1 to evaluate  $k_a$ .

The usual RRKM treatment which used models very similar to those developed by Dorer and Rabinovitch<sup>4</sup> was applied to models for MCP isomerization in order to estimate the average vibrational energies of the MCP molecules produced at several wavelengths. The best models so determined for the activated complex and the molecule are given in Table I. The average energies of the excited molecules for each photolyzing wavelength are given in Table II. For comparison, the average energy and the rate of decomposition of MCP formed by the reaction of propene and  $\text{CH}_2$  ( $^1\text{A}_1$ ) produced from the photolysis of ketene at 320 nm<sup>4</sup> are included in this table. However, it should be noted that Dorer and Rabinovitch<sup>4</sup> used unfiltered light from a GE AH-6 super pressure lamp and, on the basis of other work,<sup>10</sup> estimated that 320 nm is the effective photolyzing wavelength and so this wavelength is not as well defined as those in our present work are.

The unmistakable difference in lifetime, and hence in internal energies,  $\langle E \rangle$ , of MCP produced by radiation of different wavelengths reflects the differences in energies carried into MCP by the  $\text{CH}_2$  ( $^1\text{A}_1$ ). Several specific RRKM models tried by us gave somewhat different values of  $\langle E \rangle$  for the hot MCP molecules, so that the numbers shown as  $\langle E \rangle$  in Table II should be regarded as uncertain to a very few kcal. All these RRKM models show, how-

- (5) A. D. Jenkins, *J. Chem. Soc.*, 2563 (1962).
- (6) B. B. Saunders, Ph. D. Thesis, Harvard University, 1972.
- (7) B. A. DeGraff and G. B. Kistiakowsky, *J. Phys. Chem.*, **71**, 3984 (1967).
- (8) D. W. Setser and B. S. Rabinovitch, *J. Amer. Chem. Soc.*, **86**, 564 (1964); E. Jakubowski, H. S. Sandhu, and O. P. Strausz, *ibid.*, **93**, 2610 (1971).
- (9) J. P. Chesick, *J. Amer. Chem. Soc.*, **82**, 3277 (1960).
- (10) D. W. Setser and B. S. Rabinovitch, *Can. J. Chem.*, **40**, 1425 (1962).

**TABLE I: Models for Methylcyclopropane (Molecule and Best Complex)<sup>a</sup>**

	Molecule	Complex
C-H stretch	3015 (8)	3015 (7)
"Breathing," ring	1202	1082
CH <sub>2</sub> bend	1047	884
	889	747
CH <sub>2</sub> twist	1111	570
CH <sub>2</sub> rock	911	890
CH <sub>2</sub> bend	983	730
CH <sub>2</sub> rock	1016	790
CH <sub>2</sub> twist	810	815
	756	421
Methyl ring torsion	0	0
CH <sub>3</sub> and CH <sub>2</sub> H bends	1436 (6)	1436 (6)
Skeletal bend	320 (2)	320 (2)
CCH methyl bends	1046 (2)	1046 (2)
E <sub>0</sub>		62.5 kcal/mol

<sup>a</sup> Values given in cm<sup>-1</sup>.  $\sigma = 5.4 \text{ \AA}$  for collisions of methylcyclopropane and cyclopropane.

**TABLE II: Average Energies and the Rates of Decomposition**

Photolysis system	$\langle E \rangle_{\max}^a$ kcal/mol	$\langle E \rangle^b$ kcal/mol	$k_a^c$ sec <sup>-1</sup>
320 nm + propene <sup>d</sup>	104.5	99.6 ± 1.4	0.72 × 10 <sup>9</sup>
330 nm + cyclopropane	109.4	104.2 ± 0.7	1.59 × 10 <sup>9</sup> ± 12%
313 nm + cyclopropane	114.2	105.1 ± 0.8	1.85 × 10 <sup>9</sup> ± 12%
277 nm + cyclopropane	126.0	107.2 ± 0.1	2.55 × 10 <sup>9</sup> ± 3%
214 nm + cyclopropane	156.8	110.5 ± 0.6	3.92 × 10 <sup>9</sup> ± 8%

<sup>a</sup>  $\langle E \rangle_{\max}$  assumes that the entire photon energy in excess of that needed for the decomposition of ketene appears as internal energy of the hot methylcyclopropane. <sup>b</sup> Calculated from RRKM model. <sup>c</sup> Measured. <sup>d</sup> Reference 4.

ever, that only a fraction of the excess photon energy is carried into the MCP and that this fraction rapidly decreases as the wavelength gets shorter and the photon energy larger.

The excess photon energy is divided in an unknown manner as internal energies of CH<sub>2</sub> and CO and as their translational energies in the 2:1 ratio. We consider it

**TABLE III: Heats of Formation**

$\Delta H_f^\circ$ at 298°K, kcal/mol	Substance
92.2 <sup>a</sup>	CH <sub>2</sub>
12.7	Cyclopropane
5.7	Methylcyclopropane
-11.4 <sup>b</sup>	Ketene
-27.2 <sup>c</sup>	CO
4.9	Propylene
-3.7	Isobutene
0	1-Butene
-1.7	<i>cis</i> -2-Butene
-2.7	<i>trans</i> -2-Butene

<sup>a</sup> W. A. Chupka, and C. Livshitz, *J. Chem. Phys.*, **48**, 1109 (1968).  
<sup>b</sup> R. L. Nuttal, A. H. Laufer, and M. V. Kilday, *J. Chem. Thermodyn.*, **3**, 167 (1971). <sup>c</sup> D. D. Wagman, W. H. Evans, V. B. Parker, I. Halow, S. M. Bailey, and R. H. Schumm, *Nat. Bur. Stand. (U. S.), Tech. Note*, No. 270-3 (1968). All other values are taken from S. W. Benson, "Thermodynamics of Gas Reactions," Wiley, New York, N. Y., 1968.

highly improbable that the  $\langle E \rangle$  values shown in Table II are the measure of the total energy received by CH<sub>2</sub> in the decomposition process, for this would mean that CO receives a rapidly increasing fraction as the total energy becomes larger. The more likely explanation is that CH<sub>2</sub> (<sup>1</sup>A<sub>1</sub>) suffers several inelastic collisions before reacting with cyclopropane. In fact, it has been estimated<sup>4</sup> that the rate of this reaction is slower than that of its reaction with propene by a factor of 10. It would be consistent with the theories of collisional energy transfer to expect that the energy loss would be greater when the total energy is greater. The reaction probability, however, is large enough that CH<sub>2</sub> (<sup>1</sup>A<sub>1</sub>) does not become fully thermalized before reaction. This we consider definitely proven by this work, the earlier results of BK having been undoubtedly distorted by the presence of CH<sub>2</sub> (<sup>3</sup>B<sub>1</sub>). It might be further noted that irradiation of ketene by the 214-nm wavelength induces a  $\pi \rightarrow \pi^*$  transition and probably produces methylene in the excited <sup>1</sup>B<sub>1</sub> state. The estimated internal energies of hot methylcyclopropane, Table II, indicate that the electronic excitation energy of CH<sub>2</sub> (<sup>1</sup>B<sub>1</sub>) is not carried into the reaction with cyclopropane.

*Acknowledgment.* This work was made possible by funds provided by the National Science Foundation.



## Heteronuclear Recombination of Chlorine and Iodine Atoms in the Flash Photolysis of Iodine Monochloride

H. N. Maier and F. W. Lampe\*

Department of Chemistry, The Pennsylvania State University, University Park, Pennsylvania 16802 (Received August 30, 1972)

Publication costs assisted by The Petroleum Research Fund

The heteronuclear recombination of Cl and I atoms and the homonuclear recombination of I atoms have been studied by spectrophotometric observation of the ICl reformation and I<sub>2</sub> formation subsequent to the flash photolytic dissociation of ICl in the presence of CO<sub>2</sub> and N<sub>2</sub>. A comparison of the specific reaction rates for heteronuclear and homonuclear recombination with CO<sub>2</sub> as the third body strongly suggests that the radical complex mechanism proceeding *via* I-CO<sub>2</sub> and Cl-CO<sub>2</sub> complexes is dominant.

### Introduction

Flash photolysis studies of bromine<sup>1-8</sup> and iodine<sup>1,9-15</sup> have resulted in the establishment of absolute rate constants for the homonuclear recombination of Br and I atoms with a variety of substances acting as third bodies. In addition, a number of other kinetic studies have been reported<sup>16-21</sup> in which the specific reaction rate for the homonuclear recombination of Cl atoms was evaluated. No such fundamental data appear to be available with respect to the heteronuclear recombinations of halogen atoms that are of major importance in the chemistry of a mixture of two halogen gases (*e.g.*, Br<sub>2</sub> + Cl<sub>2</sub>)<sup>22,23</sup> or in the decomposition of a heteronuclear halogen (*e.g.*, ICl).<sup>24</sup>

The present paper describes studies of the flash photolysis of ICl in which the specific reaction rate of the heteronuclear recombination of Cl and I atoms was evaluated from spectrophotometric observation of the formation of I<sub>2</sub> and reformation of ICl subsequent to the flash.

### Experimental Section

The flash photolysis system was of conventional design. Two 10- $\mu$ F, high-voltage, fast-discharge capacitors (Bonar, Long and Co., Ltd), connected in parallel, were discharged through two FPA-8-100 xenon flash lamps which were obtained from the Xenon Corp. Either a multiple-pass photolysis cell<sup>25,26</sup> or a 10-cm, single-pass photolysis cell was mounted coaxially to the lamps, and both lamps and the cell were mounted in an elliptically shaped aluminum holder. A 200-W General Electric quartz-iodine lamp (6.6A/T4/CL), powered by a Tabtron power supply, was used to supply the analyzing light for the spectrophotometry. Collimating lenses, a Gaertner prism monochromator, and a 1P28 RCA photomultiplier tube completed the optical train. The intensity of the analyzing light transmitted by the photolysis cell at the selected wavelength (470, 520, or 570 nm) was followed as a function of time after the flash by displaying and photographing the output of the photomultiplier tube on an oscilloscope.

The concentrations of I<sub>2</sub> and ICl were followed spectrophotometrically at 520 (or 570) and 470 nm, respectively. In the photolyses of ICl, filter solutions of Cu(NH<sub>3</sub>)<sub>4</sub><sup>2+</sup><sup>27</sup> were placed around each flash lamp in order to reduce the scattered light (from the intense flash) at the detection wavelengths of 470, 520, and 570 nm to acceptable levels. In experiments in which I<sub>2</sub> was photodissociated in the

presence of ICl, filter solutions of K<sub>2</sub>Cr<sub>2</sub>O<sub>7</sub><sup>28</sup> surrounded the flash lamps. This filter effectively prevents light from the flash lamps of  $\lambda < 540$  nm from reaching the photolysis cell. The absorption coefficients of ICl<sup>29</sup> and I<sub>2</sub><sup>10</sup> are such that I<sub>2</sub> could be photodissociated to an easily measureable extent with a negligible amount of photodissociation of ICl. The absence of ICl decomposition with this filter was verified spectrophotometrically both with and without I<sub>2</sub> present in the cell.

The intensity of the light flash reached a maximum at about 50  $\mu$ sec after triggering. The intensity of the flash was fairly symmetrical in time, with a duration of 50  $\mu$ sec (full-width at half-maximum). Quite arbitrarily we define zero reaction time to correspond to the maximum in the intensity of the flash, so that all reaction times reported

- (1) R. L. Strong, J. C. W. Chien, P. E. Graf, and J. E. Willard, *J. Chem. Phys.*, **26**, 1287 (1957).
- (2) W. G. Givens and J. E. Willard, *J. Amer. Chem. Soc.*, **81**, 4773 (1959).
- (3) G. Burns and D. F. Hornig, *Can. J. Chem.*, **38**, 1702 (1960).
- (4) M. R. Basila and R. L. Strong, *J. Phys. Chem.*, **67**, 531 (1963).
- (5) J. K. K. Ip and G. Burns, *Disc. Faraday Soc.*, **44**, 241 (1967).
- (6) J. K. K. Ip and G. Burns, *J. Chem. Phys.*, **51**, 3414 (1969).
- (7) J. K. K. Ip and G. Burns, *J. Chem. Phys.*, **51**, 3425 (1969).
- (8) B. A. DeGraff and K. L. Lang, *J. Phys. Chem.*, **74**, 4181 (1970).
- (9) M. I. Christie, R. G. W. Norrish, and G. Porter, *Proc. Roy. Soc., Ser. A*, **216**, 152 (1953).
- (10) R. Marshall and N. Davidson, *J. Chem. Phys.*, **21**, 659 (1953).
- (11) M. I. Christie, A. J. Harrison, R. G. W. Norrish, and G. Porter, *Proc. Roy. Soc., Ser. A*, **231**, 446 (1955).
- (12) D. L. Bunker and N. Davidson, *J. Amer. Chem. Soc.*, **80**, 5085 (1958).
- (13) R. Engleman, Jr., and N. Davidson, *J. Amer. Chem. Soc.*, **82**, 4770 (1960).
- (14) G. Porter and J. A. Smith, *Proc. Roy. Soc., Ser. A*, **261**, 28 (1961).
- (15) J. A. Blake and G. Burns, *J. Chem. Phys.*, **54**, 1480 (1971).
- (16) J. W. Martens, *Disc. Faraday Soc.*, **33**, 297 (1962).
- (17) P. B. Ayscough, A. J. Cocker, F. S. Dainton, and S. Hirst, *Trans. Faraday Soc.*, **58**, 295 (1962).
- (18) J. W. Linnett and M. H. Booth, *Nature (London)*, **199**, 1181 (1963).
- (19) L. W. Bader and E. A. Ogryzlo, *Nature (London)*, **201**, 491 (1964).
- (20) E. Hutton and M. Wright, *Trans. Faraday Soc.*, **61**, 78 (1965).
- (21) M. A. A. Clyne and D. H. Stedman, *Trans. Faraday Soc.*, **64**, 2698 (1968).
- (22) G. Brauer and E. Victor, *Z. Elektrochem.*, **41**, 508 (1935).
- (23) M. I. Christie, R. S. Roy, and B. A. Thrush, *Trans. Faraday Soc.*, **55**, 1139 (1959).
- (24) M. I. Christie, R. S. Roy, and B. H. Thrush, *Trans. Faraday Soc.*, **55**, 1149 (1959).
- (25) J. V. White, *J. Opt. Soc. Amer.*, **32**, 285 (1942).
- (26) T. M. Edwards, *J. Opt. Soc. Amer.*, **51**, 98 (1961).
- (27) J. G. Calvert and J. N. Pitts, Jr., "Photochemistry," Wiley, New York N.Y., 1966, p 736.
- (28) References 27, p 740.
- (29) D. J. Seery and D. Britton, *J. Phys. Chem.*, **68**, 2263 (1964).

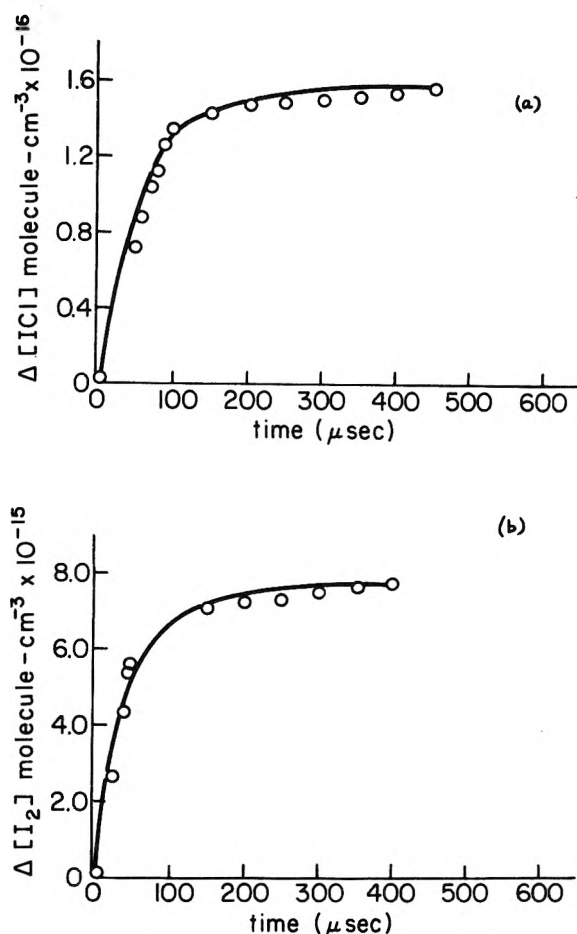


Figure 1. Formation of ICl(a) and  $I_2$ (b) subsequent to the photodissociation in the flash: (a)  $P(N_2) = 601$  Torr,  $P(ICl) = 15.3$  Torr; (b)  $P(N_2) = 606$  Torr,  $P(ICl) = 14.3$  Torr.

are measured from 50  $\mu$ sec after onset of the flash. The extent of decomposition of ICl in the flash was always in the range of 7–10%.

ICl, having a stated purity of >95%, was purchased from Alfa Inorganics. It was purified by the method described by Cornig and Karges,<sup>30</sup> degassed on a vacuum line at  $-195^\circ$ , and distilled into a storage vessel equipped with a greaseless Westef stopcock. The entire purification procedure was carried in a dim red light. The storage vessel was wrapped with aluminum foil and stored in the dark. Analytical Reagent Grade  $I_2$  was obtained from J. T. Baker Chemical Co. Prior to each use it was degassed at  $-195^\circ$ . Nitric oxide with a stated purity of >98.5% was obtained from Matheson Gas Products and was further purified using the method described by Kohout and Lampe.<sup>31</sup> Research Grade ethylene, having a stated purity of >99.9%, was obtained from the Phillips Petroleum Co.; nitrogen and carbon dioxide were obtained in high-purity from Matheson Gas Products. All three of the latter gases were used as received.

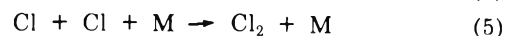
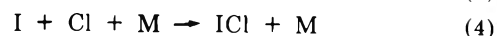
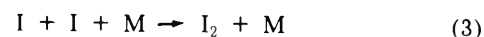
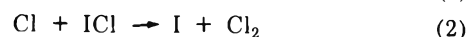
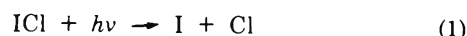
The magnitude of thermal effects resulting from a heating of the gas by the exothermicity of the reactions and a subsequent cooling of the gas at the vessel walls was examined for all photolyses by the method of Willard, *et al.*<sup>1</sup> It was concluded that negligible temperature rises of 1–2 $^\circ$  occurred in the  $I_2$  photolyses. In the ICl photolyses an average temperature rise of  $25 \pm 5^\circ$  took place, but the cool-

ing process at the walls could have only a negligible effect on the spectrophotometric measurements.

Proper operation of the apparatus was checked by examining the flash photolysis of iodine in the presence of carbon dioxide. Five separate experiments with carbon dioxide pressures in the range of 300–600 Torr led to a rate constant for the recombination of iodine atoms at 300 $^\circ$ K, with carbon dioxide as a third body, that is within  $\pm 5\%$  of the value of  $3.72 \times 10^{-32}$   $\text{cm}^6 \text{ molecule}^{-2} \text{ sec}^{-1}$  reported by Porter and Smith.<sup>14</sup> This agreement was taken as evidence of the proper functioning of the apparatus and of the validity of our techniques.

## Results and Discussion

The photochemical decomposition of ICl to  $I_2$  and  $Cl_2$  has been shown by Christie, Roy, and Thrush<sup>24</sup> to proceed by the following mechanism



and it is in terms of this mechanism that we shall consider our results.

Figure 1 shows a typical plot of the concentrations of  $I_2$  and ICl as a function of time after the photodissociation flash. The fact that the concentration of ICl increases with time and does so in a manner quite similar to that of  $I_2$  indicates that (2) is playing only a very minor role under our conditions. This is, of course, to be expected in view of the much higher atom concentrations obtaining in the flash photolysis as compared with the low-intensity, continuous photolysis.<sup>24</sup> We may, therefore, conclude that the rate equations describing the observations in Figure 1 may be written as

$$d[I_2]/dt = [I]^2 k_3(M)[M] + k_3(ICl)[ICl] \quad (6)$$

$$d[ICl]/dt = [I][Cl] k_4(M)[M] + k_4(ICl)[ICl] \quad (7)$$

$$-d[I]/dt = 2(d[I_2]/dt) + (d[ICl]/dt) \quad (8)$$

$$-d[Cl]/dt = 2(d[Cl_2]/dt) + (d[ICl]/dt) \quad (9)$$

where  $M = CO_2$  or  $N_2$ . Unfortunately we were unable to follow spectrophotometrically the formation of  $Cl_2$  in the presence of ICl, and the coupled differential equations do not lend themselves to tractable solutions. Hence, evaluation of  $k_4$ , the heteronuclear specific reaction rate, must be done somewhat indirectly from the observations of the time dependence of  $[I_2]$  and  $[ICl]$ .

Values of  $k_3(CO_2)$  and  $k_3(N_2)$  are known from the literature<sup>14,32</sup> and have been verified in our laboratory. However,  $k_3(ICl)$  is not known and must be determined independently in an experiment in which ICl is present but in which the only reaction consuming I atoms is (3). Accordingly, we flashed  $I_2$ -ICl- $CO_2$  mixtures, utilizing the  $K_2Cr_2O_7$  filter to prevent photodissociation of ICl, and followed the concentration of  $I_2$  as a function of time. Under these conditions, only (3) is occurring, and the instantaneous I atom concentration may be calculated from

(30) J. Cornig and R. A. Karges, *Inorg. Syn.*, 1, 65 (1939).

(31) F. C. Kohout and F. W. Lampe, *J. Chem. Phys.*, 46, 4075 (1967).

(32) K. E. Russell and J. Simons, *Proc. Roy. Soc., Ser. A*, 217, 271 (1953).

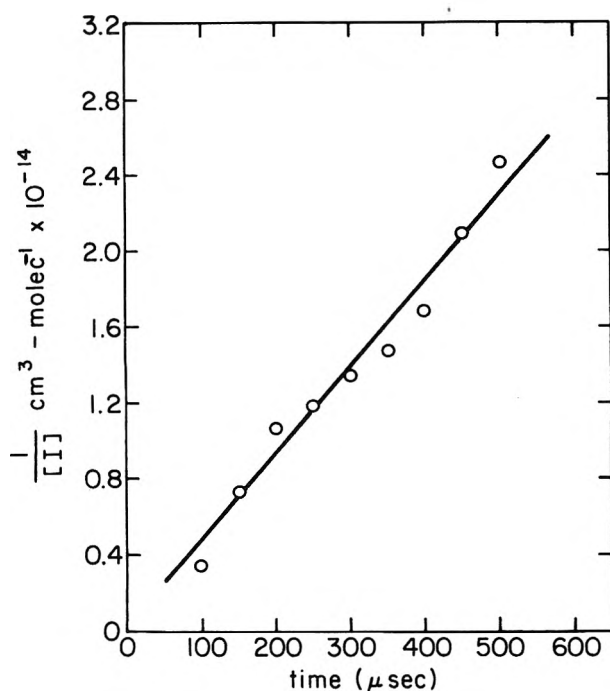


Figure 2. Second-order disappearance of I atoms by homonuclear recombination:  $P(\text{CO}_2) = 306$  Torr,  $P(\text{ICI}) = 8.8$  Torr,  $P(\text{I}_2) = 0.08$  Torr.

the measurement of  $\text{I}_2$  concentration. The integrated rate equation for I atom consumption in this case is

$$\frac{1}{[\text{I}]} = \frac{1}{[\text{I}]_0} + 2\{k_3(\text{CO}_2)[\text{CO}_2] + k_3(\text{I}_2)[\text{I}_2] + k_3(\text{ICI})[\text{ICI}]\}t \quad (10)$$

A plot according to (10) of the data from a typical flash experiment is shown in Figure 2. If one corrects the slope of the line in Figure 2 for the known contributions<sup>14</sup> from  $\text{CO}_2$  and  $\text{I}_2$ , one obtains  $k_3(\text{ICI})$ . The average value found (300°K) from 11 such experiments is

$$k_3(\text{ICI}) = 3.0 + 0.5 \times 10^{-30} \text{ cm}^6 \text{ molecule}^{-2} \text{ sec}^{-1}$$

which, as expected, is comparable to the value of  $3.80 \times 10^{-30} \text{ cm}^6 \text{ molecule}^{-2} \text{ sec}^{-1}$  reported<sup>14</sup> for  $k_3(\text{I}_2)$ .

Referring again to Figure 1, and the formation of ICl and  $\text{I}_2$  subsequent to the flash photodissociation of ICl, one may show that the time dependence of the concentrations may be written empirically as

$$\Delta[\text{I}_2] = t/(a + bt) \quad (11)$$

$$\Delta[\text{ICI}] = t/(g + ht) \quad (12)$$

when  $a$ ,  $b$ ,  $g$ , and  $h$  are constants. The validity of (11) and (12) and the evaluation of the constants may be seen from Figure 3 in which  $t/\Delta[\text{I}_2]$  and  $t/\Delta[\text{ICI}]$  are plotted as a function of  $t$ . The empirical constants evaluated from the slopes and intercepts of the straight lines are  $a = 0.57 \times 10^{-20} \text{ cm}^3 \text{ sec molecule}^{-1}$ ,  $b = 1.18 \times 10^{-16} \text{ cm}^3 \text{ molecule}^{-1}$ ,  $g = 0.28 \times 10^{-20} \text{ cm}^3 \text{ sec molecule}^{-1}$ , and  $h = 4.48 \times 10^{-17} \text{ cm}^3 \text{ molecule}^{-1}$ . It should be pointed out that (11) is the form of the integrated rate equation for  $\text{I}_2$  formation in the mathematically simple case in which I atoms react only by (3); and, since all atom combination reactions are at least comparable in rate, it is not surprising to find the same functional form, (11) and (12), being

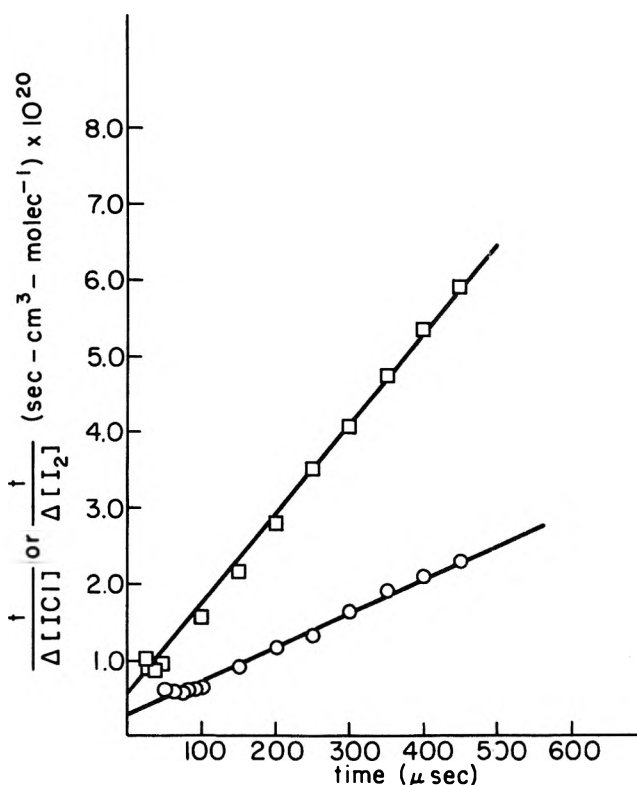


Figure 3. Kinetic plots for ICl and  $\text{I}_2$  formation according to eq 11 and 12: O, [ICI]; □,  $[\text{I}_2]$ .

obeyed in the mathematically more complex situation that precludes analytic integration of (6)–(9).

Differentiating (11) and (12), and referring to (6) and (7), we obtain for the initial rates, where the subscript zero indicates initial conditions, the following

$$(d[\text{I}_2]/dt)_0 = 1/a = [\text{I}_0]^2 \{k_3(\text{M})[\text{M}] + k_3(\text{ICI})[\text{ICI}]\} \quad (13)$$

$$(d[\text{ICI}]/dt)_0 = 1/g = [\text{I}_0][\text{Cl}]_0 \{k_4(\text{M})[\text{M}] + k_4(\text{ICI})[\text{ICI}]\} \quad (14)$$

Dividing (14) by (13) and assuming that  $[\text{I}]_0 = [\text{Cl}]_0$  yields the result

$$a/g = \{k_4(\text{ICI}) + k_4(\text{M})([\text{M}]/[\text{ICI}])\} / \{k_3(\text{ICI}) + k_3(\text{M})([\text{M}]/[\text{ICI}])\} \quad (15)$$

Since  $a/g$  is determined experimentally (cf. Figure 3) and the denominator is known, we obtain easily values of  $k_4(\text{ICI}) + k_4(\text{M})([\text{M}]/[\text{ICI}])$  as a function of the concentration ratio  $[\text{M}]/[\text{ICI}]$ . It is then simply a matter of plotting the numerical values of the numerator of (15) vs.  $[\text{M}]/[\text{ICI}]$  to obtain  $k_4(\text{ICI})$  and  $k_4(\text{M})$ . Such plots for  $\text{M} = \text{N}_2$  and  $\text{M} = \text{CO}_2$  are shown in Figure 4. The rate constants evaluated are shown in Table I where they may be compared with homonuclear recombination rate constants for I and Cl atoms.

With respect to the efficiency of the product molecule of the recombination reaction acting as a third body or chaperon, ICl falls intermediate between  $\text{I}_2$  and  $\text{Cl}_2$  as might be expected. It is a very efficient third body for the homonuclear recombination of iodine atoms, although not as efficient as  $\text{I}_2$ , again as one might expect. The most surprising result shown in Table I is the much greater effi-



TABLE I: Recombination Rate Constants for I and Cl Atoms

Reaction	$10^{32}k(M), \text{cm}^6 \text{molecule}^{-2} \text{sec}^{-1}$					
	N <sub>2</sub>	CO <sub>2</sub>	Ar	I <sub>2</sub>	ICl	Cl <sub>2</sub>
I + I + M → I <sub>2</sub> + M	1.28 <sup>a</sup>	3.72 <sup>b</sup>	0.82 <sup>b</sup>	380 <sup>b</sup>	248 ± 50 <sup>c</sup>	
I + Cl + M → ICl + M	17 ± 1 <sup>c</sup>	43 ± 8 <sup>c</sup>			119 ± 14 <sup>c</sup>	
Cl + Cl + M → Cl <sub>2</sub> + M			1.2 ± 0.1 <sup>d</sup>			5.5 ± 0.5 <sup>d</sup>

<sup>a</sup> Reference 32, 293°K. <sup>b</sup> Reference 14, 295°K. <sup>c</sup> This work, 325°K. <sup>d</sup> Reference 21, 298°K.

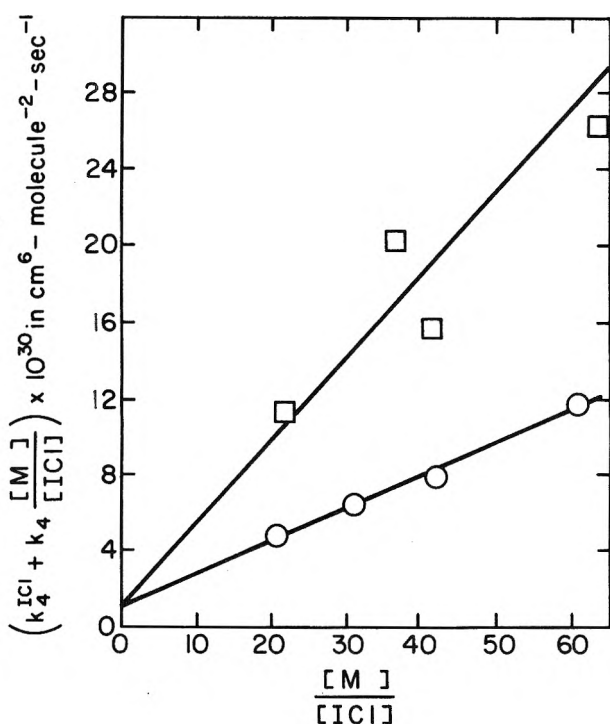
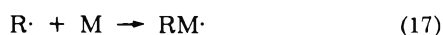


Figure 4. Dependence of heteronuclear recombination rate constant on  $[M]/[ICl]$ : O, M = N<sub>2</sub>; □, M = CO<sub>2</sub>.

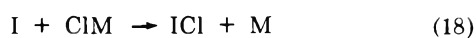
ciency of N<sub>2</sub> and CO<sub>2</sub> in promoting the heteronuclear recombination as opposed to the homonuclear recombination of I atoms. This result may be rationalized in terms of the radical-molecule complex theory<sup>12,14,33,34</sup> in which it has been shown<sup>34</sup> that the third-order rate constant may be written as

$$k_r = \alpha e^{\Delta E/RT} \quad (16)$$

where  $\Delta E$  is the exoergicity of the reaction



In general, chlorine atom bonds are stronger than iodine atom bonds and this would be reflected in a greater exoergicity for (17) when R = Cl than when R = I. Then, given essentially equal encounter frequencies for the reactions



and



one would expect, in view of (16), a greater third-order rate constant for the heteronuclear recombination, (4), than for the homonuclear recombination, (3). From stud-

ies of the temperature dependence of  $k_3(\text{CO}_2)$ , Porter<sup>34</sup> has estimated  $\Delta E$  for the formation of the I-CO<sub>2</sub> complex to be 2.35 kcal/mol. Assuming the validity of (16) one finds that the reasonable value of  $\Delta E = 3.85$  kcal/mol for the Cl-CO<sub>2</sub> exoergicity will explain the difference in the values of  $k_3(\text{CO}_2)$  and  $k_4(\text{CO}_2)$ . A similar result would also apply to  $k_3(\text{N}_2)$  and  $k_4(\text{N}_2)$  although  $\Delta E$  values for I-N<sub>2</sub> are not known. On the other hand, it would be much less likely that CO<sub>2</sub> and N<sub>2</sub> would be 11 and 13 times more efficient, respectively, in deactivating ICl\* than they would be in deactivating I<sub>2</sub>\* which would be required in terms of the energy transfer theory.<sup>35</sup>

*Excitation in the Primary Products.* With the filter employed in the ICl photolyses there is insufficient energy in the absorbed light quanta to produce I(<sup>2</sup>P<sub>1/2</sub>) atoms. It is possible that Cl(<sup>2</sup>P<sub>1/2</sub>) is formed in the primary photodissociation, but, in view of the rapid collisional spin conversion to Cl(<sup>2</sup>P<sub>3/2</sub>),<sup>36</sup> it is most probable that the excited Cl atoms will have relaxed to the ground state before combining with I atoms.

*Reaction of Atomic Chlorine with Iodine Monochloride.* Christie, Roy, and Thrush<sup>24</sup> studied the low-intensity, steady-state photolysis of iodine monochloride. From their initial photodecomposition rates and the available data at that time relative to  $k_4$ , they were able to derive values of  $k_2$  at 30 and 60°, provided the assumption that  $k_3 = k_5 = \frac{1}{2}k_4$  was valid. Inspection of Table I shows that this assumption is not a useful one in this system. We have, accordingly, recalculated  $k_2$  from their results<sup>24</sup> utilizing the data shown in Table I and assuming that over the temperature range of 30–60° the recombination rate constants are temperature independent. The result of this recalculation is that  $k_2$  is about doubled at each temperature, being  $3.2 \times 10^{-16} \text{cm}^3 \text{molecule}^{-1} \text{sec}^{-1}$  at 30° and  $6.5 \times 10^{-16} \text{cm}^3 \text{molecule}^{-1} \text{sec}^{-1}$  at 60°.

Knowledge of  $k_2$  permits us to assess more quantitatively our conclusion that (2) is playing only a very minor role under our conditions. From mechanism (1)–(5), one may write for the probability of occurrence of (2), the relation

$$P(2) = k_2[ICl]/(k_2[ICl] + k_4[M][I] + k_5[M][Cl]) \\ = 1/[1 + (k_4[M][I]/k_2[ICl]) + (k_5[M][Cl]/k_2[ICl])] \quad (20)$$

Substitution of the values of  $k_2$ ,  $k_4$ , and  $k_5$  into (20) and consideration of the fact that ~10% of ICl is decomposed in the flash leads to the conclusion that for  $P(2)$  to be as high as 0.1 some 95% of the original chlorine atoms and iodine atoms have disappeared. Thus (2) can become sig-

(33) O. K. Rice, *J. Chem. Phys.*, **9**, 258 (1941).

(34) G. Porter, *Disc. Faraday Soc.*, **33**, 197 (1962).

(35) H. B. Palmer and D. F. Hornig, *J. Chem. Phys.*, **26**, 98 (1957).

(36) R. J. Donovan, D. Husain, A. M. Bass, W. Braun, and D. D. Davis, *J. Chem. Phys.*, **50**, 4115 (1969).

nificant only in the very last stages ( $t > 300 \mu\text{sec}$ ) of the iodine and iodine monochloride formation shown in Figure 1.

*Effect of Additives.* We attempted to examine the effects of nitric oxide, oxygen, and ethylene on the flash photolysis to see if atom-scavenging reactions could be ob-

served. These attempts failed because in all three cases a very rapid dark reaction occurred, consuming the iodine monochloride.

*Acknowledgment.* Acknowledgment is made to the donors of the Petroleum Research Fund, administered by the American Chemical Society, for support of this research.

## Primary and Secondary Photolytic Processes in the Photodecomposition of Thietane Vapor

D. R. Dice and R. P. Steer\*

Department of Chemistry and Chemical Engineering, University of Saskatchewan, Saskatoon, Saskatchewan, Canada  
(Received July 14, 1972)

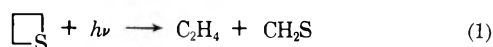
Publication costs assisted by the University of Saskatchewan

The photolysis of thietane vapor at 254 and 313 nm and at temperatures between 22 and 200° has been examined. The only primary photodecomposition forms ethylene and thioformaldehyde. Thioformaldehyde monomer is long lived and undergoes secondary photolysis to produce propylene in a sequence of reactions involving both the photoexcited monomer and a diradical. Photolysis of thioformaldehyde yields  $\text{H}_2$  with a quantum yield  $\leq 0.08$  at temperatures less than 200° and is therefore much more resistant to photodecomposition than its oxygen analog.

Extensive investigations have yielded valuable information concerning the mechanism of the primary processes involved in the photolysis of the cyclic ketones,<sup>1</sup> the pyrazolines,<sup>2</sup> the cyclic ethers,<sup>3</sup> and the cyclic sulfides.<sup>4</sup> In particular, the question of diradical *vs.* molecular decomposition pathways has been thoroughly studied and, in the cases of the cyclic ketones and the pyrazolines, tentative identifications of the excited states involved have been made. For the cyclic ethers and sulfides, however, the nature of the excited states and the photodecomposition pathways are much less certain. In part this is due to the added complication that one or more of the primary products may absorb light strongly at the photolysis wavelength.

For the particular case of the cyclic ethers, some evidence that secondary photolysis may be important has been obtained.<sup>3</sup> The carbonyl-containing fragment produced in the primary step apparently undergoes secondary photodecomposition with the production of several additional products.

Previous reports of the photolysis of thietane<sup>4b</sup> vapor have indicated that ethylene is a major product, likely arising *via* the molecular scission of an excited molecule.



Other hydrocarbon products, cyclopropane and propylene, were thought to arise from the reaction of unidentified intermediates with the substrate. It was necessary to postulate the existence of at least four different excited states and three additional intermediates to explain the results

obtained. No secondary photolysis processes were reported.

In this paper evidence that propylene is not a primary product of the photolysis of thietane vapor in its lowest energy absorption band is presented. Rather, it is demonstrated that propylene is very likely produced as a result of the secondary photolysis of monomeric thioformaldehyde. Conclusions regarding the nature of the likely primary processes in the photolysis of thioformaldehyde are also presented.

### Experimental Section

*Materials.* Thietane (Eastman) was purified by preparative gas chromatography on a 10-ft dinorolyl phthalate column. NO (Matheson) was purified by passing it through a 5-ft silica gel column at -78° followed by degassing under vacuum at -210°. It was distilled from

- (1) (a) H. A. J. Carless and E. K. C. Lee, *J. Amer. Chem. Soc.*, **94**, 1 (1972); (b) J. Metcalfe and E. K. C. Lee, *ibid.*, **94**, 7 (1972); (c) J. C. Hemminger, C. F. Rusbult, and E. K. C. Lee, *ibid.*, **93**, 1867 (1971); (d) T. F. Thomas and H. J. Rodriguez, *ibid.*, **93**, 5918 (1971); (e) W. C. Agosta and A. B. Smith, *ibid.*, **93**, 5513 (1971).
- (2) (a) E. B. Klunder and R. W. Carr, Jr., *Chem. Commun.*, 742 (1971); (b) D. S. Nowacki, P. B. Do, and F. H. Dorer, *J. Chem. Soc., Chem. Commun.*, 273 (1972); (c) J. J. Gajewski, A. Yeshurun, and E. J. Bair, *J. Amer. Chem. Soc.*, **94**, 2138 (1972).
- (3) J. D. Margerum, J. N. Pitts, Jr., J. G. Rutgers, and S. Searles, *J. Amer. Chem. Soc.*, **81**, 1549 (1959).
- (4) (a) A. Padwa and R. Gruber, *J. Org. Chem.*, **35**, 1781 (1970); (b) H. A. Wiebe and J. Heicklen, *J. Amer. Chem. Soc.*, **92**, 7031 (1970); (c) S. Braslavsky and J. Heicklen, *Can. J. Chem.*, **49**, 1317 (1971); (d) W. E. Haines, G. L. Cook, and J. S. Ball, *J. Amer. Chem. Soc.*, **78**, 5213 (1956).

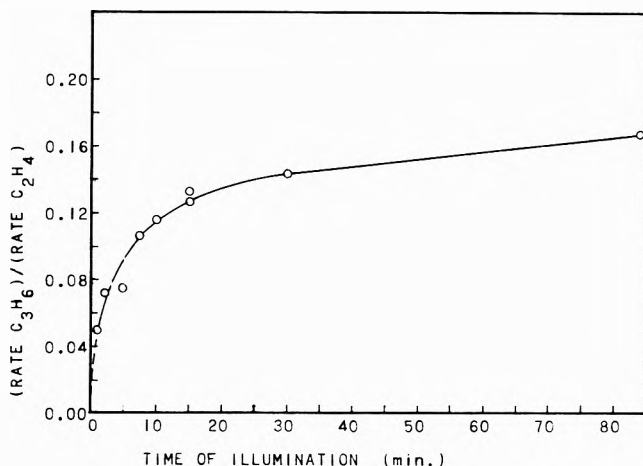


**Figure 1.** Ratio of rate of C<sub>3</sub>H<sub>6</sub> to C<sub>2</sub>H<sub>4</sub> production vs. time of illumination in the 254-nm photolysis of 30.0 Torr of thietane at 200°.

-160° prior to each run. H<sub>2</sub>S was purified by gas chromatography on a 10-ft Porapak Q column to remove traces of hydrocarbons. Ethylene and isopentane were subjected to rough fractionation and degassing under vacuum.

**Apparatus.** The reaction system was a typical mercury-containing, grease-free high-vacuum system. Photolysis was carried out in a cylindrical quartz cell 20 cm in length and of 0.216 l. total volume mounted in an aluminum block furnace. The temperature of the oven was controlled to ±1°.

In some runs a Hanovia medium-pressure lamp was used in conjunction with a Corning No. 7740 filter to isolate the λ >300-nm region, and with a Barr and Stroud U2 interference filter to isolate the 254-nm region. In most experiments a PEK Model 715 500-W high-pressure mercury lamp was used in conjunction with a Bausch and Lomb high-intensity grating monochromator, adjusted for a 10-nm bandwidth. Intensity of irradiation was monitored using an RCA 935 phototube coated with sodium salicylate. Response of the phototube was linear with light intensity at both wavelengths.

Extinction coefficients were measured using a Cary 14 spectrophotometer and were found to be nearly invariant with temperature from 25 to 230° in the 330-240-nm region.

**Analysis.** Products from the photolysis were analyzed using a Gow-Mac 69-500 gas chromatograph modified to allow the direct sampling of gases. The fraction noncondensable at -130° was separated on a 10-ft Porapak Q column, and the condensable products on a 10-ft 10% dinonyl phthalate on Gas-Chrom Z column. NO was measured using a molecular sieve 13X column using carrier gas purified by passage through a molecular sieve trap at -196°. Identification of products was made by mass spectrometry and comparison of retention times with authentic samples.

## Results

Thietane exhibits a broad, structureless absorption extending from about 240 to 330 nm. At the photolysis wavelengths of 254 and 313 nm the decadic molar extinction coefficients for thietane vapor were found to be 11.4 and 0.75 M<sup>-1</sup> cm<sup>-1</sup>, respectively, virtually independent of temperature and in excellent agreement with previous measurements.<sup>4b,5</sup>

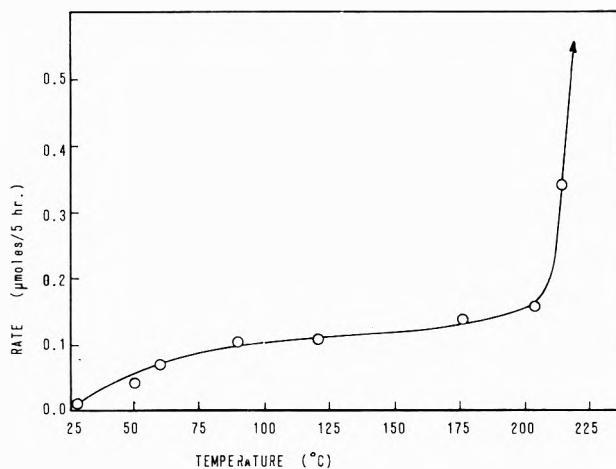


**Figure 2.** Rate of C<sub>3</sub>H<sub>6</sub> production vs. temperature from the 313-nm photolysis of 10 Torr of thietane.

Photolysis of thietane vapor at either wavelength, at temperatures from 22 to 235° and at pressures from 1 to 40 Torr produces only ethylene (and thioformaldehyde) in substantial yield when the percentage decomposition of the substrate is sufficiently small. That propylene is in fact a secondary photolysis product may be observed from Figure 1, in which a typical graph of the ratio of the rate of C<sub>3</sub>H<sub>6</sub> to the rate of C<sub>2</sub>H<sub>4</sub> production is plotted as a function of exposure time. Because the rate of production of C<sub>2</sub>H<sub>4</sub> is nearly invariant with exposure time in these experiments, it is evident that at very small percentage decompositions the rate of C<sub>3</sub>H<sub>6</sub> falls to near zero. In order to show that the presence of ethylene was not necessary for the production of propylene, a similar series of experiments was carried out in which 10 Torr of thietane with 1 Torr added ethylene was photolyzed. The rate of C<sub>3</sub>H<sub>6</sub> production still fell to near zero at short exposure times. The rates of formation of cyclopropane and of all other minor products are less than 2% of the rate of C<sub>2</sub>H<sub>4</sub> formation for photolysis in this absorption band and were not measured routinely. When 10 Torr of thietane was photolyzed at 200° with 1 atm of Ar added no significant change in the yield of cyclopropane was observed.

In order to obtain some information regarding the nature of the secondary photolysis process, experiments were carried out in which the yield of C<sub>3</sub>H<sub>6</sub> from the photolysis of thietane to about 1% conversion was measured as a function of temperature. Figure 2 indicates that there are probably two processes producing propylene. One is dominant at temperatures less than about 200° and is responsible for the slow increase in the yield with increasing temperature. The second is responsible for the rapid increase in the yield at temperatures greater than about 200°. Blank runs showed that this rapid rise in yield was photochemically and not thermally initiated.

These results were confirmed by experiments in which the yield of C<sub>3</sub>H<sub>6</sub> was measured as a function of the pressure of added nitric oxide (Figure 3). At 205° only part of the propylene is scavengable with NO. As the temperature is lowered, the fraction of the C<sub>3</sub>H<sub>6</sub> which can be scavenged increases sharply and virtually all the propylene is scavengable at temperatures less than 175°.

(5) (a) R. E. Davis, *J. Org. Chem.*, **23**, 1380 (1958); (b) D. R. Williams and L. T. Kontnik, *J. Chem. Soc. B*, 312 (1971).



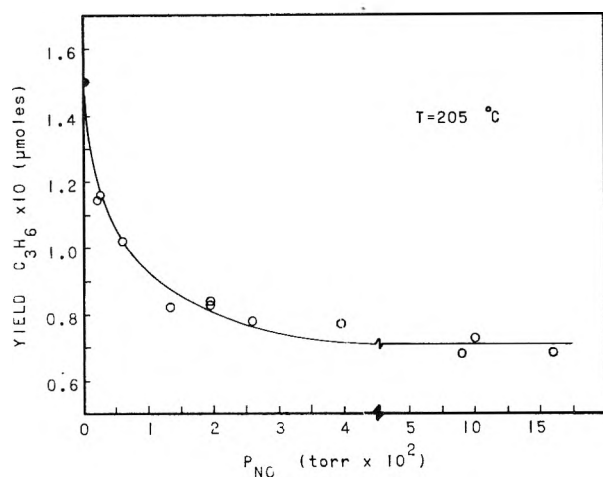


Figure 3. Yield of  $C_3H_6$  vs. pressure of added NO from the 313-nm photolysis of 10 Torr of thietane at  $205^\circ$ .

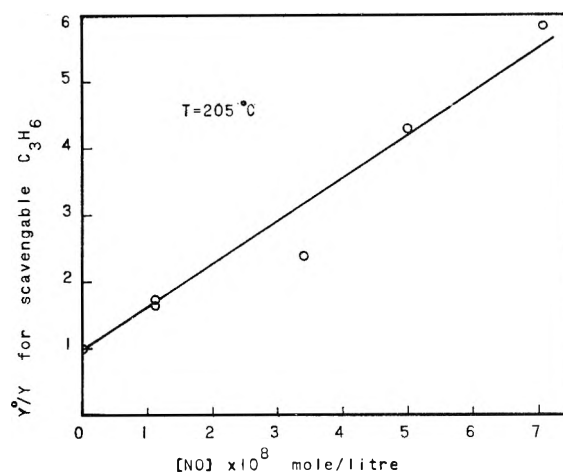


Figure 4. Stern-Volmer plot of the ratio of the yield of scavengable  $C_3H_6$  with no added NO ( $Y^0$ ) to the yield of scavengable  $C_3H_6$  with NO added ( $Y$ ) vs. concentration of added NO. Photolysis was at 313 nm and  $205^\circ$ .

Table I<sup>a</sup>

$P_{NO}$ , Torr	Rate ( $C_2H_4$ ), $\mu\text{mol}/5\text{ hr}$	Rate ( $C_3H_6$ ), $\mu\text{mol}/5\text{ hr}$	$\Delta R(NO)/\Delta R(C_3H_6)$
0	1.75	0.150	
50	1.76		
10	1.73		
$2.32 \times 10^{-2}$		0.080	1.49
$3.74 \times 10^{-2}$		0.072	1.78
$5.53 \times 10^{-2}$		0.067	2.07
$8.40 \times 10^{-2}$		0.066	2.01
$11.73 \times 10^{-2}$		0.066	2.06

<sup>a</sup>  $T = 205^\circ$ ,  $\lambda = 313\text{ nm}$ ,  $P_{\text{thietane}} = 10\text{ Torr}$ .

In order to show that NO was in fact scavenging radical- or diradical-precursors of propylene (and not just quenching some excited intermediate) experiments were carried out in which the amount of NO consumed was measured. All experiments were performed at  $205^\circ$  with 313-nm radiation. The results are presented in Table I. In these experiments the yields of ethylene (a primary product) were unchanged when up to 50 Torr of NO was added. Blank runs indicated that NO was not consumed on prolonged heating of mixtures of NO and thietane or NO, thietane, and its photolysis products. (Greater than 98% of the NO initially present was recovered in these blank runs.) At NO pressures for which scavenging of the scavengable precursor of  $C_3H_6$  was complete ( $>4 \times 10^{-2}$  Torr at  $205^\circ$ ), the ratio of the amount of NO consumed to the amount of  $C_3H_6$  scavenged,  $\Delta R(NO)/\Delta R(C_3H_6)$ , was 2:1 within an experimental error of about  $\pm 7\%$ .

## Discussion

The available evidence now indicates that the only primary products of the 254- and 313-nm photolysis of thietane vapor at temperatures from 22 to  $200^\circ$  are ethylene and monomeric thioformaldehyde. Propylene is a secondary photolysis product, one precursor of which is scavengable (at  $T < 175^\circ$ ) by nitric oxide. Other products (cyclopropane,  $CH_4$ , and  $CS_2$ ) are present in trace amounts ( $<1\%$  of the  $C_2H_4$  yield) and are not formed by a significant decomposition pathway.

The question of the nature of the secondary photolysis process and the mechanism of  $C_3H_6$  production is a particularly intriguing one. Two questions must be answered: first, what is the identity of the species which absorbs and thereby initiates the propylene-producing reactions, and second, what is the nature of the nitric oxide consuming species which is the propylene precursor?

*Identity of Absorber.* The light absorber responsible for the initiation of the propylene-producing reactions is very likely monomeric thioformaldehyde, produced in the primary process (reaction 1) in yield equal to that of ethylene. This process is analogous to that postulated by Margerum, *et al.*,<sup>3</sup> in the photolysis of oxetane vapor at  $\lambda < 200\text{ nm}$  in which formaldehyde, a primary product, absorbed light in its ( $\pi, \pi^*$ ) absorption band and decomposed to H, HCO,  $H_2$ , and CO.

Thioformaldehyde is unstable in monomeric form and has been reported to undergo trimerization to trithiane,<sup>6</sup> a crystalline material of low volatility (mp  $216^\circ$ ) which, if present, could not have been analyzed in our experiments. The rate of disappearance of the monomer is likely quite slow, however, and previous measurements<sup>7,8</sup> have indicated that the half-life of thioformaldehyde may be as long as several minutes in a static system. Because a "steady-state" concentration of thioformaldehyde monomer will only be achieved after a period of several monomer half-lives, it is evident that it may take several minutes for a steady state to be achieved in the photolysis system. This compares favorably with the observed time required for a steady state to be achieved in the rate of  $C_3H_6$  production (*cf.*, Figure 1). One therefore may conclude that the production of monomeric thioformaldehyde is a necessary preliminary step in the production of  $C_3H_6$ . Reactions leading to propylene subsequent to the initial excitation of thioformaldehyde may easily occur in a time which is short in comparison with the time necessary to establish steady-state conditions in the photolysis system.

- (6) E. E. Reid, "Organic Chemistry of Bivalent Sulfur," Vol. III, Chemical Publishing Co., New York, N. Y., 1960, Chapter 2.  
 (7) (a) A. B. Callear, J. Connor, and D. R. Dickson, *Nature (London)*, **221**, 1238 (1969); (b) A. B. Callear and D. R. Dickson, *Trans. Faraday Soc.*, **66**, 1987 (1970).  
 (8) (a) J. W. C. Johns and W. B. Olson, *J. Mol. Spectrosc.*, **39**, 479 (1971); (b) D. R. Johnson, F. X. Powell, and W. H. Kirchhoff, *ibid.*, **39**, 136 (1971).

Other evidence that thioformaldehyde monomer is the most logical choice for the secondary absorber comes from a consideration of the nature of the electronic absorption spectrum which such an absorber must have. If the absorption of light by the secondary absorber (assumed to be  $\text{CH}_2\text{S}$ ) produces  $\text{C}_3\text{H}_6$  with a maximum quantum yield of unity, then, when only a small percentage of the incident light is absorbed,  $([\text{CH}_2\text{S}]_{\text{ss}} \epsilon(\text{CH}_2\text{S})^{254})/([\text{C}_3\text{H}_6\text{S}] \epsilon(\text{C}_3\text{H}_6\text{S})^{254}) \geq (\text{rate } \text{C}_3\text{H}_6)/(\text{rate } \text{C}_2\text{H}_4)$  under steady-state conditions. The best fit of the data of Figure 1 gives a half-life for  $\text{CH}_2\text{S}$  of about 3 min (in excellent agreement with previous measurements<sup>8</sup>) and a resultant steady-state concentration of  $\text{CH}_2\text{S}$  of about  $2 \times 10^{-6} M$ , assuming that the monomer disappears by first-order or pseudo-first-order processes. Using this data, the previously determined value of  $\epsilon(\text{C}_3\text{H}_6\text{S})^{254} 11.4 M^{-1} \text{ cm}^{-1}$  and a  $[\text{C}_3\text{H}_6\text{S}]$  of  $1.61 \times 10^{-3} M$ , one calculates that  $\epsilon(\text{CH}_2\text{S})^{254} \geq 1.3 \times 10^3 M^{-1} \text{ cm}^{-1}$ .

Unfortunately the electronic absorption spectrum of thioformaldehyde has not been measured. However, in this reaction system only a  $(\pi, \pi^*)$  or a  $(n, \sigma^*)$  transition of a thiocarbonyl group is likely to have a molar extinction coefficient of the required magnitude. Furthermore, the existence of a  $(\pi, \pi^*)$  transition having a position near 254 nm and  $\epsilon^{254} \geq 1.3 \times 10^3 M^{-1} \text{ cm}^{-1}$  is not at all unreasonable. Previous measurements of the absorption spectra of aliphatic thio ketones<sup>9,10</sup> have shown that there are three absorptions in the near uv-visible region; an intense  $(n, \sigma^*)$  absorption with  $\lambda_{\text{max}}$  near 215 nm (corresponding to the long-lived absorption observed by Callear, *et al.*,<sup>7</sup> in the flash photolysis of  $\text{CH}_3\text{SSCH}_3$ ), an intense  $(\pi, \pi^*)$  absorption with  $\lambda_{\text{max}}$  near 240 nm, and a weak  $(n, \pi^*)$  absorption with  $\lambda_{\text{max}}$  about 500 nm. Since the aliphatic aldehydes and ketones exhibit similar spectra<sup>11</sup> it is not unreasonable to expect that thio aldehydes will have electronic absorption spectra similar to those of the thio ketones. Other possible light absorbers such as saturated sulfides and disulfides would not likely have large enough extinction coefficients at this wavelength. The conclusion that  $\text{CH}_2\text{S}$  is the absorber responsible for the initiation of the sequence of reactions which result in the ultimate production of  $\text{C}_3\text{H}_6$  is compelling.

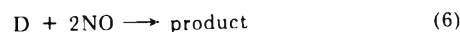
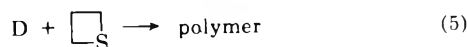
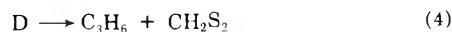
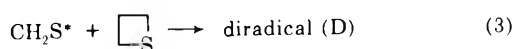
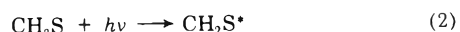
One interesting conclusion which may be drawn from these experiments is that photolysis of  $\text{CH}_2\text{S}$  at wavelengths greater than 240 nm produces little atomic or molecular hydrogen. Careful analysis of the reaction products in runs in which a narrow band of wavelengths was employed produced no measurable amount of  $\text{H}_2$  either in the photolysis at elevated temperatures of the substrate alone or in the presence of added  $\text{H}_2\text{S}$  and isopentane, commonly used as sources of readily abstractable hydrogen atoms. However, in experiments in which the full ( $\lambda > 240 \text{ nm}$ ) spectrum of the high-pressure lamp was utilized  $\text{H}_2$  was produced with a yield of about 7–8% of that of propylene at 200°. Thus at temperatures less than 200° the quantum yield of  $\text{H}_2$  from the  $\lambda > 240 \text{ nm}$  photolysis of  $\text{CH}_2\text{S}$  must be less than about 0.08 since the maximum quantum yield of  $\text{C}_3\text{H}_6$  is unity. Thioformaldehyde would therefore appear to be much more resistant to photodecomposition than its oxygen analog.<sup>12</sup> One can conclude that other radiative and nonradiative pathways for dissipating the absorbed energy must be much more important than decomposition in the photolysis of  $\text{CH}_2\text{S}$  in its  $(\pi, \pi^*)$  or  $(n, \pi^*)$  absorption bands.

*Nature of the Scavengable Precursor of  $\text{C}_3\text{H}_6$ .* It is much more difficult to identify the scavengable interme-

diolate which is the propylene precursor. The results presented do allow it to be partially characterized however.

A 2:1 ratio for  $\Delta R(\text{NO})/\Delta R(\text{C}_3\text{H}_6)$  is consistent with either (1) the scavenging of a diradical precursor of  $\text{C}_3\text{H}_6$  by 2NO, or (2) the reaction of 1NO with each of two free radicals, one of which is a precursor of  $\text{C}_3\text{H}_6$ . The latter possibility may be eliminated on the grounds that there are no products present in significant yield which could have free radical origins. Moreover, the possibility that NO is consumed in reactions involving free S atoms can be ruled out since previous work<sup>4b</sup> has demonstrated that free S atoms are not formed in this system. It is conceivable that NO could react with excited  $\text{CH}_2\text{S}$  to yield a product of formula  $\text{ONCH}_2\text{SNO}$  but it is highly unlikely that this species would be stable even if such a reaction could occur. One therefore concludes that a diradical is the most likely  $\text{C}_3\text{H}_6$  precursor.

The diradical cannot be  $\cdot\text{CH}_2\text{CH}_2\text{CH}_2\text{S}\cdot$  because such a species would almost certainly decompose to  $\text{C}_2\text{H}_4$  and  $\text{CH}_2\text{S}$ , yet the  $\text{C}_2\text{H}_4$  yield is unaffected by nitric oxide. Trimethylene is also not likely involved because cyclopropane, a major product of trimethylene ring closure,<sup>2</sup> is not present in significant quantity either at low pressure or with high pressures of inert deactivator added. Rather, we suggest that the diradical must be formed from the reaction of electronically excited thioformaldehyde either with ground state  $\text{CH}_2\text{S}$ , or with the substrate in a sequence of reactions which leads to the formation of polymer and propylene. The former process is analogous to the photodimerization of thiocarbonyls proposed by Ohno, *et al.*,<sup>12</sup> but would require subsequent reactions with substrate before propylene could be produced. The latter process is also more likely because the substrate is present in a concentration which is about a thousand times larger than that of  $\text{CH}_2\text{S}$ . A mechanism for the reaction below 175° which identifies the necessary overall reactions but which is likely quite incomplete follows.



The identity of the diradical, D, cannot be established at present because it was not possible to characterize the product of reaction 6. Either this product is unstable to gas chromatographic analysis or it is sufficiently involatile that it is impossible to remove it from the reaction cell. Some polymeric material is formed in the cell but neither photolysis nor thermolysis subsequent to its formation yields  $\text{C}_3\text{H}_6$  or  $\text{C}_2\text{H}_4$ . Any reaction in which a diradical decomposes to more than one  $\text{C}_3\text{H}_6$  can be ruled out since a  $\Delta R(\text{NO})/\Delta R(\text{C}_3\text{H}_6)$  ratio of less than 2:1 would be obtained in such a process. Hence, any product of reaction 5 cannot yield more than one  $\text{C}_3\text{H}_6$  if it decomposes. Moreover, because  $\Delta R(\text{NO})/\Delta R(\text{C}_3\text{H}_6) \approx 2$  and because nei-

- (9) J. Fabian and R. Mayer, *Spectrochim. Acta*, **20**, 299 (1964).  
 (10) D. R. Kemp, A. H. Lawrence, C. C. Liao, R. O. Loutfy, P. de Mayo, A. A. Nicholson, and S. Paszyc, *Pure Appl. Chem., Suppl.* **1**, 367 (1971).  
 (11) J. G. Calvert and J. N. Pitts, Jr., "Photochemistry," Wiley, New York, N. Y., pp 368–377.  
 (12) A. Ohno, Y. Ohnishi, and G. Tsuchihashi, *J. Amer. Chem. Soc.*, **91**, 5038 (1969).

ther  $N_2$  nor  $NO_2^{13}$  were produced in these experiments, further reaction of NO with the product of reaction 6 apparently does not occur.

At present the nature of the reactions which result in the formation of unscavengable  $C_3H_6$  at temperatures greater than  $175^\circ$  is unclear. This aspect of the work is under active investigation, however, and speculation regarding the possible results would seem to be unwarranted at present.

Finally, an estimate of the lifetime,  $\tau$ , of the scavengable diradical precursor to  $C_3H_6$  can be obtained from analysis of the data in Figure 3. Considering the scavengable portion of the  $C_3H_6$  only, a Stern-Volmer type of plot may be constructed (Figure 4). The slope of the graph gives  $\tau k = 4.3 \times 10^6 M^{-1}$ , where  $k$  is the rate constant for

the scavenging reaction. An upper limit of  $k \leq 3.6 \times 10^{11} M^{-1} \text{ sec}^{-1}$  is obtained for the case in which the scavenging reaction is diffusion controlled. Thus the average lifetime of D will be greater than  $1.2 \times 10^{-5} \text{ sec}$  at  $205^\circ$ .

*Acknowledgments.* The authors would like to thank the National Research Council of Canada for financial support. Some of the equipment was purchased through a Frederick Gardner Cottrell Grant from the Research Corporation. One of us (D. R. D.) would like to thank the National Research Council for a scholarship.

(13) B. G. Gowenlock, *Progr. React. Kinet.*, **3**, 172 (1965).

## Kinetics of Particle Growth. I. Ammonium Nitrate from the Ammonia-Ozone Reaction<sup>1a</sup>

R. G. de Pena,<sup>1b</sup> Kenneth Olszyna,<sup>1c</sup> and Julian Hecklen\*

Departments of Meteorology and Chemistry and the Center for Air Environment Studies. The Pennsylvania State University, University Park, Pennsylvania 16802 (Received August 28, 1972)

$NH_4NO_3$  particles were prepared from the reaction of  $NH_3$  and  $O_3$  at room temperature. The  $NH_3$  and initial  $O_3$  pressures ranged from 0.034 to 2.0 and from 0.020 to 0.10 Torr, respectively, their ratio being between 2 and 21.5. In all of the experiments  $N_2$  was also present. The  $O_3$  decay was monitored by ultraviolet absorption and obeyed the rate law  $-d[O_3]/dt = k[O_3]$ , where  $k$  is a function of  $[NH_3]$  and  $[O_3]_0$  (the initial value of  $[O_3]$ ). One molecule of  $NH_4NO_3$  was presumed to be produced for every four molecules of  $O_3$  consumed. The total number of particles greater than 200 or 1000 Å diameter was monitored as a function of reaction time. Initially there is a rapid production of particles in a short period of time (<10 min) until about  $10^5$  particles/cc are produced. Then particle production stops, as deduced from the fact that the number of particles between 200 and 1000 Å rapidly falls to zero. The larger particles grow, though the number,  $N$ , decays slowly according to the rate law  $N = N_0 \exp(-k't)$ . The number of particles is too small for coagulation to play any role, and the decay constant  $k'$  can be associated with diffusional loss to the wall. The number of particles at zero time,  $N_0$ , increases with the loss rate of  $O_3$  and with the  $N_2$  pressure. The particles,  $C_l$  ( $l = \text{integer}$ ), grow by reaction with the monomer, the average growth rate constant being  $\beta k[O_3]/4N$  where  $\beta$  is the fraction ( $\sim 3 \times 10^{-3}$ ) of  $NH_4NO_3$  monomers entering the gas phase. The loss of particles is entirely by diffusion to the walls, with a pressure-dependent rate constant  $k_{2,l}$ . For the simplified situation in which initially  $N_0$  particles of  $r$  monomer units each are produced, and the particle growth rate constants are all considered identical, *i.e.*,  $\beta k[O_3]/4N$  (a nearly time-independent parameter since  $N$  and  $[O_3]$  decay at similar rates), then a simplified solution for the particle size distribution results,  $[C_l] = N_0(\beta k[O_3]t/4N)^{l-r} \exp(-\alpha_l t)/(l-r)!$ , where  $\alpha_l = \beta k[O_3]/4N + k_{2,l}$ . This distribution predicts a single maximum for  $[C_l]$  at  $\tau_{\text{max}} = (l-r)/\alpha_l$ .

### Introduction

In our laboratory, we have initiated a program to examine the kinetics of particle formation, *i.e.*, both the size distribution and growth rates, as a function of time for particles produced from gas-phase chemical reactions. As far as we know, such studies have not been made before under isothermal conditions, though particle formation has been observed in numerous laboratory studies and is important in polluted urban atmospheres.

A number of studies have been made of soot formation in flames and hydrocarbon pyrolysis. Soot formation in

acetylene pyrolysis initiated at 770–1070°K and reaching 3000°K as a maximum has been discussed by Tesner.<sup>2</sup> He considered an initial distribution of carbon particles, corresponding to a commercial soot, and assumed that the particles grew upon every collision with a  $C_2H_2$  molecule until the  $C_2H_2$  was exhausted. The computed growth rate was about seven times that found experimentally, which

(1) (a) CAES Report No. 246-72. (b) Department of Meteorology. (c) Environmental Protection Agency air pollution trainee.  
(2) P. A. Tesner, *Disc. Faraday Soc.*, **30**, 170 (1960).



Tesner felt reflected the fact that every collision would not be effective.

Theoretical models have been discussed for isothermal particle growth under various conditions. Several studies have considered coagulation and wall losses,<sup>3-7</sup> whereas Goodrich<sup>8,9</sup> and Hudson and his coworkers<sup>10,11</sup> considered growth only by monomer interaction with the particles.

A number of experimental studies<sup>12-17</sup> have been reported in aging of aerosols and smokes by coagulation, but in none of these studies were gas-phase chemical reactions involved in the formation or growth process. In this paper we experimentally follow the growth rate and size distribution of NH<sub>4</sub>NO<sub>3</sub> particles produced in the reaction of NH<sub>3</sub> with O<sub>3</sub>. A previous study<sup>18</sup> from our laboratory characterized the kinetics of the loss of the gas-phase reactants.

### Experimental Section

All of the gases used were from the Matheson Co. These included Extra Dry grade O<sub>2</sub>, CP grade NH<sub>3</sub>, and prepurified N<sub>2</sub>. The nitrogen was used after passing through a glass wool filter at -196°, the only remaining impurity being trace amounts of O<sub>2</sub>. The NH<sub>3</sub> was purified by distillation from -98 to -196°. The ozone was prepared from a tesla coil discharge through O<sub>2</sub>, which had been passed through traps at -196°. The ozone was distilled at -186° and collected at -196° with continuous degassing to eliminate any impurities, particularly oxides of nitrogen.<sup>18</sup>

Before each experiment, N<sub>2</sub> was passed through the reaction vessel until the number of particles >200 Å in diameter was <6/cc. Samples of O<sub>3</sub> in N<sub>2</sub> and NH<sub>3</sub> in N<sub>2</sub> were tested periodically, and they always showed <3 particles/cc.

The O<sub>3</sub> pressure was measured by optical absorption at 2537 Å and checked with a H<sub>2</sub>SO<sub>4</sub> manometer. The NH<sub>3</sub> and N<sub>2</sub> pressures were measured by Wallace and Tiernan gauges.

The gases were introduced into the reaction vessel as follows. First O<sub>3</sub> was introduced, and then NH<sub>3</sub> and N<sub>2</sub> were added simultaneously. The reaction was monitored continually by ultraviolet absorption spectroscopy utilizing low intensities so that photochemical reaction was not induced by the monitoring lamp. The monitoring light source was a Philips 93109E low-pressure mercury resonance lamp. The radiation passed through a Corning 7-54 filter to remove radiation below 2200 and above 4200 Å and a cell filled with chlorine to remove radiation above 2800 Å before passing through the reaction vessel to a RCA 9-35 phototube.

All gases were handled in a grease-free, high-vacuum line employing Teflon stopcocks with Viton O-rings. The reaction vessel was a Pyrex cell 100 cm long and 5 cm in diameter with quartz windows sealed to the ends with epoxy resin. To ensure complete mixing the gases were introduced into the reaction vessel through a Pyrex tube (96 cm long and 8 mm diameter with several pinholes equally spaced along its length) which was placed in the vessel close to the surface.

Samples (~1.6% of total reaction volume) were withdrawn periodically during the reaction by expanding the reaction mixture into a collection tube under vacuum. The collection tube was connected through a stopcock to a tube of ~5 cc volume attached directly to the reaction vessel. The gases in the lead-in tube thus accounted for about 15% of the sample withdrawn. The sample was di-

luted with N<sub>2</sub> and analyzed for its particle content using a thermal diffusion chamber. The sampling and analyzing procedure was performed in approximately 30 sec.

The physical properties operating in such chambers had been discussed by Twomey<sup>19</sup> and more recently by Saxena, *et al.*<sup>20</sup> Basically, the chamber consists of two moistened surfaces maintained at a constant temperature difference. Water vapor is distributed through the chamber by mixing and diffusion; a linear distribution in water pressure and temperature is established between the two surfaces, which are maintained at temperatures  $T_1$  and  $T_2$ , respectively.

Since the saturation vapor pressure,  $p_s$ , described by the Clausius-Clapeyron equation

$$dp_s/dT = L_v/RT^2$$

( $L_v$  is the heat of vaporization and  $R$  is the gas constant) is not linearly related to the temperature,  $T$ , supersaturation results everywhere between the surfaces. Supersaturation,  $S$ , is defined as

$$S = (p - p_s)/p_s$$

The maximum difference between  $p$  and  $p_s$  is near the temperature  $(T_2 - T_1)/2$ , and it is expected that all the sample will pass through this region.

By changing the temperatures  $T_2$  and  $T_1$ , different supersaturations can be obtained. Soluble particles introduced in an environment where water vapor is present will form droplets whose radii are determined by the equation

$$p = p_s(1 - B/r^3) \exp(A/r) \quad (a)$$

where  $p$  is the vapor pressure in the chamber,  $r$  is the radius of the droplet, and

$$A = 2\gamma M/\rho RT$$

$$B = 3im_lM/4\pi\rho M_l$$

$\gamma$  is the surface tension of water,  $\rho$  is the density of water,  $i$  is the Van't Hoff factor,  $m_l$  is the mass of the particle,  $M$  is the molecular weight of water, and  $M_l$  is the molecular weight of the particle.

If the vapor pressure  $p$  exceeds a certain critical value, which is the maximum value computed from eq a, the

- (3) (a) J. R. Brock and G. M. Hidy, *J. Appl. Phys.*, **36**, 1857 (1965); (b) L. F. Mockros, J. E. Quon, and A. T. Hjelmfelt, Jr., *J. Colloid Interface Sci.*, **23**, 90 (1967).
- (4) J. Pich, S. K. Friedlander, and F. S. Lai, *Aerosol Sci.*, **1**, 115 (1970).
- (5) C.-M. Huang, M. Kerker, and E. Matijević, *J. Colloid Interface Sci.*, **33**, 529 (1970).
- (6) E. R. Cohen and E. U. Vaughan, *J. Colloid Interface Sci.*, **35**, 612 (1971).
- (7) G. C. Lindauer and A. W. Castleman, Jr., *Aerosol Sci.*, **2**, 85 (1971).
- (8) F. C. Goodrich, *Proc. Roy. Soc., Ser. A*, **277**, 155 (1964).
- (9) F. C. Goodrich, *Proc. Roy. Soc., Ser. A*, **277**, 167 (1964).
- (10) J. L. Hudson and J. Hecklen, *Carbon*, **6**, 405 (1969).
- (11) J. Hecklen, J. L. Hudson, and L. Armi, *Carbon*, **7**, 365 (1969).
- (12) H. S. Patterson, R. Whyllaw-Gray, and W. Cawood, *Proc. Roy. Soc., Ser. A*, **124**, 502 (1929).
- (13) R. Whyllaw-Gray, *J. Chem. Soc.*, 268 (1935).
- (14) T. Gillespie and G. O. Langstroth, *Can. J. Chem.*, **29**, 133 (1951).
- (15) T. Gillespie and G. O. Langstroth, *Can. J. Chem.*, **29**, 201 (1951).
- (16) T. Gillespie and G. O. Langstroth, *Can. J. Chem.*, **30**, 1003 (1952).
- (17) J. M. Dalla Valle, C. Orr, Jr., and B. L. Hinkle, *Brit. J. Appl. Phys., Suppl.* **3**, 5, S198 (1954).
- (18) K. Olszyna and J. Hecklen, *Advan. Chem. Ser.*, in press.
- (19) S. Twomey, *J. Rech. Atmos.*, **1**, 101 (1963).
- (20) V. K. Saxena, J. N. Burford, and J. L. Kassur, *J. Atm. Sci.*, **27**, 73 (1970).

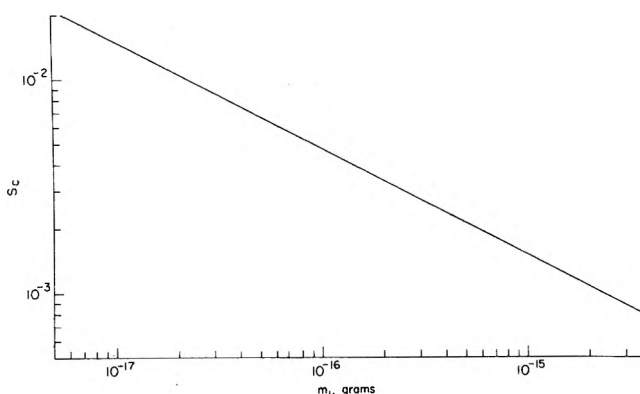


Figure 1. Plot of water vapor critical supersaturation,  $S_c$ , vs. the mass of  $\text{NH}_4\text{NO}_3$  particles.

droplets will grow indefinitely until they attain a visible size. For  $\text{NH}_4\text{NO}_3$  particles the critical supersaturation,  $S_c$ , can be computed<sup>21</sup> as a function of particle mass and is given in Figure 1.

For example, for  $S = 0.02$ , equivalent to a difference of temperature  $T_2 - T_1 \sim 7^\circ$ , all particles whose mass is larger than  $5.6 \times 10^{-18}$  g will grow to visible size. The time required to reach this size can be shown to be of the order of a few seconds.

The thermal diffusion chamber constructed at Penn State University<sup>22</sup> consists of a cylinder of clear acrylic plastic 12.7 cm in diameter by 1.9 cm high with an active volume of 240 cc. The upper and lower surfaces are aluminum disks covered by filter paper moistened with distilled water. The upper disk is maintained at room temperature and the bottom disk is cooled thermoelectrically. The turbulent motions, produced in the chamber by the introduction of the sample to be analyzed, cease after a period of about 10 sec, and a stable cloud is observed. At this moment a photograph is taken. The source of light is provided by a high-intensity mercury vapor arc lamp. The volume photographed is about 0.33 cc.

The samples to be analyzed were diluted with purified nitrogen to obtain a volume of 1 l. at atmospheric pressure. This volume, five times the active volume of the thermal diffusion chamber, was passed in whole through it in order to eliminate all gas remaining from previous samples.

Experiments were performed at different  $\text{O}_3$  decay rates by changing the initial concentrations of the reactant gases,  $\text{O}_3$  and  $\text{NH}_3$ , and at different total pressures by changing the amount of  $\text{N}_2$ . For a certain rate and total pressure, characteristic of a series, particles were analyzed at two different supersaturations, 0.018 and 0.0017, corresponding to particles larger than  $7.1 \times 10^{-18}$  and  $8 \times 10^{-16}$  g, respectively. Values of the particle size can be estimated from the specific gravity of 1.66 for  $\text{NH}_4\text{NO}_3$ .<sup>23</sup> This value leads to a monomer volume of  $80.5 \text{ \AA}^3$ . The diameters of the measured equivalent spherical particles are 200 and 1000  $\text{Å}$ , respectively.

## Results

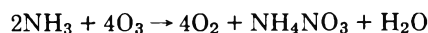
Experiments were performed in which  $\text{NH}_3$  and  $\text{O}_3$ , in the presence of excess  $\text{N}_2$ , were allowed to react to produce particles of  $\text{NH}_4\text{NO}_3$ . The reaction conditions for several series of experiments are listed in Table I. The  $\text{NH}_3$  pressure ranged from 0.034 to 2.0 Torr, the initial  $\text{O}_3$  pressure,  $[\text{O}_3]_0$ , from 0.020 to 0.10 Torr, and the  $[\text{NH}_3]/$

TABLE I: Summary of Results for  $\text{NH}_4\text{NO}_3$  Particle Production in the Reaction of  $\text{NH}_3$  with  $\text{O}_3 \pm 3^\circ$  for Particle Diameters  $> 1000 \text{ \AA}$

$10^3[\text{O}_3]_0$ , Torr	$[\text{NH}_3]/[\text{O}_3]_0$	$10^2k$ , $\text{min}^{-1}$	$10^2k'$ , $\text{min}^{-1}$	$10^{-5}N_0$ , particle/cc	$10^{-5}N_{\text{max}}$ , particle/cc	$\tau_{\text{max}}$ , $\text{min}^{-1}$	$10^3\beta$
$[\text{N}_2] = 790 \pm 10$ Torr							
89.4	4.75	1.04	1.06	1.4	0.90	44	2.8
86.3	4.90	1.20	1.19	1.6	1.0	42	3.0
97.6	5.17	1.61	1.32	1.8	1.13	42	2.2
100	10.3	1.73	1.02	1.8	1.15	38	2.2
94.8	10.0	1.74	1.28	1.5	1.12	37	2.0
40.3	2.0	1.38	0.94	1.15	0.64	37	4.5
38.4	20.8	1.43	0.96	1.3	0.96	42	4.5
40.4	20.3	1.90	0.95	1.4	0.95	40	3.7
19.7	5.1	1.92	0.82	0.68	0.57	36	4.1
20.0	5.0	1.73	1.25	0.40	0.26	40	2.4
$[\text{N}_2] = 500 \pm 20$ Torr							
101	2.0	1.53	1.54	1.35	0.90	21	3.4
100	20.4	2.38	2.52	1.8	0.95	26	2.4
40.4	20.6	2.23	1.57	1.15	0.70	27	3.8
39.2	21.1	2.87	1.52	1.20	0.82	26	3.3
18.5	5.5	1.96	1.72	0.42	0.31	20	4.7
19.9	4.7	1.97		0.42	0.27	25	3.6
$[\text{N}_2] = 117 \pm 7$ Torr							
38.8	21.5	4.37	4.42	0.90	0.40	18	2.9
40.4	20.2	6.1	3.98	0.80	0.40	16	1.6
41.3	19.7	6.1	6.42	1.1	0.37	18	1.9

$[\text{O}_3]_0$  ratio from 2.0 to 21.5. During the reaction the  $\text{O}_3$  is consumed, but since  $\text{NH}_3$  is in excess, usually in large excess, its pressure is not significantly reduced as the reaction proceeds.

In the previous work,<sup>18</sup> it was found that the main overall reaction can be represented by



Some  $\text{N}_2$  and  $\text{N}_2\text{O}$  are also produced, but they are minor products, and we shall assume for this study that the above reaction is an adequate representation of the overall chemistry. The  $\text{NH}_4\text{NO}_3$  forms as solid particles suspended in the gas. Furthermore, it was found that the rate law followed the expression

$$-d[\text{O}_3]/dt = k[\text{O}_3] \quad (I)$$

for  $[\text{NH}_3]/[\text{O}_3]$  ratios below 50. For higher ratios the rate law shifted to higher orders in  $[\text{O}_3]$ , becoming 3/2 order for ratios  $> 120$ . The reaction had a heterogeneous character and the rate constant  $k$  was a complex function of  $[\text{NH}_3]/[\text{O}_3]_0$  and the pressure of added inert gas.

In the present experiments, which utilized a much larger reaction vessel, the same results were found for any conditions except that  $k$  was smaller. This was expected since  $k$  increases with surface-to-volume ratio, and that ratio is smaller in the larger reaction vessel.

(21) B. J. Mason, "Physics of Clouds," Oxford University Press, London, 1957, p 28.

(22) R. L. Ruth, M.S. Thesis, Department of Meteorology, The Pennsylvania State University, 1968.

(23) N. A. Lange, "Handbook of Chemistry," 7th ed, Handbook Publishers, Sandusky, Ohio, 1949, p 183.

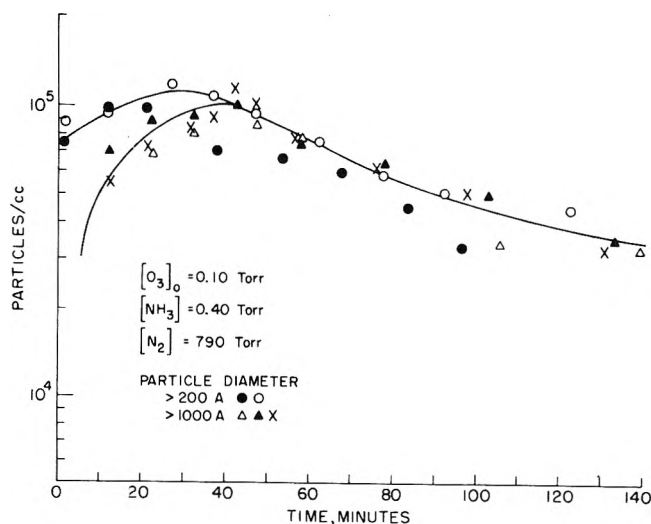


Figure 2. Semilog plots of the number density of particles exceeding 200 or 1000 Å in diameter vs. reaction time at 24° for [O<sub>3</sub>]<sub>0</sub> = 0.10 Torr, [NH<sub>3</sub>] = 0.40 Torr, and [N<sub>2</sub>] = 790 Torr.

Each series of experiments was performed as follows. Reactant mixtures were prepared, and as the reaction proceeded, [O<sub>3</sub>] was monitored by its ultraviolet absorption. Periodically samples were withdrawn from the reaction vessel for particle count analysis. In one run of each series, particles larger than 1000 Å in diameter were measured at various times. The reaction time includes that in the sampling tube (~0.5 min) prior to counting in the thermal diffusion chamber. Typically about nine samples were taken for each run. Since each sample constituted about 1.6% of the reaction mixture, the reactant pressures as well as the total pressure were reduced about 13% from the beginning to the end of the run in addition to any reduction by chemical changes. When one run was completed, other replicate runs were done, again either counting particles >1000 or >200 Å in diameter. In this way several runs were done for each experiment to obtain the number of particles greater than 200 and 1000 Å as a function of reaction time. Duplicate runs in which the number of particles of the same minimum particle size were counted generally were reproducible to ±20%.

For the several runs in each series the O<sub>3</sub> decay was monitored. It followed eq I, from which the values of *k* were obtained. In the replicate runs, the values of *k* were reproducible to ±10%, and the average values are listed in Table I for each series. To obtain *k*, corrections were made for the pressure drop due to sampling, and the values tabulated represent only chemical loss. The actual values of [O<sub>3</sub>] at any time are smaller than computed from the tabulated values of *k* using eq I, and after nine samplings, may be 13% smaller. However this effect is relatively unimportant compared to the chemical loss in most of the series.

The particle size distribution in all series shows the same general trend. Typical results are shown in Figure 2. Initially the number density of particles >200 Å rises, reaches a maximum of about 10<sup>5</sup> particles/cc, and then falls off as the reaction proceeds. The same general curve shape is observed for the number density of particles >1000 Å, but the time of the maximum, τ<sub>max</sub>, is delayed.

The most interesting (and unexpected) observation from Figure 2 is the fact that after about 40 min, there are essentially no particles between 200 and 1000 Å diameter,

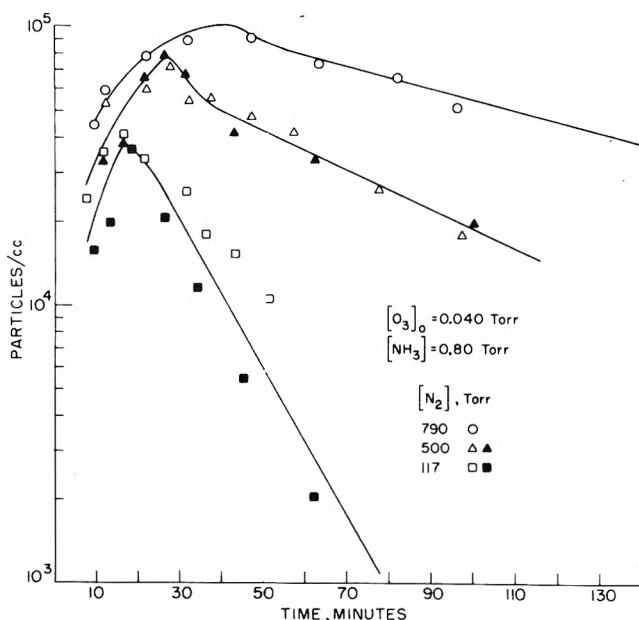


Figure 3. Semilog plots of the number density of particles exceeding 1000 Å in diameter vs. reaction time at 24° for [O<sub>3</sub>]<sub>0</sub> = 0.040 Torr, [NH<sub>3</sub>] = 0.80 Torr, and [N<sub>2</sub>] = 790, 500, or 117 Torr.

and presumably even smaller particles are also missing. In every series where particle size counts >200 and >1000 Å were taken, the same result was found. Thus in Table I we report only τ<sub>max</sub> and N<sub>max</sub> characterizing the particles >1000 Å.

The most important parameter influencing the values for both τ<sub>max</sub> and N<sub>max</sub> is the N<sub>2</sub> pressure. This effect is shown graphically in Figure 3. As the N<sub>2</sub> pressure is raised both N<sub>max</sub> and τ<sub>max</sub> are augmented. In fact the data in Table I indicate that τ<sub>max</sub> depends only on the N<sub>2</sub> pressure. It rises from 17 to 25 to 40 min as the N<sub>2</sub> pressure is increased from 117 to 500 to 790 Torr.

After τ<sub>max</sub> has been reached, the number of particles >1000 Å falls off in all the series approximately exponentially with the time, *t*

$$N = N_0 \exp(-k't) \quad (II)$$

where *N* is the total number of particles >1000 Å, and for times approximately >τ<sub>max</sub> probably represents the total number of particles, since the number of small particles has nearly disappeared. N<sub>0</sub> is the extrapolated value of *N* to zero time. Values of N<sub>0</sub> and the decay constant, *k'*, are tabulated for each series in Table I.

The values of N<sub>0</sub> vary between 0.40 × 10<sup>5</sup> and 1.8 × 10<sup>5</sup> particles/cc. N<sub>0</sub> increases with *k*[O<sub>3</sub>]<sub>0</sub> at any N<sub>2</sub> pressure, but drops as the N<sub>2</sub> pressure is lowered.

The values of *k'* the decay constant for particle depletion, are between 0.0082 and 0.013 min<sup>-1</sup> for the series with 790 Torr of N<sub>2</sub> added. There appears to be no obvious correlation with any of the parameters, and the spread may just reflect uncertainty in the results. However, it is clear that *k'* rises noticeably as the total pressure is reduced, reaching a value of 0.064 min<sup>-1</sup> for 117 Torr of N<sub>2</sub>.

### Discussion

**Nucleation.** The fact that O<sub>3</sub> decays by first-order kinetics during the whole course of a run indicates that O<sub>3</sub> consumption is not influenced by either the number or size of the particles, i.e., that the main loss of O<sub>3</sub> is not

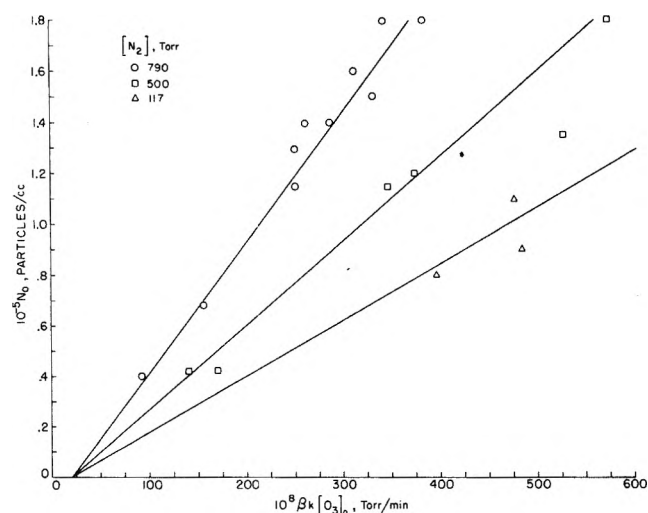
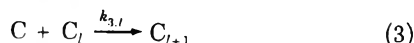


Figure 4. Plot of the initial number density,  $N_0$ , of particles vs. the initial monomer production rate for  $[N_2] = 790, 500, \text{ or } 117$  Torr.

direct chemical reaction with the particles. The main loss of  $O_3$  must be through chemical reaction with  $NH_3$  either in the gas phase or on the wall of the reaction vessel. Such a loss process can only lead to production of  $NH_4NO_3$  monomer (called C to simplify the nomenclature). The mechanism of monomer production was discussed in our previous paper.<sup>18</sup>

The monomer can disappear by three routes



where  $r$  and  $l$  are integers.  $C_r$  and  $C_l$  are particles with  $r$  and  $l$  monomer units, respectively, and  $l > r$ . Reaction 1 is not a fundamental reaction, but is some representation of the nucleation process to form stable particles of critical size, *i.e.*, containing  $r$  monomer units, which then can grow.

Reaction 2 represents loss of C to the wall *via* diffusional processes and reaction 3 represents loss of monomer by condensation on the particles. The rate constants for reaction 2 and 3 can be estimated from simple kinetic molecular theory considerations

$$k_{2,1} \sim \alpha_1 D_1 / X^2 \quad (III)$$

$$k_{3,l} = 6.9 \times 10^{-11} T^{1/2} (\sigma_1 + \sigma_l)^2 / \mu_{1,l}^{1/2} \quad (IV)$$

where  $\alpha_1$  is the accommodation coefficient for monomer depositing on the wall ( $\alpha_1 \sim 0.1$ ),  $D_1$  is the diffusion coefficient for monomer,  $X$  is the mean distance of travel for the monomer to reach the wall,  $T$  is the absolute temperature in  $^\circ K$ ,  $\sigma_1$  and  $\sigma_l$  are the diameters in  $\text{\AA}$  of C and  $C_l$ , respectively, and  $\mu_{1,l}$  is the reduced molecular weight for C and  $C_l$ . The units of  $k_{3,l}$  are  $\text{cm}^3/\text{min}$ . Values for  $\sigma_1$  and  $\sigma_l$  can be estimated from the specific gravity of 1.66 for  $NH_4NO_3$ .<sup>23</sup> This value leads to a monomer volume of  $80.5 \text{ \AA}^3$ .

The general expression for the diffusion coefficient,  $D_l$ , of any particle in 1 atm of  $N_2$  is<sup>24</sup>

TABLE II: Rate Constants for Various Size Particles in  $N_2$  at 760 Torr and 300 $^\circ K$

$\sigma, \text{\AA}$	$l$	$D_l, \text{cm}^2/\text{min}$	$k_{3,l}, \text{cm}^3/\text{min}$	$k_{l,l}, \text{cm}^3/\text{min}$
5.3	1	11.7		$2.0 \times 10^{-8}$
10	6.5	3.2	$3.0 \times 10^{-8}$	$2.9 \times 10^{-8}$
20	52	0.80	$8.2 \times 10^{-8}$	$4.1 \times 10^{-8}$
40	416	0.202	$2.68 \times 10^{-7}$	$5.7 \times 10^{-8}$
100	$6.5 \times 10^3$	$3.28 \times 10^{-2}$	$1.42 \times 10^{-6}$	$9.0 \times 10^{-8}$
200	$5.2 \times 10^4$	$8.4 \times 10^{-3}$	$5.36 \times 10^{-6}$	$1.2 \times 10^{-7}$
400	$4.16 \times 10^5$	$2.23 \times 10^{-3}$	$2.1 \times 10^{-5}$	$1.8 \times 10^{-7}$
1000	$6.5 \times 10^6$	$4.25 \times 10^{-4}$	$1.32 \times 10^{-4}$	$1.06 \times 10^{-7}$
2000	$5.2 \times 10^7$	$1.38 \times 10^{-4}$	$5.16 \times 10^{-4}$	$6.9 \times 10^{-7}$

$$D_l = [KT(1 + 2.492b/\sigma_l + 0.84(b/\sigma_l) \times \exp(-0.435\sigma_l/b))] / 3\pi\eta\sigma_l \quad (V)$$

where  $K$  is the Boltzmann constant,  $b$  is the mean free path, and  $\eta$  is the viscosity. For  $N_2$  at 1 atm,  $b = 6.5 \times 10^{-6} \text{ cm}$  and  $\eta = 1.78 \times 10^{-4} \text{ P}$ .

For various values of  $\sigma$ , the corresponding values of  $l$ ,  $D_l$ , and  $k_{3,l}$  are listed in Table II. Since in our system  $X$  is typically 2 cm, then  $k_{2,1} \sim 0.3 \text{ min}^{-1}$ .

In the initial stages, the rate law for the production of C is

$$d[C]/dt = \beta k[O_3]/4 - k_{2,1}[C] \quad (VI)$$

where the loss of C due to reactions 1 and 3 have been neglected since they are small. The factor of 4 indicates that the formation rate of C is only 1/4 the loss rate of  $O_3$ . Since C may be produced on the wall and never enter the gas phase, the constant  $\beta$  has been introduced. It represents the fraction of monomers produced that enter the gas phase. Also for the first few minutes  $[O_3]$  does not change significantly, so that eq VI can be integrated to give

$$[C] = \beta k[O_3][1 - \exp(-k_{2,1}t)] / 4k_{2,1} \quad (VII)$$

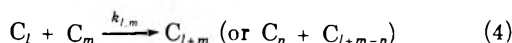
Since  $k_{2,1} \sim 0.3 \text{ min}^{-1}$ , the steady state is reached within a few minutes. Thus the initial steady-state value for  $[C]$ , called  $[C]_0$ , can then be represented as  $\beta k[O_3]_0 / 4k_{2,1}$ . As will be shown later,  $\beta \sim 3 \times 10^{-3}$ . In our experiments  $k[O_3]_0 > 10^{13} \text{ particles/cc min}$ ,  $k_{2,1} \sim 0.3 \text{ min}^{-1}$ , so that  $[C]_0 > 2.5 \times 10^{10} \text{ particles/cc}$ .

The initial production rate of particles is on the average  $< 10^5/\text{min cc}$ . Even if  $r \sim 10^3$ , particle production accounts for no more than  $10^8 \text{ monomers/cc min}$ , which is at least 2.5 orders of magnitude smaller than the production rate ( $\beta k[O_3]_0 > 3 \times 10^{10}$ ), and justifies the assumption that the rate of reaction 1 is negligible compared to reaction 2.

It is reasonable to expect that  $N_0$  will increase with  $[C]_0$ . Since  $[C]_0 = \beta k[O_3]_0 / 4k_{2,1}$ , the values of  $N_0$  were plotted *vs.*  $\beta k[O_3]_0$ , and the results are shown in Figure 4. The plots at each  $N_2$  pressure can reasonably be represented by straight lines which nearly pass through the origin. The slopes should be inversely proportional to  $k_{2,1}$ . Since  $k_{2,1}$  rises as the  $N_2$  pressure is dropped, the slopes of the curves fall from  $1.64 \times 10^{-6}$  to  $1.08 \times 10^{-6}$  to  $0.71 \times 10^{-6} \text{ min}^{-1}$  as the  $N_2$  pressure is reduced from 790 to 500 to 120 Torr.

(24) N. A. Fuchs, "Mechanics of Aerosols," Pergamon Press, New York, N. Y., 1964, p 27.

*Particle Growth.* The possible reactions of particles are



Reaction 2 is the particle removal step by diffusional loss to the walls. This rate is approximately equal to the diffusion constant, which is tabulated in Table II for various values of *l*. Reaction 3 represents particle growth terms by reaction with monomer. It should be noticed that reaction 3 does not alter the number of particles.

Reaction 4 is the coagulation term. Upper limits to these rate constants can be computed from collision rates. The limiting rate is given by kinetic molecular theory

$$k_{l,m} = 6.9 \times 10^{-11} T^{1/2} (\sigma_l + \sigma_m)^2 / \mu_{l,m}^{1/2} \quad (VIII)$$

except for particles >500 Å at 760 Torr, where diffusion is controlling. Then

$$k_{l,m} = 2\pi \times 10^{-8} (\sigma_l + \sigma_m) (D_l + D_m) \quad (IX)$$

where  $\mu_{l,m}$  is the reduced molecular weight between particles  $C_l$  and  $C_m$ ,  $\sigma_l$  and  $\sigma_m$  are their diameters in Å,  $D_l$  and  $D_m$  are their diffusion coefficients in cm<sup>2</sup>/min, and  $k_{l,m}$  has the units of cm<sup>3</sup>/min. Values of  $k_{l,l}$  for various *l* are tabulated in Table II for 300°K and 760 Torr pressure. From these values it can be seen that coagulation can play no role at all under any of our conditions, and reaction 4 can be ignored.

The only important loss process of total particles, *N*, is wall diffusion. The loss rate constant,  $k'$ , is about 10<sup>-2</sup> min<sup>-1</sup> at 760 Torr pressure. This is about 20 times larger than the value of  $D_l$  for particles of 1000-Å diameter. Apparently these large particles only travel an average distance of about 0.2 cm before deposition. At lower pressures  $k'$  goes up, but much less slowly than inversely with the pressure. Presumably the main loss has shifted to particles of larger size.

The rate law for  $C_l$  is

$$d[C_l]/dt = k_3[C]([C_{l-1}] - [C_l]) - k_{2,l}[C_l] \quad (X)$$

where the average value,  $k_3$ , has been used for  $k_{3,l}$ . When large particles are present, no new particles are formed, so that  $[C]$  must be much smaller than  $[C]_0$ . This can only be if  $C$  is removed principally by condensation, reaction 3. Under these conditions

$$[C] = \beta k[O_3]/4k_3N \quad (XI)$$

Thus eq X becomes

$$d[C_l]/dt = (\beta k[O_3]/4N)([C_{l-1}] - [C_l]) - k_{2,l}[C_l] \quad (XII)$$

Now  $[O_3]$  and  $N$  are slowly decaying functions of time, and they decay with comparable rate constants. Thus  $\beta k[O_3]/4N$  is nearly constant with time. Furthermore  $k_{2,l} \sim k_{2,l-1}$ , so that eq XII is easily integrated to give

$$[C_l] = f_l t^{l-r} \exp(-\alpha_l t) \quad (XIII)$$

where

$$\begin{aligned} \alpha_l &= \beta k[O_3]/4N + k_{2,l} \\ f_l &= \beta k[O_3] f_{l-1} / 4N(l-r) \\ &= f_r (\beta k[O_3]/4N)^{l-r} / (l-r)! \end{aligned}$$

Since  $C_r$  is produced almost exclusively at very short times,  $f_r \sim N_0$ . Thus  $[C_l]$  has the solution

$$[C_l] = N_0 (\beta k[O_3] t / 4N)^{l-r} \exp(-\alpha_l t) / (l-r)! \quad (XIV)$$

This solution is strongly peaked in *l* at any time *t* and is strongly peaked in *t* for any *l*. For any value of *l*, a maximum occurs at  $\tau_{\max} = (l-r)/\alpha_l$ . Furthermore for particles of 1000-Å diameter,  $k_{2,l}$  is much smaller than  $\alpha_l$ ,  $l-r \sim l$ , and

$$\tau_{\max} \approx 4lN_0 / \beta k[O_3]_0 \quad (XV)$$

Equation XV is readily solved for  $\beta$ , and these values are tabulated in Table I for each series. It can be seen that  $\beta \sim 3 \times 10^{-3}$  for all reaction conditions.

*Acknowledgment.* This work was supported by the Environmental Protection Agency, Office of Air Programs through Grant No. AP 00022, for which we are grateful.

## Kinetics of Particle Growth. II. Kinetics of the Reaction of Ammonia with Hydrogen Chloride and the Growth of Particulate Ammonium Chloride<sup>1</sup>

Richard J. Countess and Julian Hecklen\*

Department of Chemistry and Center for Air Environment Studies, The Pennsylvania State University, University Park, Pennsylvania 16802 (Received August 15, 1972)

$\text{NH}_3$  and  $\text{HCl}$  at 60 ppm each in  $\text{N}_2$  were allowed to react in a flow apparatus at 25° and atmospheric pressure. Solid  $\text{NH}_4\text{Cl}$  was produced and the particle size distribution measured for various reaction times. Under the conditions of the experiment both wall losses and particle coagulation were negligible. Monomer  $\text{NH}_4\text{Cl}$  is produced by the gas-phase reaction of  $\text{NH}_3$  and  $\text{HCl}$  with a rate constant of  $1.9 \times 10^{-17} \text{ cm}^3/\text{sec}$ . The monomer can then nucleate particles, though the predominant reaction is condensation of the monomer on the particles already present. The particle size distribution follows the law  $F\{l\} = N\{t\} \exp(-\beta l^{1/3})$ , where  $F\{l\}$  is the number of particles/cc containing at least  $l$  monomer units,  $N\{t\}$  is the total number of particles/cc at any reaction time  $t$ , and  $\beta = 6.24 \times 10^{-3}$ .  $N\{t\}$  first rises proportionately with reaction time, but its rate of increase falls as the reactants,  $\text{NH}_3$  and  $\text{HCl}$ , are consumed. The rate constant,  $k\{l\}$ , for condensation of the monomer on any particle with  $l$  monomer units follows the relationship  $k\{l\} - 1 = (k\{l\} + \delta)f\{l\}/f\{l-1\}$ , where  $\delta = \bar{k}\beta^3/6$ ,  $f\{l\} = \beta F\{l\}/3l^{2/3}$ , and  $\bar{k}$  is the average value of  $k\{l\}$  for all  $l$ .

### Introduction

In an attempt to learn about the dynamics of particle growth, the formation of  $\text{NH}_4\text{Cl}$  from gaseous  $\text{NH}_3$  and  $\text{HCl}$  was investigated. This reaction is well known and is a classical general chemistry experiment used to demonstrate Graham's law of gaseous diffusion. Unlike other investigators<sup>2-5</sup> who studied the  $\text{NH}_4\text{Cl}$  aerosol generation by low-temperature volatilization, atomization of an alcohol solution, irradiation by X-rays, electrical discharges, or by controlled condensation of vapor upon suitable nuclei (the La Mer generator), we studied the generation of  $\text{NH}_4\text{Cl}$  from the chemical interaction of  $\text{NH}_3$  and  $\text{HCl}$  vapors to circumvent some of the problems of the other studies (e.g., wall losses, large concentrations of electrical charges).

One important aspect that has not been resolved is the rate of reaction between the two reactant gases. The main reason for this is that the formation of  $\text{NH}_4\text{Cl}$  is more complicated than simply the homogeneous bimolecular gas-phase reaction of  $\text{NH}_3$  and  $\text{HCl}$  vapors. In addition particles are produced which might act as sites for condensation of the vapors resulting in gas-solid reactions.

In the experiments reported here  $\text{NH}_3$  and  $\text{HCl}$  are allowed to react in a flow apparatus, and the particle count and size distribution measured at various reaction times. Our results give information both about the gas-phase reaction between  $\text{NH}_3$  and  $\text{HCl}$  and the mechanism of particle growth.

### Experimental Section

Anhydrous ammonia (>99.99% purity) and Electronic Grade hydrogen chloride (>99.99% purity) gas cylinders were purchased from Matheson; prepurified nitrogen (>99.997% purity) was purchased locally from Phillip Wolf. Special equipment to handle the corrosive reactant gases included a stainless steel regulator with check valve containing a filter, Matheson No. 12-240, for the ammonia and a monel regulator with purge assembly and check

valve (also with filter), Matheson No. B15-330 K, for the hydrogen chloride. Before and after each experiment the hydrogen chloride regulator was purged with dry nitrogen. Prior to mixing the reactant gases, each gas was dried (-60° liquid  $\text{N}_2$ -propanol mixture and drierite trap in the  $\text{HCl}$  line, -30° liquid  $\text{N}_2$ -propanol mixture and glass wool trap in the  $\text{NH}_3$  line), filtered through glass wool, and diluted with  $\text{N}_2$  carrier gas that had also been dried (-196° liquid  $\text{N}_2$  and drierite trap) and filtered (glass wool). A measurement of the particulate concentration in the individual filtered gases with a Gardner Condensation Nuclei Counter indicated less than 100 particles/cc equal to or larger than 0.002- $\mu$  diameter.

Gases were metered with stainless steel Matheson N.R.S. high accuracy needle valves, Models 4176-2101 and 4181-2505, and flow rates were measured with rotameters, Matheson Models 610 and 600 (R-2-15AAA) for the reactant gases and a Matheson Model 602 and Brooks Model R-6-15A for  $\text{N}_2$ , supplied with a calibration for each gas and subsequently verified in our lab with either an American Meter Co. dry test meter (1 cf/rev) or a bubble meter (100-cc buret).

The desired ratio of carrier to reactant gas was obtained by a primary dilution of the reactant gases with  $\text{N}_2$  followed by a secondary dilution with another source of dry  $\text{N}_2$ . Excess gases from the primary dilution were exhausted into the hood while the two gas mixtures from the secondary dilution were fed through two separate mixing jets into a Pyrex reactor tube and then exhausted into the hood. Flow rates were adjusted so as to maintain laminar

- (1) CAES Report No. 264-72.
- (2) R. Whytlaw-Gray and H. S. Patterson, "Smoke," Edward Arnold, London, 1932.
- (3) J. M. DallaValle, C. Orr, and B. L. Hinkle, *Brit. J. Appl. Phys., Suppl.* 3, S198 (1954).
- (4) W. B. Kunkel, *J. Appl. Phys.*, 21, 833 (1950).
- (5) G. O. Langstroth, *Can. J. Res.*, 25, 49 (1947).



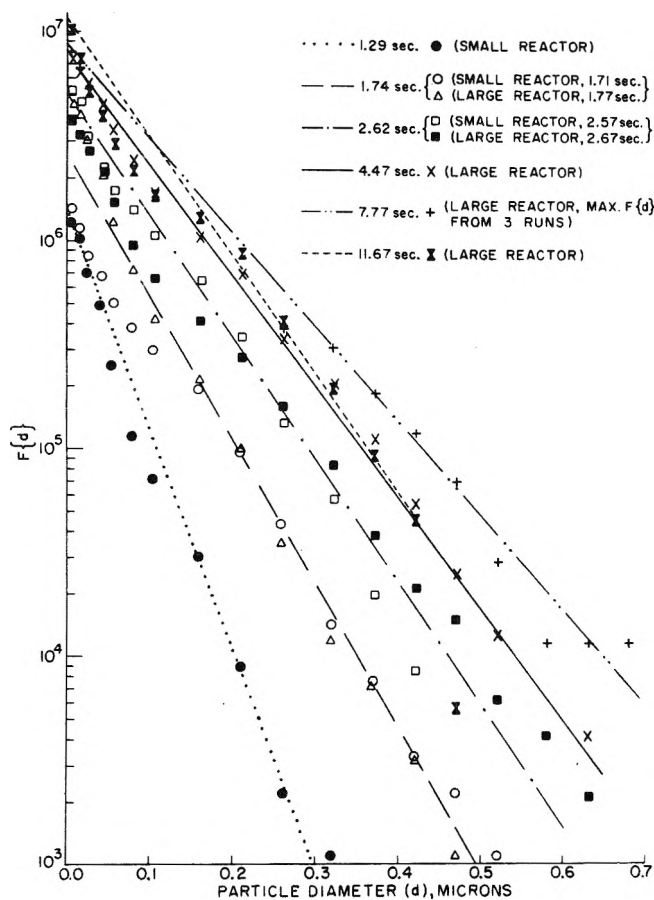


Figure 1. Plot of  $F\{d\}$ , the number of particles per cc greater than the diameter  $d$ , vs.  $d$  for various reaction times at 25°. The initial reactant concentrations were 60 ppm of NH<sub>3</sub> and 60 ppm of HCl in 1 atm of N<sub>2</sub>.

flow in the reactor. All connections were of Pyrex, stainless steel, Teflon, or polycarbonate tubing and fittings. A positive tank pressure, slightly above 1 atm (2 psig), allowed the operation of the flow experiments without the encumbrance of vacuum pumps. Also most of the particle counters operated at 1-atm pressure.

Contact time of the reacting species in the flow tube could be varied by one of two methods. In the first method, one of the gas inlets was movable along the axis of the reactor tube, with the other one rigid and thus the distance between the mixing zone of reacting species and the exit port could be varied. The second method was by varying the flow rate.

Two different size reactor vessels were constructed out of Pyrex tubing, one with an internal cross-sectional area of 3.0 cm<sup>2</sup> and 1.0 m long, the other 8.5 cm<sup>2</sup> internal cross sectional area and 2.0 m in length. Also two different inlet heads were built for the movable inlet; the first consisted simply of a Pyrex tube, 6 mm o.d., and the second one (used only with the larger of the two reactor tubes) consisted of a circular Pyrex ring (2.3 cm o.d.) with a series of finely drilled holes around the ring and pointing downstream toward the exit.

The particle size distribution was measured by precipitating the NH<sub>4</sub>Cl particles from the gas stream with an electrostatic precipitator, T.S.I. Model 3100, and obtaining the particle sizes and particle number by electron microscopy using a Phillips Model 300 transmission electron microscope. The particles were precipitated onto

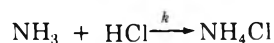
TABLE I: Particle Size Distribution Parameters<sup>a</sup>

$t$ , sec	$10^{-6}N\{t\}$ , particles/cc	$10^{-4}\alpha$ , cm <sup>-1</sup>
1.29	1.42	24.2
1.74	2.7	16.0
2.62	5.0	13.4
4.47	8.0	12.3
7.77	8.7	10.4
11.67	9.0	12.5

<sup>a</sup> [NH<sub>3</sub>] = [HCl] = 60 ppm.

small carbon-coated copper E.M. grids with the precipitator run in the intermittent mode so as to precipitate a homogeneous sample of the entire aerosol smoke on each grid. Grids were stored in a desiccator until ready for analysis.

Infrared analysis with a Beckman IR 10 spectrophotometer using both a 10-cm Pyrex cell with NaCl windows and a Beckman Multipass cell (10 cm to 10 m) with KBr windows was used to follow the disappearance of the NH<sub>3</sub> or HCl ir bands for the chemical reaction



in an attempt to obtain the rate constant  $k$ .

## Results

Experiments were done in which 120 ppm of NH<sub>3</sub> in N<sub>2</sub> was flowed into the reactor in the outer tube and 120 ppm of HCl in N<sub>2</sub> was flowed into the reactor through the inner tube. The two streams had equal flow rates so that the initial NH<sub>3</sub> and HCl concentrations were both 60 ppm after mixing. Preliminary experiments with the HCl stream on the outside and the NH<sub>3</sub> stream on the inside gave identical results. Particles of NH<sub>4</sub>Cl were produced and after a given reaction time,  $t$ , the particles were captured by the electrostatic precipitator and counted. No significant accumulation of NH<sub>4</sub>Cl occurred on the reactor walls.

The total number of particles per cc larger than a given diameter,  $d$ , was obtained, and this quantity is called  $F\{d\}$ . The particle size distribution for various reaction times are shown in Figure 1. In this figure  $\log F\{d\}$  is plotted vs. the particle diameter for six different contact times ranging from 1.29 to 11.67 sec. The semilog plots are all reasonably linear. Reactions carried out in the large and small reactors gave similar results for the same contact times. The reliability of each data point in Figure 1 may be no better than a factor of 2. However, the lines fitting the points and their intercepts are probably reliable to  $\pm 25\%$ .

Since the plots in Figure 1 are linear, the expression describing  $F\{d\}$  is

$$F\{d\} = N\{t\} \exp(-\alpha d) \quad (1)$$

where  $N\{t\}$  is the total number of particles/cc at time  $t$ , and in general  $\alpha$  might also be a function of  $t$ . The values for  $N\{t\}$  and  $\alpha$  are the intercepts and slopes, respectively, of the plots in Figure 1. They are listed in Table I for the various reaction times.

The values for  $N\{t\}$  increase from  $1.42 \times 10^6$  to  $9.0 \times 10^6$  particles/cc as  $t$  increases from 1.29 to 11.67 sec. The data are plotted in Figure 2. Initially  $N\{t\}$  is proportional to  $t$  with a proportionality constant of  $1.6 \times 10^6$  particles/cc sec. At longer times, the rise is much slower.

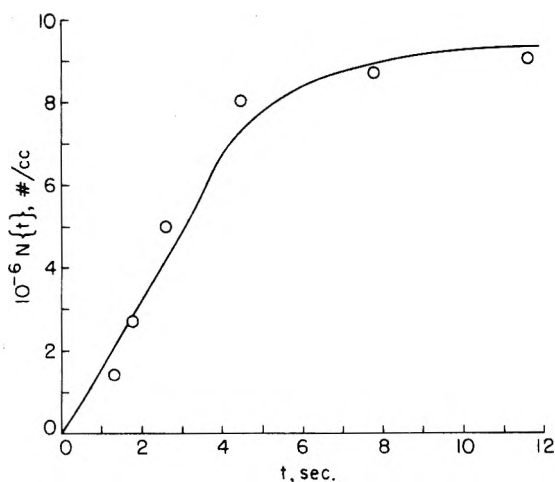


Figure 2. Plot of  $N\{t\}$ , the total number of particles/cc, vs. reaction time at 25°. The initial reactant concentrations were 60 ppm of  $\text{NH}_3$  and 60 ppm of  $\text{HCl}$  in 1 atm of  $\text{N}_2$ .

On the other hand  $\alpha$  is relatively independent of  $t$ . Except for the earliest reaction time,  $\alpha = (13 \pm 3) \times 10^4 \text{ cm}^{-1}$ . Since the density of  $\text{NH}_4\text{Cl}$  is 1.53 g/cc (at 17°),<sup>6</sup> eq 1 can be recast as

$$F\{l\} = N\{t\} \exp(-\beta l^{1/3}) \quad (2)$$

where  $l$  is the number of  $\text{NH}_4\text{Cl}$  monomers in the particle, and  $\beta = 6.24 \times 10^{-3}$ ;  $F\{l\}$  is then the total number of particles/cc containing at least  $l$  monomer units.

Equation 2 presupposes that the solid particles are entirely  $\text{NH}_4\text{Cl}$ . It is possible that either  $\text{NH}_3$  or  $\text{HCl}$  could be trapped in the particles. To check this point, deposits were obtained from reactions in which either  $\text{NH}_3$  or  $\text{HCl}$  were in excess and the  $\text{Cl}^-$  to  $\text{NH}_4^+$  ratio analyzed. In the analysis for  $\text{NH}_4^+$ , excess  $\text{HCl}$  was added to convert any free  $\text{NH}_3$  to  $\text{NH}_4^+$ . For a reaction with 500 ppm of  $\text{HCl}$  and 125 ppm of  $\text{NH}_3$ , the  $\text{Cl}^-$  to  $\text{NH}_4^+$  ratio was 1.04; whereas for a reaction with 2500 ppm of  $\text{NH}_3$  and 250 ppm of  $\text{HCl}$ , the  $\text{Cl}^-$  to  $\text{NH}_4^+$  ratio was 1.06. Both analyses are essentially stoichiometric.

## Discussion

The experiments were designed to minimize wall losses of particles and axial diffusion. Yet it was necessary that reaction times be sufficiently long so that the initial mixing time and sampling times were minimal. For this reason the reaction times were kept between about 1 and 12 sec.

From simple kinetic molecular theory considerations, the rate constant for diffusion to the walls is  $\sim D/x^2$  where  $D$  is the diffusion coefficient and  $x$  is the distance of travel. For a particle 20 Å in diameter,  $D$  is about 0.012  $\text{cm}^2/\text{sec}$ . Since  $x$  is about 1 cm, the lifetime for loss to the wall is about 80 sec. Thus for times <12 sec, wall losses should be minimal.

The experimental findings support the conclusion that wall losses were negligible. First, no significant wall deposits were observed. Second, the results were the same in the two different reactors which had different cross sectional areas.

In order to keep the reaction times between 1 and 12 sec, it was necessary to keep the reactant concentrations at (or near) 60 ppm. At significantly lower concentrations,

the rates of particle production were too slow to obtain meaningful data for the larger particle sizes, whereas at significantly higher concentrations, the  $\text{NH}_4\text{Cl}$  smoke became dense and gravitational settling became important.

Because wall losses are negligible, the total number of  $\text{NH}_3$  (or  $\text{HCl}$ ) molecules,  $n\{t\}$ , removed from the gas phase can be computed from the total particle mass. The number of particles containing  $l$   $\text{NH}_4\text{Cl}$  monomers per cc,  $f\{l\}$ , is given by

$$f\{l\} = -dF\{l\}/dl = (\beta N\{t\}/3l^{2/3}) \exp(-\beta l^{1/3}) \quad (3)$$

Then

$$n\{t\} = \int_0^\infty l f\{l\} dl = 6N\{t\}/\beta^3 \quad (4)$$

Since  $\beta = 6.2 \times 10^{-3}$ ,  $n\{t\} = 2.5 \times 10^7 N\{t\}$ . The initial  $\text{NH}_3$  (or  $\text{HCl}$ ) concentration was  $14.6 \times 10^{14}$  particles/cc. Thus the maximum value for  $N\{t\}$  is  $6.0 \times 10^7$  and this is consistent with the experimental findings as shown in Figure 2. Initially  $N\{t\}$  increases approximately linearly with time, but as the reactants are depleted,  $N\{t\}$  rises more slowly. The fact that  $N\{t\}$  is not falling at large reaction times shows that coagulation of the particles is not important. Certainly it can play no significant role at early reaction times, when  $N\{t\}$  is small and  $dN\{t\}/dt$  is constant. Straightforward computation of collision rate constants confirm this conclusion, even if every collision led to coagulation.

The growth process for any particle can occur in one of two ways. In one way,  $\text{NH}_3$  and  $\text{HCl}$  react in the gas phase to form  $\text{NH}_4\text{Cl}$  monomers and these then deposit on the particles. The other way would be for either gas-phase reactant to be adsorbed on the surface and then react with the other gas-phase reactant. Only the former process, however, can lead to production of additional particles. Thus if particle growth is by the former method, then  $n\{t\}/N\{t\}$  is independent of time, but in the latter case  $n\{t\}/N\{t\}$  should be proportional to  $N\{t\}$ . Equation 4 indicates that the former method is applicable and that  $\text{NH}_4\text{Cl}$  monomers are formed in a gas-phase reaction between  $\text{NH}_3$  and  $\text{HCl}$ .

Presumably the rate law for  $\text{NH}_3$  (or  $\text{HCl}$ ) loss is

$$dn\{t\}/dt = k[\text{NH}_3][\text{HCl}] \quad (5)$$

Now,  $dn\{t\}/dt = 2.5 \times 10^7 dN\{t\}/dt$ , which at early times is  $4.0 \times 10^{13}$  particles/cc sec since  $dN\{t\}/dt$  is  $1.6 \times 10^6$  particles/cc sec initially. With the initial values of  $[\text{NH}_3] = [\text{HCl}] = 14.6 \times 10^{14}$  particles/cc,  $k$  can be computed to be  $1.9 \times 10^{-17} \text{ cm}^3/\text{sec}$ . With this rate constant  $n\{t\}$  is computed to be  $3.1 \times 10^{14}$  particles/cc at 10 sec reaction time, leading to a predicted value of  $1.3 \times 10^7$  particles/cc for  $N\{t\}$  at 10 sec. This value is about 40% higher than observed, possibly suggesting some wall losses.

In order to check the rate constant estimated above, the  $\text{NH}_3 + \text{HCl}$  reaction was studied by monitoring the 10.4- $\mu$  infrared absorption band of  $\text{NH}_3$ . To a mixture of 0.5 Torr of  $\text{NH}_3$  in 50 Torr of  $\text{N}_2$  was added 1.0 Torr of  $\text{HCl}$  in 84 Torr of  $\text{N}_2$ . The  $\text{NH}_3$  was  $\frac{2}{3}$  consumed in 2.0 sec. This crude experiment is too rapid to obtain an accurate value for the rate constant but does lead to a value of  $2.1 \times 10^{-17} \text{ cm}^3/\text{sec}$  in fortuitously good agreement with the value obtained from particle counting.

(6) N. A. Lange, "Handbook of Chemistry," Handbook Publishers, Sandusky, Ohio, 1949, p. 181.

Finally it is of interest to examine the rate expression for individual particle growth

$$df\{l\}/dt = (k\{l-1\}f\{l-1\} - k\{l\}f\{l\})[M] \quad (6)$$

where  $k\{l\}$  is the rate constant for monomer deposition (i.e., condensation) on a particle of  $l$  monomer units and  $[M]$  is the monomer concentration. In general  $[M]$  is a function of  $t$ . From eq 3 it can be shown that

$$df\{l\}/dt = (dN\{t\}/dt)(f\{l\}/N\{t\}) \quad (7)$$

Combination of eq 6 and 7 leads to

$$k\{l-1\} = (k\{l\} + \delta)f\{l\}/f\{l-1\} \quad (8)$$

where

$$\delta \equiv (dN\{t\}/dt)(1/[M]N\{t\}) \quad (9)$$

Now  $k\{l\}$ ,  $k\{l-1\}$ , and  $f\{l\}/f\{l-1\}$  are independent of  $t$ . Thus  $\delta$  must also be independent of  $t$ . Since it is also independent of  $l$ ,  $\delta$  is a characteristic positive constant of the system.

If the steady-state hypothesis is applied to  $[M]$ , then

$$[M] = (dn\{t\}/dt) / \int_0^{\infty} k\{l\}f\{l\}dl = (dn\{t\}/dt) / \bar{k}N\{t\} \quad (10)$$

where  $\bar{k}$  is the average value of  $k\{l\}$  for all  $l$ . Then, by substitution into eq 9

$$\delta = \bar{k}dN\{t\}/dn\{t\} \quad (11)$$

which from eq 4 becomes

$$\delta = \bar{k}\beta^3/6 = 4.0 \times 10^{-8}\bar{k} \quad (12)$$

In principle every  $k\{l\}$  can now be computed if any one  $k\{l\}$  is known.

*Acknowledgment.* We wish to thank William Corbett for assistance in obtaining the electron photomicrographs, J. B. Bodkin for the  $\text{NH}_4\text{Cl}$  analyses, and Oakley Crawford and Rosa de Pena for useful discussions.

## Identification of Rate-Controlling Steps for the Water-Gas Shift Reaction over an Iron Oxide Catalyst

Shoichi Oki and

Department of Chemistry, Utsunomiya University, Utsunomiya, Japan

Reiji Mezaki\*

Department of Chemical Engineering, New York University, Bronx, New York (Received August 9, 1972)

The mechanistic study of the water-gas shift reaction was performed utilizing the hydrogen-deuterium equilibration reaction which occurs simultaneously during the course of the water-gas shift reaction. Reaction temperatures ranged from 467 to 522° and the total pressure of reaction system was 80 mm. The catalyst employed was an iron oxide. It was observed that the atomic fraction of deuterium in the total hydrogen adsorbed by the catalyst coincides with the atomic fraction of deuterium of water. Material balance equations of hydrogen and deuterium provided the estimates of the free energy changes of steps  $2\text{H}(a) \rightleftharpoons \text{H}_2$  and  $\text{CO} \rightleftharpoons \text{CO}(a)$ . These estimates were in good agreement, indicating that, on certain assumptions, these steps are rate-controlling. In addition the free energy change of hydrogen-exchange path also agrees with that of the associative desorption of hydrogen. The results obtained in the present investigation verify the conclusions, which were drawn from the previous mechanistic investigations of the water-gas shift reaction.

### Introduction

It has been widely known that the determination of stoichiometric number is one of a number of powerful tools for the identification of rate-controlling step or steps of heterogeneous catalytic reactions.<sup>1</sup> Applications of the technique can be found in several solid-catalyzed gaseous reaction systems. They include the catalytic synthesis and decomposition of ammonia,<sup>2-6</sup> the water-gas shift reaction over an iron oxide catalyst,<sup>7-9</sup> and the catalytic oxida-

tion of sulfur dioxide.<sup>10,11</sup> In those investigations the selection of the rate-determining step was based on the

- (1) J. Horiuti and M. Ikushima, *Proc. Imp. Acad. Jap.*, **15**, 39 (1939).
- (2) S. Enomoto and J. Horiuti, *J. Res. Inst. Catal., Hokkaido Univ.*, **2**, 87 (1951-1953).
- (3) S. Enomoto, J. Horiuti, and H. Kobayashi, *J. Res. Inst. Catal., Hokkaido Univ.*, **3**, 185 (1953-1955).
- (4) K. Tanaka, *J. Res. Inst. Catal., Hokkaido Univ.*, **13**, 119 (1965).

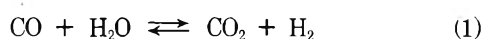
TABLE I: Possible Mechanism for the Water-Gas Shift Reaction ( $\text{CO} + \text{H}_2\text{O} = \text{CO}_2 + \text{H}_2$ ) and the Theoretical and the Apparent Stoichiometric Number

Mechanism	Elementary step		Theoretical $\nu$	Apparent stoichiometric number					
				$\text{D}^a$		$^{14}\text{C}^a$		$^{18}\text{O}^a$	
				$\text{H}_2\text{O}-\text{H}_2^b$	$\text{CO}-\text{CO}_2^b$	$\text{CO}-\text{CC}_2^b$	$\text{H}_2\text{O}-\text{CO}_2^b$		
I <sup>c</sup>	$\text{CO} \rightarrow \text{CO(a)}$	(i)	1	$\infty$	1	1	$\infty$		
	$\text{H}_2\text{O} \rightarrow 2\text{H(a)} + \text{O(a)}$	(ii)	1	1	$\infty$	$\infty$	1		
	$\text{CO(a)} + \text{O(a)} \rightarrow \text{CO}_2\text{(a)}$	(iii)	1	$\infty$	1	1	1		
	$\text{CO}_2\text{(a)} \rightarrow \text{CO}_2$	(iv)	1	$\infty$	1	1	1		
	$2\text{H(a)} \rightarrow \text{H}_2$	(v)	1	1	$\infty$	$\infty$	$\infty$		
II <sup>c</sup>	$\text{CO} \rightarrow \text{CO(a)}$	(i)	1	$\infty$	1	1	$\infty$		
	$\text{H}_2\text{O} \rightarrow \text{OH(a)} + \text{H(a)}$	(ii)	1	1	$\infty$	$\infty$	1		
	$\text{CO(a)} + \text{OH(a)} \rightarrow \text{HCOO(a)}$	(iii a)	1	$\infty$	1	1	1		
	$\text{HCOO(a)} \rightarrow \text{CO}_2\text{(a)} + \text{H(a)}$	(iii b)	1	$\infty$	1	1	1		
	$\text{CO}_2\text{(a)} \rightarrow \text{CO}_2$	(iv)	1	$\infty$	1	1	1		
III <sup>d</sup>	$2\text{H(a)} \rightarrow \text{H}_2$	(v)	1	1	$\infty$	$\infty$	$\infty$		
	$\text{H}_2\text{O} \rightarrow 2\text{H(a)} + \text{O(a)}$	(i)	1	1	$\infty$	$\infty$	1		
	$\text{CO} + \text{O(a)} \rightarrow \text{CO}_2$	(ii)	1	$\infty$	1	1	1		
IV <sup>e</sup>	$2\text{H(a)} \rightarrow \text{H}_2$	(iii)	1	1	$\infty$	$\infty$	$\infty$		
	$\text{CO} \rightarrow \text{CO(a)}$	(i)	1	$\infty$	1	1	$\infty$		
	$\text{H}_2\text{O} \rightarrow \text{H}_2\text{O(a)}$	(ii)	1	1	$\infty$	$\infty$	1		
V <sup>e</sup>	$\text{CO(a)} + \text{H}_2\text{O(a)} \rightarrow \text{CO}_2 + \text{H}_2$	(iii)	1	1	1	1	1		
	$\text{CO} \rightarrow \text{CO(a)}$	(i)	1	$\infty$	1	1	$\infty$		
	$\text{H}_2\text{O} + \text{CO(a)} \rightarrow \text{CO}_2 + \text{H}_2$	(ii)	1	1	1	1	1		

<sup>a</sup> Isotopic tracer used for the experiment. <sup>b</sup> Isotope exchange path. <sup>c</sup> Reference 18. <sup>d</sup> Reference 15. <sup>e</sup> Reference 7.

apparent stoichiometric number of the reaction, which was experimentally determined utilizing *only one kind* of isotopic tracer. It is true that the employment of an isotopic tracer is effective to select the rate-determining step in a given mechanism. However, this method does not give much assurance for the adequacy of the mechanism itself.

On the basis of the stoichiometric number concept, Oki and Kaneko<sup>7-9,12-14</sup> recently proposed a new methodology in which more than one appropriate tracer are used to identify reaction mechanisms as well as their rate-determining steps. This method, in essence, consists of the combined use of the apparent stoichiometric numbers observed by employing more than one appropriate isotopic tracer. Their method was, for the very first time, applied for the mechanistic study of the water-gas shift reaction with an iron oxide catalyst. The over-all equation for the reaction is



For this reaction system a variety of reaction mechanisms have been proposed by a number of investigators.<sup>15-17</sup> Table I shows these mechanisms along with their elementary steps. Table I also shows the theoretical stoichiometric number of each of the elementary steps. The theoretical stoichiometric numbers of all elementary steps listed in Table I are unity regardless of the reaction mechanism. On the contrary the apparent stoichiometric number which is an experimentally obtained value of the stoichiometric number varies depending on the kind of tracer employed for the experiment.

Oki and coworkers used deuterium,<sup>7</sup> carbon-14,<sup>8,9</sup> and oxygen-18<sup>12,18</sup> and observed that irrespective of the kind of isotopic tracers the apparent stoichiometric number of the water-gas shift reaction over an iron oxide catalyst

was approximately 2 for each of isotopic transfer paths with the exception of  $\text{H}_2\text{O}-\text{CO}_2$  path. On the basis of this observation, Oki concluded that in mechanism I and II of Table I both step i and v are probably rate-controlling. This implies that all the steps other than steps i and v are at equilibrium. A previous experiment<sup>7</sup> in which deuterium was used as  $\text{D}_2\text{O}$  showed that the half-deuterated hydrogen is formed in the course of the water-gas shift reaction. This fact suggests that the hydrogen-deuterium equilibration given by eq 2 proceeds *via* step v during the reaction. It was found in the present study that measurements of reaction rate of  $\text{D}_2$  and production rate of HD offers a novel method of obtaining the individual estimates of  $\Delta g_v$  and  $\Delta g_i$ . The comparison of the estimates thus obtained constitutes a quantitative justification of the earlier conclusion that steps i and v of mechanism I or II would be rate controlling. If these estimates agree, steps i and v are, indeed, rate controlling.

- (5) K. Tanaka, *J. Res. Inst. Catal., Hokkaido Univ.*, **14**, 153 (1966).
- (6) K. Tanaka, *J. Res. Inst. Catal., Hokkaido Univ.*, **19**, 63, (1971).
- (7) Y. Kaneko and S. Oki, *J. Res. Inst. Catal., Hokkaido Univ.*, **13**, 55 (1965).
- (8) Y. Kaneko and S. Oki, *J. Res. Inst. Catal., Hokkaido Univ.*, **13**, 169 (1965).
- (9) Y. Kaneko and S. Oki, *J. Res. Inst. Catal., Hokkaido Univ.*, **15**, 185 (1967).
- (10) Y. Kaneko and H. Odanaka, *J. Res. Inst. Catal., Hokkaido Univ.*, **13**, 29 (1965).
- (11) J. Happel, H. Odanaka, and P. Rosche, *Chem. Eng. Progr., Symp. Ser. N-115*, **67**, 60 (1971).
- (12) S. Oki, J. Happel, M. A. Hnatow, and Y. Kaneko, *Int. Congr. Catal., 5th.* (1972).
- (13) S. Oki, *Shokubai*, **10**, 180 (1968).
- (14) S. Oki and Y. Kaneko, *J. Res. Inst. Catal., Hokkaido Univ.*, **18**, 93 (1970).
- (15) G. G. Shchibrya, N. M. Morozov, and M. I. Temkin, *Kinet. Katal.*, **6**, 1057 (1965).
- (16) J. Nakanishi and K. Tamaru, *Trans. Faraday Soc.*, **59**, 1470 (1963).
- (17) C. Wagner, *Advan. Catal.*, **21**, 323 (1970).
- (18) S. Oki, Y. Kaneko, Y. Arai, and M. Shimada, *Shokubai*, **11**, 184 (1969).



It was also found that the use of deuterium enables one to calculate the free energy change of the hydrogen atom exchange path between  $\text{H}_2\text{O}$  and  $\text{H}_2$ , which is designated by  $\Delta g_{\text{H}}$ . In the case where steps i and v are rate controlling, the experimental estimate of  $\Delta g_{\text{H}}$  should coincide with that of  $\Delta g_{\text{v}}$ . Consequently the determination of  $\Delta g_{\text{H}}$  from experimental data obtained with deuterium furnishes an independent determination of the rate-controlling steps.

The objectives of the present investigation are threefold: (a) to obtain the values of  $\Delta g_{\text{v}}$  from experimental data gathered utilizing deuterium, (b) to calculate the values of  $\Delta g_{\text{H}}$  from the data, and (c) to definitely identify the rate-controlling step or steps of the water-gas shift reaction on the basis of the results of a and b.

### Mathematical Analysis

The chemical affinity of water-gas shift reaction 1,  $-\Delta G$ , is given by

$$-\Delta G = RT \ln \left\{ \frac{p(\text{CO})p(\text{H}_2\text{O})}{p(\text{H}_2)p(\text{CO}_2)} K_p \right\} \quad (3)$$

where  $K_p$  is the thermodynamic equilibrium constant of the reaction,  $T$  is the reaction temperature, and  $p(i)$  is the partial pressure of gaseous component  $i$ . The chemical affinity of a reaction for a single route is also expressed in terms of the stoichiometric number of elementary step, that is

$$\Delta G = \sum_{i=1}^s \nu(i) \Delta g_i \quad (4)$$

where  $\nu(i)$  and  $\Delta g_i$  are, respectively, the stoichiometric number and the free energy change of elementary step  $i$ . For the water-gas shift reaction, as stated in the previous section, the stoichiometric number of each of elementary steps considered in this study is unity (see Table I). Hence eq 4 becomes

$$\Delta G = \sum_{i=1}^s \Delta g_i \quad (5)$$

The free energy change of the  $i$ th elementary step,  $\Delta g_i$ , is given by

$$\Delta g_i = -RT \ln (v_{+i}/v_{-i}) \quad (6)$$

Substituting eq 6 into eq 5, we obtain

$$-\Delta G = RT \ln \prod (v_{+i}/v_{-i}) \quad (7)$$

Application of eq 5 to mechanism I and II of Table I yields the following relationships

$$\Delta G = \Delta g_i + \Delta g_{\text{ii}} + \Delta g_{\text{iii}} + \Delta g_{\text{iv}} + \Delta g_{\text{v}} \quad (8)$$

and

$$\Delta G = \Delta g_i + \Delta g_{\text{ii}} + \Delta g_{\text{iii-a}} + \Delta g_{\text{iii-b}} + \Delta g_{\text{iv}} + \Delta g_{\text{v}} \quad (9)$$

Oki and coworkers<sup>12,18</sup> investigated the reaction utilizing carbon-14 and oxygen-18 and found that all the steps ii through iv are in equilibrium. On the ground of this experimental result we assumed that the steps ii through iv are fast and are in equilibrium. The assumption leads to the following relationship

$$\Delta g_{\text{ii}} = \Delta g_{\text{iii}} = \Delta g_{\text{iii-a}} = \Delta g_{\text{iii-b}} = \Delta g_{\text{iv}} = 0 \quad (10)$$

Introduction of eq 10 into eq 8 and 9 gives

$$\Delta G = \Delta g_i + \Delta g_{\text{v}} \quad (11)$$

For a set of consecutive hydrogen-deuterium exchange paths of the reaction, that is, steps ii and v of mechanism I or steps ii, iii-a, iii-b, and v of mechanism II, the total free energy change of the consecutive paths,  $\Delta g_{\text{H}}$ , is expressed as

$$\Delta g_{\text{H}} = \Delta g_{\text{v}} \quad (12)$$

In the derivation of eq 12, needless to say, we assume that the relationship of eq 10 is also fulfilled in the present case. When deuterium is employed with hydrogen in kinetic experiments of water-gas shift reaction, the values of both  $\Delta g_{\text{H}}$  and  $\Delta g_{\text{v}}$  can be determined independently from material balance equations of hydrogen, deuterium, and half-deuterated hydrogen. The following describes mathematical procedures which enable one to obtain the experimental values of  $\Delta g_{\text{H}}$  and  $\Delta g_{\text{v}}$ .

Consider a closed circulating reaction system in which a gaseous mixture of carbon monoxide, water vapor, carbon dioxide, hydrogen, and deuterium is circulating through a catalyst bed. The following relationship holds between the over-all reaction rate of the system,  $V$ , and the forward and backward reaction rate of step v,  $v_{+v}$  and  $v_{-v}$ .

$$V = v_{+v} - v_{-v} = dp(\text{H}_2)/dt \quad (13)$$

In eq 13  $p(\text{H}_2)$  is the partial pressure of hydrogen in the reaction system and  $t$  is reaction time elapsed. The rates of partial pressure changes of  $\text{H}_2$ ,  $\text{D}_2$ , and  $\text{HD}$  are given by the equations

$$d(p(\text{H}_2)Y(\text{H}_2))/dt = (1 - Z(\text{H(a)}))^2 v_{+v} - Y(\text{H}_2) v_{-v} \quad (14a)$$

$$d(p(\text{H}_2)Y(\text{HD}))/dt = 2Z(\text{H(a)})(1 - Z(\text{H(a)})v_{+v} - Y(\text{HD})v_{-v} \quad (14b)$$

$$d(p(\text{H}_2)Y(\text{D}_2))/dt = (Z(\text{H(a)})^2 v_{+v} - Y(\text{D}_2)v_{-v} \quad (14c)$$

where  $Y(\text{H}_2)$ ,  $Y(\text{D}_2)$ , and  $Y(\text{HD})$  are respectively the mole fractions of  $\text{H}_2$ ,  $\text{D}_2$ , and  $\text{HD}$  in the reaction system and  $Z(\text{H(a)})$  denotes the atomic fraction of deuterium in the total number of hydrogen atoms adsorbed on the catalyst surface. Note that only two of eq 14 are independent. Equations 13, 14b, and 14c may be combined to give

$$(Z(\text{H(a)})^2 - a(Z(\text{H(a)}))) + b = 0 \quad (15)$$

in which

$$a = 2(dY(\text{D}_2)/dt) / \{dY(\text{HD})/dt + 2(dY(\text{D}_2)/dt)\}$$

$$b = \{Y(\text{HD})(dY(\text{D}_2)/dt) - Y(\text{D}_2)(dY(\text{HD})/dt)\} / \{dY(\text{HD})/dt + 2(dY(\text{D}_2)/dt)\}$$

Equation 15 should be solved to obtain the value of  $Z(\text{H(a)})$  with the condition that  $0 \leq Z(\text{H(a)}) \leq 1$ . The value of  $Z(\text{H(a)})$  so obtained may be substituted into eq 14 to calculate  $v_{+v}$  and  $v_{-v}$ . Application of eq 6, thus, gives the values of  $\Delta g_{\text{v}}$  for experimental conditions.

The forward and the backward unidirectional rate of hydrogen atom exchange path between  $\text{H}_2\text{O}$  and  $\text{H}_2$ ,  $v_{+H}$  and  $v_{-H}$ , are correlated with the over-all reaction rate  $V$  as follows

$$V = v_{+H} - v_{-H} = dp(\text{H}_2)/dt \quad (16)$$

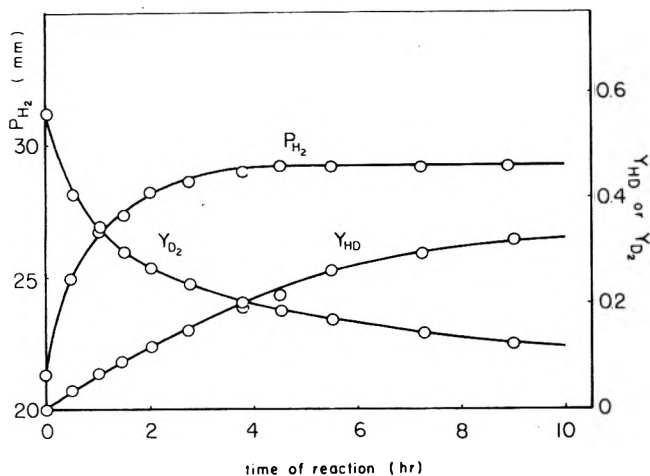


Figure 1. Time-dependent  $p(\text{H}_2)$ ,  $Y(\text{HD})$ , and  $Y(\text{D}_2)$  for run 1 (reaction temperature  $467^\circ$ ).

If it is assumed that the concentration of hydrogen atom adsorbed is constant, then, the rate of increase of deuterium content in hydrogen is given by

$$d(p(\text{H}_2)Z(\text{H}_2))/dt = Z(\text{H}_2\text{O})v_{+\text{H}} - Z(\text{H}_2)v_{-\text{H}} \quad (17)$$

where  $Z(\text{H}_2\text{O})$  and  $Z(\text{H}_2)$  are, respectively, the atomic fraction of deuterium atom in water vapor and in hydrogen. By combining eq 16 and 17, we get

$$v_{+\text{H}}/v_{-\text{H}} = 1/[1 + (Z(\text{H}_2) - Z(\text{H}_2\text{O})) (dp(\text{H}_2)/dt) / (p(\text{H}_2)dZ(\text{H}_2)/dt)] \quad (18)$$

Thus  $\Delta g_{\text{H}}$  can be readily calculated from eq 6.

### Experimental Section

Carbon monoxide, carbon dioxide, water vapor, and hydrogen were purified in the same manner as that described in earlier articles.<sup>7-9</sup> Deuterium was purchased from Takachiho Chemical Co., Ltd. The purity of the deuterium was 99.99 atom % D. It was used for the experiment without further treatment. An iron oxide catalyst ( $\text{Fe}_3\text{O}_4$ ) was supplied by Mitsubishi Kasei Co., Ltd. The physical properties of the catalyst were reported in an earlier article.<sup>7-9</sup> The catalyst was crushed and screened to about 12 mesh. The amount of the catalyst used was 0.5 g. The reaction temperature ranged from 467 to  $522^\circ$ . For all experiments feeds contained carbon monoxide, water vapor, carbon dioxide, and hydrogen. The concentrations of these component gases were varied rather widely. However, the total pressure of the reaction system was kept at about 80 mm.

In the absence of the iron oxide catalyst, a series of runs was made by employing the same experimental conditions as those of runs in the presence of the catalyst. These blank runs showed no measurable conversion for the isotopic exchange reaction between water vapor and hydrogen, the hydrogen-deuterium equilibration reaction, and the water-gas shift reaction. Thus it was established that all measurable conversion was due to the iron oxide catalyst.

A detailed description of the experimental apparatus and the procedure utilized in this study was presented elsewhere.<sup>7-9</sup> A closed recycling type reactor was used. A gaseous mixture of carbon monoxide, water vapor, carbon

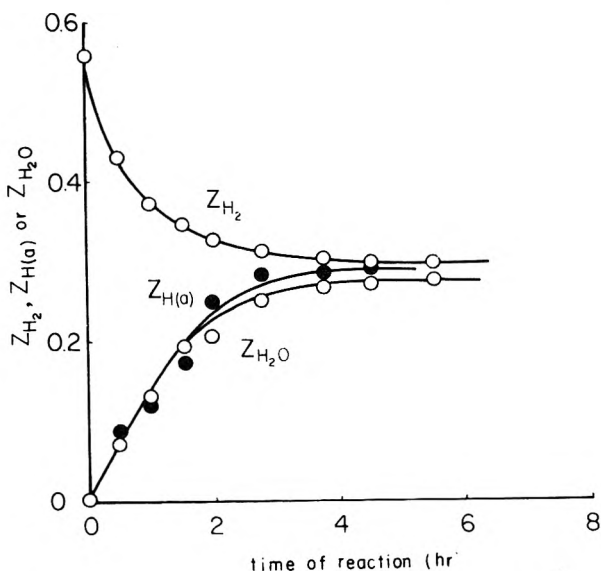


Figure 2.  $Z(\text{H}(\text{a}))$ ,  $Z(\text{H}_2)$ , and  $Z(\text{H}_2\text{O})$  vs. reaction time for run 1 (reaction temperature  $467^\circ$ ).

monoxide, hydrogen, and deuterium was circulated many times through the catalytic bed until the equilibrium of the water-gas shift reaction was reached. Gas samples were drawn into gas sampling bulbs at specific time intervals. The samples so collected were analyzed by Hitachi mass spectrometer, RMS-3B type, with a constant electron accelerating voltage of 80 V. From the gas analysis the composition of the mixture in the reaction system and the distribution of the isotopic tracers of  $\text{D}_2$  and HD were obtained.

### Results

Table II summarizes the experimental data gathered in this investigation. Figure 1 shows, as an example, the time-dependent experimental points of  $p(\text{H}_2)$  and  $Y(\text{HD})$  of run 1. For the determination of all the time derivatives which appear in eq 13 through 18, first, corresponding experimental data were fitted with a polynomial function of reaction time, and then, the derivatives were obtained analytically.

In Figure 2, for the experimental data of run 1, the estimates of  $Z(\text{H}(\text{a}))$ , which were calculated with the help of eq 15 are presented in comparison with experimental values of  $Z(\text{H}_2)$  and  $Z(\text{H}_2\text{O})$ . It is evident from Figure 2 that in a region far removed from equilibrium the value of  $Z(\text{H}_2)$  is greater than those of both  $Z(\text{H}(\text{a}))$  and  $Z(\text{H}_2\text{O})$  and that the value of  $Z(\text{H}(\text{a}))$  is in good agreement with that of  $Z(\text{H}_2\text{O})$ . For other sets of experimental data, similar results were obtained, though not shown in this article.

Figure 3 correlates the values of  $\Delta G$  with values of  $\Delta g_{\text{v}}$  calculated by eq 6, 13, 14, and 15. It can be seen from the figure that a linear relationship exists between  $\Delta G$  and  $\Delta g_{\text{v}}$  and that the slope of this relationship is approximately 2.

In Figure 4, the values of  $\Delta g_{\text{H}}$  were plotted against those of  $\Delta g_{\text{v}}$ . The relation is represented by a linear diagonal line. This indicates that  $\Delta g_{\text{H}}$  is approximately equal to  $\Delta g_{\text{v}}$  under experimental conditions employed in this investigation. It may be noticed that a slight trend exists in the relation between  $\Delta g_{\text{v}}$  and  $\Delta G$  (see Figure 2). The studies of unidirectional rate of  $v_{+\text{v}}$  and  $v_{-\text{v}}$  may explain



TABLE II: Experimental Data

Reaction time, min	P(CO), mm	P(H <sub>2</sub> O), mm	P(CO <sub>2</sub> ), mm	P(H <sub>2</sub> ), mm	Mole fraction of hydrogen		
					Y(H <sub>2</sub> )	Y(HD)	Y(D <sub>2</sub> )
Run 1. Reaction Temperature 467°							
0	20.8	19.9	20.6	21.3	0.440	0.003	0.557
30	17.4	16.6	24.1	25.0	0.552	0.038	0.410
60	15.3	14.5	26.2	26.8	0.593	0.067	0.340
90	14.9	14.0	26.6	27.3	0.609	0.093	0.298
120	13.8	13.1	27.6	28.2	0.614	0.120	0.266
165	13.5	12.8	27.9	28.5	0.610	0.152	0.238
225	13.1	12.0	28.4	29.0	0.606	0.192	0.202
270	12.9	12.1	28.6	29.2	0.594	0.217	0.189
330	12.8	12.1	28.6	29.2	0.569	0.264	0.167
435	13.0	12.2	28.5	29.1	0.563	0.291	0.144
540	12.9	12.0	28.7	29.3	0.553	0.322	0.125
630	12.9	12.2	28.5	29.1	0.537	0.346	0.117
Run 2. Reaction Temperature 489°							
0	6.04	6.10	36.96	33.60	0.455	0.002	0.542
10	7.23	7.29	35.07	32.41	0.463	0.015	0.520
20	8.10	8.16	34.81	31.40	0.460	0.028	0.511
30	9.04	9.10	33.96	30.60	0.474	0.041	0.483
40	9.73	9.79	33.27	29.91	0.479	0.054	0.466
50	10.17	10.23	32.83	29.67	0.470	0.068	0.460
60	10.64	10.71	32.36	29.00	0.470	0.079	0.450
75	10.90	10.96	32.10	28.74	0.465	0.101	0.432
90	11.14	11.20	31.86	28.50	0.465	0.123	0.410
105	11.88	11.94	31.12	27.76	0.454	0.146	0.399
120	11.93	11.99	31.07	27.71	0.454	0.166	0.379
150	12.37	12.43	30.63	27.27	0.436	0.208	0.354
180	12.33	12.39	30.67	27.31	0.427	0.238	0.333
Run 3. Reaction Temperature 522°							
0	17.93	9.95	9.55	14.68	0.250	0.003	0.750
5	17.31	9.33	10.13	15.26	0.285	0.018	0.696
18	16.15	8.17	11.33	16.46	0.356	0.045	0.597
35	15.05	7.07	12.43	17.56	0.394	0.088	0.519
47	14.41	6.43	13.07	18.20	0.407	0.121	0.471
60	13.99	6.01	13.49	18.63	0.409	0.153	0.436
80	13.63	5.65	13.85	18.98	0.408	0.197	0.393
0	15.72	7.74	25.46	30.59	0.554	0.198	0.246
10	16.00	8.02	25.18	30.31	0.560	0.206	0.232
25	16.37	8.39	24.81	29.94	0.561	0.220	0.217
40	16.59	8.61	24.59	29.72	0.561	0.233	0.204
60	16.34	8.36	24.84	29.97	0.558	0.253	0.188
80	16.74	8.76	24.44	29.57	0.550	0.273	0.176
100	16.88	8.90	24.30	29.43	0.448	0.288	0.163
130	17.05	9.07	24.13	29.26	0.545	0.306	0.147
180	17.03	9.15	24.05	29.15	0.536	0.332	0.131
230	17.27	9.29	23.91	29.04	0.527	0.353	0.119
Run 4. Reaction Temperature 511°							
0	19.50	21.10	20.24	29.65	0.720	0.002	0.276
10	19.00	20.60	20.74	30.15	0.718	0.005	0.276
25	18.40	20.30	21.34	30.75	0.729	0.008	0.262
35	17.87	19.47	21.87	31.28	0.741	0.009	0.249
45	17.65	19.25	22.09	31.50	0.743	0.012	0.244
55	17.31	18.91	22.43	31.80	0.745	0.017	0.237
70	16.70	18.30	22.74	32.45	0.743	0.021	0.234
90	16.58	18.18	23.06	32.57	0.750	0.031	0.218
110	16.47	18.07	23.27	32.68	0.751	0.037	0.210
135	16.23	17.83	23.51	32.92	0.764	0.046	0.189
155	15.93	17.53	23.81	33.22	0.754	0.054	0.190
175	15.71	17.31	24.03	33.44	0.757	0.061	0.180
195	15.46	17.06	24.28	33.69	0.757	0.069	0.172
255	15.04	16.64	24.70	34.11	0.750	0.093	0.156
285	14.37	15.97	25.37	34.78	0.757	0.097	0.143

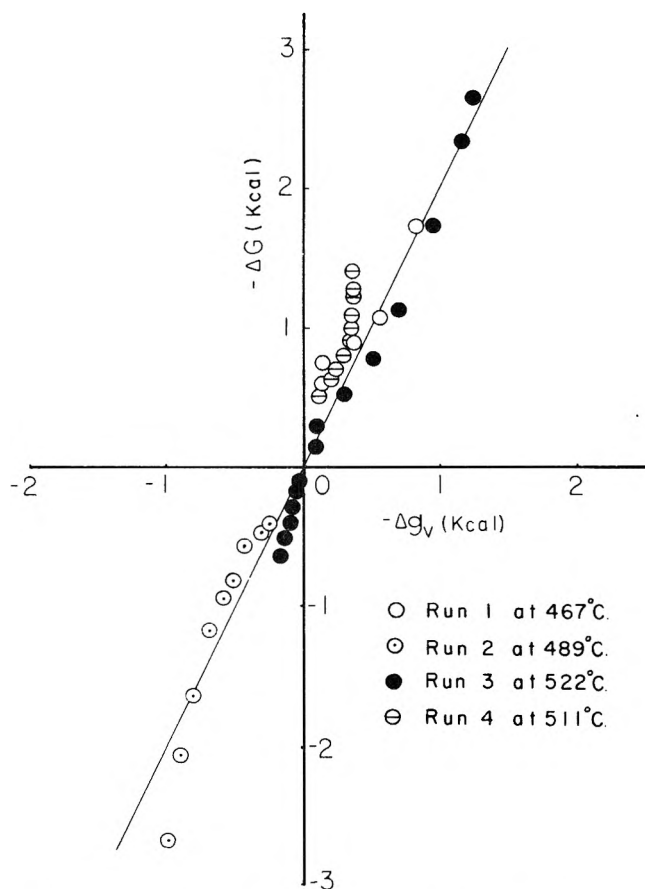


Figure 3. Gibbs free energy change of the reaction and that of step v.

the cause of the trend. A comprehensive investigation has been in progress to clarify this matter.

### Discussion

As shown in Figure 3,  $-\Delta G$  increases linearly with increasing  $-\Delta g_v$ . Moreover, the slope of this linear relation is about 2. Because the values of both  $-\Delta G$  and  $-\Delta g_v$  should be exactly zero at equilibrium and because eq 11 is assumed to be satisfied for the present system, we readily obtain

$$\Delta G = 2\Delta g_v \quad (19)$$

and

$$\Delta g_i = \Delta g_v \quad (20)$$

Equation 20 indicates that steps i and v are rate controlling. This conclusion coincides with those drawn from earlier experiments<sup>12,18</sup> conducted utilizing carbon-14 and oxygen-18. Figure 5 shows that total free energy change of hydrogen atoms exchange between  $\text{H}_2\text{O}$  and  $\text{H}_2$  is approximately equal to the free energy change of step v and that the condition of eq 12 is, indeed, fulfilled. The result also supports the validity of previously obtained experimental results<sup>12,18</sup> shown by eq 10.

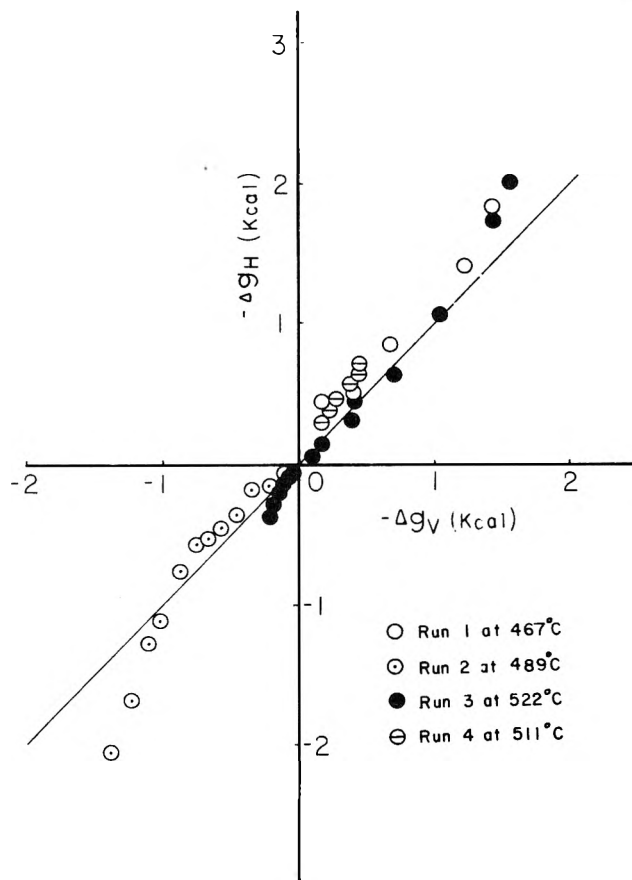


Figure 4. Gibbs free energy change of hydrogen exchange path and that of step v.

A number of investigators studied the rate of the water-gas shift reaction over an iron oxide catalyst and correlated their rate data by power function models. Their reaction rates were almost consistently first order with respect to the partial pressure of carbon monoxide. This implies that steps related to physical and chemical changes of carbon monoxide are rather significant for the reaction and that these steps could be rate controlling. Recently Nakanishi and Tamaru<sup>16</sup> measured the amount of hydrogen which was adsorbed in the course of the reverse reaction of eq 1 and concluded that the reduction process of iron oxide catalyst by hydrogen would be rate determining. More recently Temkin and coworkers<sup>15</sup> reported that two rate-controlling steps, perhaps the reaction of adsorbed water vapor with gaseous carbon monoxide and the desorption of hydrogen and carbon dioxide, may exist in the course of the water-gas shift reaction.

On the ground of the results of these investigations in conjunction with those of Oki's studies, it would be adequate to propose that the adsorption of carbon monoxide, step i, and the associative desorption of hydrogen, step v, are the rate-controlling steps of the water-gas shift reaction with the iron oxide catalyst for the experimental conditions employed in this investigation.

# g Factor and Hyperfine Coupling Anisotropy in the Electron Spin Resonance Spectra of Methyl-, Ethyl-, and Allyl-Type Radicals Adsorbed on Silica Gel

Tetsuo Shiga and Anders Lund\*

The Swedish Research Councils' Laboratory, Studsvik, 611 01 Nyköping, Sweden (Received June 30, 1972)

Public costs assisted by the Atomic Research Council of Sweden

Analysis of the asymmetric esr spectra of radicals sorbed on silica gel give the following axially symmetric parameters at 77 K; for the methyl radical  $A_{\perp} = -22.6$  G,  $A_{\parallel} = -21.9$  G,  $g_{\perp} = 2.0027$ , and  $g_{\parallel} = 2.0024$ ; for the ethyl radical  $A_{\perp} = -20.0$  G and  $A_{\parallel} = -29.9$  G; for the  $\alpha$  protons and  $A_{\perp} = 26.0$  G and  $A_{\parallel} = 27.9$  G; for the methyl protons  $g_{\perp} = 2.0029$  and  $g_{\parallel} = 2.0032$ . These data suggest that at 77 K the methyl radicals rotate about an axis perpendicular to the planes of the radical, whereas the ethyl radical rotates about the C-C bond axis. The analysis of spectra from allyl and methallyl radicals is less conclusive.

## Introduction

In contrast to the situation in the solid state,<sup>1</sup> the esr spectrum of the methyl radical which has been adsorbed on a solid surface has an asymmetric line profile.<sup>2-4</sup> Asymmetry has been observed only at an adsorbate concentration of less than a monolayer. A departure from intensities with a binomial distribution has also been observed for the ethyl radical adsorbed on silica gel.<sup>2</sup> Such departures have been accounted for in terms of an unequal line width which depends on the nuclear spin quantum number  $M_I$  and is caused by anisotropy of the hyperfine interaction and  $g$  tensors.<sup>2,5</sup> As yet, however, no quantitative analysis of these asymmetric esr spectra has been reported.

The present paper reports esr studies of the methyl, ethyl, allyl, and methallyl radicals adsorbed on silica gel as part of an attempt to obtain information about their conformation and mobility. For this purpose the anisotropy of the hyperfine couplings and the  $g$  factor were determined. Thus free motion of a radical will average out the anisotropic interactions and yield an isotropic line profile, whereas hindered rotation about a preferred axis will result in axially symmetric resonance parameters. Differentiation between these two cases is assisted by line shape simulations. In the present instance the geometries and motions of methyl, ethyl, allyl, and methallyl radicals adsorbed on silica gel were elucidated using the computer program devised by Lefebvre and Maruani.<sup>6</sup>

## Experimental Section

Silica gel used as an adsorbent was heated at 650° in air for several hours and then *in vacuo* for 12 hr. The samples were prepared by adding known amounts of adsorbate to the dried silica gel through a vacuum line. The sample tubes were sealed off under a pressure of  $10^{-5}$  Torr. Radicals were produced at 77 K by  $\gamma$ -ray radiolysis of methyl, ethyl, and allyl iodides adsorbed on silica gel. The concentration of each adsorbate was 1 mol %. Each sample received a dose of  $8 \times 10^5$  rads. The methallyl radical was produced by radiolysis at 77 K of butadiene adsorbed on silica gel at a concentration of 0.1 mol %. The butadiene cation radical is produced<sup>7</sup> under these conditions. The sample was therefore warmed initially to 200 K; at this temperature the esr spectrum of the butadiene cation radical vanishes. ESR spectra were measured with a Varian E-9 X-band spectrometer. The microwave power was maintained at 0.2-2 mW

and a magnetic field modulation of 100 kHz was used. Spectra were recorded at 77 K and also at higher temperatures for which purpose a variable temperature accessory was employed to control the temperature to within  $\pm 3^\circ$  in the range 100-300 K. The magnetic sweep was calibrated with Fremy's salt using the splitting  $a(N) = 13.0$  G. The signal from a trapped electron in the silica gel<sup>8</sup> ( $g = 2.0008$ ) was used as the standard to determine  $g$  values.

The resonance parameters were estimated by comparing the experimental line profile with computed spectra, employing a program which simulates the powder spectra of free radicals.<sup>9</sup> In the case of methyl and ethyl radicals the parameters were systematically varied to obtain the best fit on the basis of visual inspection. Derivative line shapes were computed with either Lorentzian (L) or Gaussian (G) profiles having widths  $\Delta H_{pp}$  measured peak to peak.

## Results

**Methyl Radical.** The asymmetric quartet of lines due to the methyl radical, Figure 1, which was observed at 77 K is already familiar from previous esr investigations of irradiated systems where silica gel or porous glass has been used as the adsorbent.<sup>2-4</sup> The spectrum has an apparent hyperfine splitting of 22.2 G, and an apparent  $g$  value of 2.0027. The line widths of the four lines at 77 K are 1.26, 0.92, 0.59, and 0.63 G in passing from a low to a high field. The spectrum has been analyzed in terms of axially symmetric  $g$  and hyperfine coupling tensors. The dashed profile in Figure 1 is the computed spectrum which affords the best fit with the experimental line shape. The following parameters are obtained:  $|A_{\perp}| = |a - b| = 22.6 \pm 0.2$  G,

- (1) E. L. Cochran, F. J. Adrian, and V. A. Bowers, *J. Chem. Phys.*, **34**, 1161 (1961).
- (2) V. B. Kazanskii, G. B. Pariiskii, I. V. Aleksandrov, and G. M. Zhidomirov, *Sov. Phys.-Solid State*, **5**, 473 (1963).
- (3) G. B. Garbutt, H. D. Gesser, and M. Fujimoto, *J. Chem. Phys.*, **48**, 4605 (1968).
- (4) S. Kubota, M. Iwaizumi, and T. Isobe, *Bull. Chem. Soc. Jap.*, **44**, 2684 (1971).
- (5) C. L. Gardner and E. J. Casey, *Can. J. Chem.*, **46**, 207 (1968).
- (6) R. Lefebvre and J. Maruani, *J. Chem. Phys.*, **42**, 1480 (1965).
- (7) T. Shiga, A. Lund, and P. O. Kinell, *Acta Chem. Scand.*, **25**, 1508 (1971).
- (8) P. O. Kinell, T. Komatsu, A. Lund, T. Shiga, and A. Shimizu, *Acta Chem. Scand.*, **24**, 3265 (1970).
- (9) J. Maruani, program MARU, rewritten and extended (1970) version of program described in ref 6.

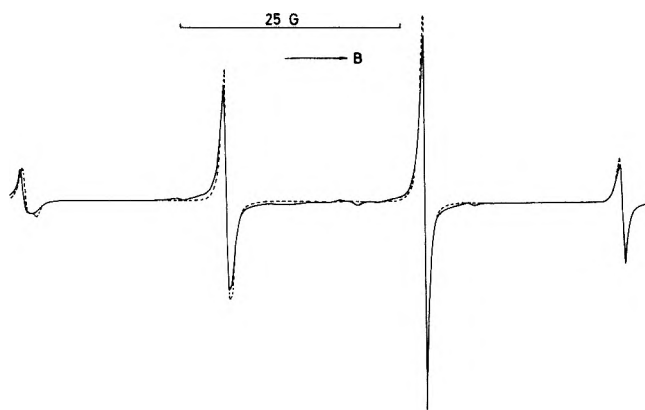


**Figure 1.** ESR spectrum at 77 K from methyl radical adsorbed on silica gel recorded with a microwave power of 0.2 mW and an amplitude of 0.2 G for the 100-kHz field modulation. The dashed spectrum is simulated with the parameters  $g_{\perp} = 2.0027$ ,  $g_{\parallel} = 2.0024$ ,  $A_{\perp} = -22.6$  G,  $A_{\parallel} = -21.9$  G, and  $\Delta H_{pp} = 0.5$  G (L).

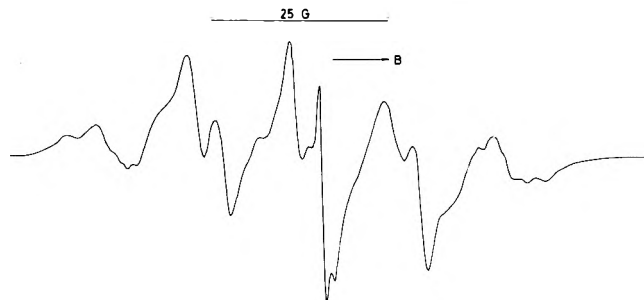


**Figure 3.** ESR spectrum at 77 K from allyl radical adsorbed on silica gel.

tropic parameters, as determined by the fitting procedure, have the following values:  $|A_{\perp}| = 20.0 \pm 0.5$  G and  $|A_{\parallel}| = 29.9 \pm 0.5$  G for the  $\alpha$  protons;  $|A_{\perp}| = 26.0 \pm 0.5$  G and  $|A_{\parallel}| = 27.9 \pm 0.5$  G for the methyl group; and  $\Delta g = (-3 \pm 1) \times 10^{-4}$  and  $g_{\text{iso}} = 2.0030 \pm 0.0002$ . The simulation represented in Figure 2a by the dashed line was obtained with  $\Delta H_{pp} = 1.8$  G(L), whereas a Gaussian profile provides a somewhat less satisfactory fit to the experimental spectrum.

Esr spectra measured at different temperatures exhibit a remarkable change in the profile of the outermost peaks with rising temperature as is illustrated in Figure 2b-d. At 178 K, Figure 2e, the altered line shape corresponds to a spectrum which is characterized by the isotropic coupling constants  $a(\text{CH}_2) = 21.5$  G and  $a(\text{CH}_3) = 26.4$  G. Another type of spectrum also appears when the sample is warmed. This spectrum, which is indicated by arrows in Figure 2e, appears to be composed of an isotropic triplet,  $a_1 = 29.4$  G of triplets,  $a_2 = 22.2$  G, and was accordingly assigned to the  $-\text{CH}_2\dot{\text{C}}\text{H}_2$  radical.

**Allyl and Methallyl Radicals.** At 77 K the spectrum from the irradiated allyl iodides-silica gel system consists of a main quintet of lines, Figure 3, which can be further resolved as the temperature increases. At 173 K the spectrum comprises a quintet  $a_1 = 13.9$  G with an additional doublet splitting of  $a_2 = 3.9$  G. The absorption, which changes reversibly to that observed at 77 K by lowering the temperature, can reasonably be attributed to the allyl radical by comparison with solution data.<sup>10</sup> The spectrum shown in Figure 3 does not afford a particularly good fit with that computed for a polycrystalline sample in a rigid medium.<sup>11</sup> Neither the structure of each line in the quintet nor the asymmetry of the spectrum with respect to its center have been reproduced.

The spectrum from the 1,3-butadiene-silica gel sample at 77 K is a poorly resolved septet with a line separation of about 14 G. As the temperature increases spectra with improved resolution are obtained and at 193 K some of the lines give  $\Delta H_{pp} = 1.0$  G or less, Figure 4. On the basis of experiments with deuterated components this spectrum has been assigned to the methallyl radical  $\text{CH}_3-\dot{\text{C}}\text{H}-\text{CH}=\text{CH}_2$  which is formed by the addition of hydrogen atoms released from surface hydroxyl groups on the silica gel.<sup>7</sup> An attempted interpretation suggests that the axially symmetric couplings  $|A_{\perp}| = 16.5$  G and  $|A_{\parallel}| = 17.5$  G for the methyl protons and  $|A_{\perp}| = 13.5$  G and  $|A_{\parallel}| = 16.5$  G for the  $\text{CH}_2$  protons are appropriate. The shape of the computed line profiles is sensitive to the degree of coupling assumed for the CH protons. No fit has been obtained using aniso-

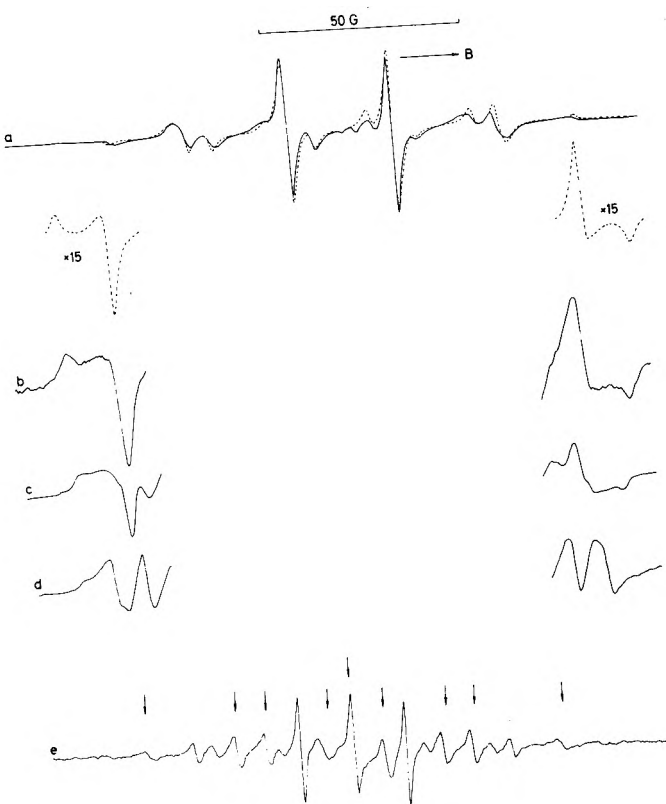


**Figure 2.** ESR line profiles of ethyl radical adsorbed on silica gel recorded with a microwave power of 2 mW and an amplitude of 1 G for the 100-kHz field modulation: (a) at 77 K, the dashed spectrum is simulated with the parameters  $g_{\perp} = 2.0029$ ,  $g_{\parallel} = 2.0032$ ,  $A_{\perp} = -20.0$  G,  $A_{\parallel} = -29.9$  G ( $\alpha$  protons),  $A_{\perp} = 26.0$  G,  $A_{\parallel} = 27.9$  G, (methyl protons),  $\Delta H_{pp} = 1.8$  G (L); (b-d) at 77, 103, and 133 K (outermost lines); (e) at 178 K. The arrows indicate a second spectrum assigned to  $-\text{CH}_2\dot{\text{C}}\text{H}_2$ .

$|A_{\parallel}| = |a + 2b| = 21.9 \pm 0.2$  G,  $\Delta g = g_{\perp} - g_{\parallel} = (3 \pm 1) \times 10^{-4}$ ,  $g_{\text{iso}} = 2.0026 \pm 0.0002$ ,  $\Delta H_{pp} = 0.5$  G(L). A Gaussian profile gave a worse agreement, particularly on the tails of the lines.

**Ethyl Radical.** The esr spectrum of the ethyl radical at 77 K, shown in Figure 2a, has for the outermost peak a line profile which is typical of the axially symmetric hyperfine interactions observed in the pure solid state.<sup>1</sup> The aniso-

(10) R. W. Fessenden and R. H. Schuler, *J. Chem. Phys.*, **39**, 2147 (1963).  
 (11) C. Chachaty and J. Maruani, *Can. J. Chem.*, **44**, 2631 (1966).

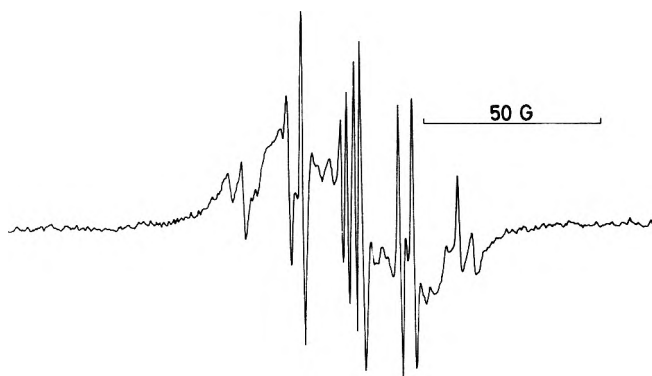


Figure 4. ESR spectrum at 193 K from methallyl radical adsorbed on silica gel.

tropic parameters while the values  $a_1 = 14.3$  G and  $a_2 = 3.9$  G give a fair agreement.

### Discussion

With the method employed here, spectral line shapes of free radicals can be analyzed only under conditions of fixed geometry, preferential reorientation about a fixed axis, or of fast isotropic tumbling. This type of analysis appears to be possible in the case of the methyl and ethyl radical. These cases are therefore considered in some detail. The results with allyl and methallyl are less conclusive.

**Methyl Radical.** The parameters  $|A_{\perp}| = 22.6$  and G  $|A_{\parallel}| = 21.9$  G inferred from the line shape analysis of the spectrum at 77 K is in good agreement with those estimated for the methyl radical trapped in a single crystal matrix of sodium acetate trihydrate.<sup>12</sup> As in that instance, the motion of the radical is restricted to a rotational diffusion, which occurs preferably about the threefold axis of the radical; this is evidenced by the small anisotropy.

In this instance the spectrum expected for a pyramidal  $C_{3v}$  structure becomes indistinguishable from that obtained for a planar  $D_{3h}$  configuration as far as the symmetry of the resonance parameters is concerned. Some support for a planar geometry is obtained by a consideration of the magnitude of the interactions. Typical values for the in-plane components of the proton dipolar coupling tensor are  $T_x = 10.9$  G and  $T_y = -11.3$  G as estimated for the malonic acid radical.<sup>13</sup> From this a value of  $b = 0.2$  G is derived in complete agreement with the experimental results. Further evidence for this type of reorientation is provided by the value of  $g_{\parallel} = 2.0024$ . This is close to the value for the free electron as might be expected for the component perpendicular to the radical plane.

In a previous analysis<sup>5</sup> Gardner and Casey attributed the departure from a binomial intensity distribution to a difference in line width which could be explained by the theory of spin relaxation in liquids. The correlation time deduced from this theory was  $\tau_c = 5.0 \times 10^{-8}$  sec, using rather large values for the parameters  $b$  and  $\Delta g$ . A more realistic estimate of the anisotropy as obtained from single-crystal studies yields a value for  $\tau_c$  which is an order of magnitude greater. This theory cannot account for the asymmetry of

the spectral lines in a simple fashion. It would appear that, at 77 K, static interactions contribute significantly to the line profile as was originally suggested by Kazanskii, *et al.*<sup>2</sup>

**Ethyl Radical.** In order to explain the equivalency and the axial symmetry of the interactions it is to be assumed that rapid reorientation occurs about the C-C bond. In the model which has been employed the H-C-H angle is  $120^\circ$ . With the dipolar components  $T_x = 10.9$  G,  $T_y = -11.3$  G, and  $T_z = 0.5$  G, a value of  $b = -2.9$  G was calculated. Here  $x$  is directed along the  $C_{\alpha}$ -H bond,  $z$  is perpendicular to the plane formed by the  $\sigma$  bonds about the  $C_{\alpha}$  position, and  $y$  is an axis perpendicular to  $x$  and  $z$ . This is fairly close to the experimental derivation of  $b = -3.3$  G based on the assumption that the isotropic coupling constant  $a = -23.3$  G, as is the case when  $A_{\perp}$  and  $A_{\parallel}$  have a negative sign. Reorientation about the axis perpendicular to the radical plane would cause a much smaller anisotropy of an order comparable to that observed for the methyl radical. Further evidence for a preferred reorientation about the  $C_{\alpha}$ - $C_{\beta}$  axis is obtained from the observation that  $\Delta g < 0$ . Since the component perpendicular to the radical frame has been observed to be smaller than the in-plane components in typical  $\pi$  electron radicals such as  $\text{CH}_2\text{COOH}$ ,<sup>14</sup> this situation could not be achieved by rotation about an axis lying perpendicular to the plane of the radical.

The magnitude of the methyl couplings  $A_{\perp} = 26.0$  G and  $A_{\parallel} = 27.9$  G obtained in the present work agrees with that obtained for couplings of methyl protons in the radical  $\text{CH}_3\text{CHCOOH}$  formed from irradiated 1-alanine.<sup>15</sup> The axial symmetry indicates that the methyl group reorients between at least three equilibrium positions.<sup>1</sup> This view is at variance with the previous observation that the outermost lines have a symmetrical line profile produced by a single equilibrium position for the ethyl radical in the adsorbed state.<sup>2</sup>

The change of the line profile into a nearly isotropic spectrum at 178 K, Figure 2e, indicates that at this temperature the ethyl radical tumbles freely. Analysis of line shapes in the region of slow diffusion, which probably prevails in the cases illustrated in Figure 2b-d and possibly also in the spectra from allyl and methallyl radicals, is much more involved and has not been attempted at this stage.

### Conclusion

The anisotropic resonance parameters for simple radicals such as methyl and ethyl radicals can be derived by line shape simulations of experimental profiles and interpreted on the assumption of rapid reorientation about a fixed axis. This fitting procedure becomes less satisfactory for larger radicals, possibly because of complications produced by slow reorientation at which point the method fails.

(12) M. T. Rogers and L. D. Kispert, *J. Chem. Phys.*, **46**, 221 (1967).

(13) T. Cole and C. Heller, *J. Chem. Phys.*, **34**, 1085 (1961).

(14) A. Horsfield, J. R. Morton, and D. H. Whiffen, *Mol. Phys.*, **4**, 327 (1961).

(15) I. Miyagawa and K. Itoh, *J. Chem. Phys.*, **36**, 2157 (1962).

## Electron Spin Resonance Spectra of the Radicals Produced in the Radiolysis of Aqueous Solutions of Furan and Its Derivatives<sup>1</sup>

Robert H. Schuler,\* Gary P. Laroff, and Richard W. Fessenden

Radiation Research Laboratories, Center for Special Studies and Department of Chemistry, Mellon Institute of Science, Carnegie-Mellon University, Pittsburgh, Pennsylvania 15213 (Received October 2, 1972)

Publication costs assisted by the U. S. Atomic Energy Commission and Carnegie-Mellon University

The esr spectra of radicals produced by addition of H atoms and OH radicals to the position adjacent to the heterocyclic oxygen atom of furan and a number of its derivatives have been observed during the continuous radiolysis of their acidic solutions. The radicals are allylic in character and exhibit hyperfine constants for the protons at the 2, 3, and 4 positions which are typical of an allylic system. The H atom adducts are characterized by hyperfine constants of the protons at the 5 position of 30–35 G. Such values are considerably larger than that of 23.0 G for the  $\beta$  protons in the structurally related hydrocarbon radical cyclopentenyl. This observed difference is attributable to the presence of a small but significant spin density on the ring oxygen atom which causes a large increase in the value of the electronic wave function at the positions of these protons. The radicals produced by addition of OH have hyperfine constants for the protons at the allylic positions which are similar to those of the H atom adducts. The CH proton of the  $-\text{CHOH}-$  group in these radicals, however, has an hyperfine constant of only 19–21 G and reflects an effect of OH substitution similar to that found in the comparison of cyclohexadienyl and hydroxycyclohexadienyl radicals. In basic solutions of furan, ring opening follows OH addition and the radical anion of butenedial is formed. Related highly conjugated radicals are produced from furfuryl alcohol, furfural, furylacetonitrile, 2-furoic acid, 3,4-furandicarboxylic acid, 2,5-furandicarboxylic acid, 2-acetylfuran, 2-furonitrile, and furylacrylic acid. Because of conjugation, these radicals can exist in a number of isomeric forms. Several isomeric radicals were observed to be produced simultaneously in the case of carboxylic acids. In very basic solutions of 2,5-dimethylfuran abstraction of one of the methyl hydrogen atoms occurs and results in the formation of a very interesting cyclic conjugated radical. The spin distribution in this radical shows that the oxygen atom induces a significant negative contribution on the atoms to which it is attached.

In a study of the esr spectra of an irradiated single crystal of furoic acid Cook, Rowlands, and Whiffen<sup>2</sup> have shown that hydrogen atoms add to the 5 position of this compound to produce a conjugated radical that exhibits an unusually large  $\beta$  proton hyperfine constant (31.4 G). From the 9.0-G hyperfine constant of the proton on the carbon atom at the 4 position one can estimate the spin density there to be 0.37. If the only contribution to the wave function at the position of the  $\text{C}_5$  protons results from spin density on this adjacent atom, one expects the observed  $\beta$  hyperfine constant to be only 12.9 G.<sup>3</sup> This situation is very much like that in cyclohexadienyl radical where the splitting by the  $\text{CH}_2$  protons is twice as large as otherwise expected from simple considerations of the spin densities on the adjacent carbon atoms. These large splittings are now understood to arise because of the nonlinear way in which the effects of the spin density on these adjacent atoms add.<sup>4,5</sup> Cyclic radicals will, in general, carry the possibility of unusual hyperfine constants at such positions. The high value in the case of furoic acid appears to be the consequence of a contribution which results from the presence of appreciable spin density on the ring oxygen atom in addition to that on the  $\text{C}_4$  carbon. It has been previously estimated that a spin density of only 0.06 on this oxygen atom would be sufficient to produce the observed effect.<sup>2,3</sup> To this point esr information on the radicals produced by H atom and OH radical addition to the furan ring system is of considerable interest. We have examined the isotropic spectra of a number of these radicals

in aqueous solution by the *in situ* radiolysis-esr approach and wish to report the results here. In acidic solutions the principal radicals observed are those which result from the addition of H and OH to the position adjacent to oxygen of the furan ring. In alkaline solutions, however, OH addition to this position results in ring opening to form conjugated radical anions having terminal aldehyde groups. Such ring opening has previously been observed by Lilie<sup>6</sup> in pulse radiolysis studies on furan where the radical anion of butenedial was shown to be an important intermediate. The esr results reported here substantiate Lilie's conclusions and show that, because of the conjugation and consequent hindered internal rotation, these radical anions can exist in a number of isomeric forms. A number of other interesting radicals are also observable during the radiolysis of solutions of derivatives of furan and the results on these are included here.

### Experimental Section

The steady-state *in situ* radiolysis-esr approach as applied to studies of aqueous systems has been described

- (1) Supported in part by the U. S. Atomic Energy Commission.
- (2) R. J. Cook, J. R. Rowlands, and D. H. Whiffen, *Mol. Phys.*, **7**, 57 (1963).
- (3) R. W. Fessenden and R. H. Schuler, *Advan. Radiat. Chem.*, **2**, 103 (1970).
- (4) D. H. Whiffen, *Mol. Phys.*, **6**, 223 (1963).
- (5) R. W. Fessenden and R. H. Schuler, *J. Chem. Phys.*, **39**, 2147 (1963).
- (6) J. Lilie, *Z. Naturforsch.*, **26**, 197 (1971).



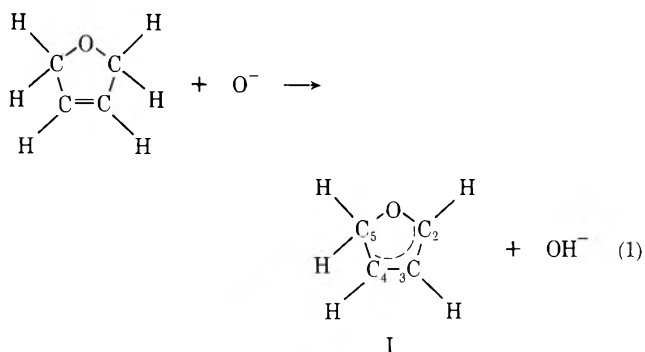
previously.<sup>7</sup> Appropriate solutions of furan and its derivatives (furan and furfuryl alcohol, Eastman Kodak Co.; furfural, Fisher Scientific Co.; 2-furonitrile, 2-furanacetone, 2-acetylfuran, 2-furylacrylonitrile, 2-furylacrylic acid, and 3,4-furandicarboxylic acid, Aldrich Chemical Co.; 2,5-dimethylfuran, Columbia Organic Chemicals Co.; 2-furoic acid, Analabs; and 2,5-furandicarboxylic acid, Pfaltz and Bauer, Inc.) were prepared and deoxygenated by bubbling either with nitrogen or nitrous oxide depending on whether or not it was desired to convert  $e_{aq}^-$  to  $\cdot\text{OH}$ . Perchloric acid and potassium hydroxide were used to adjust the pH to the desired value. Electron irradiations were continuous with radical production rates being up to  $10^{-2} M \text{ sec}^{-1}$ . Residence times of the solution within the esr cavity were  $\sim 50$  msec. Double modulation at 200 Hz and 100 kHz was used and the spectra recorded as the second derivatives of the esr absorptions. In most cases the line widths observed approached the limits of the experiment ( $\sim 0.07$  G). The magnetic field and microwave frequency were continuously monitored during the recording of the spectra as described in ref 5 and 7. Coupling constants are considered to be accurate to  $\sim 0.02$  G and absolute values of the  $g$  factors to  $\sim 0.00003$ . Comparison of two radicals within a single spectrum allows relative  $g$  factors to be determined to  $\sim 0.00001$ .

## Results and Discussion

**H Atom Addition.** Radicals formed by addition of hydrogen atoms produced in the radiolysis of water to the 2 position of furan and 3,4-furandicarboxylic acid and to the 5 position of furfuryl alcohol, 2-furoic acid, and 2-furonitrile have been observed in the irradiation of  $10^{-3}$ – $10^{-2} M$  solutions at pH 1. In each of these cases the spectrum is complicated by the presence of other radicals. However, the large hyperfine constant of the two H atoms on the carbon atom adjacent to the ring oxygen makes the spectrum of the H atom adduct sufficiently wide (80–100 G) that the outermost lines are well separated from the lines of the other radicals. The sums of the coupling constants and centers of the spectra are directly determinable from the positions of these outermost lines so that analysis of the remaining structure is readily tractable. H atom addition was also observed to occur at the 2 position of 2,5-furandicarboxylic acid. In this case the total spread of the spectrum is only 43 G because of the presence of only one proton which has a large hyperfine constant but all eight lines produced by the three nonequivalent protons are readily observable. The esr parameter of the various H atom adducts are given in Table I.

An alternative approach for producing the H atom adduct to furan is by means of H atom abstraction from 2,5-dihydrofuran. As suggested by the work of Hoffman, Simic and Neta,<sup>8</sup> a nitrous oxide saturated solution was irradiated at pH 14 (1 M KOH) under which conditions the principal reactive intermediate in the radiolysis is  $\text{O}^-$ . Preferential abstraction of one of the allylic type H atoms in the dihydrofuran occurs so that only a single radical is present in significant concentration and a simple spectrum is obtained, as is illustrated in Figure 1. The spectrum of radical I consists of a 2.20-G doublet, a 13.41-G triplet, and a 35.55-G triplet. The center lines of the large triplet are split by the appropriate second-order splitting of 0.38 G.<sup>9</sup> As is indicated in Table I an identical pattern is present in the spectrum obtained with furan at pH 1 where the reaction clearly involves H atom addition. The signal intensity in this latter case is, however, only  $\sim 5$

times the noise level. There is no evidence in the spectrum obtained in acidic solutions of furan for H atom addition at the 3 position.



Radical I is allylic in character so that the hyperfine constants of the protons at the 2 and 4 positions are expected to have values similar to those found for the terminal protons in allyl (13.9 and 14.8 G). The carbon atom at the 3 position should have a small negative spin density so that its attached proton is expected to have a hyperfine constant similar to the value for the central proton in allyl (4.1 G). The observed hyperfine constants of 13.41 and 2.20 G are assigned accordingly, as is indicated in Table I. The large hyperfine constant of 35.55 G must therefore be attributed to the two protons at the 5 position. This assignment is completely corroborated by the hyperfine splittings observed for the H atom adducts of the various derivatives of furan discussed below.

Because the allylic system in radical I is asymmetric, one does not expect the protons at the 2 and 4 positions to have identical hyperfine constants as is experimentally observed. An attempt to resolve the central line of the high-field triplet assigned to these protons showed two components separated by 0.05 G. Since this is the second-order separation expected for two equivalent protons which have a coupling constant of 13.4 G<sup>9</sup> one can only say that the two hyperfine constants are numerically equal to within this second-order splitting (0.05 G). From the studies on the other H atom adducts one can estimate that the coupling constants for these two particular atoms should differ by not more than  $\sim 0.5$  G so that the chance equivalence is, perhaps, not too surprising.

The spectrum observed with furfuryl alcohol at pH 1 is quite complex but one contributor is clearly the analog of radical I which has the H atom at position 2 replaced by a  $\text{CH}_2\text{OH}$  group. As is indicated in Table I, the coupling constants for the four H atoms at positions 3, 4, and 5 are quite similar to those for radical I so that this substitution is seen not to affect the spin distribution significantly. The protons of the side chain have a coupling constant of only 6.68 G. Interpretation of the spectrum is somewhat complicated by the fact that this coupling constant is only very slightly more than one-half that for the proton at the 4 position so that under conditions of modest resolution the fourth and fifth lines from the end of the spectrum overlap. They are, however, resolvable and the spectrum obtained at low modulation amplitude shows that  $2a^{\text{H}}(\text{CH}_2\text{OH}) - a^{\text{H}}(\text{H}_4) = 0.15$  G. The value observed for the protons on the side chain (6.68 G) is considerably smaller

- (7) K. Eiben and R. W. Fessenden, *J. Phys. Chem.*, **75**, 1186 (1971).  
 (8) M. Z. Hoffman, M. Simic, and P. Neta, *J. Phys. Chem.*, **76**, 847 (1972).  
 (9) R. W. Fessenden, *J. Chem. Phys.*, **37**, 747 (1962).

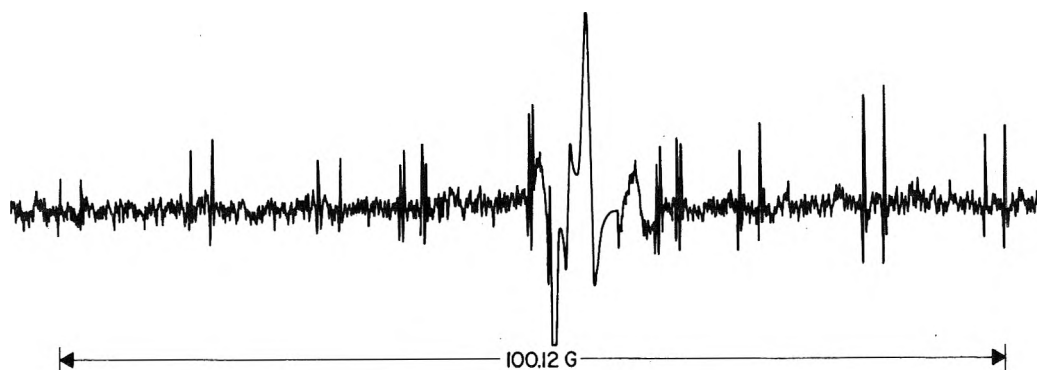


**Figure 1.** Second derivative esr spectrum taken during the irradiation of a nitrous oxide saturated  $10^{-2} M$  solution of 2,5-dihydrofuran solution at pH 14. This 24 line spectrum is identical with that of the H atom adduct to furan. The large peak to the right of the center is that of the quartz cell recorded at a 100-fold reduced gain. The esr pattern of the radical consists of a 2.2-G doublet, 13.4-G triplet, and a 35.6-G triplet with the second-order splittings (0.38 G) of the largest triplet resolved to give the additional fine structure seen in the center of the spectrum. This large triplet is typical of the radicals produced by H atom addition to the 5 position of furan derivatives and gives these spectra characteristic total spreads of 80–100 G. The increase in line intensity with increase in field (from left to right) is observed for many short-lived radicals as a result of spin polarization. This particular spectrum was taken at a relatively high scan rate (8 G/min) for presentation purposes. The individual lines are observable at a considerably increased ratio of signal-to-noise at scan rates ( $<0.1$  G/min) that can be conveniently used only to record partial spectra.

than the value expected for the protons of a methyl group at this position ( $\sim 15$  G). Favoring of rotational configurations with the OH out of the plane of the radical is indicated.

Radicals analogous to I produced by H atom addition to 2-furoic acid, 2-furonitrile, and 3,4-furandicarboxylic acid are readily observable during the irradiation of acidic solutions of these compounds. The parameters of the first of these can be compared with the isotropic values obtained in the solid-state study of Cook, *et al.*,<sup>2</sup> mentioned in the introduction (31.4 (2), 9.0, and 2.2 G) where the radical from furoic acid presumably exists in the neutral (protonated) form. All three radicals have protons at the 5 position with hyperfine constants (30.7, 31.1, and 33.9 G) which are somewhat lower than those of radical I. The hyperfine constants of the radical produced from 2-furonitrile are seen to be quite similar to those for that from 2-furoic acid. The protons at the 4 position of these radicals are only 10.0 and 9.4 G, which indicates some perturbation of spin density in the allylic system as a result of the substitution. The nitrogen hyperfine constant (2.5 G) in the first of these can be compared with the value of 3.5 G observed for  $\cdot\text{CH}_2\text{CN}$ .<sup>10</sup> A spin density of  $\sim 0.72$  in the C-CN system is indicated. The proton hyperfine constants give spin densities of 0.41 and  $-0.09$  for the 4 and 3 positions and confirm a contribution of  $\sim 0.7$  in the C-CN system. Presumably the relatively high value of the nitrogen hyperfine constant results from a small but significant contribution from the presence of spin directly on the nitrogen atom. The slightly lower  $C_4$  proton hyperfine constant for the radical from 2-furoic acid indicates an even greater perturbation by the  $-\text{CO}_2\text{H}$  group. In the radical from 3,4-furandicarboxylic acid the double substitution has a very large effect as is seen by the very low value of 8.0 G for its  $C_2$  proton hyperfine constant. In this latter case, as indicated in a footnote to Table I, line-broadening effects resulting from exchange of the  $\text{CO}_2\text{H}$  protons were observable at pH 1.

The radical produced by H atom addition to 2,5-furandicarboxylic acid is rather special in that it is related to the radical from furoic acid by substitution of one of the protons at the 5 position by a  $\text{CO}_2\text{H}$  group. It is seen that such a substitution has relatively little effect on the

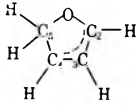
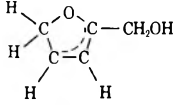
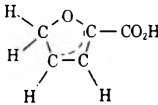
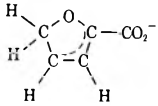
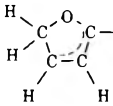
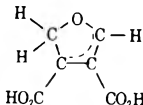
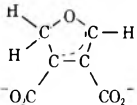
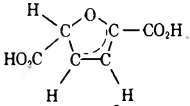
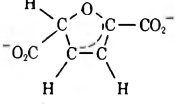
hyperfine constant of the remaining proton (29.7 *vs.* 30.8 G). This small effect is in contrast to the relatively large change produced by OH substitution (commented in the next section) where the analogous hyperfine constant drops to 21.1 G. One might expect that the 2 and 5 positions of this molecule would be blocked sufficiently that addition of H atoms to the 3 position would be observable (as for OH addition; see below). The resultant adduct is a nonconjugated radical and is expected to exhibit a 20–30-G triplet as a result of the two protons in a position  $\beta$  to the unpaired electron. No such esr pattern was present in the observable spectrum. One three proton radical ( $a = 4.19$  (2) and 2.45 G,  $g = 2.00383$ ) is present at pH 1 but the triplet spacing seems to be much too small for assignment to the H atom adduct at the 3 position.

Furoic acid, 3,4-furandicarboxylic acid, and 2,5-furandicarboxylic acid were examined at high pH in order to take advantage of a reduced recombination rate for the anionic forms. The spectra of appropriate analogs of radical I were superimposed on the other spectra reported below. In the case of furoic acid the signals of the H atom adduct were eliminated by saturation of the solution with  $\text{N}_2\text{O}$  so that electron addition followed by protonation appears to be at least one of the reaction paths by which these radicals are formed in basic solution. In the case of 2,5-furandicarboxylic acid the H atom adduct disappears upon increase of pH from 11 to 12.6 so that here the residual yield of H atoms appears to be the source. In this case the electron adduct is observable (see below) and apparently does not protonate readily. Because of ionization of the carboxyl groups, the esr parameters of the radicals produced from these acids in basic solutions are somewhat different from those observed in acidic solutions. As is indicated in Table I for the radical from furoic acid, ionization is found to result in an increase in each of the hyperfine constants with the effect on that for the proton at the 4 position being relatively large. This effect is in the opposite direction from that observed upon ionization of  $\text{HO}_2\text{C}-\text{CH}_2\dot{\text{C}}\text{HCO}_2\text{H}$  where  $a_{\alpha\text{H}}$  decreases from 20.87 to 20.41 G.<sup>11</sup> It is noted, however, that the Hammett  $\sigma$  factor for

(10) R. Livingston and H. Zeldes, *J. Magn. Resonance*, **1**, 169 (1969).

(11) H. Fischer, K.-H. Heilwege, and M. Lehnig, *Ber. Bunsenges. Phys. Chem.*, **72**, 1166 (1968).

TABLE I: Radicals Produced by H Atom Addition to Furan and Its Derivatives

Solute	pH	Radical	g factor	Assigned position	Hyperfine constants, G <sup>a</sup>
Furan 2,5-Dihydrofuran	1 14 <sup>b</sup>		2.00314 <sup>c</sup>	5 2 and 4 3	35.55(2) <sup>c</sup> 13.41(2) <sup>c,d</sup> 2.20 <sup>c</sup>
Furfuryl alcohol	1		2.00309	5 4 3 CH <sub>2</sub> OH	34.56(2) 13.21 2.21 6.68(2)
2-Furoic acid	1		2.00373	5 4 3	30.77(2) 9.43 2.15
	10		2.00378	5 4 3	31.74(2) 10.38 2.25
2-Furonitrile	1		2.00333	5 4 3 N	31.12(2) 10.00 2.26 2.52
3,4-Furandi-carboxylic acid	0.3 <sup>e</sup>		2.00348	5 2	34.86 8.04
	11.5		2.00349	5 2	33.88(2) 10.94
2,5-Furandi-carboxylic acid	1		2.00368	5 4 3	29.66 10.08 2.25
	11.2		2.00362	5 4 3	30.93 10.58 2.25

<sup>a</sup> Number of equivalent protons indicated in parentheses. <sup>b</sup> Nitrous oxide saturated to convert  $e^-_{aq}$  to  $O^-$ ; all other solutions saturated with  $N_2$ . <sup>c</sup> The esr parameters for this radical are identical at pH 1 (obtained by adding H atoms to furan) and 14 (obtained by abstraction of H atoms from 3,4-dihydrofuran). <sup>d</sup> Although the protons at the 2 and 4 position are not geometrically equivalent the esr experiment shows two protons which are magnetically identical to within the expected second-order splitting of 0.05 G. <sup>e</sup> Lines are  $\sim 0.25$ -G wide at pH 1 as a result of some broadening from the carboxyl protons. The line width narrows to 0.16 G at pH 0.3 with no change in line position.

$CO_2H$  is more positive than that for  $CO_2^-$ .<sup>12</sup> This difference implies that  $CO_2^-$  has a lesser electron-withdrawing property than  $CO_2H$ . This direction is similarly indicated by the increased coupling constants noted here. The radical from 2,5-furandicarboxylic acid behaves similarly. In the radical from 3,4-furandicarboxylic acid ionization of the carboxyl groups produces a very pronounced increase in the hyperfine constant of the proton in the 2 position and a relatively smaller decrease in that of the proton at the 5 position.

The high value of the coupling constant previously noted<sup>2</sup> for the protons at the 5 position in the radical obtained by H atom addition to furoic acid (31.4 G)<sup>2</sup> is completely corroborated by our observations on this and the other related radicals. An even higher value is observed for the radical produced from furan. The hyperfine constants of this latter radical can be compared with those of

cyclopentenyl radical ( $a_{\alpha}^H = 14.2$  G (2),  $a_{\beta}^{H(1)} = 2.8$  G,  $a_{\beta}^H = 23.0$  G (2),  $g = 2.00265$ ).<sup>13,14</sup> It is seen that the allylic protons in radical I have very similar coupling constants but that the  $CH_2$  protons have considerably larger values. From the McConnell relationship ( $a_{\alpha}^H = 24.7\rho$ ) one can estimate that the spin densities on the terminal allylic positions are 0.57 in cyclopentenyl radical and 0.54 in radical I. From these values one can in turn estimate that the coupling constant of the  $CH_2$  protons in the two radicals should be 20.0 and 19.0 G, respectively (based on a unit spin density value of 35 G for protons in the appropriate configuration as obtained from the spectrum of cy-

(12) C. D. Ritchie and W. F. Sager, *Progr. Phys. Org. Chem.*, 2, 323 (1964).

(13) T. Soylemez and R. H. Schuler, to be submitted for publication.

(14) R. H. Schuler and R. W. Fessenden, "Radiation Research," G. Sili-ni, Ed., North-Holland Publishing Co., Amsterdam, 1967, p 99 ff.

TABLE II: Radicals Produced by Addition of OH to the Furan Ring

Solute	Radical	<i>g</i> factor	Assigned position	Hyperfine constants, G
Furan		2.00277	5	21.12 <sup>a</sup>
			4	13.59 <sup>b</sup>
			3	1.97
			2	14.28
Furfuryl alcohol		2.00268	5	20.63 <sup>c</sup>
			4	13.37
			3	2.01
			CH <sub>2</sub>	8.51 7.60
2-Furoic acid		2.00339	5	19.79 <sup>d</sup>
			4	10.15
			3	2.31
2-Furonitrile		2.00303	5	19.44
			4	10.48
			3	2.37
			N	2.47
3,4-Furandi-carboxylic acid		2.00330	5	20.92
			2	9.25
2,5-Furandi-carboxylic acid		e	4	(10.6) <sup>e</sup>
			3	2.27
2,5-Furandi-carboxylic acid		2.00322	2	26.47 <sup>f</sup>
			3	1.71
			OH	0.53

<sup>a</sup> Shiga and Isomoto (ref 15) report hyperfine constants of 21.0, 14.8, 14.0, and 2.0 G for this radical. <sup>b</sup> The assignment of the 13.59-G constant to the 4 position is indicated by the similar value observed for the adduct to furfuryl alcohol. <sup>c</sup> Shiga and Isomoto (ref 15) report hyperfine constants of 20.5, 12.9, 8.3, 7.5, and 1.9 G for this radical. <sup>d</sup> Shiga and Isomoto (ref 15) report hyperfine constants of 19.1, 10.2, and 2.2 G for this radical. <sup>e</sup> At pH 0.3 two intense, otherwise unassigned, lines are observed 6.45 and 4.18 G below a center corresponding to  $g = 2.00339$ . These lines are reasonably assigned to the OH adduct at the 5 position but because their high-field counterparts are masked by the quartz signal the  $g$  factor and large coupling constant are not directly determinable. <sup>f</sup> Determined at pH 11. At pH 12.6 the 0.53-G OH splitting is lost as the result of base-catalyzed exchange. At pH 1 weak broad lines are observed at the positions corresponding to  $g = 2.00279$  and  $a^H = 25.92$  and 1.91 G.

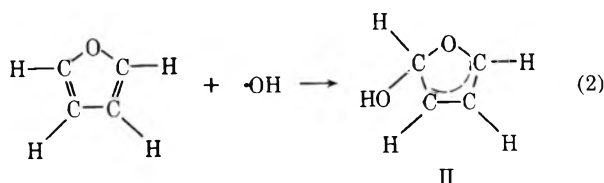
clopenty radical<sup>5</sup>). The observed value for cyclopentenyl radical (23.0 G) agrees reasonably well but the value for radical I is almost a factor of 2 larger. Cook, *et al.*,<sup>2</sup> in their treatment of the radical in-furoic acid have, in fact, discussed the electronic structure of radical I. They estimated from Hückel calculations with configuration interaction that the spin densities on the C<sub>2</sub>, C<sub>3</sub>, and C<sub>4</sub> carbon atoms are, respectively, +0.47, -0.13, and +0.48 with a spin density of 0.06 on the oxygen atom. The calculated near equivalence of the spin densities on the C<sub>2</sub> and C<sub>4</sub> carbon atoms is confirmed by the present observations. For the allylic system of radical I  $\rho Q = a^H(H_2) - a^H(H_3) + a^H(H_4) = 24.6$  G. This numerical value is similar to the value obtained for allyl (24.7)<sup>5</sup> but neglects any loss of spin density to the ring oxygen atom. The comparable value for cyclopentenyl radical is 25.6 G so that it is very evident that one is accounting for almost all of the spin density. From the observed coupling constants, a negative spin density of 0.09 is estimated for the central positions of the allylic system and positive spin densities of 0.54 for the terminal positions, in very reasonable agreement with the theoretical estimates.<sup>2</sup>

The calculations of Cook, *et al.*, indicate that the phase of the contribution from the oxygen 2s orbitals is such that a considerable increase in the wave function at the CH<sub>2</sub> protons of radical I occurs even though there is only a small spin density on the oxygen atom. Taking the coefficients of the contributions as the same, one can crudely estimate the coupling constant of these protons as  $35.0\{\rho(C_4)\}^{1/2} + (0.06)^{1/2}\}^2$  where a spin density on the oxygen atom of 0.06 is taken from the calculations indicated above. We obtain 33.6 G for radical I and 26.0 and 28.0 G for the neutral and anionic radicals produced from furoic acid (where  $\rho(C_4) \approx 0.38$  and 0.42). Quantitative agreement is obtained if one assumes a spin density on the ring oxygen atom of 0.08 in radical I and 0.09 in the radical from furoic acid.

**OH Addition.** In acidic solutions, OH adds to the furan ring system to form a stable hydroxylated radical. Certain of the OH adducts have already been observed by Shiga and Isomoto<sup>15</sup> in studies of the radicals produced by Fen-

(15) T. Shiga and A. Isomoto, *J. Phys. Chem.*, **73**, 1139 (1969).

tion reagents at low pH. In the present radiolysis studies furan at pH 1 shows, in addition to the spectrum of H adduct discussed above, lines which can be attributed to radical II. At this pH the lines of this radical are about twice as intense as those of radical I indicating about equal populations of the two (since radical I has twice as many lines as does II). The hyperfine constants of radical II given in Table II are very similar to those reported by Shiga and Isomoto.<sup>15</sup> We concur in their assignment of the largest coupling constant (21.12 G) to the proton at the 5 position. In this case the protons at the 2 and 4 positions are clearly different (14.28 and 13.59 G). By reference to the value of 13.37 G observed for the proton at the 4 position in the similar radical produced from furfuryl alcohol we assign the 13.59 G constant to the proton at the 4 position. There is no evidence in the esr spectrum of any significant population of radicals produced by OH addition at the 3 position. One experiment was carried out on an N<sub>2</sub>O saturated solution at pH 3.2 specifically to look for this adduct. Under these conditions the spectral contribution from H atoms is eliminated and one sees a very clean and moderately intense (*S/N* ~ 20:1 for the high-field lines) spectrum of radical II. A number of additional lines are present at an *S/N* of ~2:1 but they do not fall into any pattern which can be attributed to the second OH adduct. A similar result was obtained for a solution containing 10<sup>-2</sup> M KH<sub>2</sub>PO<sub>4</sub> at pH 4.7. In both of these latter cases no splitting attributable to the OH proton was observed and it is estimated that this proton must have a coupling constant <0.1 G. This result is unexpected since the analogous proton in hydroxycyclohexadienyl radical has a coupling constant of 0.42 G which is observable in this pH range.<sup>16</sup> It should be mentioned that with furan no ring opening of the type mentioned below occurs at a pH as high as 4.7.



It is noted that the *g* factor of radical II is 0.00037 less than that for radical I. Radicals I and II can, in many ways, be compared with cyclohexadienyl and hydroxycyclohexadienyl radicals. In this latter case the hydroxylated radical has a *g* factor 0.00041 less than that of its hydrogen analog.<sup>7</sup> As in the cyclohexadienyl-hydroxycyclohexadienyl comparison, replacement of one of the CH<sub>2</sub> protons by an OH group has little effect on the coupling constant of the protons in the conjugated system (a small increase is noted in the present case) but reduces that of the remaining CH<sub>2</sub> proton considerably. In the radicals from furan, substitution of OH for H causes the coupling constant of the proton at position 5 to go from 35.6 to 21.2 G whereas in the case of cyclohexadienyl the decrease is from 48.1 to 34.3 G.<sup>7</sup> One other related case exists in the comparison of H<sub>2</sub>C=N· and HC(OH)=N· where *a*<sup>H</sup> is reduced from 87.2 to 54.4 G as a result of the OH substitution.<sup>17</sup> These pronounced changes, which are not accompanied by any large changes in the spin distribution, are at this point not understood. This change seems to be specific to OH substitution since, as noted above in the discussion of the H atom adduct to 2,5-furandicarboxylic acid, replacement of an H atom at the 5 position by a CO<sub>2</sub>H group does not have a similar effect.

The OH adducts to the 5 position of furfuryl alcohol, 2-furoic acid, 2-furonitrile, 3,4-furandicarboxylic acid, and 2,5-furandicarboxylic acid have all been observed and the trends in coupling constants are seen in Table II to be very much parallel to those of the similar H atom adducts. The spectral parameters of the first two of these examples have already been reported by Shiga and Isomoto.<sup>15</sup> In the case of the adduct to furoic acid they, however, assigned the spectrum to the radical resulting from addition at the 4 position on the basis of calculations which indicate that COOH substitution has a pronounced effect on the electron distribution in the allylic system. Comparison of the parameters of this radical with those of the OH adduct to furan shows rather conclusively that the radical must be the analog to radical II with a COOH group at the 2 position. The *g* factor difference (-0.00034) between this radical and the H atom adduct is similar to that for the OH and H adducts of furan. One coupling constant has the small value characteristic of the central proton in an allylic system and the two remaining constants are similar to those of the OH adduct of furan. One must conclude, therefore, that (in spite of the calculations which purport to demonstrate such an effect) in a radical of this type COOH substitution does not have a sufficiently pronounced effect to produce a qualitative change in the distribution of spin density.

It is seen in Table II that the CH<sub>2</sub> protons of the radical produced by OH addition to furfuryl alcohol are distinctly different (7.55 and 8.51 G) as has already been reported by Shiga and Isomoto.<sup>15</sup> This difference arises because the radical framework to which the CH<sub>2</sub>OH group is referenced no longer has a plane of symmetry (as it does in the case of the H adduct). The coupling constants of these protons are somewhat higher than for the H atom adduct but still relatively small so that rotation must be severely restricted. One additional experiment on an N<sub>2</sub>O saturated solution at pH 2.7 showed a moderately intense spectrum of the above-mentioned OH addition product of furfuryl alcohol which was not complicated by lines of the H atom adduct. This spectrum enabled a determination to be made of the largest coupling constant and *g* factor. In addition, groups of lines occurred in the central region of the spectrum and ~12-15 G above the center. Detailed analysis of this additional structure was not possible because the lines were weak and they were masked in part by lines of the other radical but it seems very likely that addition of OH to the 2 position of furfuryl alcohol is responsible for this spectrum. A related experiment was carried out on 2-furonitrile in an attempt to produce a radical hydroxylated at the 2 position (pH 4.7 containing 10<sup>-2</sup> M KH<sub>2</sub>PO<sub>4</sub>, N<sub>2</sub>O saturated). No such product was, in fact, observed but rather there appeared a superposition of spectra of the OH adduct at the 5 position and the radical discussed below which is produced by opening of the furan ring. As indicated above no ring opening occurred in an identical experiment on furan. The simultaneous production of these two radicals would seem to require that OH addition at the 2 position result in spontaneous rupture of the ring even without ionization of the OH group. Presumably such an effect is promoted by the strong electron-withdrawing power of the CN group.

The only example of OH addition at the 3 position was obtained with 2,5-furandicarboxylic acid where the 2 and

(16) R. W. Fessenden, *J. Chem. Phys.*, in press.

(17) D. Behar and R. W. Fessenden, *J. Phys. Chem.*, **76**, 3945 (1972).

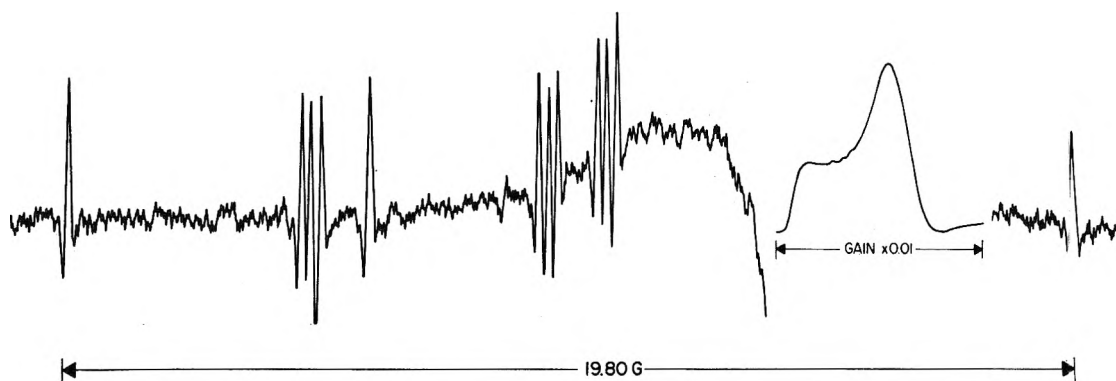
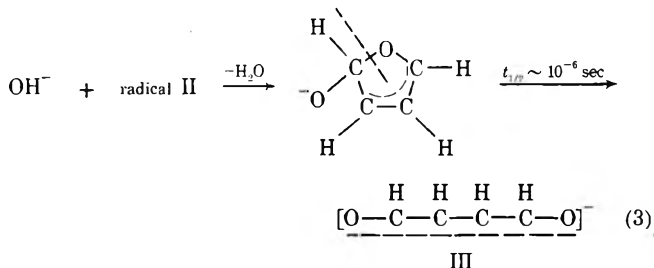


**Figure 2.** ESR spectrum during the irradiation of a nitrous oxide saturated  $10^{-2} M$  solution of furan at pH 10. The pattern of 16 equally intense lines corresponds to a radical with four nonequivalent protons (four lines are masked by the quartz signal but the three outermost of these are observable in the figure superimposed on the quartz line). The low total spread indicates a high degree of conjugation in the radical and is characteristic of spectra obtained in basic solutions of furan derivatives. The spectrum is assigned to an asymmetric form of the radical produced by addition of OH to the 2 position of furan, followed by ionization of the hydroxyl proton and opening of the furan ring (see eq 3).

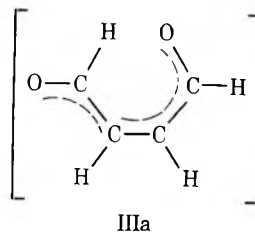
5 positions are partially blocked by the presence of the carboxyl groups. While only weak lines were observable in acidic solution a moderately intense spectrum was present in basic solutions. At pH 11 the spectrum consisted of four pairs of 0.15-G wide lines split by 0.53 G. At pH 12.6 these pairs disappeared and were replaced by single 0.08-G wide lines located at the positions central to the pairs. This spectral change provides an excellent example of the base-catalyzed exchange of OH protons which occurs at pH values above  $\sim 11$ . General aspects of this phenomenon have been treated in detail elsewhere.<sup>18</sup>

**Ring Opening of the OH Adduct in Basic Solution.** The spectrum observed in basic solutions of furan is quite different from that found in acidic solutions and it is obvious that ring opening follows OH addition and results in the formation of the radical anion of butenedial (III). Lillie<sup>6</sup> has observed this ring opening in pulse radiolysis experiments and reports a rate constant of  $1.4 \times 10^6 \text{ sec}^{-1}$  for the scission. Since the present steady-state experiments focus attention on radicals which have mean lifetimes of the order of milliseconds or longer the ESR spectrum observed in basic solution is expected to be that of radical III. The spectrum obtained with a nitrous oxide saturated solution of furan at pH 10.4 is displayed in Figure 2. This spectrum consists of 16 equally intense lines with a total spread of only 19.8 G and a center which corresponds to the  $g$  factor of 2.00416. The low total spread and a  $g$  factor in this region are characteristic of the other radicals produced by reactions of OH with furan derivatives in basic solutions. The small hyperfine constants show that the radicals are highly conjugated.



The ESR pattern from furan shows the radical to have four nonequivalent H atoms. Because of the conjugation two possible configurations can exist about each of the three partial double bonds. This leads to a total of eight

possible configurations for the radical. Of these six are unique, four which are symmetrical and two (each representing two configurations) which are nonsymmetrical. We suggest that the general configuration of the parent molecule is retained in the radical and that the anion responsible for the spectrum in Figure 2 has the structure shown in IIIa. The dominance of the spectrum of a single asymmetric radical in Figure 2 shows that ready interconversion of the various configurations does not occur within the millisecond lifetime of the radicals. Retention of configuration of the parent molecule has been observed for hydrogen abstraction from *cis*- and *trans*- $\mathcal{E}$ -butene which results in the selective production of the distinctly different *cis* and *trans* form of the 1-methyl allyl radical.<sup>19</sup>



One experiment was carried out on furan in 1 M KOH in an attempt to produce isomers of radical III other than IIIa. In this experiment a fairly intense spectrum of a radical with three nonequivalent protons ( $a^{\text{H}} = 10.7, 8.6, \text{ and } 0.4 \text{ G}$ ;  $g = 2.00367$ ) was superimposed on the spectrum of Figure 2. This radical is clearly of a different type than those produced by ring opening but the assignment is not immediately obvious. One suggestion is that  $\text{O}^-$  abstracts a hydrogen atom from furan but we would expect any vinylic radical produced from such a reaction to have considerably larger hyperfine constants. Neta<sup>20</sup> has recently observed the spectrum of the 2-carboxylic acid derivative of IV with parameters of  $a^{\text{H}} = 9.68 \text{ and } 1.15 \text{ G}$  and  $g = 2.00360$ . The similarity between the present parameters and these latter values suggests that radical IV is produced from furan at very high pH but the reaction path

- (18) G. P. Laroff, Ph.D. dissertation, Carnegie-Mellon University, 1972; G. P. Laroff and R. W. Fessenden, *J. Phys. Chem.*, submitted for publication.  
 (19) J. K. Kochi and P. J. Krusic, *J. Amer. Chem. Soc.*, **90**, 7157 (1968).  
 (20) P. Neta, to be submitted for publication.



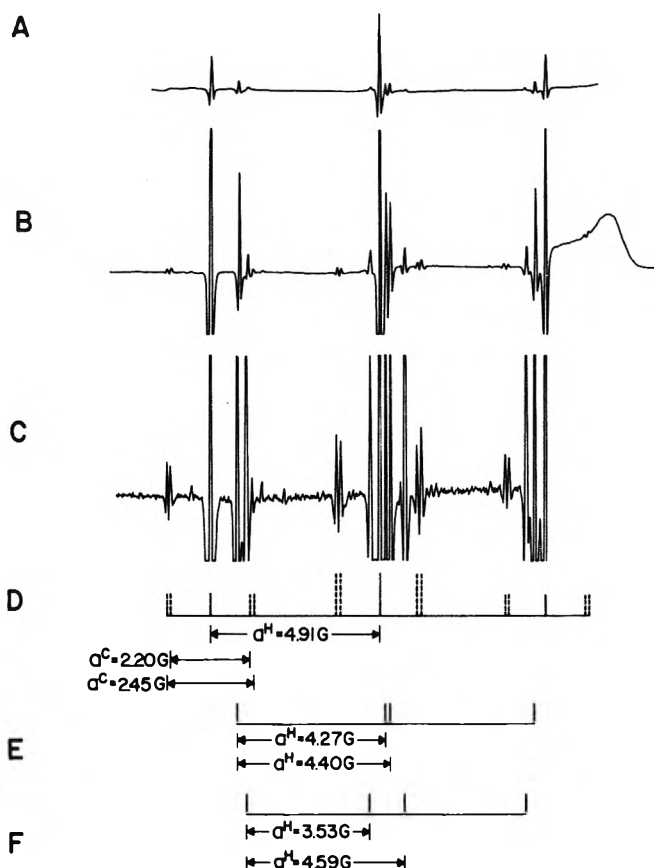
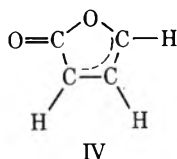


**Figure 3.** ESR spectra obtained during the irradiation of nitrous oxide saturated  $10^{-2}$  M solutions of 3,4-furandicarboxylic acid at pH 10. A, B, and C reproduce spectra obtained respectively at relative gains of 1, 10, and 100. Three radicals corresponding to the patterns D, E, and F are readily discernible. In addition the lines of the most intense spectrum have two sets of satellites of 1% intensity (as indicated in D) which corresponds to the radicals containing  $^{13}\text{C}$  at the natural abundance level. A number of other unassigned lines are also observable.

by which it is formed is not obvious. At least two additional radicals with spectra that have total spreads of  $\sim 19$  G or less are also present at pH 14. However most of their ESR lines are masked by more intense spectra so that their patterns cannot be established.



A second very important example of the radicals produced by opening of the furan ring is seen in the spectrum observed from basic solutions of 3,4-furandicarboxylic acid. In this case the analog of radical III is a trianion which recombines very slowly and as a result can be produced in very high concentrations. Stop-flow experiments show, for example, that at the concentration levels usually attained in these experiments the median radical lifetime is many minutes. Spectra recorded under normal spectrometer conditions, and at gains 10 and 100 times lower, are illustrated in Figures 3c, 3b, and 3a, respectively. The spectra of three different isomers of this dicarboxylate radical trianion are readily apparent in Figures 3a and 3b.

The most intense spectrum is one which exhibits two equivalent protons and is attributed to a symmetrical form of the radical. An experiment specifically designed to produce the electron adduct which would have a similar spectrum (pH 11,  $\text{N}_2$  saturated, 0.1 M isopropyl alcohol) gave no lines in the central region of the spectrum. It seems likely that if electron addition occurs the resultant anion radical rapidly protonates. The second and third contributing spectra, which have relative intensities of 0.2 and 0.05 at pH 11, exhibit nonequivalent protons and must be attributed to the two asymmetrical forms of the radical. At pH 14 the relative abundances increase to 0.5 and 0.2 but the intensities within the individual patterns remain the same so that the analysis of the spectrum is not open to question. From its higher relative intensity we tentatively suggest that the radical having proton coupling constants of 4.39 and 4.27 G be assigned to the carboxylated derivative of IIIa and that having constants of 4.59 and 3.53 G to the isomer rotated by  $180^\circ$  about the central C-C bond.

The radical with two equivalent 4.91-G protons is suggested to be one of the two symmetrical radicals with a cis configuration at the central bond. The spectrum of this latter radical is sufficiently intense that the  $^{13}\text{C}$  species are readily apparent at the natural abundance level. Since symmetry requires that the carbon atoms be equivalent in pairs, the spectra of the  $^{13}\text{C}$ -containing radicals should be 0.011 times as intense as that of the main radical. As is seen in Figure 3c the spectra of two of the three types of this radical containing  $^{13}\text{C}$  are observable. These radicals have  $^{13}\text{C}$  hyperfine constants of 2.20 and 2.45 G (the third type apparently has an unresolvably small splitting, *i.e.*,  $< 0.8$  G). The small, nearly equal values of these hyperfine constants show that the unpaired electron is spread over a highly conjugated system. The low total (9.30 G) shows that considerable spin density must be lost to the oxygen atoms. A fair number of other lines with relative intensities of the magnitude of 0.001–0.01 times that of principal radical are present in the spectrum but the patterns are sufficiently complex that they are not readily analyzable. Some of the lines are too intense to be attributable to  $^{13}\text{C}$ -containing species and it is clear that at least several other radicals with relative abundances  $\sim 0.01$  are present. The lines of these radicals mask the less intense spectra of the isomeric  $^{13}\text{C}$  radicals.

The other dicarboxylate studied (2,5-furandicarboxylic acid) gave an equally intense but even more complex spectrum in basic solution. The most prominent pattern was a triplet having the relatively small hyperfine constant of 3.17 G. Two other isomers of the radical produced by ring opening of the OH adduct were also discernible and their parameters are given in Table III. It is seen that the  $g$  factor and to some extent the hyperfine constants of the radicals resemble those from furoic acid. Considerable additional structure is also apparent in the spectrum. In this case we were able to produce the electron adduct by irradiation of a nitrogen-saturated solution containing 0.1 M isopropyl alcohol to remove the OH radicals. Apparently it does not protonate readily. Its spectrum consists of a 1.53-G triplet centered at  $g = 2.00394$  and is eliminated by saturating the solution with  $\text{N}_2\text{O}$ . This electron adduct is not manifest in the experiments designed to examine the products of OH addition. Individual lines of  $^{13}\text{C}$ -containing radicals are also present in the spectrum but the patterns are, to a large extent, masked by lines from other species.

TABLE III: Radicals Produced by OH Reaction in Basic Solutions of Furan Derivatives<sup>a</sup>

Solute	Radical <sup>b</sup>	Relative intensity <sup>c</sup>	<i>g</i> factor	Proton coupling constants, G
Furan	$\begin{array}{cccc} \text{O} & \text{H} & \text{H} & \text{O} \\    &   &   &    \\ \text{[H-C-C-C-C-H]}^- & & & \end{array}$	12	2.00416	5.79
				4.86
				4.66
				4.49
3,4-Furandi-carboxylic acid	$\begin{array}{cccc} \text{O} & \text{CO}_2 & \text{CO}_2 & \text{O} \\    &   &   &    \\ \text{[H-C-C-C-C-H]}^- & & & \end{array}$	1500 <sup>e</sup> 500 <sup>e</sup>	2.00449 2.00438	4.92(2) <sup>f</sup>
				4.39
				4.27
				4.59
2,5-Furandi-carboxylic acid	$\begin{array}{cccc} \text{O} & \text{H} & \text{H} & \text{O} \\    &   &   &    \\ \text{[O}_2\text{C-C-C-C-CO}_2^-]^- & & & \end{array}$	1000 200 75	2.00407 2.00411 2.00423	3.17(2)
				4.23(2)
				5.18
				3.07
Furoic acid	$\begin{array}{cccc} \text{O} & \text{H} & \text{H} & \text{O} \\    &   &   &    \\ \text{[H-C-C-C-C-CO}_2^-]^- & & & \end{array}$	140  30  6	2.00411  2.00412  2.00416	4.92
				3.80
				3.63
				4.90
Furfuryl alcohol	$\begin{array}{cccc} \text{O} & \text{H} & \text{H} & \text{O} \\    &   &   &    \\ \text{[H-C-C-C-C-CH}_2\text{OH]}^- & & & \end{array}$	15	2.00406	5.27(2)
				5.51
				4.96
				4.16
2-Furylacetonitrile	$\begin{array}{cccc} \text{O} & \text{H} & \text{H} & \text{O} \\    &   &   &    \\ \text{[H-C-C-C-C-CH}_2\text{CN]}^- & & & \end{array}$	3	2.00412	5.18(2) <sup>g</sup>
				4.91
				4.70
				4.50
2-Furylacrylic acid	$\begin{array}{ccccccc} \text{O} & \text{H} & \text{H} & \text{O} & \text{H} & \text{H} & \\    &   &   &    &   &   & \\ \text{[HC-C-C-C-C-C-CO}_2^-]^- & & & & & & \end{array}$	15	2.00397	5.43
				4.43
				2.55
				2.01
2-Furonitrile	$\begin{array}{cccc} \text{O} & \text{H} & \text{H} & \text{O} \\    &   &   &    \\ \text{[H-C-C-C-C-CN]}^- & & & \end{array}$	10	2.00423	7.20
				2.18
				0.69
				( <i>N</i> = 1.18)
Furfural	$\begin{array}{cccc} \text{O} & \text{H} & \text{H} & \text{O} & \text{O} \\    &   &   &    &    \\ \text{[H-C-C-C-C-C-H]}^- & & & & \end{array}$	10  5 <sup>h</sup>	2.00477  2.00478	6.20
				3.14
				1.27
				0.46
2-Acetylfuran	$\begin{array}{cccc} \text{O} & \text{H} & \text{H} & \text{O} & \text{O} & \text{H} \\    &   &   &    &    &   \\ \text{[H-C-C-C-C-C-C-H]}^- & & & & & \end{array}$	8	2.00457	5.84
				1.83
				1.19
				0.34

<sup>a</sup> At pH 10–11. <sup>b</sup> Radical may exist in several geometric forms. <sup>c</sup> Approximate intensities relative to a noise level of 1. <sup>d</sup> At pH 14 where the predominant reactant is O<sup>-</sup> a radical was observed which is identical with that at pH 10. In addition a radical with *g* = 2.00367 and three protons with hyperfine constants of 10.7, 8.6, and 0.40 G was observed at a *S/N* of 6. Partial spectra of at least two other radicals are also observed at signal intensities of 1–2. Insufficient detail is, however, available for analysis as a result of masking by the other spectra. <sup>e</sup> At pH 14 the same radicals are observed but with increased relative intensities of the second and third species. A number of other radicals are also present. <sup>f</sup> Carbon-13 hyperfine constants of 2.45 and 2.20 G are observable (see Figure 3c). Each represents one pair of magnetically equivalent carbon atoms. The third pair do not have a sufficiently large hyperfine constant to be observable at the natural abundance level (<0.8 G). <sup>g</sup> No nitrogen splitting was directly observed. The lines of this spectrum, however, have a width of ~0.15 G. Presumably this width is due to an unresolved nitrogen splitting which would be of the magnitude of ~0.05 G. <sup>h</sup> This second radical is observed only at low flow rates. <sup>i</sup> The spectrum clearly shows coupling to four nonequivalent protons with no evidence for involvement of a CH<sub>3</sub> group. This structure must be regarded as tentative.

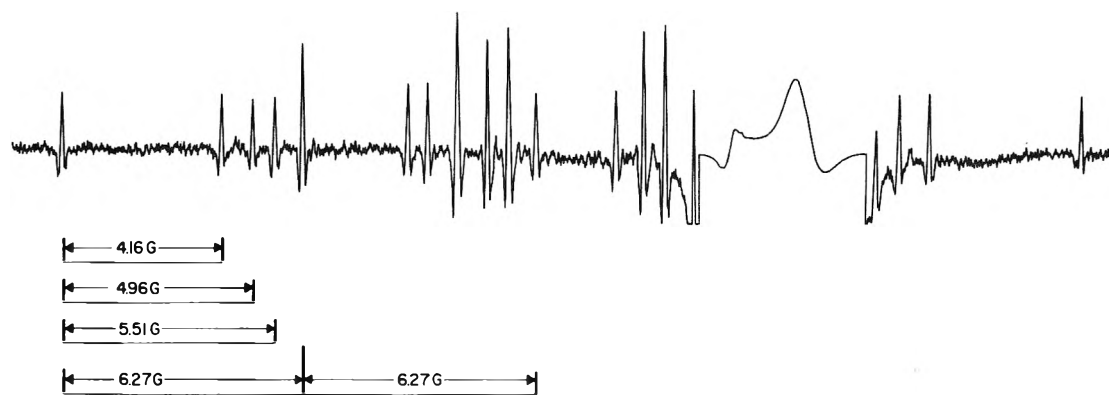
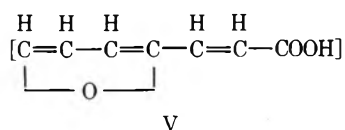
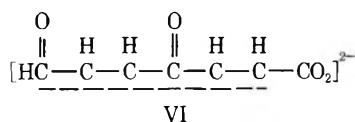


Figure 4. ESR spectrum observed during the irradiation of a nitrous oxide saturated  $10^{-2}$  M solution of furfuryl alcohol at pH 11. The pattern corresponds to the three doublets and a triplet indicated by the stick spectrum. The eighth line from the left (and right) is a compound line caused by the fact that the sum of the largest and smallest coupling constants (10.43 G) is almost identical with the sum of the two intermediate ones (10.47 G). All other features are resolved so that the pattern appears to consist of 22 lines.

Other examples of radicals with similar parameters were apparent in the spectra from basic solutions (pH 10–11) of 2-furoic acid, 2-furylacrylic acid, furfuryl alcohol, and 2-furylacetonitrile. Three different isomeric radicals are easily discernible in the furoic acid system. The spectrum obtained with furfuryl alcohol at pH 11 is illustrated in Figure 4. This spectrum very clearly shows two equivalent protons and three additional protons which are not equivalent but which differ only slightly. A summary of the ESR parameters of these various radicals, along with the approximate relative intensities under constant production and spectrometer conditions, is given in Table III. All of these radicals exhibit small coupling constants and have  $g$  factors in the range 2.0039–2.0041. Of these perhaps the most interesting is the radical obtained from 2-furylacrylic acid (V).



The spectrum consists of 32 lines of equal intensity, as expected for a radical with hyperfine couplings to five nonequivalent protons. The unpaired electron is effectively distributed over the entire radical, *i.e.*



In this case the protons provide probes of the spin density on five of the six conjugated positions. Comparison of the sum of the observed hyperfine constants (15.78 G) with the total of 19.80 G observed for radical III indicates that these five carbon atoms account for  $\sim 80\%$  of the spin density, *i.e.*, that only a few per cent is lost to the  $\text{CO}_2^-$  group.

Analyzable spectra were obtained in three additional cases: 2-furonitrile, furfural, and 2-acetylfuran. As is seen in Table III all three radicals have somewhat higher  $g$  factors than those of the radicals produced from the other monosubstituted furans. The hyperfine constants also show a considerably greater spread in values. The spectra obtained from furfural and furonitrile are reasonably attributed to the CHO and CN derivatives of radical III

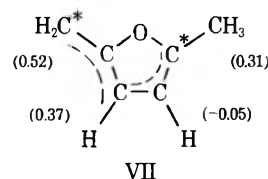
with a considerable change in spin distribution resulting from the highly polar nature of the substituent. With furfural Shiga and Isomoto<sup>15</sup> appear to have observed an identical radical in their Fenton reagent studies at pH 7 but have assigned it as a positive ion. The spectrum from 2-acetylfuran shows, unexpectedly, hyperfine interaction with only four protons and no manifestation of a  $\text{CH}_3$  group. A possible structure is suggested in Table III. This structure would result from the enolization of the radical initially produced and requires, if it is appropriate, that one of the  $\text{CH}_2$  protons exhibit an unresolvably small hyperfine constant. This structure must be regarded only as tentative and as a result, some doubt must be cast on the structural assignment of the radicals from the furonitrile and furfural because of the similarity of their parameters.

We have examined several other systems at pH 11 but have not, as yet, been able to interpret the spectra obtained. These systems include 2,5-dimethylfuran, furylacrylonitrile, and  $\beta$ -(2-furylacrolein). In the case of the dimethylfuran a moderately intense but very complex spectrum was obtained. At least two radicals are present with interlaced patterns. Most of the more intense lines lie within  $\pm 10$  G of the spectral center so that 1,4-dimethyl derivatives of radical III seem to be unquestionably present. At pH values below 12 abstraction from the methyl groups (see below) was shown to be unimportant. The other two solutes show only weak lines.

*H Abstraction from 2,5-Dimethylfuran.* In the case of 2,5-dimethylfuran it seemed possible that abstraction of an H atom from a methyl group might be an important process and as a result contribute to the complications in interpreting the spectrum. The radical resulting from such an abstraction is, in fact, observable in the radiolysis of strongly basic solutions (pH  $> 13$ ,  $\text{N}_2\text{O}$  saturated) where  $\text{O}^-$  is the reactant. Even here the central region of the spectrum is cluttered by the presence of several radicals. The lines of a radical containing three equivalent and four nonequivalent protons were apparent in the region above the quartz signal which is relatively free of interference. The total available intensity for such a radical is distributed over a pattern of 64 lines so that the individual lines are still relatively weak (signal/noise of the high-field lines is  $\sim 3$ –9) but nevertheless observable. Because of chemically induced spin polarization, the low-field lines are so weak as not to be observable. The hyperfine constants determined were 8.34 (3), 12.84, 13.19, 9.44, and

1.03 G. The  $g$  factor is 2.00261 and is typical of aliphatic radicals. At pH values below  $\sim 12$  lines of this radical are not present.

The above spectrum is clearly assignable to radical VII. This radical is extremely interesting in that it possesses conjugation of an allylic type which extends over the entire ring. Because of the conjugation the two protons of the  $\text{CH}_2$  group are not equivalent. They are, however, not expected to have very different hyperfine constants and accordingly the constants of 12.8 and 13.2 G assigned to this position. The 8.3 G of the quartet pattern is directly assignable to the methyl group and, by analogy with allyl, the 9.4- and 1.0-G hyperfine constants are assigned to the protons at the starred and unstarred positions of the ring. The 8.3-G splitting of the methyl protons indicates a spin density of 0.31 on the adjacent carbon. The other hyperfine constants indicate spin densities of 0.52 at the  $\text{CH}_2$  carbon atom, and 0.37 at the starred and  $-0.05$  at the unstarred positions of the ring to which protons are attached. The total of the above is 1.15 so that appreciable negative spin density must exist at the unprobed carbon position and on the oxygen atom. Since methyl groups are known to have little effect on spin distribution it must be concluded that it is the oxygen linkage that induces considerable asymmetry into the distribution in this particular radical.



### Summary

Furan and its derivatives provide a source of a large variety of interesting radicals, most of which exhibit a high degree of conjugation and thus are of interest in both experimental and theoretical determinations of spin distribution. It is clear that the H and OH reactions exemplified here are general and that with appropriate effort it should be possible to obtain similar information on other derivatives of furan. The esr approach can be put to extremely good use here since a large number of different radicals are producible from each single solute. It is noted, for example, that the esr parameters of nine distinguishable radicals from 2,5-furandicarboxylic are reported in this paper.

*Acknowledgment.* The authors wish to thank Dr. P. Neta for many valuable discussions and suggestions during the course of this work.

## Infrared Spectra and Geometries of Matrix Isolated Yttrium Tri- and Difluorides

R. D. Wesley and C. W. DeKock\*

Department of Chemistry, Oregon State University, Corvallis, Oregon 97331 (Received April 5, 1972)

The infrared spectra of  $\text{YF}_3$  and  $\text{YF}_2$  isolated in argon and nitrogen matrices have been measured in the region  $40\text{--}800\text{ cm}^{-1}$ . The fundamental frequency assignments in argon assuming  $C_{3v}$  symmetry for  $\text{YF}_3$  are  $\nu_3(\text{E})$   $663\text{ cm}^{-1}$ ,  $\nu_2(\text{A}_1)$   $119\text{ cm}^{-1}$ ,  $\nu_4(\text{E})$   $140\text{ cm}^{-1}$ , with  $\nu_1$  unobserved. The frequency assignments for  $\text{YF}_2$  in nitrogen assuming  $C_{2v}$  symmetry are  $\nu_3(\text{B}_1)$   $538\text{ cm}^{-1}$ ,  $\nu_1(\text{A}_1)$   $545\text{ cm}^{-1}$ , and  $\nu_2(\text{A}_1)$   $134\text{ cm}^{-1}$ . The results show that  $\text{YF}_3$  is easily reduced to  $\text{YF}_2$  in a tantalum Knudsen cell.

### Introduction

As part of a continuing study of the infrared spectra of the rare-earth halides<sup>1</sup> and dihalides<sup>2</sup> we have measured the infrared spectra of matrix isolated  $\text{YF}_3$  and  $\text{YF}_2$ . These results are of particular interest since they show that  $\text{YF}_3(\text{g})$  is easily reduced to  $\text{YF}_2(\text{g})$  at high temperatures.

$\text{YF}_3$  has recently been studied by Margrave, *et al.*,<sup>3</sup> but their reported spectrum of  $\text{YF}_3$  we attribute to  $\text{YF}_2$ . Recent work on  $\text{YF}_3$  includes mass spectrometric results showing it to be monomeric in the gas phase<sup>4</sup> and more significantly very recent molecular beam electric deflec-

tion studies<sup>5</sup> showing that  $\text{YF}_3$  has a dipole moment and therefore is presumably a pyramidal molecule. (However, in the later study the  $\text{YF}_3$  was vaporized from a tantalum Knudsen cell which as seen from the present study would give primarily  $\text{YF}_2$  *vide infra*.)

- (1) R. D. Wesley and C. W. DeKock, *J. Chem. Phys.*, **55**, 3866 (1971).
- (2) C. W. DeKock, R. D. Wesley, and D. D. Radtke, *High Temp. Sci.*, **4**, 41 (1972).
- (3) R. H. Hauge, J. W. Hastie, and J. L. Margrave, *J. Less Common Metals*, **23**, 359 (1971).
- (4) K. F. Zmbov and J. L. Margrave, *Advan. Chem. Ser.*, **No. 72**, 267 (1968).
- (5) E. W. Kaiser, W. E. Falconer, and W. Klemperer, *J. Chem. Phys.*, **56**, 5392 (1972).

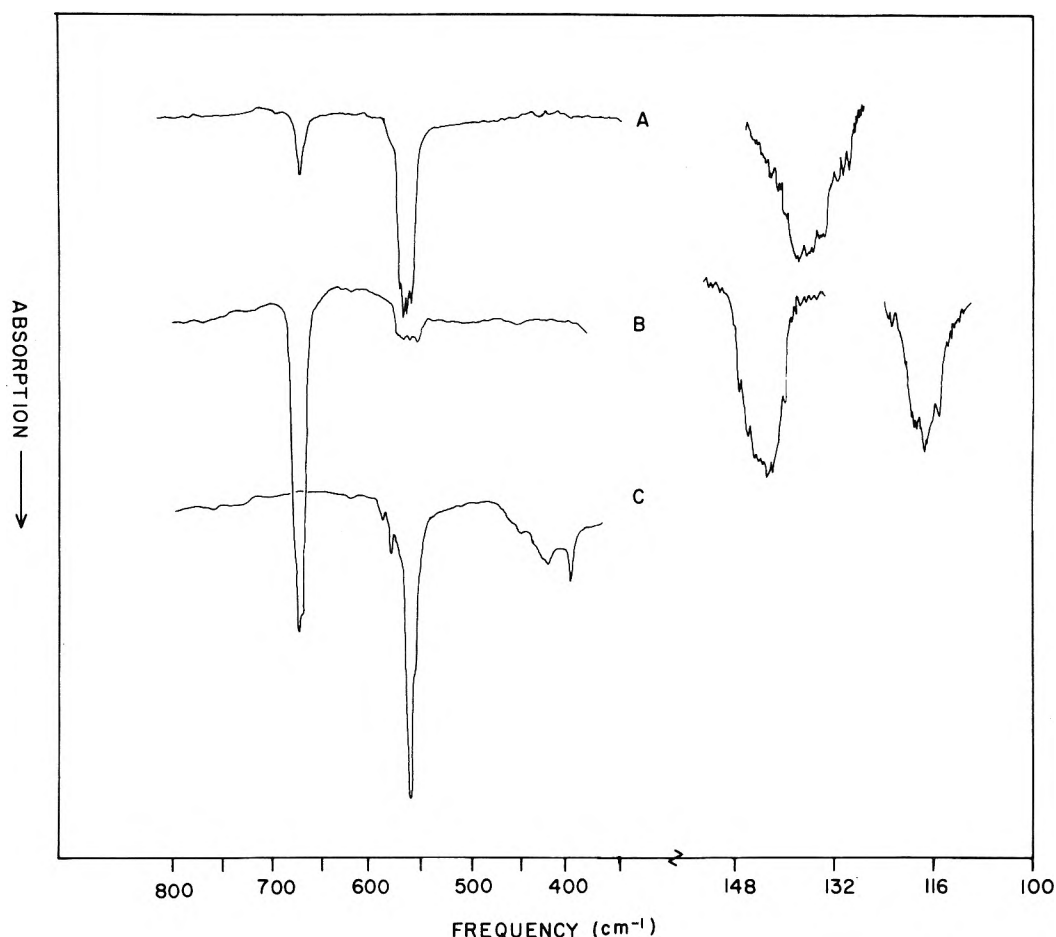


Figure 1. (A) Spectrum of YF<sub>3</sub>(s) evaporated from a tantalum Knudsen cell. (B) Spectrum of YF<sub>3</sub>(s) evaporated from a graphite Knudsen cell. (C) Spectrum of a mixture of Y metal and BaF<sub>2</sub> evaporated from a tantalum Knudsen cell. Note: the bending modes shown are for a deposit approximately five times more intense than for the stretching modes.

### Experimental Section

The techniques and apparatus used in this study are similar to those described elsewhere.<sup>1</sup> The infrared spectrum was recorded in the region 40–800 cm<sup>-1</sup> using a Beckman IR-11 spectrophotometer. YF<sub>3</sub>(s) was purchased commercially and was stated to be of 99.9% purity or greater. It was used without further purification. Both tantalum and graphite Knudsen cells were used for the YF<sub>3</sub> and YF<sub>2</sub> runs. The graphite Knudsen cells were out-gassed at 1800° for at least 8 hr under high vacuum prior to use.

### Results and Discussion

The spectrum of YF<sub>3</sub> in an argon matrix is shown in Figure 1 and recorded in Table I. Spectrum A resulted from heating YF<sub>3</sub> in a tantalum Knudsen cell (four runs); B shows the spectrum obtained with a graphite Knudsen cell (four runs). It is apparent from the alternation of intensities of the 663- and 550-cm<sup>-1</sup> absorptions between A and B that at least two different chemical species are involved. The results suggest that the 663-cm<sup>-1</sup> absorption belongs to YF<sub>3</sub>(g) while the 550-cm<sup>-1</sup> absorption may be assigned to YF<sub>2</sub>(g). This is supported by the number of low-frequency modes observed for each system. Recalling that four infrared active frequencies are expected for a pyramidal XY<sub>3</sub> molecule, two stretches and two low-frequency bends while three infrared active frequencies, two

stretches and one low-frequency bend, are expected for a bent symmetrical XY<sub>2</sub> molecule requires that two low-frequency bends be observed for YF<sub>3</sub> and only one for YF<sub>2</sub>. This is observed. Heavy deposits of YF<sub>3</sub> evaporated from a tantalum cell (YF<sub>2</sub>(g)) show only an absorption at 134 cm<sup>-1</sup> (Figure 1A) while heavy deposits of YF<sub>3</sub> from a

TABLE I: Fundamental Frequencies and Assignments for YF<sub>3</sub> and YF<sub>2</sub> (cm<sup>-1</sup>)

Molecule	Matrix		Assignment	Preparation
	Argon	Nitrogen		
YF <sub>3</sub>	663 vs	660 vs	$\nu_3$	
	140		$\nu_2$	
	119		$\nu_4$	
YF <sub>2</sub>		532 wk		Y + BaF <sub>2</sub>
	538 m	535 wk		
	546 m	538 s		
	552 s	545 m		
	558 s	555 w		
YF <sub>2</sub>		579 wk		YF <sub>3</sub> + Ta cell
		588 wk		
	134		$\nu_2$	
	546 s			
	552 m			
	554 m			
	558 m			

TABLE II: Force Constants for YF<sub>3</sub> and YF<sub>2</sub><sup>a</sup>

YF <sub>3</sub>		YF <sub>2</sub>		
K <sub>r</sub>	K, δ/l <sup>2</sup>	K <sub>r</sub>	K <sub>rr</sub>	K, δ/l <sup>2</sup>
3.76	0.048	2.70	0.05	0.088

<sup>a</sup> Units are 10<sup>5</sup> dyn/cm.

graphite cell (YF<sub>3</sub>(g)) show two low-frequency modes at 119 and 140 cm<sup>-1</sup> (Figure 1B).

To further verify this analysis two other types of experiments were performed. First, BaF<sub>2</sub> was mixed with yttrium metal and heated at 1370° in a tantalum Knudsen cell (Figure 1C); no 663-cm<sup>-1</sup> absorption was observed (only peaks in the 550-cm<sup>-1</sup> region). The weak peaks at 395 and 419 cm<sup>-1</sup> are due to BaF<sub>2</sub>,<sup>6</sup> while the two peaks at 579 and 588 cm<sup>-1</sup> may be due to other matrix sites. Second, an experiment was performed in which YF<sub>3</sub> was heated with yttrium metal in a graphite Knudsen cell (four runs); these spectra again showed no evidence of the 663-cm<sup>-1</sup> absorption (only strong transitions at 552 and 558 cm<sup>-1</sup>). The 579- and 588-cm<sup>-1</sup> absorptions were absent for these runs.

The above interpretation agrees with our previous experience for reduction of EuF<sub>3</sub>, SmF<sub>3</sub>, and YbF<sub>3</sub> by tantalum;<sup>2</sup> however, the reduction of YF<sub>3</sub> by tantalum implies an unexpected stability for yttrium in a reduced state.

It may appear that the present work is in direct conflict with the electric deflection work discussed earlier<sup>5</sup> and mass spectrometric studies of Margrave, *et al.*,<sup>7</sup> on the vapor pressure of YF<sub>3</sub>(s), both of whom interpreted their results in terms of only YF<sub>3</sub>(g) effusing from a tantalum Knudsen cell. It is very important to note, however, from Figure 1A that some YF<sub>3</sub> did effuse from the tantalum Knudsen cell. In fact, in one run from a tantalum cell the ratio of YF<sub>3</sub> to YF<sub>2</sub> is reversed from that shown in Figure 1A with considerably more YF<sub>3</sub>(g) present than YF<sub>2</sub>(g). It is also important to note that the vapor pressure and electric deflection work were carried out at temperatures from 100 to 200° lower than the present experiments which is expected to result in less reduction of YF<sub>3</sub>. The present work is in direct conflict with the mass spectrometric results of Zmbov and Margrave<sup>8</sup> on the stabilities of the mono- and difluorides of yttrium. They interpreted their experiments with yttrium metal and CaF<sub>2</sub>(s) as showing

equilibria among all the gaseous yttrium fluorides YF, YF<sub>2</sub>, and YF<sub>3</sub> together with CaF and Ca. The present results strongly indicate that no YF<sub>3</sub>(g) is present above a mixture of yttrium metal and BaF<sub>2</sub>(s). It is noteworthy that no YF<sub>3</sub><sup>+</sup> was observed in their study, but rather inferred from the ionization efficiency curve of YF<sub>2</sub><sup>+</sup>

The assignment of the YF<sub>3</sub> frequencies is as follows: ν<sub>3</sub>(E) 663 cm<sup>-1</sup>, ν<sub>2</sub>(A<sub>1</sub>) 119 cm<sup>-1</sup>, ν<sub>4</sub>(E) 140 cm<sup>-1</sup>, with ν<sub>1</sub>(A<sub>1</sub>) unobserved. The assignment of the bending modes follows our reassignment for those of the lighter rare-earth fluorides.<sup>9</sup>

The assignment of the transitions for YF<sub>2</sub> presents some peculiar difficulties since an alternation of intensities occurs for the 546- and 558-cm<sup>-1</sup> transitions in the argon matrix depending upon the method of preparation. The higher temperature methods, either Y + YF<sub>3</sub> or Y + BaF<sub>2</sub>, favor the 558-cm<sup>-1</sup> site (Figure 1C) while reduction by the tantalum cell favors the 546-cm<sup>-1</sup> (Figure 1A) transition. This same behavior has been observed for superheated BaCl<sub>2</sub> in argon matrices with the higher frequency site favored by the superheated molecule.<sup>10</sup> In nitrogen matrices only one set of transitions is observed for all methods of preparation and therefore our assignments of ν<sub>3</sub> and ν<sub>1</sub> is for the nitrogen matrix only: ν<sub>3</sub>(B<sub>1</sub>) 538 cm<sup>-1</sup>, ν<sub>1</sub>(A<sub>1</sub>) 545 cm<sup>-1</sup>, and ν<sub>2</sub>(A<sub>1</sub>) 134 cm<sup>-1</sup> (argon matrix). The ν<sub>1</sub> assignment is tentative because, as discussed earlier, additional transitions are present which cannot be assigned other than to matrix effects.

Calculated force constants, using a valence force field calculation, are shown in Table II. A 140° angle was chosen for the F-Y-F angle of YF<sub>2</sub> while a 115° angle was chosen for the F-Y-F angle of YF<sub>3</sub>. The additional electron in YF<sub>2</sub> compared to SrF<sub>2</sub> is reflected in the significantly larger force constant for YF<sub>2</sub> (2.7C) compared to SrF<sub>2</sub> (1.97).

*Acknowledgment.* We wish to thank the United States Atomic Energy Commission for support of this research.

- (6) V. Calder, D. E. Mann, K. S. Seshadri, M. Alavena, and David White, *J. Chem. Phys.*, **51**, 2093 (1969).
- (7) R. A. Kent, K. F. Zmbov, A. S. Kana'an, G. Besenbruch, J. D. McDonald, and J. L. Margrave, *J. Inorg. Nucl. Chem.*, **28**, 1419 (1966).
- (8) K. F. Zmbov and J. L. Margrave, *J. Chem. Phys.*, **47**, 3122 (1967).
- (9) M. Lesiecki, J. W. Nibler, and C. W. DeKock, *J. Chem. Phys.*, **57**, 1352 (1972).
- (10) J. W. Hastie, R. H. Hauge, and J. L. Margrave, *High Temp. Sci.*, **3**, 56 (1971).

## Vibrational Spectra and Rotational Isomerism of 1,2-Propanedithiol

S. K. Nandy, D. K. Mukherjee, S. B. Roy, and G. S. Kastha\*

Optics Department, Indian Association for the Cultivation of Science, Calcutta-32, India (Received June 20, 1972)

The Raman and infrared spectra of 1,2-propanedithiol in the liquid state and the Raman spectrum in the solid state at 93°K have been investigated and probable assignments of the observed vibrational frequencies have been made. The results indicate that the molecules exist as a mixture of three rotamers, one trans and two gauche, of which the trans form is more stable in the liquid state and is the only form in the solid state. The spectra further indicate that the fraction of the higher energy gauche form is very small and the energy difference between the trans and the more abundant gauche isomer is about 450 ± 100 cal/mol.

### Introduction

Reports on the rotational isomerism and analysis of the vibrational spectra of the molecules of 1-propanethiol,<sup>1</sup> 2-methyl-1-propanethiol,<sup>2</sup> 2-butanethiol,<sup>3</sup> and 1,2-ethanedithiol<sup>4</sup> have appeared in the literature. No such report in the case of 1,2-propanedithiol has been made so far. However, the rotational isomerism and vibrational assignments of the closely related molecule of 1,2-dichloropropane<sup>5</sup> have only recently been reported. The present work reports the results of investigations on the Raman and infrared spectra of the molecule of 1,2-propanedithiol in the liquid state and the Raman spectrum in the solid state at 93°K. Probable assignments of the observed vibrational frequencies of the molecule together with a discussion are presented in the following paragraphs.

### Experimental Section

Pure 1,2-propanedithiol procured from Schuchardt (Germany) was distilled under reduced pressure before use in the investigations. The Raman spectra of the compound in the liquid and solid state at 93°K and the polarization character of the Raman bands in the liquid state were obtained with a Fuess glass spectrograph, and the infrared spectra of a thin film of the liquid was recorded with a Perkin-Elmer Model 21 infrared spectrophotometer with rock salt optics. Temperature dependence of the intensities of the Raman lines in the liquid state was studied with a recording grating spectrometer as described earlier.<sup>6</sup>

### Results

The Raman shifts and the wave numbers of the infrared absorption bands with approximate intensities are given in Table I. The polarization character of Raman bands is also indicated in the same table.

### Discussion

*Existence of Rotational Isomerism.* The molecule of 1,2-propanedithiol, if SH groups are considered to be rigid, can exist in three isomeric forms (Figure 1) as in the case of 1,2-dichloropropane,<sup>5</sup> but because of the possibility of orientation of the SH group, each of the above three isomeric forms will have nine configurations and so the total number of configurations will be 27. However, seven of the nine possibilities of the form A and eight of the nine

possibilities of the forms B and C can be eliminated considering the steric repulsion of the CH<sub>3</sub> and SH groups. Thus we are left with two configurations of form A and one each for B and C. However, it does not appear probable that the two configurations of form A will be distinguishable spectroscopically, so only the three forms as shown in Figure 1 have been considered in the present discussion.

Investigation on the temperature dependence of the intensities of the Raman bands in the liquid state shows that the intensities of the bands at 618 and 782 cm<sup>-1</sup> increase with an increase of temperature, while those of the bands at 719 and 353 cm<sup>-1</sup> increase with a decrease of temperature. This shows that the liquid consists of at least two forms of isomeric molecules, the bands at 618 and 782 cm<sup>-1</sup> belonging to the high-energy form while those at 719 and 353 cm<sup>-1</sup> belong to the low-energy form.

Further, it was observed that the strong Raman bands at 618 and 782 cm<sup>-1</sup> in the spectrum of the liquid persist with very weak intensity in the spectrum of the solid at 93°K, though much weaker bands 213 and 353 cm<sup>-1</sup> due to the liquid appear in the solid-state spectrum with almost undiminished intensity. The appearance of the Raman bands at 618 and 782 cm<sup>-1</sup> with almost zero intensity in the spectrum of the solid indicates that a small fraction of molecules of higher energy form persists in the solid at 93°K. It was, however, observed that in the case of 1-propanethiol and 1,2-ethanedithiol the high-energy form of the molecules completely disappears in the crystalline state. Thus in the present case the persistence of the two Raman lines due to the high-energy form in the solid with much diminished intensity should be attributed to the spectrum of a glassy mass mixed with that of polycrystalline solid. Similar superposition of the spectra due to the crystalline solid and glassy mass was reported earlier.<sup>7</sup> It may be noted here that in spite of repeated at-

- (1) T. Torgrimsen and P. Kloeboe, *Acta. Chem. Scand.*, **24**, 1139 (1970).
- (2) D. W. Scott, R. E. Pennington, I. A. Hossenlopp, H. L. Finke, and G. Waddington, *J. Amer. Chem. Soc.*, **80**, 56 (1958).
- (3) J. P. McCutlar, H. L. Finke, D. W. Scott, R. E. Pennington, M. E. Gross, J. F. Messenly, and G. Waddington, *J. Amer. Chem. Soc.*, **80**, 4986 (1958).
- (4) M. Ikram and D. B. Powell, *Spectrochim. Acta.*, **21A**, 59 (1972).
- (5) A. B. Dempster, K. Price, and N. Shepperd, *Spectrochim. Acta.*, **27A**, 1563 (1971).
- (6) G. S. Kastha, S. B. Roy, and M. Mazumder, *Indian J. Phys.*, **42**, 478 (1968).
- (7) C. A. Crowder and Norwal Smyrl, *J. Mol. Struct.*, **7**, 478 (1971).



TABLE I: Raman and Infrared Data of 1,2-Propanedithiol<sup>a</sup>

Raman shifts, cm <sup>-1</sup>		Infrared band, cm <sup>-1</sup>		Assignment
Liquid	Solid	Liquid thin film		
		3010 vs		
2968 (6b)	2965 (4b)	2972 s		CH <sub>3</sub> , CH <sub>2</sub> and CH str
2912 (8) P	2912 (6)	2907 s		
2863 (4) P	2869 (3)	2848 w		
2565 (10) P	2563 (6)	2565 s		SH stretch t, g <sub>1</sub> , g <sub>2</sub>
1422 (4) D	1422 (1)	1422 s		CH <sub>2</sub> scissor t, g <sub>1</sub> , g <sub>2</sub>
1380 (3b)		1375 vs		CH <sub>3</sub> sym. def. t, g <sub>1</sub> , g <sub>2</sub>
1342 (2)				CH wag t, g <sub>1</sub> , g <sub>2</sub>
1312 (2b)		1310 vw		
1272 (6) D	1272 (3)	1265 s		
		1250 ms		CH <sub>2</sub> wag t, g <sub>1</sub> , g <sub>2</sub>
		1235 s		
1207 (2) D	1201 (1)	1190 s		CH <sub>2</sub> twist t, g <sub>1</sub> , g <sub>2</sub>
		1178 m		
1101 (6) P	1101 (3)	1105 m		CH <sub>3</sub> rock t
1080 (1)	1080 (0)	1075 m		C-C stretch t
		1055 s		C-C stretch g <sub>1</sub> , g <sub>2</sub>
1022 (4)	1022 (1)			C-C stretch t, g <sub>1</sub> , g <sub>2</sub>
		1012 s		CH <sub>3</sub> rock
		925 msh		CH <sub>2</sub> rock t, g <sub>1</sub> , g <sub>2</sub>
				C-S-H def. t, g <sub>1</sub> , g <sub>2</sub>
900 (3b) D	900 (1)			
863 (3b) D	863 (2)	865 m		
782 (5) P	782 (0)	770		CH <sub>2</sub> rock g <sub>1</sub> , g <sub>2</sub>
719 (9) D	719 (5)	715 ms		C-S stretch t
		700 m		C-S stretch t
665 (2b)	665 (0)	662 m		C-S stretch g <sub>1</sub>
		650 w		C-S stretch g <sub>2</sub>
618 (8) P	618 (0)			C-S stretch g <sub>1</sub> , g <sub>2</sub>
510 (0) D				C-C-C def.
405 (5) P				C-C-C def. g <sub>1</sub> , g <sub>2</sub>
353 (5b) P	353 (3)			C-C-C def. t
282 (5) P	282 (2)			C-C-S def. t
213 (2b) D	213 (1)			C-C-S def. t, g <sub>1</sub> , g <sub>2</sub>
126 (2b) D				C-C torsion

<sup>a</sup> t, trans; g<sub>1</sub> and g<sub>2</sub>, gauche (Figure 1); P, polarized; D, depolarized; s, strong; m, medium; w, weak; v, very; sh, shoulder.

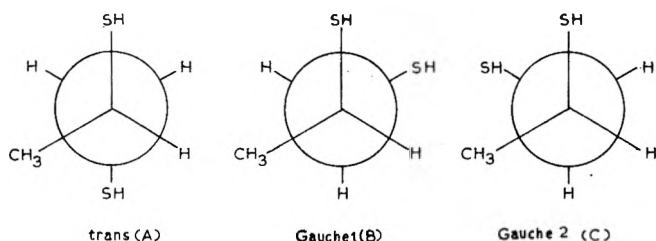


Figure 1. Three possible isomers in 1,2-propanedithiol.

tempts, perfect crystalline form of the solid could not be obtained.

**Identification of Isomers.** The C-S stretching frequencies in alkanethiols are found in the region 610–730 cm<sup>-1</sup>. In the present molecule five frequencies at 719, 700, 665, 650, and 618 cm<sup>-1</sup> are found in the Raman and infrared spectra whereas only four C-S stretching frequencies, 720, 690, 665, and 635 cm<sup>-1</sup>, are observed in the case of 1,2-ethanedithiol. This is analogous to what has been observed in the case of 1,2-dichloropropane<sup>5</sup> and 1,2-dichloroethane.<sup>8</sup> Dempster, *et al.*,<sup>5</sup> have shown that in the case of 1,2-dichloropropane, the five C-Cl stretching frequencies are to be attributed to three isomeric forms of the

molecule. By analogy with this, it is inferred that in the present molecule also, all the three rotamers are present.

In the form trans (A) (Figure 1) each sulfur atom is trans to the other sulfur atom and both the C-S stretching frequencies will be high with  $\nu(-\text{CH}_2\text{-S}) > \nu(>\text{CH-S})$ . The highest frequency, 719 cm<sup>-1</sup>, which is also observed in the Raman spectrum of the solid, is attributed to the trans form (A); the next higher frequency, 700 cm<sup>-1</sup>, is then assigned to the other C-S stretching frequency of the same form. This is justified from the assignments of bands at 720 and 690 cm<sup>-1</sup> to C-S stretching frequencies of the trans isomer in 1,2-ethanedithiol.<sup>4</sup>

The Raman band at 665 cm<sup>-1</sup> due to the liquid appears broad and may consist of two bands, corresponding to the infrared bands at 662 and 650 cm<sup>-1</sup> due to the liquid. This Raman band disappears in the solid state and is assigned to the C-S stretching vibration of gauche 1 (B) and gauche 2 (C) forms. Similarly, the strong Raman band at 618 cm<sup>-1</sup> which also is absent in the spectrum of the solid is assigned to the other C-S stretching vibration of (g<sub>1</sub>) and (g<sub>2</sub>) forms. Since the form (g<sub>2</sub>) has the highest energy of the three,<sup>3,5</sup> its population is also very small and there-

(8) S. Mizushima, "Structure of Molecules and Internal Rotation," 1954 Academic Press, New York, N. Y., 1954, p 220.

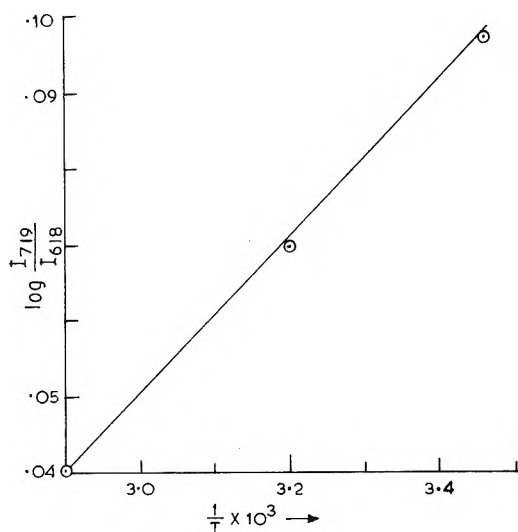


Figure 2. Plot of  $\log I_{719}/I_{618}$  vs.  $1/T$ .

fore the bands at 665 and 618  $\text{cm}^{-1}$  are mainly due to the B form. However, the weak infrared band at 650  $\text{cm}^{-1}$  may represent the C-S vibration of the form ( $g_2$ ). These assignments are consistent with those given for C-C1 stretching vibrations in 1,2-dichloropropane.

*Assignments of Other Vibration Frequencies.* The assignments of the stretching vibrations of CH and SH bonds and the deformation vibrations of CH, CH<sub>2</sub>, and CH<sub>3</sub> groups are straightforward and shown in Table I. The assignments of the frequencies due to C-S-H, C-C-S, and C-C-C bending vibrations are discussed below.

In the case of 1,2-ethanedithiol,<sup>4</sup> the bands at 890 and 800  $\text{cm}^{-1}$  were assigned to the C-S-H bending vibrations. The corresponding frequencies in 1-propanethiol<sup>1</sup> are at 883 and 816  $\text{cm}^{-1}$  and in 2-butanethiol<sup>3</sup> the band at 873  $\text{cm}^{-1}$  is assigned to the C-SH bending vibration. In the present case the broad bands at 863 and 900  $\text{cm}^{-1}$ , which

become sharper and reduced in intensity in the spectrum of the solid, are assigned to the C-S-H bending vibrations of all three rotamers of the molecule.

The frequencies 295 and 308  $\text{cm}^{-1}$  have been assigned to the C-C-S bending vibration in 1-propanethiol and 1,2-ethanedithiol, respectively. In the present molecule, the Raman bands at 282 and 213  $\text{cm}^{-1}$  due to the liquid also appear in the solid state and are assigned to a similar vibration of the form A (trans).

The frequencies 375-520  $\text{cm}^{-1}$  in the case of 2-butanethiol<sup>3</sup> have been assigned to the C-C-C bending vibrations. In the present case the Raman band at 353  $\text{cm}^{-1}$  in the liquid state persists in the solid state and may represent a C-C-C bending vibration of the form A (trans). On the other hand, the band at 405  $\text{cm}^{-1}$ , which disappears in the solid state, is assigned to the forms B ( $g_1$ ) and C ( $g_2$ ). The assignments of C-C stretching vibration have been made following those of 1-propanethiol and 1,2-dichloropropane.

*Energy Difference.* There are three Raman bands at 719, 665, and 618  $\text{cm}^{-1}$  due to C-S stretching vibrations of the present molecule in the liquid state. Of these the band at 665  $\text{cm}^{-1}$  is broad and about one-fourth as intense as the other two bands, so the Raman bands at 719 and 618  $\text{cm}^{-1}$  were used for the determination of the energy difference between the forms (t) and ( $g_1$ ). It has already been mentioned that the band at 618  $\text{cm}^{-1}$  is due to the vibration of ( $g_1$ ) and ( $g_2$ ) forms of the molecule, but as the population of the ( $g_2$ ) form is very small, its contribution to the overall intensity of the band at 618  $\text{cm}^{-1}$  will also be very small and therefore will not affect the value of the energy difference very much.

The ratio of the peak intensities of the Raman bands at 719 and 618  $\text{cm}^{-1}$  were determined at different temperatures with a recording grating spectrometer. From the straight line plot of the logarithm of intensity ratio against the reciprocal of absolute temperature, the energy difference between the forms (t) and ( $g_1$ ) is found to be  $450 \pm 100$  cal/mol.

# A Spectrophotometric Study of the Palladium(II) Chloride–Aluminum Chloride Vapor Complex

G. N. Papatheodorou

The James Franck Institute, University of Chicago, Chicago, Illinois 60637 (Received May 8, 1972)

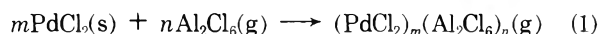
The reaction of solid  $\alpha$ -PdCl<sub>2</sub> with gaseous Al<sub>2</sub>Cl<sub>6</sub> to form a deep red gaseous complex has been studied spectrophotometrically. Thermodynamic considerations suggested the stoichiometry for the reaction PdCl<sub>2</sub>(s) + Al<sub>2</sub>Cl<sub>6</sub>(g) → PdAl<sub>2</sub>Cl<sub>8</sub>(g):  $\Delta H_R = 7.2$  kcal/mol,  $\Delta S_R = 9.45$  eu. The visible and uv electronic absorption spectrum of the PdAl<sub>2</sub>Cl<sub>8</sub> complex was interpreted in terms of a square-planar PdCl<sub>4</sub> sharing edges with two tetrachloroaluminates. The data for the above reaction were compared with the data available in the literature for the corresponding reaction of NiCl<sub>2</sub>. The electronic absorption spectrum of NiAl<sub>2</sub>Cl<sub>8</sub>(g) is reported and interpreted as a NiCl<sub>6</sub> octahedron sharing faces with two tetrachloroaluminates.

## I. Introduction

In recent years the existence of vapor complexes of metal chlorides, with highly volatile chlorides of aluminum and iron(III), has attracted the interest of different investigators. These gaseous complexes are widely distributed throughout the periodic table, including metal monochlorides to metal pentachlorides.

The first complexes to be investigated were the NaAlCl<sub>4</sub><sup>1</sup> and NaFeCl<sub>4</sub>.<sup>2-4</sup> Later the alkaline earth chlorides (Mg and Ca),<sup>5,6</sup> divalent 3d metal (Mn, Fe, Co, Ni, and Zn)<sup>5</sup> chlorides, and the chlorides of Cd<sup>5</sup> and Pb<sup>5</sup> with either Al<sub>2</sub>Cl<sub>6</sub> or Fe<sub>2</sub>Cl<sub>6</sub> have been studied by vapor pressure equilibrium methods. Representative chlorides from the lanthanides (NdCl<sub>3</sub>) and from the actinides (UCl<sub>4</sub> and UCl<sub>5</sub>) have been investigated spectroscopically by Gruen and coworkers.<sup>7,8</sup> Zvarova and Zvara<sup>9</sup> have shown the formation and separation, by means of gas chromatography, of gaseous complexes of the lanthanide (Ce, Pr, Pm, Gd, Tb, Dy, Tm, Yb, and Lu) chlorides with Al<sub>2</sub>Cl<sub>6</sub>. The general formula for the gaseous complexes with aluminum chlorides is (MCl<sub>k</sub>)<sub>m</sub>·(Al<sub>2</sub>Cl<sub>6</sub>)<sub>n</sub>. In all cases studied, the value of *m* is 1, while the value of *n* varies between 0.5 and 2.

In the present report the existence of a dark red vapor complex of palladium chloride with aluminum chloride is established. Furthermore, the equilibrium



has been studied by measuring spectrophotometrically the absorbance of the gaseous complexes over  $\alpha$ -PdCl<sub>2</sub>(s). The thermodynamic quantities for the above equilibrium and the spectroscopic properties of the Pd–Al–Cl gaseous complexes are discussed in terms of the stoichiometry and structure of the gaseous molecules.

## II. Experimental and Results

**Chemicals and Equipment.** The anhydrous aluminum chloride was prepared from high-purity aluminum metal and gaseous HCl.<sup>10</sup>

The  $\gamma$ -palladium(II) chloride was purchased from Matthey Bishop, Inc.<sup>11</sup> The salt was dried at 150° for several hours under vacuum of less than 1  $\mu$ . The anhydrous ma-

terials were handled under vacuum in tight containers or in a drybox with water vapor level less than 2 ppm.

The spectrophotometric measurements were performed on a Cary Model 14H spectrophotometer equipped with a high-temperature cell compartment<sup>12</sup> (1-cm maximum path length). The spectra were digitally recorded on paper tape, and the calculation and plotting of molar absorptivities were carried out by a digital computer. The quartz optical cells were the uv type rectangular 1-cm cells purchased from Pyrocell.

**Method.** Each optical cell was connected with a 10 cm long, 3-mm i.d., side quartz tube. A calibrated 10-cm<sup>3</sup> buret and water were then used for measuring the volume of the cell. The side tube was calibrated in cm<sup>3</sup> of the total volume (cell plus tube). These procedures permitted the determination of the cell volume with an error of less than 0.5%. The height of each cell did not exceed 9 cm and the total volume varied between 8 and 24 cm<sup>3</sup>.

In a typical experiment amounts of AlCl<sub>3</sub> and PdCl<sub>2</sub>, preweighed on a microbalance, were transferred into the dry and degassed cell. The cell was evacuated and sealed on a premarked point of the side tube. The amounts of AlCl<sub>3</sub> were adjusted so that all the AlCl<sub>3</sub> in the cell was in the vapor phase at temperatures between 500 and 600°K. The cell was then heated for 15–30 min at 700°K and finally transferred into the furnace of the spectrophotometer. The vertical and horizontal temperature gradients of the high-temperature compartment of the spectrophotometer were less than 2°. In most cases the spectra were re-

- (1) E. W. Dewing, *J. Amer. Chem. Soc.*, **77**, 2639 (1955).
- (2) C. M. Cook and W. E. Dunn, *J. Phys. Chem.*, **65**, 1505 (1961).
- (3) B. G. Korshunov, I. S. Morozov, V. I. Ionov, and M. A. Zorina, *Izv. Vyssh. Ucheb. Zaved., Tsvet. Met.*, **3**, 72 (1960).
- (4) R. R. Richards and N. W. Gregory, *J. Phys. Chem.*, **68**, 3089 (1964).
- (5) (a) E. W. Dewing, *Nature (London)*, **214**, 483 (1967); (b) *Met. Trans.*, **1**, 2169 (1970).
- (6) K. N. Semenenko, T. N. Naumova, L. N. Gorokhov, and A. V. Bovoselova, *Dokl. Akad. Nauk. USSR*, **154**, 648 (1964).
- (7) H. A. Oye and D. M. Gruen, *J. Amer. Chem. Soc.*, **91**, 2229 (1969).
- (8) D. M. Gruen and R. L. McBeth, *Inorg. Chem.*, **8**, 2325 (1969).
- (9) T. S. Zvarova and I. Zvara, *J. Chromatogor.*, **44**, 634 (1969).
- (10) N. J. Bjerrum, C. R. Boston, and G. P. Smith *Inorg. Chem.*, **6**, 2261 (1967).
- (11) Malvern, Pa. 19355.
- (12) C. R. Boston and G. P. Smith, *J. Sci. Instrum., Ser. 2*, **2**, 543 (1969).

**TABLE I: Determination of Molar Absorptivity**

E-97 <sup>c</sup>			E-101 <sup>b</sup>		E-107 <sup>c</sup>		E-109 <sup>d</sup>	
<i>T</i> , °K	$\nu_{\max}$ , $\mu^e$	$\epsilon_{\max}$	<i>T</i> , °K	$\epsilon_{\max}$	<i>T</i> , °K	$\epsilon_{\max}$	<i>T</i> , °K	$\epsilon_{\max}$
500	485.5	174	600	217	575	206	550	197
550	488	189	650	227	600	212	600	205
600	490.5	194	700	236	650	218	650	212
650	493	204	750	244	700	227	700	218
700	496	211			750	235	750	226
750	499	216			800	241		
800	502	223						

<sup>a</sup>  $P_0 = 4.65 \times 10^{-3}T$  atm;  $n_{Pd} = 1.024 \times 10^{-5}$  mol;  $V = 9.95$  cm<sup>3</sup>.  
<sup>b</sup>  $P_0 = 4.326 \times 10^{-3}T$  atm;  $n_{Pd} = 7.038 \times 10^{-5}$  mol;  $V = 15.25$  cm<sup>3</sup>.  
<sup>c</sup>  $P_0 = 4.468 \times 10^{-3}T$  atm;  $n_{Pd} = 5.906 \times 10^{-5}$  mol;  $V = 8.95$  cm<sup>3</sup>.  
<sup>d</sup>  $P_0 = 2.407 \times 10^{-3}T$  atm;  $n_{Pd} = 5.532 \times 10^{-5}$  mol;  $V = 15.95$  cm<sup>3</sup>.  
<sup>e</sup> The values of  $\nu_{\max}$  (the frequency at which the maximum absorptivity occurs) were found to be the same for all four experiments.

recorded in the range between 600 and 800°K and in intervals of 50°K. The pressure  $P'$  of  $Al_2Cl_6(g)$ , without correction for consumption due to reaction 1, was calculated from the difference  $P' = P_0 - P_D$ . Here  $P_0$  is the "ideal gas" pressure of  $Al_2Cl_6$ , and  $P_D$  is the correction<sup>7</sup> due to the dissociation<sup>13</sup> of the dimer  $Al_2Cl_6$ .

**Determination of Molar Absorptivity.** The cells were filled with small amounts of  $PdCl_2$  to ensure that all of the  $PdCl_2$  was in the gaseous complex state in the range of temperatures studied. The "apparent" molar absorptivity  $\epsilon(\lambda)$  for the gaseous complex(es) of wavelength  $\lambda$  was then determined from the relation

$$\epsilon = AV/n_{Pd}h \quad (2)$$

where  $V$  is the volume of the optical cell,  $h$  is the 1-cm optical path length,  $A$  is the absorbance at wavelength  $\lambda$ , and  $n_{Pd}$  the total number of Pd moles placed into the cell.

Four different spectrophotometric experiments were carried out for this determination of  $\epsilon(\lambda)$ . The characteristics of each of these experiments are shown in Table I. The spectra were recorded from 4 to 30 kK. No bands were found in the 4–12 kK range. A strong absorption band close to 20 kK and a very weak band close to 15 kK were observed (Figure 1). From the listed values in Table I, it appears that  $\epsilon_{\max}$  varies almost linearly with temperature. A plot of  $\epsilon_{\max}$  vs.  $T$  for all four experiments gives a set of straight lines with slopes very close to  $0.15 M^{-1} \text{ cm}^{-1} \text{ deg}^{-1}$ . However, the absolute magnitude of  $\epsilon_{\max}$  is subject to a nonsystematic variation from one experiment to another. Averaging all four experiments, we can express  $\epsilon_{\max}$  as a function of  $T$

$$\epsilon_{\max} \approx 117.5 + 0.15T M^{-1} \text{ cm}^{-1} \quad 500^\circ\text{K} \leq T \leq 800^\circ\text{K} \quad (3)$$

The constant term (117.5) is calculated with a 5% variation, which we attribute to errors associated with the weighing of the small amounts of  $PdCl_2$ . On the other hand, the second term of the equation (*i.e.*, the relative change of absorptivity with temperature) is well established with an error of less than 1%. A comparison of the last experiment (E-109 in Table I) with the other three experiments indicates that, within experimental error, the absorptivity  $\epsilon$  is independent of the  $Al_2Cl_6$  pressure. This implies that either only one gaseous species is present or that two or more species with equal "atomic absorptivi-

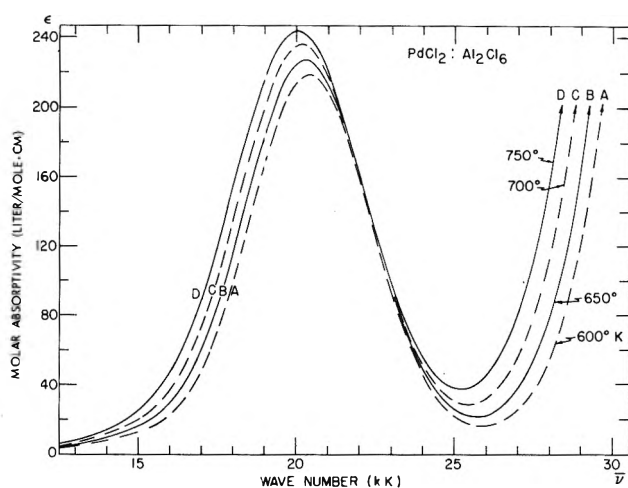


**Figure 1.** Absorption spectra of the palladium chloride-aluminum chloride vapor complex as a function of temperature.

ties" are present. Thus in a mixture of  $l$  gaseous complexes  $(PdCl_2)_m(Al_2Cl_6)_n$  ( $m = m_1, m_2, \dots, m_l$  and  $n = n_1, n_2, \dots, n_l$ ) the molar absorptivities  $\epsilon_1, \epsilon_2, \dots, \epsilon_l$  of the absorbing complexes are related to the apparent molar absorptivity  $\epsilon$

$$\epsilon_i = m_i \epsilon, \quad i = 1, 2, \dots, l \quad (4)$$

The uv spectrum of the gaseous complexes was recorded in a somewhat different way. Due to the high absorptivity of the uv bands, the number of moles of  $PdCl_2$  to be complexed in the gaseous phase (in order to give absorbances in the range permitted by the instrument) is very small and cannot be weighed accurately. However, we were able to determine the absorptivity in the uv region by preparing a very dilute, but unknown, concentration of the gas and by measuring the relative intensities of the uv and visible bands. For wavenumbers below 50 kK, there is only one uv band present at  $\sim 41$  kK. The absorbance of this band was measured with the 0 to 2 slidewire while for the same cell the absorbance of the visible band (at  $\sim 20$  kK) was measured with the 0.0 to 0.1 slidewire. It was found that at 600°K  $\epsilon_{\max}(41 \text{ kK})/\epsilon_{\max}(20 \text{ kK}) \approx 80$ . From this relation and the value of  $\epsilon_{\max}(20 \text{ kK})$  of 210 (at  $T = 600^\circ\text{K}$ ) we were able to approximate the absorptivity scale in the uv region.

**Solid  $PdCl_2$  in Equilibrium with  $Al_2Cl_6$  Gas.** In order to determine the nature of the solid phase(s) in equilibrium with gaseous  $Al_2Cl_6$  and to exclude the possibility of a  $PdCl_2-Al_2Cl_6$  solid compound above 500°K, we performed the following experiments.

Excess quantities of  $\gamma$ - $PdCl_2$ <sup>14</sup> and small quantities of  $Al_2Cl_6$  were sealed in an evacuated 10-cm long quartz tube whose volume was about 20 cm<sup>3</sup>. The quartz tube was then placed in a vertical windowed furnace and the temperature of the furnace was raised slowly to 650°K. The sample was kept at that temperature for 3 hr to ensure equilibrium. The upper end of the tube was then quenched in water, and all the aluminum chloride, with some gaseous complex, was solidified. After reaching room temperature, the tube was opened and the X-ray diffraction pattern of the solid in the lower end of the tube was

(13) JANAF Thermochemical Data, The Dow Chemical Co., Midland, Mich.

(14) J. R. Soulen and W. H. Chappell, *J. Phys. Chem.*, **69**, 3669 (1965).

taken. The pattern showed that  $\alpha$ -PdCl<sub>2</sub><sup>15,16</sup> was the only solid phase present. No additional lines, indicating either the  $\beta$ <sup>17</sup> and  $\gamma$  forms or possible solid compound formation with Al<sub>2</sub>Cl<sub>6</sub>, were present. We have repeated the same type of experiment at two different equilibration temperatures, 550 and 750°K. In all cases the only solid found (after breaking the tube) was the  $\alpha$ -PdCl<sub>2</sub>.

Finally, in a fourth experiment, the quartz tube containing the  $\alpha$ -PdCl<sub>2</sub> and Al<sub>2</sub>Cl<sub>6</sub> was placed in a vertical windowed furnace in such a way that the excess  $\alpha$ -PdCl<sub>2</sub> was maintained in the bottom of the tube at 550°K, while the other end of the sample tube was in a cooler zone at about 520°K. The tube was maintained in this way for several days. Daily visual observations indicated the formation of small red single crystals in the middle of the sample tube. These crystals were identified by X-ray diffraction as  $\alpha$ -PdCl<sub>2</sub>. This last experiment eliminated any possibility of solid complex compound formation and shows that the decomposition of the gaseous complex yields the  $\alpha$ -PdCl<sub>2</sub> form.

*Partial Pressures of the Gaseous Complex(es).* The optical cells were filled with excess quantities of PdCl<sub>2</sub>. The apparent partial pressure of the gaseous complex(es) over the solid  $\alpha$ -PdCl<sub>2</sub> was determined from the relation

$$P_c = (A_{\max}/\epsilon_{\max})RT \quad (5)$$

where  $A_{\max}$  is the measured absorbance at  $\nu_{\max}$  and  $\epsilon_{\max}$  is the apparent absorptivity of the complex(es) as given in eq 3. Measurements of  $P_c$  as a function of time and at constant temperature showed that the equilibrium was reached very fast. An equilibration time of less than 10 min was sufficient before making spectral measurements. Seven separate experiments with different pressures ( $P'$ ) of Al<sub>2</sub>Cl<sub>6</sub> were performed and the values of  $A_{\max}$ ,  $P_c$ , and  $P'$  are given in Table II.

### III. Discussion

*Thermodynamic Treatment of the Data.* According to reaction 1, the equilibrium constant of the  $i$ th gaseous complex ( $n = n_i$ ,  $m = m_i$ ) with partial pressure  $P_i$  is

$$K_i = P_i / (P' - \sum_{j=1}^l n_j P_j)^{n_i} \quad (6)$$

In the absence of information (e.g., mass spectrometric studies) regarding the principal gaseous complexes present, a thermodynamic treatment of the data for all possible reactions leading to different complex species is futile. However, the treatment can be significantly simplified from the experimental fact that the measured apparent pressure  $P_c$  is proportional to  $P'$ .

$$P_c = (1/b)P' \quad (7)$$

The validity of this proportionality is illustrated in Figure 2. Relation 7 implies<sup>18</sup> that (a) each gaseous complex contains one Al<sub>2</sub>Al<sub>6</sub> molecule per mole and that (b) there is only one predominant complex species present. The general formula of this complex is (PdCl<sub>2</sub>)<sub>m</sub>Al<sub>2</sub>Cl<sub>6</sub> with  $m = 1, 2, 3, \dots$

The, thus far, investigated gaseous<sup>1-9</sup> or solid<sup>19</sup> complexes of Al<sub>2</sub>Cl<sub>6</sub> with transition metal chlorides contain always one transition metal atom per mole of complex, while the number of Al atoms varies from 1 to 4. Thus, we consider it reasonable to make the assumption that in the

TABLE II: Partial Pressures of the Palladium Gaseous Complex

Experiment no. and characteristics	T, °K	A <sub>max</sub>	P <sub>c</sub> , atm	P', atm	10K
E-102	602.5	1.895	0.450	1.980	2.95
V = 12.2 cm <sup>3</sup>	648	2.500	0.619	2.107	4.16
P <sub>0</sub> = 3.31 × 10 <sup>-3</sup> T	702	3.280	0.848	2.137	6.59
E-103	549	0.5025	0.113	0.761	1.75
V = 21.5 cm <sup>3</sup>	601	0.7425	0.176	0.826	2.71
P <sub>0</sub> = 1.39 × 10 <sup>-3</sup> T	650	1.000	0.248	0.878	3.94
	699.5	1.280	0.330	0.914	5.66
	747.5	1.600	0.427	0.928	8.54
	801.0	1.815	0.501	0.905	12.45
E-104	601	3.02	0.717	3.110	2.99
V = 9.5 cm <sup>3</sup>	624.2	3.60	0.873	3.220	3.72
P <sub>0</sub> = 5.21 × 10 <sup>-3</sup> T	651.5	4.225	1.049	3.340	4.57
	699.5	5.125	1.311	3.530	5.90
E-105 <sup>a</sup>	651	4.545	1.128	3.587	4.59
V = 8.5 cm <sup>3</sup>	676.7	5.165	1.310	3.700	5.48
P <sub>0</sub> = 5.59 × 10 <sup>-3</sup> T	701.5	5.885	1.521	3.801	6.67
E-106	601.5	0.455	0.108	0.447	3.19
V = 24.55 cm <sup>3</sup>	651.5	0.590	0.147	0.472	4.50
P <sub>0</sub> = 0.756 × 10 <sup>-3</sup> T	700.0	0.735	0.190	0.485	6.40
	749.5	0.875	0.234	0.482	9.45
	800.5	0.980	0.271	0.455	14.69
E-111	550.5	0.385	0.087	0.588	1.74
V = 24.3 cm <sup>3</sup>	600.5	0.575	0.136	0.635	2.73
P <sub>0</sub> = 1.073 × 10 <sup>-3</sup> T	650.0	0.795	0.197	0.674	4.14
	699.5	1.055	0.272	0.701	6.35
	749	1.24	0.331	0.702	8.96
	799	1.397	0.386	0.676	13.38
E-112	600	2.040	0.484	2.196	2.83
V = 11.6 cm <sup>3</sup>	649.5	2.830	0.702	2.351	4.25
P <sub>0</sub> = 3.688 × 10 <sup>-3</sup> T	699.5	3.760	0.962	2.482	6.32
	750.5	4.775	1.278	2.570	9.89
	800.0	5.70	1.570	2.590	15.3

<sup>a</sup> A 0.5-cm path length cell was used but the absorbance is referred to 1-cm path length.

PdCl<sub>2</sub>(s)-Al<sub>2</sub>Cl<sub>6</sub>(g) system the predominant gaseous complex is a mononuclear ( $m = 1$ ) palladium species and that the equilibria leading to complexes with  $m \geq 2$  occur only to a slight extent. This view is also supported by the recent<sup>20</sup> isolation of a diamagnetic palladium aluminate compound with an 1:1 PdCl<sub>2</sub>:Al<sub>2</sub>Cl<sub>6</sub> stoichiometry.

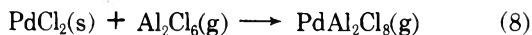
- (15) H. Schafer, U. Wiese, K. Rinke, and K. Brendt, *Angew. Chem.*, **79**, 244 (1966).  
 (16) A. F. Wells, *Z. Kristallogr. Mineralogr. Petrogr., Abt. A*, **100**, 189 (1938).  
 (17) K. Brodersen, G. Thiele, and H. G. Schnering, *Z. Anorg. Allg. Chem.*, **337**, 120 (1965).  
 (18) From eq 4-7 it follows that

$$P_c = \sum_{j=1}^l m_j P_j, P' = (P_i / K_i)^{n_i} + \sum_{j=1}^l n_j P_j = b \sum_{j=1}^l m_j P_j, i = 1, 2, \dots, l$$

This last equation, based on the experimentally determined relation 8, is an identity; thus  $n = n_1 = n_2 \dots = 1$  and  $P_j = 0$  ( $j \neq i$ ). For the only nonvanishing partial pressure (e.g.,  $P_i$ ) we have  $(1/K_i) + 1 = b$  which determine the equilibrium constant of reaction 1.

- (19) (a) J. A. Ibers, *Acta Crystallogr.*, **15**, 967 (1952); (b) R. F. Belt and H. Scott, *Inorg. Chem.*, **3**, 1785 (1964); (c) J. Brynestad, S. von Winbush, H. L. Yakel, and G. P. Smith, *Inorg. Nucl. Chem. Lett.*, **6**, 889 (1970); (d) J. Brynestad, H. L. Yakel, and G. P. Smith, *Inorg. Chem.*, **9**, 686 (1970).  
 (20) G. N. Papatheodorou, to be submitted for publication.

With the values  $m = n = 1$  equilibrium 1 becomes



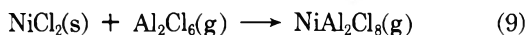
and the equilibrium constant is

$$K = P_c / (P' - P_c)$$

The values of  $K$  are listed in the last column of Table II. A deduction of the enthalpy and entropy of this equilibrium, according to the second law, is shown in Figure 3. Thirty-two experimentally determined values of  $R \ln K$  are plotted vs.  $1/T$ . The least-squares treatment of the data shown yields a value of  $\Delta H_R = 7.2 \pm 0.16$  kcal/mol for the enthalpy of reaction 8 over the range of temperature studied. For the same temperature range a value for the entropy of reaction  $\Delta S_R = 9.45 \pm 0.75$  is obtained.

A comparison between the angles and distances of the  $\text{PdCl}_4$  square in solid  $\text{PdCl}_2$ <sup>16</sup> and of the  $\text{AlCl}_4$  in gaseous<sup>13</sup>  $\text{Al}_2\text{Cl}_6$  shows that changes of bond lengths and bond angles by less than 3% make the Cl-Cl edge of the  $\text{AlCl}_4$  tetrahedron equal with the Cl-Cl side of the square-planar  $\text{PdCl}_4$ . In view of this consideration we propose in Figure 4 a structural model for the  $\text{PdAl}_2\text{Cl}_8$  gaseous complex. The angle  $\omega$  was introduced in order to determine the position of Al atom (and the  $\text{AlCl}_4$  units) with respect to the  $\text{PdCl}_4$  plane. Using this model ( $\omega = 0$ ) and the structural parameters of the  $\text{Al}_2\text{Cl}_6$  dimers<sup>13</sup> we calculated a statistical<sup>21</sup> third law translational and rotational entropy for reaction 8:  $\Delta S_{\text{TR}} = 3.8 \pm 0.3$ ,  $500^\circ\text{K} < T < 800^\circ\text{K}$ . This value, and the experimentally determined entropy, suggest a small vibrational entropy contribution of  $\sim 5$  eu.

We shall now compare the thermodynamic functions of reaction 8 with the available in the literature<sup>5b</sup> corresponding functions for the  $\text{NiCl}_2\text{-Al}_2\text{Cl}_6$  reaction.



$$\Delta H = 7.5 \text{ kcal/mol} \quad \Delta S = 9 \text{ eu}$$

It appears that the stabilities of the  $\text{PdAl}_2\text{Cl}_8$  and  $\text{NiAl}_2\text{Cl}_8$  gaseous complexes are very similar. In his work, Dewing<sup>5b</sup> concluded that the similarities of the stabilities of the  $\text{MAl}_2\text{Cl}_8$  ( $\text{M} = \text{Ca}, \text{Mn}, \text{Co}, \text{and Ni}$ ) complex can be best interpreted as implying that the bonding of the divalent ions in the complex is very similar to that in the solid. All  $\text{MCl}_2$  solids have similar structures with the divalent metal in octahedral coordination while the  $\text{PdCl}_2$  solid is a completely different structure with  $\text{Pd}^{2+}$  in square-planar coordination. These differences, however, do not alter the thermodynamic functions of reactions 8 and 9, which implies that the characteristic structure and coordination in the solid is also present in the gaseous complex. Thus we should expect that local geometry of  $\text{Ni}^{2+}$  in  $\text{NiAl}_2\text{Cl}_8$  is very close to  $O_h$  while the geometry of  $\text{Pd}^{2+}$  in  $\text{PdAl}_2\text{Cl}_8$  is very close to  $D_{3h}$ .

**Electronic Spectra.** In Figure 5 the absorption spectrum of the  $\text{PdAl}_2\text{Cl}_8$  gaseous complex is shown in the region from 4 to 5 kK. The visible and near-ir spectrum is characterized by one high-intensity band at wave number close to 20 kK. A low-intensity band can be also observed in the 14-15-kK region. The uv spectrum shows a very strong absorption band at 40.2 kK.

The only known all-chloride Pd(II) complex is  $\text{PdCl}_4^{2-}$  which is a typical example of a well-known square-planar

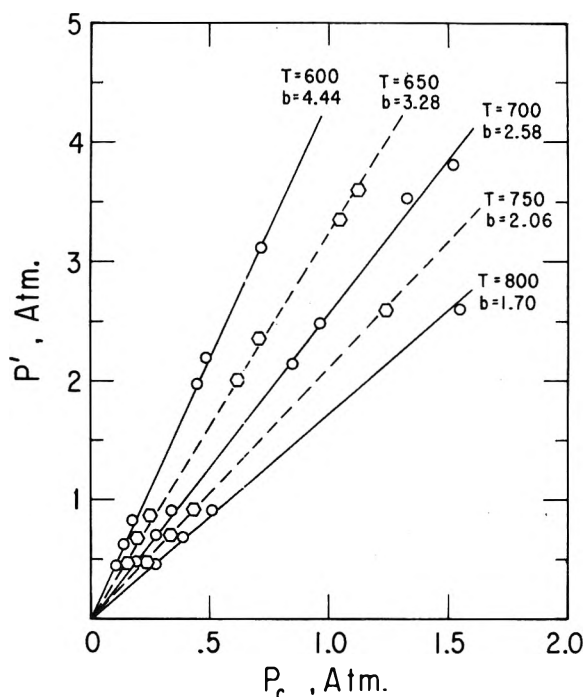


Figure 2. Plots of  $P'$  vs.  $P_c$  at different temperatures. The slopes  $b$  were determined from a least-squares treatment of the data.

diamagnetic complex. In Table III we give the absorption data of  $\text{PdCl}_4^{2-}$  in the solid state and in solution. The assignments of the  $d \rightarrow d$  transitions are based on the data of Day, *et al.*,<sup>22</sup> on  $\text{K}_2\text{PdCl}_4$  and on the data and ligand field calculations of Martin and coworkers<sup>23</sup> on solid  $\text{K}_2\text{PtCl}_4$ . The assignments of the uv band are based on MO calculations.<sup>24</sup> These high-intensity absorptions are attributed to ligand-to-metal charge transfer transitions (L  $\rightarrow$  M).

A comparison of the visible spectrum of the solid  $\text{K}_2\text{PdCl}_4$  and of  $\text{PdCl}_4^{2-}$  in solution indicates that the two first spin-allowed bands of the  $\text{K}_2\text{PdCl}_4$  are not separable in the solution, while the third spin allowed band of the solid seems to disappear under the first charge transfer band in the solution. In the last column of Table III we have listed for comparison the absorption data for the gaseous  $\text{PdAl}_2\text{Cl}_8$  complex. It appears that in the visible region the same band(s) is(are) present for both the gaseous and solution spectrum. Their main differences are a substantial enhancement of intensity, a slight red shift, and some broadening in going from the aqueous HCl solution to the gas. All these differences are reasonably attributed to temperature differences. As Figure 1 shows, the broadening of the band and the red shift increases with increasing temperature. In fact, an extrapolation of the spectrum in Figure 1 to room temperature, where the  $\text{PdCl}_4^{2-}$  solution spectrum was taken, gives  $\epsilon_{\text{max}}(300^\circ\text{K}) \approx 160$  and  $\nu_{\text{max}}(300^\circ\text{K}) \approx 21$  kK.

- (21) A calculation of the moment of inertia of the gaseous complex, as a function of  $\omega$ , shows that the entropy contribution of the moment of inertia increases by only 0.7 eu for changes of  $\omega$  between 0 and  $45^\circ$ .
- (22) P. Day, A. F. Orchard, A. J. Thompson, and R. J. P. Williams, *J. Chem. Phys.*, **42**, 1973 (1965).
- (23) D. S. Martin, M. A. Tucker, and A. J. Kassman, *Inorg. Chem.*, **4**, 1682 (1965); as amended, **5**, 1298 (1966).
- (24) (a) A. J. McCaffery, P. N. Schaltz, and P. J. Stephens, *J. Amer. Chem. Soc.*, **90**, 5730 (1968); (b) H. Ito, J. Fujita, and K. Saito, *Chem. Soc. Jap.*, **40**, 2534 (1967).

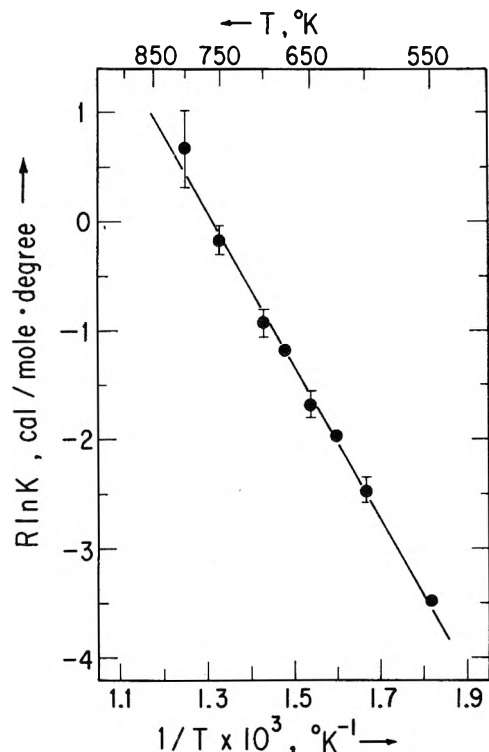


Figure 3. Plot of  $R \ln K$  vs.  $1/T$  for reaction 8.

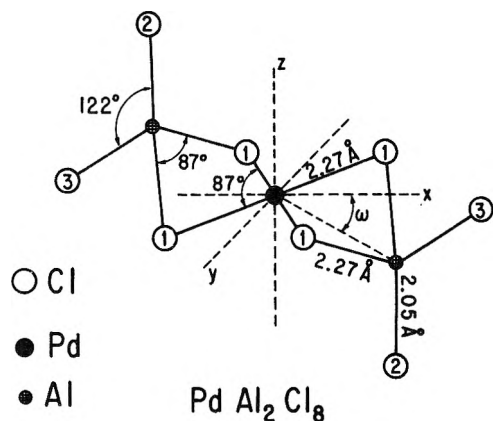


Figure 4. Molecular model of the  $\text{PdAl}_2\text{Cl}_8$  gas.

Although the effect of temperature has not been measured for  $\text{PdCl}_4^{2-}$  in solution, it has been measured in the case of  $\text{K}_2\text{PtCl}_4$  crystals<sup>23</sup> between 15 and 300°K, and in the case of  $\text{PtCl}_4^{2-}$  centers in liquid alkali chloride solvents between 600 and 1100°K.<sup>25</sup> Here, also, an increase in temperature greatly enhances the intensity, shifts the peak to the red, and broadens the band. These effects are plausibly accounted for by vibronic interactions in which asymmetric vibrational states, which destroy the center of symmetry of  $\text{MCl}_4^{2-}$  anion, become increasingly populated with increasing temperature.<sup>23</sup> Therefore, it is more likely that the broad band, occupying the visible spectrum of  $\text{PdAl}_2\text{Cl}_8$ , covers at least two spin-allowed  $d \rightarrow d$  transitions of the palladium atom in a ligand field with approximately  $D_{4h}$  local symmetry.

In contrast with the agreement observed in the visible region, a comparison of the uv spectra of  $\text{PdCl}_4^{2-}$  and  $\text{PdAl}_2\text{Cl}_8$  indicates definite differences. The three charge

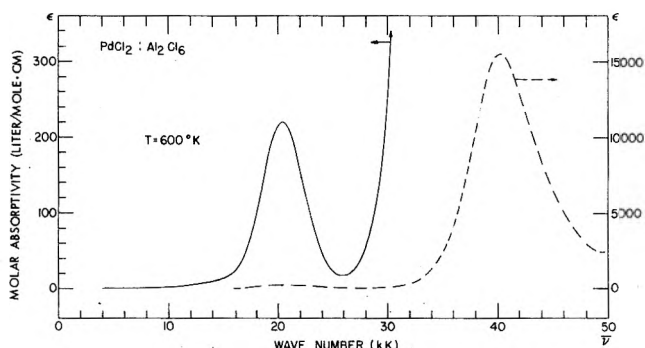


Figure 5. Absorption spectrum of  $\text{Pd}(\text{AlCl}_4)_2(\text{g})$  from 4 to 50 kK.

TABLE III: Assignments of the  $\text{K}_2\text{PdCl}_4$  Solid and  $\text{PdCl}_4^{2-}$  Solution Spectra

Assignment $^1A_{1g} \rightarrow$	$\text{K}_2\text{PdCl}_4^a$ solid, 300°K		$\text{PdCl}_4^{2- b}$ soln, 2 M HCl		$\text{PdAl}_2\text{Cl}_8$ gas, 300°K	
	$\nu$ , kK	$\epsilon_{\text{max}}$	$\nu$ , kK	$\epsilon_{\text{max}}$	$\nu$ , kK	$\epsilon_{\text{max}}$
$^3E_g, ^3B_{1g}^a$	17 (18) <sup>c</sup>	7 (19)	(16)		(~15)	
$^1A_{2g}^a$		(20)	(67)			
$^1E_g$ or $^1B_{1g}^a$	22.6 23.0	128 80		21 152	20	220
$^1B_{1g}$ or $^1E_g^a$	(29.5)	(67)				
$d$			(30.2) <sup>d</sup>	(540)		
$^1A_{2u} +$ $^1E_u(\pi)^{b,c}$			35.8	10,400		
$^1E_u(\sigma)^{b,c}$			44.9	28,300	40.2	15,800

<sup>a</sup> From ref 22. <sup>b</sup> From ref 24. <sup>c</sup> Shoulder. <sup>d</sup> Orbital forbidden charge transfer band.<sup>24b</sup>

transfer bands in aqueous HCl have been replaced in  $\text{PdAl}_2\text{Cl}_8$  by one band of intermediate energy. Since the charge transfer transitions originate essentially from ligand-based molecular orbital levels, their energies should be very sensitive to the electronic environment of the chloride ligand. Environments pulling away the electronic density of the ligand are expected to give rise to charge transfer transitions at higher energy.<sup>26</sup> In the case of the  $\text{PdAl}_2\text{Cl}_8$  molecule the bridged chloride is strongly polarized by the aluminum atom, and the Cl electronic density is substantially different from that of Cl in  $\text{PdCl}_4^{2-}$  (aqueous HCl). Thus the  $L \rightarrow M$  charge transfer is hindered by the aluminum, and the energies of the charge transfer bands occur at higher energies. From these considerations, we suggest that the only uv band in the  $\text{PdAl}_2\text{Cl}_8$  spectrum is the  $^1A_{1g} \rightarrow ^1A_{2u} + ^1E_u(\pi)$  charge transfer transition. A further support for this assignment is the similarity of the relative intensities of the uv and visible bands for the  $\text{PdAl}_2\text{Cl}_8$ , with the relative intensities of the  $^1A_{1g} \rightarrow ^1A_{2u} + ^1E_u(\pi)$  and  $^1A_{1g} \rightarrow ^1A_{2g}$  bands in the  $\text{PdCl}_4^{2-}$  (in 2 M HCl) molecule.

The association of the electronic absorption spectrum of the gaseous complex, with the spectrum of  $\text{PdCl}_4^{2-}$  in a

(25) G. N. Papatheodorou and G. P. Smith, *J. Nucl. Inorg. Chem.*, to be published.

(26) The substitution of Br in  $\text{PdBr}_4^{2-}$  by the less polarizable Cl shifts the charge transfer band toward the blue. The energy of the  $^1A_{1g} \rightarrow ^1A_{2u} + ^1E_u(\pi)$  band, for example, shifts to higher energies by ~6 kK as we go from Br to Cl.<sup>24</sup>



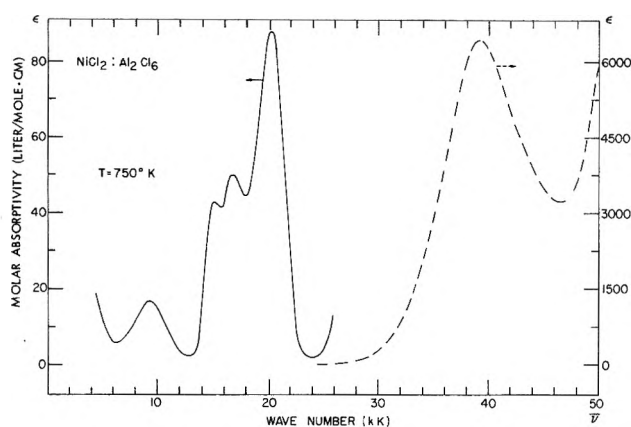


Figure 6. Absorption spectrum of  $\text{Ni}(\text{AlCl}_4)_2(\text{g})$  from 4 to 50 kK.

close to square-planar coordination, is compatible with the proposed molecular model. A  $D_{2h}$  or  $C_{2h}$  (with small) molecular symmetry for the  $\text{PdAl}_2\text{Cl}_8$  gas is anticipated.

Finally, before we close the present section we should like to compare once more the spectrum of the palladium aluminate gaseous complex with that of nickel aluminate. In Figure 6 we give the absorption spectrum of the  $\text{NiAl}_2\text{Cl}_8$  gaseous complex.<sup>27</sup> From the works of Smith and coworkers<sup>28</sup> we have identified this spectrum as either a spectrum of  $\text{Ni}^{2+}$  partitioned between an octahe-

dral and a tetrahedral coordination, the octahedral coordination being the predominant species, or as a  $\text{Ni}^{2+}$  in a distorted octahedral coordination. Both assignments suggest that the proposed molecular model for  $\text{PdAl}_2\text{Cl}_8$  (Figure 4) is also valid for the nickel chloroaluminate with the angles  $\omega$  close to  $45^\circ$ . A  $D_{3h}$  molecular symmetry for the  $\text{NiAl}_2\text{Cl}_8$  molecule is anticipated. With such a symmetry no drastic changes in the coordination of Ni occur as the gaseous complex is formed from the solid  $\text{NiCl}_2$  ( $\sim O_h$  local symmetry) according to reaction 9. Thus the spectroscopic data for the  $\text{PdAl}_2\text{Cl}_8$  and  $\text{NiAl}_2\text{Cl}_8$  gases show that the  $\text{AlCl}_4$  tetrahedra of  $\text{Al}_2\text{Cl}_6$  gas can be bound to the transition metal chloride by either an edge (*i.e.*,  $\omega = 0^\circ$  for Pd) or a plane (*i.e.*,  $\omega = 45^\circ$  for Ni). This is in agreement with the thermodynamic data and explains the similarities in the magnitudes of the thermodynamic quantities of reactions 8 and 9.

*Acknowledgment.* The author is deeply indebted to Dr. G. Pedro Smith for allowing him to use his laboratory facilities at the O. R. N. L. The kind help and advice of Drs. J. Brynestad, C. R. Boston, and G. P. Smith during the course of this investigation is also acknowledged.

- (27) The spectrum was taken by using the same experimental techniques described for the spectrum of the palladium aluminate.  
 (28) (a) W. E. Smith, J. Brynestad, and G. P. Smith, *J. Chem. Phys.*, **52**, 3890 (1970); (b) J. Brynestad, C. Boston, and G. P. Smith, *ibid.*, **47**, 3179 (1967); (c) J. Brynestad and G. P. Smith, *ibid.*, **47**, 3190 (1967); (d) J. Brynestad, H. L. Yakel, and G. P. Smith, *ibid.*, **45**, 4652 (1966).

## Dimeric Structure of a Copper Phthalocyanine Polymorph

James H. Sharp\* and Martin Abkowitz

Xerox Rochester Research Center, Xerox Corporation, Rochester, New York 14603 (Received April 5, 1972)

Publication costs assisted by Xerox Corporation

The preparation and characterization of a polymorph of copper phthalocyanine (CuPc) having a dimeric structure is described. The infrared, X-ray, electronic, and esr spectra of the new polymorph, designated x-CuPc, are compared to those of the well-known  $\alpha$ - and  $\beta$ -CuPc polymorphs. Distinct differences among the three polymorphs are observed in their infrared and X-ray spectra and these differences are useful in the general characterization of the polymorphs. The electronic spectrum of x-CuPc can be interpreted in terms of a dimer structure which is analogous to that reported for the metal-free phthalocyanine dimer, x- $\text{H}_2\text{Pc}$ . Additional support for the dimer model is obtained from a qualitative comparison of the esr envelope line shapes for the  $\alpha$ -,  $\beta$ -, and x-CuPc polymorphs.

### I. Introduction

The phthalocyanines have been reported to exist in at least three different polymorphic phases and the polymorphic form can greatly influence both the pigment<sup>1</sup> and electrical properties<sup>2,3</sup> of these materials. The  $\beta$  polymorphs are most easily studied by X-ray methods, since single crystals can be prepared by sublimation at approxi-

mately  $550^\circ$ . Robertson<sup>4</sup> found that  $\beta$ -copper phthalocyanine ( $\beta$ -CuPc) is a monoclinic crystal having the following

- (1) See, for example, F. H. Moser and A. L. Thomas, "Phthalocyanine Compounds," Reinhold, New York, N. Y., 1963.  
 (2) K. Wiksne and A. E. Newkirk, *J. Chem. Phys.*, **34**, 2184 (1961).  
 (3) C. Y. Liang and E. G. Scalco, *J. Electrochem. Soc.*, **110** (7), 779 (1963).

unit cell dimensions:  $a = 19.6 \text{ \AA}$ ,  $b = 4.79 \text{ \AA}$ ,  $c = 14.6 \text{ \AA}$ ,  $\beta = 120^\circ 36'$ ; there are two molecules per unit cell.

Preparation of single crystals of  $\alpha$ -phthalocyanine polymorphs have not been reported, but Robinson and Klein<sup>5</sup> have determined the crystal structure of  $\alpha$ -copper phthalocyanine ( $\alpha$ -CuPc) from X-ray powder diffraction data. They found that this polymorph was a tetragonal crystal, probably belonging to the  $C_{4h}-P_{4/m}$  space group, having six molecules per unit cell. The  $\alpha$  polymorph is metastable and undergoes a polymorphic transition to the stable  $\beta$  polymorph when heated<sup>6-8</sup> at ca.  $300^\circ$  or when stored in certain organic solvents.

A third polymorph of CuPc has been reported by Eastes<sup>9</sup> and was designated as  $\gamma$ -copper phthalocyanine ( $\gamma$ -CuPc). This phase was identified by a comparison of its X-ray powder diffraction pattern with those of the  $\alpha$ - and  $\beta$ -CuPc polymorphs. In more recent work, however, Assour<sup>7</sup> has presented experimental evidence that the X-ray patterns of  $\alpha$ - and  $\gamma$ -CuPc differ only in the degree of resolution and suggests that the  $\alpha$  and  $\gamma$  phases differ only in particle size. Assour<sup>7</sup> also implies that his X-ray powder diffraction data on  $\alpha$ -CuPc support an orthorhombic structure rather than a tetragonal structure as reported by Robinson and Klein.<sup>5</sup> On the other hand, Knudsen<sup>10</sup> has proposed a key, based upon infrared absorption spectra, to distinguish among the  $\alpha$ ,  $\beta$ , and  $\gamma$  modifications as well as two additional polymorphic phases, designated  $\delta$ <sup>11</sup> and  $\epsilon$ ,<sup>12</sup> which have been reported in more recent patent literature.

Recently, a new polymorph of metal-free phthalocyanine, designated as x-phthalocyanine (x-H<sub>2</sub>Pc) has been reported.<sup>13</sup> The spectroscopic characterization of this polymorph has been presented<sup>14</sup> and a dimer structure for the x phase has been proposed. The purpose of this work is to report the preparation and identification of the analogous x polymorph of copper phthalocyanine (x-CuPc). Infrared and X-ray diffraction spectra have been employed to qualitatively characterize and define the new polymorph and the electronic spectrum is interpreted in terms of a dimer model for x-CuPc. A comparison of the esr spectra of the  $\alpha$ ,  $\beta$ , and x-CuPc polymorphs is used to further support the dimer model for the x polymorph.

## II. Experimental and Results

(1) *Preparation of CuPc Polymorphs.* CuPc was obtained from Pfaltz and Bauer, Inc., Flushing, N. Y. This material was first purified by solvent extraction and sublimation techniques. For esr studies, the  $\alpha$  polymorph was prepared by precipitation from sulfuric acid solution. The  $\beta$  polymorph was prepared by heat treating the  $\alpha$  polymorph at  $320^\circ$  for several hours. Alternatively, for infrared and electronic spectra studies, thin films of the  $\alpha$  polymorph could be readily prepared by slow vacuum evaporation of the purified material onto Pyrex or KBr plates. The evaporations were carried out in a Bendix Balzers, Model BA-3 evaporator, at  $10^{-6}$  Torr. Thin films of  $\beta$ -CuPc were obtained by heat treating the  $\alpha$ -CuPc films.

The x-CuPc polymorph was prepared by evaporation of the purified commercial CuPc under a partial vacuum. The pressure range and rate of sublimation were rather critical and were determined by Griffiths and Walker<sup>15</sup> to be as follows: the x polymorph results when sublimation is carried out rapidly at pressures between 1 and 30 Torr; evaporation at pressures between  $10^{-1}$  and  $10^{-4}$  Torr gives mixtures of the  $\alpha$  and  $\beta$  polymorphs; evaporation at pressures less than  $10^{-4}$  Torr gives predominantly the  $\alpha$

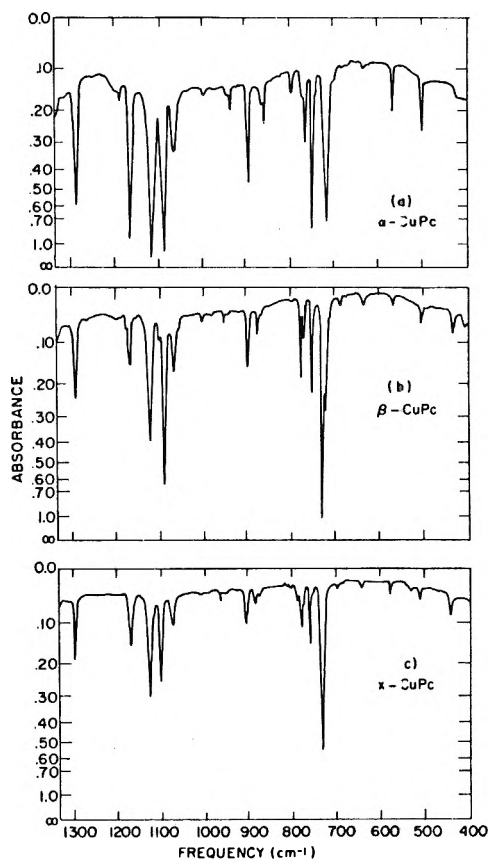


Figure 1. Infrared absorption spectra of  $\alpha$ -,  $\beta$ -, and x-CuPc films in the  $400\text{--}1300\text{-cm}^{-1}$  region.

polymorph. The x-H<sub>2</sub>Pc polymorph can also be produced by sublimation under partial vacuum and by neat milling,<sup>13</sup> but the latter preparation technique failed to produce the x-CuPc polymorph.

(2) *Spectroscopic Studies.* The room temperature infrared absorption spectra of sublimed films of the  $\alpha$ ,  $\beta$ , and x polymorphs deposited on KBr substrates were recorded with a Perkin-Elmer Model 337 spectrometer. The accuracy of the recorded infrared frequencies was  $\pm 2.0 \text{ cm}^{-1}$  throughout the  $400\text{--}1300\text{-cm}^{-1}$  region. A comparison of these infrared spectra is given in Figure 1. The X-ray powder diffraction patterns were recorded with a Phillips diffractometer employing Cu K $\alpha$  (monochromatic) radiation. The scanning speed was  $1^\circ (2\theta)/\text{min}$  and  $1^\circ$  divergence and receiving slits were used in conjunction with a  $0.006\text{-cm}$  scatter slit. The resulting X-ray diffraction patterns of the three CuPc polymorphs are shown in Figure 2.

All the electronic spectra were recorded on a Cary Model 14 automatic spectrophotometer. The absorption spectrum at room temperature of CuPc dissolved in 1-

- (4) J. M. Robertson, *J. Chem. Soc.*, 615 (1935); 1195 (1936); 219 (1937).
- (5) M. T. Robinson and G. E. Klein, *J. Amer. Chem. Soc.*, **74**, 6294 (1952).
- (6) A. N. Sidorov and I. P. Kotlyar, *Opt. Spektrosk.*, **11**, 92 (1961).
- (7) J. H. Assour, *J. Phys. Chem.*, **69**, 2295 (1965).
- (8) J. H. Sharp and R. L. Miller, *J. Phys. Chem.*, **72**, 3335 (1968).
- (9) J. W. Eastes, U. S. Patent 2,770,620 (1956).
- (10) B. I. Knudsen, *Acta Chem. Scand.*, **20**, 1344 (1966).
- (11) B. P. Brand, British Patent 912,526 (application 1960).
- (12) B. I. Knudsen and H. S. Rolskov, U. S. Patent 3,160,635 (application 1960).
- (13) J. F. Byrne and P. F. Kurz, U. S. Patent 3,357,985 (1967).
- (14) J. H. Sharp and M. Lardon, *J. Phys. Chem.*, **72**, 3230 (1968).
- (15) C. H. Griffiths and M. S. Walker, unpublished results.

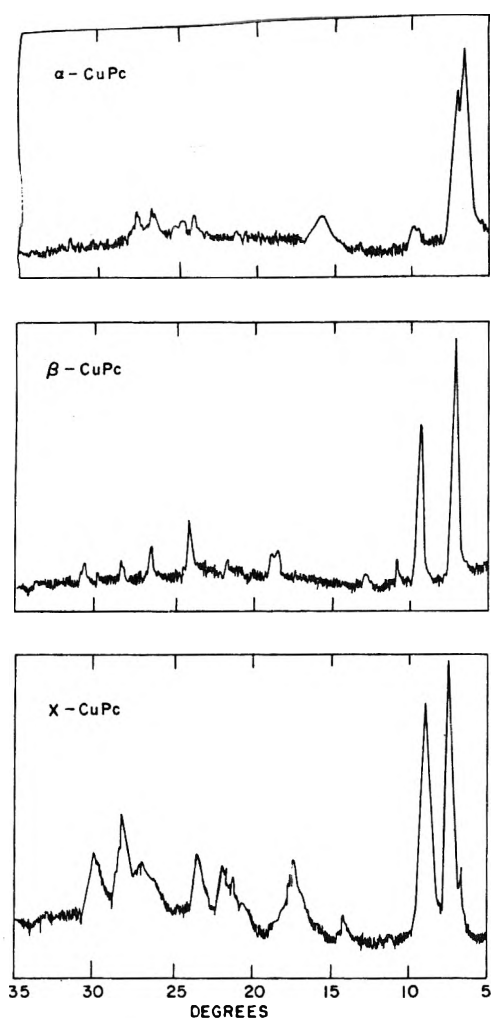


Figure 2. X-Ray diffraction spectra of  $\alpha$ -,  $\beta$ -, and  $x$ -CuPc.

chloronaphthalene is shown in Figure 3a. The absorption spectra of thin films of evaporated  $\alpha$ -,  $\beta$ -, and  $x$ -CuPc films on Pyrex substrates are shown in Figures 3a, 3b, and 3c, respectively. All the film spectra shown were recorded at room temperature. No further resolution was observed at 77°K with the  $\alpha$ - and  $\beta$ -CuPc film spectra. However, some additional structure was noted when the  $x$ -CuPc film was cooled to 77°K. Some of this material was subsequently ultrasonically dispersed in a mixture of 3-methylpentane and hexane (6:1) and the 77°K absorption spectrum of the resulting glassy matrix system is also shown in Figure 3c.

The esr spectra of the three CuPc polymorphs were obtained with an 8-mm spectrometer, which has been previously described.<sup>16</sup> Since some magnetic loading was observed for the 100% samples, diluted samples were prepared where 1 part of the  $\alpha$ ,  $\beta$ , or  $x$  polymorphs were physically mixed with 100 parts of  $\beta$ -metal-free phthalocyanine. The diluted samples showed no magnetic loading in the esr cavity and the resulting line shapes were identical with that shown in Figure 4c.

### III. Discussion

The infrared and X-ray spectra of the three polymorphs, shown in Figures 1 and 2, respectively, are quite qualitative and only very general conclusions can be drawn regarding the structure of the three CuPc poly-

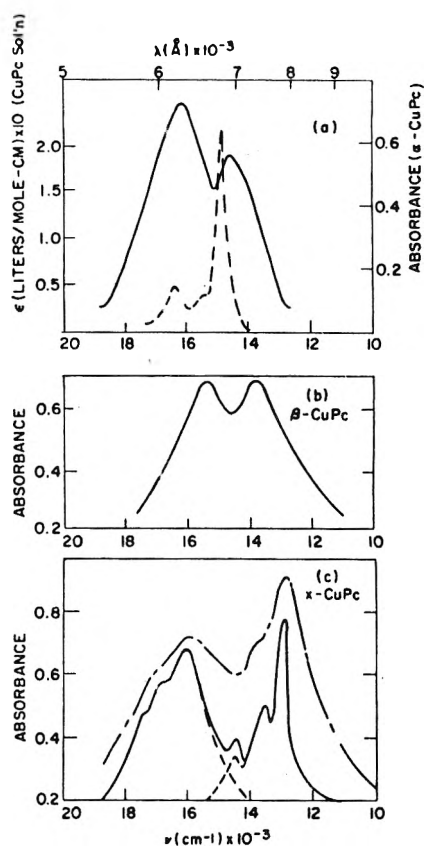


Figure 3. (a) Electronic absorption spectra of CuPc in 1-chloronaphthalene (---) and an evaporated film of  $\alpha$ -CuPc (—). (b) Electronic absorption spectrum of an evaporated film of  $\beta$ -CuPc. (c) Electronic absorption spectra of a thin evaporated film of  $x$ -CuPc (---) and a glassy dispersion of  $x$ -CuPc in 3-methylpentane-hexane (6:1) matrix at 77°K (—).

morphs. Hence, infrared and X-ray spectroscopy were used basically to characterize and define the polymorphic forms. The infrared spectra of the  $\alpha$  and  $\beta$  films, included for comparative purposes, are similar to those reported by earlier workers,<sup>6,7,10</sup> whereas that of the  $x$  film is significantly different from any previously reported polymorph. Although the three polymorphic spectra are generally similar, distinct differences among the phases are apparent. This is particularly true in the 700–800-cm<sup>-1</sup> region; the absorption frequencies are summarized in Table I. More specifically, the frequency and intensity distribution pattern of the absorption between 770 and 790 cm<sup>-1</sup> are unique for each polymorph. Since these frequencies correspond to the out-of-plane C-H bending modes of the peripheral benzene rings of the CuPc molecule, the orientation of adjacent molecules, which in turn determines the polymorphic phase, has a definite effect on these absorption frequencies. It is interesting to note that similar differences in the 700–800-cm<sup>-1</sup> region were observed in a comparison of the  $\alpha$ ,  $\beta$ , and  $x$  polymorphs of metal-free phthalocyanine.<sup>14</sup>

The X-ray diffraction patterns of the  $\alpha$ - and  $\beta$ -CuPc polymorphs are similar to those reported by Assour.<sup>7</sup> The diffraction pattern of the  $x$ -CuPc polymorph is distinctly different from those of the  $\alpha$ - or  $\beta$ -CuPc patterns. Furthermore, it is clear that these differences are not in the

(16) M. Abkowitz, I. Chen, and J. H. Sharp, *J. Chem. Phys.*, **48**, 456 (1968).

**TABLE I: Absorption Frequencies for  $\alpha$ -,  $\beta$ -, and  $\chi$ -CuPc Polymorphic Films in the 700–800- $\text{cm}^{-1}$  Infrared Absorption Region**

Polymorph	Absorption frequency, $\text{cm}^{-1}$ <sup>a</sup>							
	1	2	3	4	5	6	7	8
$\alpha$ -CuPc	724(s)		758(s)	772(m)		780(m-w)	785(w)	
$\beta$ -CuPc		731(s)	758(m)		776(w)		785(m)	
$\chi$ -CuPc		731(s)	758(m)	772(w)	778(m-w)			788(w)

<sup>a</sup> Intensities of the absorption are qualitatively described as weak (w), medium (m), or strong (s).

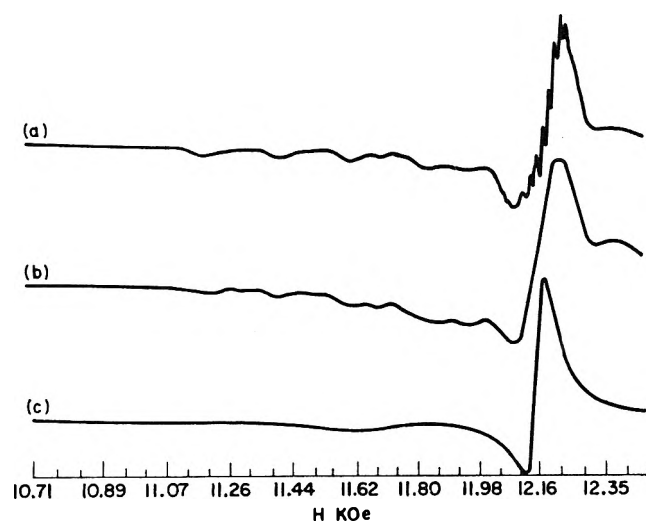


**Figure 4.** Experimental esr spectra of (a) 1 part of CuPc in 5 parts of  $\text{H}_2\text{PC}$  (1:5), (b) 1:1 sample, and (c) a sample of 100%  $\alpha$ -CuPc,  $\nu_0 = 34.74$  GHz.

degree of resolution, and that  $\chi$ -CuPc is a unique polymorph of CuPc.

The CuPc molecule has  $D_{4h}$  symmetry and the lowest allowed electronic transition is observed at 6780 Å in 1-chloronaphthalene as shown in Figure 3a. Two additional vibrational maxima, located at 6480 and 6110 Å, are also clearly evident. The former is relatively weak and appears as a shoulder on the strong (0,0) 6780-Å transition.

The absorption spectra of the  $\alpha$  and  $\beta$  polymorphic films are shown in Figures 3a and 3b, respectively. The  $\alpha$ -CuPc film shows two absorption maxima located at 6250 and 6940 Å while the  $\beta$  film shows two maxima located at 6450 and 7200 Å. For each polymorph, the two maxima are separated by approximately  $1600\text{ cm}^{-1}$ .

The double maxima observed in both the  $\alpha$ - and  $\beta$ -CuPc film spectra can be attributed to dipole-dipole excitation splitting of the 6780-Å (solution) singlet transition. In the simplest case, this splitting will result from the interaction of two molecules of a dimer. The resonance splitting,  $\Delta\epsilon(0)$ , resulting from such an interaction is observed to be  $800\text{ cm}^{-1}$  for each polymorph. For the  $\alpha$  polymorph, a crystal shift of  $480\text{ cm}^{-1}$  to the blue is observed while the  $\beta$  polymorph undergoes a  $20\text{-cm}^{-1}$  crystal shift to the red. No vibrational structure is observed in either of these film spectra.

The absorption spectrum of an evaporated film of  $\chi$ -CuPc is shown in Figure 3c. Two well-resolved absorption maxima are observed at 7820 and 6240 Å. In analogy with the proposed dimer structure of  $\chi$ -metal-free phthalocyanine,<sup>14</sup> these two transitions are compared with the 6780-Å electronic transition of the monomer (solution). The

**TABLE II: Comparison of the  $\alpha$ -,  $\beta$ -, and  $\chi$ -CuPc Film Absorption Spectra with the CuPc Solution Spectrum**

CuPc form	Absorption frequency, $\text{cm}^{-1}$			Polymorphic crystal shift, $\text{cm}^{-1}$	Observed resonance splitting, $\Delta\epsilon(0)$ , $\text{cm}^{-1}$
	$E^-$	$E^0$	$E^+$		
Solution		14,720			
$\alpha$	14,400		16,000	480	800
$\beta$	13,900		15,500	20	800
$\chi$	12,800		16,020	320	1610

**TABLE III: Correlation of the  $\chi$ -CuPc Electronic Vibrational Structure with the Solution Spectrum of CuPc**

CuPc form	Absorption maxima, $\text{cm}^{-1}$			Vibrational spacing, $\text{cm}^{-1}$	
	0,0	0,1	0,2	(0,1)-(0,0)	(0,2)-(0,0)
Solution	14,720	15,400	16,350	680	1630
$\chi$ -CuPc					
$E^-$ set	12,800	13,500	14,500	700	1700
$E^+$ set	16,000	16,650	17,500	650	1500

7820-Å absorption is red shifted  $1920\text{ cm}^{-1}$  from the monomer transition and the 6240-Å absorption is blue shifted by  $1300\text{ cm}^{-1}$ . The resonance splitting,  $\Delta\epsilon(0)$ , is therefore  $1610\text{ cm}^{-1}$ , assuming a crystal shift of  $320\text{ cm}^{-1}$  to the red, and these two absorption maxima of  $\chi$ -CuPc, designated  $E^-$  and  $E^+$ , respectively, can also be interpreted as electronic transitions. Table II compares the observed crystal shifts and resonance splittings of the  $\alpha$ -,  $\beta$ -, and  $\chi$ -CuPc polymorphs to the 6780-Å monomer transition assuming these splittings result from the dipole-dipole interaction of two molecules of a dimer.

Two additional absorption maxima are observed in the  $\chi$ -CuPc film spectrum as shoulders at 7400 and 6000 Å. In order to clarify the origin of these transitions it is helpful to consider the absorption spectrum of a dispersion of  $\chi$ -CuPc in a 3-methylpentane-hexane (6:1) glassy matrix at 77°K as shown in Figure 3c. The resulting increased resolution shows two sets of resolved maxima. The first, originating with the 7820-Å electronic transition, shows two additional, well-resolved maxima at 7400 and 6910 Å. The second set originates with the 6240-Å electronic transition and shows two shoulders at 6000 and 5700 Å. In Table III, these two sets of absorption maxima are compared with the solution absorption spectrum. The well-resolved 7820-Å dimer electronic and vibrational transition series correlates well with the solution spectrum. The resolution for the 6240-Å electronic and vibrational transition series

is not as good but the shoulder maxima correlate satisfactorily with the vibrational maxima in the solution spectrum.

The preservation of the vibrational structure of the monomer (solution spectrum) in the dimer spectrum indicates that the  $\alpha$ -CuPc polymorph can be represented by two strongly interacting molecules.<sup>17</sup> In this case the Born-Oppenheimer approximation is operative and the electronic and vibrational wave functions of the molecule are separable. The magnitude of the observed resonance splitting,  $1610\text{ cm}^{-1}$ , as opposed to  $800\text{ cm}^{-1}$  for both the  $\alpha$  and  $\beta$  polymorphs, also supports the view that the  $\alpha$  form is characterized by a much stronger dipole-dipole interaction.

In earlier work<sup>16</sup> it has been shown that when  $\alpha$ -CuPc is intimately diluted into an  $\alpha$ -H<sub>2</sub>Pc matrix (corresponding to 1 part of  $\alpha$ -CuPc to 100 parts of  $\alpha$ -H<sub>2</sub>Pc, for example) intramolecular copper-nitrogen superhyperfine splittings are observed in the esr spectra. In the current work, identical spectra were observed when intimately diluted samples of  $\beta$ -CuPc in  $\beta$ -H<sub>2</sub>Pc or  $\alpha$ -CuPc in  $\alpha$ -H<sub>2</sub>Pc (1:100) were prepared. Hence no information concerning intermolecular interactions in the three polymorphs was obtained from intimately mixed magnetically dilute samples.

Alternatively, esr spectra of 100% CuPc do not show detailed hyperfine structures. This is also true when samples of  $\alpha$ -,  $\beta$ -, or  $\alpha$ -CuPc are physically diluted with  $\beta$ -H<sub>2</sub>Pc (1:100). In this case, a composite or envelope line shape is determined by the combined effects of  $g$  factor anisotropy, unresolved hyperfine structure, and the interactions between the copper centers themselves. Since no appreciable  $g$  factor variations were observed in dilute samples of  $\alpha$ -,  $\beta$ -, and  $\alpha$ -CuPc polymorphs and identical intramolecular hyperfine interactions were observed, any differences in the esr spectra of the concentrated polymorphs must reflect some variations in the intermolecular copper-copper interactions.

A study of the effects of intermolecular exchange on the esr envelope line shape of copper phthalocyanine-metal-free phthalocyanine solid solutions has been reported recently.<sup>18</sup> In this study of series of solid solutions were pre-

pared in which the concentration of copper phthalocyanine in metal-free phthalocyanine was progressively increased. The changes observed as a function of increasing copper phthalocyanine concentration are illustrated in Figure 4 for  $\alpha$  solid solutions. One observes both the coalescence of the four low-field copper hyperfine peaks into a single weak low-field peak and the disappearance of resolvable nitrogen superhyperfine structure at high field. The strong high-field absorption is itself observed to undergo narrowing with increasing copper phthalocyanine concentration so that the separation between its minimum and maximum points is 145 Oe in (a)(1:5), 127 Oe in (b)(1:1), and 60 Oe in (c)100%  $\beta$ -CuPc. For both 100%  $\beta$ - and  $\alpha$ -copper phthalocyanine the envelope line shape resembles the one obtained for 100%  $\alpha$ -CuPc, shown in Figure 4c, but the separation between minimum and maximum points on the high-field absorption is 44 Oe for  $\beta$ -CuPc and 35 Oe for  $\alpha$ -CuPc. The changes illustrated in the envelope esr line shapes shown in Figure 4 result from the tendency of the intermolecular copper exchange interaction to effectively average the local hyperfine fields.<sup>19</sup> That is, there is a decrease with increasing copper phthalocyanine concentration, and therefore stronger intermolecular exchange, in the phenomenological copper hyperfine and nitrogen superhyperfine coupling constants. Our esr results therefore show that the intermolecular exchange interaction is strongest in the  $\alpha$ - and weakest in the  $\beta$ -copper phthalocyanine polymorph and this in turn is consistent with the hypothesis that the  $\alpha$  polymorph can be represented by two strongly interacting molecules.

*Acknowledgments.* We wish to acknowledge M. Bailey and R. L. Miller for their assistance in performing part of the experimental work. The authors wish to thank Drs. G. E. Johnson, A. R. Monahan, and D. L. Stockman for several helpful discussions. We wish to thank Dr. P. Chérin for supplying our X-ray data.

(17) M. Kasha, *Radiat. Res.* **20**, 55 (1963).

(18) M. Abkowitz and I. Chen, *J. Chem. Phys.*, **54**, 811 (1971).

(19) D. Kivelson, *J. Phys. Chem.*, **27**, 1087 (1957).

## $C\pi \rightarrow \pi^*$ Transition. III.<sup>1,2</sup> Experimental and Theoretical Verification of the Assignment

John C. Nnadi,\* Allen W. Peters,

*Mobil Research and Development Corporation, Paulsboro, New Jersey 08066*

and Shih Yi Wang

*Department of Biochemistry, The Johns Hopkins University, School of Hygiene and Public Health, Baltimore, Maryland 21205*  
(Received July 28, 1972)

*Publication costs assisted by the Mobil Research and Development Corporation*

The  $\lambda_{\max}$  and  $\epsilon_{\max}$  of the  $C\pi \rightarrow \pi^*$  transitions in the anionic forms of diethyl uracil-1-malonate, diethyl 5-methyluracil-1-malonate, diethyl 5-bromouracil-1-malonate, and diethyl 5-nitrouracil-1-malonate have been measured. Values obtained were 253 (16,500), 259 (17,000), 257 (23,000), and 255 nm (28,000), respectively, for the above compounds. Unlike the  $\pi \rightarrow \pi^*$  transition which showed a 35-nm bathochromic shift in going from C(5)-H to C(5)-NO<sub>2</sub>, the position of the  $C\pi \rightarrow \pi^*$  band was relatively constant. Extended Hückel MO calculations were used to rationalize the constancy of the  $C\pi \rightarrow \pi^*$  band. The results of the calculations showed that the energy of the lowest  $\pi^*$  orbital of uracil was nearly independent of the C(5) substituent, and that the symmetry of the lowest  $\pi^*$  orbital in all cases was essentially similar to that of the pyrimidine ring with small orbital coefficients at C(5) suggesting a near node there. This could explain why the  $C\pi \rightarrow \pi^*$  transitions, like the  $n \rightarrow \pi^*$  transitions of pyrimidine, are relatively insensitive to substitution at C(5). Finally, by shifting the  $\pi \rightarrow \pi^*$  transition to the red the  $C\pi \rightarrow \pi^*$  band was distinctly observed for the 5-bromouracil and 5-nitrouracil compounds as opposed to the case for the uracil and 5-methyluracil compounds where the two bands overlapped.

### Introduction

In two previous reports<sup>1,2</sup> the occurrence of a new transition in the uv spectra of the anionic forms of *N*-malonic esters of heteroaromatic compounds and of phenyl- and substituted phenylmalonic esters was documented. The notation of  $n_C \rightarrow \pi^*$  was used initially but was later changed to  $C\pi \rightarrow \pi^*$  in order not to confuse it with the familiar  $n \rightarrow \pi^*$  transitions.<sup>3</sup> It was suggested that this new transition involves excitation of an electron of the malonate moiety to the  $\pi^*$  orbital of the aromatic or heteroaromatic ring. This is because reasonable resonance structures delocalizing the electron pair of malonate anion are possible only within the malonate moiety and thus the two moieties do not interact appreciably in the classical sense. However, since the  $\pi$  orbital systems of the malonate and heteroaromatic are close together, interactions across space may occur and lead to typical intramolecular charge transfer transitions rather than to the bathochromic shifts expected if resonance is important.

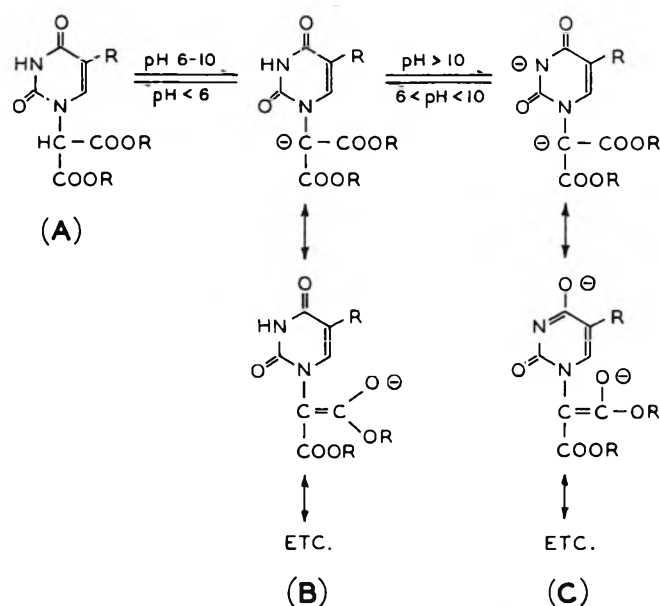
This would mean that the  $C\pi \rightarrow \pi^*$  transitions are quite similar to the  $n \rightarrow \pi^*$  transitions in pyrimidine where the excitation is from a nonbonding orbital of a heteroatom to a  $\pi^*$  orbital of the ring. Fortunately, the pyrimidine system is ideal for studies of electronic transitions similar to  $n \rightarrow \pi^*$ , since substituent effects on its  $n \rightarrow \pi^*$  transitions have been extensively studied by Mason.<sup>4</sup> Thus, an examination of the effects of substituents at the C(5) position on the  $C\pi \rightarrow \pi^*$  charge transfer transition could have a double significance. First, the  $C\pi \rightarrow \pi^*$  band may be shifted to a different degree than the  $\pi \rightarrow \pi^*$  band, allowing the separation of the  $C\pi \rightarrow \pi^*$  from the  $\pi \rightarrow \pi^*$  band in some C(5)-substituted uracil malonic esters. These two bands overlapped in the spectra of the

diethyl uracil-1-malonate anion. Secondly, the transition can be used as a probe to study the effects of substitution on the  $\pi^*$  orbital of these pyrimidine derivatives. We would like to report the results of experimental and theoretical studies of C(5)-substituted diethyl uracil-1-malonates which not only support and strengthen the previous assignment, but also suggest that the lowest  $\pi^*$  orbital of these substituted uracils has nearly the symmetry of the same orbital in pyrimidine.

### Results and Discussion

Represented in Figure 1 are the possible tautomeric structures<sup>5</sup> of these *N*-malonic esters of uracil and its C(5) derivatives. The pH regions shown in the figure are those where the neutral (A), monoanionic (B), and dianionic (C) forms exist for the uracil and the 5-methyluracil derivatives. The pH regions are expected to be lower by about one or more units for the corresponding species of the 5-bromouracil and the 5-nitrouracil compounds. The  $C\pi \rightarrow \pi^*$  transition did not occur in the neutral form (at pH <6.5) for diethyl uracil-1-malonate, but it occurred with the same intensity in both the mono- and the dianionic forms, Figure 2. Thus at pH >10, the relative ratio of mono- to dianionic forms present for the above

- (1) J. C. Nnadi and S. Y. Wang, *J. Amer. Chem. Soc.*, **92**, 4421 (1970).
- (2) J. C. Nnadi, A. W. Peters, and S. Y. Wang, *J. Amer. Chem. Soc.*, **94**, 712 (1972).
- (3) J. Sidman, *Chem. Rev.*, **58**, 689 (1958).
- (4) S. F. Mason in "Physical Methods of Heterocyclic Chemistry," Vol. II, A. R. Katritzky, Ed., Academic Press, New York, N. Y., 1963, pp 20-35 and references therein.
- (5) D. J. Brown, E. Hoerger, and S. F. Mason, *J. Chem. Soc.*, 211 (1955); D. J. Brown, *Rev. Pure Appl. Chem. (Australia)*, **3**, 115 (1953).

Figure 1. Tautomeric equilibria of *N*-malonic esters of pyrimidines.TABLE I: Uv  $\lambda_{\max}$  (nm) of  $\pi \rightarrow \pi^*$  Transitions of N(1)-Methyl- and N(1)-Diethylmalonate of C(5)-Substituted Uracils (Neutral Form A)

Compd	N(1)CH <sub>3</sub>	N(1)CH(COOC <sub>2</sub> H <sub>5</sub> ) <sub>2</sub>
C(5)H	262 (9.6)	260 (10.1)
C(5)CH <sub>3</sub>	268 (7.4)	267 (10.3)
C(5)Br	283 (8.7)	281 (8.2)
C(5)NO <sub>2</sub>	310 (11.4)	298 (11.1)
	240 (8.2)	237 (8.0)

TABLE II: C $\pi \rightarrow \pi^*$  Charge Transfer Spectra of N(1)-Diethylmalonate of C(5)-Substituted Uracils (Anionic Form C)

Compd	$\lambda_{\max}$ , nm	$10^{-3}\epsilon_{\max}^a$	pH <sup>b</sup>
C(5)H	253	16.5	10
C(5)CH <sub>3</sub>	259	17.1	10
C(5)Br	257	23.6	11
C(5)NO <sub>2</sub>	255	28.0	11

<sup>a</sup> Corrected for absorption of neutral form at the respective wavelength. <sup>b</sup> Approximate pH where maximum effect occurred.

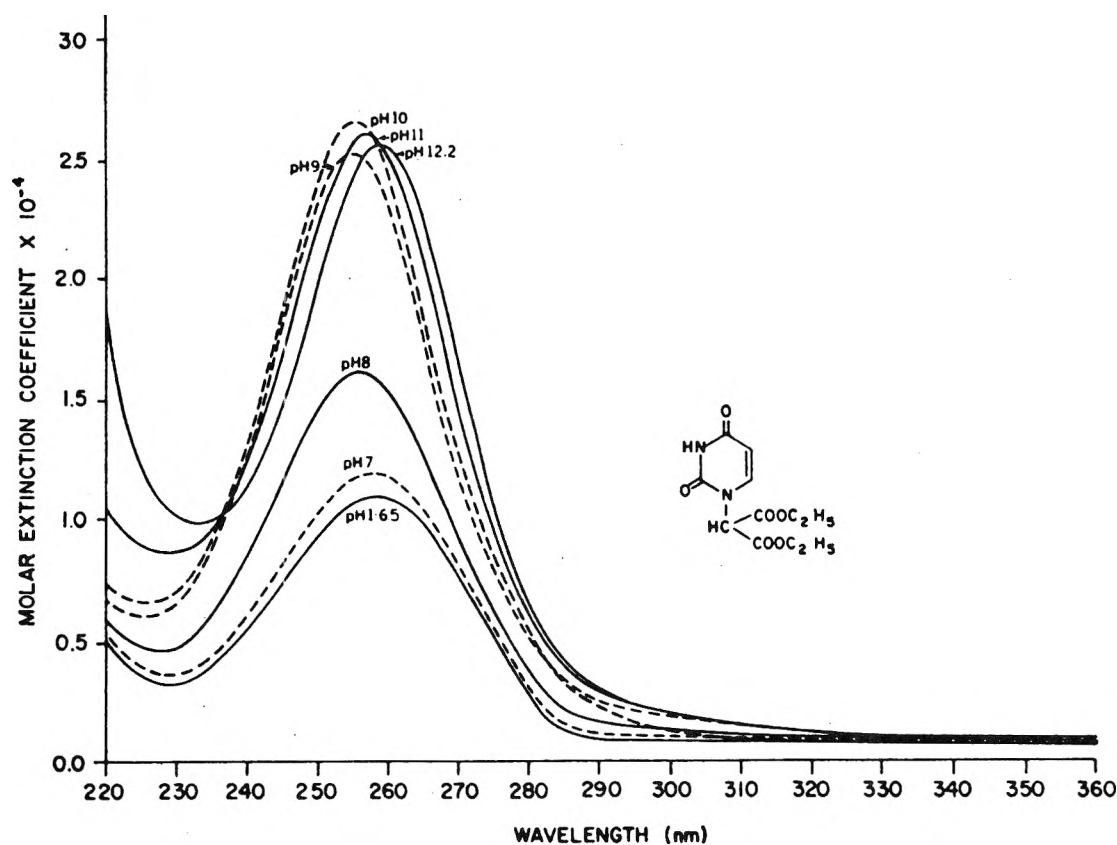


Figure 2. Uv spectra of diethyl uracil-1-malonate.

compounds should not significantly affect their  $\lambda_{\max}$  and  $\epsilon_{\max}$ . Spectral data reported in this paper for the  $\lambda_{\max}$  and  $\epsilon_{\max}$  of C $\pi \rightarrow \pi^*$  transition were obtained at the pH where maximum change occurred.

From Figure 1, it may also be seen that the electron pair of the monoanion can be classically delocalized only on the malonate moiety. Likewise when anion formation at N(3) occurs in the dianionic form, the electron pair can be classically delocalized only on the uracil ring. Thus, though bonded, the  $\pi$  systems of the two moieties do not

interact in the classical sense. This may explain why we did not see the substantial spectral shifts which would be expected if resonance interactions linked the two moieties.

Shown in Table I are the spectral parameters of various C(5)-substituted diethyl uracil-1-malonates in pH 2 buffered solution where the neutral form<sup>6</sup> (structure A, Figure 1) is important. These spectra are mainly due to  $\pi \rightarrow \pi^*$

(6) Protonation of the rings probably occur in  $>1N$  H<sub>2</sub>SO<sub>4</sub>.



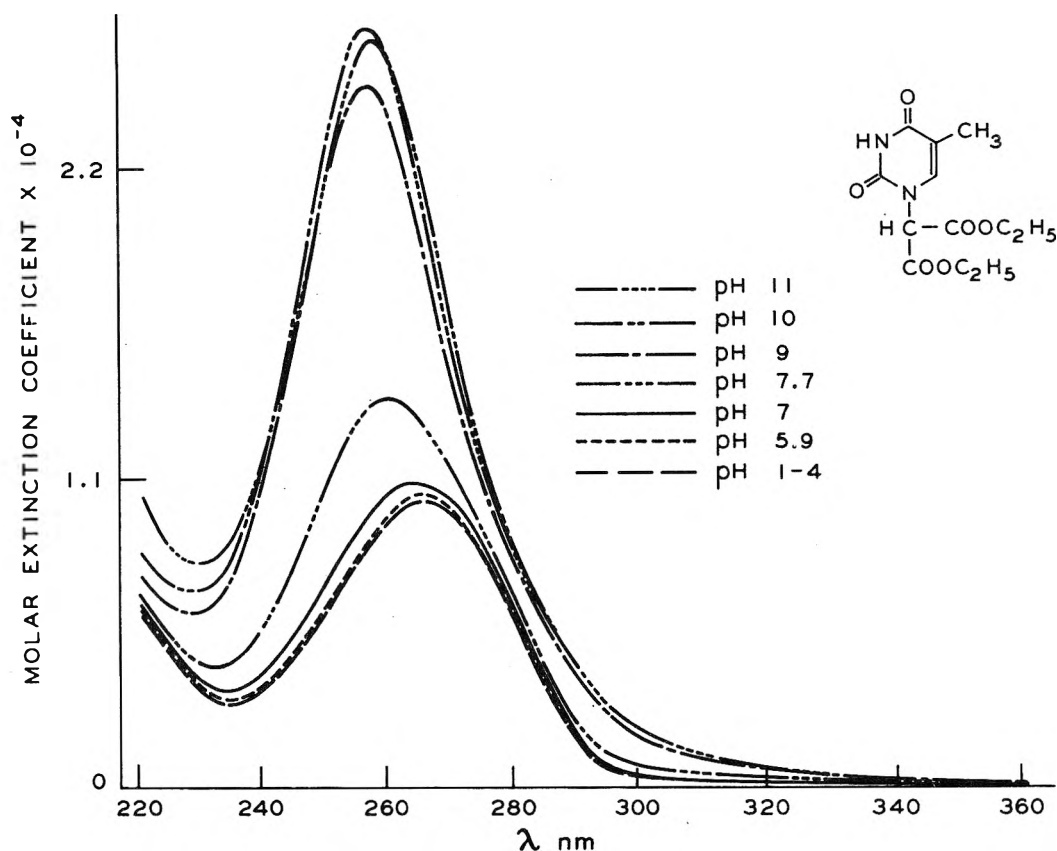


Figure 3. Uv spectra of diethyl 5-methyluracil-1-malonate.

transitions.<sup>7</sup> From this table it is seen that the neutral malonic ester substituent has essentially the same effect on the spectra of these compounds as does a simple alkyl substituent, *e.g.*, a methyl group. Thus, it is unlikely that there are any significant interactions between the two  $\pi$ -orbital systems in the neutral forms, as this would result in significant hyperchromism and possibly bathochromic shifts.

The spectra of diethyl 5-methyluracil-1-malonate (Figure 3) show about a 2.5-fold hyperchromism with an 8-nm hypsochromic shift in going from pH 2 to 11 buffered aqueous solutions. The results are similar to those in Figure 2, and this suggests that the same effects operate for both compounds. Again, the lower intensity ( $\pi \rightarrow \pi^*$  and  $n \rightarrow \pi^*$ ) normal absorption bands of the neutral form<sup>7</sup> are buried under the new intense  $C\pi \rightarrow \pi^*$  transition.

The spectra of diethyl 5-bromouracil-1-malonate (Figure 4) show the presence of the two distinct transitions. Its spectra at pH 7 and 7.7 clearly show the  $C\pi \rightarrow \pi^*$  transition,  $\lambda_{\max} \sim 258$  nm and the  $\pi \rightarrow \pi^*$  bands at  $\lambda_{\max} \sim 280$  nm. The intensity of the  $C\pi \rightarrow \pi^*$  transition continues to increase with pH up to a maximum of  $2.3 \times 10^4$  at pH 11 while that of the  $\pi \rightarrow \pi^*$  transition decreases slightly. The new intense band was not observed in the spectra of 5-bromouracil, 1-methyl-5-bromouracil, and 1,3-dimethyl-5-bromouracil from pH 1 to 14 and it is unlikely that the bromo group is directly involved. It is interesting to point out that substitution of the bromo group at C(5) sufficiently shifted the  $\pi \rightarrow \pi^*$  band to the red to make the  $C\pi \rightarrow \pi^*$  band clearly distinguishable.

The anionic form of diethyl 5-nitrouracil-1-malonate (Figure 5) also shows the  $C\pi \rightarrow \pi^*$  transition distinctly at about 255 nm in addition to spectral changes at 240 nm

and from 290 to 360 nm. The changes at 240 nm and from 290 to 360 nm are also observed in the spectra of compounds such as 1,3-dimethyl-5-nitrouracil and *N,N*-dimethyl-2,4-dinitroaniline<sup>2</sup> in basic solutions and are typical of nitroaromatic compounds. In contrast, the new band at 250 to 260 nm is clearly missing in the spectra of these nonmalonic ester substituted nitroaromatics. But, since it is observed in the uv spectra of the anionic forms of nitroaromatic malonates, such as diethyl *p*-nitroanilino-malonate<sup>2</sup> and diethyl 5-nitrouracil-1-malonate, and of the *N*-malonic ester derivatives of uracils and other heteroaromatic compounds<sup>1,2</sup> a general mechanism involving charge transfer interaction between the malonate anion (donor) and the heteroaromatic moieties (acceptor) seems to be operating.

The experimental results are summarized in Table II where the values of  $\lambda_{\max}$  and  $\epsilon_{\max}$  for the  $C\pi \rightarrow \pi^*$  bands of the various C(5)-substituted uracils are listed. The  $\lambda_{\max}$  of this new transition is relatively insensitive to substitution at C(5) but its  $\epsilon_{\max}$  increased in order  $-H < CH_3 < -Br < -NO_2$ . This is contrary to the behavior of the  $\pi \rightarrow \pi^*$  transitions which show about a 35-nm bathochromic shift in the same direction but with little increase in intensity (Table I).

The lack of shift in the  $C\pi \rightarrow \pi$  band with substitution at C(5) is similar to the results Mason<sup>4</sup> obtained for  $n \rightarrow \pi$  transitions in pyrimidine. These results suggest that the lowest  $\pi^*$  orbital of these substituted pyrimidines, as in pyrimidine, have small or zero coefficients at C(5). Thus carbonyl groups at C(2) and C(4) do not appear to have

(7) See M. Kasha in "Light and Life," W. D. McElroy and B. Glass, Ed., Johns Hopkins Press, Baltimore, Md., 1961, pp 31-67.

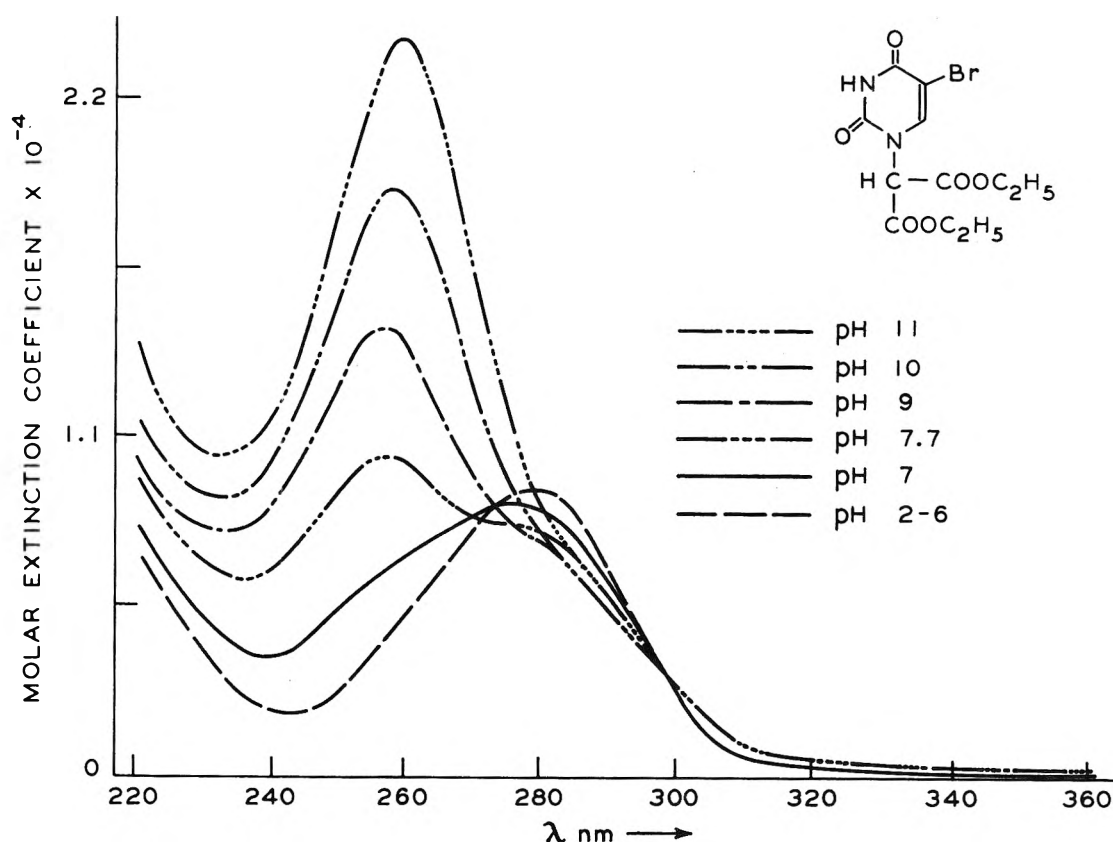


Figure 4. Uv spectra of diethyl 5-bromouracil-1-malonate.

altered the symmetry of the lowest  $\pi^*$  orbital of pyrimidine appreciably.

In order to test this possibility, a version of extended Hückel MO procedure<sup>8,9</sup> was used to obtain molecular orbitals and energies of pyrimidine, uracil, and its C(5) methyl, bromo, and nitro derivatives. The parameters used in the calculations are those given by Basch, *et al.*<sup>10</sup> Assumed structures were obtained from the Tables of Interatomic Distances<sup>11</sup> and the off-diagonal elements were computed from the relations

$$H_{ij} = S_{ij}(H_{ii} + H_{jj})$$

Listed in Table III are the energies of the frontier orbitals for these compounds, where  $E_{hi}$  is the energy of the highest occupied orbital and  $E_{lo}$  is the energy of the lowest unoccupied orbital. From this table it may be seen that  $E_{hi}$  varies appreciably while  $E_{lo}$  does not. Thus the shifts in their  $\pi \rightarrow \pi$  transitions (*i.e.*,  $E_{hi} \rightarrow E_{lo}$ ) is mainly due to differences in the energy of their highest occupied orbital,  $E_{hi}$ . Calculated values of  $\lambda$  for  $\pi \rightarrow \pi$  transition agree reasonably well with experimental values and the predicted shifts are in the right order. Our results are comparable to those of others.<sup>12-14</sup>

The fact that  $E_{lo}$  for these compounds did not vary would suggest that transitions from a nonbonding orbital, such as a C $\pi$  of the malonate, to the lowest  $\pi^*$  orbital of these C(5)-substituted uracils should occur at about the same wavelength. This is indeed what was observed (Table II).

Our MO calculations yielded very low values for the orbital coefficients at C(5) for the lowest  $\pi^*$  orbital and would support our earlier suggestion of a near node at C(5). The orbital coefficients of the lowest  $\pi^*$  orbital at

the various positions for the C(5)-substituted uracils and uracil-1-malonates were similar in magnitude and sign to those we obtained for the lowest  $\pi^*$  orbital of pyrimidine, again supporting our earlier suggestion that for these 2,4-dioxypyrimidines the  $\pi^*$  orbitals have the same symmetry as the same orbital in the parent compound, pyrimidine. If these results are indeed correct, then Mason's<sup>4</sup> rationalization of the apparent lack of effect of substitution of electron-donating or electron-withdrawing groups at C(5) on the  $n \rightarrow \pi^*$  transition in pyrimidine can be used to strengthen the C $\pi \rightarrow \pi^*$  assignment.

In the case of 5-nitrouracil, the lowest unoccupied orbital ( $-9.1$  eV) is primarily on the nitro group, while the next lowest unoccupied orbital ( $-7.3$  eV) is primarily on the uracil ring and thus corresponds to orbitals of similar energy in uracil and its other derivatives studied. Thus, it is consistent with the experiment in that this new transition was observed for the nitro compound in the same wavelength region as for the others.

Though all the above results support the view that the C $\pi \rightarrow \pi^*$  transition occurs between two weakly interacting  $\pi$  systems, it seemed worthwhile to us to carry out MO calculations of an isolated malonate and a malonate sub-

- (8) R. Hoffmann, *J. Chem. Phys.*, **39**, 1397 (1963); **40**, 3247, 2474, 2480 (1964). The Program was received from Dr. L. S. Bartell.
- (9) E. C. Clementi and D. C. Raimondi, *J. Chem. Phys.*, **38**, 2686 (1963).
- (10) H. Basch, A. Viste, and H. B. Gray, *Theor. Chim. Acta.*, **3**, 438 (1965).
- (11) "Tables of Interatomic Distances and Configurations in Molecules and Ions," *Chem. Soc., Spec. Publ.*, No. 11 (1958); No. 18 (1965).
- (12) H. Berthod, H. C. Geissrer-Prettre, and A. Pullman, *Int. J. Quantum Chem.*, **1**, 123 (1967), and references therein.
- (13) A. Pullman and B. Pulman, *Advan. Quantum Chem.*, **4**, 267 (1969).
- (14) F. Jordan and B. Pullman, *Theor. Chim. Acta.*, **9**, 242 (1968).

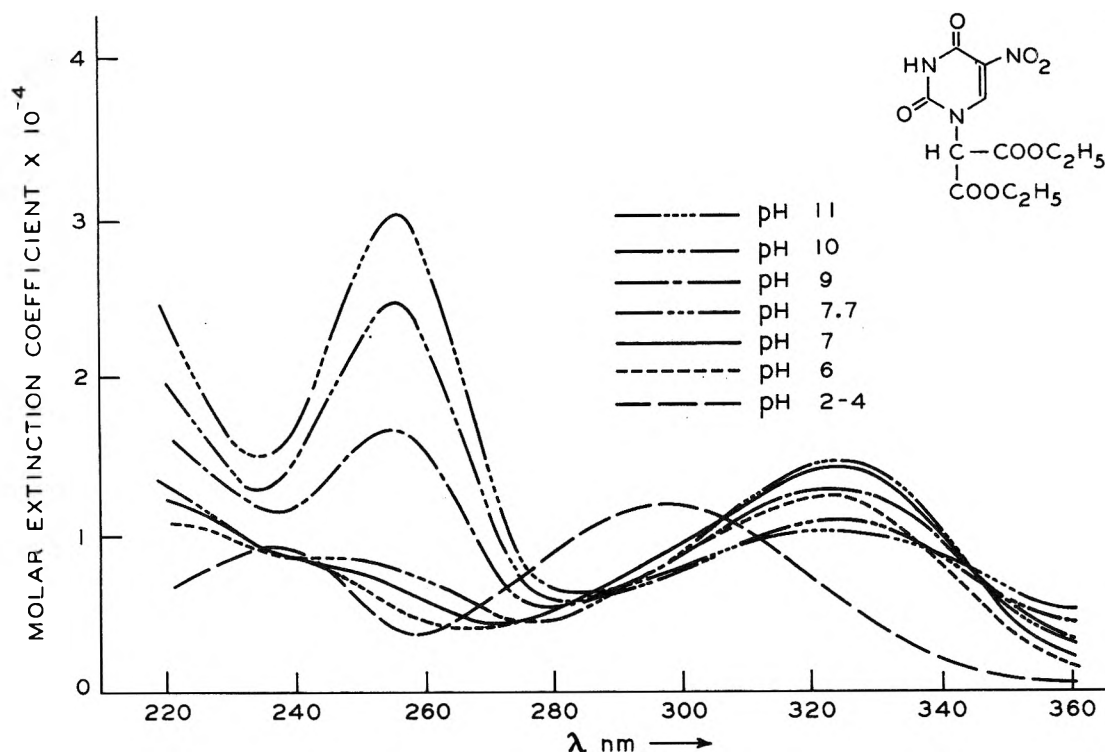


Figure 5. Uv spectra of diethyl 5-nitrouracil-1-malonate.

stituted on the N(1) position of the pyrimidine ring. Attempts to include the diethyl malonate moiety in this series of calculations is complicated by some structural uncertainties. Although one might expect the diethyl malonate to be planar, it cannot be coplanar with the uracil ring since this would require a nonbonded O...O distance of 1.56 Å. There are numerous other possibilities. Three of these are, first, the diethyl malonate may be planar but twisted out of the plane of the uracil ring; second, the diethyl malonate may be coplanar with the ring except for the interacting  $-\text{COOC}_2\text{H}_5$  group which may be twisted out of the molecular plane; or third, the diethyl malonate may exist in a number of nonplanar configurations. Complicating the above are the inherent limitations in applying the Hückel procedure to charged species.<sup>15</sup> Calculations to examine all possibilities would be prohibitive. In spite of the problems involved, it seemed reasonable to try to estimate the degree of interaction between the  $\pi$  systems of the uracil and the planar diethyl malonate anion. Experimentally no shifts were observed in the  $\pi \rightarrow \pi^*$  bands when going from the neutral to the anionic forms, implying that the  $\pi$  systems are weakly interacting and give rise only to a charge transfer type of effect. Calculations were carried out on the planar malonic acid anion (as the diacid rather than as the ethyl ester for the sake of convenience), 1-methyluracil, and the uracil-1-malonic acid anion, in which the malonic acid anion moiety was planar and  $45^\circ$  from coplanarity with the uracil ring. From the results shown in Table IV, it may be seen that the energy levels of uracil-1-malonic acid are essentially the sum of the levels calculated for 1-methyluracil and the malonic acid anion separately. This suggests that the malonate and the uracil  $\pi$  systems are relatively isolated and that spectral shifts are not expected in going from the neutral to the anionic forms, in agreement with the experimental results.

Electron distributions for uracil, malonic acid anion,<sup>16</sup> and the anion of uracil-1-malonic acid obtained from our MO calculations are shown in Figure 6. They are comparable to results obtained for uracil by others<sup>12-14</sup> and indicate that the most noticeable changes in charge distribution in going from the components to uracil-1-malonate are localized at  $>\text{N}(1)-\text{C}<$ . Also, it may be seen that the net charge on the pyrimidine moiety,  $z_p$ , is  $-0.20$  while that on the malonate moiety,  $z_m$ , is  $-0.80$ , and that the charge distribution on the malonate (Figure 6B) remained largely unchanged in its uracil derivative (Figure 6C). This is consistent with the fact that there is no appreciable resonance delocalization of the charge of the malonate anion to the pyrimidine ring as shown experimentally by the lack of bathochromic spectral shifts.

The possibility that the  $\text{C}\pi \rightarrow \pi^*$  band might be a  $\pi \rightarrow \pi^*$  malonate transition was discarded because the band was not observed in solutions of acetamidomalonic or bromomalonic at more than ten times the concentration reported above.<sup>1</sup> It is unlikely that substituting the uracil ring in the malonic ester could enhance the intensity of the  $\pi \rightarrow \pi^*$  malonate transition sufficiently to be observed as the new, intense band reported here. Also, the differences in the values of  $\lambda_{\text{max}}$  and  $\epsilon_{\text{max}}$  for the  $\text{C}\pi \rightarrow \pi^*$  transitions in *N*-malonic esters of heteroaromatic compounds and in phenylmalonic esters<sup>2</sup> are inconsistent with the suggestion that the new band is due to a  $\pi \rightarrow \pi^*$  transition in the malonate moiety.

### Conclusion

Experimental results show that the position of  $\lambda_{\text{max}}$  of the newly identified  $\text{C}\pi \rightarrow \pi^*$  transition in the anionic

(15) M. J. S. Dewar in "Molecular Orbital Theory of Organic Chemistry," McGraw-Hill, New York, N. Y., 1969.

(16) The ethyl group of the ester is not expected to significantly alter the electron distribution of the malonate moiety.

TABLE III: Electronic Transition Energies of C(5)-Substituted Uracil-1-malonic Esters and Malonate Anion

Compound	$E_{H1}$ , eV	$E_{I0}$ , eV	Calculated energies, eV		Observed $\lambda_{max}$ , nm	
			$\pi \rightarrow \pi^*$	C $\pi \rightarrow \pi^*$	$\pi \rightarrow \pi^*$	C $\pi \rightarrow \pi^*$
Uracil	-12.82	-7.52	5.30 (234) <sup>b</sup>	4.91 (253) <sup>b</sup>	260	253
5-Methyluracil	-12.22	-7.46	4.76 (261)	4.97 (250)	268	257
5-Bromouracil	-11.39	-7.44	3.95 (318)	4.99 (249)	281	259
5-Nitrouracil	-12.96	-9.15 <sup>a</sup>	5.64 (221)		237	
		-7.32	3.81 (326)	5.11 (243)	297	255
Malonate anion	-12.43	-7.07	5.33			

<sup>a</sup> Orbital centered on the NO<sub>2</sub> group. <sup>b</sup> Figures inside the parentheses are the corresponding wavelengths (nm).

TABLE IV: Energy Values Obtained by Extended Hückel MO Calculations for the Anion of Malonic Acid, 1-Methyluracil, and the Anion of Uracil-1-malonic Acid (see Figure 6)

Malonic acid anion	1-Methyluracil	Anion of uracil-1-malonic acid	Type of orbital <sup>a</sup>
$E_{I0}$ (eV) of Lowest Unoccupied Orbitals			
	-5.91	-5.91	$\pi_{pyr}$
-7.07		-7.06	$\pi_{mal}$
	-7.49	-7.48	$\pi_{pyr}$
$E_{H0}$ (eV) of Highest Occupied Orbitals			
-12.40		-11.33	$\pi_{mal}$
	-12.58	-12.64	$\pi_{pyr}$
	-13.08	-12.99	$\sigma_{pyr}$
-13.75			$\sigma_{pyr}$
	-13.79	-13.81	$\pi_{pyr}$
	-14.03	-14.07	$\sigma_{pyr}$
	-14.35	-14.32	$\sigma_{pyr}$
-14.81		-15.00	$\sigma_{mal}$

<sup>a</sup> Pyr = pyrimidine; mal = malonate.

form of diethyl uracil-1-malonnate is not affected by substitution of -CH<sub>3</sub>, -Br, and -NO<sub>2</sub> groups at C(5) of the uracil ring, but the intensity is almost doubled in going from the C(5)-H to the C(5)-NO<sub>2</sub> compound. In contrast, the  $\pi \rightarrow \pi^*$  transitions showed about 35-nm bathochromic shift with little change in intensity in the same direction. This allowed the separation of the two transitions in the C(5)-Br and the C(5)-NO<sub>2</sub> compounds which are overlapped in the C(5)-H and the C(5)-CH<sub>3</sub> compounds. The lack of shift in the  $\lambda_{max}$  of the new transition has been interpreted as due to relatively small  $\pi^*$  orbital coefficients at C(5), suggesting that the lowest  $\pi^*$  orbital has a near node there. This interpretation is supported by the results of extended Hückel calculations. The C $\pi \rightarrow \pi^*$  transition can be considered similar to  $n \rightarrow \pi^*$  transitions, since both involve the excitation of an electron from a nonbonding orbital (C $\pi$  malonnate is nonbonding with respect to the pyrimidine ring) to the  $\pi^*$  orbital. Finally it is pointed out the effects of substitution at C(5) of the pyrimidine ring on both the newly identified C $\pi \rightarrow \pi^*$  and the  $n \rightarrow \pi^*$  transitions are similar and that the same rationalizations are applicable to both.

### Experimental Section

**Uv Spectra.** All uv spectra were obtained at room temperature from freshly prepared solutions (0.03 mM)<sup>17</sup> of these compounds in the appropriate buffer solutions in a Cary 14 spectrophotometer using 1-cm cells. The buffer

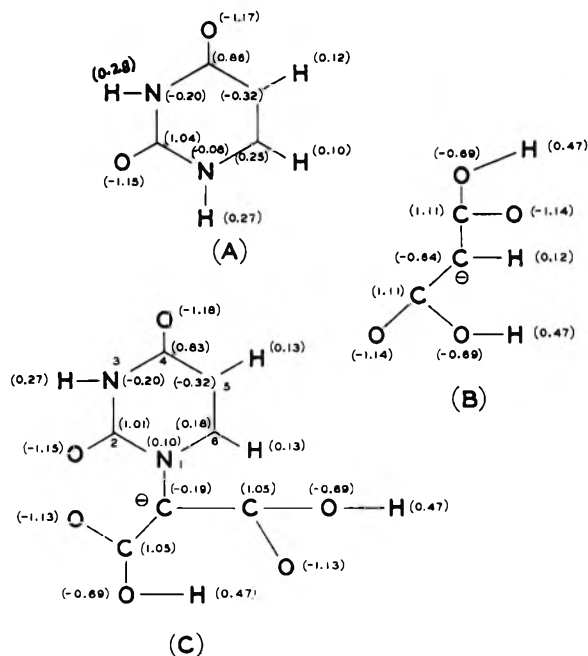


Figure 6. Electron distribution from MO calculations for (A) uracil, (B) anion of malonic acid, and (C) anion of uracil-1-malonic acid.

system, which has been previously described,<sup>1</sup> was used as a solvent and reference.

**Melting Points.** Melting points were obtained in a Fischer-Johns melting point apparatus and are uncorrected.

**Elemental Analysis.** Elemental analyses were performed at Mobil Research and Development Laboratory, Paulsboro, N. J.

**Nmr Spectra.** Nmr spectra were obtained in a Varian A60 nmr spectrometer using (CD<sub>3</sub>)<sub>2</sub>SO as a solvent.

**Synthesis. Diethyl Uracil-1-malonnate (I).** The synthesis of this compound has been previously reported.<sup>1</sup>

**Diethyl 5-Methyluracil-1-malonnate (II).** The reaction of stoichiometric amounts of monopotassium salt of 5-methyluracil and diethyl bromomalonate in DMF as described for compound I resulted in a 75% yield of compound II. It was recrystallized to constant melting point (88°) from absolute ethanol: *m/e* (mass spectrum) 284. *Anal.* Calcd for C<sub>12</sub>H<sub>16</sub>N<sub>2</sub>O<sub>6</sub>: C, 50.70; H, 5.63; N, 9.85. Found: C, 50.89; H, 5.59; N, 9.97.

(17) Since these compounds may be unstable on prolonged storage in highly basic solutions, spectral determinations were usually made within 5 min of preparation of the fresh solutions.

*Diethyl 5-Nitrouracil-1-malonate (III).* 5-Nitrouracil (3.9 g, 0.025 M) was introduced in a round-bottomed flask containing about 250 ml of DMF at 40–50° and equipped with a condenser bearing a drying tube and magnetic stirrer. After the nitrouracil had dissolved, 2.1 g (0.025 M) of NaHCO<sub>3</sub> was added and the solution was allowed to stir at the above temperature for about 1 hr. Upon addition of 6 g (0.025 M) of diethyl bromomalonate, and allowing the reaction to proceed for about 8 hr, the solvent was removed by distillation under reduced pressure under nitrogen atmosphere and the residue cooled to room temperature. The residue was extracted twice with 25 ml of ice-cooled distilled water and dried in air; the yield was 7.5 g (~90%). It was recrystallized to constant melting point (178°) from absolute ethanol: *m/e* (mass spectrum) 315. *Anal.* Calcd for C<sub>11</sub>H<sub>13</sub>N<sub>3</sub>O<sub>8</sub>: C, 41.91; H, 4.12; N, 13.33. Found: C, 42.08; H, 4.27; N, 13.18.

*Diethyl 5-Bromouracil-1-malonate (IV).* From the reaction of 0.02 M each of 5-bromouracil, NaHCO<sub>3</sub>, and diethyl bromomalonate as described for compound III above, 82% yield of compound IV was obtained and recrystallized to constant melting point (101–102°) from absolute ethanol: *m/e* (mass spectrum) 349. *Anal.* Calcd for C<sub>11</sub>H<sub>13</sub>N<sub>2</sub>O<sub>6</sub> Br: C, 37.82; H, 3.72; N, 8.02. Found: C, 37.74; H, 3.86; N, 8.16.

*Acknowledgments.* The authors would like to thank Dr. P. S. Landis of Mobil Research and Development Corporation and Professor L. S. Bartell for their helpful suggestions. This work was supported in part by U. S. Atomic Energy Commission, Contract No. AT(11-1)-3276, and is identified as COO-3276-5(67).

## Theory of Simple Electron Transfer Reactions

P. P. Schmidt<sup>1</sup>

William Ramsay and Ralph Forster Laboratories, University College, London W.C. 1 and Department of Chemistry, Oakland University, Rochester, Michigan 48063 (Received June 30, 1972)

Publication costs assisted by Oakland University

This paper reports a reexamination of the simple model of the electron transfer process first examined quantum mechanically by Levich and Dogonadze. This new analysis of an old model employs nonequilibrium statistical mechanics, as embodied in the Yamamoto chemical reaction rate theory, to obtain a generally valid expression for the rate constant. In contrast to the Levich–Dogonadze quantum mechanical treatment, our result applies uniformly to the electron transfer process in all limits from chemically adiabatic to nonadiabatic. As a result, it is possible rigorously to define the adiabatic limit. The analysis further examines the consequences of making and dropping the Condon approximation. Finally, on the basis of the calculations as well as on physical considerations we attempt to clarify and make more understandable the results of the general theory of electron transfer processes, a theory which for complicated model systems yields very complicated and often difficult to understand results.

### Introduction

This note presents a reexamination of the simple model system for the electron transfer reaction studied in some detail by Levich and Dogonadze.<sup>2</sup> Their work was based on the use of quantum mechanical time-dependent perturbation theory. This paper, on the other hand, employs an analysis based on the use of nonequilibrium statistical mechanics. In particular, the theory this paper reports develops as an application of the Yamamoto<sup>2a</sup> theory of chemical reactions to the Levich–Dogonadze system. The theory provides a general expression for the electron transfer rate constant; it is general for the model system only. Moreover, the theoretical analysis yields only one rate constant which, in contrast to the perturbation theory result, is valid independent of the type of reaction; that

is, it holds for all reaction types from those classified as chemically adiabatic to the nonadiabatic cases.

The Levich–Dogonadze model<sup>2</sup> utilizes the concept of an electron transfer between ionic electron donor and acceptor species dissolved in a simple solution. Further, the solution is approximated as a structureless dielectric continuum. This model representation rightly has come under criticism recently<sup>3b</sup> for its over simplification; it

- (1) Correspondence concerning this article should be addressed to the Oakland University. This research was supported in part by a grant from Oakland University.
- (2) (a) V. G. Levich and R. R. Dogonadze, *Collect. Czech. Chem. Commun.*, **26**, 193 (1961); (b) R. R. Dogonadze, *Proc. Acad. Sci. USSR, Phys. Chem. Sect.*, **142**, 156 (1961).
- (3) (a) T. Yamamoto, *J. Chem. Phys.*, **33**, 281 (1960); (b) J. O'M. Bockris, K. L. Mittal, and R. K. Sen, *Nature (London). Phys. Sci.*, **234**, 118 (1971).

especially ignores dynamical contributions to the electron transfer process arising from changes in the molecular solvate shells surrounding the reactants. As a result, this simple theory apparently fails to agree with experimental data in a number of instances.<sup>3b</sup>

However, the model is not totally wrong. It is a reasonable first step to a more exacting and rigorous accounting for the process of electron transfer which takes place in oxidation-reduction reactions and at electrodes as well. Indeed, there is a physical transparency to the Levich-Dogonadze model representation of the electron transfer process, which while definitely over simple, nevertheless, points the way to an understanding of the dynamics of the electron transfer process at a molecular level.

The Levich type perturbation theory and other theories as well,<sup>4,5</sup> based on transition state concepts, do not provide the only theoretical means for understanding these systems. There is a developing theory of these reactions<sup>6</sup> based on the use of nonequilibrium statistical mechanics of which this paper is a part. A portion of the growing theoretical rigor derives from the use of the Yamamoto rate theory,<sup>3a</sup> and the rest derives from the use of improved and more detailed model system representations.<sup>6</sup> The object of the combined contributions to the theory is to obtain general rate constant expressions which accurately account for the important dynamical contributions to the electron transfer process. These rate constant expressions can be exceedingly complex for model systems which are complicated to start. It seems reasonable, therefore, to present this comparatively simple analysis now as an introduction to the work to come (and some already published<sup>6</sup>) to assist the reader in understanding this work, as well as for its original content, *per se*.

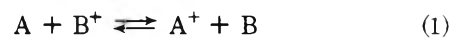
## Theory

The theory which unfolds in this paper is semiclassical (from the point of view of the quantum mechanical correspondence limit) in that it deals exclusively with the high-temperature limit. That is, we treat a system in the temperature range normally encountered by the practicing chemist (ambient temperature). As a result, averages over system variables associated with the environment around the reactants, *i.e.*, the solution surrounding them, are carried out classically. The result is formally identical with the Landau-Zener result<sup>2,7</sup> for the nonadiabatic, weak interaction limit. Our result differs from the Landau-Zener type result, however, in that, although it has the same form, it applies to all limits at once, adiabatic to nonadiabatic. This is a direct consequence of the use of nonequilibrium statistical mechanics in the analysis. Quantum mechanical perturbation theory, used by Levich and Dogonadze,<sup>2</sup> is valid only for weak interaction between the initial and final states.

The Levich-Dogonadze theory develops from the simplest possible model representation of the system, that of ionic electron donor and acceptor species dissolved in a simple solvent. The charged species interact with the polarizable solution medium surrounding them; this interaction is characterized through the solution electric polarization vector  $\mathbf{P}$ . The ions themselves have finite size, due in part to their solvation sheaths, but are assumed not to materially distort the surrounding solution. That is, dielectric saturation effects are not allowed in their model. The interaction between the donor and acceptor species which leads to the electron transfer event appears, by

virtue of a Born-Oppenheimer adiabatic separation analysis, as the matrix element of the Coulomb exchange operator; the operator is the potential energy function for the interaction between the electron on the donor and the acceptor ionic center. Moreover, this matrix element connects initial and final states.

The model system described above is the one we treat. The general chemical representation of the reaction is



For such a reaction Yamamoto's<sup>3a</sup> general expression for the rate constant provides the starting point for this analysis.

$$k = 1/2 \int_{-\infty}^{\infty} dt \langle \dot{N}^\dagger(0) \dot{N}(t) \rangle \quad (2)$$

The  $\dot{N}$  operator appearing in the correlation function in (2) is the time rate of change of the occupation number operator defined by<sup>6</sup>

$$N = a_i^\dagger a_i \quad (3)$$

In the following discussion the subscript  $i = 1$  indicates an initial state operator, here characterized by the set of reactants A and B<sup>+</sup>. The subscript 2 applies to the final state. The  $a_i^\dagger$  and  $a_i$  operators create and annihilate the appropriate states indicated by their subscript. Moreover, these operators are taken to be fermion operators, *i.e.*, they satisfy the commutation relations

$$\{a_i, a_i^\dagger\} = 1, \{a_i, a_j\} = \{a_i^\dagger, a_j^\dagger\} = 0$$

The following calculations apply only to the forward rate constant. On application of the detailed balance condition the reverse rate constant results, hence it need not directly enter the discussion.

The  $\dot{N}$  operator derives from the  $N$  operator through the use of the Heisenberg equation of motion<sup>6</sup>

$$i\hbar \dot{N} = [N, H] \quad (4)$$

The correlation function is evaluated as

$$\langle \dot{N}^\dagger(0) \dot{N}(t) \rangle = \text{Tr} \{ \rho(0) \dot{N}^\dagger(0) \dot{N}(t) \} \quad (5)$$

where the density operator is

$$\rho(0) = Z^{-1} \exp(-\beta H), \beta = 1/k_B T \quad (6)$$

and  $Z$  is the partition function

$$Z = \text{Tr} \exp(-\beta H) \quad (7)$$

In order to evaluate the equation of motion (4) an expli-

- (4) N. S. Hush, *J. Chem. Phys.*, **28**, 962 (1958); *Trans. Faraday Soc.*, **57**, 557 (1961).
- (5) R. A. Marcus, *J. Chem. Phys.*, **26**, 867 (1957); *Discuss. Faraday Soc.*, **29**, 21 (1960); *J. Chem. Phys.*, **43**, 679 (1965).
- (6) (a) P. P. Schmidt, *J. Chem. Phys.*, **56**, 2775 (1972); (b) **57**, 3749 (1972); (c) *J. Solution Chem.*, submitted for publication; (d) *Z. Naturforsch.*, in press.
- (7) (a) V. G. Levich, *Advan. Electrochem. Electrochem. Eng.*, **4**, 249 (1965); (b) "Physical Chemistry, an Advanced Treatise," Vol. IXB, H. Eyring, D. Henderson, and W. Jost, Ed., Academic Press, New York, N. Y., 1970, pp 985-1074.

cit expression for the Hamiltonian operator is necessary. The adopted operator is a considerably simplified form of the general Hamiltonian operator found in a previous paper.<sup>6a</sup> Thus, the Hamiltonian operator for this system is

$$H = \sum_{i=1,2} (\epsilon_i + V_i/2) a_i^\dagger a_i + H_f + \sum_{i,i'} C_{ii'} a_i^\dagger a_{i'} + \text{hermetian conjugate} \quad (8)$$

in which  $\epsilon_i$  is the energy of the electron, including solvation effects, in either state. More in particular, the energy  $\epsilon_1$  is the energy of the electron in the highest filled state of the A species together with the Born solvation energies for the ionic species A and B<sup>+</sup>. A similar argument applies to the final state energy  $\epsilon_2$ . The potential energy term contains all solvent interactions with the electron as well as interactions between reactants, apart from the exchange interaction. As it is a combined potential for the system of two reactants, the factor  $1/2$  avoids double counting. Furthermore, it is necessary to obtain the correct result later on. The  $C_{ii'}$  term is the matrix element of the Coulomb interaction which induces the electron transfer. Finally,  $H_f$  is a part of the total Hamiltonian which contains terms to account for the motions of the reactants mass centers and dynamical factors in the solution generally. No further specification of that operator is made here.

By means of eq 3, 4, and 8 the equation of motion for  $N$  follows.

$$\dot{N} = (i/\hbar) C_{12} a_1 a_2^\dagger \quad (9)$$

The correlation function now has the form

$$\langle \dot{N}^\dagger(0) \dot{N}(t) \rangle = \langle C_{12}^\dagger(0) e^{-i\epsilon_1 t/\hbar} C_{12}(t) e^{i\epsilon_2 t/\hbar} \rangle \quad (10)$$

with

$$\epsilon_i' = \epsilon_i + 1/2 V_i \quad (11)$$

For generality the time dependence of the exchange matrix elements also appears. As these elements depend on the relative separation between the reactant mass centers, the time dependence can be an important factor influencing the rate. To consider the time dependence in these matrix elements is equivalent to dropping the Condon approximation typically made in these types of calculations, cf. ref 7. The time dependence in the Heisenberg representation is

$$C_{12}(t) = e^{iH_f t/\hbar} C_{12}(0) e^{-iH_f t/\hbar} \quad (12)$$

and, more specifically, it appears as a time dependence of the  $R$  coordinate for the interparticle separation:<sup>6a</sup> viz.,  $C_{ii'}[R(t)]$ . We shall return to a consideration of the implication of this time dependence. However, for the immediate calculations application of the Condon approximation yields the result

$$k = (|C_{12}|^2 / 2\hbar^2) \int_{-\infty}^{\infty} dt \langle \exp[i(\epsilon_2' - \epsilon_1')t/\hbar] \rangle \quad (13)$$

for the rate constant expression.

As the energy factors  $\epsilon_i'$  depend on the potential energy function  $V_i$ , a function of system variables including the interreactant separation, an average is implied. For the moment the averaging operation is restricted to system

variables other than those for the separation between reactants. A reversal of the time integration and averaging operations enables us to write

$$k = (\pi |C_{12}|^2 / \hbar) \langle \delta(V_2/2 - V_1/2 + \Delta\epsilon) \rangle \quad (14)$$

where for simplicity

$$\Delta\epsilon = \epsilon_2 - \epsilon_1 \quad (15)$$

Define a system coordinate variable  $Q$  as that variable, apart from the interreactant separation, which undergoes change in the course of the electron transfer. The physical implication of this definition is clearly illustrated in Chapter VIII of Levich's review article.<sup>7a</sup> As a consequence of this definition of  $Q$ , the potential functions  $V_1$  and  $V_2$  are functions of  $Q$ :  $V_1(Q)$  and  $V_2(Q)$ . At this point the argument necessarily invokes the requirement that at the transition point,  $Q_0$ , the potential energy functions are equal

$$V_1(Q_0) = V_2(Q_0) \quad (16)$$

The properties of the delta ( $\delta$ ) function allow expression of the rate constant as

$$k = \frac{\pi |C_{12}|^2}{\hbar \left| \frac{\partial}{\partial Q} (V_2 - V_1) \right|} \left\langle \delta \left[ \frac{1}{2} (Q - Q_0) + \frac{\Delta\epsilon}{\frac{\partial}{\partial Q} (V_2 - V_1)} \right] \right\rangle \quad (17)$$

The remaining calculations require the evaluation of the statistical mechanical average in eq 17. This averaging operation has the form

$$\begin{aligned} \left\langle \delta \left[ \frac{1}{2} (Q - Q_0) + \frac{\Delta\epsilon}{\frac{\partial}{\partial Q} (V_2 - V_1)} \right] \right\rangle &= \frac{1}{n} \int_{-\infty}^{\infty} dQ \times \\ \exp[-\beta V_1(Q)] \delta \left[ \frac{1}{2} (Q - Q_0) + \frac{\Delta\epsilon}{\frac{\partial}{\partial Q} (V_2 - V_1)} \right] &= \frac{1}{n} \times \\ \exp \left\{ -\beta V_1 \left[ \frac{1}{2} Q_0 - \frac{\Delta\epsilon}{\frac{\partial}{\partial Q} (V_2 - V_1)} \right] \right\} &\quad (18) \end{aligned}$$

where  $n$  is a normalization factor which depends on the nature of the potential energy function  $V_1(Q)$ . It of course arises from the partition function  $Z$ , eq 7.

At this point the analysis makes a direct contact with the Levich-Dogonadze analysis.<sup>2</sup> The Hamiltonian function (classical) for the system modes represented as a dielectric continuum is<sup>2,7</sup>

$$\begin{aligned} \mathcal{H}_{s1} &= \frac{\hbar\omega_s}{2} \sum_{Q_k \neq Q} [P_k^2 + Q_k^2] + \frac{\hbar\omega_s}{2} [P^2 + Q^2] \\ \mathcal{H}_s &= \frac{\hbar\omega_s}{2} \sum_{Q_k \neq Q} [P_k^2 + Q_k^2] + \frac{\hbar\omega_s}{2} [P^2 + (Q^2 - Q_0)^2] \end{aligned} \quad (19)$$

where  $\omega_s$  is the zero point frequency for the dielectric continuum. The potential energy function for the initial state,  $V_1$ , is

$$V_1(Q) = (\hbar\omega_s/2)Q^2 \quad (20)$$

The expression for this function at the intersection point,



as required by eq 18, is

$$V_1 \left[ \frac{1}{2} Q_0 - \frac{\Delta\epsilon}{\partial Q (V_2 - V_1)} \right] = \frac{\hbar\omega_s}{2} \left[ \frac{1}{2} Q_0 - \frac{\Delta\epsilon}{\partial Q (V_2 - V_1)} \right]^2 \quad (21)$$

The Hamiltonian functions (19) imply the following

$$\frac{\partial}{\partial Q} (V_2 - V_1) = -\hbar\omega_s Q_0 \quad (22)$$

with which we find

$$V_1 \left[ \frac{1}{2} Q_0 - \frac{\Delta\epsilon}{\partial Q (V_2 - V_1)} \right] = \frac{1}{2\hbar\omega_s Q_0^2} \left[ \frac{\hbar\omega_s}{2} Q_0^2 + \Delta\epsilon \right] \quad (23)$$

Following Levich and Dogonadze,<sup>2</sup> the solvent repolarization energy is defined as

$$E_s = (\hbar\omega_s/2)Q_0^2 \quad (24)$$

Thus, with the definition of the normalization factor  $n$

$$n = (\hbar\omega_s/2\pi k_B T)^{1/2} \quad (25)$$

the rate constant is

$$k = |C_{12}|^2 (\pi/\hbar^2 E_s k_B T)^{1/2} \exp[-(\Delta\epsilon + E_s)^2/4E_s k_B T] \quad (26)$$

This expression for the rate constant is complete only after the final evaluation of the average over all interreactant separations, as specified by Levich.<sup>7</sup> As expression 26 corresponds with that obtained by Levich, we omit this final averaging. Our results are the same as his results. The interested reader should consult Levich's review article<sup>7</sup> for the details.

The expression (eq 26) for the rate constant is general for this system. It applies, in contrast to the Levich-Dogonadze result, to both adiabatic and nonadiabatic reactions, as has been stressed already. Typically, the application of the Landau-Zener semiclassical theory of collisions to these types of reactions leads to the result<sup>2b,7</sup>

$$k = (\omega_s/2\pi) \exp[-(\Delta\epsilon + E_s)^2/4E_s k_B T] \quad (27)$$

There is of course no reduction of expression 26 to the form of eq 27. However, because eq 26 applies generally, it implies that for absolute values of the square of the exchange interaction matrix element which satisfy the relation

$$|C_{12}|^2 = (\hbar\omega_s/2\pi)[E_s k_B T/\pi]^{1/2} \quad (28)$$

the separation of the potential energy surfaces is sufficiently great that the dynamics of the electron transition process are entirely those of the dynamics of the inertial system(s), *viz.*, the environment surrounding the reactant ions as well as the motions of the ions themselves. This is nothing more than the usual statement of the chemical adiabatic limit anyway. Thus, systems for which relation 28 holds need only be treated analytically with respect to the classical motions of the heavy particles. Quantum mechanical considerations enter only in the determination of the intersection of the potential energy surfaces. Such a

limiting process as this, developed for a more general type of system, brings this theoretical approach into correspondence with the unified theory Marcus has presented in recent years.<sup>5</sup> It is still more general than Marcus's theory in that electronically dependent factors needed to calculate the rate of passage through the intersection region appear automatically; presumably they are correctly chosen provided the correct Hamiltonian operator is chosen to start. In the Marcus theory,<sup>5</sup> on the other hand, some necessary physical representation of the system configuration at the point of intersection of the potential energy surfaces is needed to calculate a transmission factor. This requirement invokes the concept of a transition state.

In concluding this section we remark that the origin of the  $\omega_s/2\pi$  dependence in the adiabatic limit is an interesting one, one which certainly deserves further investigation from a rigorous point of view. No such analysis is attempted here. However, we point out that the nature of this dependence can better be seen through an examination of rate processes in solids, *cf.* ref 8. It would be of considerable interest to extend Glyde's arguments to rate processes in solution.

#### Comment on Non-Condon Contributions

Non-Condon contributions to any radiative or nonradiative process arise as a result of the significant dependence of the transition matrix elements on dynamical variables connected with the motions of heavy particles of the system. Typically, in molecular nonradiative processes non-Condon effects arise due to the dependence of the transition matrix element on normal mode coordinates of the molecule. The electron transfer problem we consider here has a similar non-Condon dependence as well. However, the major dependence of the matrix elements, at least for this simple model system, is on the interreactant separation. It is well known, moreover, that the Born repolarization energy  $E_s$  is also  $R$  dependent,<sup>2,5,7</sup>  $R$  being the interreactant separation. Thus, the average over the  $R$  variable is complicated even in the relatively simple result (eq 26) obtained by the use of the Condon approximation. In the non-Condon treatment, as this discussion soon shows, the averaging process is even more complicated.

The discussion to follow is intended merely as an illustration of the types of situations to be expected if this more general, and certainly more complete, approach is taken. A detailed consideration of the non-Condon effect has been completed and will be reported elsewhere. It deals with the general question of inner *vs.* outer sphere reactions as well as with the non-Condon effect. The succeeding discussion follows the approach of the first paper<sup>6a</sup> of this series. The analysis here is intended as an illustration of the application of the general approach of that first paper.

We return to eq 10 which expresses the time dependence of the matrix elements as well as the time dependence due to other solution variables. In line with the general scheme for separating motions of the system into separate subsystem contributions, the correlation function appears as

$$\langle C_{12}^\dagger(0) e^{-i\epsilon_1' t/\hbar} C_{12}(t) e^{i\epsilon_2' t/\hbar} \rangle = \langle C_{12}^\dagger(0) C_{12}(t) \rangle e^{-\epsilon_1' t/\hbar} e^{i\epsilon_2' t/\hbar} \rangle_R \quad (29)$$

in which the internal average (signified by the brackets) is

(8) H. R. Glyde, *Rev. Mod. Phys.*, **39**, 373 (1967).

over solution variables and the outer average is over the relative center of mass momentum and coordinate variables. This ordering of the averaging operations is needed as the solution average produces terms which still have an  $R$  dependence.

As indicated in the discussion following eq 10, the time dependence of the matrix elements appears as a time dependence of the  $R$  variable. A method of calculating matrix elements from the appropriate molecular wave functions makes use of the convolution of several Fourier transforms of the components in the matrix element.<sup>6a,9</sup> As a result, the matrix elements can be expressed as Fourier transforms in the  $k$ -space conjugate to the coordinate  $R$  space. Thus, the matrix element, together with its time dependence is

$$C_{12}[R(t)] = \int d^3k c(k) \exp[ik \cdot R(t)] \quad (30)$$

The correlation function now takes the form

$$\langle \dot{N}^+(0) \dot{N}(t) \rangle = \int d^3k_1 d^3k_2 c(k_1) c(k_2) \langle e^{-ik_1 \cdot R(0)} e^{-ik_2 \cdot R(t)} \exp[i(\epsilon_2' - \epsilon_1')t / \hbar] \rangle_R \quad (31)$$

By means of a reordering of the various integrations and averaging operations, the rate constant has the form

$$k = \frac{(\pi\beta)^{1/2}}{\hbar^2} \int d^3k_1 d^3k_2 d\omega dt c(k_1) c(k_2) e^{-i\omega t} \times \exp\left[-\frac{\Delta\epsilon + \hbar\omega}{2k_B T}\right] \langle e^{-ik_1 \cdot R(0)} e^{-ik_2 \cdot R(t)} I(\omega, R) \rangle_R \quad (32)$$

where use has been made of the results obtained in the last section. In eq 32 the  $I(\omega, R)$  and function is

$$I(\omega, R) = \exp\left\{-\frac{1}{2} \ln [E_s(R)] - \frac{1}{4k_B T} \left[ \frac{(\Delta\epsilon + \hbar\omega)}{E_s(R)} - E_s(R) \right]\right\} \quad (33)$$

which is eq 26 with the  $R$ -dependent  $E_s$  terms separated.

We now employ the technique presented in the first paper<sup>6a</sup> to write the rate constant as

$$k = \frac{(\pi\beta)^{1/2}}{\hbar^2} \int d^3k_1 d^3k_2 d\omega dt c(k_1) c(k_2) \times \exp\left[-\frac{\Delta\epsilon + \hbar\omega}{2k_B T}\right] \exp[-1/2k_2^2 \gamma(t) - i\omega t] \quad (34)$$

with

$$\gamma(t) = -(i\hbar t / \mu) - 2/3 \int_0^t du (t-u) \langle \mathbf{v}(0) \cdot \mathbf{v}(u) \rangle' \quad (35)$$

where  $\mu$  is the reduced mass, and

$$\langle \mathbf{v}(0) \cdot \mathbf{v}(u) \rangle' = (1/Z) \int d^3v d^3R e^{-\beta H(\mathbf{v}(0), \mathbf{v}(u))} \times \exp[-i(\mathbf{k}_1 - \mathbf{k}_2) \cdot \mathbf{R}(0)] I(\omega, R) \quad (36)$$

where  $\mathbf{v}(u)$  is the relative velocity of the reactants. This velocity correlation function is even more complicated than the typical cases encountered in transport theory.<sup>10</sup> This is due to the influence of solvent reorientation factors. It is possible to approximate this contribution in terms of a random walk model.<sup>11</sup> The result, discussed in the first paper,<sup>6a</sup> is

$$|t| \int_0^\infty du \langle \mathbf{v}(0) \cdot \mathbf{v}(u) \rangle' = 2/3 \bar{v} L I(\omega, R) |t| (\mathbf{k}_1 \cong \mathbf{k}_2) \quad (37)$$

where  $L$  is the most probable separation for the electron transfer.  $L$  can be obtained from (36) by means of a steepest descents analysis, for example,  $\bar{v}$  is the average relative interreactant velocity.

As a result of the approximations made, the integrations can be carried out. The rate constant is

$$k = c^2(\kappa) (2\mu^2 \bar{v} L / 3\hbar^4 \kappa^2) [\pi / E_s k_B T]^{1/2} \times \exp[-(\Delta\epsilon + \hbar\omega)^2 / 4E_s k_B T] \quad (38)$$

In this particular treatment the effect of considering contributions to the motions of the system governed by the  $R$  dependence of the matrix element produced some dependencies not expected for the simple result. There is the term  $(2\mu/\hbar^2 k^2)^2$  as well as  $\bar{v} L$  due to the motions of the reactants together to the electron transfer configuration.

The result (38) was obtained here by means more rigorous than those used in the first paper.<sup>6a</sup> There is an error in the expression in that first paper; the volume factor  $V_m$  should not appear in eq 63. Apart from a difference in numerical factors, which arises from the specific consideration of the  $c(\kappa)$  factors in part I, expression 38 is equivalent to (63) of I.

The same general questions concerning adiabaticity apply here as in the earlier Condon approximation expression derived in this paper. In particular

$$|c^2(\kappa)| \geq (\omega_s / 2\pi) [E_s k_B T / \pi]^{1/2} (3\hbar^4 \kappa^2 / 2\mu^2 \bar{v} L) \quad (39)$$

In this case the question of adiabaticity depends on the relative velocity of the reactants as well as on the solvent repolarization factors.

## Discussion

An observation concerning the general approach<sup>6</sup> deserves comment in this discussion. The Gaussian limit expression for the rate constant in part I is

$$k = (1/2\hbar^2) \int_{-\infty}^{\infty} dt \exp[-it\Delta\epsilon/\hbar] \iint d^3k_1 d^3k_2 c(k_1) c(k_2) \times \exp[-1/2k_2^2 \gamma(t)] \quad (40)$$

It is easy to see that with eq 40 and some reasonable form for the velocity autocorrelation function

$$T = \int_0^\infty du \langle \mathbf{v}(0) \cdot \mathbf{v}(u) \rangle' = T(\mathbf{k}_-, \mathbf{k}_2) \quad (41)$$

$$\gamma(t) = -(i\hbar t / \mu) + \frac{2}{3} |t| T$$

the time integration leads to a "Lorentzian" form for the rate constant

$$k = (1/2\hbar) \iint d^3k_1 d^3k_2 c(k_1) c(k_2) \{1/3\hbar k_2^2 T / [(\hbar^2 k_2^2 / 2\mu - \Delta\epsilon)^2 + (\hbar k_2^2 T / 3)^2]\} \quad (42)$$

- (9) H. J. Silverstone, *J. Chem. Phys.*, **45**, 4337 (1966).  
 (10) P. Egelstaff, "An Introduction to the Liquid State," Academic Press, New York, N. Y., 1967.  
 (11) F. Reif, "Fundamentals of Statistical and Thermal Physics," McGraw-Hill, New York, N. Y., 1965.

The solvent repolarization factors, expressed in  $E_s$ , appear as activation energy contributions to the transport factor  $T$ . The difference between the adiabatic electronic energies,  $\Delta\epsilon$ , appears in the Lorentzian part of the rate constant expression. This result is somewhat disconcerting in view of its lack of correspondence with the Arrhenius form so familiar to chemists. However, the origin of this unusual dependence of the rate constant on  $\Delta\epsilon$  in a Lorentzian manner can be traced to the approach used. As the treatment seems general and rigorous, it suggests that this Lorentzian form is entirely a result of the model chosen. In general, there is no peremptory reason to expect an Arrhenius form for the rate constant expression. However, in line with this treatment and its Gaussian limit it is relatively easy to demonstrate that if the reactants' relative motion is governed by a harmonic potential interaction, such that the relative motion is that of a harmonic oscillator, then an Arrhenius form results for the high-temperature limit.

That non-Arrhenius type behavior may be expected, is seen in the following short argument. Even without the benefit of the exact solution to the electron transfer problem one can see that the exact rate constant expression may have a Lorentzian or near Lorentzian dependence, *i.e.*, a dependence in which the adiabatic electronic energies appear in terms outside the exponential with the general form  $(\Delta\epsilon + A)^{-n}$  where  $A$  is some parameter. The general rate constant is

$$k = (1/2\hbar^2) \int_{-\infty}^{\infty} dt \times \exp[-i\Delta\epsilon/\hbar] \int d^3k_1 d^3k_2 c(k_1)c(k_2) \int d\{N'\} \times e^{-ik_1 R} P(t \leftarrow 0) e^{-ik_2 R} f_0 d\{N\} \quad (43)$$

where  $P(t \leftarrow 0)$  is the complete propagator for the system; it takes the system from the phase space  $N$  at  $t = 0$  to  $N'$  at  $t$ . Expression 43 implies that the motions of the reactants is classical. Clearly, this expression generalizes to include any quantum effects; a quantum mechanical propagator is used in such cases. Expression 43 employs the classical propagator used by Friedman<sup>12</sup> in his analysis of ionic diffusion in solution. The singular feature of eq 43, apart from the  $k$ -space integrations, is the fact that it has a number of similarities to the ionic diffusion problem as formulated by Friedman. An examination of Friedman's results and a comparison with this problem immediately suggests that there is some correspondence between the electron transfer process and the ionic diffusion process in the presence of an oscillating externally applied field. The frequency factor in the electron transfer case is  $\Delta\epsilon/\hbar$ . On the basis of this observation one suspects that there is no clear reason the adiabatic electronic energies should appear in an Arrhenius exponent.

The above remarks apply to the reaction of hard, or outer, sphere electron donor and acceptor species. The soft, or inner, sphere case, as opposed to atomic, electron donor and acceptor species, may have a different than Lorentzian form. This follows because the rate constant is expressible as a convolution of the contribution due to the internal molecular dynamics and the contribution from reactant transport, *viz.*

$$k = (1/4\pi\hbar^2) \int_{-\infty}^{\infty} d\omega \int d^3k_1 d^3k_2 c(k_1)c(k_2) \int_{-\infty}^{\infty} dt_1 \exp[-i(\Delta\epsilon + \hbar\omega)t/\hbar] \int d\{n'\} e^{-ik_1 R} P_1(t_1 \leftarrow 0) e^{-ik_2 R} f_{10} d\{n\} \times \int_{-\infty}^{\infty} dt_2 e^{-i\omega t_2/\hbar} \int d\{m'\} e^{-ik_1 R} P_0(t_2 \leftarrow 0) e^{-ik_2 R} f_{00} d\{m\} \quad (44)$$

Phase space in this case is partitioned into inner, molecular contributions,  $m$ , and outer, interreactant transport contributions,  $n$ :  $N = m + n$ .  $R_i$  is the set of coordinates associated with internal molecular degrees of freedom, while  $R_0$  is the set of coordinates pertaining to the relative motions of the reactants. A Lorentzian type form may arise for the transport contributions. In such a situation the convolution variable will have roughly the dependence  $(\hbar\omega + A)^{-n}$ ; again  $A$  is a parameter. The difference in adiabatic electronic energies appears in the expression for the internal molecular contributions; this expression may have an essentially Arrhenius form. In such a soft sphere system the adiabatic electronic energies may once again reappear in an expression which is recognizably of Arrhenius form. Of course, the convolution integration places the electronic energy difference elsewhere as well, so the end result is not entirely Arrhenius in its traditional form.

## Summary

This paper has presented an examination of the simple electron transfer system originally defined and analyzed by Levich and Dogonadze.<sup>2</sup> This work, in contrast to the Levich-Dogonadze treatment, employs the statistical mechanics of nonequilibrium systems to obtain a general form of the rate constant expression for the electron transfer process. By means of this analysis rate constant expressions resulted for two cases: one involved the use of the Condon approximation, the other dropped that approximation. The analysis showed, by means of general arguments, that the form of the rate constant is the same as that obtained by Levich and Dogonadze using both the general time-dependent quantum mechanical perturbation theory and the semiclassical Landau-Zener variety. The implication of our result is that only one expression applies to all commonly encountered cases. However, the adiabatic limit for the rate constant usually has the form embodied in eq 27. As this is the case, the distinction between adiabatic and nonadiabatic reactions, either eq 28 or 39, is rigorous and physically meaningful. That is, in the adiabatic limit, the separation between potential energy surfaces in the intersection region is equal to or greater than certain values given by the relations 28 or 39. When these relations are satisfied, the dynamics of the system are governed by the motions of the heavy particles in the system.

Further, we showed that dropping the Condon approximation introduced a dependence of the rate constant expression on transport factors associated with the solution. The dependence we got cannot be found by means of the averaging techniques employed by Levich.<sup>7</sup>

Finally, in the Discussion section, we further clarified the physical content of the general forms of the rate constant. In particular, we asserted that for hard sphere reactions, typified by the truly outer sphere examples, the rate constant need not possess the simple Arrhenius form.

(12) H. L. Friedman, *Physica*, **30**, 509, 537 (1964).

The correct form may be very nearly Lorentzian. However, we also asserted that in the soft sphere cases, characterized by the inner sphere cases, the Arrhenius form may reappear. Clearly, the form of the rate constant in an exact treatment is largely a function of the type of model representation of the system chosen.

It is my hope that these few simple physical and mathematical arguments provided in this paper will serve to make understandable the underlying concepts common to

the growing and increasingly complicated general theory of these reactions.

*Acknowledgments.* I should like to thank Professor A. G. Davies and Dr. Thirunamachandran for their hospitality and generosity in accommodating me during my stay in London. I also acknowledge a number of stimulating conversations with Professor Allen Maccoll which had an indirect bearing on this work.

## INDO Theoretical Studies.<sup>1</sup> The Geometry of 1-Substituted Vinyl Radicals and 1-Fluorovinyl Cations

Charles U. Pittman, Jr.,\* Lowell D. Kispert, and Thurman B. Patterson, Jr.

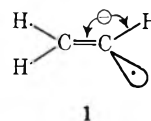
Department of Chemistry, University of Alabama, Tuscaloosa, Alabama 35486 (Received September 5, 1972)

Publication costs assisted by The University of Alabama

LCAMO-SCF calculations, in the INDO approximation, have been performed on a series of 1-substituted vinyl radicals,  $\text{CH}_2=\text{CX}$  where X is F (4),  $\text{OCH}_3$  (5), and  $\text{BH}_2$  (6). Also the *cis*- and *trans*-1,2-difluorovinyl radicals 7 and 8 were examined. When X is more electronegative than carbon, the bent ( $\text{sp}^2$ ) geometry is more stable than the linear ( $\text{sp}$ ) geometry. However, the linear geometry is more stable when X is  $\text{BH}_2$ . The most stable geometries of both bent and linear 6 were those where the plane of the  $\text{BH}_2$  group was rotated out of the molecular plane ( $xz$  plane, with  $\text{C}_2-\text{C}_1$  defined along the  $z$  axis) by 52 and 45°, respectively. In these out-of-plane geometries the  $\pi$  bonding from the "empty" boron p orbital to carbon was greatly reduced in both  $x$  and  $y$  planes. Barriers to inversion,  $\sigma$  and  $\pi$  electron distributions, and the unpaired spin densities were studied. In the bent geometry of 4, 5, 7, and 8 the bulk of the unpaired spin density is in the  $p_x$  orbitals at both C-1 and the 1 substituent. The amount of spin density in the C-1  $p_x$  orbital increases sharply as the geometry approaches linearity. However, in 6 where  $\text{BH}_2$  is the substituent, the majority of the spin density is found in the  $p_y$  orbitals of C-2 and boron in both linear and bent all-planar geometries. Rotation of the  $\text{BH}_2$  plane results in a marked increase in the C-1  $p_x$  spin density. Calculations were also performed on both the 1-fluoro and the 1,2-difluorovinyl cations 9 and 10. The linear geometry is strongly favored in both 9 and 10 where strong  $\pi_x$  back-bonding from F-1 to C-1 takes place. However,  $\pi_x$  back-bonding is also found in the bent geometries. In both cases the  $\text{C}_1-\text{F}_1$   $\sigma$  bond is still strongly polarized toward fluorine. Unlike  $\text{CH}_2\text{CH}^+$ , very little polarization of  $\pi_y$  electron density at C-2 toward C-1 takes place in 9 or 10. The instability of the bent geometry largely results from the necessity of promoting electron density from the 2s to the 2p orbital.

### Introduction

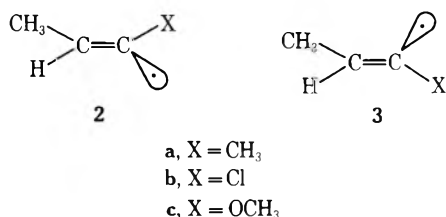
Vinyl radicals are readily available from the thermal and photochemical decompositions of  $\alpha,\beta$ -unsaturated peresters and diacyl peroxides,<sup>2-5</sup> from radical additions to alkynes,<sup>6-9</sup> from the photolysis of vinyl iodides,<sup>10</sup> and from electrochemical generation.<sup>11</sup> Previous studies of vinyl radicals have been reviewed.<sup>12</sup> ESR studies<sup>13-15</sup> of the unsubstituted ethylene radical (1) definitively supported a bent ( $\text{sp}^2$ ) structure in the condensed state with a low ( $\sim 2-3$  kcal/mol) barrier to inversion.<sup>13</sup> Detailed molecular orbital calculations,<sup>16,17</sup> in which all angles and bond lengths were optimized, predicted the bent planar structure of 1 would be the most stable. *Ab initio* calculations, using Gaussian-type basis sets,<sup>16</sup> gave  $\theta = 130.8^\circ$ . Many other theoretical calculations also favored the bent geometry for 1.<sup>18</sup>



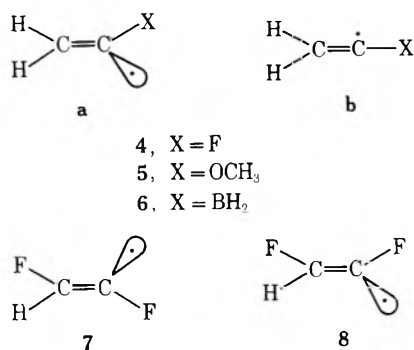
The configurational stability of *cis* and *trans* 1-substituted 1-alkenyl radicals, such as 2 and 3, have been stud-

- (1) INDO Theoretical Studies part IV. For papers I-III in this series see (a) L. D. Kispert, C. Engelman, C. Dyas, and C. U. Pittman, Jr., *J. Amer. Chem. Soc.*, **93**, 6948 (1971); (b) C. U. Pittman, Jr., C. Dyas, C. Engelman, and L. D. Kispert, *J. Chem. Soc., Faraday Trans. 2*, **68**, 345 (1972); (c) L. D. Kispert, C. U. Pittman, Jr., D. L. Allison, T. B. Patterson, Jr., C. W. Gilbert, Jr., C. F. Hains, and J. Prather, *J. Amer. Chem. Soc.*, **94**, 5979 (1972).
- (2) J. A. Kampmeier and R. M. Fantazier, *J. Amer. Chem. Soc.*, **88**, 1959 (1966).
- (3) L. A. Singer and N. P. Kong, *J. Amer. Chem. Soc.*, **88**, 5213 (1966).

ied in solution by competition studies.<sup>12,19</sup> Kampmeier, *et al.*,<sup>19</sup> generated **2c** and **3c** by thermal decomposition of their corresponding *tert*-butyl *cis*- and *trans*-1-methoxyperoxyprotonates in cumene. The radicals were quenched by hydrogen abstraction from cumene to give the *cis*- and *trans*-methyl-1-propenyl ethers with retention of stereochemistry. Thus, hydrogen abstraction was faster than the isomerization (**2c**  $\rightleftharpoons$  **3c**) of these radicals. Conversely, the isomerization of 1-alkylvinyl radicals (**2a**  $\rightleftharpoons$  **3a**) is much faster than hydrogen transfer from cumene, and these two processes are competitive for 1-chlorovinyl radicals.<sup>12</sup> While these experimental results actually reflect the ratio of the rate of hydrogen abstraction to the rate of isomerization, it was suggested that the main effect is the rate of isomerization.<sup>19</sup> It was postulated that this rate depends on the nature of the 1 substituent and that the isomerization rate was a function of the electronegativity of the 1 substituent.<sup>19</sup> However, it is quite possible that the rate of hydrogen abstraction is affected by the 1 substituent and by the nature of the radical's solvation. The character of the solvent shell would depend, in part, on the 1 substituent. Thus, the argument that the rate of isomerization is greatly reduced as the electronegativity of the 1 substituent increases, while attractive, needs further study.



In this regard it is interesting that extended Hückel molecular orbital calculations have indicated the barrier to isomerization is greater for 1-hydroxy and 1-fluorovinyl radicals than for the 1-methylvinyl radical.<sup>20</sup> It is well known that the INDO technique includes repulsion integrals which permit a description of the unpaired spin density in s orbitals. Thus, in this paper we report molecular orbital calculations, in the INDO approximation, on the series of 1-substituted vinyl radicals where the 1 substituent is fluorine, methoxy, and BH<sub>2</sub>. The bent-planar (sp<sup>2</sup>) (**4a**-**6a**) and linear-planar (sp) (**4b**-**6b**) structures were compared in order to approximate the barrier to gas-phase isomerization and, more importantly, to illustrate the trend as the electronegativity of the 1 substituent was varied. Calculations were also performed on the *cis*- and *trans*-1,2-difluorovinyl radicals **7** and **8** and the barrier to their interconversion.



The structures of the fluorine-substituted vinyl cations

CH<sub>2</sub>CF<sup>+</sup> (**9**) and CHF<sub>2</sub>C<sup>+</sup> (**10**) were studied using the INDO technique, and they are also reported here. The parent cation in this series, CH<sub>2</sub>CH<sup>+</sup> was studied previously by two groups using *ab initio*<sup>16,21</sup> and extended Hückel methods.<sup>22</sup> It was shown to be planar with C<sub>2v</sub> symmetry. Thus, in contrast to CH<sub>2</sub>CH, a planar linear (sp) structure is favored for vinyl cation, CH<sub>2</sub>CH<sup>+</sup>. The "empty" p orbital was stabilized through delocalization of electron density out of the σ framework into this orbital.<sup>21</sup> The thermodynamic stability of the vinyl cation, as determined by appearance and ionization potential studies,<sup>23,24</sup> lies between that of the methyl and ethyl cations. Vinyl cations have been generated in solution in an enormous number of studies,<sup>25,26</sup> especially *via* the solvolysis of vinyl trifluoromethanesulfonates,<sup>27,28</sup> but their short lifetimes, have, to date, made direct spectroscopic observations impossible, even in strongly acidic media. This paucity of spectroscopic data prompted us to study the structure of **9** and **10**.

### Method

The INDO program (CNINDO), QCPE No. 141, was obtained from the Quantum Chemistry Program Exchange, Indiana University, and was modified for use on a Univac 1108. Structures were generated using the Gordon-

- (4) O. Simamura, K. Tokumaru, and H. Yui, *Tetrahedron Lett.*, 5141 (1966).
- (5) P. G. Webb and J. A. Kampmeier, *J. Amer. Chem. Soc.*, **93**, 3730 (1971).
- (6) P. S. Skell and R. G. Allen, *J. Amer. Chem. Soc.*, **86**, 1559 (1964).
- (7) A. A. Oswald, K. Griesbaum, B. E. Hudson, Jr., and J. M. Bregman, *J. Amer. Chem. Soc.*, **86**, 2877 (1964).
- (8) J. A. Kampmeier and G. Chen, *J. Amer. Chem. Soc.*, **87**, 2608 (1965).
- (9) R. M. Kopchik and J. A. Kampmeier, *J. Amer. Chem. Soc.*, **90**, 6733 (1968).
- (10) R. C. Neuman, Jr., and G. D. Holmes, *J. Org. Chem.*, **33**, 4317 (1968).
- (11) A. I. Fry and M. A. Mitnick, *J. Amer. Chem. Soc.*, **91**, 6207 (1969).
- (12) W. G. Bentrude, *Annu. Rev. Phys. Chem.*, **18**, 300 (1967).
- (13) R. W. Fessenden and F. H. Schuler, *J. Chem. Phys.*, **39**, 2147 (1963).
- (14) E. Cochran, F. J. Adrian, and V. A. Bowers, *J. Chem. Phys.*, **40**, 213 (1964).
- (15) P. H. Kasai and E. B. Whipple, *J. Amer. Chem. Soc.*, **89**, 1033 (1967).
- (16) W. A. Lathan, W. J. Hehre, and J. A. Pople, *J. Amer. Chem. Soc.*, **93**, 808 (1971).
- (17) P. Millie and G. Berthier, *Int. J. Quantum Chem., Symp.*, **No. 2**, 67 (1968).
- (18) G. A. Peterson and A. D. McLachlan, *J. Chem. Phys.*, **45**, 628 (1966); T. Yonezawa, H. Nakatsumi, T. Kawamura, and H. Kato, *Bull. Chem. Soc. Jap.*, **40**, 2211 (1967); R. S. Drago and H. Peterson, Jr., *J. Amer. Chem. Soc.*, **89**, 5774 (1967); J. A. Pople, D. L. Beveridge, and P. A. Dobosh, *J. Amer. Chem. Soc.*, **90**, 4201 (1968); M. J. S. Dewar and M. Shansal, *J. Amer. Chem. Soc.*, **91**, 3654 (1969).
- (19) M. S. Liu, S. Soloway, C. K. Wedegaerter, and J. A. Kampmeier, *J. Amer. Chem. Soc.*, **93**, 3809 (1971); L. A. Singer and N. P. Kong, *ibid.*, **89**, 5251 (1967).
- (20) R. M. Kopchik, Ph.D. Thesis, University of Rochester, Rochester, N. Y., 1967; D. K. Wedegaertner, R. M. Kopchik, and J. A. Kampmeier, *J. Amer. Chem. Soc.*, **93**, 6890 (1971). In this last reference, brief mention is made of a CNDO study showing the most stable form of the 1-methoxyvinyl radical is bent and this is favored over the linear structure by 2.4 kcal/mol.
- (21) R. Sustmann, J. E. Williams, M. J. S. Dewar, L. C. Allen, and P. v. R. Schleyer, *J. Amer. Chem. Soc.*, **91**, 5350 (1969).
- (22) R. H. Hoffmann, *J. Chem. Phys.*, **40**, 2480 (1964).
- (23) A. Maccoll, *Chem. Soc., Spec. Publ.*, **No. 16**, 159 (1962).
- (24) F. P. Lossing, "Mass Spectrometry," C. A. McDowell, Ed., McGraw-Hill, New York, N. Y., 1963, Chapter 11.
- (25) For a review see H. G. Richey, Jr., and J. M. Richey in "Carbonium Ions," Vol. II, G. A. Olah and P. v. R. Schleyer, Ed., Wiley-Interscience, New York, N. Y., 1970, Chapter 21.
- (26) M. Hanack, *Accounts Chem. Res.*, **3**, 209 (1970).
- (27) A. G. Martinez, M. Hanack, R. H. Summerville, P. v. R. Schleyer, and P. J. Stang, *Angew. Chem.*, **82**, 323 (1970).
- (28) W. M. Jones and D. D. Maness, *J. Amer. Chem. Soc.*, **91**, 4314 (1969).

**TABLE I: Relative Energies of the Optimized Linear and Bent Geometries of 1-Substituted Vinyl Radicals**

Radicals	1 substituent	$\Delta E$ , kcal/mol	Most stable geometry
<b>4a vs. 4b</b>	F	6.9	Bent
<b>7 vs. 7-linear</b>	F	8.6	Bent
<b>8 vs. 8-linear</b>	F	8.8	Bent
<b>5a vs. 5b</b>	OCH <sub>3</sub>	4.8	Bent
<b>6a vs. 6b</b>	BH <sub>2</sub>	18.6	Linear
<b>6a' vs. 6b'</b>	BH <sub>2</sub>	8.1	Linear

**TABLE II: Calculated  $\pi$  Bond Orders of Vinyl Radicals<sup>a</sup>**

Radical	Bond	$\pi$ bond order	
		$\pi_y$	$\pi_x$
<b>4a</b>	C <sub>2</sub> -C <sub>1</sub>	0.936	0.332
	C <sub>1</sub> -F <sub>1</sub>	0.248	0.289 <sup>b</sup>
<b>4b</b>	C <sub>2</sub> -C <sub>1</sub>	0.968	0.430
	C <sub>1</sub> -F <sub>1</sub>	0.234	0.249
<b>5a</b>	C <sub>2</sub> -C <sub>1</sub>	0.958	0.353
	C <sub>1</sub> -O	0.237	0.010
<b>5b</b>	C <sub>2</sub> -C <sub>1</sub>	0.958	0.420
	C <sub>1</sub> -O	0.236	0.311
<b>7</b>	C <sub>2</sub> -C <sub>1</sub>	0.953	0.300
	C <sub>1</sub> -F <sub>1</sub>	0.217	0.294 <sup>b</sup>
	C <sub>2</sub> -F <sub>2</sub>	0.191	0.150
<b>8</b>	C <sub>2</sub> -C <sub>1</sub>	0.953	0.316
	C <sub>1</sub> -F <sub>1</sub>	0.217	0.302 <sup>b</sup>
	C <sub>2</sub> -F <sub>2</sub>	0.194	0.145 <sup>c</sup>
<b>6a</b>	C <sub>2</sub> -C <sub>1</sub>	0.644	0.424
	C <sub>1</sub> -B	0.693	0.313
<b>6b</b>	C <sub>2</sub> -C <sub>1</sub>	0.597	0.411
	C <sub>1</sub> -B	0.743	0.432
<b>6a'</b>	C <sub>2</sub> -C <sub>1</sub>	0.848	0.392
	C <sub>1</sub> -B	0.455	0.569
<b>6b'</b>	C <sub>2</sub> -C <sub>1</sub>	0.909	0.383
	C <sub>1</sub> -B	0.364	0.413
<b>d</b>	C <sub>2</sub> -C <sub>1</sub>	0.945	0.415
	C <sub>1</sub> -B	0.308	0.507

<sup>a</sup> The z axis is defined along the C<sub>2</sub>-C<sub>1</sub> bond unless otherwise noted.

<sup>b</sup> The z axis is defined along the C<sub>1</sub>-F<sub>1</sub> bond. <sup>c</sup> The z axis is defined along the C<sub>2</sub>-F<sub>2</sub> bond. <sup>d</sup> Radical **6** where the plane of the BH<sub>2</sub> group is rotated perpendicular to the molecular plane defined by B, C-1, C-2, H-1, and H-2.

Pople model builder program, QCPE No. 135. Initial estimates of the structure of 1-substituted vinyl radicals and 1-fluorovinyl cations were taken from available microwave data of vinyl fluoride<sup>29</sup> and *cis*-1,2-difluoroethylene.<sup>30</sup> Then the C<sub>1</sub> = C<sub>2</sub> and C<sub>1</sub>-X bond lengths and the C<sub>2</sub>C<sub>1</sub>X bond angle were varied systematically for minimum<sup>31</sup> energy resulting in the minimized structures given in the results. The H<sub>1</sub>C<sub>2</sub>H<sub>2</sub> and HC<sub>2</sub>C<sub>1</sub> angles and H-C<sub>2</sub> lengths for radicals **4**, **5**, and **6** and for cation **9** were not optimized but were assumed equal to those given for vinyl fluoride.<sup>29</sup> Similarly the H<sub>1</sub>C<sub>2</sub>F<sub>2</sub>, F<sub>2</sub>C<sub>2</sub>C<sub>1</sub>, and H<sub>1</sub>C<sub>2</sub>C<sub>1</sub> angles and C<sub>2</sub>-F<sub>2</sub> and C<sub>2</sub>-H lengths for radicals **7** and **8** and for cation **10** were obtained from those given for *cis*-1,2-difluoroethylene.<sup>30</sup> Sample calculations demonstrated that varying these angles and lengths had negligible effects on the results.

Calculations were carried out for each optimized geometry in different coordinate systems to obtain the bond order perpendicular and parallel to the bonds of interest. Unless otherwise indicated, the xz plane is the molecular

plane. For all radicals and cations, the letters a and b were used to indicate a bent geometry and a linear geometry, respectively, at the 1-substituent position. In the case of X = BH<sub>2</sub>, primes were also added to indicate the additional presence of an out-of-plane geometry.

## Results and Discussion

*1-Substituted Vinyl Radicals.* The calculated optimized geometries and total excess charge densities of both linear (**4b** and **5b**) and bent (**4a**, **5a**, **7**, and **8**) vinyl radicals are given in Figure 1. Figure 2 summarizes these data for four geometries (bent-planar (**6a**), linear-planar (**6b**), bent-out-of-plane (**6a'**), and linear-out-of-plane (**6b'**)) of vinyl radical **6**. The major feature to emerge is that the bent geometries are more stable in **4**, **5**, **7**, and **8** where either F or OCH<sub>3</sub> is the 1 substituent. Only when the 1 substituent is BH<sub>2</sub> does the linear geometry become more stable. The geometrical preference is expressed in Table I where the energy differences,  $\Delta E$ , between bent and linear geometries are listed. These values of  $\Delta E$  are also the barriers to isomerization for the radicals. It is clear that the bent geometry is stabilized, relative to linear, when the 1 substituent is an electronegative atom such as fluorine or oxygen. The more electropositive boron atom has the opposite effect. Thus, these INDO results strongly support Kampmeier's<sup>19</sup> postulate that the rate of isomerization is a function of the 1-substituent's electronegativity. Also the INDO results support the trend suggested by extended Hückel calculations on vinyl radicals showing the barrier to isomerization is greater for 1-OH and 1-F than for 1-CH<sub>3</sub>.<sup>20</sup>

A second major feature immediately apparent is that in both the linear or bent geometries of radical **6**, the plane defined by the BH<sub>2</sub> substituent prefers to be rotated out of the molecular plane (by 45° in the linear, (**6b**) geometry and 52° in the bent ( $\theta = 160^\circ$ , geometry), (**6a**)). This is a manifestation of the electronegativity difference between carbon and boron. The less electronegative boron may avoid accepting  $\pi$ -electron density donated from the carbon by undergoing partial rotation. The BH<sub>2</sub> plane does not rotate a full 90° because this would bring the vacant boron p orbital into conjugation with the p<sub>x</sub> orbital on C-1.<sup>32</sup> The relative energies of several optimized geometries of this radical are shown in Figure 3. The most stable geometry, **6b'**, is linear with the BH<sub>2</sub> plane rotated 45° to the molecular plane. Rotating 90° increases the energy 14.6 kcal/mol while the maximum energy for the linear geometry is the all-planar species **6b** which is 24.7 kcal/mol less stable than **6b'**. The all-planar-bent geometry, **6a**, is 43.3 kcal/mol less stable than **6b'** while rotating the BH<sub>2</sub> plane 52° (**6a'**) sharply increases the stability to within 8.1 kcal/mol of **6b'**.

The energy difference between the *trans*- and *cis*-1,2-difluorovinyl radicals (**7** and **8**) is negligible (*cis* is 0.2 kcal/mol more stable). The geometry at C-1, for both **7** and **8**, closely resembles that of **4a** ( $\theta = 136.7$ , 142.5, and 140° for **7**, **8**, and **4a**, respectively).

*$\pi$ -Bond Orders of Vinyl Radicals (see Table II).* In the 1-fluorovinyl radical (**4**), the C<sub>1</sub>-F<sub>1</sub>  $\pi_y$  bond order is about

(29) D. R. Lide, Jr., and D. Christensen, *Spectrochim. Acta*, **17**, 665 (1961).

(30) V. W. Laurie, *J. Chem. Phys.*, **34**, 291 (1961).

(31) J. A. Nelder and R. Mead, *Comput. J.*, **7**, 308 (1964).

(32) The interaction of the occupied carbon orbital with the empty boron orbital is not, in itself, destabilizing. Rather, this interaction reduces C-C  $\pi$  overlap and the net result is destabilizing.

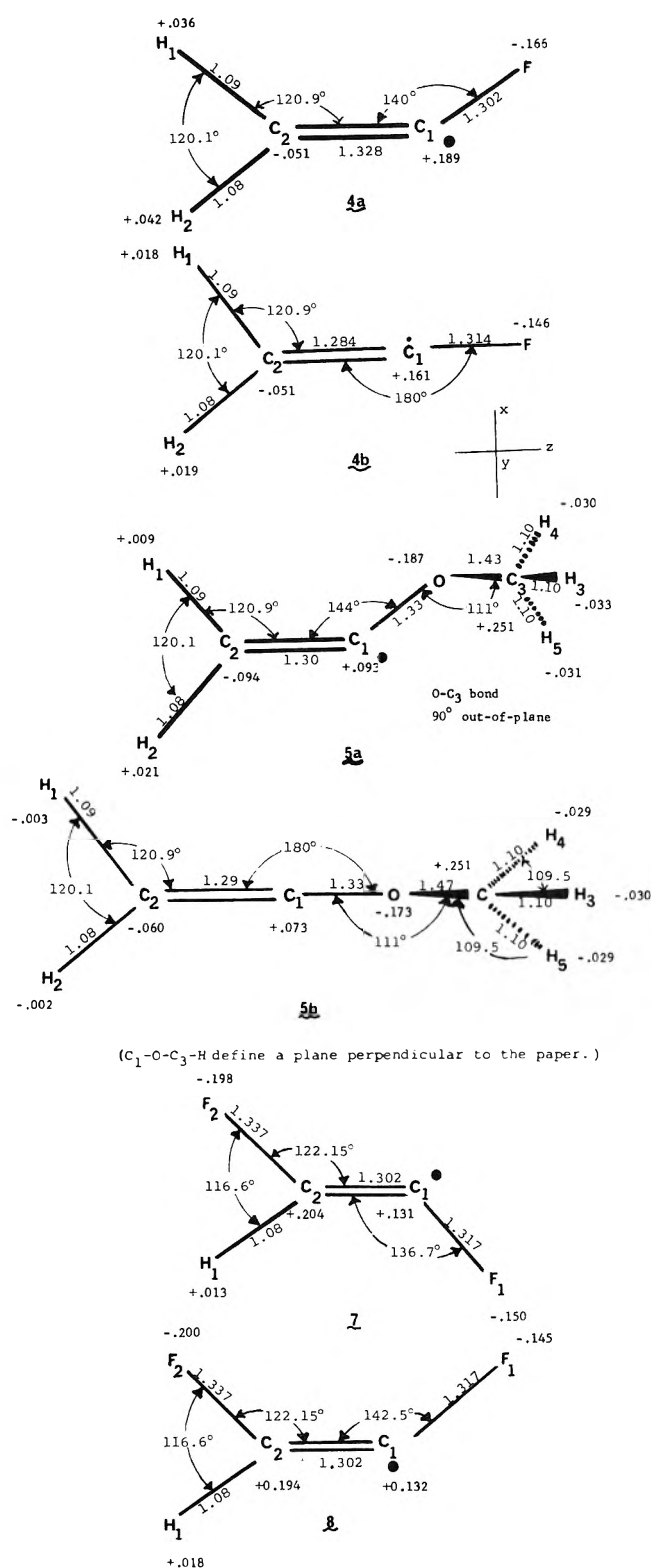


**Figure 1.** INDO optimized geometries and total charge densities of 1-substituted vinyl radicals 4a, 4b, 5a, 5b, 7, and 8.

the same in both the bent (4a) and linear (4b) geometries (0.248 and 0.234, respectively). This is also true of  $\pi_x$  bond orders (0.289 and 0.249). The magnitude of the  $\pi_y$  and  $\pi_x$  bond orders are about equal in both geometries of this radical. Since the  $C_1-F_1$  bond length changes only slightly ( $\Delta l = 0.012$  Å between 4a and 4b), the decrease in the  $\pi_x$  bond order going from bent to linear (where the  $C_1$   $p_x$  orbital is now of the proper symmetry for maximizing

$\pi_x$  bonding) is surprising. The same trends and magnitudes are found for  $C_1-F_1$   $\pi$  orders in both *trans*- and *cis*-1,2-difluorovinyl radicals 7 and 8. The  $C_2-F_2$   $\pi_y$  orders in 7 and 8 are of about the same magnitude as the  $C_1-F_1$   $\pi_y$  orders in 4a, 4b, 7, and 8. However, the  $\pi_x$  orders for  $C_1-F_1$  are greater than the  $\pi_x$  orders for  $C_2-F_2$  when this comparison is made. In the 1-methoxyvinyl radical, the values of  $\Delta\pi_y$  (*i.e.*, change in  $\pi_y$  bond order) for the  $C_2-C_1$  and  $C_1-O$  bonds is negligible going from bent 5a to linear 5b. Again, the bond lengths change little in this process.

When the 1 substituent is  $BH_2$  (6), the  $C_1-B$   $\pi_y$  bond order is very large in both the bent-planar (6a) and linear-planar (6b) geometries (*i.e.*,  $\pi_y = 0.693$  and 0.743, respectively). This effective "conjugation" greatly reduces the  $C_2-C_1$   $\pi_y$  bond order (0.544 in 6a and 0.597 in 6b). By rotating the  $BH_2$  plane in the bent or linear structures out of the plane, the  $C_1-B$   $\pi_y$  bond order is sharply decreased (to 0.455 in 6a' and 0.364 in 6b'). Simultaneously the  $C_2-C_1$   $\pi_y$  bond orders increase to 0.848 in 6a' and 0.909 in 6b'. For the linear geometry the  $\Delta\pi_y$  bond orders on rotation (6b  $\rightarrow$  6b') are  $-0.379$  for  $C_1-B$  and  $+0.312$  for  $C_2-C_1$ . Rotating the  $BH_2$  plane still further to  $90^\circ$  in the linear geometry results in a further decrease in the  $\pi_y$  order of the  $C_1-B$  bond and an increase in  $\pi_y$  order of the  $C_2-C_1$  bond. However, the changes are now much smaller and are accompanied by an increase in the  $\pi_x$  bond order for the  $C_1-B$  bond. It is clear that the minimum energy for radical 6 is achieved when the  $C_1-B_1$   $\pi$  bond orders are reduced to a minimum while achieving as much  $C_1-C_2$   $\pi_y$  bond order as possible. The less available boron is to accept electron density *via*  $\pi$  bonding at the expense of C-C  $\pi$  bonding, the more stable 6 becomes.

**Charge Distribution in 1-Substituted Vinyl Radicals.** The total charge densities on the vinyl radicals are summarized in Figures 1 and 2. Very little change in the total charge densities accompanies the geometry change from bent to linear. This is true when the 1 substituent is F,  $OCH_3$ , or  $BH_2$ . Also there is a negligible change in total charge densities accompanying the *trans* to *cis* isomerization of 7 to 8. As expected the positive charge density at C-1 decreases in the series where the 1 substituent changes from F to  $OCH_3$  to  $BH_2$ .

Examining the  $p_x$ ,  $p_y$ , and  $p_z$  charge densities (see Table III) shows that converting bent radicals 4a, 5a, or 6a to their linear forms 4b, 5b, or 6b causes only small changes in the  $p_x$ ,  $p_y$ , or  $p_z$  charge densities. Isomeric radicals 7 and 8 also have charge distributions similar to each other. By defining the  $z$  axis along the C-F bonds in 4a, 7, and 8 a view of the  $\sigma$  bond is obtained by comparing the carbon and fluorine  $p_z$  densities. At both C-1 and C-2 the  $\sigma$  bonds to fluorine are highly polarized toward fluorine (*i.e.*,  $1 - q$  for  $p_{z(C-1)} = +0.273$  and for  $p_{z(F-1)} = -0.474$  in 4a). The magnitude of this polarization is about the same for the  $C_1-F_1$  and the  $C_2-F_2$   $\sigma$  bonds. Apparently the radical center at C-1 does not seriously perturb the  $\sigma$  bond. The magnitude of the total charge densities at C-1 (+0.131 in 7 and +0.132 in 8) and C-2 (+0.204 in 7 and +0.194 in 8) are due largely to the highly polarized  $\sigma$  bond with some  $\pi_x$  and  $\pi_y$  back donation from fluorine reducing the magnitude of the overall charge separation. In 7 and 8 the extent of  $\pi_x$  and  $\pi_y$  back donation from fluorine is slightly greater at C-1 than at C-2. This accounts for the lower positive charge density at C-1.

There is a marked change in total charge distribution in 6 as the  $BH_2$  plane is rotated out of the molecular plane



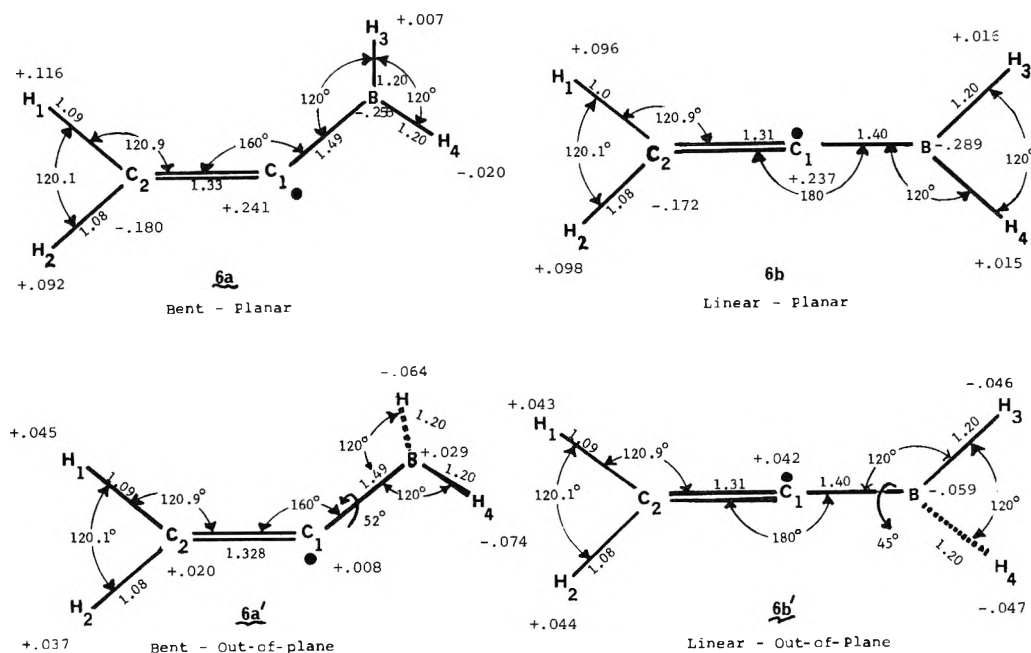


Figure 2. INDO geometries and total charge densities of 1-BH<sub>2</sub>-substituted vinyl radicals.

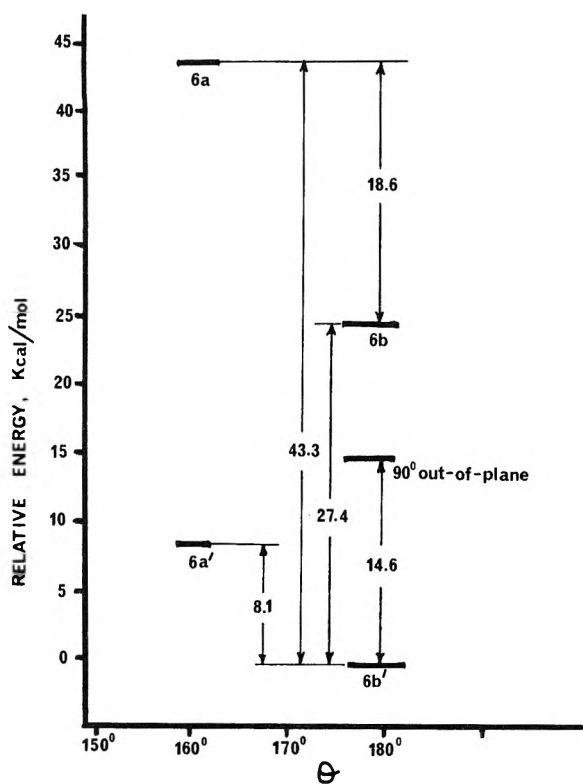


Figure 3. Relative energies for several geometries of the 1-BH<sub>2</sub>-substituted vinyl radical.

(by 52 and 45° in 6a' and 6b', respectively) for both linear and bent forms. In both cases there is (1) a sharp reduction of electron density at boron, (2) a parallel increase in electron density at C-1, (3) a decrease in electron density at C-2, and (4) an increase at H-1 and H-2. When the BH<sub>2</sub> plane becomes perpendicular to the molecular plane, the electron densities at boron and C-1 decrease while that at C-2 increases slightly. Rotation of the BH<sub>2</sub> plane

also produces large changes in the C-1 p<sub>x</sub> and B p<sub>x</sub> charge densities and moderate changes in the C-2 p<sub>y</sub> and B p<sub>y</sub> orbitals. For example, the electron density in the C-1 p<sub>x</sub> orbital increases as the rotation of the BH<sub>2</sub> plane takes place going from 6a → 6a' and then decreases slightly on further rotation to 90° (see Table III).

*Unpaired Spin Distribution in 1-Substituted Vinyl Radicals.* In the bent geometries of 4, 5, 7, and 8 the s orbital spin density is greater at C-1 (and F-1 for 4, 7, and 8) than in the corresponding linear geometries. The amount of s orbital spin density at C-2, H-1, and H-2 increases going to the linear geometry. These changes, summarized in Table IV, result in the predicted hyperfine couplings shown there. However, the calculations predict a remarkable difference in the s orbital spin density when the 1 substituent is BH<sub>2</sub>. In the bent-planar (6a) and linear-planar (6b) geometries, much larger s orbital spin densities are predicted at C-2 and B. On rotating the BH<sub>2</sub> plane (6a → 6a' and 6b → 6b') the C-2 and B s orbital spin densities decrease while those on H-1, H-2, H-3, and H-4 increase. The predicted esr spectra of the bent- and linear-planar geometries differ only slightly, but the predicted spectra of bent and linear out-of-plane (6a' and 6b') differ markedly from each other as well as from 6a and 6b.

Changes in the p<sub>x</sub>, p<sub>y</sub>, and p<sub>z</sub> orbital unpaired spin densities follow the same general pattern. When the 1 substituent is F or OCH<sub>3</sub>, the greatest spin density is found in the C-1 p<sub>x</sub> orbital for the bent geometries, and large spin densities are also found in the F or O p<sub>x</sub> and the C-1 p<sub>z</sub> orbitals. In the linear geometries the p<sub>x</sub> spin density increases substantially. Again, it is when BH<sub>2</sub> is the 1 substituent that entirely different spin distributions are calculated. In both bent 6a and linear 6b planar structures, the largest spin densities are found in the C-2 and B p<sub>y</sub> orbitals! For 6a and 6b the C-2 p<sub>y</sub> spin densities are 0.604 and 0.658 while those for B p<sub>y</sub> are 0.477 and 0.422, respectively. The sum of the unpaired p<sub>x</sub>, y, and z unpaired spin density at C-1 is less than 0.1. This is in sharp con-

**TABLE III: Charge Densities and Unpaired Spin Densities in the  $p_x$ ,  $p_y$ , and  $p_z$  Orbitals of Vinyl Radicals<sup>a</sup>**

Radical atom	Charge density			Unpaired spin density		
	$p_x$	$p_y$	$p_z$	$p_x$	$p_y$	$p_z$
<b>4a</b>	0.175					
C-1	0.050 <sup>b</sup>	0.068	0.273 <sup>b</sup>	0.453 (0.587 <sup>b</sup> )	0.074	0.155 (0.021 <sup>b</sup> )
C-2	0.063	-0.125	0.035	-0.041	-0.079	0.005
F	0.091 <sup>b</sup>	0.058	-0.474 <sup>b</sup>	0.112 (0.076 <sup>b</sup> )	0.005	-0.016 (0.020 <sup>b</sup> )
<b>4b</b>						
C-1	-0.090	0.073	0.253	0.758	0.052	0.016
C-2	0.075	-0.124	0.050	-0.078	-0.055	-0.046
F	0.071	0.051	-0.426	-0.068	0.003	-0.028
<b>5a</b>						
C-1	0.081	0.085	0.115	0.485	0.057	0.111
C-2	0.080	-0.142	0.031	-0.049	-0.061	-0.005
O	1.654 <sup>d</sup>	1.381 <sup>d</sup>	1.525 <sup>d</sup>	0.145	0.005	-0.012
<b>5b</b>						
C-1	-0.121	0.190	0.191	0.721	0.048	0.015
C-2	0.086	-0.147	0.048	-0.074	-0.052	-0.043
O	1.854 <sup>d</sup>	1.383 <sup>d</sup>	1.315 <sup>d</sup>	0.114	0.001	-0.025
<b>7</b>						
C-1	0.181 (0.069 <sup>b</sup> )	-0.0084	0.265 <sup>b</sup>	0.442	0.075	0.184
C-2	0.196	-0.0786	0.243 <sup>c</sup>	-0.039	-0.074	0.018
F-1	0.095 <sup>b</sup>	0.0474	-0.448 <sup>b</sup>	0.101	0.005	-0.012
F-2	0.023 <sup>c</sup>	0.0396	-0.409 <sup>c</sup>	0.026	-0.006	0.003
<b>8</b>						
C-1	0.165 (0.063 <sup>b</sup> )	-0.014	0.270 <sup>b</sup>	0.498 (0.596 <sup>b</sup> )	0.072	0.127 (0.029 <sup>b</sup> )
C-2	0.188	-0.075	0.255 <sup>c</sup>	-0.042	-0.071	-0.017
F-1	0.100 <sup>b</sup>	0.0478	-0.449 <sup>b</sup>	0.114 (0.086 <sup>b</sup> )	0.004	-0.017 (0.11 <sup>b</sup> )
F-2	0.024 <sup>c</sup>	0.0406	-0.408 <sup>c</sup>	0.066	-0.005	0.061
<b>6a</b>						
C-1	0.622	-0.139	-0.077	-0.001	-0.081	-0.016
C-2	0.063	-0.185	0.010	0.017	0.604	-0.017
B	0.168	0.324	0.196	0.011	0.477	0.011
<b>6b</b>						
C-1	0.604	-0.140	-0.084	-0.001	-0.080	-0.017
C-2	0.061	-0.169	-0.004	0.018	0.658	0.019
B	0.151	0.308	0.184	0.009	0.422	0.009
<b>6a'</b>						
C-1	0.156	0.048	-0.049	0.502	-0.030	0.012
C-2	0.079	0.020	-0.008	-0.042	-0.118	-0.024
B	0.594 <sup>d</sup>	0.632 <sup>d</sup>	0.793 <sup>d</sup>	0.049	0.116	0.021
<b>6b'</b>						
C-1	0.173	0.047	-0.054	0.422	-0.076	-0.000
C-2	0.072	0.046	-0.018	-0.030	0.253	-0.015
B	0.683 <sup>d</sup>	-0.612 <sup>d</sup>	0.829 <sup>d</sup>	0.042	0.156	-0.013

<sup>a</sup> Unless otherwise noted, the z axis is defined along the C<sub>2</sub>-C<sub>1</sub> bond and the y axis perpendicular to the molecular plane (xz is the plane of vinyl group).  
<sup>b</sup> The z axis is defined along the C<sub>1</sub>-F<sub>1</sub> bond. <sup>c</sup> The z axis is defined along the C<sub>2</sub>-F<sub>2</sub> bond. <sup>d</sup> Electron density  $q$  (not charge density).

trast to the bent and linear forms of 4, 5, 7, and 8 where the  $p_y$  spin densities are very small.

When either the bent or planar geometries of 6 have the BH<sub>2</sub> plane rotated out of the molecular plane to 6a' or 6b', a large increase in the C-1  $p_x$  spin density occurs (from -0.001 in 6a or 6b to 0.422 in 6a' or 0.502 in 6b'). This is accompanied by marked decreases in both the C-2 and B  $p_y$  spin densities. The C-2  $p_y$  spin density, for example, decreases from 0.604 and 0.658 in 6a and 6b to -0.118 and 0.253 in 6a' and 6b', respectively. Thus, partial BH<sub>2</sub> rotation is forcing unpaired spin density back into the C-1  $p_x$  orbital. Rotating the BH<sub>2</sub> plane to 90°, in the linear geometry, causes only a small further increase in the C-1  $p_x$  orbital (to 0.491) but a continued large decrease in C-2 and B  $p_y$  spin densities (to -0.033 and +0.005) is noted. With the BH<sub>2</sub> plane perpendicular to the molecular plane, the vacant p orbital on boron lies parallel to the x axis in the proper geometry for maximum C-B  $\pi_x$  overlap. Thus, it is not surprising to see a sharp increase (from 0.042 to 0.329) in the boron  $p_x$  unpaired spin density on rotation of the EH<sub>2</sub> plane from 45° (6b') to 90°.

Summarizing, when the BH<sub>2</sub> plane coincides with the

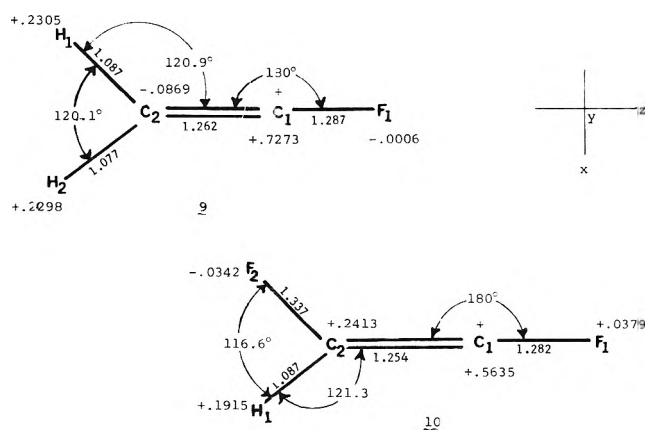


**Figure 4.** INDO optimized geometries and excess charge densities on fluorovinyl cations 9 and 10.

molecular plane, the unpaired spin is concentrated largely in the C-2 and B  $p_y$  orbitals, whether the geometry is bent or linear. Upon rotating the BH<sub>2</sub> plane 45° (52°), the radical is stabilized and the spin density in the C-1  $p_x$  orbital increases sharply at the expense of the C-2 and B  $p_y$  spin

TABLE IV: Calculated s Orbital Unpaired Spin Densities and ESR Hyperfine Coupling Constants for Radicals

Radical atom	s orbital spin density	Hyperfine coupling constant, G	Radical atom	s orbital spin density	Hyperfine coupling constant, G	
4a	C-1	0.1762	8	C-1	0.1684	
	C-2	-0.0075		C-2	0.0084	
	F	0.0039		F-1	0.0030	
	H-1	0.1223		F-2	0.0047	
	H-2	0.0375		H-1	0.0248	
4b	C-1	0.0420	6a bent-planar	C-1	-0.0115	
	C-2	-0.353		C-2	0.0285	
	F	-0.0013		B	0.0208	
	H-1	-0.1518		H <sub>1</sub>	-0.0226	
	H-2	-0.1510	H <sub>2</sub>	-0.0218		
5a	C-1	0.1392	6b linear planar	C-1	-0.0112	
	C-2	-0.0094		C-2	0.0312	
	C-3	0.0004		B	0.0176	
	O	0.0085		H <sub>1</sub>	-0.0249	
	H-1	0.1370	H <sub>2</sub>	-0.0241		
	H-2	0.0492	H <sub>3</sub>	-0.0129		
	H-3	0.0006	H <sub>4</sub>	-0.0130		
	H-4	0.0019	Bent 6a'	C-1	0.0282	
	H-5	0.0024		out-of-plane	C-2	-0.0152
5b	C-1	0.0385		B	-0.0020	
	C-2	-0.0331		H-1	0.1085	
	C-3	0.0006		H-2	0.0988	
	O	0.0044	H-3	0.0419		
	H-1	0.1438	H-4	0.0183		
	H-2	0.1429	Linear 6b'	C-1	0.0103	
	H-3	-0.0006		out-of-plane	C-2	-0.0048
	H-4	-0.0007		B	-0.0057	
	H-5	-0.0006		H-1	0.0514	
7	C-1	0.1652	H-2	0.0506		
	C-2	-0.0137	H-3	0.0790		
	F-1	0.0030	H-4	0.0804		
	F-2	0.0017				
	H-1	0.1207				

densities. Further rotation to 90° returns a significant amount of unpaired spin to boron via  $\pi_x$  overlap.

*Fluorovinyl Cations.* The bond angles, bond lengths, and total excess charge densities in vinyl cations **9** and **10** are shown in Figure 4. The calculated  $\pi$  bond orders are compiled in Table V along with the  $p_x$ ,  $p_y$ , and  $p_z$  charge densities. The most striking feature of cations **9** and **10** is their linear (*sp* at  $C_1$ ) structure. The preference for this linear geometry is large. For example, the energy of cation **9** increases by 2.0 kcal/mol when the  $C_1-F_1$  bond is bent 10° in the molecular plane (*i.e.*,  $\theta = 170^\circ$ ). Bending still further to  $\theta = 160, 140,$  and  $120^\circ$  increases the energy of **9** by 7.3, 29.7, and 70.0 kcal/mol, respectively. Although the energy of the bent geometry of cation **9** ( $\theta = 120^\circ$ ) is much greater than that of the linear geometry, the charge distribution was found to change only slightly. The  $C_1-F$   $\pi_y$  bond order decreases by 0.02 and the  $C_1-C_2$   $\pi_y$  order increases by 0.0032 on decreasing  $\theta$  to  $120^\circ$ .

Significant back  $\pi$  bonding from fluorine to C-1 occurs in both **9** and **10**. This takes place between the fluorine and carbon  $p_x$  orbitals. In spite of the large charge on C-1 in both **9** and **10**, the  $\sigma$  bond between C-1 and fluorine is still strongly polarized toward fluorine ( $1 - q$  for  $F_1 p_z$  orbital = -0.402). Unlike the unsubstituted vinyl cation,  $CH_2=CH^+$ , studied by Dewar, Allen, and Schleyer,<sup>21</sup> separation of the charge for **9** into  $\sigma$  and  $\pi$  contributions indicates very little polarization of the C-2  $\pi$  electrons

toward C-1 takes place ( $1 - q$  for  $p_y = -0.360$  for C-1 and -0.015 for C-2). The lack of charge transmission from C-2 to C-1 is also illustrated by the total charge densities. In vinyl cation **9** the charge at C-2 is -0.087 ( $4 - q$ ). The same is true in **10** where the larger positive charge density at C-2 ( $+0.241 = 4 - q$ ) results, largely, from the strongly polarized  $C_2 \rightarrow F$   $\sigma$  bond and not from a strong interaction with C-1.

There are two major sources of stabilization of the empty  $p_x$  orbital at C-1 in **9**. The first is a hyperconjugative interaction of the  $C_2-H_1$  and  $C_2-H_2$   $\sigma$  bonds with the vacant  $p_x$  orbital. This results in large plus charge densities at H-1 (+0.231) and H-2 (+0.230).<sup>33</sup> Second, the availability of back  $\pi$  donation from  $p_x$  on fluorine supplies a substantial portion of the electron density found in the  $p_x$  orbital of C-1. This results in a large  $\pi_x$  bond order between  $C_1$  and  $F_1$  in both **9** (0.512) and **10** (0.592), respectively. Finally, it is instructive to compare the total charge densities ( $7 - q$ ) at F-1 in ions **9** (-0.0006) and **10** (+0.0379) with that of vinyl fluoride (-0.182).<sup>34</sup> This difference results from F-1  $\rightarrow$  C-1  $\pi_x$  back donation in cations **9** and **10**.

(33) In ethylene, the charge density on hydrogen is +0.015. See ref 34, p 118.

(34) From INDO calculations cited in J. A. Pople and D. L. Beveridge, "Approximate Molecular Orbital Theory," McGraw-Hill, New York, N. Y., 1970.

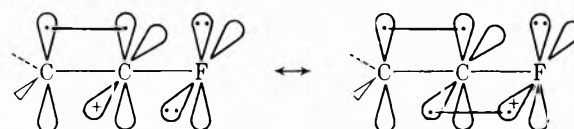
**TABLE V:  $\pi$  Bonding Orders and Excess Charge Densities in  $p_x$ ,  $p_y$ , and  $p_z$  Orbitals for 9 and 10**

Quantity	Cation	
	9	10
$\pi$ Bond Orders		
$\pi_y$ C <sub>1</sub> -C <sub>2</sub>	0.9744	0.9478
$\pi_y$ C <sub>1</sub> -F <sub>1</sub>	0.2220	0.1921
$\pi_x$ C <sub>1</sub> -F <sub>1</sub>	0.5121	0.5923
$\pi_y$ C <sub>2</sub> -F <sub>2</sub>		0.2338
Excess Charge Densities		
C <sub>1</sub> $p_x$	+0.5476	+0.5886
1 - q $p_y$	-0.0360	-0.1414
$p_z$	+0.2121	+0.2136
C <sub>2</sub> $p_x$	-0.0127	+0.1066
1 - q $p_y$	-0.0152	+0.0462
$p_z$	+0.0277	+0.1135
F <sub>1</sub> 2 - q $p_x$	+0.1800	+0.2279
2 - q $p_y$	+0.0511	+0.0430
1 - q $p_z$	-0.4017	-0.4052
F <sub>2</sub> 2 - q $p_y$		+0.0522
3 - (q( $p_x$ ) + q( $p_z$ ))		-0.2302

The C<sub>1</sub>-F<sub>1</sub> bond distances in both 9 and 10 are substantially shorter than normal vinyl carbon-fluorine distances. For example, the C<sub>1</sub>-F<sub>1</sub> distance in 10 of 1.2815 Å is 0.055 Å shorter than the C<sub>2</sub>-F<sub>2</sub> distance of 1.337 Å found in 1,2-

difluoroethylene. This contraction is expected due to (1) the greater s character in the C-1 bonding orbital, (2) the reduced C-1 van der Waal radius which results from its high positive charge density, and (3) the increased  $\pi_x$  bonding between C-1 and F-1. The latter effect is represented by the allenic resonance hybrid.

It may be concluded that the linear geometry of the 1-fluorovinyl cations results from the sp hybridization at C-1 which permits the bonding orbitals to utilize a maximum of s character. The "vacant" p orbital, as in the methyl cation, is at a maximum distance from the nucleus. Conversion from linear (sp) to in-plane bent (sp<sup>2</sup>) geometry formally requires promotion of 1/3 of an electron from an s to a p orbital. There is no advantage gained by this promotion since the charge distribution and  $\pi$  bond orders do not change markedly upon bending. Thus, this promotion is unfavorable and the linear geometry prevails.



*Acknowledgments.* We wish to thank the Alabama Computer Center for making available an extensive amount of computer time and John Prather for some preliminary calculations on the fluoro substituents.

## The Determination of the Intermolecular Forces of Attraction between Macroscopic Bodies for Separations down to the Contact Point

A. I. Bailey\* and H. Daniels

*Institute für Physik und Chemie der Grenzflächen der Fraunhofer-Gesellschaft, 7000 Stuttgart 1, West Germany  
(Received May 22, 1972)*

An analysis of the forces of attraction between two sheets of mica forming a double cantilever beam system has been made. The intermolecular attraction acting in the gap near the bifurcation point causes the sheets to be drawn toward each other. Distributed loads which account for this additional deflection are discussed. Within the limits of accuracy of this experiment the intermolecular attraction between elementary areas may be described as the superposition of (i) the sum of ionic forces varying as the inverse square of the separation for very small separations and dying off exponentially and (ii) dispersion forces varying as the inverse cube of the separation for separations less than about 30 nm and as the inverse fourth power of the separation for larger separations. The results show that the energy of interaction is due primarily to the ionic structure of the crystal even when the patterns of positive and negative charge sites on the adjacent sheets do not match each other. The contribution of the dispersion forces to the cleavage energy is only about 8% of the total energy. At separations greater than 550 nm the attraction is almost entirely due to dispersion forces.

### Introduction

During the past decade great progress has been made in our understanding of the processes occurring at surfaces

and interfaces. This has been stimulated partly by interest in neighboring fields such as investigations on colloid systems and adhesion between solids. Measurements of surface and interfacial energies, heats of wetting, contact

angles, and adsorption have provided a large body of knowledge which has contributed to this progress.

The forces giving rise to surface and interfacial energy can be any of the intermolecular attractions which exist between atoms and molecules or a superposition of a number of these. Detailed information about the magnitude and range of intermolecular forces, besides being of fundamental interest, is important in the study of the structure of large molecules, for instance polymers and proteins, and of assemblies of molecules such as we have in membranes, micelles, and so on.

Theoretical expressions for the various kinds of intermolecular interactions have been in existence for a long time. The success of the many equations for surfaces and interfaces which assume that these expressions hold, leads us to expect that they must be largely true. Many experiments have been designed to verify the theory by measuring the forces directly. The complex nature of actual solid surfaces, their shape, deformation, roughness, the presence of adsorbed films, stray electric charges, and so on have made this a difficult field to work in.

The double-cantilever beam method for measuring the surface energy of elastic solids<sup>1</sup> may be used also to examine the strength of the forces of interaction. This is done, as will be shown in detail, by observing the shape of the cantilevers in the region where they separate from each other. The method has a great advantage over other methods in that the precise value of the energy of interaction is determined at the same time. It also allows measurements to be made for separations of several hundred nanometers down to the contact point and thus the region where the forces have their maximum strength is included.

Some of the problems inherent in previous work can be eliminated by using mica. This material has such perfect cleavage that large areas can be produced in which the cleavage has run true to a single plane of atoms on both sides of the sheet. Such sheets when first cleaved are covered only with a layer of adsorbed water.

The first experiments were designed to see whether the forces were large enough to cause bending in thin sheets of mica. An arrangement consisting of two sheets bent into cylindrical shape and mounted so that their axes were at right angles to each other<sup>2</sup> was used to test this. The lower sheet was relatively thick and the upper one was as thin as could be handled conveniently. The inner surfaces of the cylinders were coated with a highly reflecting layer of silver and the multiple-beam interference pattern formed between the two was observed. In monochromatic light this pattern resembles Newton's rings while the fringes of equal chromatic order consist of arcs. Near the upper specimen a small reference mirror was fixed. This mirror was also silvered and its curvature was arranged to be such that the Fizeau fringe pattern formed between it and the upper cylinder was hyperbolic so that the two patterns could be distinguished readily.

The tilt and position of the small mirror were adjustable. The upper specimen was rigidly fixed to a micromanipulator so that the specimens could be moved through the smallest observable amounts. As the cylindrical specimens approached each other, a point was reached when the hyperbolic fringe pattern showed that the upper cylinder was beginning to deflect. The separation at this point could be determined from the Newton's rings pattern or from the fringes of equal chromatic order. The de-

flexion increased as the distance of closest approach decreased, until arriving at a point of instability when the upper cylinder flew into contact with the lower one. This effect has since been used very successfully by Tabor and Winterton<sup>3</sup> to measure the forces of interaction at separations, down to 5 nm.

A considerable part of the initial attraction may be due to stray electrostatic charging of the sheets unless an ionizing source is present. Introduction of such a source reduced the distance of instability from 200 to 20 nm in one experiment. An ionizing source was present in all subsequent measurements made in air.

The intermolecular attractions were thus shown to be large enough to cause distortion in thin sheets. It follows, therefore, that when two sheets of mica are in contact over part of their area, the mica near the region of contact must be distorted by the action of one sheet on the other.

### Experimental Section

(a) *Model Experiments.* To check this we examined the fringes of equal chromatic order formed by a strip of mica partially cleaved at one end and held open with a small cylindrical spacer. The fringes showed that the deflection of the strips near the line of bifurcation was less than that expected for a cantilever having the same dimensions and Young's modulus as the sample. In other words the sheets are closer together near the origin than they would be if no attractive forces were acting between them where the separation is small.

Treating the strips as elastic beams of length,  $L$ , and breadth,  $b$ , the attraction can be simulated by a load per unit length,  $wb$ , along the strip. This loading will not be linear and will be some function of the separation,  $Y$ , at any point along the beams.

When mica is cleaved the energy required to do so is partly used in overcoming these attractive forces. This component is the surface energy,  $\gamma$ , so that

$$2\gamma = \int_0^{\infty} bw(Y)dY$$

or, since the system is symmetrical, we may consider only one of the pair of strips, then for  $y = Y/2$

$$\gamma = \int_0^{\infty} bw(y)dy \quad (1)$$

If  $x$  represents the distance along the beam from the point of contact between the two beams, let us consider what type of function  $w(x)$  is likely to be. In the region where the mica strips are joined, each atom in the solid is in an equilibrium position determined by the mutual attractions and repulsions between the atoms constituting the solid. Once we move into the region of separation, these forces are no longer in equilibrium and the solids would approach one another unless restrained from doing so by the elastic forces in the beam resulting from the externally applied loads. Hence at the origin where each atom is again in its equilibrium position, the distributed load must be zero. At some point along the beam where the separation is sufficiently large the attraction will again be

(1) A. I. Bailey, *Proc. Int. Congr. Surface Activ.*, 2nd 189 (1957).

(2) A. I. Bailey and J. S. Courtney-Pratt, *Proc. Roy. Soc., Ser. A*, **227**, 500 (1955).

(3) D. Tabor and R. Winterton, *Proc. Roy. Soc., Ser. A*, **312**, 435 (1969).

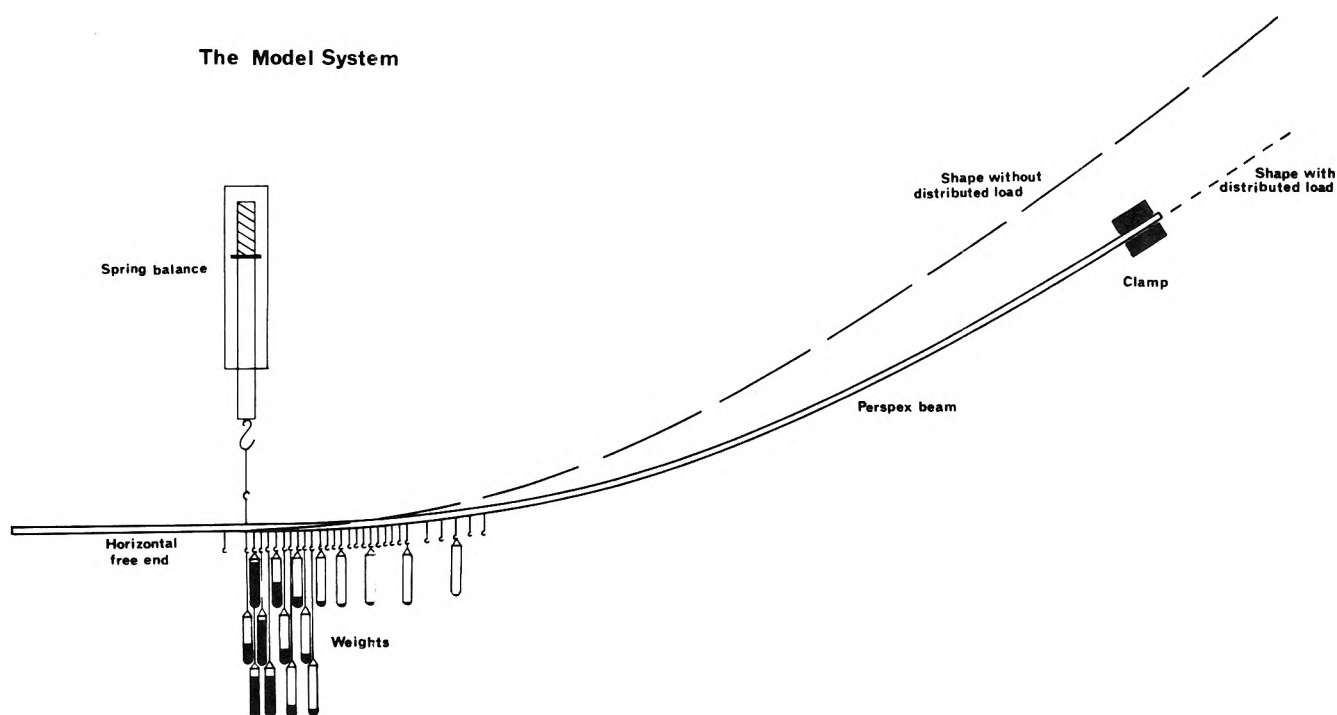


**Figure 1.** The model system consisting of a long Perspex beam loaded with tubes containing lead shot used to explore the type of loading required to cause the observed deflection.

zero. The function will therefore have a maximum somewhere along the length of the beam and presumably very close to the origin.

Dr. D. Ashwell suggested to us that one might readily obtain some idea of the magnitude and distribution of the loading by performing simple experiments using model beams. Thus the arrangement shown in Figure 1 was set up. The beams consisted of strips of Perspex about 1.5 cm wide and 75 cm long. A thickness of 2.5 mm was found to be suitable. Hooks from which weights could be hung were attached at 5-mm intervals from the point which was to serve as the origin. A graph of the observed shape was drawn on paper and fixed to a vertical board. The theoretical shape of a cantilever of corresponding length with no distributed load was also drawn on this sheet, the two curves having the same origin. The Perspex beam was then held up by a spring balance at the origin and the far end was clamped so as to have the same slope as the observations at that point. Narrow plastic tubes were attached to the hooks and lead shot poured into them and adjusted from one tube to another until the Perspex assumed the shape of the graph and the unloaded portion beyond the origin showed the slope to be zero at the origin.

It was found that with no distributed loading but with a force and a couple at the origin, the beam assumed the theoretical shape for no distributed load. The loading required to produce the observed shape is shown in Figure 2 and the effect of reducing this distributed load to an equivalent load and a couple at the origin is also shown. The Perspex strips have a slight tendency to deform plastically if the loads are left on for any length of time so that experiments of this kind do not give results which are quantitatively reproducible. The general shape of the load, with a high peak very close to the origin and tailing off more slowly, was always observed. The other striking

feature of the experiment is the large value of the load necessary to produce this relatively small distortion.

(b) *Experiments on Mica Cantilevers.* It is desirable that the interfacial energy of the mica should be determined at the same time as the observations on the shape are made. This is because slight variations in the experimental conditions can produce measurable changes in the interfacial energy, and it is important that the energy should relate exactly to the forces causing the distortions if eq 1 is to be valid.

Specimens were prepared by cleaving a piece of mica to a suitable thickness, such as 4 to 6  $\mu\text{m}$ . A facet of constant thickness was chosen and cut into two portions, the cut being made parallel to the direction of one of the refractive indices of the crystal. The two halves were then aligned, placed in contact, and allowed to adhere to each other. This process was carried out in a dust-free chamber. Strips about 2 cm long and 3 mm wide were cut following the direction of the refractive index. They were then silvered and the high-dispersion Fizeau fringes were examined. The sample should appear of perfectly uniform intensity over its entire area and should transmit light of a wavelength of 546 nm (Hg green) with approximately half maximum intensity.

The experimental arrangement is essentially the same as that used previously by Bailey and Kay<sup>4</sup> to measure surface and interfacial energies. A strip of mica is partially cleaved at one end and the ends so formed were fitted into a pair of parallel, horizontal clamps. The other end of the strip is free (see Figure 3). By separating the clamps the strip may be cleaved further. For any particular separation between the clamps the cleavage proceeds until it attains a position where all the forces acting on the mica are in equilibrium. This equilibrium is perfectly stable as

(4) A. I. Bailey and S. M. Kay, *Proc. Roy. Soc. Ser. A.*, **301**, 47 (1967).

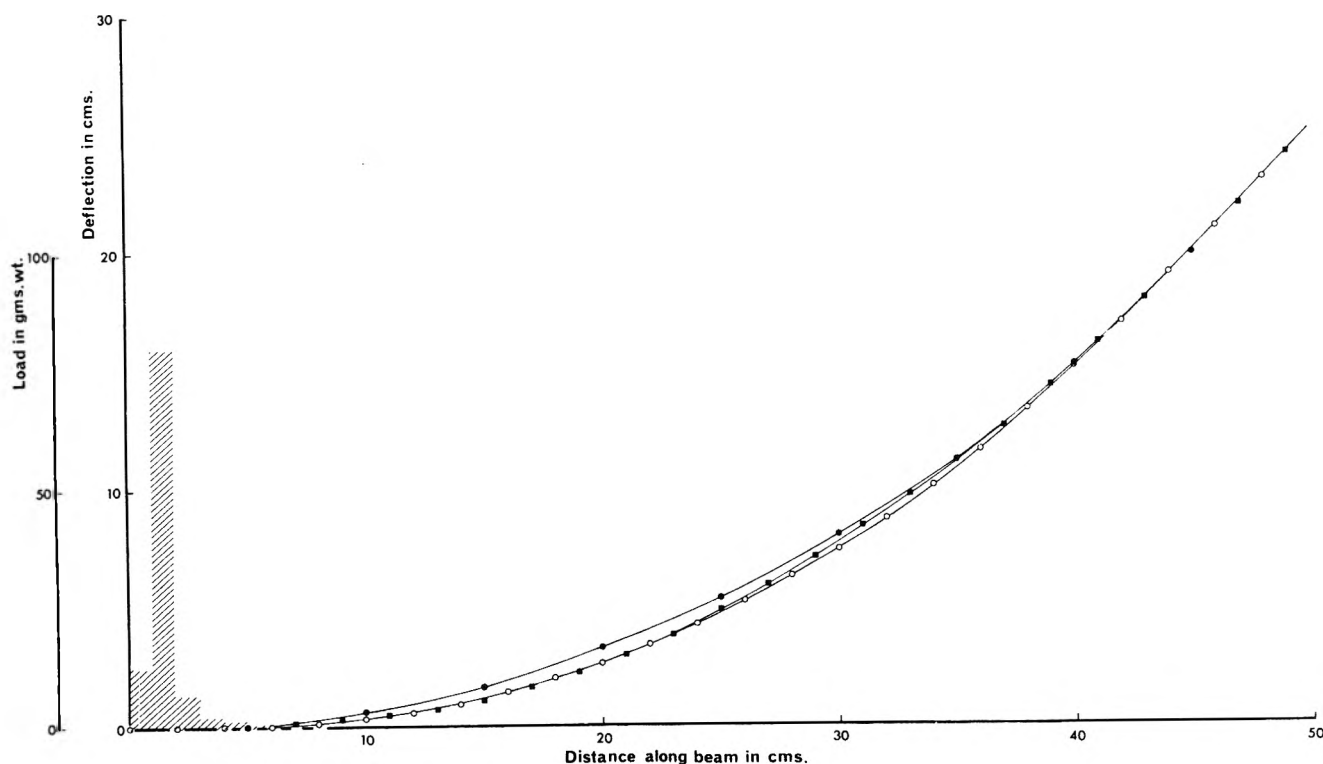


Figure 2. Results obtained using the model system. The deflection under the action of the distributed load (■) is in good agreement with the observed deflection (O). The upper curve (●) shows the effect of replacing the distributed load by an equivalent couple concentrated at the origin.

long as the environment remains unaltered. The applied load,  $P$ , the separation between the clamps, and the Fizeau fringe pattern of the bifurcation region, which enables the length of cleaved portion of the sample to be determined, were measured. A knowledge of  $P$  and the separation at its point of application permits us to determine the work done in moving from one equilibrium position to the next. Part of this energy is stored as additional strain energy in the mica. After allowance has been made for this we obtain the energy associated with the formation of the two new interfaces. This energy is found to be constant along the strip and is reproducible from specimen to specimen provided the conditions of the experiment are maintained constant. Since the energy is the integrated effect of the forces acting between the sheets, reproducibility of  $\gamma$  values implies similar reproducibility of the forces themselves.

When the cleavage had proceeded to a suitable position, collimated white light was substituted for the monochromatic light and the fringes of equal chromatic order were observed and recorded. From these, as described below, the shape of the sheets near the origin was determined. At the end of the experiment the sheets were allowed to re-seal as a test of their cleanliness. Experiments in which sheets failed to re-seal satisfactorily were discarded. Later, the sample was reopened a given amount and the surfaces were dusted with talc to prevent resealing. By observing the bending in the absence of cleavage, the value of the Young's modulus,  $E$ , was obtained for the sample. This was  $11.668 \times 10^{13} \text{ N/m}^2$ .  $E$  varies from crystal to crystal. A source of  $\beta$  rays was placed to the side and near the bifurcation point.

An accurate measure of the shape of the deflected sheets is essential and was achieved by interpreting the

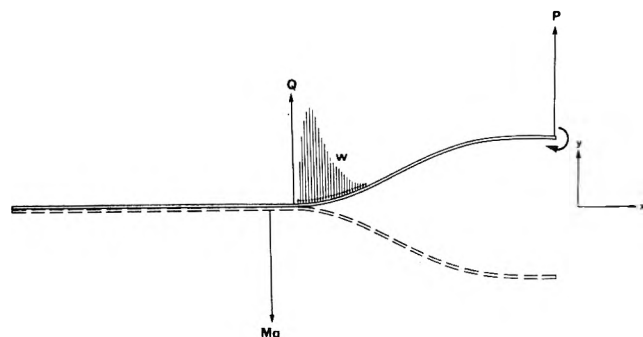


Figure 3. The forces acting on a partially cleaved strip of mica.  $P$  is the externally applied load,  $Q$  is the reaction between the strips, and  $w$  is the distributed load per unit length arising from the intermolecular attraction. The uncleaved end is free.

fringes of equal chromatic order. These fringes are shown in Figure 4. The portion of each fringe which is of constant wavelength corresponds to that region of the sample where the two strips are in contact. As they separate, the fringes move toward the red end of the spectrum. The modulations in position and intensity visible in this pattern do not represent oscillatory variations in the separation between the sheets.

Such modulations of fringes formed in multiple-beam interference systems were first observed by Glauert.<sup>5</sup> She observed that modulations on Fizeau fringes formed when a piece of mica was placed between two silvered optical flats. The appearance of the pattern was explained in an analysis carried out by Hunter and Nabarro.<sup>6</sup> They showed that the modulations result from the superposition of patterns formed by interference of light reflected from

(5) A. N. Glauert, *Nature (London)*, **168**, 861 (1951).

(6) S. C. Hunter and R. R. Nabarro, *Phil. Mag.*, **43**, 58 (1952).



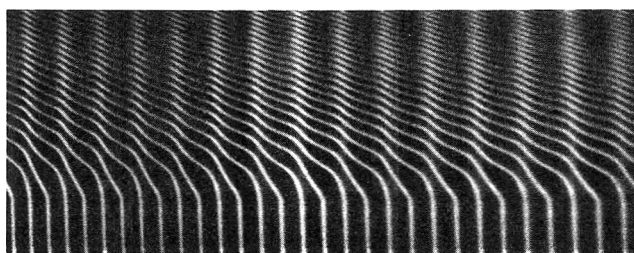


Figure 4. Fringes of equal chromatic order used to determine the shape of the mica in the region of the bifurcation point. Magnification is about 400X.

the various boundaries which arise when there are materials of different refractive index in the interferometer gap. The detailed appearance is a function of the relative separation, slope, and position of these boundaries.

The modulations seen in Figure 4 are also of this kind. The wedge of air between the two mica sheets forms a region of low refractive index between the two parallel sided regions of high refractive index. If this wedge is filled with water whose refractive index is closer to that of mica, the fringe pattern changes as is shown in Figure 5a and b. Figure 5a shows a sample in air and Figure 5b shows a similar sample totally immersed in water. The amplitude of the modulations is seen to be reduced although they are still present. In all of these examples alternate fringes have the same shape. This is a consequence of the fact that the system is symmetrical since the two sheets are of identical thickness. Fringes produced when the sheets differ in thickness are more complex. The pattern may reproduce itself after a few orders if the thicknesses bear some simple ratio to each other or each fringe in the visible may oscillate in a different way from its neighbors if there is no simple relationship between the thicknesses. It is clearly desirable to keep the pattern as simple as possible and it is also advantageous in the analysis of the mechanics of the system that the strips should be of equal thickness. The specimens were therefore made from portions of a single facet of constant thickness.

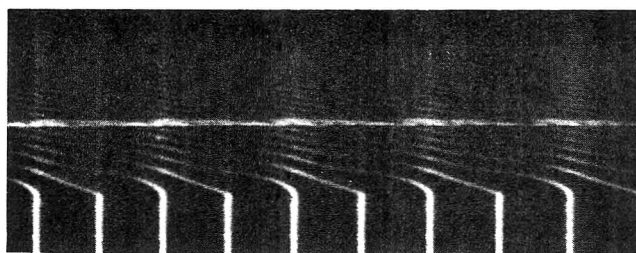
An analysis similar to that of Hunter and Nabarro for the propagation of electromagnetic waves through this system gives for the equation of a fringe formed by light at normal incidence

$$kY = \tan^{-1} \left[ \frac{r'[\sin k\mu(G - Y)](1 - r^2)}{2rr' - r[\cos k\mu(G - Y)](1 + r^2)} \right] + N\pi \quad (2)$$

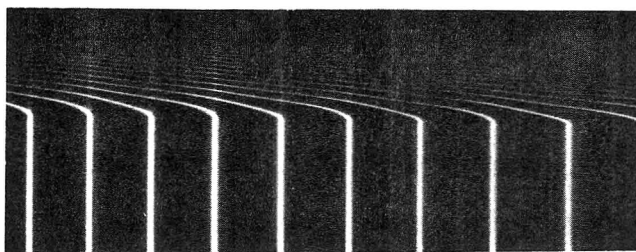
where  $r$  is the reflection coefficient at a mica-air interface,  $r'$  is the reflection coefficient at a mica-silver interface,  $\mu$  is the refractive index of the mica,  $k$  is the wavelength constant,  $G$  is the distance between the silver surfaces, and  $Y$  is the distance between the inner surfaces of the mica.

Correction was made for non-normal incidence when the angle of incidence exceeded 0.001 radian. The thicknesses  $G$  and  $Y$  include the phase change on reflection,  $\tau$ , at the mica-silver interface. Both  $\tau$  and  $\mu$  are functions of the wavelength,  $\lambda$ , and since these fringes are chromatic, appropriate corrections were made at all points along the fringes. Values of  $\tau$  and  $d\tau/d\lambda$  were taken from observations by Eisner.<sup>7</sup>

The refractive index,  $\mu$ , and  $d\mu/d\lambda$  were measured by the method described by Bailey and Kay.<sup>8</sup> Mica is bire-



(a)



(b)

Figure 5. Fringe pattern produced by a sample (a) in air and (b) immersed in water. Since the refractive index of water is closer to that of mica than that of air, the oscillation of the fringes is greatly reduced.

fringent and the fringe pattern normally consists of doublets. Care was taken that the directions of  $\mu_\beta$  and  $\mu_\gamma$  remained the same after the sheets were placed in contact. If the components are rotated with respect to each other in the two sheets, the light is refracted as though the refractive index has some intermediate value. In addition to this, the strips must be cut so that the direction of either  $\mu_\beta$  or  $\mu_\gamma$  lies accurately perpendicular to the length of the sheet.

The separation between the sheets determined in this way is shown in Figure 6 (and magnified detail in the inset) the dots corresponding to the readings which were taken on the fringes. The fringes were measured several times and an average was taken, the accuracy being about  $\pm 0.4$  nm. Also shown in this diagram is the shape of a sheet of mica having the same dimensions, slope, and displacement at each end as the sample but bent by the action of concentrated shear forces and couples at the two ends and having no distributed load. This shape was calculated using simple beam theory. It can thus be seen that the effect of the intermolecular interactions is to reduce the separation between the sheets.

The loads acting on the upper component of the pair of cantilevers of length,  $L$ , are as shown in Figure 3.  $P$  is the externally applied force and  $Q$  is the shearing force resulting from the reaction of the lower beam on the upper.<sup>9</sup> The mutual reaction between the sheets causes a small elastic compression which may be detected by careful measurement of the interference fringes. It must be remembered that the interference in this system takes place between the outer silvered surfaces of the mica whereas the separation naturally refers to the space between the inner surfaces. Since the cleavage is so perfect in mica, the thickness of the sheets may in general be assumed constant. In the region of the large shear force  $Q$ , the fringes indicate a thickness less than that of the uncleaved re-

(7) E. Eisner, *Research*, 4, 183 (1951).

(8) A. I. Bailey and S. M. Kay, *Brit. J. Appl. Phys.*, 16, 39 (1965).

(9) S. P. Timoshenko, "Theory of Plates and Shells," 2nd ed. McGraw-Hill, New York, N. Y., 1959.

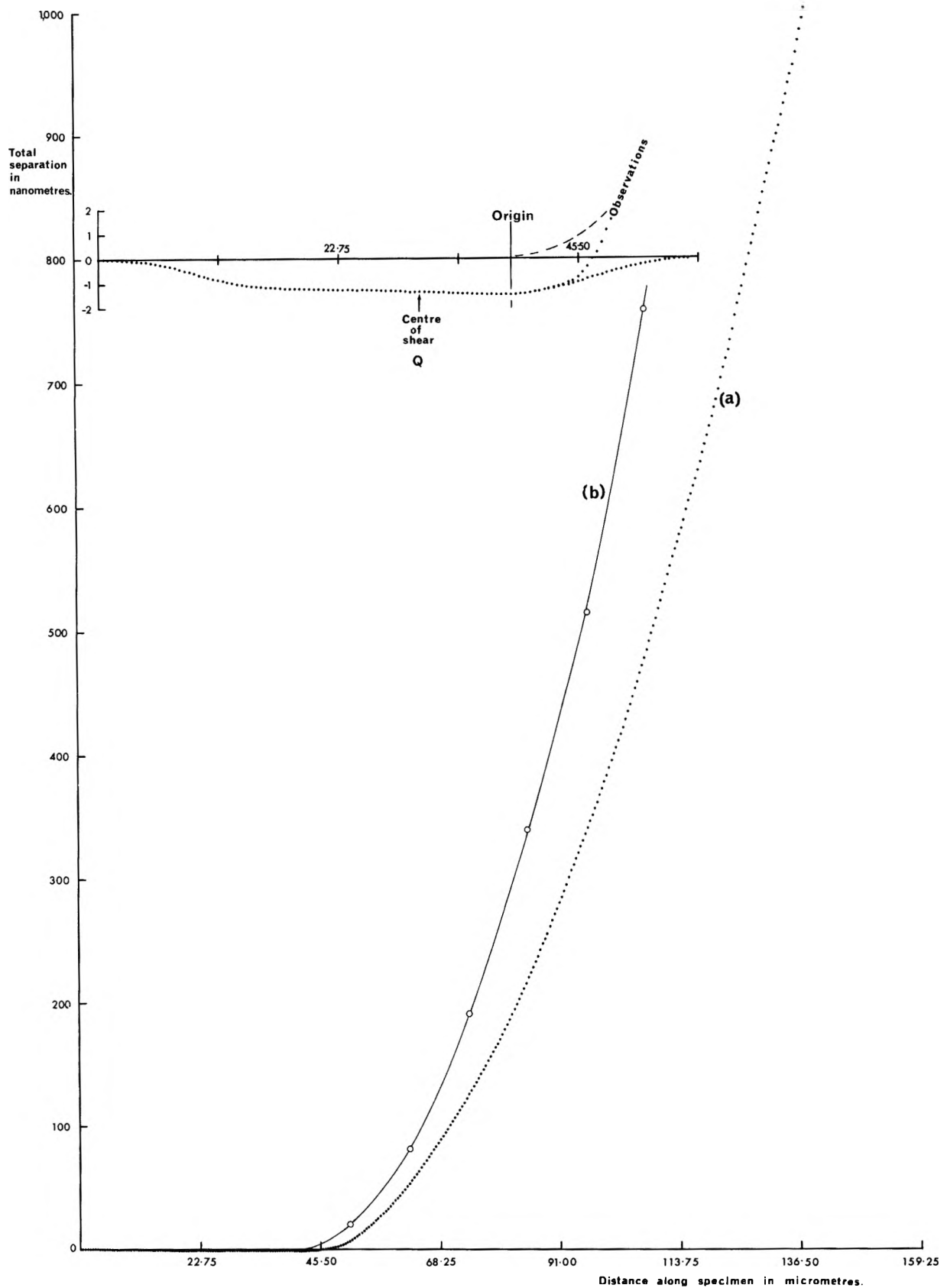


**Figure 6.** The shape of the sheet of mica determined from the fringes shown in Figure 4. Curve a represents experimental points calculated using eq 2. The mutual reaction of one sheet on the other causes a small compression as indicated in Figure 7 and the corresponding decrease in thickness is shown here in the inset. Curve b is the calculated shape of a cantilever of identical dimensions with two horizontally built-in ends coinciding with those of the sample but having no distributed load.

gion. This can only mean a compression of the sheets (see Figure 7). Since the constant thickness of the sheets is subtracted from the total thickness to obtain the separation, the values of separation here appear to be negative. The experimental points for distance along the specimen from 0 to 45  $\mu\text{m}$  have been plotted at higher magnification in the inset of Figure 6. In order to fix the position of the origin, *i.e.*, the point at which separation begins, as accurately as possible, it is desirable to correct for the effects of this compression. In order to do so, since no forces are in reality ideally concentrated, we have assumed that the force  $Q$  is distributed symmetrically about the point indicated in the inset. The displacements to the left of this point represent pure compression. Assuming symmetry, the same compression will occur on the right, so these values have been subtracted point by point from all observations to the right of the center of the shear force, yielding the origin shown with an accuracy of  $\pm 0.5 \mu\text{m}$ . The corrected separation is given by the dashed curve. Only the first few points in the region of separation are sensibly affected.

Considering again the beam shown in Figure 3, we see that the sealed portion to the left of the origin, *i.e.*, the free end, contains no bending moment, so the bending moment just at the origin is zero. The fact that the free end is horizontal is due to the combined effect of the shear,  $Q$ , and the distributed load  $\int_0^L w(x) dx$ ; *i.e.*, there is no externally applied moment concentrated at the origin. One can imagine therefore that if the intermolecular attraction were weak enough and the mica thick, an equilibrium might be impossible. This was confirmed by the following observations. Samples were constructed from sheets of mica which had been coated with an oriented monomolecular film of perfluorodecanoic acid, a substance which has a surface energy of  $12 \text{ mJ m}^{-2}$ , one of the lowest known values. It was found that the intermolecular forces were strong enough to bend only the thinnest sheets. For thick samples even a small separation at the open end caused the sheets to fall apart.

(c) *Equilibrium of the Cantilever System.* The deflection of any elastic beam under the influence of a distributed load  $w(x)$  per unit length which becomes vanishingly small at a point  $x = X$  along its length, and in equilibrium with externally applied loads, is given by

$$\begin{aligned} \frac{EI}{b} \frac{d^4 y}{dx^4} &= w(x) \quad (x < X) \\ \frac{EI}{b} \frac{d^4 y}{dx^4} &= 0 \quad (x \geq X) \end{aligned} \quad (3)$$

This equation may be solved by successive integration if four end conditions are known. For the beam under consideration whose length is  $L$  and width  $b$ , we have the following: (1)  $y = 0$  at  $x = 0$ ; (2)  $y = h$  at  $x = L$ ; (3)  $dy/dx = 0$  at  $x = 0$ ; (4)  $dy/dx = 0$  at  $x = L$ ; (5)  $(EI/b)(d^2 y/dx^2) = 0$  at  $x = 0$ . Using the first four of these end conditions the solution of eq 3 is

$$\begin{aligned} \frac{EI}{b} y &= -F_4(x) + A \frac{x^3}{6} + B \frac{x^2}{2} \quad (x < X) \\ \frac{EI}{b} y &= -F_4(X) - F_3(X)(x - X) - \\ &F_2(X) \frac{(x - X)^2}{2} - F_1(X) \frac{(x - X)^3}{6} + \\ &A \frac{x^3}{6} + B \frac{x^2}{2} \quad (x \geq X) \end{aligned}$$

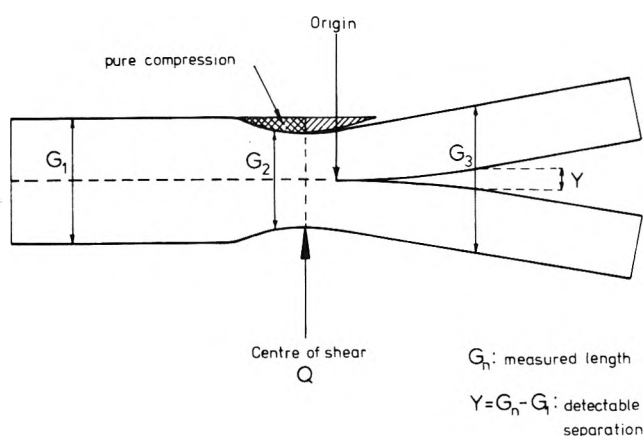


Figure 7. Diagrammatic representation of compression effect caused by mutual reaction of sheets of mica.

where

$$\begin{aligned} F_4(x) &= \int \int \int \int_0^x w(x) dx dx dx dx; \quad F_1(X) = \int_0^X w(x) dx, \\ F_2(X) &= \int \int_0^X w(x) dx dx; \quad F_3(X) = \int \int \int_0^X w(x) dx dx dx; \\ F_4(X) &= \int \int \int \int_0^X w(x) dx dx dx dx \end{aligned}$$

The constants  $A$  and  $B$  are given by

$$\begin{aligned} A &= -\frac{12EIh}{bL^3} - F_4(X) \frac{12}{L^3} - 6F_3(X) \frac{(L - 2X)}{L^3} + \\ &6F_2(X) \frac{X(L - X)}{L^3} + F_1(X) \frac{(L - X)^2(L + 2X)}{L^3} \end{aligned}$$

and

$$\begin{aligned} B &= \frac{6EIh}{bL^2} + F_4(X) \frac{6}{L^2} + F_3(X) \frac{2(2L - 3X)}{L^2} + \\ &F_2(X) \frac{(L - X)(L - 3X)}{L^2} - F_1(X) \frac{X(L - X)^2}{L^2} \end{aligned}$$

If  $w(x)$  is known or if it can be represented by a suitable function, eq 3 can be solved and the result compared with the observed shape. The extra end conditions not used in the calculation serve as an additional check on the solution.

From the shearing force equation we have, neglecting the weight of the beam

$$\frac{EI}{b} \frac{d^3 y}{dx^3} = -F_1(x) + A$$

At  $x = 0$ ,  $A = Q$  and at  $x = L$ ,  $A = -P + F_1(X)$ . This is in agreement with the result

$$Q + P = F_1(X)$$

required for statical equilibrium.  $P$  is a measured quantity, so in principle could be used as one of the end conditions. It turns out to be very small in comparison with  $Q$  and  $F_1(X)$  and so is not, in fact, suitable.

(d) *Force Functions.* It is necessary to choose some suitable function to represent the attraction  $w(x)$ . As we have seen  $w(x)$  must be zero at the origin, rise steeply for values of  $x$  corresponding to small separations, and, after reaching a maximum, fall off again as the separation be-

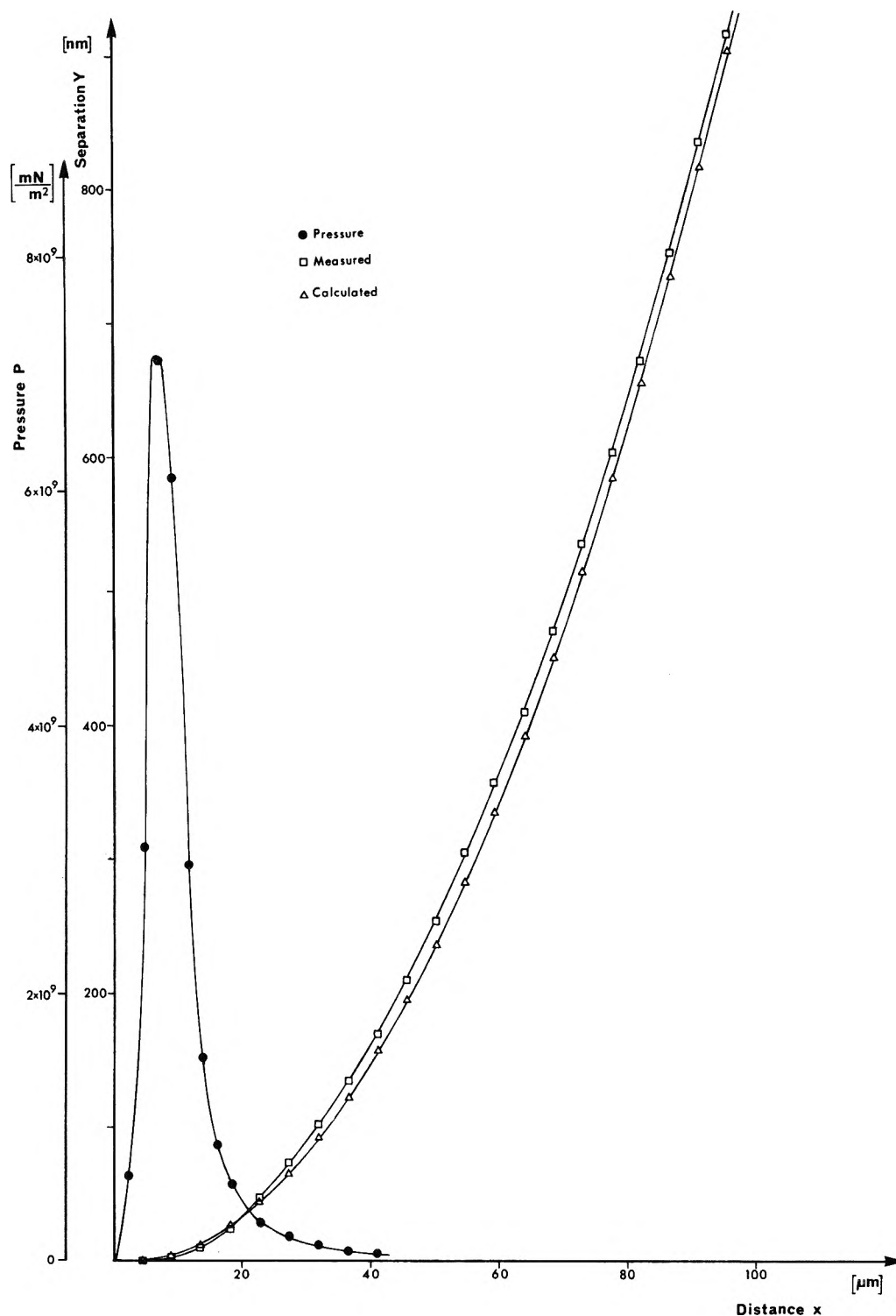


Figure 8. A solution of the beam equation ( $\Delta$ ) for a load function,  $P(x)$  ( $\bullet$ ), for values of the parameters  $n = 1.1$ ,  $\epsilon\delta = 5$ .

comes large. Such a function is

$$w(x) = \frac{\alpha}{[y(x) + \epsilon\delta]^n} - \eta e^{-\beta[y(x) + \epsilon\delta]} \quad (4)$$

where  $\alpha$  and  $\eta$  are constants governing the magnitude of the attractive and repulsive terms respectively.  $\delta$  is the distance of closest approach of the sheets. It was measured by cleaving very thin facets of mica over part of their area and allowing them to reseal. The thickness of the cleaved portions was found to be  $0.6 \pm 0.2$  nm larger than the uncleaved portions. This increase represents the

thickness of the monomolecular layers of water vapor adsorbed on the sheets.  $\beta$  and  $n$  are parameters which control the rate at which the loading rises to and falls from its maximum value. The value of  $n$  should give information about the nature of the attractive forces. The load  $w(x)$  may also be represented conveniently by the force/unit area,  $P(x)$  acting at any point  $x$ .

The energy of attraction given by eq 1 is constant and is divided between the attractive and repulsive terms in such a way that a fraction  $R\gamma$  is associated with the repulsive term and  $(1 + R)\gamma$  with the attractive term. We also

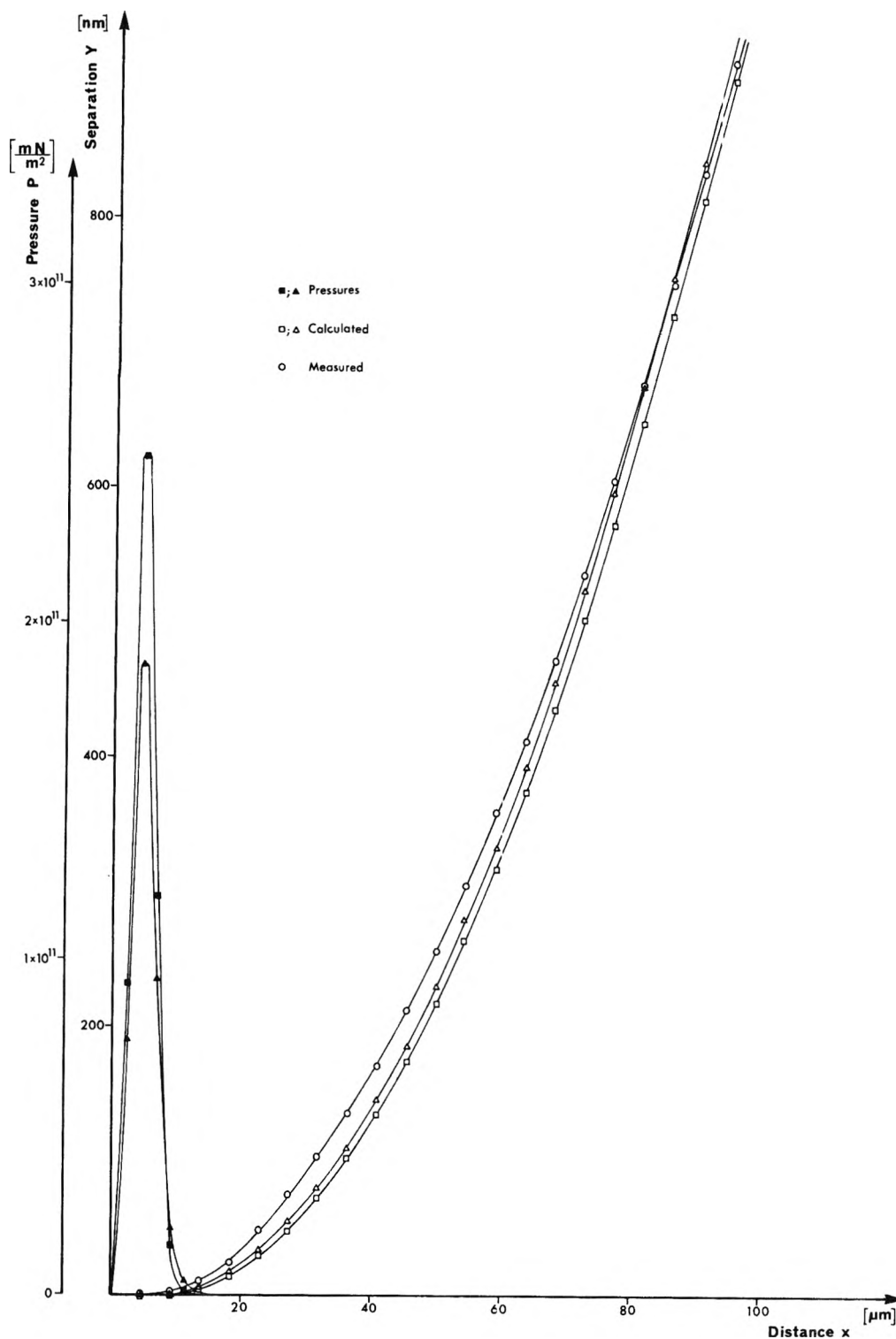


Figure 9. Similar solutions ( $\Delta$ ) for  $n = 2$ ,  $\epsilon\delta = 3$ , and ( $\square$ ) for  $n = 3$ ,  $\epsilon\delta = 4$ , obtained using the corresponding load functions,  $P(x)$  ( $\blacktriangle$ ) and ( $\blacksquare$ ), respectively.

know that the loading is always positive and that it is zero at the origin. These conditions give  $w(x) = 0$  at  $x = 0$  and  $dw/dx \geq 0$  at  $x = 0$ . Integrating eq 1 and applying these conditions gives for the attractive pressure between elements on the two sheets

$$P(x) = \frac{b(1 + R)\gamma(n - 1)\delta^{(n-1)}}{[y(x) + \epsilon\delta]^n} - bR\gamma\beta \frac{e^{-[y(x) + \epsilon\delta]}}{e^{-\beta\epsilon\delta}} \quad (4a)$$

with

$$R = \frac{n - 1}{\beta - (n - 1)}; \beta > \frac{n}{\epsilon\delta}$$

$P(x)$  was substituted in eq 3 which was then integrated four times using Simpson's rule, for elements along the sheet and taking various values of the parameters  $\epsilon\delta$ ,  $n$  and  $\beta$ . The resulting values of  $Y$  were compared with the observed ones. If only dispersion forces act in the gap  $n$  should assume the value 3, while lower values would indicate the presence of other interactions.

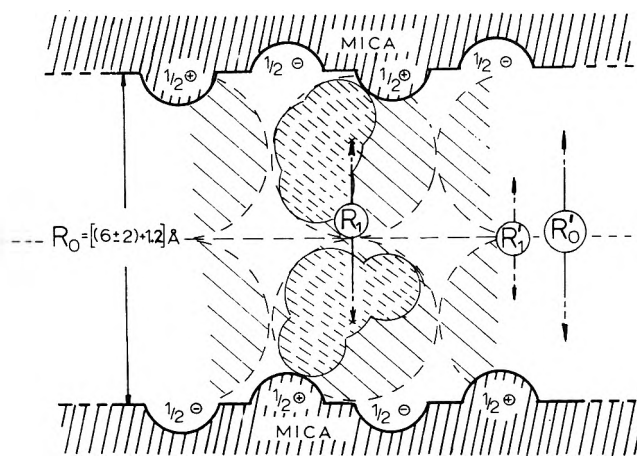


Figure 10. Diagrammatic representation of the contact between two sheets of mica each covered with an adsorbed monolayer of water.

The load at any point,  $P(x)$ , corresponding to a solution of eq 3 is shown in Figure 8. Also shown on the diagram are the calculated and observed values of the separation  $Y$ . For all separations greater than the equilibrium lattice spacing the intermolecular interactions will be positive (attractive). The force function was, therefore, constrained to be positive for all  $x$ . The parameters  $n$  and  $\epsilon\delta$  were 1.1 and 0.5 nm, respectively. Using eq 4a it was not possible to obtain a closer fit.

For any assumed value of one of the parameters,  $\epsilon\delta$  say, values of the other parameters can be found which represent a force function which produces a solution which fits the observed shape more or less closely. The sum of the modulus of all deviations from the observations,  $\sigma$ , taken over 237 points lie in the range  $3.2 \times 10^3$  to  $6.5 \times 10^3$  nm. Figure 9 shows two such functions the values of the parameters being  $n = 3$ ,  $\epsilon\delta = 4$  nm and  $n = 2$ ,  $\epsilon\delta = 3$  nm as indicated. The distributed load functions having the lowest values of  $\sigma$  all correspond to low values of  $n$ . Hence a function like eq 4a which consists of a single attractive term and a single repulsive term is insufficient to fix the value of  $n$  unambiguously.

In reality the attractive force is the sum of a number of different types of interaction which decay at different rates and it is desirable to develop a model force function which takes account of this. Assuming that Hamaker's formula,<sup>10</sup> in which the attraction between macroscopic bodies is proportional to the inverse cube of the distance between them, still holds at distances of less than 5 nm, low values of  $n$  suggest that forces other than dispersion forces are playing a large part in the interaction. We may again consider the sheets to be made up of a series of parallel-spaced elements. Since the cleavage plane of mica is ionic in character, the force acting between the elements may then be treated as the sum of ionic and dispersion forces, these forces acting independently of each other.<sup>11</sup> This procedure would enable us to interpret the attractive force in terms of well established theoretically predictable components and indicate whether these formulas still hold at the very small separations used in these experiments.

We have assumed, therefore, that eq 1 may be expressed as

$$2\gamma = \int_0^{\infty} [P'_i(Y) + P_d(Y) - P'_r(Y)] dY \quad (5)$$

where  $P'_i$  and  $P_d$  are the ionic and dispersive attractive

pressures between elements, respectively.  $P'_r$  is chosen to be equal to the sum of  $P'_i$  and  $P_d$  at  $Y = R_0$ . For the evaluation of  $P'_i$  it is necessary to make certain assumptions with regard to the surface of the mica after cleavage has taken place. The  $K^+$  ions, which before cleavage are embedded in an aluminosilicate lattice, are divided equally between the two surfaces after cleavage, each leaving a negatively charged site on the opposite surface. The ionic attractive pressure results from the interaction of the  $K^+$  ions with these sites. The possibility that there is an additional attraction due to stray charges, or to unequal division of  $K^+$  ions between the surfaces, has been excluded by the following simple experiment. A sheet of mica was cleaved into two separate pieces, one of which may be supposed to be negatively charged and the other positively charged. Two samples were made, one consisting of a part of each of these two sheets and the other of two parts of the same sheet. Both samples gave the same value of the surface energy, from which we deduce that any stray charge which may have been present had been dissipated. We assume, therefore, that both sheets may be regarded as neutral. We have also assumed a symmetrical and alternating distribution of charges in the cleavage plane as indicated in Figure 10.

The contribution of this specific arrangement of charges to the net attraction between non-matching elements of area was accounted for by the introduction of a two dimensional Madelung constant,  $A_M$ . This constant was calculated following the method due to Evjen<sup>12</sup> and taking into account neighbors up to the fifth order. The value of  $A_M$  deduced is 1.3. A rotation of the charge patterns relative to each other through an angle of 0.4 radian has little effect (less than 5%) on the value of  $A_M$ .

In order to set the limits for the value of the contact separation we must consider not only the thickness of the adsorbed monolayers of water but also the alteration in the lattice spacing of the outer layer of mica after cleavage. In addition we must allow for the reduction in the ionic attraction which results from the shielding of the charge site by these water films. For this purpose we introduce the quantity,  $\epsilon R_0$ , where  $\epsilon$  represents the effective dielectric constant of the film. The influence of the air in the gap may be neglected since the dielectric constant of dry air is very nearly equal to the value *in vacuo*.

The charge corresponding to the positive and negative sites is equal to half the elementary charge, since the  $K^+$  ions are in [12] coordination with the oxygen atoms of two aluminosilicate layers. The number of ion pair interactions,  $M$ , which is equal to the number of  $K^+$  ions per unit area of the crystal, is  $4.193 \times 10^{14}$  cm<sup>-2</sup>. Hence, the ionic component of the attractive pressure,  $P_i$ , is given by

$$P_i(x) = \frac{(e/2)^2 z^2 A_M M}{[\epsilon R_0 + Y(x)]^2}$$

This equation does not, however, describe the attraction exactly. At large distances, since the surfaces are neutral, a charge on one surface experiences the attraction and repulsion of a large number of ions on the opposite surface.<sup>13</sup> This smearing out of charge effect can be repre-

(10) H. C. Hamaker, *Physica*, **4**, 1058 (1937).

(11) J. H. de Boer, *Trans. Faraday Soc.*, **32**, 10 (1936).

(12) H. M. Evjen, *Phys. Rev.*, **39**, 665 (1932).

(13) J. E. Lennard-Jones and B. M. Dent, *Proc. Roy. Soc., Ser. A*, **121**, 247 (1928).

sented by an exponential function having a logarithmic decrement  $R_L$ .

Since the sheets are in equilibrium at the bifurcation point the attractive pressure must be balanced by a repulsive pressure. This decays very rapidly with distance, and following Born and Mayer<sup>14</sup> we have represented it by an exponential function. Thus the net ionic attractive pressure becomes

$$P'_i(x) = e^{-Y(x)/R_L} [P_i(x) - P_r e^{-Y(x)/R'_0}] \quad (6)$$

where  $P_r$  is given by

$$P_r = \frac{(e/2)^2 z^2 A_M M}{(\epsilon R_0)^2}$$

Let us now consider the contribution of the dispersive forces to the attraction. According to microscopic theory,<sup>10,15,16</sup> the dispersion pressure,  $P_d$ , between two semiinfinite solids separated by a distance  $R_1$  is given by

$$P_d = \frac{A_H}{6\pi R_1^3} \quad (7)$$

Since in our experimental arrangement the gap between the mica strips increases with distance from the contact point, eq 7 becomes

$$P_d(x) = \frac{A_H}{6\pi [R_1 + Y(x)]^3} \quad (0 < Y \lesssim 30 \text{ nm}) \quad (8)$$

For separations greater than about 30 nm retardation effects cause the force to fall off more rapidly than is represented by eq 8. For large distances  $P_d(x)$  becomes<sup>17</sup>

$$P_d(x) = \frac{B_L}{[R_1 + Y(x)]^4} \quad (30 \text{ nm} \lesssim Y < \infty) \quad (8a)$$

The repulsive pressure was accounted for in a similar manner to that used for the ionic component of the interaction, using an exponential function having a logarithmic decrement  $R'_1$ .

The constants  $A_H$  and  $B_L$  were obtained from the results of Tabor and Winterton,<sup>3</sup> whose experiments were also carried out using mica in air. Their values, therefore, correspond to mica covered with an adsorbed water film and no correction for this is required.

The complete expression used to evaluate the force function at separations of less than 30 nm is

$$P(x) = e^{-[Y(x)/R_L]} \times \left\{ \frac{e^2 z^2 A_M M}{[\epsilon R_0 + Y(x)]^2} - \frac{e^2 z^2 A_M M}{(\epsilon R_0)^2} e^{-[Y(x)/R'_0]} \right\} + \left\{ \frac{A_H}{6\pi [R_1 + Y(x)]^3} - \frac{A_H}{6\pi R_1^3} e^{-[Y(x)/R'_1]} \right\} \quad (9)$$

Using this relation for  $P(x)$  the beam equation (3) was again solved. The parameters  $R_L$ ,  $\epsilon$ ,  $R_0$ ,  $R'_0$ ,  $R_1$ , and  $R'_1$  can only take on values which lie within limits specified by the thickness of the water film and the structure of mica. These ranges are:  $2 \text{ nm} < R_L < 100 \text{ nm}$ ;  $1.7 < \epsilon < 6$ ;<sup>18,19</sup>  $0.6 \text{ nm} < R_0 < 0.95 \text{ nm}$ ;  $R'_0 \leq 0.6 \text{ nm}$ ;  $0.1 \text{ nm} < R_1 < R_0$ ;  $R'_1 < R_1$ . These parameters were first varied until  $\gamma$  attained the measured value of  $106.4 \text{ mJ m}^{-2}$ . An iterative procedure was evolved for solving eq 3 such that the sum of the deviations,  $\sigma$ , of the calculated values of  $Y(x)$  from the observed values attained a minimum. The

force function corresponding to this solution is shown in Figure 11 together with the shape of the beam under this loading. The values of the parameters are:  $R_L = 37 \pm 4 \text{ nm}$ ;  $\epsilon = 2.14 \pm 0.07$ ;  $R_0 = 0.7 \pm 0.01 \text{ nm}$ ;  $R'_0 = 0.6 \pm 0.01 \text{ nm}$ ;  $R_1 = 0.45 \pm 0.03 \text{ nm}$ ;  $R'_1 = 0.124 \pm 0.002 \text{ nm}$ .

It is possible that the reaction between the sheets,  $Q$ , still has some effect near the origin since, in reality, no forces are ideally concentrated at a point. The effect of the local distribution of so-called concentrated loads requires further investigation and it is possible that a better fit could have been obtained if these effects had been taken into consideration. However, the deflection at points far from the concentrated load must be the same as though the load were concentrated as a point.

## Discussion

The general survey of the solutions carried out using a general force function, given by eq 4a, showed that it was not possible to fix the power of the attractive potential unambiguously. From Figures 8 and 9 one can see how a change in the force function changes the computed shape of the beams. In the subsequent investigations we assumed that the currently accepted theoretical expressions for the various types of intermolecular interactions hold over the whole range of distances used in the experiment as expressed in the force function given by eq 9. With these restrictions one, and only one, solution of eq 3 can be found and is shown in Figure 11.

If any one of the parameters was allowed to take another value, then either  $\sigma$  was larger, the curvature was incorrect, or the solution did not satisfy the mechanical end conditions. It should be emphasized perhaps that all solutions pass with the correct slope through the point corresponding to the clamp some  $9 \times 10^3 \mu\text{m}$  from the origin. Typically, a change in  $R_0$  of  $\pm 0.02 \text{ nm}$  increases  $\sigma$  by a factor of 2.  $R_0$  and  $R_1$  should also take on values which are physically significant.

It is a fundamental assumption in this work that the surface energy,  $\gamma$ , is the integrated effect of the forces of interaction. The values of  $\gamma$  are found to be constant for any particular specimen of mica to better than 1%<sup>4</sup> and vary from specimen to specimen by not more than 4%. The high reproducibility of these values is also evidence for the reproducibility of the total force function acting between the mica sheets.

This force, distributed along the beam, gives rise to the observed shape. The fringes used to determine the shape were measured many times at high magnification and the results of adjacent fringes were averaged. The shape is accurate to  $\pm 0.4 \text{ nm}$ . The best solution we have obtained fits this observed shape to  $\pm 5 \text{ nm}$  for each beam over the whole length. The later calculations have been an attempt to create a model load from the superposition of dispersion forces using known values for  $A_H$  and  $B_L$  and an ionic force function.

The accuracy with which each parameter  $R_0$ ,  $R_1$  etc. is known is given with the values of the parameters. The parameters themselves hold only for the particular  $A_H$  and

(14) M. A. Born and K. Mayer, *Z. Phys.*, **75**, 1 (1932).

(15) F. London, *Trans. Faraday Soc.*, **33**, 19 (1937).

(16) H. Krupp, *Advan. Colloid Interface Sci.*, **1**, 113 (1967).

(17) L. Landau and E. M. Lifschitz, "Electrodynamics of Continuous Media," Pergamon Press, Oxford, 1960.

(18) D. C. Graham, *Chem. Rev.*, **41**, 441 (1947).

(19) J. Gregory, *Advan. Colloid Interface Sci.*, **2**, 396 (1969).



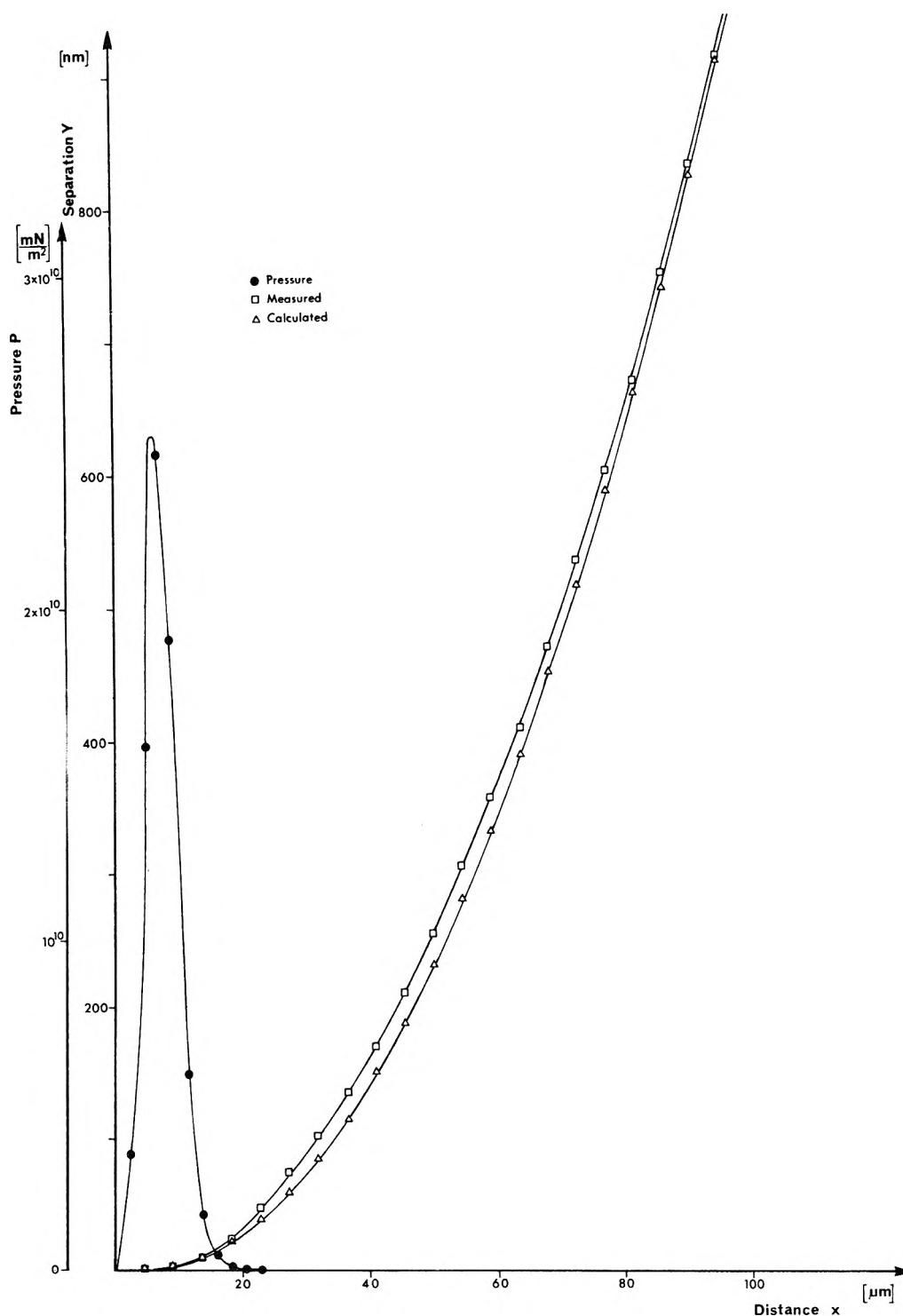


**Figure 11.** A solution of the beam equation ( $\Delta$ ) for a load function ( $\bullet$ ),  $P(x)$ , given by eq 9, consisting of an attractive term due to the sum of ionic and dispersion forces and a corresponding repulsive term which brings the net attraction at the contact point to zero.

$B_L$  used. If  $A_H$ , for example, were chosen larger, the parameters would assume other values within the specified ranges. This case would correspond to a higher contribution of dispersion forces which would mean that the ionic forces would decay more rapidly thus influencing  $R_L$ . The position of the maximum in the total force function is sensitive and was found to lie at  $Y = 0.86 \pm 0.38$  nm for all solutions having  $\sigma < 5.0 \times 10^3$  nm.

Let us now consider the equilibrium separation between the two sheets of mica in the contact region assuming that

each is covered with an adsorbed monomolecular layer of water. Referring to Figure 10 this separation is represented by the parameter  $R_0$  and for the solution shown in Figure 11 has the value 0.70 nm. When a sheet of mica has been cleaved we may expect the outer  $K^+$  ions remaining on the sheets to be attracted more strongly toward the oxygen atoms of the aluminosilicate layer than they were in the uncleaved crystal. The distance between the planes containing the  $K^+$  ions and oxygen atoms will be reduced by about 30% or 0.05 nm. If we assume that the surface of

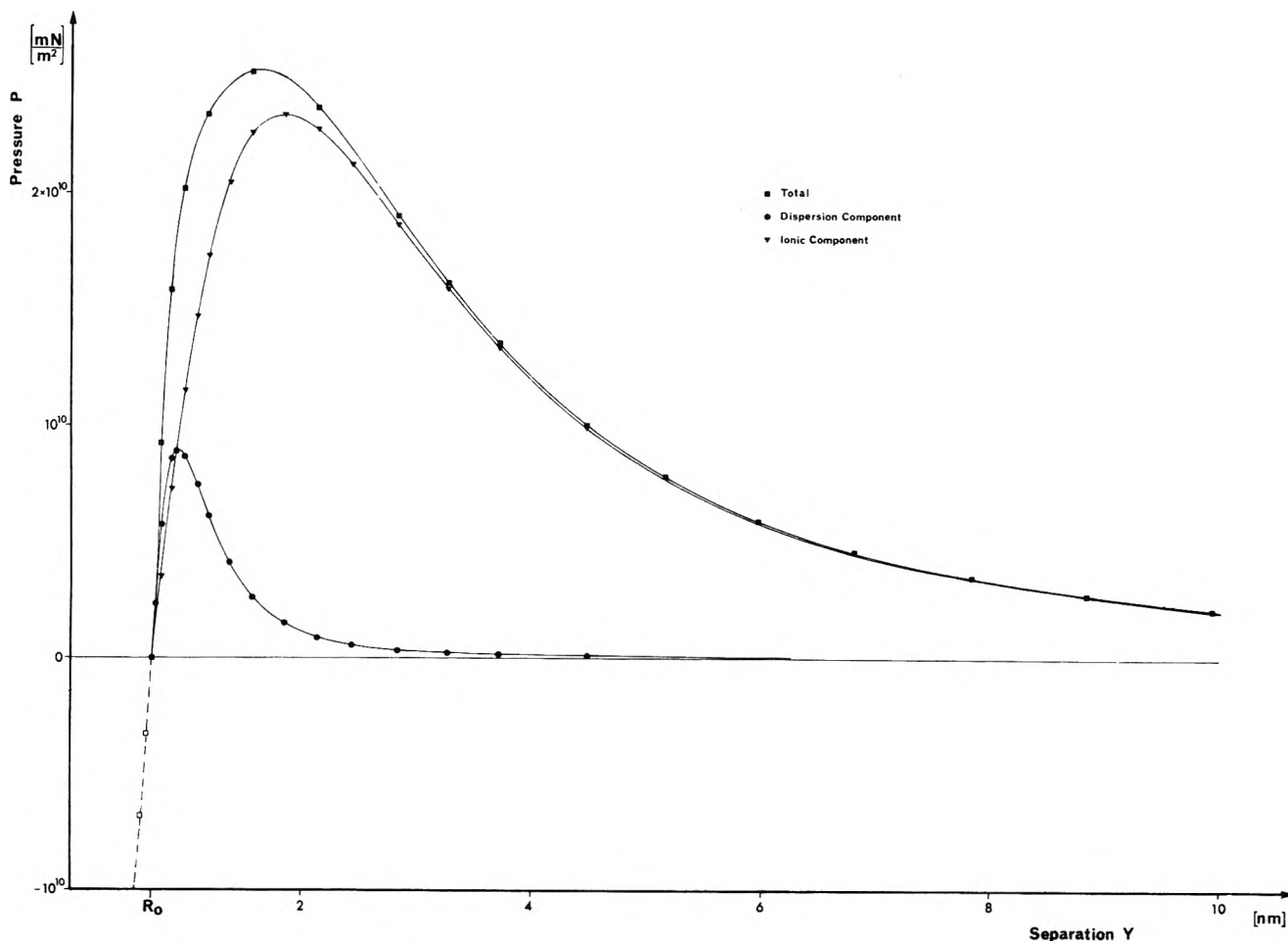


Figure 12. The distributed load shown in Figure 11, given as a function of the separation,  $Y$ , between the sheets at any point. The contributions due to ionic ( $\blacktriangle$ ) and dispersion forces ( $\bullet$ ) are also shown. The dispersion forces contribute some 8% to the total surface energy.

the crystal lies halfway between these two planes, then we may interpret the value of the parameter  $R_0$  as the thickness of the two adsorbed films of water. The value of 0.70 nm is in good agreement with the accepted value for the diameter of the water molecule and with the value of 0.6 nm obtained by partially cleaving a crystal and measuring the increase in thickness. If we correct this measurement for the movement of the  $K^+$  ions we obtain the value 0.72 which agrees even better.

The calculated parameter  $R_1$  represents the distance between the planes of highest electron density in the adsorbed water layers. If the molecules were randomly oriented with respect to the solid surface we would expect a value of 0.35 nm. We obtain the value 0.45 nm and conclude, therefore, that the mica imposes a strong orientation on the adsorbed molecules. The effective dielectric constant,  $\epsilon$ , of the adsorbed water films comes out to be 2.14, which would correspond to a material having a refractive index of 1.46. It is interesting to note that the refractive index of ice VI is 1.48.<sup>20</sup>

The value of the constants  $A_H$  and  $B_L$  are  $1.15 \times 10^{-16}$  mJ and  $1.20 \times 10^{-19}$  mJ m, respectively. They lie in the upper range of the values of Tabor and Winterton and were found to give a better fit than lower values. Figure 12 shows the total force/unit area acting between the beams as a function of the distance between the surfaces. Also shown are the components due to ionic and dispersion forces. The ionic attraction is responsible for some 90–92%

of the total energy of separation while the dispersion forces contribute the remaining 8–10%. Previous measurements showed that the presence of a monomolecular layer of perfluorodecanoic acid deposited on mica reduces the total energy of separation to about 11% of the value for clean mica in which the charge sites on the sheets do not match. The forces of interaction between the monolayers of perfluorodecanoic acid are dispersive in character. The close agreement of these two results suggests that the perfluorodecanoic acid monolayers are very effective at shielding the charge sites in the mica substrate. However, neglecting the contribution due to the dispersion forces in eq 9 and solving again for the best fit gave a solution having a much higher value of  $\sigma$ .

The maximum value of the attractive pressure is very high,  $2.5 \times 10^{10}$  mN m<sup>-2</sup>, while that due to the dispersion forces alone is more than a third of this value. The two components of attraction reach their maximum values at slightly different separations. The resultant attraction is strongest at a distance of 0.86 nm and falls to a third of its maximum value by 3.5 nm separation. That portion of the total force operating in the first 4 nm separation accounts for more than 60% of the total energy of separation. By 6 nm separation this proportion has reached 83%, while at separations exceeding 10 nm less than 10% of the total energy remains to be accounted for. It is in this re-

(20) M. E. Hobbs, M. S. Jhon, and H. Eyring, *Proc. Nat. Acad. Sci. U. S.*, **56**, 31 (1966).

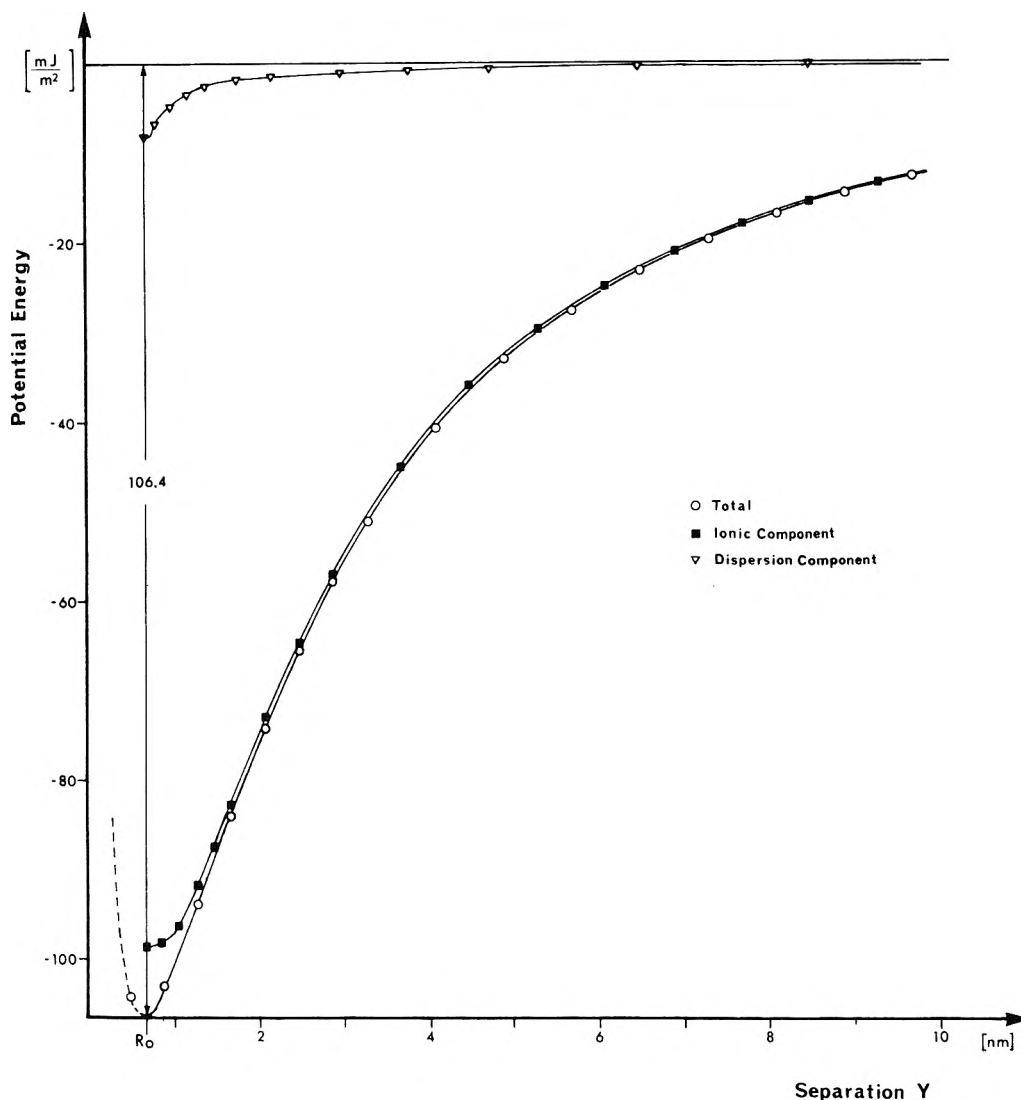


Figure 13. The potential distributions for the total and component force functions.

gion, where only the remnants of the forces are still acting, that most previous measurements have been made.<sup>21-25</sup> Since the ionic forces decay much faster than the dispersion forces, the components will be equal at some value of the separation. This value is 470 nm and for values of the separation greater than this the dispersion forces dominate the field. At distances from the surface greater than 550 nm the attraction is almost entirely dispersion in character. The value of the total force at this point is  $2 \text{ mN m}^{-2}$ . The potential functions corresponding to the component and resultant forces are shown in Figure 13. A close inspection of Figure 12 shows that in the region of very small separations, *i.e.*, less than 0.5 nm, the dispersion forces are larger than the ionic forces.

Capillary condensation in the tip of the crack should be considered since surface tension forces could give rise to forces of attraction nearly as large as the observed ones. That these are the origin of the attraction measured here must be rejected by careful scrutiny of the fringes shown in Figure 4. Let us assume a relative humidity even as high as 50%. Then Kelvin's formula predicts a capillary radius of about 6 nm. If such a meniscus formed in the wedge it would occur at a distance of  $10 \mu\text{m}$  from the contact point. No discontinuity in the fringes of equal chro-

matic order due to an abrupt change in refractive index has been detected there or indeed anywhere. Fizeau fringes show irregularity in their spacing when condensation occurs<sup>4</sup> and again no such effect was observed here. In practice, as shown by Cohan,<sup>26</sup> a very much smaller radius than that predicted by Kelvin is required before capillary condensation occurs.

Since this work was submitted two other papers dealing with the forces acting between sheets of mica have appeared. The first is by Metsik<sup>27</sup> who, following the wedge method of Obreimov, obtains a value of  $380 \text{ mJ m}^{-2}$  for the energy required to form new surfaces in air. He assumes a model for the mica crystal which treats the structure as an assembly of internal dipoles, but which takes

- (21) J. Th. G. Overbeek and M. J. Sparnaay, *Discuss. Faraday Soc.*, **18**, 12 (1954).
- (22) G. C. J. Rouweler and J. Th. G. Overbeek, *Trans. Faraday Soc.*, **67**, 2117 (1971).
- (23) B. V. Derjaguin, A. S. Titijevskia, I. I. Abricisova, and A. D. Malinka, *Discuss. Faraday Soc.*, **18**, 24 (1954).
- (24) B. V. Derjaguin and I. I. Abricisova, *J. Exp. Theor. Phys.*, **30**, 933 (1956); **31**, 3 (1956).
- (25) J. A. Kitchener, and A. P. Prosser, *Proc. Roy. Soc. Ser. A*, **242**, 403 (1957).
- (26) L. H. Cohan, *J. Amer. Chem. Soc.*, **66**, 98 (1944).
- (27) M. S. Metsik, *J. Adhesion*, **3**, 307 (1972).

no account of the adsorbed films of water. The contribution of the dispersion forces to the energy is neglected.

The second, by Israelachvili and Tabor,<sup>28</sup> extends the work of Tabor and Winterton down to separations of 2 nm and gives a slightly higher value of  $A_H$ . They assume that only dispersion forces are effective at this distance. As a matter of interest we have calculated the value of  $\epsilon R_0$  using the first term of eq 9 and choosing  $R_1$ , so that the ionic forces are a thirtieth of the value of the dispersion forces at 2 nm separation. This force must give rise to the energy of  $94 \text{ mJ m}^{-2}$  which still remains to be accounted for when the effect of the dispersion forces has been subtracted. The value obtained is 0.3 nm. If we assume that the adsorbed monolayers have the same refractive index as bulk water, then  $\epsilon$  is about 1.8 and  $R_0$  must have the value of 0.17 nm compared with the measured value of 0.6 nm. It may be that the Hamaker constant requires revision, or that other forces than those considered are also acting, or that the physical conditions prevailing in the two investigations were not identical. Our mica surfaces were formed during the experiment and hence were much newer than those of Tabor and Winterton and may well correspond to a higher value of  $A_H$ . This point is being investigated.

The results of this work are consistent with the supposition that the interaction between the sheets can be represented by the superposition of two systems of intermolecular forces. These are (i) an ionic attraction which may be summed for small macroscopic elements with the aid of a Madelung constant and which decays exponentially for neutral bodies and (ii) an attraction due to dispersion forces which is proportional to the inverse cube of the separation for separations up to 30 nm and to the inverse fourth power of the separation for separations greater than this. The main advantages of these experiments lie in the close distances of approach made possible by working with molecularly smooth mica and the use of a simple mechanical system which not only adjusts itself so that it is always in equilibrium but also allows the energy of the interaction to be determined.

*Acknowledgments.* We wish to thank the Deutsche Forschungsgemeinschaft for support for this work. A. I. B. also wishes to thank the Royal Society of London for the award of the Smithson Research Fellowship during the tenure of which many of the basic ideas for the experiment were developed. She also has much pleasure in acknowledging many stimulating discussions with colleagues,

especially Miss Gillian Vaisey, Dr. Susan Kay, Dr. Alan Wonacott, and Dr. David Dover.

#### Appendix. Nomenclature

$\gamma$	surface energy
$\mu$	refractive index $\mu_\beta, \mu_\gamma$ components of refractive index
$\lambda$	wavelength
$k$	wavelength constant
$r, r'$	reflection coefficients at mica/air and mica/silver interfaces
$\tau$	phase change on reflection of light at mica/silver interphase
$N$	order of interference
$G$	distance between highly reflecting silver films
$P$	end load
$Q$	shear force at bifurcation point
$Y$	distance between mica surfaces
$L$	length of mica strip
$E$	Young's modulus
$I$	second moment of area of mica strip
$b$	breadth of mica strip
$w(x)$	distributed load per unit length on mica strip of unit breadth
$x$	distance along mica strip
$y(x)$	deflection of mica strip at point $x$ [ $Y(x) = 2y(x)$ ]
$n, \alpha, \beta,$ $\eta, R$	parameters in model force function
$\delta$	separation of mica surfaces at contact point [ $R_0 = 2\delta$ ]
$\epsilon$	effective dielectric constant of adsorbed water film
$A_M$	Madelung constant
$A_H$	Hamaker constant
$B_L$	Lifschitz constant
$R_0, R_1$	constants for dispersion and ionic attractive terms of interaction
$R'_0, R'_1$	constants for repulsive term of interaction
$R_L$	separation at which ionic forces are mainly shielded
$P_i$	ionic component of attractive pressure
$P_d$	dispersive component of attractive pressure
$P_r$	repulsive pressure in contact region
$M$	number of potassium ions per unit area in mica cleavage plane
$\sigma$	sum of modulus of all deviations of calculated curves from observed curve

(28) Israelachvili and D. Tabor, *Nature (London)*, **236**, 106 (1972).

# Nonstoichiometric Interactions of Long-Chain Ammonium Salts in Organic Solvents<sup>1</sup>

Y. Marcus

Department of Inorganic and Analytical Chemistry, The Hebrew University, Jerusalem, Israel (Received June 27, 1972)

Several phenomena observed in solutions of long-chain substituted ammonium salts in nonpolar or slightly polar organic diluents cannot be reconciled with the ideal associated mixture approach commonly used. These phenomena include liquid-liquid immiscibilities and apparent average molecular weights of the aggregated salt that decrease with increasing concentrations. Nonspecific interactions between the solute and the solvent can account for them. These interactions are a plausible alternative to the assumption of the presence of higher oligomers (octa-, dodeca-, docosamers, etc.), besides a simple dimer or trimer, required to interpret osmometric data by the ideal association model. An expression has been derived which can fit the nominal molal activity coefficient  $\log \gamma_A$  as a function of the ammonium salt molality  $m_A$ , for such systems as triaurylammonium tetrahaloferrates in benzene and tetraisopentylammonium thiocyanate in chloro aromatic solvents recently studied, with a single interaction parameter  $\alpha$  and one association constant  $\beta_j$ .

Several years ago the author pointed out that the use of the mass action law in extraction equilibria with no regard paid to nonspecific interactions may lead to serious errors.<sup>2a</sup> Unfortunately, general interactions in polar organic mixtures are not at all well understood. Many authors are therefore persuaded to ignore nonspecific interactions altogether, and resort to the Dolezalek approach,<sup>2b</sup> of assigning all the deviations from ideal behavior to the formation of definite chemical species. Modern computers, which facilitate least-squares fitting of ideal association complex formation functions to experimental data, compound the error, by letting the statistical goodness-of-fit argument prevail over chemical common sense.

Leaving generalities aside (the present paper is concerned with long-chain substituted ammonium salts in nonpolar organic solvents) it is worthwhile to explore whether an alternative approach is possible. The best argument for the necessity to include a consideration of nonspecific interactions is the fact that the systems studied show liquid-liquid immiscibilities. It has been shown conclusively that in systems where phase separation occurs, no ideal association model can account for it, and nonspecific interactions must occur.<sup>3</sup> This means that the monomeric and associated species themselves have activity coefficients which differ from unity. Evidence for liquid-liquid immiscibility for the present kind of systems that has been published is summarized in Table I.<sup>4-15</sup> Most of the systems shown are "wet," *i.e.*, are obtained by extraction from an aqueous phase, hence are water saturated, but some are "dry," that is binary solutions of the salt in the diluent. Noteworthy is the fact that carbon tetrachloride and aromatic hydrocarbons, which are usually not considered to be as inert as the aliphatic hydrocarbons, also give rise to liquid-liquid immiscibility with appropriate salts. There is no doubt that many more systems with miscibility gaps may be found, particularly if the temperature is lowered.

A different kind of evidence for nonspecific interactions is that the apparent molecular weight of the aggregates decreases with increasing concentration of some salts, after a maximum aggregation has been reached. No ideal association model with any choice of species and association constants can account for this behavior. Some information is obtained from cryoscopy<sup>16,17</sup> and ebullioscopy<sup>16</sup>

in benzene (at 5 and 80°, respectively) of trihexyl- and trioctylammonium salts of perchlorate, hydrogen dichloride, hydrogen dinitrate, hydrogen sulfate, nitrate, and chloride (the maximal average association decreasing in this order),<sup>16</sup> and of pentyltributylammonium iodide, and tetraisopentyl- and tetrabutylammonium thiocyanates.<sup>17</sup> Other information comes from the extraction behavior of triaurylammonium thiocyanate in benzene, carbon tetrachloride, and cyclohexane, the iodide in carbon tetrachloride and cyclohexane, and the bromide in carbon tetrachloride at 23°. <sup>18</sup> In all cases have the authors explained the results correctly by pointing out that the association equilibrium quotients do not remain constant (they decrease) when the salt concentration increases, since the nature of the medium changes, so that the activity coefficients of the species do not remain constant at unity. Therefore, colligative properties of the systems yield only apparent degrees of association, rather than the true ones.

On the other hand, there is no doubt that in the present systems there occurs extensive association to dimers or trimers, due to dipole-dipole interactions. The main question is whether the observed behavior is explained best by

- (1) A paper presented at the International Symposium on Ion-Pair Partition, Stockholm, Oct 1972.
- (2) (a) Y. Marcus, *Pure Appl. Chem.*, **20**, 85 (1969); (b) F. Dolezalek, *Z. Phys. Chem.*, **64**, 727 (1908).
- (3) I. Prigogine and R. Defay, "Chemical Thermodynamics," Longmans, London, 1954, pp 432 and 518.
- (4) Y. Marcus, E. Hoffman, and A. S. Kertes, *J. Inorg. Nucl. Chem.*, **33**, 863 (1971).
- (5) S. S. Choi and D. G. Tuck, *J. Phys. Chem.*, **68**, 2712 (1964).
- (6) A. S. Kertes and Y. E. Habousha, *J. Inorg. Nucl. Chem.*, **25**, 1531 (1963).
- (7) A. S. Kertes and Y. E. Habousha, *Proc. Int. Conf. Peaceful Uses At. Energy*, **3rd**, 1964, **10**, 392 (1965).
- (8) M. L. Good and S. E. Bryan, *J. Inorg. Nucl. Chem.*, **20**, 140 (1961).
- (9) C. Boirie, French Report No. CEA-1262 (1960).
- (10) C. F. Coleman, K. B. Brown, J. G. Moore, and D. J. Crouse, *Ind. Eng. Chem.*, **50**, 1756 (1958).
- (11) V. M. Vdovenko, T. V. Kovaleva, and M. A. Ryazanov, *Radiokhimiya*, **4**, 609 (1962).
- (12) J. M. P. J. Versteegen, *J. Inorg. Nucl. Chem.*, **26**, 1589 (1964).
- (13) H. L. Friedman, *J. Phys. Chem.*, **66**, 1595 (1962).
- (14) U. Bertocci and G. Rolandi, *J. Inorg. Nucl. Chem.*, **23**, 323 (1961).
- (15) A. S. Wilson, American Report No. HW-68207 (1961).
- (16) V. V. Fomin and V. T. Potapova, *Zh. Neorg. Khim.*, **8**, 990 (1963).
- (17) J. Copenhafer and C. A. Kraus, *J. Amer. Chem. Soc.*, **73**, 4557 (1951).
- (18) W. Müller and R. M. Diamond, *J. Phys. Chem.*, **70**, 3469 (1966).

**TABLE I: Substituted Ammonium Salts in Nonpolar Organic Solvents that Show Liquid-Liquid Immiscibility**

Solvent	Salts <sup>a</sup>
<i>n</i> -Pentane	MDOAHNO <sub>3</sub> <sup>b</sup>
Isopentane	MDOAHNO <sub>3</sub> <sup>b</sup>
<i>n</i> -Hexane	MDOAHNO <sub>3</sub> , <sup>b</sup> TiOAHCl, <sup>c</sup> alamine HCl, <sup>c,d</sup> TNAHCl, <sup>c,e</sup> TH <sub>x</sub> AHCl <sup>f</sup>
<i>c</i> -Hexane	MDOAHNO <sub>3</sub> , <sup>b</sup> MDOAHCl, <sup>b</sup> MDOAHB, <sup>b</sup> MDOAHHSO <sub>4</sub> , <sup>b</sup> MDOAHClO <sub>4</sub> , <sup>b</sup> TiOAHCl, <sup>c</sup> alamine HCl, <sup>c,d</sup> TNAHCl <sup>c</sup>
Decane (? , white spirit)	MDOAHHSO <sub>4</sub> , <sup>g</sup> TOAHHSO <sub>4</sub> , <sup>g</sup> MDDAHHSO <sub>4</sub> <sup>g</sup>
Dodecane (kerosene)	TiOAHCl, <sup>c</sup> alamine HCl, <sup>c</sup> TNAHCl, <sup>c</sup> DDAH <sub>2</sub> HSO <sub>4</sub> , <sup>h</sup> TDAHHSO <sub>4</sub> , <sup>h</sup> LDBAHHSO <sub>4</sub> , <sup>h</sup> DLAH <sub>2</sub> HSO <sub>4</sub> , <sup>h</sup> BzLAH <sub>2</sub> HSO <sub>4</sub> , <sup>h</sup> Ph- PLAH <sub>2</sub> HSO <sub>4</sub> , <sup>h</sup>
Carbon tetrachloride	TH <sub>x</sub> AHCl, <sup>f</sup> MDOAHClO <sub>4</sub> , <sup>b</sup> TOAHNO <sub>3</sub> <sup>i</sup>
Benzene	(TOAH) <sub>2</sub> Th(NO <sub>3</sub> ) <sub>6</sub> , <sup>j</sup> TtiAAPic <sup>k</sup>
Xylene	TOAHHSO <sub>4</sub> , <sup>l</sup> (TOAH) <sub>2</sub> Pu(NO <sub>3</sub> ) <sub>6</sub> <sup>m</sup>

<sup>a</sup> The abbreviations used to designate the substituted ammonium salts follow ref 4. <sup>b</sup> Reference 5. <sup>c</sup> Reference 6. <sup>d</sup> Alamine 336 is a mixture of tertiary C<sub>8</sub> to C<sub>10</sub> amines. <sup>e</sup> Reference 7. <sup>f</sup> Reference 8. <sup>g</sup> Reference 9. <sup>h</sup> Reference 10. <sup>i</sup> Reference 11. <sup>j</sup> Reference 12. <sup>k</sup> Reference 13. <sup>l</sup> Reference 14. <sup>m</sup> Reference 15.

the additional existence of higher oligomers, such as the octamer, dodecamer, docosamer, etc., or whether the small species alone, combined with the nonspecific interactions, describe better the true state of the system. In the following, it will be shown that this second approach presents an adequate interpretation of some recent osmometric and dielectric constant data.<sup>19,20</sup>

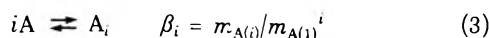
The regular associated mixture approach will be used.<sup>21,22</sup> It has been found useful for the associated hydrogen fluoride in aliphatic hydrocarbon systems, among others.<sup>23</sup> It permits phase separation to occur and association equilibrium quotients to decrease with increasing concentrations.<sup>22</sup> The excess Gibbs free energy of a mixture of  $n_A$  moles of substituted amine salt A and  $n_B$  moles nonpolar diluent B is written as the sum of two terms,  $G^E = G_{\text{nonspec}}^E + G_{\text{assoc}}^E$ , and differentiation gives the activity coefficient of the nominal component A

$$RT \ln f_A = (\partial G^E / \partial n_A)_{n_B, T} \\ = v_A \phi_B^2 \alpha + RT \ln (n_{A(1)} / n_A) / x_{A(1)}^0 - RT \ln (x_B + x_A / \chi) \quad (1)$$

where  $v$  is the molar volume,  $\phi$  the volume fraction,  $\alpha$  the regular solution interaction parameter,  $A(i)$  is the  $i$ -mer of A,  $x_{A(1)}^0$  is the mole fraction of monomeric A in pure liquid (supercooled) A,  $x$  is the nominal mole fraction, and  $\chi$  is the average degree of oligomerization

$$\chi = \sum i n_{A(i)} / \sum n_{A(i)} \quad (2)$$

The first term on the right-hand side of (1) represents the total contribution of the nonspecific interactions. That is, the self-association reactions



are assumed to proceed ideally, so that the molal association constants  $\beta_i$  are independent of the composition. The

parameter  $\alpha$  may be written<sup>24</sup> as

$$\alpha = (\delta_A - \delta_B)^2 + (\omega_A - \omega_B)^2 \quad (4)$$

where  $\delta$  is the solubility parameter, and  $\omega$  is given by

$$\omega^2 = 8\pi N_0 p^4 / 9r^6 k T v \quad (5)$$

where  $p$  is the dipole moment,  $r$  the dipole length, and  $N_0$ ,  $k$ , and  $T$  have their usual significance.<sup>24</sup> The chemical potential of the amine salt A is independent of the concentration scale, so that

$$\ln \gamma_A = \ln f_A + \ln (x_A / m_A) + (\mu^0 - \mu^*) / RT \quad (6)$$

where superscript zero denotes pure A as the standard state and the asterisk superscript denotes infinitely dilute A in B,  $m$  is the molality, and  $\gamma$  the molal activity coefficient. The conversion formula

$$x_A = 1 / (1 + 1000 / m_A M_B) \quad (7)$$

where  $M$  is the molar weight, permits the unknown quantities  $x_{A(1)}^0$  in (2) and  $(\mu^0 - \mu^*)$  in (6) to be eliminated by going to the limit

$$\lim_{x_A \rightarrow 0} \ln f_A = \ln (1000 / M_B) - (\mu^0 - \mu^*) / RT \\ = v_A \alpha / RT - \ln x_{A(1)}^0 \quad (8)$$

where the first equality results from (6) and (7) and the second from (1). From (1), (6), and (8) now results the expression for the molal activity coefficient of the nominal component A

$$\ln \gamma_A = v_A \alpha (\phi_B^2 - 1) / RT + \ln (n_{A(1)} / n_A) - \\ \ln (1 + m_A M_B / 1000) - \ln (x_B + x_A / \chi) \quad (9)$$

This, it should be noted, differs from the activity coefficients of the true species in the mixture, monomeric A and the oligomers  $A_i$ , for which it is possible to write suitable expressions. However, the activity coefficient of the nominal component is directly available from thermodynamic data, such as osmometric measurements. It is necessary now to convert all the concentration terms to the molal scale

$$\phi_B = n_B v_B / (n_B v_B + n_A v_A) = 1 / (1 + m_A M_B v_A / 1000 v_B) \quad (10)$$

$$n_{A(1)} / n_A = m_{A(1)} / m_A \quad (11)$$

$$\chi = m_A \sum \beta_i m_{A(i)}^i \quad (12)$$

$$-\ln (x_B + x_A / \chi) = \ln (1 + m_A M_B / 1000) - \\ \ln (1 + (M_B / 1000) \sum \beta_i m_{A(i)}^i) \quad (13)$$

- (19) O. Levy, Ph.D. Thesis, Hebrew University, Jerusalem, 1970; O. Levy, G. Markovits, and A. S. Kertes, *J. Inorg. Nucl. Chem.*, **33**, 551 (1971); A. S. Kertes, O. Levy, and G. Markovits, *J. Phys. Chem.*, **74**, 3568 (1970).  
 (20) J. David-Auslaender, Ph.D. Thesis, Hebrew University, Jerusalem, 1972.  
 (21) Reference 3, pp 394 and 409.  
 (22) H. Kehiaian and A. Fajans, *Bull. Acad. Pol. Sci. Ser. Chim. Sci.*, **12**, 255 (1964); A. Treszczanowicz and H. Kehiaian, *ibid.*, **14**, 413 (1966).  
 (23) Y. Marcus, J. Shamir, and J. Soriano, *J. Phys. Chem.*, **74**, 133 (1970).  
 (24) A. E. Van Arkel, *Trans. Faraday Soc.*, **42B**, 81 (1946); R. F. Weimer and J. M. Prausnitz, *Hydrocarbon Process.*, **44**(9), 237 (1965); J. H. Hildebrand, J. M. Prausnitz, and R. L. Scott, "Regular and Related Solutions," Van Nostrand-Reinhold, New York, N. Y., 1970, p 213.

TABLE II: Parameters  $\alpha$  and  $\beta_j$  of Eq 14 Which Fit Osmometric Data for Several Substituted Ammonium Salt-Aromatic Diluent Systems<sup>a</sup>

Salt	Diluent (conc range, $10^{-3} m$ )	Temp, °C	$\alpha, ^b \text{ cal ml}^{-1}$	$\log \beta_2$ (molal scale)
$(C_{12}H_{25})_3NHFeCl_4$	$C_6H_6$ (6-123)	25	$10.8 \pm 1.1$	2.11
	$C_6H_6$ (18-125)	37	$7.7 \pm 0.8$	1.84
	$C_6H_6$ (24-126)	50	$7.3 \pm 0.7$	1.70
$(C_{12}H_{25})_3NHFeBr_4$	$C_6H_6$ (6-125)	37	$10.8 \pm 1.2$	2.04
	$(i-C_5H_{11})_4NSCN$			
	$C_6H_5Cl$ (16-107)	65	$27.8 \pm 1.5$	1.78
	$C_{10}H_7Cl$ (12-93)	100	$19.6 \pm 2.6$	1.20
	$C_{10}H_7Cl$ (40-116)	132	$15.5 \pm 1.3$	1.31

<sup>a</sup> References 19 and 20. <sup>b</sup> The limits of error given are twice the standard deviation of the mean of 10-15 individual estimates for different concentrations in the range given, assuming that  $\beta_2$  is exact.

TABLE III: Aggregation Constants  $\beta_i$  Calculated for the Ideal Association Model Involving the Oligomers  $i = a + b + c$ 

Salt	Solvent (temp, °C)	Model $a + b + c$	$\log \beta_a$	$\log \beta_b$	$\log \beta_c$
$(C_{12}H_{25})_3NHFeCl_4^a$	$C_6H_6$ (25)	2 + 8 + 22	$2.14 \pm 0.05$	$14.94 \pm 0.05$	$44.55 \pm 0.06$
	$C_6H_6$ (37)	2 + 8 + 22	$1.95 \pm 0.03$	$14.32 \pm 0.01$	$42.06 \pm 0.06$
	$C_6H_6$ (50)	2 + 8 + 22	$1.81 \pm 0.06$	$13.45 \pm 0.03$	$39.39 \pm 0.10$
$(C_{12}H_{25})_3NHFeBr_4^a$	$C_6H_6$ (37)	2 + 8 + 10	$2.21 \pm 0.09$	$15.32 \pm 0.27$	$20.04 \pm 0.04$
	$(i-C_5H_{11})_4NSCN^b$				
	$C_6H_5Cl$ (65)	2 + 8	$1.78 \pm 0.06$	$14.13 \pm 0.04$	
	$C_{10}H_7Cl$ (100)	2 + 6	$1.44 \pm 0.04$	$8.66 \pm 0.02$	
	$C_{10}H_7Cl$ (132)	2 + 6	$1.26 \pm 0.06$	$7.95 \pm 0.02$	

<sup>a</sup> Reference 19. <sup>b</sup> Reference 20.

When (10) to (13) are introduced into (9), and the approximations

$$(\phi_B^2 - 1)' \approx -2m_A v_A M_B / 1000 v_B = 2m_A v_A \rho_B^0 / 1000$$

where  $\rho_B^0 = M_B / v_B$  is the density of the pure diluent B, and

$$-\ln(1 + (M_B/1000) \sum \beta_i m_{A(i)}^i) \approx -(M_B/1000) \sum \beta_i m_{A(i)}^i$$

are made for dilute solutions, the final result is

$$\log \gamma_A = -2m_A v_A^2 \rho_B^0 \alpha / 2303RT + \log(m_{A(1)} / m_A) - (M_B/2303) \sum \beta_i m_{A(i)}^i \quad (14)$$

All the terms in (14) are negative, and  $\log \gamma_A$  is seen to fall both due to the nonspecific interactions with the solvent (first term) and because of the self aggregation (last two terms).

Osmometric data give  $\log \gamma_A$  and  $m_A$  as functions of  $m_A$ , and (14) may therefore be compared to the data.<sup>19,20</sup> In particular, it is attempted to make the fit on the simplest assumption that but a single oligomer is formed so that the sum in the last term of (14) is replaced by a single term  $\beta_j m_A^j$ . For the tertiary amine salts in aromatic diluents, dielectric constant measurements<sup>25</sup> show that the dimer is the predominating oligomer. The data were fitted with the nonlinear least-squares program,<sup>19</sup> and yielded the parameters  $v_A^2 \alpha$  and  $\beta_j$ . For lack of information, it will be assumed that  $v_A(T) \approx v_A(30^\circ)$ , for the following three salts (calculated from densities of benzene solutions<sup>25</sup>):  $v((C_{12}H_{25})_3NHFeCl_4) = 640$  ml,  $v((C_{12}H_{25})_3NHFeBr_4) = 706$  ml, and  $v((C_7H_{15})_4NCl) = 482$  ml, and that  $v(T) = v(114.65^\circ)$  for  $(i-C_5H_{11})_4NSCN$ , where for the liquid tetrafluoroborate  $v = 413.9$  ml,<sup>26</sup> and  $v(SCN^-) - v(BF_4^-) \approx -3$  ml, so that  $v((i-C_5H_{11})_4NSCN) = 411$  ml. The results are shown in Table II. For comparison, the association constants for the species cal-

culated with the same non-linear least-squares program on the assumption of ideal association were obtained from previous publications,<sup>19,20</sup> and are shown in Table III. The precision of  $\alpha$  in Table II, around  $\pm 10\%$  corresponding to 0.04 log units, is comparable with that of the association constants when higher species are assumed, as in Table III. The inherent improbability of the existence of just octamers and docosamers, for instance, beside the dimer, and the necessity for inclusion of nonspecific interactions proven above, make the present interpretation, by the criterion of Occam's razor, preferable. It is always possible to multiply entities to fit the data, but such interpretations are not unique. A better claim to uniqueness has the interpretation which recognizes the existence of the dimer, and nonspecific interactions, described in the accepted manner<sup>21,22</sup> by the parameter  $\alpha$ .

For further interpretation of the  $\alpha$  values, the validity of (4) and (5) may be assumed, and proper values for  $p$  and  $r$  must then be assigned. Some estimates are available,<sup>25,26</sup> but these, inserted in (5), yield  $\omega_A^2$  values one to two orders of magnitude higher than  $\alpha$ , and even accounting for  $\omega_B$  for the polar chlorobenzene and chloronaphthalene does not bring them down to the experimental values. On the other hand, the Van Arkel expression is not particularly successful also in many other cases.<sup>24</sup> The  $\alpha$  values themselves, however, are similar in magnitude to those found, e.g., for the interaction of HF with  $C_nH_{2n+2}$  ( $n = 3-7$ ),  $\alpha \sim 40 \text{ cal ml}^{-1}$ . There is also agreement between the trends in  $\alpha$  and in  $\omega_A^2$ , in that the values decrease with increasing temperatures, and are higher for the tetrabromoferrate than the tetrachloroferrate at the same temperature. If  $\alpha$  is taken as representing the square of a difference of empirical "solubility parameters," i.e.,  $\alpha^{1/2} + \delta_B \sim \delta_A$  (empirical), with  $\delta(C_6H_6) = 9.2$ ,  $\delta(C_6H_5Cl) =$

(25) O. Levy, G. Markovits, and A. S. Kertes, *J. Phys. Chem.*, **75**, 542 (1971).

(26) J. E. Lind, Jr., and D. R. Sageman, *J. Phys. Chem.*, **74**, 3237 (1970).



9.5, and  $\delta$  ( $C_{10}H_7Cl$ ) = 10.4 (in  $\text{cal}^{1/2} \text{ ml}^{-1/2}$ , the latter calculated from the group contributions<sup>27</sup>), leads to reasonable values for  $\delta_A$  (empirical) = 12.6 for the tetrahaloferrates and 14.8 for the tetraisopentylammonium thiocyanate (in  $\text{cal}^{1/2} \text{ ml}^{-1/2}$ ).

In conclusion, although the theories of solutions of polar liquids are not yet sufficiently advanced to permit an *a priori* estimate of nonspecific interactions, the theory of regular associated solutions provides an alternative approach that seems to have more conceptual merit than that used hitherto, the ideal associated solutions. It pro-

vides a comparably "good" fit to the data, and allows for phase separation and decreasing average molecular weights that have been observed in long-chain substituted ammonium salt solutions in nonpolar or slightly polar organic diluents.

*Acknowledgment.* Thanks are due to Dr. O. Levy, the Negev University, Beer-Sheva, and to Mrs. J. David-Auslaender, Soreq Nuclear Research Center, Yavneh, for providing me with the data from their Ph.D. Theses.

(27) P. S. Small, *J. Appl. Chem.*, **3**, 75 (1953).

## Conductance and Ion-Pair Formation of Bis(2,9-dimethyl-1,10-phenanthroline)copper(I) Perchlorate. II. In Nitrobenzene–Carbon Tetrachloride and Methanol–Carbon Tetrachloride Mixtures

Katsuhiko Miyoshi\* and Toshihiro Tominaga

Department of Chemistry, Faculty of Science, Hiroshima University, Hiroshima, Japan (Received August 15, 1972)

Conductance of bis(2,9-dimethyl-1,10-phenanthroline)copper(I) perchlorate was measured at 25° in nitrobenzene–carbon tetrachloride and methanol–carbon tetrachloride mixtures which cover the range of 35–11 in dielectric constant. Experimental data were analyzed with the Fuoss–Onsager–Skinner 1965 conductance theory. The derived parameters indicated that the chelate salt is more dissociated at a given dielectric constant in nitrobenzene–carbon tetrachloride mixtures than in methanol–carbon tetrachloride mixtures, whereas both hydrodynamic radius  $R$  and  $a_k$  from the association constants are nearly the same in both mixtures. These facts were interpreted in terms of the specific interaction of the chelate cation with nitrobenzene and the decrease in charge density on the chelate cation arising from the coordination bond between Cu(I) and the aromatic ligands. The parameters were compared with those of tetrabutylammonium bromide obtained by Fuoss, *et al.*, in both mixtures and also with those of the chelate salt obtained previously in *n*-alcohols.

### Introduction

Conductance measurements in binary mixed solvents have been widely used for the investigation of solute–solvent interactions in electrolyte solutions. Generally accepted conductance theories are based on a model of "charged spheres in a continuum" and therefore the decrease of conductance with increasing salt concentration arises from the electrostatic forces between ions, *i.e.*, electrophoresis, relaxation, and ionic association. However, many interesting departures from the theory have been observed which have been interpreted in terms of some kinds of solute–solvent interactions by many workers. Strictly speaking, however, these interactions cannot be taken into account in the framework of a continuum theory.

Fuoss, Kraus, *et al.*, have focused their attention on the tetraalkylammonium salts, especially on tetrabutylammonium bromide, which is a unique model electrolyte in that the cation has tetrahedral symmetry and its structure is described as a point charge embedded in a sphere of par-

affin, while the anion is spherical with the charge uniformly distributed over the peripheral volume. In addition, the hydrophobic nature of the cation has recently been discussed by Kay, *et al.*,<sup>1</sup> in relation to the transport properties. Fuoss, *et al.*, have extensively studied the conductance behavior of this salt in various binary mixed solvents, namely, MeOH–PhNO<sub>2</sub>,<sup>2</sup> MeOH–benzene,<sup>3</sup> MeOH–CH<sub>3</sub>NO<sub>2</sub>,<sup>3</sup> MeOH–methyl ethyl ketone,<sup>4</sup> MeOH–CCl<sub>4</sub>,<sup>5</sup> MeOH–heptane,<sup>5</sup> EtOH–CCl<sub>4</sub>,<sup>6</sup> PhNO<sub>2</sub>–CCl<sub>4</sub>,<sup>7</sup> and dioxane–water<sup>8,9</sup> mixtures. They found that the initial effect

- (1) R. L. Kay, "Trace Inorganics in Water," R. A. Baker, Ed., American Chemical Society, Washington, D. C., 1968, p 1.
- (2) H. Sadek and R. M. Fuoss, *J. Amer. Chem. Soc.*, **72**, 301 (1950).
- (3) R. C. Miller and R. M. Fuoss, *J. Amer. Chem. Soc.*, **75**, 3076 (1953).
- (4) F. M. Sacks and R. M. Fuoss, *J. Amer. Chem. Soc.*, **75**, 5172 (1953).
- (5) H. Sadek and R. M. Fuoss, *J. Amer. Chem. Soc.*, **76**, 5897 (1954).
- (6) H. Sadek and R. M. Fuoss, *J. Amer. Chem. Soc.*, **76**, 5902 (1954).
- (7) H. Sadek and R. M. Fuoss, *J. Amer. Chem. Soc.*, **76**, 5905 (1954).
- (8) R. W. Martel and C. A. Kraus, *Proc. Nat. Acad. Sci. U. S.*, **41**, 9 (1955).
- (9) P. L. Mercier and C. A. Kraus, *Proc. Nat. Acad. Sci. U. S.*, **41**, 1033 (1955).

of adding another solvent to methanol was to decrease the degree of association of the salt despite the accompanying decrease in dielectric constant and to decrease the Walden products. They interpreted this effect in terms of solvation to ions, especially to the anion by monomeric methanol molecules produced by the addition of another solvent. Among these binary mixtures, methanol-carbon tetrachloride and nitrobenzene-carbon tetrachloride systems<sup>10</sup> seem to be suitable for the investigation of solute-solvent interactions since the polar component is protic (hydrogen-bonded) for the former and is dipolar aprotic (nonhydrogen-bonded) for the latter and the common nonpolar component is expected to behave only as a diluent of the corresponding polar component unless its mole fraction is considerably high.<sup>11,12</sup> Therefore the difference between the interactions of these polar components with ions is expected to be revealed clearly.

Bis(2,9-dimethyl-1,10-phenanthroline)copper(I) perchlorate was chosen as a sample electrolyte which is stable in solvents with dielectric constant higher than 10 and is composed of tetrahedrally symmetrical ions. It is, therefore, suitable as a sample electrolyte. Moreover, it has been found that the chelate cation is hydrodynamically equivalent to the tetrabutylammonium ion<sup>13</sup> and that the charge on the chelate cation is considerably decreased by the aromatic ligands. Therefore interesting differences are expected to appear with regard to ionic association behavior of these electrolytes.

### Experimental Section

**Materials.** Bis(2,9-dimethyl-1,10-phenanthroline)copper(I) perchlorate was recrystallized from acetone solution. Its purity was checked by analysis. The analytical data were as follows. *Anal.* Calcd: C, 58.03; H, 4.17; N, 9.67. Found: C, 58.05; H, 4.11; N, 9.67. The purity was quite satisfactory for the present purpose and was better than that of the early lot.<sup>13</sup> Stability of the complex in solution was confirmed by spectrophotometry using a charge-transfer band in a visible region with absorption maximum at 455 m $\mu$ . Reagent grade methanol was refluxed over calcium oxide, distilled, and then refluxed over magnesium methoxide. Finally it was purified by distillation and a middle fraction was collected. All the procedures were done under nitrogen gas to avoid the oxidation of methanol. Its specific conductance was less than  $6 \times 10^{-8}$  mho cm<sup>-1</sup>. Nitrobenzene was washed three times with conductivity water. It was then kept over anhydrous calcium chloride for several days and the filtrate was passed through molecular sieve, followed by distillation at reduced pressure (below 10 mm). The product was still slightly yellow though its specific conductance was negligibly small. Carbon tetrachloride was washed with conductivity water and was kept over anhydrous calcium chloride for several days. The filtrate was distilled through a 50-cm column packed with glass beads. Its specific conductance was negligibly small. Water contents in these solvents were examined by titration with Karl Fischer reagent and were found to be less than 0.01 wt% for MeOH and 0.005 wt% for PhNO<sub>2</sub> and CCl<sub>4</sub>. The solvent mixtures employed in conductance measurements were individually prepared by weight just before the measurements. Densities of the mixture were determined in a 50-ml single-neck capillary tube pycnometer by calibration with water at 25°. Observed values were in good agreement with the values interpolated from the data by

Hirsch and Fuoss<sup>14</sup> for PhNO<sub>2</sub>-CCl<sub>4</sub> mixtures and by Sadek and Fuoss<sup>5</sup> and by Pistoia, *et al.*,<sup>11</sup> for MeOH-CCl<sub>4</sub> mixtures. Therefore other physical properties of these mixtures were interpolated from their values. Mixtures of methanol with carbon tetrachloride showed somewhat higher conductance than either of the starting solvents. Usually it was  $5 \times 10^{-7}$  mho cm<sup>-1</sup> but it increased slightly on standing and also increased slightly with the concentration of carbon tetrachloride. Such a phenomenon was observed by Sadek and Fuoss<sup>6</sup> in EtOH-CCl<sub>4</sub> mixtures but not in MeOH-CCl<sub>4</sub> mixtures. The cause of increased solvent conductance in the former mixtures was attributed to the generation of hydrogen chloride but it is not known to us in the latter case. Accordingly when the content of carbon tetrachloride was relatively high, all runs were made by solution addition technique since measurements must be carried out at low salt concentrations owing to the limitation of applicability of the conductance theory ( $\kappa a < 0.2$ ).

**Apparatus and Procedure.** Conductance measurements were carried out by a conductometer, Type MY-7, from Yanagimoto Mfg. Co. Ltd., with the Wheatstone bridge at the frequency of 800 Hz. All the resistances were calibrated by a resistance box from Yokogawa Electric Works Ltd., which was standardized by Shinkawa Electric Co. Pyrex conductance cells were of erlenmeyer type with lightly platinized electrodes, containing about 200 ml of solution, and were standardized with aqueous KCl solutions, using the Lind, Zwolenik, and Fuoss constants.<sup>15</sup> Potassium chloride was recrystallized three times from conductivity water and dried at 500°. The cells were cleaned with chromic acid mixtures to eliminate traces of organic materials (solvents and complex salt) and with nitric acid. They were fully washed with conductivity water and with steam before each run. Cell solutions were thermostated to  $25 \pm 0.01^\circ$  in a double water bath with a mercury-in-glass thermoregulator. In order to hasten the temperature equilibrium and to avoid the polarization effect, a stirring bar was rotated very slowly by a magnet situated in the bath below the cell during the measurement. All the solutions were prepared by weight since the molecular weight of the complex salt is very high (579.522). In the case of nitrobenzene-carbon tetrachloride systems, a sample of 100-110 mg was directly added to the solvent of known conductivity in the cell for each run. After a constant value of resistance was attained, about 20 ml of solution was siphoned out and an equal volume of the solvent was added to the cell. This procedure was continued to an appropriate concentration. On the other hand, in the case of methanol-carbon tetrachloride mixtures with relatively low dielectric constant, solution addition technique was applied to vary the salt concentration. A sample of 100-110 mg accurately weighed was dissolved in about 20 ml of mixed solvent accurately weighed. Successive portions of this stock solution were then added to the same mixed solvent in the cell after the first determination of the solvent conductance, so that the

- (10) H. Sadek and R. M. Fuoss, *J. Amer. Chem. Soc.*, **81**, 4507 (1959).
- (11) F. Conti, P. Delogu, and G. Pistoia, *J. Phys. Chem.*, **72**, 1396 (1968).
- (12) (a) R. Mecke, *Discuss. Faraday Soc.*, **9**, 161 (1950); (b) F. Franks and D. J. G. Ives, *Quart. Rev. Chem. Soc.*, **20**, 1 (1966).
- (13) K. Miyoshi, *J. Phys. Chem.*, **76**, 3029 (1972).
- (14) E. Hirsch and R. M. Fuoss, *J. Amer. Chem. Soc.*, **82**, 1018 (1960).
- (15) J. E. Lind, J. Zwolenik, and R. M. Fuoss, *J. Amer. Chem. Soc.*, **81**, 1557 (1959).

TABLE I: Derived Parameters

No.	$\Lambda_0$	$a, \text{\AA}$	$K_A$	$L$	$\sigma$	$D$
1 <sup>a</sup>	107.95 ± 0.07	3.27 ± 0.25	3.48 ± 1.9	630 ± 80	0.024	32.62
2	100.55 ± 0.08	3.45 ± 0.53	10.1 ± 4.1	670 ± 190	0.035	30.4
3	96.46 ± 0.21	3.52 ± 0.66	15.3 ± 6.8	690 ± 260	0.021	29.0
4	91.33 ± 0.04	4.32 ± 0.18	21.4 ± 1.9	990 ± 70	0.015	27.4
5	85.53 ± 0.18	4.38 ± 0.60	32.3 ± 8.4	1020 ± 260	0.015	25.2
6	71.96 ± 0.15	9.07 ± 0.68	144 ± 15	3610 ± 350	0.017	19.35
7	31.865 ± 0.004	4.33 ± 0.04	0	264.0 ± 3.3	0.008	34.69
8	32.48 ± 0.01	4.51 ± 0.09	0	307 ± 8	0.016	32.80
9	33.98 ± 0.01	4.58 ± 0.06	0	406 ± 9	0.019	27.85
10	34.94 ± 0.02	4.97 ± 0.08	0	561 ± 15	0.028	24.0
11	35.66 ± 0.01	4.90 ± 0.05	0	620 ± 13	0.011	20.9
12	36.44 ± 0.02	4.81 ± 0.04	0	603 ± 17	0.024	18.2
13	36.59 ± 0.03	5.35 ± 0.21	28 ± 11	770 ± 110	0.019	16.0
14	37.16 ± 0.03	5.66 ± 0.05	131 ± 6	739 ± 38	0.007	13.9
15	37.26 ± 0.13	6.23 ± 0.16	407 ± 32	770 ± 150	0.010	12.2
16	36.69 ± 0.14	6.31 ± 0.17	963 ± 56	-130 ± 230	0.010	10.6

<sup>a</sup> Parameters in no. 1 mixture are quoted from ref 13.

uncertainty in the conductance at the most dilute solutions due to the relatively high and slightly changing solvent conductance might be minimized. In the case of nitrobenzene-carbon tetrachloride mixtures with considerably low dielectric constant, the increase in resistance with time was observed, probably due to the slight decomposition of the chelate. The rate of the increase was about 0.063%/hr in the mixture with the most low dielectric constant, for example. Therefore a small correction for resistance was made by extrapolating to  $t = 0$ .

## Results

The physical properties of the mixed solvents used (mole fraction  $x_2$ , weight per cent  $w_2$  of carbon tetrachloride, density  $d$ , viscosity  $\eta$ , and dielectric constant  $D$ ) are given in the microfilm editions of this journal.<sup>16</sup> The code numbers are used to identify the mixtures. Equivalent conductance and the corresponding concentration in equivalents per liter  $C$  are also given in the microfilm editions.<sup>16</sup> These data were analyzed with the Fuoss-Onsager-Skinner 1965 conductance equations for both associated and unassociated electrolytes.<sup>17</sup> No viscosity correction was made. All the calculations were performed on a TOSBAC 3400 electronic computer using the least-squares method proposed by Kay.<sup>18</sup> The derived parameters are summarized in Table I together with those obtained previously in pure methanol.<sup>13</sup>

## Discussion

Figure 1 shows the dependence of association constant  $K_A$  on dielectric constant  $D$  of the solvent medium. It is clearly seen from the figure that bis(2,9-dimethyl-1,10-phenanthroline)copper(I) perchlorate is more dissociated at a given dielectric constant in  $\text{PhNO}_2\text{-CCl}_4$  mixtures than in  $\text{MeOH-CCl}_4$  mixtures in the range of dielectric constants examined here. In Figure 1 are included the data of the chelate salt in  $n$ -alcohols and in methyl ethyl ketone obtained previously<sup>13</sup> for comparison together with those of tetrabutylammonium bromide in the both mixtures obtained by Sadek and Fuoss<sup>10</sup> which were recomputed with the 1965 equation.

It has been reported by conductance studies on mixed solvent systems that the variation of solvent composition

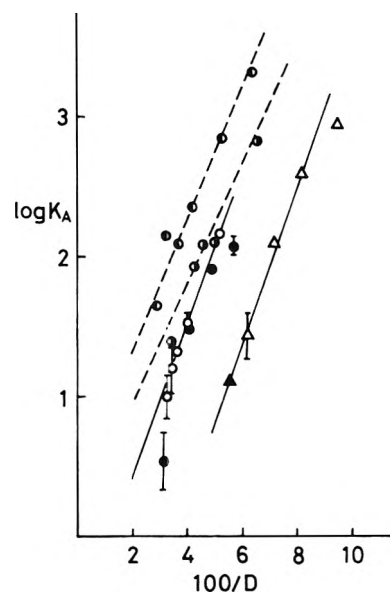


Figure 1. The dependence of  $K_A$  on dielectric constant: the chelate salt in  $\text{PhNO}_2\text{-CCl}_4$  ( $\Delta$ ); in  $\text{MeOH-CCl}_4$  ( $\circ$ ); in  $n$ -alcohols ( $\bullet$ ); in MEK ( $\blacktriangle$ );  $\text{Bu}_4\text{NBr}$  in  $\text{PhNO}_2\text{-CCl}_4$  ( $\bullet$ ) and in  $\text{MeOH-CCl}_4$  ( $\bullet$ ).

has a special effect on the association of electrolytes in different ways<sup>2,4,11,19-22</sup> which cannot be explained easily by a simple electrostatic theory.<sup>23</sup> However, Figure 1 indicates that the chelate salt has approximately the same magnitude of association constants in  $\text{MeOH-CCl}_4$

- (16) The data will appear following these pages in the microfilm edition of this volume of the journal. Single copies may be obtained from the Business Operation Office, Books and Journal Division, American Chemical Society, 1155 Sixteenth St., N. W., Washington, D. C. 20036. Remit check or money order for \$3.00 photocopy or \$2.00 for microfiche, referring to code number JPC-73-519.
- (17) R. M. Fuoss, L. Onsager and J. F. Skinner, *J. Phys. Chem.*, **69**, 2581 (1965).
- (18) R. L. Kay, *J. Amer. Chem. Soc.*, **82**, 2099 (1960).
- (19) A. D'Aprano and R. M. Fuoss, *J. Phys. Chem.*, **67**, 1704, 1722, 1871 (1963); **73**, 400 (1969); *J. Amer. Chem. Soc.*, **91**, 211 (1969); H. K. Bodenseh and J. B. Ramsey, *J. Phys. Chem.*, **67**, 140 (1963).
- (20) F. Conti and G. Pistoia, *J. Phys. Chem.*, **72**, 2245 (1968).
- (21) G. Pistoia and G. Pecci, *J. Phys. Chem.*, **74**, 1450 (1970).
- (22) D. F. Evans, J. Thomas, J. A. Nadas, and S. M. A. Matesich, *J. Phys. Chem.*, **75**, 1714 (1971).
- (23) R. M. Fuoss, *J. Amer. Chem. Soc.*, **80**, 5059 (1958).

TABLE II: Derived Distances in Å and Values of  $E_s/kT$ 

	CH <sub>3</sub> OH-CCl <sub>4</sub>		C <sub>6</sub> H <sub>5</sub> NO <sub>2</sub> -CCl <sub>4</sub>	
	Chelate salt	Bu <sub>4</sub> NBr	Chelate salt	Bu <sub>4</sub> NBr
$a_k$	4.4 (no. 3-6)	5.7	(4.4)	5.1
$R_{\infty}^+$	3.3 <sup>a</sup>	3.4	3.2 <sup>a</sup>	3.6
$R_{\infty}^-$	1.7 <sup>a</sup>	2.4	1.7 <sup>a</sup>	1.3
$R = R_{\infty}^+ + R_{\infty}^-$	5.0	5.8	4.9	4.9
$E_s/kT$	+0.09	-0.86	+3.1	-1.8

<sup>a</sup> Limiting equivalent conductances were split according to ref 13.

mixtures as that in *n*-alcohols in which the salt has been found to form a contact ion pair.<sup>13</sup> This fact seems to be interpreted reasonably by assuming that methanol structure is not changed by the addition of CCl<sub>4</sub> unless the mole fraction of CCl<sub>4</sub> is considerably high and that therefore the chelate salt forms a contact ion pair in the mixtures. Nmr,<sup>11</sup> ir,<sup>12a</sup> heats of mixing,<sup>12b</sup> and vapor pressure<sup>12a</sup> measurements have shown that CCl<sub>4</sub> has little effect on the structure of methanol when the content of CCl<sub>4</sub> is relatively small.

The striking feature observed in the figure is that the complex perchlorate is more dissociated in PhNO<sub>2</sub>-CCl<sub>4</sub> mixtures than in MeOH-CCl<sub>4</sub> mixtures, whereas Bu<sub>4</sub>NBr shows the reverse association behavior and that  $K_A$  values in MeOH-CCl<sub>4</sub> mixtures are approximately the same for the two salts, despite the fact that Br<sup>-</sup> ion is smaller than ClO<sub>4</sub><sup>-</sup> ion in size and that the cations in these salts are hydrodynamically equivalent.<sup>13</sup> Fuoss and Sadek<sup>10</sup> attributed the difference in  $K_A$  values of Bu<sub>4</sub>NBr in the two mixtures to the difference in the Gilkerson's  $E_s$  values<sup>24</sup> in eq 1 and found them to be of a reasonable order of magnitude (see Table II).

$$\log K_A = \log K_A^0 + 0.4343e^2/a_k Dkt - 0.4343E_s/kT \quad (1)$$

There seem, however, to be three causes responsible for the phenomena seen in Figure 1. The first is that as Fuoss, *et al.*,<sup>2-6</sup> suggested, solvation to Br<sup>-</sup> ion by methanol decreases the association, while solvation to ClO<sub>4</sub><sup>-</sup> ion does not take place owing to its low charge density. That is, Bu<sub>4</sub>NBr forms a solvent-separated ion pair in MeOH-CCl<sub>4</sub> mixtures, whereas the chelate salt forms a contact ion pair in the mixtures. Also the stabilization of the ion pair of the bulky chelate salt by the structure of methanol may take place in MeOH-CCl<sub>4</sub> mixtures as suggested by Kay, *et al.*<sup>25</sup> The second is that the two hydrodynamically equivalent cations are not equivalent electrostatically. The charge on the chelate cation is well distributed over the chelate through the coordination bond between Cu(I) and the aromatic ligands and therefore its charge density seems to be decreased considerably. On the other hand, for Bu<sub>4</sub>N<sup>+</sup> ion its charge is located chiefly on the nitrogen atom,<sup>5</sup> so that an affinity for anions is stronger in the latter than in the former. The  $K_A$  value of Bu<sub>4</sub>NClO<sub>4</sub> in PrOH and BuOH has been reported to be  $769 \pm 6^{26}$  and  $2200 \pm 20^{27}$  respectively, while that of the chelate salt is  $82 \pm 10^{13}$  and  $119 \pm 34^{13}$  respectively. Great difference in these values is attributable to the difference in charge density on the cations. Therefore marked solvation of methanol to Br<sup>-</sup> ion, which has been confirmed on the basis of ir investigation by Hyne and Levy,<sup>28</sup> seems to compensate the difference between Bu<sub>4</sub>N<sup>+</sup> ion and the chelate cation in the affinity for the corresponding anions

and decrease the degree of association of Bu<sub>4</sub>NBr to that of the chelate salt. On the other hand, in PhNO<sub>2</sub>-CCl<sub>4</sub> mixtures, Bu<sub>4</sub>NBr forms a contact ion pair so that the  $K_A$  is larger than that in MeOH-CCl<sub>4</sub> mixtures.

Hyne<sup>29</sup> tried to explain the abnormally large association constant of Bu<sub>4</sub>NBr in PhNO<sub>2</sub> and proposed the special structure of the ion pair in which PhNO<sub>2</sub> acts as a template for the absorption. Kay and Evans<sup>30</sup> reinvestigated this salt in pure MeOH, PhNO<sub>2</sub>, and CH<sub>3</sub>NO<sub>2</sub><sup>31</sup> and found that the salt is associated in PhNO<sub>2</sub> but not in MeOH or CH<sub>3</sub>NO<sub>2</sub> despite the fact that these solvents have about the same dielectric constant. Furthermore, Evans, *et al.*,<sup>32</sup> reported that a more likely explanation is to assume an almost complete lack of solvation of small Br<sup>-</sup> ion in PhNO<sub>2</sub>. We feel their explanation to be most likely since the order of the Walden product of halide ions is the same as that of the crystallographic radius in PhNO<sub>2</sub>-CCl<sub>4</sub> mixtures,<sup>12</sup> while that in MeOH,<sup>25</sup> CH<sub>3</sub>NO<sub>2</sub>,<sup>31</sup> and CH<sub>3</sub>CN<sup>32,33</sup> is the reverse order owing to the solvation of these solvents to halide ions. Recently, Petrucci, *et al.*,<sup>34</sup> measured the ultrasonic absorption of Bu<sub>4</sub>NBr in MeOH-CCl<sub>4</sub> and PhNO<sub>2</sub>-CCl<sub>4</sub> mixtures and found that the association is a single process in the latter mixtures, whereas it is a two-step process in the former. This is one of the supports for the validity of the assumptions that strong solvation to Br<sup>-</sup> ion by methanol leads to small association in the former mixtures and that a lack of solvation leads to large association in the latter.

Finally we must examine the large difference in the  $K_A$  value between the chelate salt and Bu<sub>4</sub>NBr in PhNO<sub>2</sub>-CCl<sub>4</sub> mixtures. If both ions of the chelate salt are not solvated and/or not stabilized by PhNO<sub>2</sub> and form a contact ion pair as Bu<sub>4</sub>NBr does in these mixtures, the  $K_A$  value of the chelate salt will be smaller than that of Bu<sub>4</sub>NBr because it is natural that the larger the ions, the smaller will be the  $K_A$  value in these aprotic solvents according to the electrostatic theory and because the affinity of the chelate cation for anions is weakened by the decrease in charge density on it. However, the remarkable difference

- (24) W. Gilkerson, *J. Chem. Phys.*, **25**, 1199 (1956).  
 (25) R. L. Kay, C. Zawoyski, and D. F. Evans, *J. Phys. Chem.*, **69**, 4208 (1965).  
 (26) D. F. Evans and P. Gardam, *J. Phys. Chem.*, **72**, 3281 (1968).  
 (27) D. F. Evans and P. Gardam, *J. Phys. Chem.*, **73**, 158 (1969).  
 (28) J. B. Hyne and R. M. Levy, *Can J. Chem.*, **40**, 692 (1962).  
 (29) J. B. Hyne, *J. Amer. Chem. Soc.*, **85**, 304 (1963).  
 (30) R. L. Kay and D. F. Evans, *J. Amer. Chem. Soc.*, **86**, 2748 (1964).  
 (31) R. L. Kay, S. C. Bulm, and H. I. Schiff, *J. Phys. Chem.*, **67**, 1223 (1963).  
 (32) D. F. Evans, C. Zawoyski, and R. L. Kay, *J. Phys. Chem.*, **69**, 3878 (1965).  
 (33) C. H. Springer, J. F. Coetzee, and R. L. Kay, *J. Phys. Chem.*, **73**, 471, (1969).  
 (34) S. Petrucci and G. Atkinson, *J. Phys. Chem.*, **70**, 2550 (1966); S. Petrucci and M. Battistini, *ibid.*, **71**, 1181 (1967).

is not explained by the difference in anion size and charge density on the cations alone since the chelate salt is more dissociated in  $\text{PhNO}_2\text{-CCl}_4$  mixtures than in  $\text{MeOH-CCl}_4$  mixtures where the chelate salt is thought to form a contact ion pair as described above. Therefore it must be concluded that any specific interaction between the chelate cation and  $\text{PhNO}_2$  may play an important role in decreasing the association in  $\text{PhNO}_2\text{-CCl}_4$  mixtures. This is the third explanation.

In Table II are given the distance  $a_k$  from  $K_A$ ,  $R_\infty^\pm$  from Stokes' law corrected for the dipole relaxation<sup>35</sup> of solvent molecules, and the values of the Gilekson's term calculated with the corresponding  $a_k$  values. The corresponding values of  $\text{Bu}_4\text{NBr}$  derived from the recomputation of the data by Fuoss, *et al.*, with the 1965 conductance theory are also given for comparison. Judging from the plots in Figure 1,  $a_k$  was set equal to 4.4 Å in both mixtures. It is seen in the table that a larger value of  $E_s/kT$  in  $\text{PhNO}_2\text{-CCl}_4$  mixtures than in  $\text{MeOH-CCl}_4$  mixtures suggests the specific interaction of the chelate cation with  $\text{PhNO}_2$ . The hydrodynamic radius, however, is nearly the same in both mixtures. Therefore the interaction between the chelate cation and  $\text{PhNO}_2$  decreases the ionic association but does not retard the ionic migration. On the other hand, the interaction of the chelate with methyl ethyl ketone which is also dipolar aprotic, has been found to retard it,<sup>13</sup> though the  $K_A$  in MEK is approximately the same as that in  $\text{PhNO}_2\text{-CCl}_4$  mixtures at the same dielectric constant, as seen in Figure 1. We

assume that this interaction is a kind of ion-dipole interactions since  $\text{PhNO}_2$  molecules have large dipole moment (3.99 D). Kay, *et al.*,<sup>36</sup> reported from the conductance study on alkali metal perchlorates and tetraphenylborides in  $\text{CH}_3\text{CN}$  that the degree of solvation of large ions is determined predominantly by the dipole moment of the solvent molecules, whereas that of small ions is determined predominantly by the acid-base properties of the solvent molecules. Preliminary measurements of the chelate salt in  $\text{CH}_3\text{CN-CCl}_4$  mixtures indicated that the salt is also more dissociated in these mixtures than  $\text{MeOH-CCl}_4$  mixtures. This fact seems to support the above assumption since  $\text{CH}_3\text{CN}$  molecules have also large dipole moment (3.37 D).

It is seen in Table II that  $R_\infty^-$  value of  $\text{Br}^-$  ion in  $\text{MeOH-CCl}_4$  mixtures is considerably larger than that in  $\text{PhNO}_2\text{-CCl}_4$  mixtures and still larger than that of  $\text{ClO}_4^-$  ion in both mixtures despite the fact that  $\text{ClO}_4^-$  ion is much larger than  $\text{Br}^-$  ion in crystallographic radius. Therefore marked solvation of  $\text{Br}^-$  ion by methanol assumed by Fuoss, *et al.*, seems to be justified.

*Acknowledgment.* The authors would like to express their deep gratitude to Professor Y. Yamamoto of Hiroshima University for his interest and encouragement in this study.

(35) R. M. Fuoss, *Proc. Nat. Acad. Sci. U. S.*, **45**, 807 (1959).

(36) R. L. Kay, B. J. Hales, and G. P. Cunningham, *J. Phys. Chem.*, **71**, 3925 (1967).

## Medium Activity Coefficient of Iodate in Methanol, Acetonitrile, and Dimethyl Sulfoxide with Reference to Water

I. M. Kolthoff\* and M. K. Chantooni, Jr.

School of Chemistry, University of Minnesota, Minneapolis, Minnesota 55455 (Received August 30, 1972)

Values of  $\text{p}K^{\text{sp}}(\text{AgIO}_3)$  at 25° in water (W), methanol (M), acetonitrile (AN), and dimethyl sulfoxide (DMSO) were found equal to 7.5, 12.7, 10.6, and 9.8, respectively. Values of  $\text{p}K^{\text{sp}}(\text{KIO}_3)$  in W, M, and DMSO are 1.6, 7.3, and 7.7, respectively, while those of  $\text{p}^{\text{w}}\gamma^{\text{M}}(\text{IO}_3^-)$ ,  $\text{p}^{\text{w}}\gamma^{\text{AN}}(\text{IO}_3^-)$ , and  $\text{p}^{\text{w}}\gamma^{\text{DMSO}}(\text{IO}_3^-)$  are 3.9, 6.9, and 8.3, respectively. The value of  $\text{p}^{\text{w}}\gamma^{\text{S}}(\text{IO}_3^-)$  is unusually large as compared to corresponding values of nitrate, chloride, and acetate, indicating unusually large solvation of iodate in water as compared to that in M, AN, and DMSO. The mean ionic activity coefficient  $f^\pm(\text{KIO}_3)$  is only 0.38 in 0.44 M (saturated) solution in water, indicating some  $\text{KIO}_3$  association of ions.

### Introduction

On the basis of the tetraphenylborate assumption we reported in a previous paper<sup>1</sup> values of medium activity coefficients  $^{\text{w}}\gamma^{\text{Si}}$  of a number of cations and anions with reference to water (W) in the solvents (S), methanol (M), acetonitrile (AN), and dimethyl sulfoxide (DMSO). In unpublished work we found from the solubility of silver iodate in W and M,  $\text{p}^{\text{w}}\gamma^{\text{M}}(\text{IO}_3^-)$  of the order of 3.9, a value much larger than that of any other anion studied. In the

present paper we have made more accurate estimates of  $K^{\text{sp}}(\text{AgIO}_3)$  and also have determined  $K^{\text{sp}}(\text{KIO}_3)$  in the above solvents,  $\text{p}^{\text{w}}\gamma^{\text{S}}(\text{K}^-)$  being known.<sup>1</sup> The large value of  $\text{p}^{\text{w}}\gamma^{\text{M}}(\text{IO}_3^-)$  is discussed in relation to the structure of the ion. The solubility of potassium iodate in AN was found to be too small to allow an accurate determination of its  $\text{p}K^{\text{sp}}$ .

(1) I. M. Kolthoff and M. K. Chantooni, Jr., *J. Phys. Chem.*, **76**, 2024 (1972).

The values of  $pK^{sp}(\text{AgIO}_3)$  in W, M, AN, and DMSO were estimated potentiometrically with the silver wire and silver|silver iodate electrodes in saturated silver iodate solutions containing tetraethylammonium iodate. To check the value of  $(pK^{sp}(\text{AgIO}_3))_M$  a chemical exchange method involving chloride was used. Values of  $pK^{sp}(\text{KIO}_3)$  were found potentiometrically in water with the cation sensitive electrode in suitable cells without liquid junction (cells I and II), and in DMSO in a cell with liquid junction (cell III). Independent estimates of  $pK^{sp}(\text{KIO}_3)$  in M and DMSO were made from the total solubility and/or conductivity of the saturated solutions. Activity coefficients were calculated from the partially extended Debye-Hückel equation taking  $\bar{a} = 3 \text{ \AA}$  for  $\text{K}^{+2}$  and  $4.5 \text{ \AA}$  for  $\text{IO}_3^{-2}$  when  $\mu < 0.02$ .

### Experimental Section

**Chemicals.** Methanol,<sup>3</sup> acetonitrile,<sup>4</sup> and dimethyl sulfide<sup>5</sup> were purified as described elsewhere. Tetraethylammonium iodate was prepared by neutralization of aqueous tetraethylammonium hydroxide with Merck Reagent Grade iodic acid, evaporating the solution to dryness, and recrystallizing the solid from ethyl acetate. Assay by iodometric titration showed 99.3% purity. Tetraethylammonium chloride was a product prepared by F. G. Thomas in this laboratory.<sup>6</sup> Potassium chloride was Baker's Analyzed Reagent Grade. Silver chloride and iodate were prepared in the conventional way. All salts were dried *in vacuo* at 70° for 3 hr.

**Potentiometry.** The silver|silver chloride electrode was prepared by the method of Brown and McInnes<sup>7</sup> by anodization of a silver plated platinum wire in 0.1 M HCl while the silver|silver iodate electrode was fabricated from a silver plated platinum wire by anodizing for 20 min at 1 mA/cm<sup>2</sup> in 0.05 M potassium iodate by a method similar to that for silver|silver bromide electrodes.<sup>8</sup> It had a light tan color and was prepared daily. The potentiometric cell and 0.01 M  $\text{AgNO}_3|\text{Ag}$  reference electrodes (both half-cells containing the same solvent) were those described previously<sup>9</sup> for pH measurements with the glass electrode. A Beckman No. 39137 cationic glass electrode was used for  $a(\text{K}^+)$  measurements. It was calibrated in 0.01–0.6 M aqueous potassium chloride solutions using values of  $f(\text{K}^+)$  calculated by Bates, *et al.*,<sup>10</sup> on the basis of ionic hydration theory. It was also calibrated in  $1 \times 10^{-4}$ – $1 \times 10^{-2}$  M potassium perchlorate solutions in DMSO. All emf measurements were made on a Corning Model 10 pH meter.

**Other Operations.** Conductivity measurements were made as described previously.<sup>4</sup> A conductivity cell having a cell constant of 16.40 was used in the determination of the conductivity of saturated potassium iodate in water. It was calibrated in 0.1 and 1.0 demal potassium chloride solutions of known specific conductivity.<sup>11</sup> Exchange experiments between tetraethylammonium chloride and silver iodate in methanol were performed in a similar way as those involving tetraphenylborate and bromide.<sup>12</sup>

### Results

**Mobility of the Iodate Ion.** Conductance data of tetraethylammonium iodate in AN, M, and DMSO are presented in Table I. The observed slopes of the  $\Lambda$  vs.  $c^{1/2}$  plots and theoretical Onsager slopes are 230 and 241, respectively, in M, 460 and 368 in AN, and 57 and 54.1 in

**TABLE I: Conductivity of Tetraethylammonium Iodate in Various Solvents<sup>a</sup>**

M		AN		DMSO	
$C(\text{Et}_4\text{NIO}_3), 10^3 M$	$\Lambda$	$C(\text{Et}_4\text{NIO}_3), 10^3 M$	$\Lambda$	$C(\text{Et}_4\text{NIO}_3), 10^3 M$	$\Lambda$
1.88	98	1.27	170.5	1.98	36
3.45	94	2.12	165	3.76	34.1
5.90	89	6.35	149	8.50	33.2
12.4	82	10.6	139	17.5	30.4

<sup>a</sup>  $\Lambda_0(\text{Et}_4\text{NIO}_3) = 107 \pm 2$  in M,  $186 \pm 3$  in AN, and  $38.2 \pm 0.5$  in DMSO.

**TABLE II: Ionic Mobilities of Iodate and Several Anions in Various Solvents**

Solvent	$\lambda_0(\text{IO}_3^-)$	$\lambda_0(\text{ClO}_4^-)$	$\lambda_0(\text{NO}_3^-)$	$\lambda_0(\text{Cl}^-)$	$\lambda_0(\text{Br}^-)$	$\lambda_0(\text{I}^-)$
W	40.5 <sup>a</sup>	67.3 <sup>a</sup>	71.4 <sup>a</sup>	76.4 <sup>a</sup>	78.2 <sup>a</sup>	76.9 <sup>a</sup>
M	49 <sup>b</sup>	71 <sup>c</sup>	60.8 <sup>h</sup>	54.7 <sup>c</sup>	56.5 <sup>c</sup>	62.8 <sup>g</sup>
AN	101 <sup>b</sup>	103.4 <sup>d</sup>	104 <sup>e</sup>	91 <sup>e</sup>	100.1 <sup>d</sup>	102.0 <sup>d</sup>
DMSO	23.5 <sup>b</sup>	25.2 <sup>f</sup>	27.7 <sup>f</sup>		24.7 <sup>f</sup>	24.3 <sup>f</sup>

<sup>a</sup> Reference 22. <sup>b</sup> This work. <sup>c</sup> J. Prue and P. J. Sherrington, *Trans. Faraday Soc.*, 1795 (1951); ref 13. <sup>d</sup> J. F. Coetzee and G. P. Cunningham, *J. Amer. Chem. Soc.*, 87, 2529 (1965). <sup>e</sup> P. Walden and E. Birr, *Z. Phys. Chem.*, 144, 269 (1929). <sup>f</sup> P. Sears, G. Lester, and L. Dawson, *J. Phys. Chem.*, 60, 1433 (1956). <sup>g</sup> R. E. Jervis, D. Muir, J. P. Butler, and A. Gordon, *J. Amer. Chem. Soc.*, 75, 2855 (1953). <sup>h</sup> M. Barak and H. Hartley, *Z. Phys. Chem.*, 165, 290 (1933).

DMSO, indicating practically complete dissociation in these three solvents in the concentration range studied. Resulting values of  $\lambda_0(\text{IO}_3^-)$  in M, AN, and DMSO tabulated in Table II were found using  $\lambda_0(\text{Et}_4\text{N}^+) = 58.2$  in M<sup>13</sup> and 85 in AN.<sup>14</sup> Since  $\lambda_0(\text{Et}_4\text{N}^+)$  is unavailable in DMSO, a value of 14.7 was calculated from the relation  $\eta\lambda_0 = (Fe/1800\pi)/(R_\infty + S/D)$ ,<sup>14</sup> assuming the constants  $R_\infty$  and  $S$  found for  $\text{Et}_4\text{N}^+$  in acetonitrile-carbon tetrachloride mixtures<sup>14</sup> (equal to 2.748 and 4.20, respectively) to be the same in DMSO. In the above relation  $D$  refers to the dielectric constant while the other symbols have their usual significance.

**Solubility Product of Silver Iodate.** Potentiometric data of the emf of cells composed of the silver|silver iodate electrode in water, M, AN, and DMSO solutions saturated with silver iodate and containing tetraethylammonium iodate and  $\text{Ag}|0.01 \text{ M } \text{AgNO}_3$  in S as reference electrode are presented in Table III. In water and methanol the po-

- (2) J. Kielland, *J. Amer. Chem. Soc.*, 59, 1675 (1937).
- (3) I. M. Kolthoff and M. K. Chantooni, Jr., *Anal. Chem.*, 44, 194 (1972).
- (4) I. M. Kolthoff, S. Bruckenstein, and M. K. Chantooni, Jr., *J. Amer. Chem. Soc.*, 83, 3927 (1961).
- (5) I. M. Kolthoff, M. K. Chantooni, Jr., and S. Bhowmik, *J. Amer. Chem. Soc.*, 90, 23 (1968).
- (6) I. M. Kolthoff and F. G. Thomas, *J. Phys. Chem.*, 69, 3049 (1965).
- (7) A. S. Brown and D. A. McInnes, *J. Amer. Chem. Soc.*, 57, 1356 (1935).
- (8) D. J. Ives and G. J. Janz, "Reference Electrodes," Academic Press, New York, N. Y., 1961, p 207.
- (9) I. M. Kolthoff and M. K. Chantooni, Jr., *J. Amer. Chem. Soc.*, 87, 4428 (1965).
- (10) R. G. Bates, B. R. Staples, and R. A. Robinson, *Anal. Chem.*, 42, 867 (1970).
- (11) G. Jones and B. C. Bradshaw, *J. Amer. Chem. Soc.*, 55, 1780 (1933).
- (12) I. M. Kolthoff and M. K. Chantooni, Jr., *Anal. Chem.*, 44, 194 (1972).
- (13) E. C. Evers and A. G. Knox, *J. Amer. Chem. Soc.*, 73, 1739 (1951).
- (14) D. S. Berns and R. M. Fuoss, *J. Amer. Chem. Soc.*, 82, 5585 (1960).

tentials with the silver wire electrode were irreproducible, while reproducible potentials to within  $\pm 2$  mV, which agree to within  $\pm 2$  mV with those of the  $\text{AgIO}_3|\text{Ag}$  electrode, were obtained in AN and DMSO. In all solutions in Table III tetraethylammonium iodate was taken as completely dissociated. Under our experimental conditions no indication was obtained of complexation between iodate with silver iodate. From the value in water of  $K^f(\text{Ag}(\text{IO}_3)_2^-) = a(\text{Ag}(\text{IO}_3)_2^-)/a(\text{Ag}^+)a^2(\text{IO}_3^-) = 8 \times 10^3$ ,<sup>15</sup> we find in the aqueous solutions in Table III  $a(\text{IO}_3^-)/a(\text{Ag}(\text{IO}_3)_2^-) = 4 \times 10^3$ , taking  $\text{p}K^{\text{sp}}(\text{AgIO}_3) = 7.5$ . From the data in Table III the average value of  $\text{p}K^{\text{sp}}(\text{AgIO}_3)$  in water equal to 7.5 is in good agreement with the values reported by other workers<sup>16-19</sup> (7.45 to 7.52) using various methods, thus attesting to the reliability of the silver|silver iodate electrode. The potentiometric value of  $\text{p}K^{\text{sp}}(\text{AgIO}_3)$  in methanol was checked by a chemical exchange method involving silver iodate and tetraethylammonium chloride. When the initial concentrations were  $7.85 \times 10^{-3}$  and  $1.44 \times 10^{-2}$  M, the iodometrically determined concentrations of iodate in the equilibrated solutions were  $2.00 \times 10^{-3}$  and  $3.84 \times 10^{-3}$  M, respectively. From the value of  $\text{p}K^{\text{sp}}(\text{AgCl})$  in methanol equal to 13.2<sup>20</sup> an average value of 12.7 is calculated for  $\text{p}K^{\text{sp}}(\text{AgIO}_3)$ , in satisfactory agreement with the potentiometric value of 12.6 in Table III. A value of  $(\text{p}K^{\text{sp}}(\text{AgIO}_3))_{\text{W}}$  equal to 7.5<sub>5</sub>, also in good agreement with the potentiometric value, is obtained in the present study from the specific conductivity of a saturated solution of silver iodate in water,  $1.53 \times 10^{-5}$  ohm<sup>-1</sup> cm<sup>-1</sup>. To summarize,  $\text{p}K^{\text{sp}}(\text{AgIO}_3)$  has been found in the present study to be 7.5 in W, 12.6 in M, 10.6 in AN, and 9.8 in DMSO.

**Solubility Product of Potassium Iodate.** The solubility product of potassium iodate was estimated in water from the difference in emf of cells II and I without liquid junction.

$\text{Ag} \text{AgIO}_3$	sat. $\text{KIO}_3$ sat. $\text{AgIO}_3$	$\text{K}(\text{gl})$	I
$\text{Ag} \text{AgCl}$	0.44 M $\text{KCl}$ sat. $\text{AgCl}$	$\text{K}(\text{gl})$	II

$$E_{\text{II}} - E_{\text{I}} = 0.0591[(\text{p}K^{\text{sp}}(\text{AgCl}) - \text{p}K^{\text{sp}}(\text{AgIO}_3)) + \text{p}K^{\text{sp}}(\text{KIO}_3) + 2 \log C(\text{KCl})f^{\pm}(\text{KCl})]$$

In cells I and II the same cation sensitive glass electrode,  $\text{K}(\text{gl})$ , was used. The concentration of potassium chloride in cell II was equal to the total solubility of potassium iodate in water. In this way no large difference in  $C(\text{K}^+)$  in cells I and II are expected, obviating checking the linear response of the cation glass electrode with  $\text{p}a(\text{K}^+)$ . With our particular cation glass electrode  $E_{\text{I}} = +0.051$  V and  $E_{\text{II}} = +0.213$  V, which combined with the accepted values in water of  $\text{p}K^{\text{sp}}(\text{AgCl}) = 9.7$ ,  $\text{p}K^{\text{sp}}(\text{AgIO}_3) = 7.5$ , and the mean ionic activity coefficient  $f^{\pm}(\text{KCl})$ , in 0.44 M potassium chloride equal to 0.65 (interpolated from values calculated from hydration theory by Bates, *et al.*,<sup>10</sup>) yield  $\text{p}K^{\text{sp}}(\text{KIO}_3) = 1.64$ . In DMSO  $\text{p}a(\text{K}^+)$  was determined in the saturated potassium iodate solution with the cation glass electrode in cell III with liquid junction



A value of  $\text{p}a(\text{K}^+) = 3.8_5$  was found, yielding  $(\text{p}K^{\text{sp}}(\text{KIO}_3))_{\text{DMSO}} = 7.7$ , assuming  $a(\text{IO}_3^-) = a(\text{K}^+)$ . The liquid

TABLE III: Potentiometric Determination of  $\text{p}K^{\text{sp}}(\text{AgIO}_3)$  in Various Solvents

Solvent	$C(\text{Et}_4\text{NIO}_3)$ , $10^3 \text{ M}$	$E^a$ , mV $\text{Ag} \text{AgIO}_3$ electrode	$f(\text{IO}_3^-)$	$\text{p}K^{\text{sp}}(\text{AgIO}_3)$ $\text{Ag} \text{AgIO}_3$ electrode
W	1.15	-152	0.95	7.5 <sub>5</sub>
	2.90	-172	0.94	7.5 <sub>4</sub>
	4.83	-185	0.93	7.4 <sub>8</sub>
	8.70	-190	0.89	7.3 <sub>7</sub>
				Av 7.5
M	2.16	-444	0.84	12.5 <sub>0</sub>
	21.6	-507	0.64	12.6 <sub>5</sub>
				Av 12.6
AN	3.17	-338	0.82	10.5 <sub>7</sub>
	9.51	-370	0.75	10.7 <sub>0</sub>
				Av 10.6
DMSO	4.32	-312	0.85	9.8 <sub>2</sub>
	21.6	-347	0.74	9.7 <sub>7</sub>
				Av 9.8

<sup>a</sup> Vs. 0.00947 M  $\text{AgNO}_3|\text{Ag}$  in W, salt bridge 0.01 M  $\text{Et}_4\text{NPI}$  in W; vs. 0.010 M  $\text{AgNO}_3|\text{Ag}$  in M, AN, and DMSO, salt bridges 0.010 M  $\text{Et}_4\text{NClO}_4$  in respective solvents. No liquid junction correction estimation applied.

junction potential of cell III, calculated from the Henderson equation to be -5 mV, was neglected.

The molar solubilities of potassium iodate in water and methanol were found iodometrically to be 0.44 and  $2.70 \times 10^{-4}$  M. The specific conductivities of the saturated potassium iodate solutions in W, M, and DMSO were  $2.6_8 \times 10^{-2}$ ,  $2.7_3 \times 10^{-5}$ , and *ca.*  $0.8_5 \times 10^{-5}$  ohm<sup>-1</sup> cm<sup>-1</sup>, respectively. The following equivalent conductivities of potassium iodate were measured in undersaturated aqueous solutions: 94.0, 83.3, 80.7, and 79.0 in 0.05, 0.10, 0.14, and 0.20 M potassium iodate, respectively.

In the calculation of  $\text{p}K^{\text{sp}}(\text{KIO}_3)$  from the conductivity data values of  $\lambda_0(\text{IO}_3^-)$  from Table II,  $\lambda_0(\text{K}^+) = 50.2$  in M,<sup>21</sup> 73.5 in W,<sup>22</sup> and 13.9 in DMSO,<sup>23</sup> were used. The following values of  $\text{p}K^{\text{sp}}(\text{KIO}_3)$  were obtained in W, 1.6 (potentiometric); in M, 7.2 (total solubility, assuming complete dissociation) and 7.3<sub>5</sub> (conductometric); in DMSO, 7.7 (potentiometric, from  $a(\text{K}^+)$ ) and 7.4 (conductometric). The uncertainties in the reported values of  $\text{p}K^{\text{sp}}(\text{KIO}_3)$  and  $\text{p}K^{\text{sp}}(\text{AgIO}_3)$  are  $\pm 0.05$  in W and  $\pm 0.1$  in the organic solvents.

## Discussion

The use of the silver|silver iodate electrode for the measurement of  $a(\text{IO}_3^-)$  is not mentioned in the literature. From our results it appears to be reliable in the solvents used.

From the values of  $\text{p}^{\text{W}}\gamma^{\text{S}}(\text{K}^+)$  and  $\text{p}^{\text{W}}\gamma^{\text{S}}(\text{Ag}^+)$ <sup>1</sup> based on the tetraphenylborate assumption and the present values of  $(\text{p}K^{\text{sp}}(\text{AgIO}_3))_{\text{s}}$  the following  $\text{p}\gamma$  values are found:

- (15) J. J. Renier and D. S. Martin, *J. Amer. Chem. Soc.*, **78**, 1833 (1956).
- (16) A. Noyes and D. Kohr, *Z. Phys. Chem.*, **42**, 336 (1902).
- (17) N. C. Li and Y. Lo, *J. Amer. Chem. Soc.*, **63**, 394 (1941).
- (18) I. M. Kolthoff and J. J. Lingane, *J. Phys. Chem.*, **42**, 133 (1938).
- (19) P. Derr, R. Stockdale, and W. Vosburgh, *J. Amer. Chem. Soc.*, **63**, 2670 (1941).
- (20) P. Buckley and H. Hartley *Phil. Mag.*, **8**, 320 (1929).
- (21) E. C. Evers and A. G. Knox, *J. Amer. Chem. Soc.*, **73**, 1739 (1951).
- (22) H. Harned and B. Owen, "Physical Chemistry of Electrolytic Solutions," 3rd ed, Reinhold, New York, N. Y., 1958.
- (23) P. G. Sears, G. R. Lester, and L. R. Dawson, *J. Phys. Chem.*, **60**, 1433 (1956).



$p^W\gamma^M(\text{IO}_3^-) = 3.9$ ,  $p^W\gamma^{\text{AN}}(\text{IO}_3^-) = 6.9$ ,  $p^W\gamma^{\text{DMSO}}(\text{IO}_3^-) = 8.3$ ; and from  $pK^{\text{sp}}(\text{KIO}_3)$ ,  $p^W\gamma^M(\text{IO}_3^-) = 3.9$  and  $p^W\gamma^{\text{DMSO}}(\text{IO}_3^-) = 8.2$ . The values of  $p^W\gamma^S(\text{IO}_3^-)$  from silver and potassium iodate are in good agreement. From a comparison of  $p^W\gamma^M(\text{IO}_3^-) = 3.9$  with  $p^W\gamma^M(\text{OAc}^-) = 2.8$ ,<sup>1</sup>  $p^W\gamma^M(\text{Cl}^-) = p^W\gamma^M(\text{NO}_3^-) = 2.2$ ,<sup>1</sup> and  $p^W\gamma^M(\text{ClO}_4^-) = 1.0$ <sup>1</sup> we conclude that with reference to M the solvation of iodate in water is unexpectedly large as compared to that of the other anions. The same is true with reference to AN and DMSO. This conclusion is substantiated by a comparison of ionic mobilities of iodate and other anions in W, M, AN, and DMSO (Table II). In water  $\lambda_0(\text{IO}_3^-) \sim \frac{1}{2}\lambda_0(\text{Br}^-)$ , while in M, DMF, and DMSO they are of the same order of magnitude. As a further indication of the hydration of iodate, the  $\bar{a}$  parameter in the partially extended Debye-Hückel activity coefficient relation is 4–4.5 Å for  $\text{IO}_3^-$  but only 3 Å for nitrate and the halides.<sup>2</sup> In comparison, a relatively large distance,  $a$ , from the center of the sodium ion to the electrostatic center of the dipole of the bromate ion, equal to 4.00 Å, was also derived from precise conductivity data of sodium bromate<sup>24</sup> by application of the Fuoss-Onsager conductance equation for associated electrolytes, in contrast to  $\bar{a} = 3.30$  Å calculated from the Bjerrum ion pair theory.<sup>24,25</sup> This led Fuoss to postulate that the bromate ion possesses a permanent  $\text{Br}^{2+}-\text{O}^-$  dipole. Slater<sup>26</sup> states that, since 26 electrons are involved in the halates, a pyramidal structure results with  $\text{X}^{2+}$  at an apex. Consequently, water molecules can coordinate to  $\text{X}^{2+}$  with their oxygens, while the oxygen end of the  $\text{X}^{2+}-\text{O}^-$  dipole can serve as a good hydrogen bond acceptor, which manifests itself in the ease of crystallization of  $\text{KH}(\text{IO}_3)_2$  from aqueous solution. Since sulfite and arsenite have similar pyramidal structures,<sup>26</sup> it is expected that they are considerably more hydrated than their planar  $\text{XO}_3$  counterparts, nitrate, carbonate, and borate, respectively.

An unsuccessful attempt has been made to arrive at a fair estimate of the degree of ionic association in the saturated aqueous solution of potassium iodate. From comparison of conductivity data in solutions 0.10–0.44 M (saturation) of potassium iodate with the conductivities calculated from the Falkenhagen equation<sup>27</sup> using  $\Lambda_0(\text{KIO}_3) = 114$  and  $\bar{a}$  of 4.5 and 3.0 Å for iodate and potassium ion, respectively, it appears that this salt is extensively dissociated in concentrated aqueous solution. In the saturated solution  $\alpha \sim 0.9_6$ , yielding  $K^d(\text{KIO}_3)$  of the order of 1. From conductivity data in dilute solutions ( $1.8 \times 10^{-4}$ – $3.91 \times 10^{-3}$  M) Monk<sup>28</sup> calculated  $K^d(\text{KIO}_3) = 1.7$ . We consider the fair agreement between the  $K^d(\text{KIO}_3)$  values fortuitous; the true value may be much smaller. Considering potassium iodate as 96% dissociated in its saturated solution, and taking  $K^{\text{sp}}(\text{KIO}_3) = 0.025$ , we find a mean ionic activity coefficient  $f^\pm(\text{KIO}_3) = 0.38$ , a value much lower than  $f^\pm(\text{KBrO}_3) = 0.75$ ,<sup>29</sup>  $f^\pm(\text{KClO}_3) = 0.59$ ,<sup>30</sup> and  $f^\pm(\text{KCl}) = 0.66$ <sup>10</sup> at the same concentration.

Because of the tight binding of water molecules by the iodate ion the microscopic dielectric constant in the vicinity of this ion may be lowered much more than by other anions. It is beyond the scope of this paper to provide a quantitative interpretation of the abnormally low  $f^\pm$  value of potassium iodate in its saturated solution in water.

*Acknowledgment.* We thank the National Science Foundation for a grant (No. GP-20605) in support of this work.

- (24) R. M. Fuoss and C. A. Kraus, *J. Amer. Chem. Soc.*, **79**, 3304 (1957).  
 (25) N. Bjerrum, *Kgl. Dan. Vidensk. Selsk.*, **1**, No. 9 (1926).  
 (26) J. C. Slater, *Phys. Rev.*, **38**, 325 (1936).  
 (27) G. Kortum, "Treatise on Electrochemistry," Elsevier, New York, N. Y., 1965, p 195.  
 (28) C. B. Monk, *J. Amer. Chem. Soc.*, **70**, 3281 (1948).  
 (29) J. H. Jones, *J. Amer. Chem. Soc.*, **69**, 2066 (1947).  
 (30) J. H. Jones and H. R. Froning, *J. Amer. Chem. Soc.*, **66**, 1672 (1944).

## Medium Activity Coefficients in Methanol and Some Aprotic Solvents of Substituted Benzoic Acids and Their Anions as Related to Their Hydrogen Bonding Properties

M. K. Chantooni, Jr., and I. M. Kolthoff\*

School of Chemistry, University of Minnesota, Minneapolis, Minnesota 55455 (Received October 5, 1972)

Hydrogen bond accepting capacities of solvents (S) relative to that of acetonitrile (AN), expressed as  $p^{AN}\gamma^S(H_a)$ , were obtained by assuming that  $p^{AN}\gamma^S(H_a) = p^{AN}\gamma^S(HA) - p^{AN}\gamma^S(MeA) = p^{AN}\gamma^S(HA) - p^{AN}\gamma^S(n)$ , HA denoting substituted benzoic acids, MeA, their methyl esters, and  $p^{AN}\gamma^S(n)$  the nonhydrogen bonded part of  $p^{AN}\gamma^S(HA)$ . The same value of  $p^{AN}\gamma^S(H_a)$  was found from  $\log {}^{AN}\Delta^S K^f(HA_2^-)$  or  ${}^{AN}\Delta^S K^f(HACl^-)$  using eq 7a. The following average values of  $p^{AN}\gamma^S(H_a)$  were obtained: -1.9, -1.5, -1.4, +0.1, +0.4, and +3.0 for S = dimethyl sulfoxide (DMSO), methanol (M), *N,N*-dimethylformamide (DMF), acetone (Ac), methyl isobutyl ketone (MIBK), and nitrobenzene (NB), respectively. The electrostatic part of  $p^{AN}\gamma^{DMF,DMSO}(A^-)$ ,  $p^{AN}\gamma^{DMF,DMSO}(A^-)_{el}$ , calculated from eq 3, has been found to be small and independent of the basic strength of  $A^-$ , being +0.8 and -0.3, respectively. On the other hand, both  $p^{M,AN,DMF,DMSO}(A^-)$  and  $p^{M,AN,DMF,DMSO}(A^-)_{el}$  are large and increase with increasing basic strength of  $A^-$ , the organic contribution to the former being small and of the order of  $-0.7 \pm 0.2$ . Acetic acid and its methyl ester are miscible in all proportions with the organic solvents used. Indirectly it was found that  $p^{AN}\gamma^{M,DMF,DMSO}(H_a)$  values of this acid are the same as of the substituted benzoic acids, but that  $p^{AN}\gamma^{M,DMF,DMSO}(n)$  are 0.5, 1.5, and 1.7 units more positive than those of the substituted benzoic acids.

### Introduction

In a previous study,<sup>1</sup> dissociation constants of substituted benzoic acids (HA) have been determined in the three polar aprotic solvents, acetonitrile (AN), *N,N*-dimethylformamide (DMF), and dimethyl sulfoxide (DMSO). It was found that  ${}^{DMF,DMSO}\Delta^{AN} pK^d(HA)$  is a constant, indicating no difference in resolution of acid strength between the three solvents, or expressed in terms of medium activity coefficients  $p^{AN}\gamma^{DMF,DMSO}(HA) - p^{AN}\gamma^{DMF,DMSO}(A^-) = \text{constant}$  in

$${}^S\Delta^{AN} pK^d(HA) = (pK^d(HA))_S - (pK^d(HA))_{AN} = p^{AN}\gamma^S(H^+) + p^{AN}\gamma^S(A^-) - p^{AN}\gamma^S(HA) \quad (1)$$

In order to gain some insight into the relative hydrogen bond accepting properties of the three aprotic solvents and methanol (M), expressed as  $p^{AN}\gamma^{DMF,DMSO,M}(H_a)$ , we have determined the solubility of various substituted benzoic acids and their methyl esters (MeA) in these solvents. Parker, *et al.*,<sup>2</sup> considered  $p\gamma(HA)$  to be the sum of a nonhydrogen bond accepting component, denoted by us as  $p\gamma(n)$ , and of  $p\gamma(H_a)$ . We assume that  $p\gamma(n) = p\gamma(MeA)$  and write

$$p^{AN}\gamma^S(HA) = p^{AN}\gamma^S(n) + p^{AN}\gamma^S(H_a) = p^{AN}\gamma^S(MeA) + p^{AN}\gamma^S(H_a) \quad (2)$$

the ester having similar size and structure as HA.

In order to arrive at an estimate of the relative hydrogen bond donating capacities of M and the aprotic solvents toward  $A^-$ , we assume

$$p^{AN}\gamma^S(A^-) = p^{AN}\gamma^S(A^-)_{el} + p^{AN}\gamma^S(A_n) \quad (3)$$

as was done by Alfenaar and de Ligny<sup>3,4</sup> for the solvent

pair water and methanol. In eq 3,  $p^{AN}\gamma^S(A^-)_{el}$  denotes the sum of the hydrogen bond donating effect of the solvent and ion-dipole and ion-quadrupole interactions. The Born effect is small, as M, AN, DMF, and DMSO are close to isodielectric. Also in eq 3  $p^{AN}\gamma^S(A_n)$  refers to the neutral component of the medium transfer coefficient of  $A^-$ . Introducing eq 2 and 3 into eq 1 and assuming that  ${}^{AN}\gamma^S(n) = {}^{AN}\gamma^S(A_n)$ , eq 4 results

$${}^S\Delta^{AN} pK^d(HA) = p^{AN}\gamma^S(H^+) + p^{AN}\gamma^S(A^-)_{el} - p^{AN}\gamma^S(H_a) \quad (4)$$

In an independent way,  $p^{AN}\gamma^{DMF,DMSO}(H_a)$  has been estimated from

$${}^{AN}\Delta^S \log K^f(HAA'^-) = p^{AN}\gamma^S(HAA'^-) - p^{AN}\gamma^S(A'^-) - p^{AN}\gamma^S(HA) \quad (5)$$

from values of  ${}^{AN}\Delta^S \log K^f(HA_2^-)$  and  ${}^{AN}\Delta^S \log K^f(HACl^-)$ , denoted by  ${}^{AN}\Delta^S \log K^f(HAA'^-)$ . We consider that  $p^{AN}\gamma^S(HAA'^-)$  consists of the neutral nonhydrogen bonded component of HA, the nonelectrostatic (neutral) part of  $A'^-$  plus the electrostatic part of the conjugate, *viz.*

$$p^{AN}\gamma^S(HAA'^-) = p^{AN}\gamma^S(A_n) + p^{AN}\gamma^S(A')_n + p^{AN}\gamma^S(HAA'^-)_{el} \quad (6)$$

(1) I. M. Kolthoff and M. K. Chantooni, Jr., *J. Amer. Chem. Soc.*, **93**, 3843 (1971).

(2) B. Clare, D. Cook, E. Ko, Y. Mac, and A. J. Parker, *J. Amer. Chem. Soc.*, **88**, 1911 (1966).

(3) M. Alfenaar and C. L. de Ligny, *Recl. Trav. Chim. Pays-Bas*, **86**, 929 (1967).

(4) D. Bax, C. de Ligny, and M. Alfenaar, *Recl. Trav. Chim. Pays-Bas*, **91**, 452 (1972).

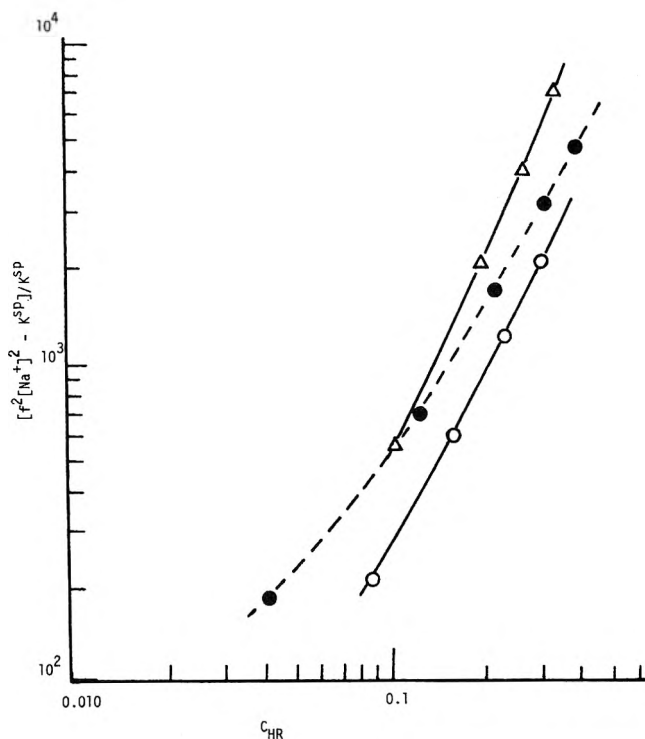


Figure 1. Plots of  $[f^2[\text{Na}^+]^2 - K^{\text{SP}}]/K^{\text{SP}}$  vs.  $C(\text{HR})$  on logarithmic scales for sodium salts in AN: ●, *p*-bromobenzoate; ○, 3,4-dichlorobenzoate; Δ, 3,4-dimethylbenzoate.

In eq 6 it is assumed that hydrogen bonding of  $\text{HAA}'^-$  to the solvent is negligible. Substituting eq 2, 3, and 6 into eq 5, the following results

$${}^{\text{AN}}\Delta^{\text{S}} \log K^{\text{f}}(\text{HAA}'^-) = -p^{\text{AN}}\gamma^{\text{S}}(\text{H}_a) + p^{\text{AN}}\gamma^{\text{S}}(\text{HAA}'^-)_{\text{el}} - p^{\text{AN}}\gamma^{\text{S}}(\text{A}'^-)_{\text{el}} \quad (7)$$

In deriving eq 7 it is not necessary to assume  ${}^{\text{AN}}\gamma^{\text{S}}(n) = {}^{\text{AN}}\gamma^{\text{S}}(\text{A}'^-)_n$ . When the values of the electrostatic medium transfer coefficients  $p^{\text{AN}}\gamma^{\text{S}}(\text{A}'^-)_{\text{el}}$  and  $p^{\text{AN}}\gamma^{\text{S}}(\text{HAA}'^-)_{\text{el}}$  are small, as is encountered between close to isodielectric aprotic solvents, they may be taken equal in eq 7. Hence

$${}^{\text{AN}}\Delta^{\text{S}} \log K^{\text{f}}(\text{HAA}'^-) = -p^{\text{AN}}\gamma^{\text{S}}(\text{H}_a) \quad (7a)$$

Equation 7a states that the difference in the logarithm of the formation constant of a 1:1 conjugate in a given pair of solvents is a measure of the relative hydrogen bond accepting properties of the solvents. A similar treatment for the 2:1 conjugate  $(\text{HA})_2\text{A}'^-$  yields

$${}^{\text{AN}}\Delta^{\text{S}} \log K^{\text{f}}((\text{HA})_2\text{A}'^-) = -2p^{\text{AN}}\gamma^{\text{S}}(\text{H}_a) + p^{\text{AN}}\gamma^{\text{S}}((\text{HA})_2\text{A}'^-)_{\text{el}} - p^{\text{AN}}\gamma^{\text{S}}(\text{A}'^-)_{\text{el}} \approx -2p^{\text{AN}}\gamma^{\text{S}}(\text{H}_a) \quad (8)$$

where  $K^{\text{f}}((\text{HA})_2\text{A}'^-)$  denotes the overall formation constant of  $(\text{HA})_2\text{A}'^-$ .

### Experimental Section

**Solvents, Acids, and Salts.** Acetonitrile,<sup>5</sup> *N,N*-dimethylformamide,<sup>5</sup> dimethyl sulfoxide,<sup>5</sup> methanol,<sup>5</sup> and acetone<sup>6</sup> were purified as described elsewhere, while methyl isobutyl ketone was a product purified in this laboratory.<sup>7</sup> Substituted benzoic acids<sup>8</sup> and acetic acid<sup>9</sup> were products used previously, while *p*-dimethylaminobenzoic

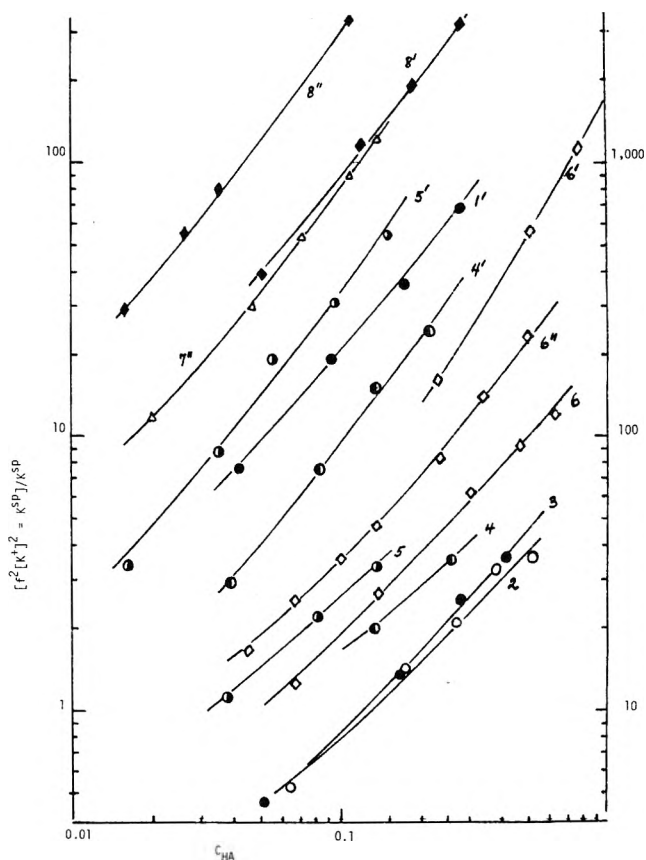


Figure 2. Plots of  $[f^2[\text{K}^+]^2 - K^{\text{SP}}]/K^{\text{SP}}$  vs.  $C(\text{HA})$  on logarithmic scales for potassium chloride with substituted benzoic acids, and acetic and dichloroacetic acids in AN, Ac, and DMF: 1, benzoic; 2, *p*-bromobenzoic; 3, 3,4-dichlorobenzoic; 4, *p*-nitrobenzoic; 5, 3,5-dinitrobenzoic; 6, acetic; 7, monochloroacetic; and 8, dichloroacetic acids: unprimed, in DMF; singly primed, in Ac, and doubly primed, in AN. Left-hand scale constructed for curves 2-6, 1', and 7''; right-hand scale for curves 4'-6', 8', 6'', and 8''.

and 4-chloro-3,5-dinitrobenzoic acids were Aldrich products recrystallized from ethanol-water mixtures. Mono- and dichloroacetic acids were Eastman Kodak White Label products distilled at 20 mm pressure. Sodium and potassium chlorides were Merck Reagent Grade, while the sodium salts of the substituted benzoic acids were prepared in the same way as the *p*-bromobenzoate.<sup>5</sup>

**Esters.** Methyl *p*-bromo-, *p*-iodo-, and *p*-nitrobenzoates were Eastman Kodak White Label products. All the other methyl esters except *p*-dimethylaminobenzoate were prepared by reaction of the acid with Eastman White Label phosphorus pentachloride followed by treatment with methanol.<sup>10</sup> The *p*-dimethylaminobenzoate ester was prepared by esterification of 1 *M* solution of the acid in boiling methanol in presence of 0.05 *M* sulfuric acid (in excess). Ethyl and isopropyl *p*-nitrobenzoates were prepared by reacting Aldrich *p*-nitrobenzoyl chloride with the appropriate alcohol at the boiling point.<sup>10</sup> All esters were recrystallized from ethanol-water mixtures and dried at 50°

- (5) I. M. Kolthoff and M. K. Chantooni, Jr., *J. Phys. Chem.*, **76**, 2024 (1972), and references therein.
- (6) T. Jasinski and Z. Pawlak, *Rocz. Chem.*, **41**, 1943 (1967).
- (7) J. Juillard and I. M. Kolthoff, *J. Phys. Chem.*, **75**, 2496 (1971).
- (8) M. K. Chantooni, Jr., and I. M. Kolthoff, *J. Amer. Chem. Soc.*, **92**, 7025 (1970).
- (9) I. M. Kolthoff, M. K. Chantooni, Jr., and S. Bhowmik, *J. Amer. Chem. Soc.*, **90**, 23 (1968).
- (10) R. L. Shriner and R. C. Fuson, "The Systematic Identification of Organic Compounds," Wiley, New York, N. Y., 1948, p 165.

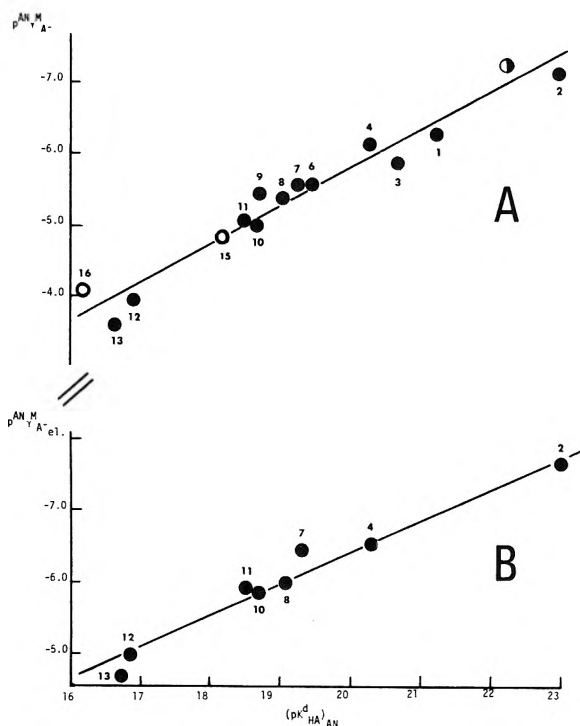


Figure 3. Plots of  $p^{AN} \gamma^M(A^-)$  and  $p^{AN} \gamma^M(A^-)_{el}$  vs.  $(pK^d(HA))_{AN}$  (A and B, respectively) for substituted benzoates and acetate: filled in circles, meta- and para-substituted benzoates; open circles, ortho-substituted benzoates; half-filled circles, acetate. Numbers are those in Table III. Least-squares slopes of A and B are  $-0.54$  and  $-0.43$ ; the intercepts are  $+4.9_5$  and  $+2.2_3$ , respectively.

at atmospheric pressure. Their melting points were 102, 80, 113, 78, 46.5, 95, 55.5, 110, 82, 110, and 105.5°, the esters listed in order of appearance in Table III. These melting points agree within 1–2° with the literature values.<sup>11</sup>

**Crystal Solvates of Salts and Acids.** Crystal solvates of sodium 3,4-dichloro-, 3,4-dimethyl-, *p*-dimethylamino-, *p*-bromo-, *p*-nitro- and 3-nitro-4-chlorobenzoates with DMF and DMSO (Table I, footnote *a*) were prepared by filtering a slurry of the salt in DMF or DMSO and washing with *n*-hexane or ethyl ether, as described previously.<sup>5</sup> Assay, by dissolving the salt in 0.3 ml dry acetic acid, adding 5 ml AN, and titrating the benzoate with standard 0.5 *M* perchloric acid in acetic acid using  $\alpha$ -naphtholbenzein as indicator<sup>12</sup> corresponds to NaA·0.2<sub>5</sub>DMF,DMSO for 3,4-dichloro- and *p*-bromobenzoate and to NaA·1.0<sub>0</sub> ± 0.0<sub>5</sub>DMF,DMSO for the other solvates. Blanks were run with the corresponding amounts of DMF and DMSO in AN.

Crystalline solvates of benzoic acids with DMF or DMSO were prepared in the same way as those of the salts. Their melting points were not sharp. Assay by alkalimetric titration in water-ethanol mixtures using phenolphthalein as indicator corresponded to monosolvate of mononitro-substituted and disolvate of dinitro-substituted benzoic acids. Crystalline solvates with DMF or DMSO were not formed with benzoic acids having other substituents. It was also found that all the solid benzoic acids and their sodium salts studied remained unsolvated in M and AN.

**Techniques.** The conductometric determination of ionic solubilities of sodium benzoates in the various solvents was the same as for sodium acetate,<sup>5</sup> while that of potas-

TABLE I: Specific Conductivity of Saturated Solutions,  $L_{sat.}$ , and  $pK^{SP}$  of Sodium Salts

Salt	AN $pK^{SP}$	DMF		DMSO	
		$L_{sat.}$ $\times 10^4$	$pK^{SP}$	$L_{sat.}$ $\times 10^4$	$pK^{SP}$
<i>p</i> -Dimethylamino- benzoate	10.0 <sup>b</sup>		6.5 <sup>a,b</sup>		4.7 <sup>b</sup> 5.3 <sup>a,b</sup>
3,4-Dimethylbenzoate	8.1 <sup>e</sup>	1.83 <sup>e</sup>	5.2 <sup>e</sup>	4.78 <sup>e</sup>	3.8 <sup>a,e</sup>
Benzoate	8.7 <sup>b</sup>	1.28 <sup>e</sup>	5.4 <sup>e</sup>		
<i>p</i> -Bromobenzoate	8.4 <sup>e</sup>	1.82 <sup>e</sup>	5.3 <sup>a,e</sup>	8.45 <sup>e</sup>	3.1 <sup>e</sup>
3,4-Dichlorobenzoate	8.1 <sup>e</sup>	3.15 <sup>e</sup>	4.8 <sup>a,e</sup>	9.35 <sup>a,e</sup>	3.2 <sup>a,e</sup> 9.3 <sup>e</sup>
<i>p</i> -Nitrobenzoate	8.2 <sup>d</sup>	3.88 <sup>e</sup>	4.6 <sup>a,e</sup> 4.1 <sup>c</sup>		
<i>m</i> -Nitrobenzoate	7.9 <sup>d</sup>	5.78 <sup>e</sup>	4.3 <sup>e</sup>		
3-Nitro-4-chlorobenzoate	7.4 <sup>d</sup>	10.6 <sup>e</sup>	3.7 <sup>a,e</sup>		
Acetate	9.1 <sup>b</sup>		6.7 <sup>b</sup>		4.8 <sup>b</sup>

<sup>a</sup> Salt solvated in solid phase. <sup>b</sup> Reference 5. <sup>c</sup>  $pK^{SP}$  of potassium salt; ref 19. <sup>d</sup> Reference 8. <sup>e</sup> This work.

sium chloride in presence of HA was described elsewhere.<sup>8</sup> Solubilities of benzoic acids in the various solvents were determined by titrating alkalimetrically in ethanol-water mixtures aliquots of the filtered saturated solutions, phenolphthalein serving as indicator.

Methods involving distribution of HA between S (AN, DMF, DMSO, etc.) and a hydrocarbon for the estimation of  $p^{AN} \gamma^S(HA)$  were found to be subject to complications due to complex formation between HA and DMSO or DMF in the hydrocarbon layer saturated with S. Such a solution became considerably undersaturated in the presence of HA and a long study<sup>13</sup> for each acid would be necessary to calculate the solubility of S in hexane containing a known concentration of HA.

Solubilities of esters in M and AN were found by taking the filtered saturated solutions to dryness under a heat lamp and weighing the residue to constant weight, taking care not to volatilize the esters. Solubilities of the esters in DMF, DMSO, and MIBK were found by introducing aliquots of the filtered saturated solutions into 10 volumes of water, in which the esters are sparingly soluble, removing the water together with DMF or DMSO by means of a filter stick, washing the ester with water, drying at 50°, and weighing. The MIBK was removed as an azeotrope with water by carefully heating after flooding the saturated MIBK solution with water.

## Results

**Ionic Mobilities.** In the calculation of  $K^{SP}(NaA)$  and  $K^t(HA Cl^-)/(K^t((HA)_2 Cl^-))$  from conductance data the following values of ionic mobilities at infinite dilution have been used previously: Na<sup>+</sup>, 70 in AN,<sup>14</sup> 30 in DMF,<sup>15</sup> 13.1 in DMSO;<sup>16</sup> K<sup>+</sup>, 85 in AN,<sup>17</sup> 80.6 in Ac;<sup>18</sup>

- (1) J. Pollock and R. Stevens, Ed., "Dictionary of Organic Compounds," Vol. 1–5, Oxford University Press, London, 1965.
- (2) I. M. Kolthoff, M. K. Chantooni, Jr., and S. Bhowmik, *Anal. Chem.*, **39**, 1627 (1967).
- (3) R. van Duyne, S. Taylor, S. Christian, and H. Afsprung, *J. Phys. Chem.*, **71**, 3427 (1967).
- (4) S. Minc and L. Werblan, *Rocz. Chem.*, **40**, 1537 (1966).
- (5) J. E. Prue and P. J. Sherrington, *Trans. Faraday Soc.*, **57**, 1795 (1961).
- (6) P. J. Sears, G. Lester, and L. Dawson, *J. Phys. Chem.*, **60**, 1433 (1956).

TABLE II: Homo- and Heteroconjugation Constants with Chloride of Substituted Benzoic, Acetic, and Chloroacetic Acids in Aprotic Solvents<sup>a</sup>

Acid	AN		DMF		DMSO	Ac		NM
	Log $K^f$ (HA <sub>2</sub> <sup>-</sup> ) <sup>b</sup>	Log $K^f$ (HACl <sup>-</sup> )	Log $K^f$ (HA <sub>2</sub> <sup>-</sup> ) <sup>b,f</sup>	Log $K^f$ (HACl <sup>-</sup> ) <sup>b,d</sup>	Log $K^f$ (HA <sub>2</sub> <sup>-</sup> ) <sup>b,g</sup>	Log $K^f$ (HA <sub>2</sub> <sup>-</sup> ) <sup>b,h</sup>	Log $K^f$ (HACl <sup>-</sup> )	Log $K^f$ (HA <sub>2</sub> <sup>-</sup> ) <sup>b,h</sup>
Benzoic	3.6 <sub>0</sub> <sup>c</sup>	2.2 <sup>c</sup> [-0.1] <sup>c</sup>	2.4		1.8		2.2 <sub>5</sub> <sup>d</sup> [0.0] <sup>d</sup>	
<i>p</i> -Bromobenzoic		2.3 <sup>e</sup>		0.9				
3,4-Dichlorobenzoic		2.5 <sup>e</sup>		1.0				
<i>p</i> -Nitrobenzoic	3.8 <sub>5</sub> <sup>c</sup>	2.5 <sup>c</sup> [0.3] <sup>c</sup>	2.6	1.2			2.8 <sub>5</sub> <sup>d</sup> [0.4] <sup>d</sup>	
3,5-Dinitrobenzoic <sup>j</sup>	4.0 <sup>c</sup>	2.9 <sup>c</sup> [0.6] <sub>5</sub> <sup>c</sup>		1.5		4.1	3.2 <sup>d</sup> [1.0] <sup>d</sup>	4.6
Acetic	3.6 <sup>g</sup>	2.5 <sub>5</sub> <sup>b,d</sup>	2.6	1.3	1.5		2.0 <sup>b,i</sup>	
Monochloroacetic		2.7 <sub>3</sub> <sup>d</sup> [0.7] <sup>d</sup>				3.2 <sub>5</sub>	2.6 <sup>d</sup> [0.5] <sup>d</sup>	3.7 <sub>5</sub>
Dichloroacetic <sup>k</sup>		3.4 <sup>d</sup> [0.4] <sup>d</sup>				3.5	2.8 <sup>b,i</sup>	
							3.7 <sup>b,i</sup>	
							3.8 <sub>3</sub> <sup>d</sup> [0.5] <sup>d</sup>	

<sup>a</sup> Ac = acetone, NM = nitromethane. <sup>b</sup> No data available of  $K^f$ ((HA)<sub>2</sub>A<sup>-</sup>) or  $K^f$ ((HA)<sub>2</sub>Cl<sup>-</sup>); values expected to be very small. <sup>c</sup> Reference 8. <sup>d</sup> This work. <sup>e</sup> From Hammett plot of log  $K^f$ (HACl<sup>-</sup>) vs.  $\sigma$ , ref 8. <sup>f</sup> I. M. Kolthoff, M. K. Chantooni, Jr., and H. Smagowski, *Anal. Chem.*, **42**, 1622 (1970). <sup>g</sup> Reference 9. <sup>h</sup> T. Jasinski and Z. Pawlak, *Rocz. Chem.*, **43**, 605 (1969), and references therein. <sup>i</sup> Reference 18. <sup>j</sup> Log  $K^f$ (HA<sub>2</sub><sup>-</sup>) = 4.3, ref 7. <sup>k</sup> Log  $K^f$ (HA<sub>2</sub><sup>-</sup>) = 6.3, log  $K^f$ (HACl<sup>-</sup>) = 6.7 in NB, ref 18.

Cl<sup>-</sup>, 105.2 in Ac;<sup>18</sup> A<sup>-</sup> (acetate or substituted benzoate) in AN assumed the same as 3,5-dinitrobenzoate, 100.<sup>5</sup> Values of  $\lambda_0$ (A<sup>-</sup>) in DMF and DMSO equal to 43 and 17.6, respectively, were calculated from that in AN from the Walden product. The Walden product for anions holds for our three aprotic protophobic solvents. Previously, the value of  $\lambda_0$ (HACl<sup>-</sup>) = 55 in AN<sup>8</sup> was used, while those in Ac and DMF equal to 63 and 24, respectively, were calculated from the Walden products.

**Solubilities of Sodium Salts.** Specific conductivities of saturated solutions and values of  $pK^{sp}$  of sodium salts of substituted benzoic acids in DMF and DMSO are listed in Table I. Since these salts are not sufficiently soluble in AN to allow the direct determination of ionic solubility from the conductivity of their saturated solutions, values of  $pK^{sp}$ (NaA) in Table I were found conductometrically from the ionic solubility in presence of *p*-bromophenol as described previously.<sup>8</sup> Plots of  $[f^2[Na^+]^2 - K^{sp}(NaA)]/K^{sp}(NaA)$  vs.  $C(HA)$  are presented in Figure 1.

**Conjugation of HA with Chloride.** The formation constants of HACl<sup>-</sup> and (HA)<sub>2</sub>Cl<sup>-</sup> in AN, DMF and Ac were estimated as previously in AN<sup>8</sup> conductometrically from the ionic solubility of potassium chloride in presence of substituted benzoic acids, acetic or dichloroacetic acid. Plots of  $[f^2[K^+]^2 - K^{sp}(KCl)]/K^{sp}(KCl)$  vs.  $C(HA)$  are presented in Figure 2. Values of  $pK^{sp}(KCl)$  were reported previously as 8.0,<sup>5</sup> 5.5,<sup>5</sup> and 9.2<sup>18</sup> in AN, DMF, and Ac, respectively. In the present investigation the specific conductivity of a saturated solution of potassium chloride in acetone was found to be  $2.3 \times 10^{-6}$  ohm<sup>-1</sup> cm<sup>-1</sup>, yielding  $pK^{sp}(KCl) = 9.8$ , this value being used in our calculations. Previously<sup>18</sup> Pawlak reported  $pK^{sp}(KCl) = 9.2$ . Because of the low solubility of this salt in acetone and the possible effect of small amounts of water, values of  $pK^{sp}(KCl)$  are approximate. Evidence of formation of (HA)<sub>2</sub>Cl<sup>-</sup> is found in the present study in acetone, as in AN,<sup>5</sup> but not in the stronger hydrogen bond acceptor DMF. Values of log  $K^f$ (HACl<sup>-</sup>) and log  $\beta$ (HACl<sup>-</sup>) (in brackets) are presented in Table II where  $\beta$ (HACl<sup>-</sup>) =  $[(HA)_2Cl^-]/[HA][HACl^-]$  ( $f((HA)_2Cl^-) = f(HACl^-)$ ). Since the effect of HA on the total solubility of potassium chloride in DMSO is very small,<sup>18</sup> considerable uncertainty is involved in the estimation of  $K^f$ (HACl<sup>-</sup>) in this sol-

vent; consequently these values have been omitted from Table II.

**Solubility of Benzoic Acids and Their Esters.** The molar solubilities of substituted benzoic acids in M, AN, DMF, and DMSO are listed in Table III, the ionic solubilities being negligible. Solubilities of the methyl esters of the substituted benzoic acids in the four solvents are also entered in Table III. Not included in Table III are the solubilities of 3,5-dinitrobenzoic acid and its methyl ester in methyl isobutyl ketone, 0.37<sup>7</sup> and 0.53 M, respectively. To account for the effect of the alcohol residue on the medium activity coefficient of the ester, solubilities of methyl-, ethyl-, and isopropyl-*p*-nitrobenzoates in M, AN, and DMSO were determined and the data reported in Table III. Hardly any effect of the alcohol residue containing three carbon atoms or less on  $p^{AN}\gamma^S$ (ester) is encountered among the aprotic solvents and M,  $p^{AN}\gamma^M$ (MeA),  $p^{AN}\gamma^M$ (EtA),  $p^{AN}\gamma^M$ (*i*-PrA) being 0.8<sub>4</sub>, 0.7<sub>7</sub>, and 0.6<sub>9</sub>, respectively. Between AN and DMSO the corresponding values are 0.0<sub>5</sub>, 0.0<sub>6</sub>, and 0.2<sub>4</sub>, respectively.

**Dissociation and Homoconjugation Constants of Acids.** Values of the dissociation constants of substituted benzoic acids and acetic acid in M,<sup>19</sup> AN,<sup>1</sup> DMF,<sup>1</sup> and DMSO<sup>1</sup> were used in the calculation of  $p^{AN}\gamma^S(HA)$  from eq 1 and

$${}^S\Delta^{AN} pK^{sp}(NaA) = p^{AN}\gamma^S(Na^+) + p^{AN}\gamma^S(A^-) \quad (9)$$

Since the values of  $pK^d(HA)$  of *p*-dimethylaminobenzoic acid in M, AN, DMF, and DMSO are not available in the literature, they were determined in the present study. In M the following *paH* values were found in mixtures of the acid and its potassium salt at constant ratio  $C_a(M)/C_s(M)$ :  $C_a = 1.86 \times 10^{-3}$ ,  $C_s = 2.50 \times 10^{-3}$ , 10.3<sub>2</sub>;  $4.4 \times 10^{-3}$ , 5.98  $\times 10^{-3}$ , 10.2<sub>5</sub>;  $8.25 \times 10^{-3}$ ,  $1.11 \times 10^{-2}$ , 10.2<sub>0</sub>; and  $1.09 \times 10^{-2}$ ,  $1.47 \times 10^{-2}$ , 10.1<sub>8</sub>. Extrapolation to zero concentration as recommended by Juillard<sup>19</sup> yields  $pK^d(HA) = 10.4_0$ . The *paH* of equimolar mixtures *p*-dimethylaminobenzoic acid and its tetrabutylammonium salt was 22.8<sub>9</sub> in AN when  $C = 3.64 \times 10^{-3}$  M, 14.4<sub>0</sub> in DMF when  $C = 2.80 \times 10^{-3}$  M, and 13.0<sub>2</sub> in DMSO when

- (17) J. Forcier and J. Olver, *Electrochim. Acta*, **7**, 257 (1962).  
 (18) Z. Pawlak, *Rocz. Chem.*, **46**, 249 (1972).  
 (19) J. Juillard, *J. Chim. Phys. Physicochim. Biol.*, **69**, (1970).

TABLE III: Solubilities of Substituted Benzoic Acids (HA) and Their Methyl Esters (MeA) in Various Solvents

Acid or ester	M		AN		DMF		DMSO	
	S(HA)	S(MeA)	S(HA)	S(MeA)	S(HA)	S(MeA)	S(HA)	S(MeA)
1. 3,4-Dimethyl-	0.59 <sub>5</sub> <sup>c</sup>		0.091		1.19		3.0 <sub>7</sub>	
2. <i>p</i> -Dimethylamino-	0.086 <sup>c</sup>	0.27 <sub>3</sub>	0.023	0.86	1.10	2.2 <sub>2</sub>	1.9 <sub>5</sub>	1.9 <sub>6</sub>
3. Unsubstituted	3.16 <sup>a</sup>		0.85		5.3 <sub>5</sub>			
4. <i>p</i> -Bromo-	0.12 <sup>c</sup>	0.31	0.018	0.80	0.93	1.69	2.4 <sub>5</sub>	0.93
5. <i>p</i> -Iodo-	0.06 <sub>8</sub> <sup>c</sup>	0.07 <sub>6</sub>	0.0098	0.15 <sub>6</sub>	0.72	0.60 <sub>5</sub>	2.1 <sub>4</sub>	0.41
6. <i>m</i> -Bromo-	1.51 <sup>c</sup>		0.16 <sub>7</sub>					
7. <i>m</i> -Nitro-	3.4 <sub>6</sub> <sup>a</sup>	0.26 <sub>5</sub>	0.78	2.02	1.90 <sup>b</sup>	2.2 <sub>9</sub>	2.5 <sub>1</sub> <sup>b</sup>	1.60
8. 3,4-Dichloro-	0.27 <sup>c</sup>	0.95	0.028	2.38	2.8 <sub>6</sub>	3.7 <sub>5</sub>	2.1 <sub>4</sub>	2.6 <sub>6</sub>
9. 3,5-Dichloro-	1.25 <sup>c</sup>		0.085					
10. <i>p</i> -Nitro-	0.20 <sup>a</sup>	0.18	0.041	1.26	0.29 <sup>b</sup>	1.7 <sub>3</sub>	0.80 <sup>b</sup>	1.1 <sub>1</sub>
		0.75 <sub>7</sub> <sup>d</sup>		4.4 <sub>1</sub> <sup>d</sup>				3.80 <sup>d</sup>
		0.11 <sup>e</sup>		0.55 <sup>e</sup>				0.31 <sub>2</sub> <sup>e</sup>
11. 3-Nitro-4-chloro-	0.70 <sub>5</sub> <sup>c</sup>	0.21	0.13 <sub>3</sub>	1.44	1.42 <sup>b</sup>	2.1 <sub>6</sub>	2.4 <sub>7</sub> <sup>b</sup>	1.1 <sub>5</sub>
12. 3,5-Dinitro-	1.23 <sup>c</sup>	0.10 <sub>7</sub>	0.23	1.15	1.30 <sup>b</sup>	1.8 <sub>6</sub>	1.5 <sub>7</sub> <sup>b</sup>	1.3 <sub>3</sub>
13. 4-Chloro- 3,5-dinitro-	1.55 <sup>c</sup>	0.12 <sub>7</sub>	1.22	1.70				
14. <i>o</i> -Chloro-	2.53 <sup>c</sup>		0.53		4.7 <sub>4</sub>			
15. <i>o</i> -Nitro-	2.99 <sup>a</sup>		0.98		2.5 <sub>8</sub> <sup>b</sup>			
16. 2,4-Dinitro-	3.2 <sub>3</sub> <sup>c</sup>		1.0 <sub>2</sub>					
17. 2,4-Dichloro-	1.34 <sup>c</sup>		0.16 <sub>8</sub>		2.9 <sub>3</sub>			

<sup>a</sup> I. M. Kolthoff, J. J. Lingane, and W. Larson, *J. Amer. Chem. Soc.*, **60**, 2512 (1938). <sup>b</sup> Acid solvated in solid phase. <sup>c</sup> This work; all esters this work. <sup>d</sup> Ethyl ester. <sup>e</sup> Isopropyl ester.

$C = 4.0 \times 10^{-3} M$ , yielding  $pK^d(HA) = 23.0, 14.5,$  and  $13.1$  in AN, DMF, and DMSO, respectively.

Previously reported values of homoconjugation constants of substituted benzoic and acetic acids in the various solvents are tabulated in Table II.

## Discussion

*Hydrogen Bond Accepting Properties of Solvents.* The agreement of  $p^{AN\gamma_{DMF,DMSO,MIBK}}(H_a)$  values found for benzoic acids from solubility data in Table III using eq 2 with those from  $K^f(HA_2^-)$  and  $K^f(HACl^-)$  (Table II, eq 7a) is gratifying, considering the different assumptions on which these equations are based.  $p^{AN\gamma_{DMF,DMSO,Ac,NM}}(H_a)$  values derived from  $K^f(HACl^-)$ ,  $K^f(HA_2^-)$  values in Table II for acetic and chloroacetic acids are the same as for the benzoic acids. It is of interest to note that  $p^{AN\gamma_{DMF,DMSO}}(H_a)$  equal to  $-1.2$  and  $-1.8$ , respectively, derived from  $K^f(HRA^-)$  values previously reported<sup>1</sup> using eq 7a ( $HR = p$ -bromophenol) agree well with those from carboxylic acids. Average values of  $p^{AN\gamma^S}(H_a)$  equal to  $-1.9, -1.5, -1.4, +0.1, +0.4,$  and  $+3.0$  were found, S being DMSO, M, DMF, Ac, MIBK, and NB, respectively, in order of decreasing hydrogen bond accepting capacity toward HA.

The values of the stepwise formation constants of  $(HA)_2Cl^-$  in Table II are approximately the same in AN and Ac and much smaller in DMF as predicted from eq 7a and 8 using the average values of  $p^{AN\gamma_{Ac,DMF}}(H_a)$ .

It is of interest to compare our data of  $p\gamma(H_a)$  with values of the enthalpy of formation  $\Delta H^f(H_a)$  of the hydrogen bond between phenol and various solvent bases by Arnett, *et al.*<sup>20</sup> They applied the pure base method, taking  $\Delta H^f(H_a) = \Delta H^f(\text{phenol}) - \Delta H^f(\text{anisole})$ , the latter accounting for the nonhydrogen bonded contribution. They found  $\Delta H^f(H_a)(DMF) - \Delta H^f(H_a)(2\text{-butanone}) = -1.67$

and  $\Delta H^f(H_a)(DMSO) - \Delta H^f(H_a)(2\text{-butanone}) = -1.9_8$  kcal/mol as compared to  $p^{MIBK\gamma_{DMF,DMSO}}(H_a)$  free energy values of  $-1.3$  and  $-2.0$  kcal/mol, respectively, found in this study. It may be concluded, therefore, that  $\Delta\Delta S^f(H_a)$  between DMF, DMSO, and MIBK is equal or close to zero, within experimental error, assuming that  $p^{MIBK-\gamma^2\text{-butanone}}(H_a) = 0$ .

From *ir* studies of  $\Delta\nu(OH)$  and  $K^f$  in carbon tetrachloride<sup>20</sup> and <sup>19</sup>F nmr studies of  $\Delta$  and  $K^f$  in cyclohexane<sup>21</sup> of the hydrogen bonded complex between *p*-fluorophenol and various bases, the same order of hydrogen bond accepting capacity DMSO > DMF > 2-butanone, benzonitrile was found, as given above. The latter two bases have comparable hydrogen bond accepting capacities as AN.

For acetic acid,  $p^{AN\gamma_{M,DMF,DMSO}}(n)$  has been evaluated in the present study, using eq 2, from known values of  $p^{AN\gamma_{M,DMF,DMSO}}(HAc)$  equal to  $-0.4, -0.2,$  and  $-1.2$  (Table IV) and the average values of  $p^{AN\gamma_{M,DMF,DMSO}}(H_a)$  given above. The value of  $p^{AN\gamma^M}(HOAc)$  has been calculated from eq 1 using previously reported values of  $p^{AN\gamma^M}(H^+) = -6.2,$ <sup>5</sup>  $p^{AN\gamma^M}(Ac^-) = -7.0,$ <sup>5</sup> and  $^{AN}\Delta^M pK^d(HAc) = 12.8$ . Resulting values of  $p^{AN\gamma_{M,DMF,DMSO}}(n)$  are 0.5, 1.5, and 1.7 unit, respectively, more positive for acetic acid than for the average of the benzoic acids.

*Medium Transfer Coefficient of A<sup>-</sup>.* Values of  $p^{AN\gamma^S}(A^-)$  and  $p^{AN\gamma^S}(A^-)_{e1}$  reported in this paper are based on the tetraphenylborate assumption. Among the aprotic solvents AN, DMF, and DMSO, values of  $p^{AN\gamma_{DMF,DMSO}}(A^-)_{e1}$  in Table IV are found essentially independent of the basic strength of the substituted benzo-

(20) E. M. Arnett, L. Joris, E. Mitchell, S. Murty, T. Gorrie, and P. v. R. Schleyer, *J. Amer. Chem. Soc.*, **92**, 2365 (1970).

(21) L. Joris, J. Mitsky, and R. W. Taft, *J. Amer. Chem. Soc.*, **94**, 3438 (1972).

TABLE IV: Medium Activity Coefficients of Substituted Benzoic Acids, Methyl Esters, and Benzoates between AN, DMF, and DMSO<sup>a</sup>

Benzoic acid	$^s\Delta^{AN}pK^d(HA)$	$^s\Delta^{AN}pK^{sp}(NaA)$		$p^{AN}\gamma^S(HA)$		$p^{AN}\gamma^S(MeA)$	$p^{AN}\gamma^S(A^-)$	$p^{AN}\gamma^S(A^-)_{el}$	$p^{AN}\gamma^S(H_a)$
		Obsd	Calcd	Obsd	Calcd				
S = DMF									
3,4-Dimethyl-	-8.2	-2.9		-1.1			1.1		
<i>p</i> -Dimethylamino-	-8.5	-3.5		-1.7		-0.4	0.5	0.9	-1.3
Unsubstituted	-8.4	-3.3		-1.3			0.7		
<i>p</i> -Bromo-	-8.2	-3.1 <sup>c</sup>	-3.3	-1.7		-0.3	0.7	1.0	-1.4
<i>p</i> -Iodo-	-8.2			-1.9		-0.6			-1.3
3,4-Dichloro-	-8.1	-3.3 <sup>c</sup>	-3.5	-2.0		-0.2	0.5	0.7	-1.8
<i>p</i> -Nitro-	-8.1	-3.6 <sup>c</sup>		-0.9 <sup>b</sup>		-0.14			
3-Nitro-4-chloro-	-8.5	-3.7 <sup>c</sup>		-1.0 <sup>b</sup>		-0.2			
<i>m</i> -Nitro-	-8.5	-3.6		-0.4 <sup>b</sup>	-1.7	-0.1	0.4	0.5	-1.6
3,5-Dinitro-	-8.0			-0.7 <sup>b</sup>		-0.2			
Acetic	-8.8	-2.4			-0.2		1.6		
						Av -0.3		Av +0.8 ±0.2	Av -1.5 ±0.2
S = DMSO									
3,4-Dimethyl-	-9.8	-4.3 <sup>c</sup>	-4.7	-1.5			+0.1		
<i>p</i> -Dimethylamino-	-9.9	-5.3		-1.9		-0.3	-0.5	-0.2	-1.6
<i>p</i> -Bromo-	-9.8	-5.3		-2.1		0.0	-0.5	-0.5	-2.1
<i>p</i> -Iodo-	-9.8			-2.3		-0.4			-1.9
3,4-Dichloro-	-9.8	-4.9		-1.9		0.0	-0.1	-0.1	-1.9
<i>p</i> -Nitro-	-9.7			-1.3 <sup>b</sup>		+0.1			
3-Nitro-4-chloro-	-10.0			-1.3 <sup>b</sup>		+0.1			
3,5-Dinitro-	-9.5			-0.8 <sup>b</sup>		-0.1			
<i>m</i> -Nitro-	-10.1			-0.5 <sup>b</sup>		+0.1			
Acetic	-9.7	-4.3			-1.2		+0.5		
						Av -0.1		Av -0.3 ±0.2	Av -1.9 ±0.2

<sup>a</sup>  $p^{AN}\gamma^{DMF}(H^+) = -10.6$ , <sup>5</sup>  $p^{AN}\gamma^{DMSO}(H^+) = -11.4$ , <sup>5</sup>  $p^{AN}\gamma^{DMF}(Na^+) = -4.0$ , <sup>5</sup>  $p^{AN}\gamma^{DMSO}(Na^+) = -4.8$ . <sup>b</sup> Acid solvated in solid phase;  $p\gamma(HA)$  calculated as described in Discussion. <sup>c</sup> Salt solvated in solid phase;  $^s\Delta^{AN}pK^{sp}(NaA)$  calculated as described in Discussion.

ate. Furthermore, they are numerically small as compared to those of the aprotic solvents and methanol. Average values of  $p^{AN}\gamma^{DMF,DMSO}(A^-)_{el}$  are found equal to  $+0.8 \pm 0.2$  and  $-0.3 \pm 0.2$ .

On the other hand, values of  $p^{AN}\gamma^M(A^-)$  as well as those of  $p^{AN}\gamma^M(A^-)_{el}$  are very negative (indicating strong solvation in M) and become increasingly so with increasing basic strength of the substituted benzoate ion, as illustrated by the plots of  $p^{AN}\gamma^M(A^-)$  and  $p^{AN}\gamma^M(A^-)_{el}$  vs.  $(pK^d(HA))_{AN}$  in Figure 3. The slopes of these plots are  $-0.54$  and  $-0.43$ , respectively, as compared to  $(\rho(M) - \rho(AN))/\rho(AN) = -0.44$  predicted from combining the Hammett  $\rho\sigma$  relation of  $pK^d(HA)$  with eq 1 or 4, respectively, and taking  $p\gamma(HA)$  or  $p\gamma(H_a)$ , respectively, as constant. Values of  $\rho(M) = -1.36$ <sup>19</sup> and  $\rho(AN) = -2.4$ <sup>1</sup> have been previously reported. It is therefore evident that the effect of substituent on  $^s\Delta^{AN}pK^d(HA)$  is accounted almost entirely for by changes in  $p^{AN}\gamma^M(A^-)_{el}$ . It follows from eq 4 that for two acids

$$\Delta^M \Delta^S pK^d(HA) = \Delta p^S \gamma^M(A^-)_{el} - \Delta p^S \gamma^M(H_a) \sim \Delta p^S \gamma^M(A^-)_{el}$$

In an excellent and thought provoking paper Parker, *et al.*,<sup>2</sup> attributed the large changes in  $\Delta pK^d(HA)$  with the basic strength of  $A^-$  going from M to DMF to changes in the hydrogen bond accepting property of  $A^-$  expressed by them as  $\gamma(A^-)H$ . In fact, from  $S_N2$  reaction rates Parker reported  $p^M\gamma^{DMF}(A^-)H$  equal to 6.2 and 5.5 for unsubsti-

tuted acetate and benzoate, respectively, as compared to  $p^M\gamma^{DMF}(A^-)_{el}$  values of 8.4 and 7.3 in the present paper. The difference of about 2 units in  $p^M\gamma^{DMF}(A^-)H$  and  $p^M\gamma^{DMF}(A^-)_{el}$  is probably due to nonhydrogen bonding ion-solvent interactions (ion-dipole, etc.), but may be accounted for in part or entirely by the validity of the  $\gamma(MeA) = \gamma(n)$  assumption, the tetraphenylborate assumption, and Parker's assumption that  $k^M/k^{DMF} = \gamma(A^-)H$ .

*Crystalline Solvates of HA and NaA.* In systems in which either the acid or its sodium salt forms solid solvates in DMF and DMSO either  $p^{AN}\gamma^{DMF,DMSO}(HA)$  or  $p^{AN}\gamma^{DMF,DMSO}(A^-)$  has been estimated from eq 2 using the data in Table IV. No crystalline solvates of HA or NaA are found in AN. From  $p\gamma(HA)$  (or  $p\gamma(A^-)$ ) thus found the solubility of HA (or  $K^{sp}(NaA)$ ) is calculated; hence  $p^{AN}\gamma^{DMF,DMSO}(HA)$  or  $p^{AN}\gamma^{DMF,DMSO}(A^-)$  of the unsolvated species become known. The free energy of solvation (in kcal/mol) is equal to  $1.36 (p^{AN}\gamma^{DMF,DMSO}(HA)_{unsolv} - p^{AN}\gamma^{DMF,DMSO}(HA)_{solv})$  for HA and  $1.36 (p^{AN}\gamma^{DMF,DMSO}(A^-)_{unsolv} - p^{AN}\gamma^{DMF,DMSO}(A^-)_{solv})$  for NaA. For the three sodium salts which form solvates calculated values of  $^s\Delta^{AN}pK^{sp}$  are presented in Table IV. Considering the uncertainties in values of  $p\gamma(HA)$  and  $p\gamma(A^-)$  of  $\pm 0.1$  to  $\pm 0.2$ , we may conclude that  $\Delta F_{solv}$  of these sodium salts in DMF and DMSO is equal to  $-0.3 \pm 0.2$  kcal/mol.

From the data in Table IV an average value of  $p^{AN}\gamma^{DMF}(HA)$  of the unsolvated acid, excluding 3,4-dimeth-



ylbenzoic acid is  $-1.7$ . Assuming this value for  $p^{AN\gamma DMF}$  ( $HA$ ) of unsolvated *m*-nitrobenzoic acid,  $\Delta F_{solv} = -1.6$  kcal/mol for this acid in DMF.

From the observation that a considerable quantity of heat is evolved accompanying solvate formation of  $HA$  and  $NaA$  and that values of  $\Delta F_{solv}$  are small, it appears that large negative entropy changes are involved. On the other hand, dissolution of the esters in all solvents studied

(saturated solutions) is considerably less exothermic than the corresponding acids which indicates that the former do not form crystalline solvates.

*Acknowledgment.* We thank the National Science Foundation for a grant (No. GP-20605) in support of this work.

## Solubilities of Alkali Metal Chlorides in Some Amine and Ether Solvents

J. Strong and T. R. Tuttle, Jr.\*

Department of Chemistry, Brandeis University, Waltham, Massachusetts 02154 (Received June 16, 1972)

Solubilities of alkali metal chlorides except lithium were determined in ammonia, EDA, methyl- and ethylamines, DME, and THF at three different temperatures. From these data, standard thermodynamic functions of solution and solvation with respect to ion formation were calculated. The standard free energies of solvation increased linearly as a function of  $D^{-1}$ . However, the requirements of the Born equation were not satisfied because the slopes and intercepts of these plots were not equal. Values of the entropies of solvation are roughly accounted for on the basis of the freezing out of a fixed number of solvent molecules. The superiority of ammonia as an agent for solvating ions is attributed to its relatively low molecular entropy compared to other solvents. A criterion for salt-like behavior is introduced and used to suggest that saturated alkali metal solutions are salt like and are probably dominated by the  $M^+ \cdot M^-$  ion pairs. On this basis solubilities of metals in ammonia are too large to be accounted for without introducing additional species.

### Introduction

Solubilities of alkali metal halides have been measured in liquid ammonia,<sup>1</sup> but not in alkylated amines, although these solvents exhibit somewhat similar properties. In order to compare the behavior of ionic solutes in these solvent systems solubility measurements of slightly soluble alkali chlorides, with the exception of  $LiCl$ , have been made. From this information standard free energies of solution and solvation are calculated, and comparisons made of trends with respect to changes in solvent dielectric constant and trends with respect to cation size in a given solvent system.

The measurements were carried out in ammonia, methylamine, ethylamine, and ethylenediamine (EDA), as well as in two ethers, tetrahydrofuran (THF) and 1,2-dimethoxyethane (DME). The ethers were included due to their similarity to amines with respect to formation of alkali metal solutions and were also of interest with respect to specific solvent effects as they have dielectric constants which are very close to that of ethylamine.

A major stimulus for these solubility measurements was our interest in metal solutions in these polar solvents. The question of whether the metal solutions behave like solutions of salts is of considerable importance and interest in assessing the nature of the metal solutions.

### Experimental Section

*Materials.* Solutes were of the highest purity commercially available.  $NaCl$  and  $KCl$  were Fisher Reagent Grade,  $CsCl$  was 99.97% from K & K Laboratories, and  $RbCl$  was Mann analyzed, optical grade from Mann Research Laboratories. All salts were dried over  $P_2O_5$  *in vacuo* at  $100^\circ$  for 24 hr and stored over drierite.

Ammonia from Matheson was dried *in vacuo* over Na-K alloy and used without further purification. Ethylamine and methylamine from Matheson were treated to remove ammonia impurities.<sup>2</sup> Gas chromatographic analysis<sup>3</sup> showed the final ammonia content of each to be less than 0.01 mol %. These solvents were dried *in vacuo* over Na-K alloy prior to use. EDA from Eastman Organic Chemicals was predried over  $CaH_2$  for several months and fractionally distilled from  $CaH_2$  onto sodium pieces in a dry nitrogen atmosphere. The fraction boiling at  $115.9$ – $116.0^\circ$  was collected and vacuum distilled onto Na-K alloy for final drying. The characteristic deep blue color of alkali metal solution in EDA was taken as an indication of dryness.

(1) G. Heymer and A. Schneider, *Z. Anorg. Allg. Chem.*, **302**, 306 (1959). See also ref 11.

(2) Ian Hurley, Thesis, Brandeis University, Waltham, Mass., 1970.

(3) I. Hurley, T. R. Tuttle, Jr., and S. Golden, *J. Chem. Phys.*, **48**, 2818 (1968).

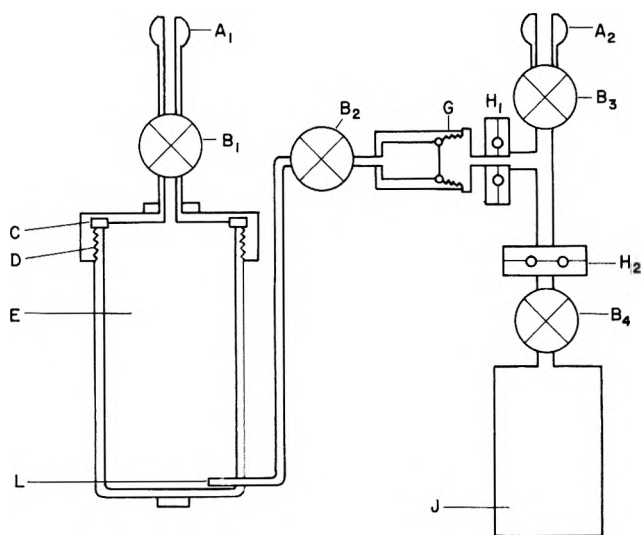


Figure 1. Stainless steel solubility apparatus: (A) 18/19 ball joints, (B) needle valves, (C) O-ring seal, (D) cap threads, (E) main cylinder, (G) filter assembly, (H) flange connectors with O-ring seals, (J) sample collection cylinder, (L) transfer tube.

THF, Baker analyzed reagent, was predried over  $\text{CaH}_2$  and fractionally distilled in a nitrogen atmosphere. The fraction boiling at  $65.8^\circ$  was collected and allowed to react with potassium metal and anthracene until a deep blue color characteristic of the anthracene negative ion had formed. Finally the THF was vacuum distilled into a storage bulb containing Na-K alloy. The resulting light blue color characteristic of the alkali metal solution indicated dryness. DME, from Eastman Organic Chemicals, was treated as described for THF. The fraction boiling at  $82.2\text{--}83.0^\circ$  was collected. Dryness was indicated by the unstable deep blue color which was generated by shaking the solvent with Na-K alloy.

**Apparatus and Procedure.** In order to avoid alkali metal contamination which was observed with Pyrex systems<sup>2-4</sup> and to facilitate operation at higher total pressures, the salt solutions were formed and manipulated in the stainless steel apparatus diagrammed in Figure 1. Measurements were made in the following manner. Solute was introduced into the equilibration vessel, E, and then the cap was replaced to form a vacuum tight seal *via* the flat Teflon O-ring, C. The system was evacuated and dry solvent distilled in through valve B-1. The resulting solution was frozen and a known quantity of argon gas added. Valve B-1 was closed and the vessel placed on a platform shaker at room temperature for about 24 hr to facilitate equilibration. The vessel was placed in a constant temperature bath maintained within  $0.04^\circ$  or less. The apparatus was assembled as shown in Figure 1 for sampling. The sampling vessel, J, was evacuated and a known pressure of argon, ranging from 100 to 500 Torr, was added to inhibit distillation of solvent during the sampling operation. A sample of the solution in vessel E was taken by opening valve B-2. The excess pressure above the solution forced the solution up tube L and through the filter assembly G, which contained a Teflon millipore filter, and into vessel J. Sample size was regulated by the quantities of argon added and that period of time B-2 remained open and varied between 10 and 150 g of solution. After the sample was taken valve B-4 was closed and the apparatus disassembled. The quantity of solvent present in cylinder J was determined by quantitative transfer by vacuum distilla-

tion into a glass bulb which was then weighed. The amount of solute was determined by flame photometry,<sup>2</sup> or by a modification of the Volhard method.<sup>5</sup> In most cases where both methods were used, the analyses agreed to within 5% or less.

Attainment of equilibrium was tested from under saturation by agreement between data obtained for successive samples of a solution taken at intervals of 24 hr or more. In some cases equilibrium was approached from supersaturation by removal of a known quantity of solvent from the solution in vessel E soon after a sample had been taken. After 24 hr another sample was taken for analysis. The procedure was then repeated several times. Equilibration of some solutions, notably CsCl and RbCl in ethylamine, was relatively slow (*ca.* 3-5 days) and supersaturated solutions were readily obtained which required 24 hr or more to reach saturation. Further details on apparatus and procedures are given elsewhere.<sup>6</sup>

## Results

The solubility results at the temperatures investigated are given in Table I. Values reported are the mean of all determinations at a given temperature. The average deviation from the mean is also given.

The systems investigated were checked for solvate formation by comparison of X-ray powder patterns of the dry salt with those of the salt in contact with the appropriate solvent for several months or more. No indications of solvate formation were observed. It is of note that in all instances where a nonzero temperature coefficient of solubility is observed within experimental error, namely, RbCl and CsCl in ammonia, and NaCl in EDA and methylamine, it is negative. This is in accord with the observations of Heymer and Schneider<sup>1</sup> who found negative temperature coefficients of solubility of the alkali halides in liquid ammonia when the solid phase was solvent free, and positive temperature coefficients when solvates were present.

Standard free energies of solution were obtained from the relationship

$$\Delta G^\circ(\text{soln}) = -RT \ln \gamma_{\pm}^2 m_{\pm}^2 = -RT \ln K_s \quad (1)$$

where  $\gamma_{\pm}$  is the mean molal ionic activity coefficient,  $m_{\pm}$  the concentration of each ion in the saturated solution, and  $K_s$  the solubility product. If the concentration of salt is sufficiently low, activity coefficients may be calculated from the Debye-Hückel theory. However, in solvents of low dielectric constant the concentration of free ions may differ appreciably from  $m$ , the molality of salt in the saturated solution, due to ion association. Thus it is necessary to include  $\alpha$ , the degree of dissociation of the ion pair, in eq 1 to obtain

$$\Delta G^\circ(\text{soln}) = -RT \ln \alpha^2 \gamma_{\pm}^2 m^2 \quad (2)$$

Due to lack of experimentally determined ion association constants for the present systems, Bjerrum theory<sup>7</sup> was used to calculate these quantities. The values of the

- (4) I. Hurley, T. R. Tuttle, Jr., and S. Golden, "Metal-Ammonia Solutions. Pure and Applied Chemistry," Butterworths, London, 1970, p 449.
- (5) G. H. Ayres "Quantitative Analysis," Harper and Row, New York, N. Y., 1958.
- (6) J. Strong, Thesis, Brandeis University, Waltham, Mass., 1970.
- (7) N. Bjerrum, *K. Dan. Vidensk. Selsk.* 7, No. 9, 108 (1926).

TABLE I: Solubilities<sup>a</sup> of Alkali Chlorides in Some Amine and Ether Solvents

Solvent	Solute	5.0°	25.0°	50.0°
NH <sub>3</sub>	RbCl	1.86 ± 0.10 × 10 <sup>-2</sup>	1.69 ± 0.09 × 10 <sup>-2</sup>	
	CsCl	1.66 ± 0.09 × 10 <sup>-2</sup>	1.47 ± 0.12 × 10 <sup>-2</sup>	
EDA	NaCl	6.63 <sup>b</sup> ± 0.15 × 10 <sup>-2</sup>	5.04 ± 0.12 × 10 <sup>-2</sup>	3.56 ± 0.09 × 10 <sup>-2</sup>
	KCl	1.10 <sup>b</sup> ± 0.05 × 10 <sup>-3</sup>	1.12 ± 0.05 × 10 <sup>-3</sup>	1.13 ± 0.05 × 10 <sup>-3</sup>
	RbCl	1.59 <sup>b</sup> ± 0.04 × 10 <sup>-3</sup>	1.67 ± 0.10 × 10 <sup>-3</sup>	1.51 ± 0.04 × 10 <sup>-3</sup>
	CsCl	1.86 <sup>b</sup> ± 0.05 × 10 <sup>-3</sup>	1.95 ± 0.05 × 10 <sup>-3</sup>	2.02 ± 0.05 × 10 <sup>-3</sup>
CH <sub>3</sub> NH <sub>2</sub>	NaCl	2.24 ± 0.06 × 10 <sup>-3</sup>	1.93 ± 0.05 × 10 <sup>-3</sup>	1.16 ± 0.03 × 10 <sup>-3</sup>
	KCl	5.05 ± 0.22 × 10 <sup>-5</sup>	5.14 ± 0.25 × 10 <sup>-5</sup>	4.56 ± 0.05 × 10 <sup>-5</sup>
	RbCl	8.90 ± 0.19 × 10 <sup>-5</sup>	8.90 ± 0.30 × 10 <sup>-5</sup>	8.33 ± 0.22 × 10 <sup>-5</sup>
	CsCl	1.15 ± 0.05 × 10 <sup>-5</sup>	0.94 ± 0.15 × 10 <sup>-5</sup>	1.03 ± 0.06 × 10 <sup>-5</sup>
C <sub>2</sub> H <sub>5</sub> NH <sub>2</sub>	NaCl	1.43 ± 0.12 × 10 <sup>-4</sup>	1.25 ± 0.15 × 10 <sup>-4</sup>	1.30 ± 0.24 × 10 <sup>-4</sup>
	KCl	4.21 ± 0.32 × 10 <sup>-6</sup>	4.48 ± 0.10 × 10 <sup>-6</sup>	4.36 ± 0.10 × 10 <sup>-6</sup>
	RbCl	9.10 ± 1.00 × 10 <sup>-6</sup>	7.52 ± 0.88 × 10 <sup>-6</sup>	7.44 ± 0.40 × 10 <sup>-6</sup>
	CsCl	6.50 ± 0.50 × 10 <sup>-6</sup>	7.00 ± 0.50 × 10 <sup>-6</sup>	6.50 ± 0.50 × 10 <sup>-6</sup>
DME	NaCl	5.46 ± 2.00 × 10 <sup>-7</sup>	6.34 ± 2.00 × 10 <sup>-7</sup>	6.05 ± 2.00 × 10 <sup>-7</sup>
	KCl	1.34 ± 0.53 × 10 <sup>-6</sup>	0.90 ± 0.09 × 10 <sup>-6</sup>	1.71 ± 0.17 × 10 <sup>-6</sup>
	RbCl		7.95 ± 0.32 × 10 <sup>-7</sup>	6.97 ± 0.78 × 10 <sup>-7</sup>
	CsCl	1.30 ± 0.10 × 10 <sup>-6</sup>		1.33 ± 0.10 × 10 <sup>-6</sup>
THF	NaCl		2.66 ± 0.27 × 10 <sup>-6</sup>	1.38 ± 0.14 × 10 <sup>-6</sup>
	KCl		2.48 ± 0.50 × 10 <sup>-7</sup>	3.72 ± 0.90 × 10 <sup>-7</sup>
	RbCl	3.5 ± 1.5 × 10 <sup>-8</sup>	6.1 ± 3.5 × 10 <sup>-8</sup>	
	CsCl	4.50 ± 0.50 × 10 <sup>-7</sup>	3.51 ± 0.74 × 10 <sup>-7</sup>	5.54 ± 0.75 × 10 <sup>-7</sup>

<sup>a</sup> Given in molality of salt. <sup>b</sup> At 10.0°.

ion size parameters were determined by the requirement that Bjerrum theory fit experimentally determined ion pairing constants in liquid ammonia.<sup>8,9</sup> Since no experimental value of the ion association constant for NaCl in liquid ammonia was available the size parameter was determined by requiring that the difference in size parameters between KCl and NaCl be equal to that between KBr and NaBr.<sup>8</sup> A similar method was used for RbCl and CsCl.<sup>9</sup> The size parameters so obtained were 4.11 Å for NaCl, 3.03 Å for KCl, 2.77 Å for RbCl, and 2.60 Å for CsCl.

The same size parameters were used for all the solvents. Comparison of measured ion pair dissociation constants in solvents of nearly the same dielectric constants<sup>10</sup> suggests that this procedure can lead to an error of an order of magnitude in the dissociation constant. However, where solvents of similar structural characteristics are concerned, such as the amines in this work, the error introduced will probably be less.

Computations were carried out on an IBM 1130 computer to facilitate iteration between values of the ionic activity coefficient and degree of dissociation of ion pairs. Literature results for solubilities of KCl and NaCl in liquid ammonia<sup>11</sup> were used in addition to the present results. Values of solvent density and dielectric constant used in the computations are collected in Table II.<sup>11-18</sup>

As the solubility data were obtained over a range of temperature, the standard enthalpy of solution was obtained from

$$\Delta H^\circ(\text{soln}) = -2R[\Delta \ln \alpha\gamma_{\pm}m/\Delta(1/T)]_p \quad (3)$$

and the entropy of solution from the enthalpy and the free energy in the usual manner. Because the values of the enthalpy obtained in this way depend heavily on the temperature dependence of  $\alpha\gamma_{\pm}$  they cannot be considered to be very reliable. The error involved is difficult to estimate, but may easily amount to several kilocalories/mole.

TABLE II: Physical Constant of the Solvents at 298°K

Solvent	$\rho$ , g/cm <sup>3</sup>	Ref	$D$	Ref
NH <sub>3</sub>	0.6105	16	16.9	12
EDA	0.8906	17	13.7	13
MA	0.6562	18	9.4	14
EA	0.6793	11	6.26	14
DME	0.859	15	7.20	15
THF	0.883	15	7.39	15

Nevertheless, the sign of  $\Delta H^\circ(\text{soln})$  is probably correct in most cases since ion pairing, which is the controlling factor in determining the temperature dependence of  $\alpha\gamma_{\pm}m$ , almost invariably increases with increasing temperature. The standard enthalpies reported in Table III are averages over the temperature range studied. Standard free energies and entropies at 25° are also given in Table III. The degree of dissociation of dissolved salt into ions is included to show the extent of ion pairing for the saturated solutions.

- (8) V. F. Hnizda and C. A. Kraus, *J. Amer. Chem. Soc.*, **71**, 1565 (1949); R. L. Kay, *ibid.*, **82**, 2099 (1960).  
 (9) A. M. Monsoszon and V. A. Pleskov, *Z. Phys. Chem.*, **A156**, 176 (1931).  
 (10) C. A. Kraus, *J. Phys. Chem.*, **58**, 673 (1954).  
 (11) H. M. Elsey, *J. Amer. Chem. Soc.*, **42**, 2454 (1920); "The Handbook of Chemistry and Physics," 41st ed, Chemical Rubber Publishing Co., Cleveland, Ohio, 1959; L. Lange "Handbook of Chemistry," 5th ed, Handbook Publishers, Sandusky, Ohio, 1944.  
 (12) H. M. Grubb, J. F. Chittum, and H. Hunt, *J. Amer. Chem. Soc.*, **58**, 776 (1936).  
 (13) A. H. White and S. O. Morgan, *J. Chem. Phys.*, **5**, 655 (1937).  
 (14) H. Ulrich and W. Nespital, *Z. Phys. Chem.* **B16**, 221 (1932); Schlundt, *J. Phys. Chem.*, **5**, 157, 503 (1901); R. J. W. LeFevre and P. Russell, *Trans. Faraday Soc.*, **43**, 374 (1947).  
 (15) C. Carvajal, K. J. Tolle, J. Smid, and M. Szwarc, *J. Amer. Chem. Soc.*, **87**, 5548 (1965); D. J. Metz and A. Glines, *J. Phys. Chem.*, **71**, 1158 (1967).  
 (16) C. S. Cragoe and D. R. Harper, *Bull. Std. Sci. Papers Nr.*, **420**, 313 (1921).  
 (17) M. J. Timmermann and Hennant-Roland, *J. Chim. Phys.*, **56**, 984 (1959).  
 (18) W. A. Felsing and A. F. Thomas, *Ind. Engl. Chem.*, **21**, 1269 (1969).

TABLE III: Thermodynamic Functions of Solution at 298°K

Solvent	Solute	$\Delta G^\circ$ <sup>a</sup>	$-\Delta H^\circ$ <sup>a</sup>	$\Delta S^\circ$ <sup>a</sup>	$\alpha$ <sup>b</sup>	$K_A$ <sup>c</sup>
NH <sub>3</sub>	NaCl	3.7	7.8	39	0.12	$5.67 \times 10^2$
	KCl	7.0	2.8	33	0.41	$1.73 \times 10^3$
	RbCl	7.1	3.6	35	0.21	$3.68 \times 10^3$
	CsCl	7.5	4.9	42	0.16	$6.66 \times 10^3$
EDA	NaCl	6.4	4.9	38	0.17	$2.31 \times 10^3$
	KCl	9.8	2.9	43	0.26	$1.62 \times 10^4$
	RbCl	10.1	4.1	48	0.15	$3.94 \times 10^4$
	CsCl	10.3	4.4	49	0.10	$7.82 \times 10^4$
MA	NaCl	10.3	5.2	52	0.10	$1.04 \times 10^5$
	KCl	14.5	4.3	63	0.094	$3.36 \times 10^6$
	RbCl	15.3	5.4	70	0.028	$2.12 \times 10^7$
	CsCl	17.3	7.3	83	0.050	$6.23 \times 10^7$
EA	NaCl	15.9	7.6	79	0.011	$8.57 \times 10^7$
	KCl	21.4	9.7	104	0.0032	$3.27 \times 10^{10}$
	RbCl	22.9	12.0	117	0.00054	$6.68 \times 10^{11}$
	CsCl	24.0	11.3	119	0.00023	$4.12 \times 10^{12}$
DME	NaCl	17.9	2.1	67	0.42	$6.07 \times 10^6$
	KCl	20.4	4.4	83	0.038	$8.40 \times 10^8$
	RbCl	22.0	12.1	114	0.011	$1.13 \times 10^{10}$
	CsCl	23.0	6.4	99	0.003	$5.29 \times 10^{10}$
THF	NaCl	16.7	7.3	81	0.28	$3.80 \times 10^6$
	KCl	20.8	-1.2	66	0.095	$4.66 \times 10^8$
	RbCl	23.1	-1.3	73	0.056	$5.62 \times 10^9$
	CsCl	23.0	3.3	88	0.011	$2.63 \times 10^{10}$

<sup>a</sup> Errors are discussed in the text. The uncertainty in  $\Delta G^\circ$  is 2 kcal/mol for NH<sub>3</sub>, EDA, and MA, 5 kcal/mol for EA and higher for the ethers. The uncertainty in  $\Delta H^\circ$  amounts to several kcal/mol. <sup>b</sup> Degree of dissociation. <sup>c</sup> Ion pairing association constant in liters/mole.

Uncertainties in the standard free energies arise primarily from use of theory to account for ion association effects. A factor of 10 change in ion association constant yields a change of about 1.4 kcal/mol at 298°K in the free energy. Our estimated errors from this source are about 2 kcal/mol for ammonia, EDA, and methylamine, about 5 kcal/mol for ethylamine and higher for the ethers.

Comparison of the above results with literature values is possible for liquid ammonia solutions. The standard functions of solution are readily converted to standard free energies and enthalpies of formation and standard entropies using the tabulations of Latimer<sup>19</sup> of free energies and enthalpies of formation and entropies of the crystalline chlorides. Table IV gives the functions of formation in liquid ammonia from the present results and those obtained by Jolly.<sup>20</sup> The functions listed for NaCl and KCl were obtained using the results of previous solubility studies.<sup>21</sup> For the standard free energies of formation,  $\Delta G_f^\circ$ , the present results and those of Jolly agree well within the bounds of experimental error. Even for RbCl and CsCl the differences are not large. These differences may be accounted for in part by slightly different values of the free energies of formation of the crystalline chlorides  $\Delta G_f^\circ(\text{MCl})$  being used in the two computations. The values of  $\Delta G_f^\circ(\text{MCl})$  used here in conjunction with Jolly's values<sup>20</sup> for  $\Delta G^\circ(\text{soln})$  yield -91.0 and -90.8 kcal/mol respectively for RbCl and CsCl. In addition, the estimates of Jolly involved an extrapolation from solubility data at 0°. This extrapolation may also account for part of the differences. In any event, the differences between Jolly's adjusted estimates and ours are again well within the uncertainties incurred in estimating ion pairing for RbCl and CsCl.

Comparison of the values of  $\Delta H_f^\circ$  given in Table IV shows that the estimates from this work are consistently

TABLE IV: Thermodynamic Functions of Formation in Liquid Ammonia at 298° K

Solute	NaCl	KCl	RbCl	CsCl
	$\Delta H_f^\circ$ , kcal/mol			
This work	-106.0	-107.0	-106.5	-108.4
Reference 20	-103.8	-106.2	-105.0	-106.2
	$\Delta G_f^\circ$ , kcal/mol			
This work	-88.1	-90.6	-89.7	-89.1
Reference 20	-87.7	-91.1	-91.6	-92.0
	$S^\circ$ , cal/deg mol			
This work	-22	-13	-12	-19
Reference 20	-15	-9	-1	-1

1-2 kcal/mol lower than those of Jolly. Considering the uncertainties involved in obtaining each of the two sets of estimates these differences cannot be considered to be significant. The differences in the absolute entropies given in Table IV reflect an accumulation of the differences in the enthalpies and free energies. Consequently, the fact that the average difference between corresponding members of the two sets of entropies is about 10 eu simply reflects the uncertainty in our knowledge of the true values of these quantities.

The enthalpies and free energies of solvation of the alkali metal chlorides with respect to ion formation were

- (19) W. M. Latimer, "The Oxidation States of the Elements and Their Potentials in Aqueous Solutions," 2nd ed, Prentice-Hall, Englewood Cliffs, N. J., 1952.
- (20) W. M. Latimer and W. L. Jolly, *J. Amer. Chem. Soc.*, **75**, 4147 (1953).
- (21) M. Linhard and M. Stephan, *Z. Phys. Chem.*, **A167**, 87 (1933); P. R. Marshall and H. Hunt, *J. Chem. Eng. Data*, **4**, 217 (1959); P. W. Schenk and H. Tuihoff, *Chem. Ber.*, **71**, 206 (1967); G. Patscheke and C. Tanne, *Z. Phys. Chem.*, **A174**, 135 (1935); G. Patscheke, *ibid.*, **A163**, 340 (1933); S. Abe and R. Hara, *J. Soc. Chem. Ind. Jap.*, **36**, supplemental binding 557 (1933); G. W. Watt, W. A. Jenkins, and C. V. Robertson, *Anal. Chem.*, **22**, 330 (1959).

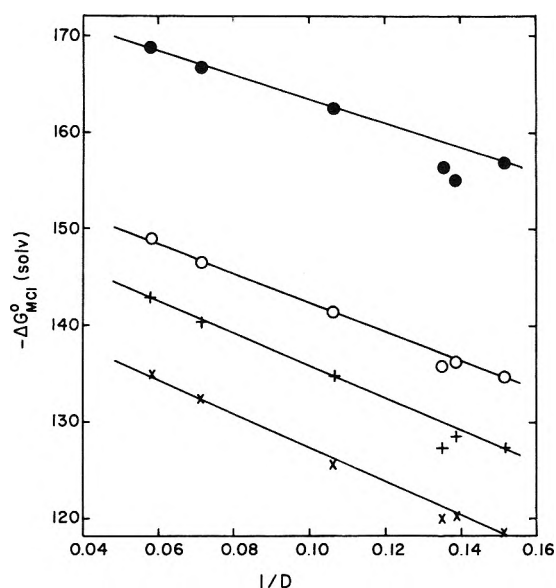
**TABLE V: Thermodynamic Functions of Solvation at 298°K (SS = 1 atm)**

Solvent	Solute	$-\Delta G^\circ$ , kcal/mol	$-\Delta H^\circ$ , kcal/mol	$-\Delta S^\circ$ , eu
NH <sub>3</sub>	NaCl	168.5	196.3	93
	KCl	148.0	174.2	88
	RbCl	142.3	168.9	89
	CsCl	134.1	162.6	96
EDA	NaCl	165.8	193.4	93
	KCl	145.1	174.3	98
	RbCl	139.3	169.4	101
	CsCl	131.3	162.1	103
MA	NaCl	161.9	193.7	107
	KCl	140.5	175.7	118
	RbCl	134.1	170.3	121
	CsCl	124.3	165.0	136
EA	NaCl	156.3	196.1	134
	KCl	133.6	181.1	159
	RbCl	126.5	177.3	170
	CsCl	117.6	169.0	172
DME	NaCl	154.3	190.6	122
	KCl	134.6	175.8	138
	RbCl	127.4	177.4	168
	CsCl	118.6	164.1	153
THF	NaCl	155.5	195.8	135
	KCl	134.2	170.2	121
	RbCl	126.3	164.0	127
	CsCl	118.6	161.0	142

**TABLE VI: Free Energies and Heats of Solvation with Respect to Ion Formation in Liquid Ammonia**

Source and temperature	NaCl	KCl	RbCl	CsCl
$-\Delta G^\circ$ , kcal/mol				
This work, 298°K	168.4	148.4	142.4	134.2
Reference 24, 298°K	164.5	145.0	139.0	131.0
Reference 25, 298°K	164.8	145.8	141.2	134.1
$-\Delta H^\circ$ , kcal/mol				
This work, 298°K	196.2	174.3	169.0	162.7
Reference 24, 273°K	190.0	168.0	161.0	152.0
Reference 26, 240°K	190.0	167.0	159.0	140.0

obtained from the corresponding quantities of formation of ions in solution and the enthalpies and free energies of formation of the gaseous ions. The enthalpies of formation of the gaseous alkali metal ions were taken from the tabulations of Latimer.<sup>20</sup> The enthalpy of formation of the gaseous chloride ion was calculated to be  $-54.4$  kcal/mol using the value of the electron affinity of Cl measured by Berry and Reimann<sup>22</sup> and the value of the dissociation energy of Cl<sub>2</sub> given by Rossini, *et al.*<sup>23</sup> Corresponding free energies were calculated from these enthalpies, the appropriate entropies from Rossini, *et al.*, and the absolute entropies of the gaseous ions calculated from the Sakur-Tetrode equation. Enthalpies and free energies of solvation of alkali metal chlorides with respect to ion formation in liquid ammonia from this work and from the literature are presented in Table V. Part of the differences between the free energies and enthalpies of the present work on the one hand, and those of previous workers on the other can be accounted for on the basis of older values of the electron affinity of chlorine being used in the computations of previous workers. In order to correct for the newer value of this electron affinity,<sup>22</sup> 3.9 kcal/mol should be added to

**Figure 2.** Plots of standard free energies of solvation at 298°K with respect to ion formation vs. reciprocal of dielectric constant, ●, NaCl; ○, KCl; +, RbCl; ×, CsCl.

the values of  $-\Delta G^\circ$  and  $-\Delta H^\circ$  from previous works recorded in Table VI.<sup>24-26</sup> After this correction is applied the differences remaining among corresponding values of the free energy are insignificant. However, the enthalpies of Makishima<sup>27</sup> and of Coulter<sup>26</sup> remain appreciably less negative than the present values. At least part of this difference may be accounted for by the different temperatures of measurement. As expected on the basis of a large decrease in heat capacity accompanying the dissolution of the gaseous ions, the enthalpy decreases with increasing temperature.

## Discussion

The relationship of the present data to the Born equation is made clear by examining plots of the solvation free energies given in Table V vs.  $1/D$ . A nearly linear plot is obtained for each metal chloride, with the exception of points for THF and DME which appear to be consistently low, (see Figure 2) so that a relationship of the form

$$\Delta G^\circ(M^+, \text{soln}) + \Delta G^\circ(A^-, \text{soln}) = A + (B/D) \quad (4)$$

is followed. However the intercepts  $A$  and slopes  $B$  differ appreciably from each other so that any attempt to fit the data to the Born equation, or its modified version proposed by Latimer and Slansky,<sup>28</sup> is bound to fail. As a consequence the method employed by these authors to obtain individual ion solvation energies may not be applied to the present data. While individual ion solvation energies may be obtained on the basis of a simple assumption such as  $\Delta G^\circ(\text{Cl}^-, \text{soln}) = \Delta G^\circ(\text{Cs}^+, \text{soln})$  as found by Izmailov<sup>24</sup> these quantities will not be required in the considerations which follow.

- (22) R. S. Berry and C. W. Feimann, *J. Chem. Phys.*, **38**, 1543 (1968).  
 (23) F. D. Rossini, D. D. Wagman, W. H. Evans, S. Levine, and I. Jaffe, NBS Circular No. 500 (1961).  
 (24) N. A. Izmailov, *Russ. J. Phys. Chem.*, **34**, 1142 (1960).  
 (25) J. A. Plambek, *Can. J. Chem.*, **47**, 1401 (1969).  
 (26) I. V. Coulter, *J. Phys. Chem.*, **57**, 553 (1953).  
 (27) S. Makishima, *J. Fac. Eng., Tokyo Imp. Univ.*, **21**, 115 (1938).  
 (28) W. M. Latimer and C. Slansky, *J. Amer. Chem. Soc.*, **62**, 2019 (1940).

The entropies of solvation with respect to ion formation given in Table V appear to be inordinately large compared to the corresponding quantities when water is the solvent.<sup>29</sup> Although the uncertainty in these entropies is large, perhaps amounting to as much as 20 eu, the trend of increasing values of  $-\Delta S^\circ(\text{solv})$  with decreasing solvent dielectric constant is no doubt real. The same trend is revealed in the corresponding entropies calculated with respect to ion pair formation<sup>6</sup> except perhaps in the case of the sodium chloride. Consequently, this trend reflects the solubility data directly and is not simply an artifact introduced on account of the ion pairing theory used in the computations. The trend is certainly enhanced through the use of ion pairing theory and through the particular manner in which the association constants have been calculated. The enhancement arises essentially because the theory<sup>7</sup> requires that the extent of ion association increase as the quantity  $DT$  decreases. Since changes in ion association quite generally satisfy this criterion, the enhancement of the trend in  $-\Delta S^\circ(\text{solv})$  due to the use of ion pairing theory may be accepted as arising from a reasonable extrapolation of present knowledge. Latimer and Slansky<sup>28</sup> have reported a similar trend in  $-\Delta S^\circ(\text{solv})$  for alkali halides in changing from water to methanol as solvent. In order to provide a rough interpretation of the entropies of solvation of the alkali halides in various solvents it is useful to compare values of  $-\Delta S^\circ(\text{solv})$  with corresponding entropies of fusion of the solvents involved. Without regard to the particular alkali halide, the average values of  $-\Delta S^\circ(\text{solv})$  for water, methanol, ammonia, EDA, and MA are about 20, 60, 90, 100, and 120 eu, respectively. Corresponding values of the entropies of fusion<sup>29</sup> are 5.5, 4.3, 6.9, 16.4, and 8.2 eu, respectively. Thus, the values of  $-\Delta S^\circ(\text{solv})$  in the respective solvents correspond to freezing out 4, 13, 13, 6, and 15 mol of solvent per mol of dissolved ions. Considering that the low number for EDA may be attributed to the chelating ability of this solvent, the changes in  $-\Delta S^\circ(\text{solv})$  are roughly accounted for simply on the basis of changes in molar entropies of the respective solvents, except in the case of water. Apparently, with water, structure breaking effects<sup>30</sup> of the ions are rather important, but with the remaining solvents considerably less so. Unfortunately insufficient data on heats of fusion are available to extend this comparison to the remaining solvents.

For the majority of solvents studied  $-\Delta S^\circ(\text{solv})$  increases with increasing cation radius. However, this trend has been entirely introduced by the requirement that ion association increase with increasing cation size. The opposite trend is observed for the entropies of solvation with respect to ion pair formation.<sup>6</sup> Consequently, the reality of this tendency of  $-\Delta S^\circ(\text{solv})$  to increase with increasing cation radius is highly questionable. Presumably, such an effect could result from the greater surface area, on which solvent molecules condense, of the larger ions. Further speculation appears to be unwarranted at this time.

One further interesting feature of the data presented in Table V is that the values of  $\Delta H^\circ(\text{solv})$  change very little from one solvent to another. If anything a slight tendency of  $-\Delta H^\circ(\text{solv})$  to increase in going from ammonia to solvents of lower dielectric constant may be detected. Since  $-\Delta H^\circ(\text{solv})$  decreases markedly as solvent dielectric constant decreases it is clear that the controlling factor in the relative abilities of the solvents to solvate the ions is the entropy. Accordingly, in the context of what has been

written above relative to the variation in  $\Delta S^\circ(\text{solv})$  with changing solvent, the superiority of ammonia as an ionizing solvent rests in its low molar entropy relative to the other solvents rather than in its stronger interaction with the ions. In extending these considerations to water and methanol, again the entropy is the controlling factor,<sup>28</sup> however, the effect in water is appreciably enhanced through the structure breaking factor.<sup>30</sup>

Our results on the solubilities of alkali metal chlorides may be used to define salt-like behavior in the group of solvents studied. For example, the solubilities of NaBr may be expected to parallel those of NaCl, and of CsI those of CsCl. Such relationships may be summarized simply as

$$\sigma_{\text{MX}} = k_{\text{MX}}\sigma_{\text{MCl}} \quad (5)$$

in which  $\sigma$  is the solubility of the subscripted salt. Generally  $k_{\text{MX}}$  will depend on MX and the solvent as well. If the dependence on the solvent is too strong then eq 5 is not useful. This will occur when there are different species in the saturated solutions of MCl and MX, or when activity coefficients differ widely. When the saturated solutions are dominated by similar species,  $k_{\text{MX}}$  may be nearly constant, independent of solvent. Under these conditions eq 5 may be used as a reference to define salt-like behavior. These conditions appear to be fulfilled for the saturated chloride solutions studied in which the ion pairs predominate (see Table III). Consequently, the measured solubilities of the chlorides may be used with eq 5 as a test of salt-like behavior, *i.e.*, a test of whether the saturated solutions of MX consist principally of  $\text{M}^+\cdot\text{X}^-$ .

The objects of our concern with salt-like qualities are solutions of alkali metals in amines and ethers. The question is whether saturated solutions of the metals behave in a salt-like manner. Unfortunately, solubility data for the metals are relatively sparse. Measured solubilities are available only for  $\text{NH}_3$  and EDA solutions.<sup>31,32</sup> However, qualitative observations are sufficient to establish trends. For example, sodium is apparently insoluble in DME and THF while the heavier alkali metals are slightly soluble<sup>33</sup> ( $\sim 10^{-5}$ – $10^{-6}$  M). For the amines, solubility decreases with decreasing dielectric constant from the order of 10 M for ammonia solutions to  $10^{-4}$ – $10^{-5}$  M for ethylamine solutions.<sup>34</sup> To test whether this constitutes salt-like behavior for the saturated metal solutions  $k_{\text{M}}$  is determined using solubility data for the metals in EDA. The values of  $k_{\text{M}}$  are 0.048 for Na, 9.3 for K, 7.9 for Rb, and 28 for Cs. With these values of  $k_{\text{M}}$  and the solubilities of the chlorides  $\sigma(\text{M})$  may be calculated using eq 5. Metal solubilities calculated in this way agree with the trends described above. For example, for the ethers solubility of Na is calculated to be  $10^{-7}$ – $10^{-8}$  M, probably too small to be easi-

(29) Landolt-Bornstein, Part 4, pp 188, 349, 350.

(30) H. S. Frank and W. Y. Wen, *Discuss. Faraday Soc.*, **24**, 133 (1957).

(31) R. Caterall, "Metal-Ammonia Solutions," W. A. Benjamin, New York, N. Y., 1964, pp 57 and 58.

(32) R. R. Dewald and J. L. Dye, *J. Phys. Chem.*, **68**, 128 (1964).

(33) F. A. Cafasso and B. R. Sundheim, *J. Chem. Phys.*, **31**, 809 (1959), found  $K(\text{solubility}) = 1.7 \times 10^{-3}$  M at  $-40^\circ$ . Solubility decreases markedly at higher temperatures as is indicated in ref 34. See also T. R. Tuttle, Jr., and S. I. Weissman, *J. Amer. Chem. Soc.*, **80**, 5342 (1958).

(34) I. Hurley, T. R. Tuttle, Jr., and S. Golden, "Metal-Ammonia Solutions," Butterworths, London, 1970, p 449; I. Hurley, Thesis, Brandeis University, 1970. Estimate of solubility is based on maximum values of absorbances obtained in a 1-cm path length optical cell of  $\sim 1.0$  with an extinction coefficient of between  $10^4$  and  $10^5$   $\text{M}^{-1}$   $\text{cm}^{-1}$ .

ly observed, while for the heavier metals  $\sigma(M)$  is  $10^{-5}$ – $10^{-6}$   $M$  in agreement with the observation that dilute solutions of these metals may be prepared. Similarly, the trend for the amines is well reproduced in the calculated solubilities. Nevertheless, the calculated solubilities for  $NH_3$  are about 2 orders of magnitude lower than the measured ones.

The success of this comparison between the metal chloride and metal solutions, except for  $NH_3$ , suggests that the saturated metal solutions are salt like and consequently composed of ion pairs. These ion pairs cannot be between metal cations and solvated electrons because other properties of the solutions rule out this possibility.<sup>35</sup> The only reasonable alternatives are  $M^+ \cdot M^-$ . This conclusion is in agreement with indications from measure-

ments on electrical conductivity<sup>36</sup> and optical spectra<sup>37</sup> of alkali metal amine solutions that the metal anion is an important constituent of these solutions.

*Acknowledgments.* This work was supported in part through a grant from the National Science Foundation. The authors are grateful for many helpful discussions and suggestions by Professor Sidney Golden.

(35) Dilute solutions often show properties attributable to solvated electron, but other species grow in importance as metal concentration increases. See, for example, R. R. Dewald and J. L. Dye, *J. Phys. Chem.*, **68**, 121 (1964). See also ref 32 and 34.

(36) R. R. Dewald and J. L. Dye, *J. Phys. Chem.*, **68**, 121 (1964).

(37) S. Matalon, S. Golden, and M. Ottolenghi, *J. Phys. Chem.*, **73**, 3098 (1969).

## A Comparative Study of the Enthalpy of Ionization of Polycarboxylic Acids in Aqueous Solution

V. Crescenzi,\* F. Delben, F. Quadrioglio, and D. Dolar<sup>1</sup>

*Institute of Chemistry, University of Trieste, Trieste, Italy (Received September 18, 1972)*

Calorimetric data are reported on the enthalpy of dissociation of the maleic acid–ethylene copolymer, the maleic acid–propylene copolymer, and of the maleic acid–ethyl vinyl ether copolymer, together with additional data for poly(acrylic acid), in water at 25°. These data with the aid of potentiometric ones afford a rather complete thermodynamic description of the ionization behavior of the four polycarboxylic acids in dilute aqueous solution. In the case of the maleic acid copolymers our present results (from the uncharged state to half-neutralization) point out the strong influence of chain substituents on value and sign of the enthalpy of dissociation. A simplified approach is attempted to account for the fraction of the total observed enthalpy due to the buildup of the charge density along the polyelectrolyte chains.

### Introduction

In previous papers from this laboratory, enthalpy of dissociation data for two polycarboxylic acids, namely poly(methacrylic acid)<sup>2a</sup> and the maleic acid–butyl vinyl ether copolymer<sup>2b</sup> in water, have been reported. The calorimetric results were essentially employed to derive, in conjunction with potentiometric data, a thermodynamic picture of the globule  $\rightarrow$  coil conformational transition which the two polyacids mentioned above undergo upon increasing their degree of dissociation in dilute aqueous solution.

We wish to report here a set of enthalpy of dissociation data for other polycarboxylic acids which are assumed gradually to expand and solvate upon increasing charge density along the chains and which therefore may provide an insight into the energetics of proton ionization from weak polyacids devoid of complications due to conformational transitions.

The ultimate aim of our research is that of describing with the aid of direct microcalorimetric measurements how free energy changes associated with the ionization of weak polyacids are built up by enthalpy and entropy con-

tributions, a basic type of physicochemical information which is lacking in the realm of polymer solutions. Data reported here represent to our knowledge the first attempt in this direction. Polymers considered are poly(acrylic acid), maleic acid–ethylene copolymer, maleic acid–propylene copolymer, and maleic acid–ethyl vinyl ether copolymer.

The results of the microcalorimetric measurements indicate that nature of side chains, extent of hydration, and charge density of polyions would be the main factors controlling the absolute value and sign of the enthalpy of dissociation of polycarboxylic acids. The interplay of such factors whose relative entity depends on the degree of neutralization, as typical of any property of polyelectrolytes, is difficult to grasp, however, on the basis of our limited number of data. Difficulties encountered in the

(1) Chemistry Department, University of Ljubljana, Ljubljana, Yugoslavia.

(2) (a) V. Crescenzi, F. Delben, and F. Quadrioglio, *J. Polym. Sci., Part A-2*, **10**, 357 (1972); (b) V. Crescenzi, F. Quadrioglio, and F. Delben, paper presented at the 9th IUPAC Microsymposium on Macromolecules, Prague, Sept 1971; *J. Polymer. Sci., Part C*, in press.



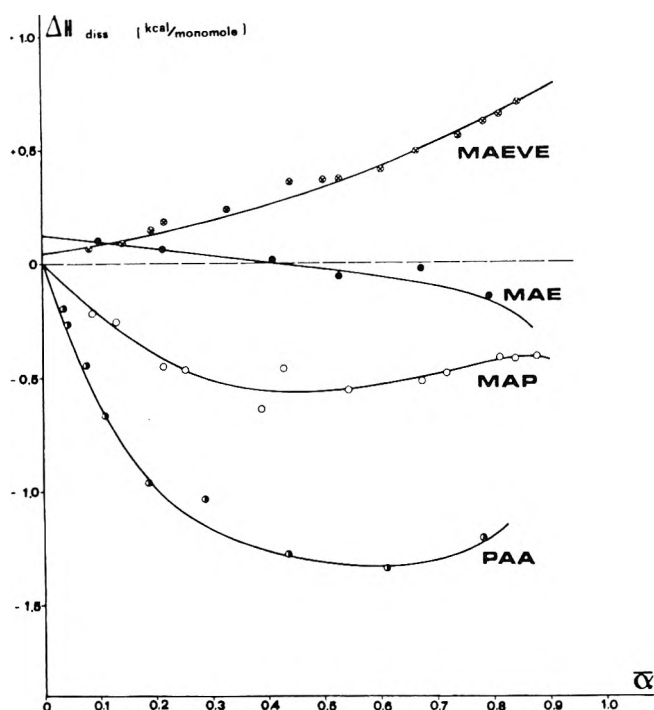


**Figure 1.** Dependence of the enthalpy of dissociation,  $\Delta H_{\text{diss}}$  (see text), upon the degree of neutralization  $\bar{\alpha}$ , for aqueous solutions of:  $\bullet$ , poly(acrylic acid), PAA;  $m_p = 4.3 \times 10^{-2}$ ;  $\circ$ , maleic acid-propylene copolymer, MAP;  $m_p = 1.3 \times 10^{-2}$ ;  $\ominus$ , maleic acid-ethylene copolymer, MAE;  $m_p = 1.7 \times 10^{-2}$ ;  $\oplus$ , maleic acid-ethyl vinyl ether copolymer, MAEVE;  $m_p = 1.7 \times 10^{-2}$ .

interpretation of the enthalpy of dissociation data are discussed. Finally, an estimate of the contribution of electrostatic interactions to the observed ionization behavior of four polyacids considered is attempted.

### Experimental Section

(a) *Materials.* Poly(acrylic acid), PAA, was a conventional sample prepared and characterized as previously specified<sup>2a</sup> ( $M_v = 3 \times 10^5$ ). Maleic acid-propylene copolymer, MAP, and maleic acid-ethylene copolymer, MAE, samples were received from the Monsanto Chemical Co. ( $M_v \sim 10^5$ ). The maleic acid-ethyl vinyl ether copolymer, MAEVE, was a high molecular weight sample obtained from Professor U. P. Strauss.

Aqueous solutions of the three maleic acid copolymer were prepared following essentially the procedure outlined by Bianchi, *et al.*<sup>3a</sup> Solutions of the sodium salts of the copolymers were dialyzed, passed through a cation-exchange column in the  $\text{H}^+$  form, dialyzed again, and concentrated under reduced pressure at *ca.* 40°.

The titre of the polyacids stock solutions was determined by means of potentiometric titrations in *ca.* 0.1 M NaCl. In these experiments as well as in the preparation of the (salt-free) polyelectrolyte solutions for the calorimetric measurements standard NaOH solutions were used. The concentration of polyelectrolyte is given as the number of moles of repeating units (or monomoles) per liter of solution,  $m_p$ , at 25°.

All the copolymers used are of the 1:1 alternating type.<sup>3a,b</sup> In view of the free radical process of synthesis they are believed to be essentially "atactic."

(b) *Microcalorimetric Experiments.* The experiments were carried out at 25° using an LKB Model 10700 batch-

type microcalorimeter. For the study of MAP, an LKB flow-type microcalorimeter was used.

The procedure followed with the batch-type calorimeter has been described elsewhere.<sup>2a</sup> With the flow-type apparatus a polyelectrolyte solution ( $m_p = 0.200$ ; see Figure 1) at a given initial degree of neutralization ( $\alpha_1$ ) was allowed to flow through the apparatus at a constant flow rate and was first mixed with water (to determine the heat of dilution of the polyelectrolyte) and then with a  $2.5 \times 10^{-3}$  N HCl solution, both flowing at a rate half of that of the polyelectrolyte solution. All flow rates were controlled by weighing. The output of the calorimeter was amplified using a Keithley Model 150B microvoltmeter and recorded with a Perkin Elmer Model 165 pen recorder. Electrical calibrations were performed routinely before and after each run. Corrections were made for the heat of dilution of HCl.<sup>4</sup>

The recorded heat exchange,  $q_{\text{obsd}}$ , obtained by adding  $m_{\text{H}^+}$  moles of hydrogen ions to the solution of the partially neutralized polyelectrolyte, was in all cases corrected for the heat of dilution of the polyelectrolyte and of HCl to calculate the heat of dissociation,  $q_{\text{diss}}$

$$q_{\text{diss}} = - \left\{ q_{\text{obsd}} - q_{\text{dil}}^{\text{pol}} - q_{\text{dil}}^{\text{HCl}} \right\}$$

The change of degree of neutralization from  $\alpha_1$  to  $\alpha_2$  was not greater than 0.06 in each experiment. The  $q_{\text{diss}}$  thus obtained was recalculated per mole of hydrogen ions giving the enthalpy of dissociation as function of  $\bar{\alpha}$

$$(q_{\text{diss}}/m_{\text{H}^+}) \equiv \Delta H_{\text{diss}}(\bar{\alpha})$$

where  $\bar{\alpha} = (\alpha_1 + \alpha_2)/2$ .

In the range of  $\alpha$  values between 0.1 and 1.0 the true degree of dissociation  $\alpha_{\text{diss}}$  of the polyelectrolytes considered in our study may be taken with good approximation as equal to the degree of neutralization,  $\alpha$ . Appropriate corrections using  $\alpha_{\text{diss}} \approx \alpha + [\text{H}^+]/m_p$  resulted in small shifts of both the  $\Delta H_{\text{diss}}$  and  $\bar{\alpha}$  values which were within experimental error.

(c) *Potentiometric Titrations.* Potentiometric titrations were performed at 25° using a Radiometer PHM4d pH meter with Radiometer "combination" electrodes, GK-2301 C.

### Results

The results of the microcalorimetric measurements on aqueous solutions of PAA, MAP, MAE, and MAEVE are reported in Figure 1. In the case of the maleic acid copolymers,  $\alpha = 1$  is defined to correspond to half-neutralization. The data lead to the following conclusions.

(1) In general,  $\Delta H_{\text{diss}}$  depends upon  $\alpha$ . The dependence is particularly strong in the case of PAA, while only slight in the case of MAE.

(2) For PAA, MAP, and MAE the difference between  $\Delta H_{\text{diss}}$  and  $\Delta H_{\text{diss}}^0$  (the extrapolated  $\Delta H_{\text{diss}}$  value for  $\alpha \rightarrow 0$ ) becomes more negative with increasing  $\alpha$ . In analogy with the conventional treatment of the free energy of ionization of polyions, we shall designate this difference as the excess enthalpy of dissociation.

(3) (a) E. Bianchi, A. Ciferri, R. Parodi, R. Rampone, and A. Tealdi, *J. Phys. Chem.*, **74**, 1050 (1970); (b) P. L. Dubin, and U. P. Strauss, *ibid.*, **74**, 2842 (1970).

(4) D. D. Wagman, W. H. Evans, V. B. Parker, I. Halow, S. M. Bailey, and R. H. Schumm, *Nat. Bur. Stand. (U. S.) Tech. Note*, No. 270-3, 27 (1968).

**TABLE I: Thermodynamics of Dissociation of Polycarboxylic Acids in Water at 25°**

$\alpha$	$\Delta H_{diss}^a$ kcal/mol	$pK_a$	$\Delta G_{diss}$ kcal/mol	$-\Delta S_{diss}$ eu
PAA				
0.0	0.0	4.40	6.00	20.1
0.1	-0.61	5.10	6.95	25.4
0.2	-0.96	5.46	7.44	28.2
0.3	-1.15	5.71	7.78	30.0
0.4	-1.25	5.91	8.06	31.3
0.5	-1.30	6.11	8.34	32.4
0.6	-1.32	6.30	8.60	33.3
0.7	-1.29	6.48	8.84	34.0
0.8	-1.18	6.64	9.06	34.4
MAE				
0.0	0.13	3.80	5.18	17.0
0.1	0.10	4.21	5.74	19.0
0.2	0.07	4.34	5.92	19.6
0.3	0.04	4.44	6.05	20.2
0.4	0.00	4.50	6.14	20.6
0.5	-0.02	4.55	6.20	20.9
0.6	-0.06	4.58	6.25	21.2
0.7	-0.09	4.61	6.28	21.4
MAP				
0.0	0.0	3.50	4.77	16.0
0.1	-0.22	3.92	5.35	18.7
0.2	-0.40	4.09	5.58	20.1
0.3	-0.51	4.20	5.73	21.0
0.4	-0.56	4.29	5.84	21.5
0.5	-0.56	4.36	5.95	21.8
0.6	-0.53	4.41	6.01	22.0
0.7	-0.49	4.44	6.06	22.0
MAEVE				
0.0	0.05	3.500	4.773	15.8
0.1	0.09	4.090	5.577	18.4
0.2	0.14	4.500	6.136	20.1
0.7	0.52	5.193	7.082	22.0

<sup>a</sup> Interpolated or extrapolated from the curves drawn in Figure 1.

(3) For PAA a flat minimum in the plot of  $\Delta H_{diss}$  against  $\alpha$  occurs at around  $\alpha \sim 0.6$ . A very slight minimum may also be noticed in the case of MAP.

(4) The absolute value and sign of  $\Delta H_{diss}$  (as well as the trend of  $\Delta H_{diss}$  with increasing  $\alpha$ ) depend in a striking manner on the chemical structure of the polymer.

(5) Among the polycarboxylic acids studied so far, only MAEVE is characterized by  $\Delta H_{diss} > 0$  over the entire range of  $\alpha$ .

To make more complete the thermodynamic characterization of the dissociation behavior of the different polycarboxylic acids, we take recourse to a number of potentiometric data obtained working with the same polymer solutions used in the microcalorimetric experiments. From these data, with the aid of the potentiometric equation

$$pH + \lg \frac{1-\alpha}{\alpha} \equiv pK_a = pK_0 + 0.434 \frac{\Delta G^{exc}}{RT} \quad (1)$$

where  $K_0$  is the limiting value of the dissociation constant of the polyelectrolyte for  $\alpha \rightarrow 0$  and  $\Delta G^{exc}$  is the change of the excess free energy (electrostatic, conformational, etc.) when the charge on every polyion is increased by one, one readily obtains for the total free energy of dissociation for

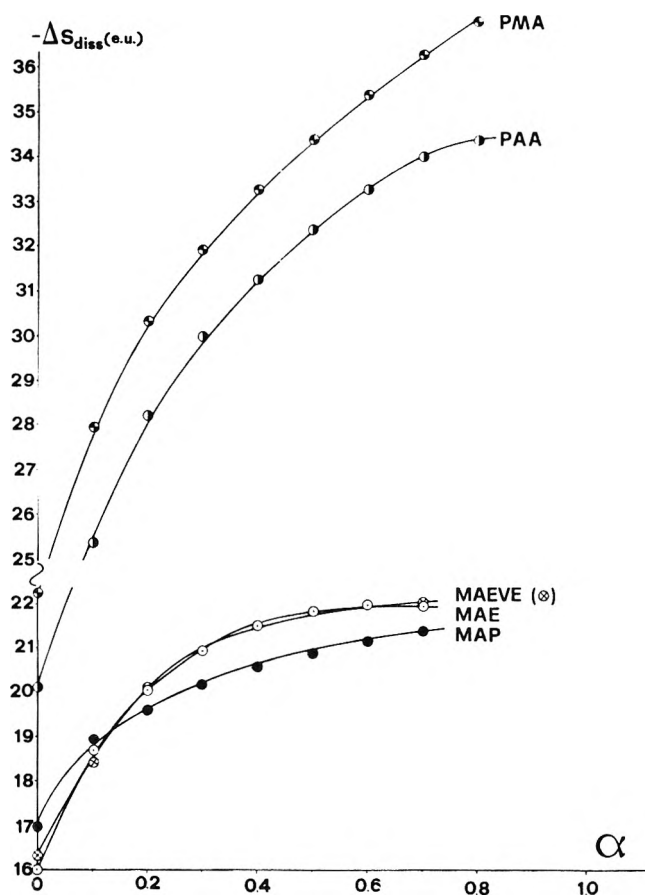


Figure 2. The entropy of dissociation of poly(acrylic acid), PAA, of poly(methacrylic acid), PMA,<sup>2a</sup> and of the maleic acid copolymers (see text and Figure 1) in water at 25°.

each given  $\alpha$  value

$$\Delta G_{diss} = 2.303RT(pK_a) \quad (1')$$

Combined use of the microcalorimetric and potentiometric data, which are also reported in Table I, finally yields a set of entropy of dissociation values

$$\Delta S_{diss} = \frac{\Delta H_{diss} - \Delta G_{diss}}{T}$$

which are reported in Figure 2 (see also Table I). Data of Figure 2 clearly show that the entropy of ionization is distinctly more negative for PAA than for the maleic acid copolymers at least for  $\alpha \leq 1$ . (The data for poly(methacrylic acid), PMA, were calculated from microcalorimetric and potentiometric results already reported in the literature.<sup>2a</sup>) This fact should be at least in part connected with a stronger water molecule immobilization during the charging process of PAA (and of PMA) than for the copolymers in the range of values considered so far. This hypothesis appears in agreement with the results of dilatometric experiments recently reported by Begala and Strauss<sup>5</sup> for MAE and PAA.

## Discussion

The interpretation of the ionization behavior of polymeric carboxylic acids in water is fraught with a number of difficulties additional to those encountered in the rela-

(5) A. J. Begala and U. P. Strauss, *J. Phys. Chem.*, **76**, 254 (1972).

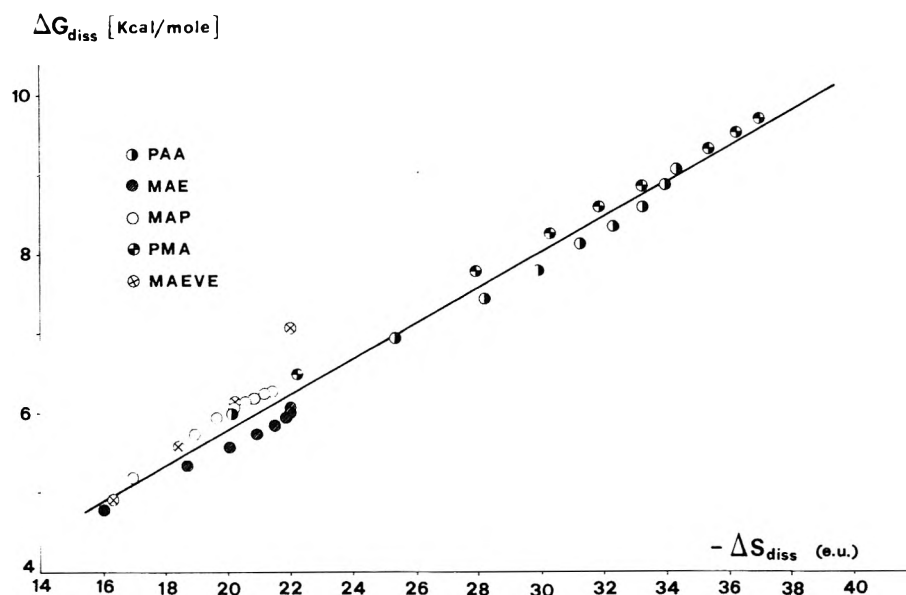


Figure 3. Free energy–entropy of dissociation relationship for poly(carboxylic acids) (see Figures 1 and 2 and text) in water at 25°. The data for PMA are from ref 2a.

tively simpler case of mono- and dicarboxylic acids considered so far in the literature.<sup>6,7</sup>

We refer in particular to the fact that polyions in dilute aqueous solution are highly charged species each of which may be thought of as a local very high concentration of carboxylate residues. The energy required for the ionization of each carboxylic group will thus depend on the number of fixed charges already present along the chain and on their relative distances. These, in turn, are a function of the stoichiometric degree of neutralization the chain-backbone flexibility and its more or less favorable interactions with water.

Furthermore, the specific influence of nonionizable chain substituents on value and sign of  $\Delta H_{\text{diss}}$  may be very important, as already shown in the case of substituted dicarboxylic acids<sup>7</sup> and as also dramatically demonstrated by the difference in behavior exhibited by the maleic acid copolymers (see Figure 1). Chain substituents will in fact influence the conformational distribution of polymeric electrolytes, and thus the mean distance between ionized groups, as well as their hydration, and will diversely control also the local effective dielectric constant.

In other words, the observed ( $\Delta H_{\text{diss}} - \Delta H^0_{\text{diss}}$ ) values may be thought as made up by different contributions arising from changes in (a) the electrostatic enthalpy, (b) the hydration, and (c) the conformational energy of the chains and from changes in the extent of interaction of the polyions with sodium counterions, upon varying  $\alpha$ .

The associated differential enthalpy changes are difficult to evaluate and may be of course of different relevance passing from one polyelectrolyte to another.

Pending more experimental data which might furnish all quantitative information necessary for an evaluation of the different enthalpic terms mentioned above (for each given polyelectrolyte), we shall confine attention on a possible estimate of the contribution of electrostatic interactions to the ionization behavior of polyelectrolytes studied in this work.

(1) Let us first consider that we may express the electrical free energy of polyion ionization in water by

$$\Delta G_{\text{el}} = \frac{e_0^2 Q}{D}; \quad Q = \sum \left( \frac{1}{r_i} \right) \quad (2)$$

where  $r_i$  are the distances of the ionic charges from a carboxyl group undergoing ionization. ( $e_0$  is the unit charge and  $D$  is the dielectric constant of the medium.) We have then, by straightforward manipulation of eq 2, the following expressions for the electrostatic entropy,  $\Delta S_{\text{el}}$ , and the electrostatic enthalpy,  $\Delta H_{\text{el}}$ , respectively

$$\Delta S_{\text{el}} = \left( \frac{d \ln D}{dT} - \frac{d \ln Q}{dT} \right) \Delta G_{\text{el}} \quad (3)$$

$$\Delta H_{\text{el}} = \left[ \left( 1 + \frac{d \ln D}{d \ln T} \right) - \frac{d \ln Q}{d \ln T} \right] \Delta G_{\text{el}} \quad (4)$$

If the  $d \ln Q/dT$  and  $T d \ln Q/dT$  terms are neglected, eq 3 and 4 reduce to the well known relationships derived by Bjerrum<sup>8</sup> for simple polyprotic acids, which lead to a linear plot of  $\Delta G_{\text{el}}$  against  $\Delta S_{\text{el}}$  with a slope equal to  $-217^\circ\text{K}$  at 25°. A plot of  $\Delta G_{\text{diss}}$  against  $\Delta S_{\text{diss}}$  using our experimental data is reported in Figure 3.

It is seen that the experimental points reported for different polyacids, in steps of 0.1  $\alpha$  unit for each, may be fitted with reasonable approximation by a single line (with the exception of the data for MAEVE) having a slope equal to  $-222^\circ\text{K}$ , quite close to that predicted by Bjerrum's theory.

These results would reinforce the hypothesis that the interactions involved in proton ionization for the polyacids studied by us are primarily electrostatic. This is no proof, of course, that the  $d \ln Q/d \ln T$  term is indeed negligible, the qualitative correlation depicted by the plot of Figure 3 being possibly somewhat fortuitous.

Calculation of absolute  $\Delta H_{\text{el}}$  values on the basis of eq 3 would require, besides a knowledge of the  $d \ln Q/d \ln T$

(6) J. J. Christensen, R. M. Izatt, and L. D. Hansen, *J. Amer. Chem. Soc.*, **89**, 213 (1967).

(7) J. J. Christensen, M. D. Slade, D. E. Smith, R. M. Izatt, and J. Tsang, *J. Amer. Chem. Soc.*, **92**, 4164 (1970).

(8) E. J. King, "Acid Base Equilibria," Macmillan, New York, N. Y. 1965, p 211.

term, which is related to the temperature coefficient of polyion dimensions, the evaluation of  $\Delta G_{ei}$  values.

Consistent with the line of reasoning schematized in a previous paragraph for  $(\Delta H_{diss} - \Delta H^0_{diss})$ , the excess enthalpy of ionization, we assume that  $\Delta G_{ei}$  represents only a portion of the total excess free energy of ionization as derivable from potentiometric ( $pK_a - pK^0$ ) data (see eq 1), and consider it as an entity not yet unambiguously derivable from experimental data.

(2) Let us now consider the rod-like electrostatic model for the polyions,<sup>9,10</sup> a model which has been applied with considerable success also to the interpretation of heat of dilution of polyelectrolytes.<sup>11</sup>

The macroions are thus assimilated to rods of fixed radius  $a$ , in contact with a medium (containing the counterions) of dielectric constant  $D$  invariant with the charge density on the rods. A dilute solution of a polyelectrolyte may be formally divided into parallel cylindrical domains of radius  $R$ , each containing a macroion and its counterions. For this cylindrical cell the Poisson-Boltzmann equation has been solved<sup>9,10</sup> giving the electrostatic potential as a function of distance from the axis of the polyion,  $\psi(r)$ . Using this model, we shall have to calculate the enthalpy  $\Delta H_{ei}$  of the process



in which a proton is removed from an already broken OH bond on a partially ionized rod-like polyion ( $\bar{\alpha}$ ) and brought to a distance  $R$  where the electrical force of the macroions vanishes.

For process (5) the free energy change would be

$$\Delta G_{ei} = e_0[\psi(R) - \psi(\mathbf{a})] \quad (6)$$

which according to theory for rod-like macroions in water becomes

$$\Delta G_{ei} = RT \ln \{e^{2\gamma}[(\lambda - 1)^2 - \beta^2]/(1 - \beta^2)\} \quad (7)$$

where  $\lambda = \alpha e_0^2/DK T b =$  charging parameter  $= \alpha \lambda^0$  and  $b$  is the length of the monomer unit. In eq 7  $\beta$  is a constant, related to  $\lambda$  and  $\gamma$  by eq 9, and  $\gamma$  is the concentration parameter

$$\gamma = \frac{1}{2}[\ln(10^3/\pi a^2 b N_A) - \ln m_p] \quad (8)$$

where  $N_A$  is Avogadro's number and  $m_p$  is the concentration of the polymer in moles of monomer units per liter.

$$\lambda = (1 - \beta^2)/[1 + \beta \coth \beta \gamma] \quad (9)$$

The expression for  $\Delta H_{ei}$  may then be derived from eq 7 according to the Gibbs-Helmholtz relationship. The final equation reads

$$\begin{aligned} \Delta H_{ei} = & 2RT\lambda \left[ \left( 1 + \frac{d \ln D}{d \ln T} \right) + \right. \\ & \left. \frac{d \ln b}{d \ln T} \right] \left\{ \frac{\lambda - 1}{[(\lambda - 1)^2 - \beta^2]} + \beta^2(\lambda - 2)\lambda / \{\lambda(\lambda - 1 - \beta^2) + \right. \\ & \left. \gamma(1 - \beta^2)[(\lambda - 1)^2 - \beta^2][(\lambda - 1)^2 - \beta^2] \right\} - \\ & RT \frac{d \ln V}{d \ln T} + RT \left[ 2 \frac{d \ln a}{d \ln T} + \frac{d \ln b}{d \ln T} \right] \quad (10) \end{aligned}$$

where all symbols have their previously defined meaning and where  $V$  is the volume of the solution.

Use of eq 7 and 10 requires that we adopt appropriate values of both the charging parameter  $\lambda^0$  and the so-called concentration parameter  $\gamma$  (see eq 8 and 9).

Calculations of  $\Delta H_{ei}$  and  $\Delta G_{ei}$  have been carried out for different sets of  $\lambda^0$  and  $\gamma$  values, neglecting the derivatives with respect to temperature of the parameters  $a$  and  $b$  and taking for the terms

$$RT \left( 1 + \frac{d \ln D}{d \ln T} \right); RT \frac{d \ln V}{d \ln T}$$

the values  $-220.4$  and  $44.9$  cal/mol, respectively, *i.e.*, those for pure water at  $25^\circ$  ( $D = 78.54$ ).

In Figure 4 three representative  $\Delta H_{ei}$  against  $\alpha$  plots, according to eq 10, are reported for two  $\lambda^0$  values. These two values ( $\lambda^0 = 3.0$  and  $1.5$ ) use  $b = 2.52$  Å and  $b = 5.0$  Å, which correspond to the spacing of nearest-neighbor carboxyls in PAA and next-to-nearest-neighbor carboxyls in the maleic acid copolymers if the polyions chains are represented in the all *trans* conformation. The associated  $\gamma$  values were also chosen consistent with the structural parameters of the polymers and experimental concentrations ( $\gamma \sim 3$  for all polymers considered assuming a common value for  $a$  equal to 3 Å).

Other curves calculated for higher  $\lambda^0$  values are not drawn in Figure 4 since it was found that an increase in  $\lambda^0$  beyond 3 only moderately influences the  $\Delta H_{ei}$  values and in the same time shifts the minimum in the  $\Delta H_{ei}$ - $\alpha$  plots to lower  $\alpha$  values.

Comparison with the experimental  $\Delta H_{diss}$  vs.  $\alpha$  curves of Figure 1 shows that the trend exhibited by the data for MAP and MAE happen to fall within predictions of the approximate electrostatic theory outlined above.

One could then be led to assume that the differences between calculated  $\Delta H_e$  values and experimental  $\Delta H_{diss}$  values might be essentially a measure of others than coulombic interactions to the enthalpy of polyions dissociation, for each given  $\alpha$  value.

Our limited confidence in the accuracy of the electrostatic approach outlined above (as employed by us) which besides the inherent weakness of the rod-like model at low  $\alpha$  values entails the choice of an adjustable parameter ( $\lambda^0$ ) as well as a number of approximations, prevents us from tackling this more advanced stage of the problem.

At this stage we can only qualitatively conclude that the behavior of PAA should be markedly influenced by a strong dependence of the hydration of the chains upon  $\alpha$ , which would contribute an increasingly negative term to the observed enthalpy of dissociation, while for MAEVE ( $\Delta H_{diss} > 0$ ) the electrostatic interactions between fixed charges and the hydration of ionized groups would play a minor role with respect to the ion-dipole and/or dipole-dipole interactions between side chain and ionizable groups in determining the  $\Delta H_{diss}$  values (for  $\lambda \leq 1$ ).

In conclusion, it appears that more data should be accumulated before a less qualitative picture of the thermodynamics of dissociation of weak polyelectrolytes may be achieved. Data using other than calorimetric and po-

(9) T. Alfrey, P. W. Berg, and H. Morawetz, *J. Polym. Sci.*, **7**, 543 (1951).

(10) R. M. Fuoss, A. Katchalsky, and S. Lifson, *Proc. Nat. Acad. Sci. U. S.*, **37**, 579 (1951).

(11) J. Skerjanc, D. Dolar, and D. Leskovsek, *Z. Chem.*, **56**, 207, 218 (1967); **70**, 31 (1970).

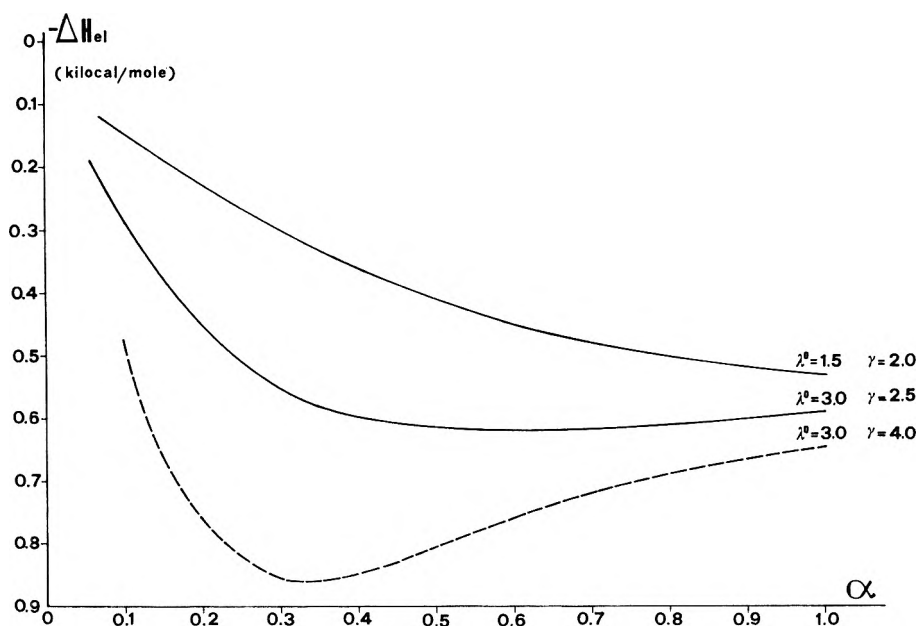


Figure 4. Dependence of  $\Delta H_{e1}$  on  $\alpha$  (eq 11).

tentiometric techniques, in particular experiments from which reliable information on polyions hydration and on the temperature dependence of polyions dimensions and charge densities for different  $\alpha$  values might be derived, should prove valuable in this context.

*Acknowledgments.* This work has been carried out with financial support of the Italian Consiglio Nazionale delle Ricerche. The authors wish to express their gratitude to Professor H. Morawetz for much stimulating advice and many helpful discussions.

## Calorimetric Investigation of the Association of Various Purine Bases in Aqueous Media<sup>1</sup>

Michael G. Marenchic<sup>2</sup> and Julian M. Sturtevant\*

Department of Chemistry, Yale University, New Haven, Connecticut 06520 (Received September 25, 1972)

Publication costs assisted by the National Institutes of Health and the National Science Foundation

The thermodynamics of association of 6-dimethylaminopurine in aqueous media have been investigated by flow microcalorimetry. The presence of charges on the solute molecules at high and low pH decreases the association, but the changes in enthalpy and entropy are both of sign opposite to that expected on the basis of simple electrostatic considerations. Results obtained with added organic solvents suggest contributions to the binding free energy resulting both from hydrophobic forces (W. Kauzmann, *Advan. Protein Chem.*, **14**, 1 (1959)) and from surface forces (O. Sinanoğlu and S. Abdunur, *Fed. Proc., Fed. Amer. Soc. Exp. Biol.*, **24**, 5 (1965)). It is not, however, possible to give a fully satisfactory analysis of the data in terms of presently accepted views of solute-solvent interactions. Preliminary data have been obtained for five additional purine derivatives.

### Introduction

The association in aqueous solution of pyrimidine and purine bases, and the nucleosides and nucleotides derived from them, has received much study because of the bearing of this association on the interactions between the

stacked pyrimidine and purine rings in helical nucleic acids. Current information on this association has been well summarized by Ts'o.<sup>3</sup> Gill and his coworkers<sup>4-6</sup> have

(1) From the Ph.D. thesis of M. G. Marenchic.

shown that the thermodynamics of the association can be conveniently investigated by flow microcalorimetry. We have employed this method in further work on the association of certain purine derivatives, with emphasis on a study of the effects of pH, solvent composition, and nature and concentration of anionic species on the association of 6-dimethylaminopurine.

### Experimental Section

The bases and nucleosides used were obtained from various sources, and were in most cases used without further purification since paper chromatography with *n*-butyl alcohol-water (86:14) gave only one spot. In some cases it was ascertained that recrystallization led to no observable variation of dilution properties.

Heats of dissociation were measured in a flow modification<sup>7</sup> of the Beckman Model 190B microcalorimeter. Analysis of the resulting data is based on a treatment developed by Stoesser and Gill.<sup>4</sup> This treatment assumes, first, that all solute species behave ideally; second, that polymerization of the monomeric solute proceeds to an indefinite degree; and, third, that all polymerization steps are characterized by the same dissociation constant  $K$  and dissociation enthalpy  $\Delta H$ . Stoesser and Gill employed molality as concentration unit, but if the first assumption is valid, there will be no volume changes on dilution and molarity can equally well be employed. It was shown that at the concentration levels used in our work any volume changes on dilution were indeed negligible.

It is found on this basis that the heat of dilution  $\Delta Q_i$  from a total monomer molarity of  $M_i$  to zero molarity is

$$\Delta Q_i = \Delta H - (K\Delta H)^{1/2}(\Delta Q_i/M_i)^{1/2} \quad (1)$$

From this expression it follows that for a finite dilution experiment from initial molarity  $M_i$  to final molarity  $M_f$

$$\Delta Q = \Delta Q_i - \Delta H + (K\Delta H)^{1/2}[(\Delta Q_i - \Delta Q)/M_f]^{1/2} \quad (2)$$

where  $\Delta Q_i$  is the heat of dilution from  $M_i$  to zero concentration.

As pointed out by Gill, *et al.*,<sup>5</sup> if osmotic coefficient data are available, an estimate of  $\Delta H$  is obtained by combination of osmotic and calorimetric data, in effect using the former type of data for the evaluation of  $K$ , which may differ numerically from the purely calorimetric estimate. For example, for 6-methylpurine in water at 25°, Stoesser and Gill<sup>4</sup> reported  $K = 0.116 \pm 0.030 m$  and  $\Delta H = 5.6 \pm 0.2 \text{ kcal mol}^{-1}$  from calorimetric data alone, and  $K = 0.149 m$  and  $\Delta H = 6.0 \pm 0.4 \text{ kcal mol}^{-1}$  on the basis of combined osmotic and calorimetric data. We have employed only calorimetric data in the evaluation of  $K$  and  $\Delta H$  since osmotic data are not available for most of the systems studied.

In each set of experiments a stock solution was diluted to a number of lower concentrations. Trial values of  $\Delta Q_i$  were assumed until a value was found which gave the best least-squares fit of the data to a straight line plot of  $\Delta Q$  vs.  $X \equiv [(\Delta Q_i - \Delta Q)/M_f]^{1/2}$ . Values of  $K$  and  $\Delta H$  were then obtained from the intercept and slope of the straight line. Since more than one initial solution was usually employed, each corresponding set of data points was treated as outlined above, and then combined with the curve of highest initial concentration by addition to the experimental dilution heats of a constant heat quantity equal to the weighted mean difference between the smoothed dilution curve for the lower initial concentration and that for

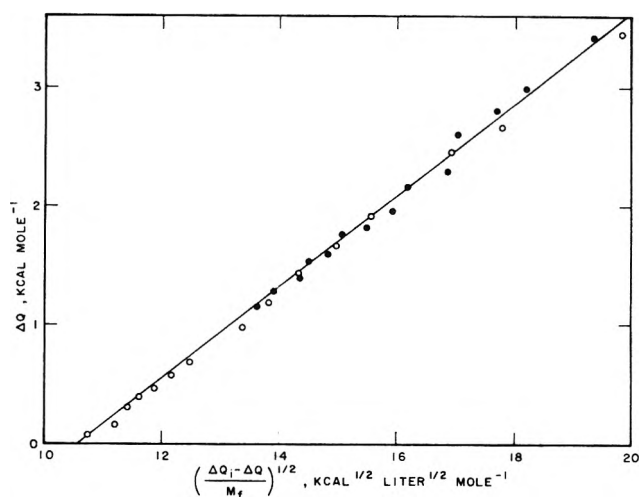


**Figure 1.** Data for two series of experiments on the heat of dilution of 6-dimethylaminopurine in water at 25° plotted to show adherence to eq 2.  $\Delta Q$  is the observed heat of dilution per mole of monomer from a fixed initial molarity,  $M_i$ , to a series of final molarities,  $M_f$ , and  $\Delta Q_i$  is a value for the heat of dilution from  $M_i$  to zero molarity selected as outlined in the text to give optimum fit of the data to a straight line plot: O, series 1,  $M_i = 0.0457 M$ ,  $\Delta Q = \Delta Q_{\text{obsd}}$ ; ●, series 2,  $M_i = 0.0221 M$ ,  $\Delta Q = \Delta Q_{\text{obsd}} + 1.090 \text{ kcal mol}^{-1}$ ;  $\Delta Q_i = 5.086 \text{ kcal mol}^{-1}$ . The line is drawn for  $K = 0.0162 M$ ,  $\Delta H = 9.15 \text{ kcal mol}^{-1}$ .

the highest initial concentration. The combined data were then again treated by least squares to obtain refined values for  $K$  and  $\Delta H$ .

A typical group of experimental data for the dilution of 6-dimethylaminopurine in water is presented in Figure 1, and is seen to fit well the assumed polymerization scheme. It should be pointed out, however, that a simple dimerization would also lead to a linear dependence of  $\Delta Q$  on  $(\Delta Q/M_0)^{1/2}$ . In the present case, indefinite polymerization seems more likely than dimerization.<sup>8</sup>

In many cases the observable heats were too small, because of low solubility and/or small heat of dissociation, to enable a satisfactory selection of  $\Delta Q_i$  to be made as outlined above. In these cases the observed heats of dilution were least squared to the equation

$$\Delta Q = \Delta Q_i - \Delta H(1 + (K/2M_f)\{1 - [1 + (4M_f/K)]^{1/2}\}) \quad (3)$$

which is based on the same model for the polymerization, for various assumed values of  $K$ . It was found that  $\Delta H$  could then be expressed to better than  $\pm 5\%$  accuracy as a function of  $K$ , over a full range of probable values for  $K$ , by the empirical equation

$$\Delta H = A + (B/K) + CK \quad (4)$$

where  $A$ ,  $B$ , and  $C$  are constants. Thus, if the value for  $K$  for any of these cases is determined by other means such as osmometry, the value of  $\Delta H$ , consistent with our calori-

- (2) Predoctoral Trainee, USPHS GM No. 00748, from the National Institutes of Health.
- (3) P. O. P. Ts'o in "Fine Structure of Proteins and Nucleic Acids," G. D. Fasman and S. N. Timasheff, Ed., Marcel Dekker, New York, N. Y., 1970, p 49.
- (4) R. Stoesser and S. J. Gill, *J. Phys. Chem.*, **71**, 564 (1966).
- (5) S. J. Gill, M. Downing, and G. F. Sheats, *Biochemistry*, **6**, 272 (1967).
- (6) E. L. Farquhar, M. Downing, and S. J. Gill, *Biochemistry*, **7**, 1224 (1968).
- (7) J. M. Sturtevant, *Fractions*, No. 1 (1969).
- (8) P. O. P. Ts'o, I. S. Melvir, and A. C. Olson, *J. Amer. Chem. Soc.*, **85**, 1289 (1963).

TABLE I: Thermodynamic Parameters for a Single Step in the Dissociation of Polymers of 6-Methylpurine in Water and of 6-Dimethylaminopurine in Various Solvents at 25°

Solvent	$10^2 K$ , M	$\Delta H$ , kcal mol <sup>-1</sup>	$\Delta G^\circ$ , kcal mol <sup>-1</sup>	$\Delta S^\circ$ , cal deg <sup>-1</sup> mol <sup>-1</sup>
6-Methylpurine				
H <sub>2</sub> O	12.9 ± 1.6	5.56 ± 0.05	1.21 ± 0.07	14.6 ± 0.1
6-Dimethylaminopurine				
H <sub>2</sub> O	1.62 ± 0.03	9.1 ± 0.1	2.44 ± 0.01	22.5 ± 0.3
0.01 M NaCl	1.47 ± 0.02	9.02 ± 0.08	2.50 ± 0.01	21.9 ± 0.2
0.1 M NaCl	1.72 ± 0.04	9.1 ± 0.1	2.40 ± 0.01	22.5 ± 0.3
1.0 M NaCl	1.71 ± 0.04	9.2 ± 0.2	2.41 ± 0.01	22.8 ± 0.6
0.1 M Na <sub>2</sub> SO <sub>4</sub>	1.72 ± 0.05	9.3 ± 0.2	2.40 ± 0.02	23.3 ± 0.6
1.0 M Na <sub>2</sub> SO <sub>4</sub>	1.07 ± 0.04	9.5 ± 0.2	2.68 ± 0.02	22.9 ± 0.6
0.1 M NaTCA <sup>a</sup>	2.36 ± 0.06	9.1 ± 0.1	2.22 ± 0.02	22.9 ± 0.3
1.0 M NaTCA	6.92 ± 0.02	7.3 ± 0.1	1.58 ± 0.01	19.2 ± 0.3
0.1 M NaOH	27.8 ± 1.2	5.2 ± 0.1	0.76 ± 0.03	15.1 ± 0.2
0.64 M dioxane	3.80 ± 0.05	9.4 ± 0.1	1.93 ± 0.01	25.1 ± 0.2
1.2 M CH <sub>3</sub> CN	3.81 ± 0.07	9.8 ± 0.1	1.93 ± 0.01	26.2 ± 0.3
4.8 M CH <sub>3</sub> CN	21.6 ± 0.1	8.0 ± 0.1	0.90 ± 0.01	23.7 ± 0.3

<sup>a</sup> Sodium trichloroacetate.

metric measurements, can be calculated with an accuracy largely determined by the accuracy of the measured equilibrium constant.

### Results and Discussion

The values of  $K$  and  $\Delta H$ , and derived values for  $\Delta G^\circ$  and  $\Delta S^\circ$ , are given in Table I for all systems for which a convergent calculation was possible. The values for 6-methylpurine agree well with those reported by Stoesser and Gill<sup>4</sup> on the basis of calorimetric data alone, namely,  $K = 0.116 \pm 0.030 m$  and  $\Delta H = 5.6 \pm 0.2 \text{ kcal mol}^{-1}$ .

In all cases the standard entropy of dissociation is positive. The cratic contribution,<sup>9</sup> arising from the unit increase in mole number at each dissociation step, lies between  $+8.0 \text{ cal deg}^{-1} \text{ mol}^{-1}$  in water and  $+7.7 \text{ cal deg}^{-1} \text{ mol}^{-1}$  in 4.8 M acetonitrile.

Gill, *et al.*,<sup>5</sup> reported for the dissociation of polymers of purine itself, the quantities  $\Delta H = 4.2 \pm 0.2 \text{ kcal mol}^{-1}$ ,  $\Delta G^\circ = 0.44 \text{ kcal mol}^{-1}$ , and  $\Delta S^\circ = 12.6 \text{ cal deg}^{-1} \text{ mol}^{-1}$ . We thus see a steady trend in all three thermodynamic parameters toward more positive values in the series purine, 6-methylpurine, and 6-dimethylaminopurine. It is usually considered<sup>3</sup> that interactions of hydrophobic origin are of importance in the association of purine derivatives in H<sub>2</sub>O, and some part of the increased association in this series is presumably to be attributed to such interactions. However, that this cannot be the full story is indicated by the fact that both  $\Delta H$  and  $\Delta S^\circ$  change in the direction opposite to that expected on the basis of increased orientation of water molecules on dissociation of the bases.<sup>10</sup> After deduction of the cratic contributions from the entropies, and  $-5$  to  $-10 \text{ cal deg}^{-1} \text{ mol}^{-1}$  from the value for 6-dimethylaminopurine to allow for additional structuring of water around the dimethylamino group, the entropy of dissociation for the substituted purine is seen to be four-five times as large as that for the parent substance. The origin of this significant difference cannot be specified at the present time.

A part of the increased association of 6-dimethylaminopurine as compared with purine can probably be attributed to the increased polarizability of the  $\pi$ -electron system of the former substance.<sup>3,11</sup>

The data in Table I show that the dissociation process in the case of 6-dimethylaminopurine is not significantly affected by sodium chloride up to a concentration of 1 M, as expected for the dissociation of a substance into two uncharged products. The effects produced by sodium sulfate and sodium trichloroacetate can be rationalized if it is assumed that the stacked bases are unaffected by the added salts while the monomeric base is salted out by sodium sulfate and salted in by sodium trichloroacetate.<sup>12</sup> On this basis

$$\Delta G_{\text{salt}}^\circ - \Delta G_{\text{H}_2\text{O}}^\circ = RT \ln (f_i/f_i^\circ) = K_s C_s \quad (5)$$

where  $f_i$  and  $f_i^\circ$  are respectively the molar activity coefficients in salt solution and in water,  $K_s$  is the salting out constant, and  $C_s$  is the salt concentration in moles per liter. The data for molar salt solutions give  $K_s = 0.41$  for sodium sulfate and  $K_s = -1.5$  for sodium trichloroacetate. From measurements of the solubility of adenine, Robinson and Grant<sup>12</sup> found values of 0.24 and  $-0.31$  for  $K_s$  for these two salts. Robinson and Grant suggest that salting in results from direct interaction of the salt anion with the base monomer. The decreased enthalpy and entropy of dissociation are consistent with this mechanism.

In 0.1 M NaOH (pH  $\approx 13$ ) 6-dimethylaminopurine carries a single negative charge, so that the tendency toward association is decreased by electrostatic repulsions. However, the changes observed for  $\Delta H$  and  $\Delta S^\circ$  are both of sign opposite to that expected on the basis of the simplest view of charged spheres interacting in a dielectric continuum, according to which

$$T\Delta\Delta S^\circ / \Delta\Delta G^\circ = \partial \ln D / \partial \ln T$$

$$\Delta\Delta H / \Delta\Delta G^\circ = 1 + (\partial \ln D / \partial \ln T) \quad (6)$$

where  $\Delta\Delta S^\circ = \Delta S^\circ(\text{uncharged}) - \Delta S^\circ(\text{charged})$  and  $D$  is the dielectric constant of the continuum. The value of  $\partial \ln$

(9) R. W. Gurney, "Ionic Processes in Solution," McGraw-Hill, New York, N. Y., 1953, p 90.

(10) W. Kauzmann, *Advan. Protein Chem.*, **14**, 1 (1959).

(11) H. DeVoe and I. Tinoco, Jr., *J. Mol. Biol.*, **4**, 500 (1962).

(12) D. R. Robinson and M. E. Grant, *J. Biol. Chem.*, **241**, 4030 (1966).



TABLE II: Empirically Determined Constants for Eq 4 at 25°

System	A, cal mol <sup>-1</sup>	B, cal mol <sup>-2</sup> l.	C, cal l. <sup>-1</sup>	Lower limit of K, <sup>a</sup> M
Adenosine-H <sub>2</sub> O	1050	0.55	38,500	0.002
6-Chloropurine-H <sub>2</sub> O	1440	2.0	20,980	0.002
6-Cyanopurine-H <sub>2</sub> O	670	1.6	3,375	0.003
6-Dimethylaminopurine-HCl (pH 2)	410	1.5	2,800	0.004
2'-Deoxyadenosine-H <sub>2</sub> O	1295	0.80	36,750	0.002
6-Methoxypurine-H <sub>2</sub> O	1065	0.65	37,950	0.002

<sup>a</sup> Minimum value of K for ±5% accuracy in ΔH.

TABLE III: Thermodynamic Parameters Calculated Using the Constants of Table II with Indicated<sup>a</sup> Assumed Values

Base	10 <sup>2</sup> K, M	ΔH, kcal mol <sup>-1</sup>	ΔG <sup>o</sup> , kcal mol <sup>-1</sup>	ΔS <sup>o</sup> , kcal deg <sup>-1</sup> mol <sup>-1</sup>
Adenosine	<b>22<sup>b</sup></b>	9.6	0.89	29
6-Chloropurine	19	5.4	1.02	15
6-Chloropurine	26	6.8	0.81	20
6-Cyanopurine	110	4.4	-0.06	15
6-Cyanopurine	150	5.7	-0.24	20
2'-Deoxyadenosine	<b>13<sup>c</sup></b>	6.1	1.19	16
2'-Deoxyadenosine	<b>21<sup>c</sup></b>	9.2	0.92	28
6-Dimethylaminopurine (pH 2)	140	4.3	-0.2	15
6-Methoxypurine	13	5.8	1.23	15
6-Methoxypurine	16	7.1	1.09	20

<sup>a</sup> Assumed values are given in boldface type. <sup>b</sup> Reference 17; K actually has the units moles per kg of water. <sup>c</sup> Reference 17; K actually has the units moles per kg of water; the lower value of K applies to concentrations below about 0.02 m, the higher value to higher concentrations.

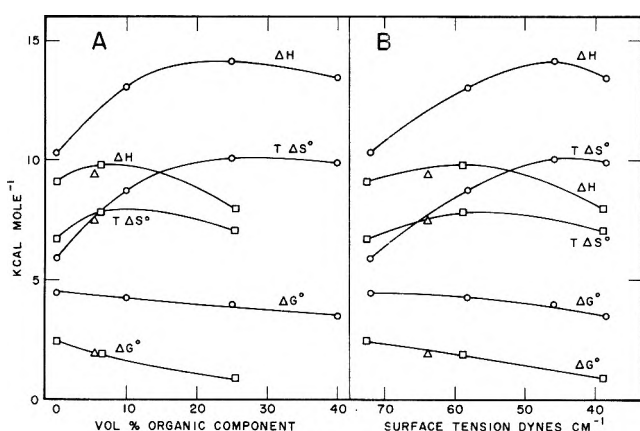


Figure 2. Influences of the addition of organic components on the thermodynamic parameters of dissociation reactions at 25°. Data of Crothers and Ratner<sup>14</sup> (O) on the dissociation of the complex of actinomycin and deoxyguanosine in methanol-water mixtures; present data on the dissociation of 6-dimethylaminopurine polymers in acetonitrile-water mixtures (□) and in 0.64 M dioxane (Δ). ΔH, TΔS<sup>o</sup>, and ΔG<sup>o</sup> are plotted as functions of the volume fraction of organic component in A, and of the solvent surface tension (interpolated to 25° (O); at 20° (□ and Δ)) in B.

$D/\partial \ln T$  for water at 25° is -1.36. Evidently, and not surprisingly, the effective dielectric constant for this system is very different from that of bulk water. In this connection it is interesting that a communication of Andrews and Haydon quoted by Howarth, *et al.*,<sup>13</sup> gives  $T\Delta S/\Delta G = +0.45$  for films of glycerol monoleate plus *n*-decane.

If it is assumed that the entropy of dissociation at low pH, where 6-dimethylaminopurine carries a positive charge, is the same as that when it is negatively charged,

the data of Table II give  $K = 1.4 M$ ,  $\Delta H = 4.3 \text{ kcal mol}^{-1}$ ,  $\Delta G^{\circ} = -0.2 \text{ kcal mol}^{-1}$ , and  $\Delta S^{\circ} = +15 \text{ cal deg}^{-1} \text{ mol}^{-1}$  (Table III). However, even if this assumption is correct, this calculation represents a long extrapolation from the very small heats of dilution observed with solutions approximately 0.05 M in base.

6-Dimethylaminopurine is less associated in solutions containing dioxane or acetonitrile than in pure water. The initial increase in the enthalpy and entropy of dissociation followed by a decrease in both quantities as the concentration of acetonitrile is increased (Table I and Figure 2A) is similar to that observed by Crothers and Ratner<sup>14</sup> for the dissociation of the complex of actinomycin with deoxyguanosine in methanol water mixtures. These authors interpreted the initial rise in the enthalpy and entropy of dissociation as indicative of a significant hydrophobic<sup>10</sup> contribution to the association reaction.

Sinanoğlu<sup>15,16</sup> has proposed as an important source of binding energy for large molecules the surface energy required to form cavities around the molecules in the system. In an association reaction, the cavities around the two reactant species have a larger total surface area than the single cavity around the product, so that surface forces literally squeeze the reactants together. This picture leads to enthalpy and entropy changes of opposite sign to those expected to result from hydrophobic interactions, and the decrease of enthalpy and entropy observed in 4.8 M acetonitrile may thus be an indication that this mecha-

(13) J. V. Howarth, R. D. Keynes, and J. M. Ritchie, *J. Physiol.*, **194**, 745 (1968).

(14) D. M. Crothers and D. I. Ratner, *Biochemistry*, **7**, 1823 (1968).

(15) O. Sinanoğlu and S. Abdulnur, *Federation Proc.*, **24**, 5 (1965).

(16) O. Sinanoğlu in "Molecular Associations in Biology," B. Pullman, Ed., Academic Press, New York, N. Y., 1968, p 427.

nism is also operative. Additional support for this view may be drawn from the fact that our data and those of Crothers and Ratner<sup>14</sup> exhibit greater qualitative similarity when plotted as functions of surface tension (Figure 2B) than as functions of volume fraction (Figure 2A).

Broom, *et al.*,<sup>17</sup> have reported equilibrium data for the association of adenosine ( $K = 0.22 M$ ) and 2'-deoxyadenosine ( $K = 0.13-0.21 M$ ) in water at 25°. Using these values and the constants in Table II, we obtain the thermodynamic parameters given in Table III. Preliminary values for 6-chloropurine, 6-cyanopurine, and 6-methoxypurine are also given in Table III, based on assignment of the values 15 and 20 cal deg<sup>-1</sup> mol<sup>-1</sup> for the entropy of dissociation. The equilibrium constant calculated in this way for cyanopurine is surprisingly high; as-

sumption of a lower value for the entropy lowers the equilibrium constant, for example,  $\Delta S^\circ = 0$  gives  $K = 0.37 M$ .

It is to be emphasized that we are still very far from being able to give a satisfactory interpretation of the thermodynamics of association of molecules such as the purine bases in qualitative terms, to say nothing of quantitative explanations.

*Acknowledgments.* This research was aided by grants from the National Science Foundation (GB 23545) and the National Institutes of Health of the United States Public Health Service (GM 04725).

(17) A. D. Broom, M. P. Schweizer, and P. O. P. Ts'o, *J. Amer. Chem. Soc.*, **89**, 3612 (1967).

## The Association of Heptanol-1 in Carbon Tetrachloride from Static Dielectric Measurements

P. Bordewijk,\* M. Kunst, and A. Rip

*Gorlaeus Laboratories, Department of Physical Chemistry II, University of Leiden, Leiden, The Netherlands*  
(Received July 12, 1972)

Static dielectric constants have been determined of solutions of heptanol-1 in carbon tetrachloride in the concentration range from 0.1 to 3 mol % at temperatures from 25 to 45°. Possible interpretations are a monomer-dimer-trimer equilibrium (heats of association for dimer and trimer 9 and 17 kcal/mol, respectively) and a monomer-dimer-tetramer equilibrium (heats of association for dimer and tetramer 9 and 26 kcal/mol, respectively). The measurements confirm Ibbitson and Moore's conclusion that the dimer is linear.

### Introduction

In spite of many investigations with different techniques, still no general agreement has been obtained concerning the structure of the multimers formed due to the self-association of the mono-alcohols.<sup>1-9</sup> An important type of technique is the measurement of a physical quantity that is built up from contributions of the various types of multimers as a function of the formal concentration in a nonpolar solvent. The physical quantity may be the infrared absorption at some deliberately chosen frequency,<sup>10-13</sup> the chemical shift in nuclear magnetic resonance,<sup>14-17</sup> the vapor pressure,<sup>4</sup> or the apparent value of the square of the molecular dipole moment.<sup>18-20</sup> Measurements of the lowering of the freezing point, of the partition coefficient with respect to water, and of the osmotic pressure fall under the same category. Also investigations combining different methods<sup>21-23</sup> have been reported.

The physical quantity under investigation need not depend on all multimers present in all cases. For instance, the ir absorption may only depend on the concentration of open multimers, and both the vapor pressure in a nonvolatile solvent and the partition coefficient for organic solvents with respect to water<sup>22</sup> depend only on the concen-

tration of monomers. This simplifies the calculations, but not enough to get unambiguous results.

Apart from incidental failures in the application of the measuring technique, and from unjustified *a priori* as-

- (1) S. N. Vinogradov and R. H. Linell, "Hydrogen Bonding," Van Nostrand-Reinhold, New York, N. Y., 1971.
- (2) P. Bordewijk, Thesis, University of Leiden, 1968.
- (3) P. Bordewijk, F. Gransch, and C. J. F. Böttcher, *J. Phys. Chem.*, **73**, 3255 (1969).
- (4) E. Tucker, S. B. Farnham, and S. D. Christian, *J. Phys. Chem.*, **73**, 3820 (1969).
- (5) J. Crossley, *Advan. Mol. Relaxation Processes*, **2**, 69 (1970).
- (6) W. Dannhauser and A. F. Flueckinger, *Phys. Chem. Liquids*, **2**, 37 (1970).
- (7) J. Dos Santos, J. Biais, and P. Pineau, *J. Chim. Phys.*, **67**, 814 (1970).
- (8) J. Crossley, L. Glasser, and C. P. Smyth, *J. Chem. Phys.*, **55**, 2197 (1971).
- (9) A. N. Fletcher, *J. Phys. Chem.*, **75**, 1808 (1971).
- (10) A. Ens and F. C. Murray, *Can. J. Chem.*, **35**, 70 (1957).
- (11) W. C. Coburn, Jr., and E. Grunwald, *J. Amer. Chem. Soc.*, **80**, 1318 (1958).
- (12) G. Geiseler and E. Stockel, *Spectrochim. Acta*, **17**, 1185 (1961).
- (13) H. Dunken and H. Fritzsche, *Spectrochim. Acta*, **20**, 785 (1964).
- (14) L. K. Patterson and R. M. Hammaker, *Spectrochim. Acta*, **23A**, 2333 (1967).
- (15) W. Storek and H. Kriegsmann, *Ber. Bunsenges. Phys. Chem.*, **72**, 706 (1968).
- (16) W. D. Dixon, *J. Phys. Chem.*, **74**, 1396 (1970).

sumptions concerning the association of the alcohols, two reasons may be given why most conclusions of the work on the self-association of the mono-alcohols published until now are unreliable.

(1) In a great number of articles measurements in the complete concentration range from diluted solutions up to the pure alcohols are analyzed as if the association were ideal; *i.e.*, all equilibria are assumed to be determined by equilibrium constants, independent of the medium.<sup>24</sup> It is known, however, that quantities depending on the association of an alcohol differ for different nonpolar solvents; moreover, the dielectric constant of the solution changes with the concentration making considerable changes of the equilibrium constants over the whole concentration range plausible.

(2) When the quantity studied as a function of the formal concentration increases or decreases monotonously with this concentration (as is the case in most experiments), one needs very accurate measurements to discriminate between different association schemes proposed.

To be able to draw more reliable conclusions we have turned to a quantity that does not vary monotonously with the formal concentration, *i.e.*, the apparent value of the square of the dipole moment. It has been known for a long time<sup>25</sup> that for the normal alcohols this quantity shows a minimum as a function of the concentration in solvents like cyclohexane and carbon tetrachloride. More recently,<sup>26</sup> a maximum at very low concentrations was found. Since this maximum lies within the concentration range where it seems plausible that the deviations of the ideal association may be neglected, we have studied the association of one alcohol (heptanol-1) in carbon tetrachloride in the concentration range up to 3 mol % with the help of static dielectric measurements at 25, 30, 35, 40, and 45°.

### Experimental Procedure

*a. Materials.* Heptanol-1 was supplied by Fluka (purum), dried on CaSO<sub>4</sub> and afterward distilled. Carbon tetrachloride was supplied by Baker (pA quality) also dried on CaSO<sub>4</sub> and distilled over a glass column.

*b. Experimental Equipment.* Dielectric constants were determined with a two-terminal cell described by De Vos.<sup>27</sup> Use was made of a water thermostat, with a capacity of 45 l., that made possible a temperature control to within 0.02° by circulation of the water through the outer electrode of the cell. To diminish the influence of variations of the cell constant and of the connecting wires as far as possible, before and after each determination of the capacity of the cell filled with the solution under investigation, the capacity of the cell was determined when filled with the pure solvent from the same sample as used to prepare the solution (the dielectric constant of the pure solvent was assumed to be equal to its literature value<sup>28</sup>). Only those measurements were considered where the capacity of the cell, filled with the pure solvent, as determined after the measurement of the solution did not differ by more than 0.004 pF from its value before the measurement, corresponding to a variation in  $\epsilon$  of 0.00006. In this way not only variations of the capacity of the empty cell and the connecting wires over more than 5 min but also the direct influence of impurities of the solvent were eliminated. The cell constant was determined from the difference between the capacity of the empty cell and the cell filled with carbon tetrachloride, using the dielectric constant of carbon tetrachloride given in the literature.<sup>28</sup>

For each temperature densities were determined for a few concentrations only with pycnometers of about 10 ml, calibrated with distilled water. At each temperature the specific volume was considered to depend linearly on the concentration for the concentration range studied.

### Experimental Results

From the values of  $\epsilon$  determined experimentally,<sup>29</sup> apparent values of the square of the molecular dipole moment,  $(\mu^2)_{app}$ , were calculated with the help of the equation

$$\langle \mu^2 \rangle_{app} = \frac{9kT(2\epsilon + \epsilon_\infty)^2}{4\pi N_A x(\epsilon_\infty + 2)^2(2\epsilon + 1)} \left[ \frac{\phi(\epsilon - 1)}{\epsilon} - \frac{3(1-x)(\epsilon_0 - 1)\phi_1}{2\epsilon + \epsilon_0} - \frac{3x(\epsilon_x - 1)\phi_2}{2\epsilon + \epsilon_x} \right] \quad (1)$$

Here  $\epsilon$  is the dielectric constant of the solution,  $\epsilon_\infty$  is the dielectric constant of induced polarization for the pure solute, estimated<sup>30</sup> to be  $\epsilon_\infty = 1.05n_D^2$ ,  $\epsilon_0$  is the dielectric constant of the pure solvent,  $x$  is the formal concentration of the solute expressed in molar fractions,  $\phi$  is the molar volume of the solution,  $\phi_1$  is that of the pure solvent, and  $\phi_2$  is that of the pure solute. Equation 1 is equivalent with the equation given by Huyskens and Cracco<sup>31</sup> except for the fact that these authors take  $\epsilon_\infty = n_D^2$ . The equation is based on Onsager's treatment<sup>32,33</sup> of the internal field, applied to a mixture consisting of the solvent and different types of multimers, assuming that the polarizability of a multimer is proportional to the number of alcohol molecules it contains.

For all temperatures the experimental values of  $(\mu^2)_{app}$  are given in Figure 1. It appears from this figure that the value of the formal concentration where  $(\mu^2)_{app}$  has a maximum increases with increasing temperature, as could be expected since an increase of the temperature reduces the association.

At 25° an inflexion point occurs within the concentration range studied. At higher temperatures there is no inflexion point visible; it can be presumed to occur at higher concentrations since it is known that for the pure hep-

- (17) J. Biais, J. Dos Santos, B. Lemanceau, *J. Chim. Phys.*, **67**, 806 (1970).
- (18) Th. Clerboux and Th. Zeegers-Huyskens, *Bull. Soc. Chim. Belges*, **75**, 366 (1966).
- (19) R. van Loon, J. P. Dauchot, and A. Bellemans, *Bull. Soc. Chim. Belges*, **77**, 397 (1968).
- (20) H. A. Rizk and N. Youssef, *Z. Phys. Chem. (Leipzig)*, **244**, 413 (1969).
- (21) P. Huyskens, Th. Huyskens-Zeegers, and J. Capart, *Bull. Soc. Chim. Belges*, **68**, 515 (1959).
- (22) E. Meeuwse and P. Huyskens, *J. Chim. Phys.*, **63**, 845 (1966).
- (23) J. Dos Santos, F. Cruege, and P. Pineau, *J. Chim. Phys.*, **67**, 826 (1970).
- (24) I. Prigogine and R. Defay, "Chemical Thermodynamics," Longmans, Green and Co., New York, N. Y., 1954 p 411.
- (25) G. Oster, *J. Amer. Chem. Soc.*, **68**, 2036 (1946).
- (26) D. A. Ibbotson and L. F. Moore, *J. Chem. Soc. B*, **76** (1967).
- (27) F. C. De Vos, Thesis, University of Leiden, 1958.
- (28) A. A. Maryott and E. R. Smith, "Table of Dielectric Constants of Pure Liquids," *Nat. Bur. Stand. (U. S.) Circ.* **514**, (1951).
- (29) Listings of experimental values of  $\epsilon$  and  $(\mu^2)_{app}$ , together with values of  $(\mu^2)_{app}$  calculated with the various models considered, will appear immediately following this article in the microfilm edition of this volume of the journal. Single copies may be obtained from the Business Operations Department, Books and Journals Division, American Chemical Society, 1155 Sixteenth St., N.W., Washington, D. C., 20036. Remit check or money order for \$3.00 for photocopy or \$2.00 for microfiche, referring to code number JPC-73-548.
- (30) W. Dannhauser, *J. Chem. Phys.*, **48**, 1911 (1968).
- (31) P. Huyskens and F. Cracco, *Bull. Soc. Chim. Belges*, **69**, 422 (1960).
- (32) L. Onsager, *J. Amer. Chem. Soc.*, **58**, 1486 (1936).
- (33) C. J. F. Böttcher, "Theory of Electric Polarisation," Elsevier, Amsterdam 1952.

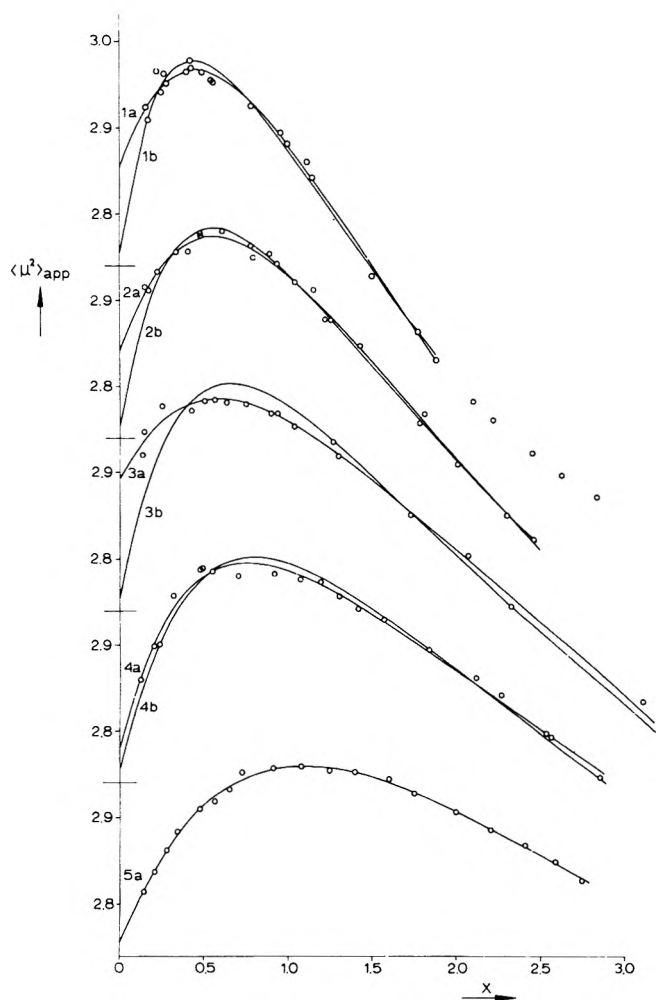


Figure 1. Values of  $\langle \mu^2 \rangle_{app}$  ( $D^2$ ) as a function of the concentration in mol %. Ordinates shifted consecutively over 0.2 scale unit: 1, 25°; 2, 30°; 3, 35°; 4, 40°; 5, 45°; O, experimental values; —, calculated best fits for the monomer-dimer-trimer model, (a) with variation of  $\mu_1$ ,  $K_2$ ,  $g_2$ , and  $K_3$ , and  $g_3 = 0$ , and (b) with variation of  $K_2$  and  $K_3$  and  $\mu_1 = 1.660$  D,  $g_2 = 2.26$ ,  $g_3 = 0$ .

tanol the apparent value of the square of the dipole moment lies above the value in dilute solutions.<sup>34</sup>

#### Numerical Adjustment to Simple Association Models.

From the method of derivation it follows that the apparent value of the square of the molecular dipole moment as it can be calculated from eq 1 is an average over all types of multimers present, in the following way

$$\langle \mu^2 \rangle_{app} = \frac{\sum_i C_i \langle \mu^2 \rangle_i}{x} \quad (2)$$

The symbol  $\langle \mu^2 \rangle_i$  denotes the average of the square of the dipole moment of the multimers containing  $i$  molecules; it must be mentioned that it is not necessary that all multimers with  $i$  molecules have the same structure. The amount of multimers containing  $i$  molecules is denoted by  $C_i$ ;  $C_i$  denotes the fraction of multimers containing  $i$  molecules with respect to the total number of solvent molecules and monomeric units; thus one has

$$x = \sum_i i C_i \quad (3)$$

We now introduce quantities  $g_i$  given by

$$g_i = \frac{\langle \mu^2 \rangle_i}{i \mu_1^2} \quad (4)$$

where  $\mu_1$  is the dipole moment of the monomer. If  $g_i > 1$ , the formation of multimers with  $i$  molecules from monomers tends to increase the dielectric constant; for  $g_i < 1$ , it tends to decrease the dielectric constant. It is also possible to define a quantity  $g$  which characterizes the effect on the dielectric constant of the association equilibrium for a given temperature and formal concentration

$$g = \frac{\sum_i i C_i g_i}{x} = \frac{\langle \mu^2 \rangle_{app}}{\mu_1^2} \quad (5)$$

This quantity is chosen in such a way that for the pure alcohol eq 1 changes into the Kirkwood-Fröhlich equation<sup>35,36</sup>

$$g \mu_1^2 = \frac{9kTM}{4\pi N_A d} \frac{(\epsilon - \epsilon_\infty)(2\epsilon + \epsilon_\infty)}{\epsilon(\epsilon_\infty + 2)^2} \quad (6)$$

It may be noted in passing that in this way eq 6 is obtained by applying the Onsager treatment to a mixture of multimers. It follows that eq 1 may be considered a generalization of the Kirkwood-Fröhlich equation for solutions.

Assuming ideal association we can write

$$C_i = K_i (C_1)^i \quad (7)$$

It must be mentioned that the  $C_i$ 's are not exactly equal to the concentrations in molar fractions, since according to eq 3  $C_i$  is obtained by dividing the amount of  $i$ -mers by the sum of the number of solvent molecules and the number of monomeric units instead of the sum of the number of solvent molecules and the total number of multimers. For this reason in eq 7 every  $C_i$  should be corrected by a factor  $(1 - x - \sum_i C_i)^{-1}$  that was neglected to make the calculations not more intricate than necessary. The error introduced in this way is of the same order as the neglect of deviations of ideality, or perhaps even smaller.

After substitution of eq 7, eq 2 and 3 change into

$$\langle \mu^2 \rangle_{app} = \frac{1}{x} \sum_i K_i (C_1)^i g_i \mu_1^2 \quad (8)$$

$$x = \sum_i i K_i (C_1)^i \quad (9)$$

Considering eq 9 as a power series in  $C_1$ , the series can be inverted to obtain an expression for  $C_1$  as a power series in  $x$  that can be substituted into eq 8. This leads to a general expression for  $\langle \mu^2 \rangle_{app}$  as a power series in  $x$  with coefficients expressed in terms of  $\mu_1^2$ ,  $K_i$  and  $g_i$

$$\begin{aligned} \langle \mu^2 \rangle_{app} = & \mu_1^2 [1 + 2K_2(g_2 - 1)x + \{3K_3(g_3 - 1) - \\ & 8K_2^2(g_2 - 1)\}x^2 + \{4K_4(g_4 - 1) - 13K_2K_3(g_3 - 1) + \\ & (40K_2^3 - 12K_2K_3 + 2K_2^2)(g_2 - 1)\}x^3 + \dots] \quad (10) \end{aligned}$$

(In this equation the correction factors for the  $C_i$  have also been taken into account.)

It did not appear to be possible, however, to use a polynomial fit of  $\langle \mu^2 \rangle_{app}$  as a function of  $x$  to obtain values of

(34) P. Bordewijk, F. Gransch, and C. J. F. Böttcher, *Trans. Faraday Soc.*, **66**, 293 (1970).

(35) J. G. Kirkwood, *J. Chem. Phys.*, **7**, 911 (1939).

(36) H. Fröhlich, "Theory of Dielectrics," Oxford University Press, London, 1949.

TABLE I: Parameters for the Monomer-Dimer-Trimer Model

	t, °C				
	25	30	35	40	45
$\mu_1, D$	1.690	1.686	1.701	1.666	1.660
$K_2, (\text{mol } \%)^{-1}$	0.039	0.056	0.082	0.181	0.068
$g_2$	3.45	2.69	1.78	1.82	2.26
$K_3, (\text{mol } \%)^{-2}$	0.073	0.058	0.038	0.071	0.028
$g_3$	0.00	0.00	0.00	0.00	0.00
$\sigma$	0.009	0.006	0.008	0.008	0.003
$\sqrt{v}$	0.007	0.006	0.007	0.006	0.003

these coefficients, since the extrapolation to  $x = 0$  that is involved leads to large uncertainties. Reduction of the uncertainties through measurements at still lower concentrations is not feasible because of the increased inaccuracy of the measurements.

Therefore, we decided to consider  $C_1$  in eq 8 and 9 as a parameter and optimize eq 8 and 9 simultaneously for a number of simple association models. When  $n$  is the maximum size of the multimers present to a nonnegligible extent in the concentration range studied, the values of  $\mu_1, K_2, \dots, K_n$  and  $g_2, \dots, g_n$  have to be determined. Such a determination is possible with the help of a computer program in which the deviation between experimental and calculated values of  $\langle \mu^2 \rangle_{\text{app}}$  and  $x$  is minimized. As the quantity to be minimized we have taken  $d^2 = \sum_j \{(\Delta x_j)^2 / x_j^2 + (\Delta \langle \mu^2 \rangle_{\text{app},j})^2\}$  where the index  $j$  indicates the measurements at different formal concentrations at each temperature and  $\Delta$  denotes the difference between the experimental and calculated values.

It appeared that the relation between  $\langle \mu^2 \rangle_{\text{app},j}$  and  $x_j$  (via  $C_{1,j}$ ) was too complicated to admit simultaneous variation of all unknown parameters during the minimization procedure. Therefore, another computer program was used in which the values of the equilibrium constants only were varied for given values of  $\mu_1$  and  $g_2, \dots, g_n$ . Minimization now easily led to the "best" values for  $K_2, \dots, K_n$  adjusted to the given values of  $\mu_1$  and  $g_2, \dots, g_n$ . Then other combinations of values for  $\mu_1$  and  $g_2, \dots, g_n$  were tried until a minimum value for  $d^2$  was reached. Since this adjustment by trial and error demands a large amount of computer time, we performed the calculations in the simplest possible manner.

To account for the occurrence of a maximum in the values of  $\langle \mu^2 \rangle_{\text{app}}$ , at least two types of multimers have to be used. The simplest model compatible with this condition is the monomer-dimer-trimer model with  $g_3 = 0$ . The values of  $\mu_1, g_2, K_2$ , and  $K_3$  obtained for this model are given in Table I. (In the calculation the points at 25° above 2 mol % were discarded, since the occurrence of an inflexion point at about 2 mol % indicates the influence of larger multimers with a high dipole moment). The assumption  $g_3 = 0$  has been checked at 45° where a slight increase of  $g_3$  leads to higher values of  $d^2$ .

The graphs of  $\langle \mu^2 \rangle_{\text{app}}$  as a function of  $x$  corresponding to the values of the parameters in Table I are given in Figure 1 (curves denoted by a). With the help of these graphs values of  $\langle \mu^2 \rangle_{\text{app}}$  were interpolated at the formal concentrations at which the measurements were made. From these values the standard deviation  $\sigma$ , defined by

$$\sigma^2 = \frac{1}{l} \sum_{j=1}^l (\Delta \langle \mu^2 \rangle_{\text{app},j})^2$$

has been calculated (see Table I).

For comparison we also entered in Table I the standard deviation obtained when polynomial fitting is applied for  $\langle \mu^2 \rangle_{\text{app}}$  as a function of  $x$ , using polynomials of an increasing degree  $m$ , until the error variance<sup>37</sup>

$$v = \frac{1}{l-m} \sum_{j=1}^l (\Delta \langle \mu^2 \rangle_{\text{app},j})^2$$

is minimal.

Since the monomer-dimer-trimer model leads to standard deviations only slightly larger than the square root of the minimal error variance for polynomial fitting, it can be concluded that the parameters of the model given in Table I contain almost all information contained in the experimental values of  $\langle \mu^2 \rangle_{\text{app}}$  as a function of  $x$ .

It is not possible, however, to attach a physical meaning to the values of the parameters in Table I in view of the absence of a systematic temperature dependence of the values of  $K_2$  and  $K_3$ , and the rather improbable temperature dependence of  $g_2$ . The reason for this behavior is that rather large complementary shifts in the values of the parameters are possible that do not affect the deviation  $d$ . It is clear from the experimental points, especially for the lower temperatures, that unequivocal extrapolation to  $x = 0$  is not possible. Thus a shift in *e.g.*,  $K_2$  can be compensated by a shift in  $\mu_1$ . Compensating shifts in the values of the parameters are restricted to the smallest range at 45°, where the experimental points show the smallest scatter, and the extrapolation to  $x = 0$  is more reliable than at lower temperatures since the maximum in  $\langle \mu^2 \rangle_{\text{app}}$  is found at higher values of  $x$ .

To obtain information on the temperature dependence of the equilibrium constants, fixed values for  $\mu_1, g_2$ , and  $g_3$  have been chosen, based on the values of these parameters at 45°, for the minimization procedure at the lower temperatures. This implies that whereas in the foregoing calculation the possibility was kept open of an equilibrium between dimers of different structure (*e.g.*, open and closed), leading to different values of  $g_2$  at different temperatures, in this calculation only one kind of dimers is supposed to be present. It must be pointed out that the value of  $g_2$  used in the calculation ( $g_2 = 2.26$ ) cannot be obtained by vector addition of the dipole moments of the monomeric units, which leads to a maximum value  $g_2 = 2$  in the case of parallel dipole moments; it is possible, however, that due to the formation of the hydrogen bond an enlargement of one of the dipole moments occurs, as calculated by Hoyland and Kier for the methanol dimer.<sup>38</sup>

With regard to the value  $g_3 = 0$ , this value can be made plausible by assuming the trimer to be cyclic. Assuming tetrahedral bond angles for the oxygen atom, one finds an H...O-H bond angle of 109°, leading to a hydrogen bond angle (O-H...O) of 131°. One then has complete compensation of the OH dipole moments, and of the components of the OR dipole moments in the plane of the hydroxyl groups. Assuming two aliphatic chains at one side of this plane, and one at the other side, the dipole moment of the cyclic trimer is equal to the component of one OR dipole perpendicular to the plane of the hydroxyl groups, that is<sup>39</sup>

(37) J. Mandel, "The Statistical Analysis of Experimental Data," 1964, p 163.

(38) J. R. Hoyland and L. B. Kier, *Theoret. Chim. Acta.* **15**, 1 (1969).

(39) C. P. Smyth, "Dielectric Behavior and Structure," McGraw-Hill, New York, N. Y., 1955, p 301.

$$\mu_3 = 1.14 \cos 55^\circ = 0.65 D \quad (11)$$

and

$$g_3 = \mu_3^2 / 3\mu_1^2 = 0.05 \approx 0 \quad (12)$$

The values of  $K_2$  and  $K_3$  obtained in this way are given in Table II; the corresponding graphs for  $\langle \mu^2 \rangle_{app}$  as a function of  $x$  are given in Figure 1 (curves denoted by b). The standard deviations (calculated on the basis of interpolated  $\langle \mu^2 \rangle_{app}$  values) are somewhat larger than in the case of arbitrary  $\mu_1$  and  $g_2$ , as could be expected. Only at  $35^\circ$  is the adjustment rather bad; at this temperature, however, the experimental points show a large scatter at low values of  $x$ .

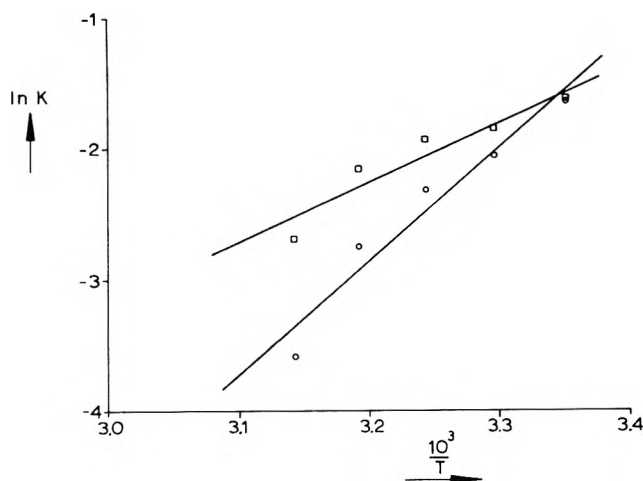


Figure 2. Arrhenius plots for the equilibrium constants calculated with the monomer-dimer-trimer model:  $\square$ ,  $K_2$ ;  $\circ$ ,  $K_3$ .

TABLE II: Equilibrium Constants for the Monomer-Dimer-Trimer Model Calculated on the Basis of  $\mu_1 = 1.660 D$ ,  $g_2 = 2.26$ ,  $g_3 = 0$

	$t, ^\circ C$				
	25	30	35	40	45
$K_2, \text{mol } \%^{-1}$	0.190	0.158	0.145	0.117	0.068
$K_3, (\text{mol } \%)^{-2}$	0.192	0.127	0.098	0.064	0.028
$\sigma$	0.012	0.011	0.023	0.012	0.003

The values of the equilibrium constants in Table II show a regular trend, decreasing with increasing temperature. Plotting  $\log K$  against  $1/T$  (see Figure 2), apparent heats of association can be obtained of 8.9 kcal/mol for the dimers and 17.2 kcal/mol for the trimers.

To check the significance of these results, other models with an equal number of parameters must be considered. For methanol in the vapor phase, Fletcher<sup>9</sup> found with the help of infrared measurements that there occurs association to dimers and tetramers. For this reason we also analyzed our data on the basis of a monomer-dimer-tetramer model. The measurements at  $45^\circ$  then lead to the following values of the parameters:  $\mu_1 = 1.657 D$ ,  $g_2 = 1.34$ ,  $g_4 = 0.19$ ,  $K_2 = 0.304 (\text{mol } \%)^{-1}$ ,  $K_4 = 0.0280 (\text{mol } \%)^{-3}$  with a standard deviation of 0.003, that is to say, of the same magnitude as in the case of the monomer-dimer-trimer model.  $K_2$  and  $K_4$  were determined at the lower temperatures with the help of the minimization procedure and with  $\mu_1$ ,  $g_2$ , and  $g_4$  held fixed at the values obtained

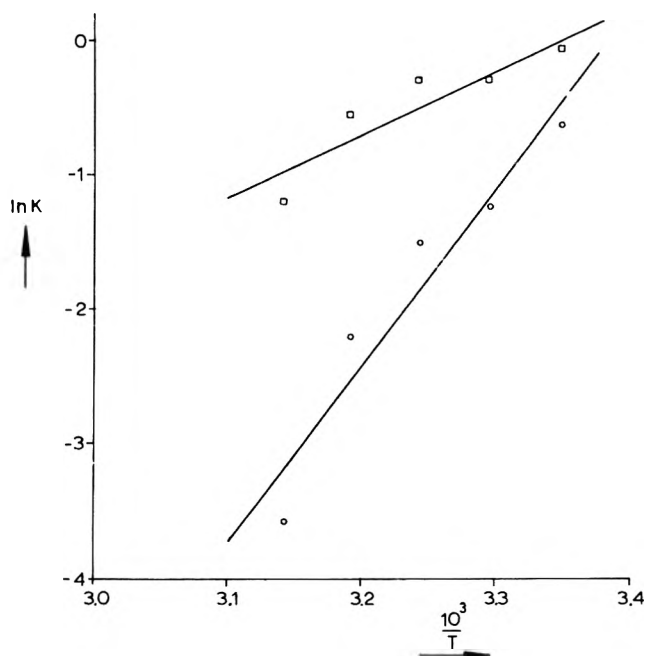


Figure 3. Arrhenius plots for the equilibrium constants calculated with the monomer-dimer-tetramer model:  $\square$ ,  $K_2$ ;  $\circ$ ,  $K_4$ .

TABLE III: Equilibrium Constants for the Monomer-Dimer-Tetramer Model Calculated on the Basis of  $\mu_1 = 1.657 D$ ,  $g_2 = 1.34$ ,  $g_4 = 0.19$

	$t, ^\circ C$				
	25	30	35	40	45
$K_2, (\text{mol } \%)^{-1}$	0.87	0.74	0.74	0.57	0.304
$K_4, (\text{mol } \%)^{-3}$	0.52	0.290	0.217	0.107	0.0280
$\sigma$	0.011	0.010	0.025	0.009	0.003

at  $45^\circ$ . The results are given in Table III. Standard deviations have been calculated with the help of interpolated values of  $\langle \mu^2 \rangle_{app}$ .

The standard deviations are comparable with the standard deviations in the case of the monomer-dimer-trimer model. The values of  $K_2$  and  $K_4$  in Table III show a regular temperature dependence; an Arrhenius plot (see Figure 3) leads to values for the apparent heats of association of 9.0 kcal/mol for the dimers and 26 kcal/mol for the tetramers.

Figures 4 and 5 show the distribution of the heptanol-1 molecules over the multimers of different sizes assumed to be present, as a function of the formal concentration at 25 and  $45^\circ$ , for the monomer-dimer-trimer, and the monomer-dimer-tetramer model, respectively, based on the values of the parameters given in Tables II and III. In accordance with the higher values of  $K_2$  and  $K_4$  for the monomer-dimer-tetramer model compared with the values of  $K_2$  and  $K_3$  for the monomer-dimer-trimer model, the average multimer size is much smaller for the latter model. This corresponds to the higher values for the dipole moments found for this model.

## Discussion

A number of conclusions can be drawn from the general features of the experimental results independent of the results of the numerical adjustment to simple association models. Our measurements confirm the results of Ibbitson

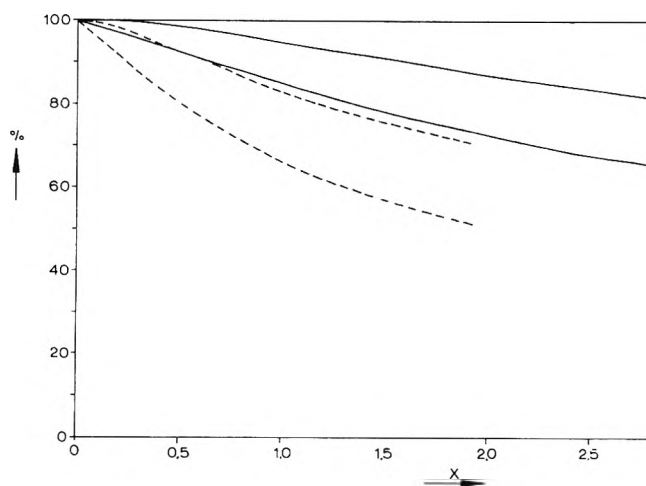


**Figure 4.** Distribution of the heptanol-1 molecules over monomers (lower), dimers (middle), and trimers (upper): . . . , 25°; —, 45°.

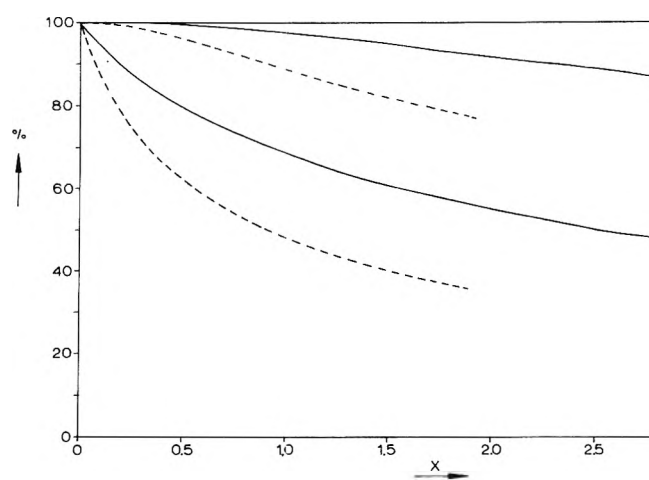


**Figure 5.** Distribution of the heptanol-1 molecules over monomers (lower), dimers (middle), and tetramers (upper): . . . , 25°; —, 45°.

and Moore<sup>26</sup> in that at low concentrations a maximum is found for the apparent value of the square of the molecular dipole moment. It follows that, for the mono-alcohols, at least three kinds of multimers must be distinguished: large multimers with a high dipole moment (dominating for the normal alcohols in the pure state), a smaller multimer with a low dipole moment, and a very small multimer with again a relatively high dipole moment. This is contrary to the assumption, made by one of us in former publications<sup>2,34</sup> as well as by Dannhauser and Johari,<sup>30,40</sup> that the multimers with a low dipole moment should be identified as cyclic dimers. It follows from our results that if dimers occur to a nonnegligible extent, they must have a relatively high dipole moment. Furthermore, if no dimers were formed, the limiting value  $(\partial\langle\mu^2\rangle_{\text{app}}/\partial x)_{x\rightarrow 0}$  would be zero, as follows from eq 10 for  $K_2 = 0$ . Since the values of  $\langle\mu^2\rangle_{\text{app}}$  found at the highest temperature where measurements were done do not show any indication of this behavior it is plausible that the dimers play an important role indeed; the high dipole moment of these associates then leads to the assumption that their structure is linear. This is in agreement with CNDO/2 calculations on the association of methanol by Murthy, *et al.*,<sup>41</sup> and by Hoyland and Kier,<sup>38</sup> who also found a linear structure for the dimer.

Not all papers on the association of the mono-alcohols published recently report the occurrence of dimers. Tucker, *et al.*,<sup>4</sup> concluded from their vapor pressure measurements on methanol in *n*-hexadecane that the association could be described using monomers, trimers, and octomers only. Fletcher<sup>9</sup> has criticized the experiments; apart from that, one may object to the calculations. It appears<sup>42</sup> that if one considers only three kinds of associates like Tucker, *et al.*, did, not the monomer-trimer-octomer model but the monomer-tetramer-decamer model gives the best adjustment. If one allows four kinds of associates one finds the best adjustment for the monomer-dimer-pentamer-hendecamer model. It is clear that numerical calculations of this type cannot decide whether or not dimers occur in the solution of methanol in *n*-hexadecane. Dixon<sup>16</sup> concluded from nmr measurements on methanol in cyclohexane and cyclopentane that only monomers and tetramers would occur. Taking into account the relative

insensibility of the chemical shift to changes in multimer composition, as compared with dielectric measurements, it appears that their conclusion is rather ill-founded.

From nmr measurements on alcohols with a strongly branched carbon skeleton, like<sup>43,44</sup> 2,2,3-trimethylpentanol-3 and 2,2,4,4-tetramethylpentanol-3, it was concluded that these alcohols would only associate to dimers. If this conclusion is correct, these alcohols, on the basis of our results, are expected to show at higher concentrations a dielectric constant higher than would be expected if also greater multimers were formed.

From the above argument we conclude that the existence at low concentrations of open dimers is reasonably well founded. Whether the next higher multimer is the trimer or the tetramer cannot be decided with the help of the numerical analysis of our experimental results. Since the differences between the results for the monomer-dimer-trimer and the monomer-dimer-tetramer adjustment are much smaller than the differences between these adjustments and the experimental values,<sup>29</sup> it may not be expected that it will be possible to discriminate between the association models mentioned by improving the experimental accuracy. Data on the average multimer size would be very valuable, since we find this quantity to be much higher for the monomer-dimer-tetramer model than for the monomer-dimer-trimer model.

On the basis of the results of Fletcher,<sup>9</sup> as well as on the basis of the calculations of Hoyland and Kier,<sup>38</sup> one might prefer the monomer-dimer-tetramer model. Then one may use our result that the heat of association amounts to 9 kcal/mol for the dimers. From the *g* factor we obtain a dipole moment of the dipole of 2.71 D. If one wants to use the results of the numerical adjustment for the tetramers, the small dipole moment of 1.45 D (calculated from  $g_4 = 0.19$ ) indicates that these multimers are cyclic, leading to an energy per bond of 6.5 kcal/mol.

(40) G. P. Johari and W. Dannhauser, *J. Chem. Phys.*, **48**, 5114 (1968).

(41) A. S. N. Murthy, R. E. Davis, and C. N. R. Rao, *Theoret. Chim. Acta*, **13**, 81 (1969).

(42) R. J. J. Jongschaap, private communication.

(43) J. Biais, B. Lemanceau, and C. Lussan, *J. Chim. Phys.*, **64**, 1019 (1967).

(44) L. K. Patterson and R. M. Hammaker, *Spectrochim. Acta*, **23A**, 2333 (1967).



# Studies on the Properties of Large Ions in Solvents of High Dielectric Constant. III. Refractive Index of Solutions of Some Salts Containing an Ion with a Long Alkyl Chain in Formamide, *N*-Methylacetamide, *N,N'*-Dimethylformamide, and *N,N'*-Dimethylacetamide

Ram Gopal\* and Jug Raj Singh

Department of Chemistry, Lucknow University, Lucknow, India (Received July 5, 1972)

Refractive indices of solutions of sodium oleate, sodium stearate, sodium palmitate, sodium deoxycholate, and cetyltrimethylammonium bromide have been measured in formamide, *N*-methylacetamide (NMA), *N,N'*-dimethylformamide (DMF), and *N,N'*-dimethylacetamide (DMA) at 30° and different concentrations. The study indicates micelle formation in formamide and NMA but not in DMF and DMA. These results support the conclusions arrived at from the conductance measurements that the cation- and anion-active colloidal electrolytes form charged micelles in strongly hydrogen-bonded solvents of high dielectric constant, namely, formamide and NMA (as in water), but not in the solvents of medium dielectric constant and weak hydrogen bonding like DMF and DMA (as also ethanol and methanol). Thus it appears that the high dielectric constant of the medium ensures complete dissociation of the electrolyte into ions which then associate to form charged micelles through the hydrogen bonds.

## Introduction

Recent studies on electrical conductance<sup>1,2</sup> of solutions of some anion- and cation-active colloidal electrolytes, containing an ion having a large alkyl chain, *viz.*, oleate, stearate, palmitate, deoxycholate, and cetyltrimethylammonium, indicate the presence of charged micelles in formamide and NMA (both having high dielectric constant and strong hydrogen bonding) and their absence in DMF and DMA (both having medium dielectric constant and negligible hydrogen bonding). These observations clearly indicate that ionic micelle formation is favored by high dielectric constant and strong hydrogen bonding of the solvent. For a better understanding of the process of ionic micelle formation and the factors governing the phenomenon of micellization, it appears desirable to examine some other property of these solutions to make sure that the micelle formation does occur in formamide and NMA and not in DMF and DMA. A very appropriate property which can be accurately measured in dilute solutions is the refractive index.<sup>3</sup> The results obtained from refractive index measurements on solutions of the salts mentioned earlier in formamide, NMA, DMF, and DMA are reported in this paper. Sodium oleate, sodium stearate, and sodium palmitate could not be studied in DMF and DMA, due to solubility restrictions.

## Experimental Section

Sodium oleate, sodium palmitate, sodium stearate, and sodium deoxycholate were fractionally recrystallized from ethanol and cetyltrimethylammonium bromide from acetone. These were dried in an oven to a constant weight. Formamide was left overnight on freshly ignited quicklime and then distilled under reduced pressure. The middle fraction of the distillate was collected and fractionally crystallized; the crystals were melted and the resulting liquid was vacuum distilled, the middle fraction being collected again. The process of purification was repeated until the conductance of the middle fraction was reduced

to 10<sup>-5</sup> mho or less. *N*-Methylacetamide (NMA), *N,N'*-dimethylformamide (DMF), and *N,N'*-dimethylacetamide (DMA), after drying on freshly ignited quicklime, were repeatedly vacuum distilled. The specific conductance of the purified samples of these chemicals ranged between 10<sup>-6</sup> and 10<sup>-7</sup> mho. A stock solution of the salt in question was prepared and other solutions were made by suitable dilutions of the stock solution with the same sample of the solvent concerned in a drybox. The Brice-Phoenix differential refractometer<sup>4</sup> (Model BP-2000V) was used for determining the difference,  $\Delta n$ , in the refractive indices of the solution and the solvent for the different salts at various concentrations. The temperature was maintained at 30 ± 0.5° by circulating hot water in the outer jacket of the cell holder. Measurements were made with the light of 436-m $\mu$  wavelength. The instrument was calibrated with standard KCl solutions.<sup>5</sup> From the procedure detailed elsewhere,<sup>5</sup> the difference  $\Delta n$  between the refractive indices of the solvent and solution was obtained<sup>6</sup> for different solutions. The  $\Delta n$  values were plotted against concentration *C* of solutions and the curves thus obtained are given in Figures 1-4.

## Results and Discussion

From Figures 1-4, it appears that  $\Delta n$  *vs.* *C* plots are linear in DMF and DMA and the salts appear to behave like common binary electrolytes. On the other hand,  $\Delta n$  *vs.* *C*

- (1) R. Gopal and J. R. Singh, *Kolloid-Z. Z. Polym.*, **239**, 699 (1970).
- (2) R. Gopal and J. R. Singh, *J. Indian Chem. Soc.*, **49**, 667 (1972).
- (3) C. A. Browne and F. W. Zerban, "Physical and Chemical Methods of Sugar Analysis," 3rd ed, Wiley, New York, N. Y., 1941, p 1206.
- (4) B. A. Brice and M. Halwer, *J. Opt. Soc. Amer.*, **41**, 1033 (1951).
- (5) A. Kruis, *Z. Phys. Chem.*, **34B**, 13 (1936).
- (6) The difference  $\Delta n$  in the refractive indices of solution and solvent for different salts in formamide, NMA, DMF, and DMA will appear following these pages in the microfilm edition of this volume of the journal. Single copies may be obtained from the Business Operations Office, Books and Journals Division, American Chemical Society, 1155 Sixteenth St., N.W., Washington, D. C. 20036. Remit check or money order for \$3.00 for photocopy or \$2.00 for microfiche, referring to code number JPC-73-554.
- (7) K. W. Herrmann, *J. Phys. Chem.*, **66**, 295 (1962).

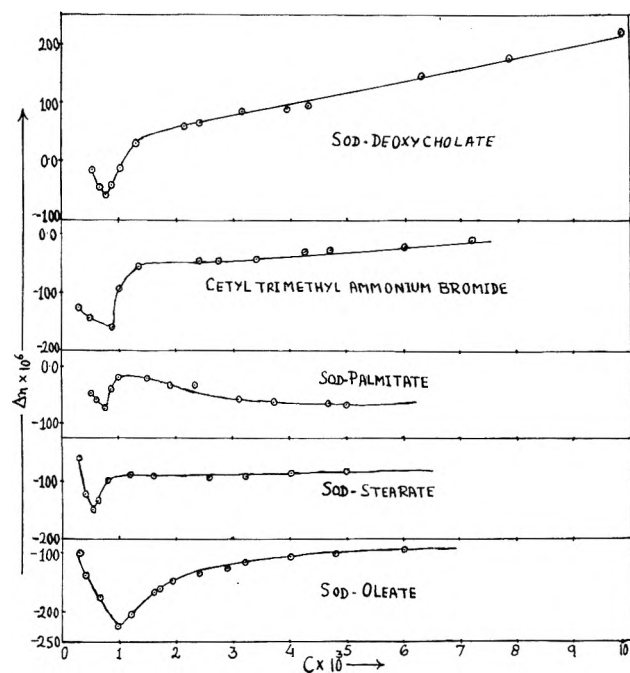


Figure 1.  $\Delta n$  vs.  $C$  plots for different salts in formamide at  $30 \pm 0.5^\circ$ .

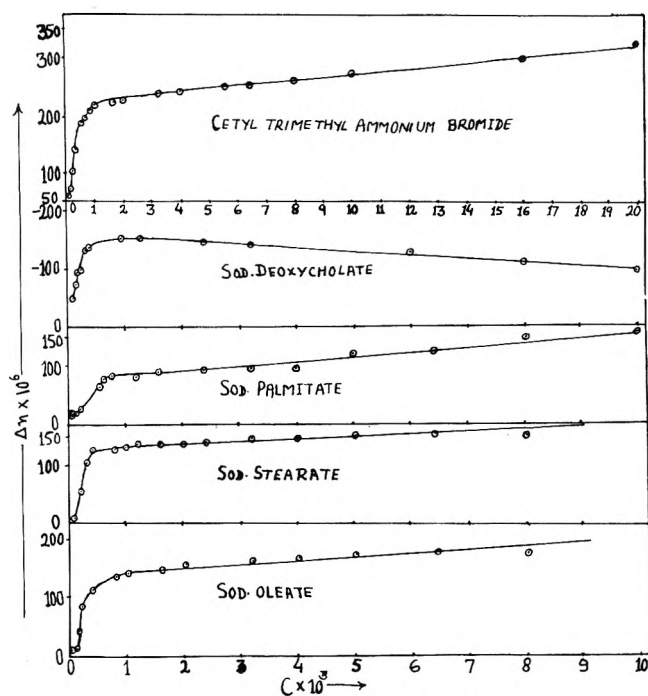


Figure 2.  $\Delta n$  vs.  $C$  plots for different salts in NMA at  $30 \pm 0.5^\circ$ .

curves in formamide and NMA are not linear. Inflexion occurs in all the curves and the critical micelle concentration (cmc) corresponds to the point of inflexion.<sup>7</sup> The cmc values for different salts studied here are given in Table I in which the cmc values, obtained from conductance measurements, are also included for the sake of comparison.

It may be noted from Table I that the cmc values, obtained from refractive index measurements, are, in general, appreciably higher than those obtained from the conductance method but are of the same order, the difference being presumably due to the difference in precision obtainable in the two methods. Also the cmc values in

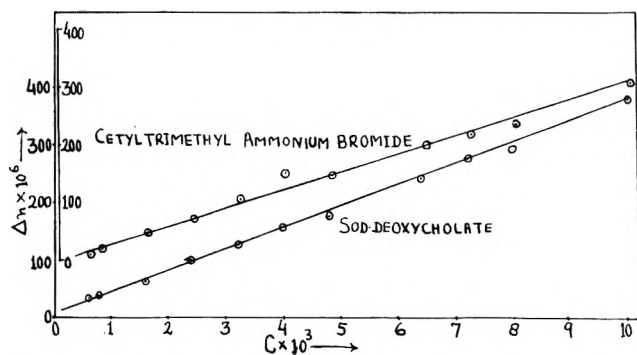


Figure 3.  $\Delta n$  vs.  $C$  plots for different salts in DMF at  $30 \pm 0.5^\circ$ .

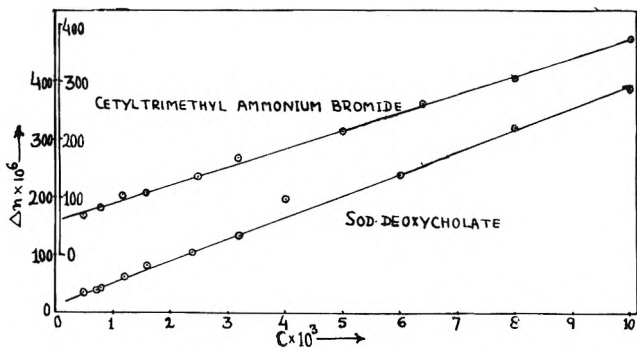


Figure 4.  $\Delta n$  vs.  $C$  plots for different salts in DMA at  $30 \pm 0.5^\circ$ .

TABLE I: Cmc Values of Some Salts in Formamide and NMA at  $30^\circ$

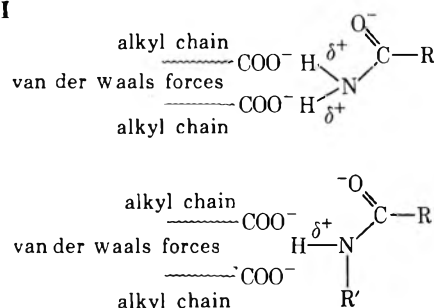
Salt	$10^4$ cmc. $M$			
	Formamide		NMA	
	Conductance	Refractive index	Conductance	Refractive index
Sodium oleate	5.1	9.5	0.822	1.6
Sodium stearate	5.2	5.3	0.80	2.0
Sodium palmitate	6.0	7.5	0.90	1.5
Sodium deoxycholate	4.0	8.0	0.70	1.6
Cetyltrimethyl-ammonium bromide	5.0	8.8	0.80	1.0

NMA, obtained from both the methods, are lower than those in formamide. Hence the micelle formation in NMA and formamide and its absence in DMF and DMA appears to be established beyond doubt. A reference to the properties of the two sets of solvents suggests that the ionic micelle formation is favored by high dielectric constant and strong hydrogen bonding of the solvent. The high dielectric constant makes the micelle a charged one as it brings about complete dissociation of the salt concerned so that micelle forming units are ions and not molecules. The ion-solvent interaction in water, formamide, and NMA, in terms of a molecular picture, can be looked upon somewhat as follows. The negatively charged anion ( $RC(=O)O^-$ ) offers strong repulsion to the exposed negative end of the solvent dipole and there is attraction between the anions and the positive end of the dipole, leading to solvation; this situation forces the alkyl chains of the anions to come into somewhat closer proximity of one another than would have been possible on account of random thermal distribution. The alkyl chains would attract each other by dispersion forces, as in solids, to form ionic aggregates or micelles whose size would depend on tem-

perature. Since all the salts under study exhibit, in very dilute solutions, random thermal ionic distribution and no detectable micelles appear to be formed, it is quite apparent that the micelle formation occurs only when the ions are in close proximity at the higher concentrations, so that the dispersion forces between the alkyl chains may become effective. In both the anion- and cation-active colloidal electrolytes, the alkyl chains are forced to orient themselves near each other in the presence of the solvent dipoles. The formation of micelles in solutions of these salts in formamide and NMA and their absence in DMF and DMA suggests that in formamide and NMA, the micelles are formed by interlinking of long anions through the hydrogen bonds between the hydrogen atoms of  $-\text{NH}_2$  and  $>\text{NH}$  groups and the anions. The process may be pictured somewhat as shown in Scheme I. The dialkyl substitution in DMF and DMA does not favor micelle formation, presumably due to shielding of the positive charge on the dipole and the absence of the hydrogen bonding. It may be remembered that in methyl and ethyl alcohols, ionic micelle formation does not occur because of their

low dielectric constant and weak hydrogen bonding. In such solvents, association between the oppositely charged ions occurs in preference to the ion-solvent dipole interaction.

Scheme I



*Acknowledgment.* The authors are grateful to the Council of Scientific and Industrial Research, India, and the Society of the Sigma Xi (U. S. A.), for financial aid.

## Charge Transfer of Adsorbed Ozone

H. Kiess and T. Freund\*<sup>1</sup>

David Sarnoff Research Center, RCA Laboratories, Princeton, New Jersey 08540 (Received July 3, 1972)

Publication costs assisted by RCA Laboratories

The interaction of ozone with semiconducting inorganic and organic solids has been examined. Evidence is presented that a charge-transfer complex is formed of the type,  $\text{O}_3^- \cdot \text{solid}^+$ . Electrical measurements support the formation of the complex by a transfer of a valence-band electron of the solid to the adsorbed species; such a process is known as hole injection. Both porous and nonporous solids were investigated.

### Introduction

The interdependence of the electronic properties of wide bandgap semiconducting materials and the chemical properties of sorbed chemical species has been of interest in many fields including electrochemistry,<sup>2,3</sup> heterogeneous catalysis,<sup>4</sup> and the photolysis of solids.<sup>5</sup> Two of the most basic questions are what is the sign of the charge on the adsorbed species and whether the charge transfer is between the sorbed species and the conduction or valence band of the solid. We wish to report evidence for hole injection from sorbed ozone into the valence band of several solids. This process is equivalent to the abstraction of an electron from the valence band of the solid with the formation of a negative sorbed species, possibly sorbed  $\text{O}_3^-$ . We believe the report of our studies is timely because the type of charge-transfer complex, molecule<sup>-</sup>·solid<sup>+</sup>, in contrast to molecule<sup>-</sup>·molecule<sup>+</sup>, has been largely neglected in chemistry and because of the increasing interest in the reactions of ozone in connection with smog problems.

### Experimental Section

Basically, our primary experimental technique was borrowed from electrophotography and consisted of two steps: electrostatic charging of the gas/semiconductor interface and second, contacting the semiconductor with a gas stream containing ozone. The change in surface voltage is a measure of the net change of surface charge and hence a quantitative measure of the change in the number of charged adsorbed species on the surface. Three Kelvin-type surface voltage detectors were used: electrostatic voltmeter,<sup>6</sup> rotating disk electrometer,<sup>7</sup> and a probe connected to a high-impedance voltmeter.<sup>8</sup> The back surface

- (1) Present address: Xerox Corporation, Xerox Square-114, Rochester, N. Y. 14644.
- (2) R. Memming and H. Tributsh, *J. Phys. Chem.*, **75**, 562 (1971).
- (3) T. Freund, *J. Phys. Chem.*, **73**, 468 (1969).
- (4) S. R. Morrison and T. Freund, *J. Chem. Phys.*, **4**, 1543 (1967); T. Freund and W. P. Gomes, *Catal. Rev.*, **3**, 1 (1969).
- (5) S. R. Morrison, *J. Vac. Sci. Technol.*, **7**, 84 (1970).
- (6) Monroe Electronic Company, Middleport, N. Y.
- (7) E. C. Giaimo, *RCA Rev.*, **22**, 780 (1961).
- (8) Model 602, Kiethley Instrument Company, Cleveland, Ohio.

of the semiconductor was grounded and masked from the ambient atmosphere. The charging step was carried out by exposure of the sample to an atmospheric pressure corona discharge which creates<sup>9</sup> either  $\text{H}(\text{H}_2\text{O})_n^+$  or  $\text{CO}_3^-$ . Typical surface voltages ranged from 50 to 2000 V giving fields as high as  $10^6$  V/cm through the semiconducting layer.

Two types of auxiliary measurements were made. Direct current conductivity measurements were made on samples prepared by coating a glass plate upon which had been deposited two conducting stripes of tin oxide. The current was measured at a fixed voltage as a function of the gaseous ambient. The second type of auxiliary measurement was the differential capacitance. The differential capacitance measurement<sup>10</sup> was made by carrying out the following steps: positively charging a layer with a positive corona discharge, measuring the surface voltage, depositing a small amount of measured negative charge on the layer from a negative corona, remeasuring the surface voltage; the cycle of deposition of measured negative charge and the surface voltage measurement is repeated until a zero surface voltage is obtained.

Films on Al or other conducting substrates were prepared from sucrose benzoate containing partially oxidized Leuco Malachite Green (LMG),<sup>11</sup> poly(*N*-vinyl)carbazole (PVK),<sup>12</sup> poly(*N*-vinyl)carbazole containing rhodamine B (PVK-RhB), equimolar poly(*N*-vinyl)carbazole and trinitrofluorenone (PVK-TNF), and zinc oxide dispersions<sup>13</sup> in various commercial electrophotographic grade organic resins such as silicone, acrylic, or vinyl acetate based polymers. Conducting zinc oxide single crystals were obtained from 3M Co. and the sputtered zinc oxide films were prepared at RCA.

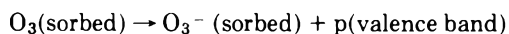
Except for single crystal zinc oxide, some of the sputtered layers, and some of the ZnO-resin layers all samples could be and were charged with both polarities before exposure to  $\text{O}_2$  containing up to 4 mol %  $\text{O}_3$ . In all cases, the positively charged samples were discharged by  $\text{O}_3$  except for sputtered ZnO. In the case of negatively charged samples, only the ZnO-resin layers were discharged. For both positively and negatively charged ZnO-resin layers, the initial rate of decrease in voltage was found to be proportional to the ozone concentration in the range of 1 to 1000 ppm; for typical layers, assuming first order in voltage, the rate constant was  $10^2$  (atm sec)<sup>-1</sup>. For the lower concentrations of ozone, the discharge process could be arrested by switching the gas stream to pure oxygen. In general, exposure to ozone caused no permanent damage to the layers with respect to light or ozone discharge characteristics. The dark decay discharge rates in  $\text{O}_2$ , air,  $\text{CO}_2$ , or other ambients with very low  $\text{O}_3$  concentrations depended on the detailed history of the sample including factors such as light exposure and humidity. For many of the ZnO-binder layers the dark decay rate was below that of 0.5 ppm of ozone. As expected, resin layers accepted charge of both polarities but were not discharged by ozone.

One other configuration of ZnO-binder layers was used: semiconductor-Mylar-metal. In this configuration it was found that the same increment of the initial surface voltage was discharged by light or ozone. For corona-charged LMG it was found that either constant intensity light or ozone discharged the layer to 60% of initial surface voltage but that for the last 40% of the voltage both agents were very ineffective. For positively charged PVK, differential capacitance measurements were made on samples partial-

ly discharged by either light or ozone; the differential capacitance curves were the same for samples prepared by either discharge method. With ZnO-binder layers, the dc conductivity (tin oxide contacts) was found to decrease in the order  $\text{CO}_2 > \text{air} > \text{C}_2 > \text{O}_3\text{-O}_2$ .

## Discussion

The discharge of positively charged surfaces that is associated with ozone may be attributed to the formation of a negatively charged chemical species on the surface; the simplest example is an electrically neutral adsorbed ozone yielding a negative species such as  $\text{O}_3^-$ . In principle, this process could occur by one of two electronic mechanisms: reaction of an electron from the conduction band of the solid with  $\text{O}_3$  or hole injection from neutral adsorbed  $\text{O}_3$  into the valence band of the solid. We propose the hole injection mechanism, an essential part of which is the relationship of the energy level of the electron of the adsorbed charged species to that of the electron levels just inside the surface. Electron transfer from the valence band of the solid to a neutral sorbed species, such as  $\text{O}_3$ , will be energetically favorable if the electronic energy level of the least tightly bound electron of the sorbed species  $\text{O}_3^-$  is below the top of valence band of the solid. This process is equivalent to a transfer of a positive charge from the sorbed species and is called hole injection



The negative charge on the ozone compensates the positive surface charge which was formed during the electrostatic charging. In order for the discharge process to be observed, the injected hole must move from the gas-semiconductor interface toward the grounded rear interface. The alternative mechanism, electron capture from the conduction band by neutral sorbed  $\text{O}_3$ , is ruled out because during the positive electrostatic charging step any mobile electrons that may be present in the conduction band are removed from the bulk of the solid to the ground side of the sample.

Since, at least in the gas phase, the decomposition of  $\text{O}_3$  is highly exothermic, another possible mechanism for the discharge by adsorbed ozone of charged surfaces involves the transfer of this decomposition energy to a surface state. For this type of mechanism to be operative, the decomposition energy must be at least as large as the activation energy for charge injection from the surface state to the appropriate band of the solid. Such a mechanism could be postulated for the ozone discharge of either positively or negatively charged surfaces.

Support for the negative charge on the ozone was obtained from dc electrical conductivity measurements with solid contacts performed on ZnO-binder layers (known electron conductors) in various ambients;  $\text{O}_3$  decreased the conductivity even more than  $\text{O}_2$ . Further evidence for the electronic nature of the discharge process was obtained from two types of experiments in which the discharge by ozone and light was shown to be similar. The first, obtained with LMG, concerns the similarity of the voltage-time dependence for photo and ozone discharge. The second type of evidence, obtained on positively

- (9) M. M. Shahin, *Advan. Chem. Ser.*, No. 80, 1 (1969); *Appl. Opt., Suppl.*, 106 (1969).
- (10) R. B. Comizzoli, *Photogr. Sci. Eng.*, 14, 210 (1970).
- (11) W. Mehl and N. E. Solif, *J. Phys. Chem. Solids*, 25, 1221 (1964).
- (12) C. A. Queener, *Photogr. Sci. Eng.*, 15, 423 (1971).
- (13) R. B. Comizzoli, G. Lozier, and D. A. Ross, *Proc. IEEE*, 60, 348 (1972).

charged PVK, is the similarity of the differential capacitance of samples partially discharged either by light or ozone.

The results obtained with two types of samples, namely, the positively charged sputtered ZnO and the negatively charged ZnO-binder layers, need further comment. The lack of discharge of the positively charged sputtered layers was not unexpected since their photobehavior indicated a very low carrier mobility, *i.e.*, if positive charge were injected at the surface, it would not move far before being trapped.

The discharge of negatively charged ZnO-binder layers by ozone can be explained by the hole injection mechanism since these layers are known to have a very large pore volume.<sup>14</sup> The charge distribution of a porous layer after the corona charging step is the same as a nonporous layer, *i.e.*, negative charge on the outer surface of the layer and counter positive charge at the semiconductor-metal interface.<sup>15</sup> For the discharge of a porous layer, we suggest three steps: (1) penetration of the layer by ozone with the adsorption of ozone on the pore walls, (2) hole injection with the formation of immobile adsorbed  $O_3^-$ , and (3) limited movement of the hole toward the negative surface under the influence of the electric field. The number of ozone molecules needed to discharge each charge on the outer surface depends on the distance that the hole travels before trapping. Our proposed model is equally applicable to the discharge of negatively charged porous layers since

the positive counter charge of these layers, located at the semiconductor-metal interface, is accessible through the pores. That the discharge process is not connected with an ozone-metal interaction at the metal-semiconductor interface was shown by experiments with the three-layer structure, semiconductor-Mylar-metal.

We have no direct evidence for the chemical formula of the negative species that is formed on the surface but  $O_3^-$  has been identified recently on the semiconducting oxide, MgO.<sup>16</sup> Since the layers are not permanently damaged by  $O_3$  with respect to electrophotographic or ozone discharge properties, one suspects that there may not be any chemical attack by ozone. However, since the ratio of negative species to surface atoms of the layer in an experiment is typically less than 1/1000, our electrical measurements may be too insensitive. With regard to the neutral species, it appears that ozone is weakly adsorbed since the discharge process was found to be stopped by flushing with an ozone-free gas stream.

*Acknowledgment.* We wish to thank R. B. Comizzoli for many instructive discussions and H. Azarian for technical assistance in carrying out some of the experiments.

(14) E. C. Hutter, *Photogr. Sci. Eng.*, **15**, 456 (1971).

(15) The more complex model to include volume charge<sup>12</sup> is equally applicable to porous and nonporous layers and does not change any of the conclusion of our mechanism.

(16) N.-B. Wong and J. H. Lunford, *J. Chem. Phys.*, **56**, 2664 (1972).

## Formation Constants and Enthalpies of Some Organomercury-Nitrogen Base Adducts

Warren H. Puhl<sup>1</sup> and H. F. Henneike\*

Chemistry Department, Georgia State University, Atlanta, Georgia 30303 (Received July 24, 1972)

Publication costs assisted by Petroleum Research Fund

Enthalpies and equilibrium constants for the interaction of pyridine (py) and 2,2'-bipyridyl (bipy) with bis(pentafluorophenyl)mercury in  $CCl_4$  and  $C_6H_6$  have been determined calorimetrically. The equilibrium constant for the  $py-(C_6F_5)_2Hg$  adduct formation in  $CCl_4$  has been independently determined by an nmr method thus enabling calculation of the statistical dispersion independent of the high correlation coefficients between the calorimetrically determined  $\Delta H$  and  $K$ . Discrepancies encountered in the use of  $CCl_4$  and  $C_6H_6$  as solvents for these systems are noted. The enthalpy and equilibrium constant for the formation of the pyridine adduct of diphenylmercury is also reported. Organomercurials are indicated to be very weak Lewis acids.

### Introduction

In recent years there has been sufficient qualitative data establishing the formation of neutral mercurial complexes of the type  $R_2HgL_n$ ,  $n = 1, 2$  where  $R =$  aryl, perfluoroalkyl, fluoroalkyl, or perfluoroaryl, and  $L =$  monodentate (or bidentate<sup>2</sup>) neutral ligand. Oscillometric titrations,<sup>3</sup> infrared spectra,<sup>3</sup> and conductance measurements<sup>4</sup> have suggested 1:1 complexes of bidentate bases together with 1:1 and possibly 1:2 complexes with monodentate bases. Bis(perfluoroorganomercurial) complexes have been

isolated where  $R = CF_3$ ,  $C_2F_5$ ,  $C_3F_7$ , and  $C_6F_5$ ,  $L = 2,2'$ -bipyridine,<sup>5</sup> *o*-phenanthroline,<sup>5</sup> and 1,2-bis(diphenylphosphino)ethane,<sup>6</sup> and  $n = 1$ . In addition, complexes where  $R$

(1) Abstracted in part from the Ph.D. Thesis of W. H. Puhl, University of Minnesota, 1970.

(2) G. B. Deacon and A. J. Canty, *Inorg. Nucl. Chem. Lett.*, **5**, 183 (1969).

(3) H. B. Powell, M. T. Maung, and J. J. Lagowski, *J. Chem. Soc.*, 2484 (1963).

(4) J. E. Connett, A. G. Davies, G. B. Deacon, and J. H. S. Green, *J. Chem. Soc.*, 106 (1966).

=  $\text{CF}_3\cdot\text{CFH}-$ ,  $\text{CF}_3\text{CH}_2-$ , and  $(\text{CF}_3)_2\text{CF}-$ , and L = pyridine *N*-oxide, tetramethylene sulfoxide, piperidine, and ethylenediamine have been isolated and characterized by infrared spectroscopy and elemental analysis.<sup>7</sup> No bisalkyl mercurial complexes have been indicated; however, the isolation of a diphenylmercury- $\text{L}_2$  complex has been suggested where L = *o*-phenanthroline, 2,9-dimethyl-*o*-phenanthroline, and 2,4,7,9-tetramethyl-*o*-phenanthroline<sup>2</sup> indicating a coordination number of 6 for mercury.

Thus far oscillometric, conductometric, spectroscopic, analytic, and molecular weight evidence has indicated a maximum coordination of 4 for mercury in such neutral complexes. It is interesting to note that molecular weight measurements<sup>5</sup> show that both the bisperfluoroalkyl and bisperfluoroaryl mercury-phenanthroline complexes are 1:1 and monomeric in benzene whereas the corresponding 2,2'-bipyridine complexes dissociate to a larger degree. The R group effect on the dissociation of the 2,2'-bipyridine complexes is given as  $-\text{C}_6\text{F}_5 > -\text{CF}_3 > -\text{C}_3\text{F}_7 > -\text{C}_2\text{F}_5$ .<sup>5</sup> It is interesting to note here that the electronegativity of the  $-\text{C}_6\text{F}_5$  group has been suggested to be between that of chlorine and that of bromine.<sup>8</sup>

Hg(II) halides often form tetrahedral species such as  $\text{HgCl}_2\cdot 2\text{py}$  which is partially dissociated in dioxane; however, polarization and dipole moment studies strongly suggest a three-coordinate  $\text{HgCl}_2\cdot\text{O}_2\text{C}_4\text{H}_8$  with Cl-Hg-Cl angle of about  $160^\circ$  in a HgCl-dioxane solution.<sup>9</sup> Three coordinate group IIb halides such as  $\text{CdI}_2\cdot\text{P}(\text{CH}_3)_2(\text{C}_6\text{H}_4\text{N}(\text{CH}_3)_2)$ ,  $\text{HgBr}_2\cdot\text{P}(\text{C}_2\text{H}_5)_2(\text{C}_6\text{H}_5)$  in equilibrium with their dimers have been indicated.<sup>10</sup> Also,  $\text{Pt}^0$ , which is isoelectronic with Hg(II), has been shown to exist in a three-coordinate form as  $\text{Pt}(\text{P}(\text{C}_6\text{H}_5)_3)_3$ .<sup>11,12</sup>

The original intent of this study was to provide enough thermodynamic data on adduct formation reactions of an organomercurial that accurate *E* and *C*<sup>13</sup> parameters could be calculated. It was deemed probable that the mercury site would act as a soft<sup>14</sup> acceptor. The characterization of a soft metallic acceptor would usefully extend the present list of acids for which *E* and *C* numbers are available. It would also make possible the prediction of enthalpies for a large variety of donor-acceptor systems.

However, solubility limitations and surprisingly small formation constants and enthalpies have served to restrict the suitable electron pair donors to the strong (protonic) nitrogen bases.

## Experimental Section

**Materials.** Matheson Coleman and Bell Spectroquality carbon tetrachloride and benzene were dried over Linde 4A molecular sieves for at least 24 hr. Mallinckrodt SpectAR pyridine was refluxed over barium oxide for 3 hr at  $60^\circ$  and distilled onto Linde 4A sieves; the middle fraction, 93–95° (400–420 Torr), was retained. Eastman White Label 2,2'-bipyridine was recrystallized from ethanol and dried *in vacuo* over  $\text{P}_2\text{O}_5$ . The Grignard route to bispentafluorophenylmercury is described elsewhere.<sup>6</sup> The crude product of the Grignard preparation was sublimed at  $110^\circ$ , recrystallized from benzene, resublimed at 90–95°, and dried *in vacuo* over  $\text{P}_2\text{O}_5$  (mp 141–143, lit.<sup>4</sup> mp 142.3°).

**Apparatus and Procedure.** All chemicals were handled in a dry, inert atmosphere. The bases were added (neat or as a solution) in 0.2–0.4 ml aliquots to 205.9 ± 0.2 ml of organomercurial solution in the calorimeter dewars. The dewars had previously been flushed with dry nitrogen gas.

The calorimeter design was similar to that utilized by Arnett<sup>15</sup> and Drago.<sup>16</sup> A base addition tube, resistance heating coil, 5000-ohm thermistor, and rotary Teflon stirring blades were positioned in each of two 200-ml silvered dewar flasks *via* a Teflon cover.

The sensitivity of the Wheatstone bridge circuit was such that 8 cal of heat generated in 200 ml of  $\text{CCl}_4$  produced a 10-cm recorder pen deflection. The accuracy of the system was evaluated by measuring the heat of reaction between tris(hydroxymethyl)aminomethane and HCl. The agreement with literature<sup>17</sup> values was better than 1%.

After making electrical and mechanical connections to the dewar flasks, the filled base addition bulbs were inserted through the dewar caps so that liquid levels inside and outside the bulb were equal.

Initially a drifting base line was adjusted to zero drift by changing the relative stirring speeds in the dewar flasks. In order to assume linearity in deflections the bridge circuitry was adjusted to zero potential across the recorder before each set of measurements. The thermistors were matched to within 250 ohms and to maintain an approximate equality in resistance, the dewars were counterheated after each deflection of more than 5–6 cm.

After establishing thermal equilibrium, the calorimeter was calibrated before and after the chemical reaction. The average of these calibrations was used to calculate the heat liberated. This procedure was repeated with up to six aliquots being added to each dewar. Heats of solution for the bases were determined in the same way. All experiments were conducted at 25°.

The nmr studies utilized a Varian A60A instrument.

## Calculations

The equations and method utilized in the simultaneous calculation of enthalpies and equilibrium constants from calorimetric data have been described.<sup>16,18</sup> Programs HEAT11 and HEAT12<sup>19</sup> using STEPIT<sup>20</sup> as the minimization algorithm were written to handle data for one-to-

- (5) J. E. Connett and G. B. Deacon, *J. Chem. Soc. C*, 1058 (1966).
- (6) R. D. Chambers, G. E. Coates, J. G. Livingstone, and W. K. R. Musgrave, *J. Chem. Soc.*, 4367 (1962).
- (7) H. B. Powell and J. J. Lagowski, *J. Chem. Soc. A*, 1282 (1966).
- (8) R. D. Chambers and T. Chivers, *Organometal. Chem. Rev.*, **1**, 297 (1966), and references therein.
- (9) S. R. Jain and S. Soundarajan, *J. Inorg. Nucl. Chem.*, **26**, 1255 (1964).
- (10) R. C. Cass, G. E. Coates, and R. G. Hayter, *J. Chem. Soc.*, 4007 (1955).
- (11) R. Ugo, *Coord. Chem. Rev.*, **3**, 319 (1968).
- (12) L. Malatesta and C. Cariello, *J. Chem. Soc.*, 2323 (1958).
- (13) (a) R. S. Drago and B. B. Wayland, *J. Amer. Chem. Soc.*, **87**, 3571 (1965); (b) R. S. Drago, G. C. Vogel, and T. E. Needham, *ibid.*, **93**, 6014 (1971).
- (14) R. G. Pearson, *J. Chem. Educ.*, **45**, 581, 643 (1968).
- (15) E. M. Arnett, W. G. Bentrude, J. J. Burke, and P. M. Duggeby, *J. Amer. Chem. Soc.*, **87**, 1541 (1965).
- (16) T. F. Bolles and R. S. Drago, *J. Amer. Chem. Soc.*, **87**, 5015 (1965).
- (17) R. J. Irving and I. Wadso, *Acta Chem. Scand.*, **18**, 195 (1964).
- (18) (a) R. S. Drago and T. D. Epley, *J. Amer. Chem. Soc.*, **91**, 2883 (1969). (b) The calculation of equilibrium constants from both calorimetric and nmr measurements employs concentrations rather than activities. Since the two types of experiments cover concentration ranges which are nonoverlapping yet yield essentially the same value for *K*, the usual assumption of a constant activity coefficient quotient  $\gamma_{\text{AB}}/\gamma_{\text{A}}\cdot\gamma_{\text{B}}$  seems reasonable.
- (19) Details given in the Ph.D. Thesis of W. H. Puhl, University of Minnesota, 1970.
- (20) STEPIT (copywrite 1965 by J. P. Chandler, Physics Department, Indiana University) was obtained from the Quantum Chemistry Program Exchange (QCPE), Department of Chemistry, Indiana University, Bloomington, Ind.

TABLE I: Summary of Results

Solvent	Base	$K, M^{-1}$	$\Delta H_f^\circ, \text{kcal/mol}$	$\Delta S_f^\circ, \text{eu}$	$\Delta G_f^\circ, \text{kcal/mol}$
			(C <sub>6</sub> F <sub>5</sub> ) <sub>2</sub> Hg		
CCl <sub>4</sub>	Py	20.1 ± 1.0	-5.40 ± 0.11	-11.4 ± 0.6	-1.77 ± 0.03
CCl <sub>4</sub>	Bipy	55.5 ± 3.0	-7.28 ± 0.12	-15.4 ± 0.4	-2.39 ± 0.03
C <sub>6</sub> H <sub>6</sub>	Py	2.1 ± 0.1	-4.32 ± 0.11	-13.0 ± 0.4	-0.44 ± 0.03
C <sub>6</sub> H <sub>6</sub>	Bipy	19.2 ± 2.0	-4.19 ± 0.25	-8.2 ± 1.0	-1.75 ± 0.06
			(C <sub>6</sub> H <sub>5</sub> ) <sub>2</sub> Hg		
CCl <sub>4</sub>	Py	~0.3	~-2.9		

TABLE II: Summary of Experimental Conditions

Solvent	Acid	Base solution	No. of data points	Base:acid ratio	max. % acid complexed
CCl <sub>4</sub>	(C <sub>6</sub> F <sub>5</sub> ) <sub>2</sub> Hg	3.6 M py	12	0.1:3.3	63
CCl <sub>4</sub>	(C <sub>6</sub> F <sub>5</sub> ) <sub>2</sub> Hg	3.6 M bipy	11	0.2:3.6	78
C <sub>6</sub> H <sub>6</sub>	(C <sub>6</sub> F <sub>5</sub> ) <sub>2</sub> Hg	Neat py	24	0.2:11.8	43
C <sub>6</sub> H <sub>6</sub>	(C <sub>6</sub> F <sub>5</sub> ) <sub>2</sub> Hg	1.4 M bipy	11	0.2:2.2	42
CCl <sub>4</sub>	(C <sub>6</sub> H <sub>5</sub> ) <sub>2</sub> Hg	Neat py	8	0.5:2.2	9

one (A + B → AB) and two-to-one (A + 2B → AB<sub>2</sub>) systems, respectively.

In each case  $\Delta H_{\text{obsd}}$  is the measured enthalpy change including any heat of dilution term for the added base and  $\Delta H_{\text{corr}}$  is the experimental heat corrected for dilution effects. The values of  $K$  and  $\Delta H_f$  are varied by STEPIT and used to calculate enthalpy changes ( $\Delta H_{\text{calcd}}$ ) to be compared with  $\Delta H_{\text{corr}}$ . The following relationships are used in the one-to-one case

$$K = AB/(A_0 - AB)(B_0 - AB)$$

$$\Delta H_{\text{calcd}} = AB\Delta H_f V$$

where  $V = 0.2059l + V_B$  where  $V_B$  is the volume of added base.

The concentration dependence of the heats of solution was determined through the use of ORTHON,<sup>21</sup> a library routine for general fitting of orthogonal functions obtained from the University of Minnesota Computer Center.

STD ERR is a confidence limit calculated by STEPIT in conjunction with a correlation indicator which is given in parentheses. A value of unity for the correlation parameter (which is given in parentheses after STD ERR) implies any increase in CHISQ (the functional minimized by STEPIT, in this case =  $\sum_{i=1}^n (\Delta H(i)_{\text{corr}} - \Delta H(i)_{\text{calcd}})^2$ ) due to a change in one variable ( $K$  or  $\Delta H$ ) can be completely offset by an appropriate change in the other variable. EST ERR is the more usual dispersion indicator and is calculated assuming a diagonal correlation matrix.

A sharpness of fit<sup>22,23</sup> value of 20 or greater has been used as a criterion for a reliably determined parameter.

The value of  $\chi_{(0.1)}^2$  is calculated using an estimated reliability for any observed heat of  $\pm 0.1$  cal; thus a good fit for  $n$  measurements should give a value of unity or less for  $\chi_{(0.1)}^2$  defined as

$$\chi_{(0.1)}^2 = \frac{1}{n} \sum_{i=1}^n \left[ \frac{\Delta H(i)_{\text{corr}} - \Delta H(i)_{\text{calcd}}}{0.1} \right]^2$$

## Results

Table I contains a summary<sup>24</sup> of all the thermodynamic parameters evaluated in this study. Table II presents a summary of the experimental conditions employed. Table

III summarizes data for experiments on the heat of solution of pyridine in benzene, carbon tetrachloride, and cyclohexane.

## Discussion

These results clearly indicate the very weak Lewis acidity of diphenylmercury and the sizeable increase brought about by substitution of C<sub>6</sub>F<sub>5</sub> groups for C<sub>6</sub>H<sub>5</sub> groups. This greater acidity of the perfluoroorgano-substituted mercurial is consistent with the reported group electronegativity for C<sub>6</sub>F<sub>5</sub>.<sup>8</sup>

The calorimetric data for the pyridine-(C<sub>6</sub>F<sub>5</sub>)<sub>2</sub>Hg systems were carefully checked against the predictions of both a 1:1 and a 2:1 model for adduct formation. The fit for the 1:1 model was always well within estimations of experimental errors. The second equilibrium constant and second enthalpy change were almost completely indeterminate for the 2:1 model. The data for 2,2'-bipyridyl systems were also fit satisfactorily with a 1:1 model. However, one disturbing feature about the parameters found from the fit of the 1:1 model was often large values of the correlation coefficient between  $K$  and  $\Delta H$ .

In an attempt to provide independent support for the values of  $K$  and  $\Delta H$  found calorimetrically, the pyridine-(C<sub>6</sub>F<sub>5</sub>)<sub>2</sub>Hg system was investigated *via* proton nmr. It was found that the chemical shift difference between the ortho and meta protons of pyridine was sensitive to the presence of (C<sub>6</sub>F<sub>5</sub>)<sub>2</sub>Hg. The observed chemical shift was arbitrarily taken as the separation in Hz between the major downfield signal of the ortho protons and a major upfield spike of the meta proton multiplets. The assumption of only a 1:1 complex is warranted on the basis of the fit of the calorimetric data and assuming that the observed average chemical shifts are proportional to the fraction of pyridine complexed. The equations of Li, *et al.*,<sup>25</sup> were used to relate the observed chemical shift to a value for the equilibrium constant at the probe temperature of 40°.

The chemical shift difference ( $\delta_{\text{obsd}}$ ) for ten solutions ranged from 83.0 (no (C<sub>6</sub>F<sub>5</sub>)<sub>2</sub>Hg) to 70.1 Hz for a pyridine

- (21) Programmed by J. Carlson, R. Hotchkiss, and L. Liddiard to perform a linear least-squares approximation using orthonormalized arbitrary functions with recall ability to continue to higher order approximation. Accuracy of this method is much greater than with the standard matrix least-squares technique.
- (22) E. Coburn and W. C. Grunwald, Jr., *J. Amer. Chem. Soc.*, **80**, 1322 (1958).
- (23) K. Conrow, G. D. Johnson, and R. E. Bowen, *J. Amer. Chem. Soc.*, **86**, 1025 (1964).
- (24) Listings of solution concentrations and measured heats will appear following these pages in the microfilm edition of this volume of the journal. Single copies may be obtained from the Business Operations Office, Books and Journals Division, American Chemical Society, 1155 Sixteenth St., N.W., Washington, D. C. 20036. Remit check or money order for \$3.00 for photocopy or \$2.00 for microfiche, referring to code number JPC-73-558.
- (25) R. Mathur, S. M. Wang, and N. C. Li, *J. Phys. Chem.*, **68**, 2140 (1964).



to acid ratio of 3:1. As shown in Figure 1, a plot of the standard deviations of the differences ( $\delta_{\text{calcd}} - \delta_{\text{obsd}}$ ) obtained from a linear least-squares fit of  $\delta_{\text{obsd}}$  vs. per cent pyridine complexed for a series of equilibrium constant result in a minimum for  $K = 15$  where eq 1 holds. The amount of pyridine complexed ranges from 0 to 52%.

$$\delta_{\text{calcd}}(\text{Hz}) = 82.98 (\pm 0.32) - (0.274 \pm 0.008)(\% \text{ py complexed}) \quad (1)$$

This value for the equilibrium constant compares favorably with a value of 13 calculated from the calorimetric data corrected to 40°.

A 1 M solution of  $\text{I}_2$  in pyridine reportedly exhibits no change in the position of the ortho proton peaks and only a small downfield shift for the meta and para resonances.<sup>26</sup>  $\text{MgI}_2 \cdot 6\text{py}$  has been reported as exhibiting downfield shifts for the meta and para positions similar to those in the  $\text{I}_2$  case along with a small downfield shift for the ortho proton signals.<sup>27</sup> The pyridinium ion exhibits a marked but unequal downfield shift for all three proton types; para and meta signals being shifted 73 and 44 Hz compared to 15 Hz for the ortho signals.<sup>28,29</sup> In this work the meta and para signals shifted downfield while the ortho signals shifted upfield about the same distance (13 Hz). Inspection of molecular models for possible adduct stereochemistries and the use of tabularized ring current anisotropy effect data suggest that the upfield shift found for the ortho protons could be due to the aromatic rings of the organomercurial. In that case the pattern of shifts found would resemble strongly that found for the soft acid  $\text{I}_2$ . This and the small  $\Delta H$  suggest only a small positive charge resides on the mercury center.

From the relative  $\Delta H_f$  values for the two bases in  $\text{CCl}_4$  it appears most likely that 2,2'-bipyridyl is acting as a bidentate ligand. One would not expect the overall enthalpy change to be double that for one pyridine molecule since the coordination by the first nitrogen should serve to reduce the acidity at the mercury site with respect to a second interaction, e.g., no evidence of the existence of a 2:1 pyridine- $(\text{C}_6\text{F}_5)_2\text{Hg}$  complex was found in this work. Also the free 2,2'-bipyridyl molecule may have a dihedral angle as large as 162°<sup>30</sup> between the planes of the two rings. For chelation to occur these two rings would have to be coplanar or nearly so. The energy necessary to accomplish this would presumably be associated with the second step of the chelation process and would serve to reduce the exothermicity of the overall  $\Delta H_f$  reported here.

In comparing the formation enthalpies of  $(\text{C}_6\text{F}_5)_2\text{Hg} \cdot \text{bipy}$  of this work with the reported dissociation enthalpies of +10.8 kcal/mol for  $\text{Zn}(\text{C}_4\text{H}_9)_2 \cdot \text{bipy}$  and +35.1 kcal/mol for  $\text{Zn}(\text{C}_2\text{H}_5)_2 \cdot \text{bipy}$ <sup>31</sup> in toluene, the marked differences in the Lewis acidity of the organozinc and organomercury compounds is quantitatively shown. Previous qualitative data<sup>32-36</sup> has also suggested that the Lewis acidities of the group IIb organometallics decrease significantly as one proceeds from Zn to Hg.

The data of Table I show that both bases give less exothermic enthalpies of interaction in  $\text{C}_6\text{H}_6$  as solvent than in  $\text{CCl}_4$ . It is not unusual to find that adduct formation enthalpies are less exothermic in benzene than in carbon tetrachloride and less exothermic still in cyclohexane.<sup>37-39</sup> The heats of solution data in Table III agree well with values reported by Purcell and Sherry<sup>40</sup> for  $\text{CCl}_4$  and pyridine.

These authors suggested that  $\text{CCl}_4$  forms a weak complex with pyridine which serves to reduce the endothermic

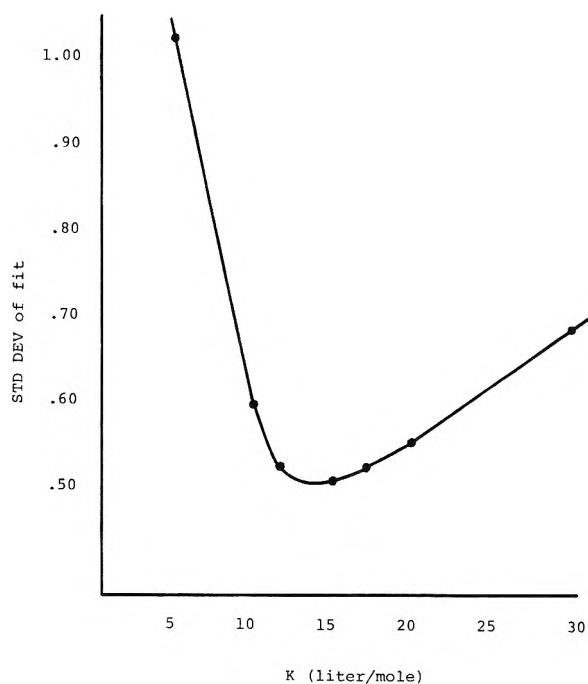


Figure 1. Least-squares fit of chemical shift difference between ortho and meta protons of pyridine as a function of  $K$  at 40°.

TABLE III: Experimental Heats of Solution for Pyridine (cal/mol)<sup>a</sup>

$\Delta H_{\text{sol}}$	=	$(36.9 \pm 1.6) - (23.4 \pm 8.2)[\text{py}]$	in $\text{C}_6\text{H}_6$
$\Delta H_{\text{sol}}$	=	$(245.6 \pm 1.2) - (119.4 \pm 4.8)[\text{py}]$	in $\text{CCl}_4$
$\Delta H_{\text{sol}}$	=	$(1961 \pm 2) - (399 \pm 14)[\text{py}]$	in $\text{C}_6\text{H}_{12}$

<sup>a</sup> These are least-squares fits of the experimental data for neat pyridine being dissolved in the solvent indicated to give solutions in the range 0.0–0.5 M pyridine concentration.

effect of deaggregating pyridine molecules in going from the neat liquid. Dipole moment,<sup>41</sup> nuclear quadrupole resonance,<sup>42</sup> and heat of mixing<sup>43</sup> data have also suggested the acceptor properties of  $\text{CCl}_4$ . Data from nmr studies<sup>44</sup> have suggested that pyridine is solvent tetrachloride more strongly in benzene than in carbon tetrachloride which is consistent with our relative heats of solution.

The existence of a stronger solvent base interaction in benzene than in carbon tetrachloride would account for

- (26) A. Fratiello, *J. Chem. Phys.*, **41**, 2204 (1964).  
 (27) C. B. Storm and A. H. Corwin, *J. Org. Chem.*, **29**, 3700 (1964).  
 (28) I. C. Smith and W. G. Schneider, *Can. J. Chem.*, **39**, 1158 (1961).  
 (29) B. Kotowicz, T. Schaefer, and E. Bock, *Can. J. Chem.*, **42**, 2541 (1964).  
 (30) C. W. N. Cumper, R. F. A. Genman, and A. I. Vogel, *J. Chem. Soc.*, 1188 (1962).  
 (31) V. H. Rau and K. H. Thiele, *Z. Anorg. Allg. Chem.*, **355**, 253 (1967).  
 (32) K. H. Thiele, *Z. Anorg. Allg. Chem.*, **330**, 8 (1964).  
 (33) K. H. Thiele, *Z. Anorg. Allg. Chem.*, **319**, 183 (1962).  
 (34) K. H. Thiele, *Z. Anorg. Allg. Chem.*, **322**, 71 (1963).  
 (35) K. H. Thiele, *Z. Anorg. Allg. Chem.*, **325**, 156 (1963).  
 (36) G. E. Coates and S. I. Green, *J. Chem. Soc.*, 3340 (1962).  
 (37) W. Partenheimer, T. D. Epley, and R. S. Drago, *J. Amer. Chem. Soc.*, **90**, 3886 (1968).  
 (38) W. Partenheimer and R. S. Drago, *Inorg. Chem.*, **9**, 47 (1970).  
 (39) R. S. Drago, *Chem. Brit.*, 3, 516 (1967).  
 (40) A. D. Sherry and K. F. Purcell, *J. Amer. Chem. Soc.*, **92**, 6386 (1970).  
 (41) A. N. Sharp and S. Walker, *J. Chem. Soc.*, 2974 (1961).  
 (42) V. S. Grechishkin and I. A. Kyuntsel, *J. Struct. Chem.*, *USSR*, **7**, 113 (1966).  
 (43) K. W. Morcom and D. N. Travers, *Trans. Faraday Soc.*, **62**, 2063 (1966).  
 (44) J. N. Murrell and V. M. S. Gil, *Trans. Faraday Soc.*, **61**, 402 (1965).

the less exothermic nature of the enthalpies measured in benzene; however, we are unable to completely rule out a more exothermic solvation of the organomercurial acid by benzene as the cause of this discrepancy. Since the differences in enthalpies between the two solvents differ for the two base systems studied, it does seem more probable that the difference is connected with the bases (and their solvation) rather than the acid which is constant to all systems. It is unfortunate that solubility limitations prevented us from using  $C_6H_{12}$  as a solvent since this would have provided an additional test of the hypothesis presented.

### Conclusions

Bis(perfluorophenyl)mercury is indicated to be a very weak Lewis acid, although noticeably stronger than

diphenylmercury. When complexed with pyridine in solution both are apparently examples of three coordinate mercury since only a 1:1 complex is observed.

It appears probable from a comparison of heats of solution and the adduct formation enthalpies in  $C_6H_6$  and  $CCl_4$  that  $CCl_4$  is the more nearly inert solvent for these systems.

*Acknowledgments.* Acknowledgment is made to the donors of the Petroleum Research Fund, Grant No. 874G, administered by the American Chemical Society, for partial support of this work. Our thanks are also due to the Graduate School Research Fund. W. H. P. expresses his appreciation for a Dupont Summer Fellowship.

## Empirical Study of Heavy-Atom Collisional Quenching of the Fluorescence State of Aromatic Compounds in Solution<sup>1</sup>

Isadore B. Beriman<sup>2</sup>

Radiological and Environmental Research Division, Argonne National Laboratory, Argonne, Illinois 60439

(Received August 28, 1972)

Publication costs assisted by the Argonne National Laboratory

The values of the rate constant  $k_x$  for heavy atom quenching of 57 aromatic compounds, induced by bromine in bromobenzene solutions, have been measured and found to vary from  $0.7 \times 10^7$  to  $3.0 \times 10^9$   $\text{sec}^{-1}$ . This quenching constant is composed of two independent rate constants:  $k_t$ , a rate constant for intermolecular *singlet-triplet* energy transfer (chromophore to quencher), and  $k_i$ , a rate constant for induced intramolecular intersystem crossing (in the chromophore). Our results are consistent with the concept that collisional quenching is of short range and that a close encounter between chromophore and quencher is necessary. During their intimate collision, the p orbital of the halogen overlaps the  $\pi$  orbital of the chromophore and the perturbation produced by the bromine leads to a breakdown of the spin-selection rules. Steric hindrance is believed to interfere with this close approach and to reduce the efficiency of the quenching process. Substituents that are noncoplanar with the basic chromophore and produce a large spectral red shift are very effective in shielding the chromophore from being quenched. Finally, many planar compounds that are sensitive to heavy-atom quenching are also susceptible to concentration quenching (*e.g.*, anthracene) or excimer formation (*e.g.*, naphthalene).

### Introduction

High Z atoms, whether as components of a fluorescent compound or of a solvent, are assumed to perturb and quench the fluorescence state by increasing the spin-orbit coupling<sup>3</sup> and possibly forming a charge-transfer complex.<sup>4</sup> In order to learn more about fluorescence quenching, the relative yield,  $R$ , of each of a series of compounds in benzene, B, and in bromobenzene, BrB, has been systematically measured, where  $R$  is the ratio of the fluorescence intensity from a benzene solution to that from a bromobenzene solution. Selected compounds were also measured in ethyl bromide. The compounds that have

been investigated are those on which spectroscopic information is already available<sup>5</sup> and whose absorption spectra are of longer wavelengths than those of BrB.

- (1) Work performed under the auspices of the U. S. Atomic Energy Commission.
- (2) Present address: Racah Institute of Physics, Hebrew University, Jerusalem, Israel.
- (3) M. Kasha, *J. Chem. Phys.*, **20**, 71 (1952).
- (4) S. Lipsky, W. P. Helman, and J. F. Merklin in "Luminescence of Organic and Inorganic Materials," H. P. Kallmann and G. M. Spruch, Ed., Wiley, New York, N. Y., 1962, p 83.
- (5) I. B. Beriman, "Handbook of Fluorescence Spectra of Aromatic Molecules," 2nd ed, Academic Press, New York, N. Y., 1971.

## Procedure

Certain fluorescence parameters of aromatic compounds in cyclohexane have been measured,<sup>5</sup> among these are the decay time  $\tau$  and the quantum yield  $Q_y$ . It is assumed herein that the values of these parameters (and of those derived below) are essentially unchanged in benzene solutions. From these values of  $\tau$  and  $Q_y$ , the rate constants for emission  $k_e$ , for nonradiative transitions  $k_n$ , and for induced (by heavy atom) intersystem crossing  $k_i$ , have been calculated according to the equations

$$\tau^{-1} = k_e + k_n$$

$$Q_y = k_e / (k_e + k_n)$$

$$Q_y' = k_e / (k_e + k_n + k_x)$$

$$R = Q_y / Q_y' = 1 + \tau k_x$$

or

$$k_x = (R - 1) \tau^{-1}$$

The rate constant  $k_x$  is composed of two independent components, a rate constant for transfer  $k_t$  and a rate constant for induced intersystem crossing  $k_i$ .

An average wave number,  $\nu_{av}$ , of each fluorescence spectrum was also available.<sup>5</sup> The quantity  $\nu_{av}$  is defined as

$$\int_{\nu_{min}}^{\nu_{av}} f(\nu) d\nu = \frac{1}{2} \int_{\nu_{min}}^{\nu_{max}} f(\nu) d\nu$$

where  $f(\nu)$  is the photon flux per unit wave number increment,  $\nu_{min}$  is the smallest wave number of the fluorescence band, and  $\nu_{max}$  is the largest. From these values a quantity,  $\Delta\nu_s$ , representative of the shift in the spectrum in wave numbers was calculated according to

$$\Delta\nu_s = \nu_{av}^0 - \nu_{av}$$

where  $\nu_{av}^0$  is the average wave number of the fluorescence spectrum of a basic chromophore, and  $\nu_{av}$  that of the compound listed. Since  $\Delta\nu_s$  is intended to represent the shift in the fluorescence spectrum, its value will be useful only when the same type of transition is measured. It is for this reason that the compounds in Table I are listed as groups containing the same type of fluorescence transition.

A quantity,  $\Delta\nu_{ph}$ , is used to indicate the energy gap between the fluorescence state and the next lower triplet state, and was computed from

$$\Delta\nu_{ph} = \nu_{av} - \nu_{ph}$$

where  $\nu_{ph}$  is the value of the 0-0 transition of the phosphorescence spectrum.<sup>6</sup> In a few cases, several triplet states may be below the first excited singlet state, e.g., anthracene,<sup>7</sup> and  $\Delta\nu_{ph}$  is then taken as the energy gap between the average fluorescence wave number and the higher triplet state. Although Pariser<sup>8</sup> has predicted the existence of various triplet levels below the first excited singlet level for some of the compounds studied, their energy values are in question. For many compounds, the energy of the first triplet level is not available.

Each compound, in dilute ( $<10^{-3}$  mol) B and BrB solutions, was excited by monochromatic uv radiation, and the fluorescence emission was reproduced on a Beckman DK-2 spectrophotometer. An attempt was made to keep the concentration of the solute in both B and BrB the same, so as to avoid having to make a geometrical correction in the yield measurements.<sup>9</sup>

Because BrB is a polar aromatic solvent, the spectra are often red shifted (extreme cases  $\sim 40$  Å) relative to those in B. Ethyl bromide has a tendency to blue shift the spectra. No adjustment has been made to correct for the wavelength sensitivity of the spectrometer, nor has a correction been made to the intensity values to take into account the effect produced by a difference in index of refraction among the solutions on the light collection efficiency of the apparatus. The corrections are assumed to be about the same small value for each compound and are neglected. Finally, an attempt was made *not* to use an exciting wavelength that fell at the onset of the absorption spectrum so as to avoid the possibility of the exciting radiation being more readily absorbed in the spectrum-shifted solutions and the necessity of making a geometrical correction for the light collection efficiency of the equipment. The estimated error in  $k_x$  is about  $\pm 15\%$ .

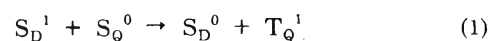
Our experimental techniques<sup>10</sup> are very sensitive to the presence of impurities in compounds. A new procedure for detecting the presence of an impurity can now be added to those listed in the above reference. If an impurity contributes peaks to the recorded spectrum in benzene, the spectrum in BrB will be modified because the degree of quenching will usually be different for the two species. In the present work, any compound that contained a perceptible impurity was omitted.

## Discussion

The compounds investigated and their calculated and measured parameters are assembled in Table I. They are grouped according to certain fluorescence features of the basic chromophore, particularly according to a similarity in their fluorescence transition. As an example, naphthalene is assumed to be the basic chromophore in the first group, and the remaining compounds of the group are substituted analogs of naphthalene. The fluorescence transition of each of these compounds is relatively weak so that the decay time is relatively long. Fluoranthene and 3-phenylfluoranthene are included because spectroscopically these compounds can be considered as substituted naphthalenes.<sup>11,12</sup>

Some general remarks can be made before each of the groupings is considered separately. The character of the transition is not of major importance in determining the value of  $k_x$  because the fluorescence transitions in naphthalene, anthracene, and *p*-terphenyl are  $^1L_b-^1A$ ,  $^1L_a-^1A$ , and  $^1B_b-^1A$ , respectively,<sup>13,14</sup> and these compounds each have large and approximately equal values of  $k_x$ .

Two major mechanisms appear to be enhanced by the breakdown of the spin selection rules and are responsible for large values of  $k_x$ . One is a singlet-triplet energy transfer process whose rate constant is  $k_t$  and can be represented as follows



where  $S_D^1$  and  $S_D^0$  represent the donor molecule in its

(6) Reference 5, p 425.

(7) R. E. Kellogg, *J. Chem. Phys.*, **44**, 411 (1966).

(8) R. Pariser, *J. Chem. Phys.*, **24**, 250 (1956).

(9) Reference 5, p 25.

(10) Reference 5, p 29.

(11) Reference 5, p 81.

(12) E. Heilbronner, J. P. Weber, J. Michl, and R. Zahradnick, *Theor. Chim. Acta*, **6**, 141 (1966).

(13) J. R. Platt, *J. Chem. Phys.*, **17**, 484 (1949).

(14) I. B. Berlman, *J. Chem. Phys.*, **52**, 5616 (1970).

TABLE I: Parameters of Compounds in Bromobenzene

Compound	Decay time, nsec	Quantum yield	$k_e \cdot 10^7$ , sec <sup>-1</sup>	$k_m \cdot 10^7$ , sec <sup>-1</sup>	<i>R</i>	$k_x \cdot 10^9$ , sec <sup>-1</sup>	$\Delta\nu_s$ , cm <sup>-1</sup>	$\Delta\nu_{ph}$ , cm <sup>-1</sup>
Naphthalene	96	0.23	0.23	0.77	295	3.1	0	(8,604)
Acenaphthene	46	0.60	1.32	0.88	44.4	0.94	204	8,820
2,3-Dimethylnaphthalene	76	0.38	0.5	0.82	68.6	0.88	151	
2-Phenylnaphthalene	114	0.26	0.23	0.65	19.4	0.16	2149	
Phenanthrene	57	0.13	0.23	1.5	16.8	0.28	2649	5,615
2-Phenylphenanthrene	90	0.17	0.2	0.9	14.2	0.15	3753	
3,4-Benzophenanthrene	76	0.12	0.2	1.1	13	0.15	4954	4,930
Chrysene	44.7	0.14	0.3	1.9	31	0.67	3699	(6,165)
Triphenylene	36.6	0.08	0.22	2.5	28.3	0.74	2701	3,953
Fluoranthene	53	0.30	0.57	1.3	19	0.34	8953	2,441
3-Phenylfluoranthene	34.5	0.65	1.9	1.0	8.1	0.21	8900	
Azulene	1.4	0.03	2.1	69	1.9	0.64	3549	(12,055)
1,1'-Binaphthyl	3.0	0.77	26	7	2.3	0.43	2401	
1,4,5,8-Tetraphenylnaphthalene	1.5	0.33	22	45	1.3	0.18	7203	
Perylene	6.4	0.94	14.7	0.9	1.4	0.056	8403	8,901
Anthracene	4.9	0.36	7.3	13.1	14.5	2.7	0	1,200
9-Methylantracene	4.6	0.35	7.6	14.4	2.1	0.25	699	
9-Phenylantracene	6.5	0.49	7.5	7.8	2.0	0.15	1045	
9-Vinylantracene	10.1	0.76	7.6	2.3	1.2	0.02	1746	
9,10-Diphenylantracene	9.4	1.0	11	<2	1.1	0.011	1546	
9,10-Dichloroanthracene	8.5	0.55	6.6	5.4	1.1	0.007	1651	
Tetracene	6.4	0.21	3.2	12.4	11.3	1.61	0	
Rubrene	16.5	1.0	6.1	<1	1.2	0.01	2397	
Fluorene	10	0.80	8	2	22	2.2	-253	8,158
Dibenzofuran	7.3	0.53	7.3	6.4	18.7	2.4	248	
Carbazole	16.1	0.38	2.4	3.8	15.6	0.91	3002	4,153
<i>N</i> -Phenylcarbazole	10.3	0.37	3.6	6.1	12.1	1.1	3549	
Triphenylbenzene	42.6	0.28	0.6	1.7	22	0.49	3454	5,581
2-Phenylindole	2.0	0.86	43	7	3	1.0	0	
1,2-Diphenylindole	2.0	0.90	45	5	3.4	1.2	500	
2,3-Diphenylindole	3.8	0.64	17	9.6	1.4	0.09	3059	
<i>p</i> -Terphenyl	0.95	0.93	98	7	3.7	2.8	0	8,687
4-Methyl- <i>p</i> -terphenyl	1.0	0.94	94	6	3	2.0	305	
3,3'-Dimethyl- <i>p</i> -terphenyl	1.0	0.90	90	10	3.2	2.2	355	
2,2'-Methylene- <i>p</i> -terphenyl	1.5	0.91	61	6	4.1	2.1	102	
2,2'-Ethylene- <i>p</i> -terphenyl	1.4	0.84	60	11.4	3.5	1.8	800	
3-Phenyldibenzofuran	1.8	1.0	56	<3	5.8	2.7	102	
4,4''-Dihexahydrofarnesoxy- <i>p</i> -terphenyl	0.95	0.97	102	3	2.1	1.2	1456	
<i>p</i> -Quaterphenyl	0.8	0.89	111	14	1.4	0.54	1905	
3,3'''-Dimethyl-3',2''-methylene- <i>p</i> -quaterphenyl	1.05	1.0	95	<5	1.3	0.32	2157	
2,2''''-Diethyl- <i>p</i> -quinquephenyl	0.88	0.92	104	10	1.3	0.34	2354	
3,3''''-Di(ethylheptyl)- <i>p</i> -quinquephenyl	0.8	1.0	125	<10	1.2	0.25	3202	
Tetramethyl- <i>p</i> -sexiphenyl	0.65	0.94	145	9	1.2	0.31	2753	
(PPD) 2,5-Diphenyloxadiazole	1.35	0.89	66	8.2	2.6	1.17	0	
(PPF) 2,5-Diphenylfuran	1.2	1.0	83	<7	2.3	1.1	1898	
(PPO) 2,5-Diphenyloxazole	1.4	1.0	71	<5	2.1	0.78	1847	
( $\alpha$ NPO) 2-(1-Naphthyl)-5-phenyloxazole	2.06	0.94	46	3	1.6	0.30	4100	
(BBO) 2,5-Diphenyloxazole	1.15				1.4	0.32	4900	
(POPOP) <i>p</i> -Bis[2-(5-phenyloxazolyl)]benzene	1.26	0.93	74	5	1.2	0.16	4750	
(Dimethyl POPOP) 1,4-Bis-2-(4-methyl-5-phenyloxazolyl)benzene	1.5	0.93	62	4.7	1.2	0.16	5449	
(BPSB) Bis(isopropylstyryl)benzene	1.1	0.94	86	5	1.2	0.14	4951	
(BBOT) 2,5-Bis[5- <i>tert</i> -butylbenzoxazolyl(2)]thiophene	1.1	0.74	67	24	1.04	0.036	6099	
1,3,6,8-Tetraphenylpyrene	2.67	0.90	34	3.7	1.5	0.18	1180	
Diphenylstilbene (B)	1.1				2.9	1.7	0	
Tetraphenylbutadiene	1.76	0.60	34	23	1.7	0.39	2853	
1,6-Diphenylhexatriene	12.4	0.80	6.5	1.6	1.7	0.053	2502	
1,8-Diphenyloctatetraene	6.2	0.09	1.5	14.6	0.95		5506	

first excited singlet and ground states, respectively, and  $S_Q^0$  and  $T_Q^1$  represent the quenching molecule in its ground state and first excited triplet state. The second mechanism (process two) is the enhancement of intersystem crossing in the fluorescent molecule with rate constant  $k_1$ .

When the fluorescence level of the donor has an energy greater than that of the triplet level of the quencher, both of the above quenching processes are operative, but when it is of lower energy, only the latter process is active.

Process one, represented by eq 1, has been reported<sup>15,16</sup> but has not been extensively studied. Transfer in this case is by means of an exchange mechanism and is short range. The efficiency of this process is dependent on the overlap between the fluorescence spectrum of the donor and the singlet-triplet absorption spectrum of the quencher. In other words, the efficiency increases as the intermolecular energy interval between the excited singlet of the donor and the triplet of the quencher becomes larger. On the other hand, the efficiency of intersystem crossing becomes larger as the intramolecular energy gap  $\Delta\nu_{ph}$  becomes smaller. Steric hindrance prevents a close approach of the heavy atom and thereby inhibits quenching in both processes.

The value of the triplet state of BrB is not known, but it is assumed to be slightly less than that of benzene. Therefore, an arbitrary value of  $28,000\text{ cm}^{-1}$  is assumed for discussion purposes.

Values of  $\Delta\nu_s$  are listed in Table I. It is noted that in each group of compounds  $\Delta\nu_s$  is somewhat inversely related to  $k_x$ . As  $\Delta\nu_s$  becomes sufficiently large so that energy transfer to the BrB is negligible,  $k_x$  becomes small. In those cases where  $k_x$  is even smaller than would be expected from the large values of  $\Delta\nu_s$ , steric factors are generally operative and interfering with the quenching process. On the other hand, when  $k_x$  is larger than expected, the value of  $\Delta\nu_{ph}$  is usually smaller than about  $6000\text{ cm}^{-1}$  and  $k_1$  is large.

Although substituents and bridging groups cause the singlet levels to be displaced toward lower energy and thereby to increase  $\Delta\nu_s$ , they, at the same time, displace the triplet manifold either upward or downward and thereby change  $\Delta\nu_{ph}$ . The direction of relative change of the two manifolds can often be gauged by comparing  $\Delta\nu_{ph}$  of the substituted analog with that of the basic chromophore. Since  $\Delta\nu_{ph}$  has been defined as the energy gap between the fluorescence level and the nearest lower triplet level (not always the lowest triplet level), there are cases where  $\Delta\nu_{ph}$  becomes much larger with substitution due to level crossing, e.g.,  $\Delta\nu_{ph}$  for anthracene is about  $1200\text{ cm}^{-1}$  and for 9,10-diphenylanthracene,<sup>17</sup> it is a factor of 5-6 times larger. In many other cases,  $\Delta\nu_{ph}$  becomes smaller with substitution.

The appendages and bridging groups that red shift the fluorescence spectrum and are noncoplanar with the basic chromophore are the ones most effective in reducing the efficiency of collisional quenching by BrB. Phenyl groups are generally not coplanar with the chromophore, and produce the greatest red shift when positioned along the axis of the fluorescence transition. The compound 9,10-diphenylanthracene and anthracene are examples of this. The phenyl groups of this substituted anthracene are positioned along the axis of the transition, which is short-axis polarized.<sup>13</sup> Moreover, the phenyl groups are noncoplanar with the chromophore both in the ground state and the

excited state.<sup>18,19</sup> In a similar case, the vinyl group in 9-vinylanthracene may also interfere with quenching because its conformation changes on excitation.<sup>20</sup>

On the other hand, substituents that do not affect the spectroscopic characteristics of the chromophore have little effect on the value of  $k_x$ , e.g., the values of  $k_x$  of carbazole and *N*-phenylcarbazole are essentially the same (Table I) and so are those of 2-phenylindole and 1,2-diphenylindole.

Selected compounds in Table I will now be treated individually. Naphthalene has been taken as the basic chromophore of the second series of compounds, as well as of the first, because its  $^1L_a$  state is very close to its  $^1L_b$  state. The fluorescence transition in the first series is similar to a  $^1L_b \rightarrow ^1A$  transition, in the second series it is similar to a  $^1L_a \rightarrow ^1A$  transition.

Naphthalene has a large value of  $k_x$  probably because  $k_t$  is large. The value of  $\Delta\nu_{ph}$  is in parentheses because there is some evidence that there may be a second triplet below the first excited singlet state.<sup>21</sup> The phenyl group in 2-phenylnaphthalene is very effective in immunizing the chromophore against being quenched. By being positioned along the axis of the fluorescence transition, this substituent is very effective in shifting the spectrum so that there is little overlap between the fluorescence spectrum of the donor and the singlet-triplet absorption spectrum of the quencher molecule, and  $k_t$  is almost zero. Steric hindrance by the noncoplanar phenyl group is an additional factor contributing to a low value of  $k_x$ .

The compound 3,4-benzophenanthrene is nonplanar both in its ground<sup>22</sup> and first excited state<sup>17</sup> because of the steric hindrance. In spite of this nonplanarity and a large value  $\Delta\nu_s$ , the relatively large value of  $k_x$  appears to be determined mainly by the small value  $\Delta\nu_{ph}$ , i.e., large  $k_t$ .

Chrysene has a much larger value of  $k_x$  than would be expected from the large value of  $\Delta\nu_s$ . This result is consonant with other experimental results that support the existence of another triplet level below the first excited level, i.e., a large value of  $k_n$  and a large value of 0.70 for the phosphorescence yield.<sup>23</sup> Because the value of  $\Delta\nu_{ph}$  is in question, it is in parentheses.

The last three compounds of the series, triphenylene, fluoranthene, and 3-phenylfluoranthene, have larger values of  $k_x$  than would be expected from their  $\Delta\nu_s$  values. Here, too, these larger values can be explained by the relatively small values of  $\Delta\nu_{ph}$ . What is surprising is that fluoranthene and its substituted analogs are known to be relatively immune to oxygen quenching,<sup>24</sup> yet they have these relatively large values of  $k_x$  (because of large  $k_t$ ).

Azulene is listed in the second series of compounds because it has been treated theoretically<sup>25</sup> as a modified

- (15) A. N. Terenin and V. L. Ermolaev, *Trans. Faraday Soc.*, **52**, 1042 (1956).
- (16) V. L. Ermolaev and E. B. Sveshnikova, *Opt. Spectrosc.*, **28**, 324 (1970).
- (17) C.-H. Ting, *Chem. Phys. Lett.*, **1**, 335 (1967).
- (18) I. B. Berlman, *J. Phys. Chem.*, **74**, 3085 (1970).
- (19) R. N. Jones, *J. Amer. Chem. Soc.*, **67**, 2127 (1945).
- (20) A. S. Cherkasov and K. G. Voldaikina, *Bull. Acad. Sci. USSR, Phys. Ser.*, **27**, 630 (1963).
- (21) N. Hirota and C. A. Hutchison, Jr., *J. Chem. Phys.*, **42**, 2869 (1965).
- (22) F. H. Herbstein and G. M. J. Schmidt, *J. Chem. Soc.*, 3302 (1954).
- (23) M. W. Windsor and W. R. Dawson, *Mol. Cryst.*, **3**, 165 (1967).
- (24) I. B. Berlman, H. O. Wirth, and O. J. Steingraber, *J. Amer. Chem. Soc.*, **90**, 566 (1968).
- (25) D. E. Mann, J. R. Platt, and K. B. Klevans, *J. Chem. Phys.*, **17**, 481 (1949).

form of naphthalene. It is a nonalternant and its fluorescence transition is anomalous in that it is from the second excited singlet state to the ground state. The very large value of  $k_n$  and the relatively large value of  $k_x$  (for  $\Delta\nu_s$ ) would indicate that there is another triplet below the second singlet. Therefore, the value of  $\Delta\nu_{ph}$  is in parentheses. Perylene is also included in this series of compounds because, spectroscopically, it can also be considered a substituted naphthalene or bridged binaphthyl.<sup>11</sup>

Anthracene is taken as the basic chromophore of the third series of compounds. All of these compounds have values of  $k_t$  approximately equal to zero. Therefore,  $k_x$  is composed almost totally of  $k_1$ , in agreement with Medinger and Wilkinson.<sup>26</sup> The low value of  $k_x$  for 9,10-dichloroanthracene may be aided by the fact that chlorine atoms are electronegative, as discussed below.

Rubrene is also called 5,6,11,12-tetraphenyltetracene. Here, too,  $k_t \cong 0$  and  $k_x \cong k_1$ .

The following group, headed by fluorene, is considered as composed of compounds that are bridged or substituted biphenyl and the values of  $\Delta\nu_s$  are computed using the value of  $\nu_{av}^0$  for biphenyl, the basic chromophore. Those compounds with small values of  $\Delta\nu_s$  have large values of  $k_x$  because  $k_t$  is large. Those compounds with large values of  $\Delta\nu_s$ , such as carbazole and *N*-phenylcarbazole, have large values of  $k_x$  because  $k_1$  is large ( $\Delta\nu_{ph}$  is small). Triphenylbenzene has a smaller value of  $k_x$  than the carbazoles because  $k_1$  is smaller and because of conformational considerations.

The results from the three indole derivatives indicate that this type of experiment can be employed to find where the sensitive positions on the chromophore are located. From the values of  $\Delta\nu_s$  it is noted that substitution on the 3 position of 2-phenylindole is more effective in red shifting the fluorescence spectrum than substitution on the 2 position. Likewise, the value of  $k_x$  is much smaller (because  $k_t$  is smaller) for 2,3-diphenylindole than for 1,2-diphenylindole.

The basic chromophore of the next series is *p*-terphenyl. A large value of  $k_x$  for this chromophore is the result of a large value of  $k_1$  and the fact that this chromophore is planar in the excited state.<sup>27</sup> Since the fluorescence transition is long-axis polarized, substituents on the para positions are especially effective in shielding the chromophore from being quenched. It is of interest that 3-phenyldibenzofuran and 2,2'-methylene-*p*-terphenyl have values of  $k_x$  and fluorescence characteristics that resemble *p*-terphenyl rather than phenyl-substituted dibenzofuran and fluorene, respectively. For the remainder of the *p*-oligophenylenes the larger values of  $\Delta\nu_s$  are associated with smaller values of  $k_x$ .

The following group, containing five-membered rings such as the oxazoles, etc., do not have a basic chromophore. Yet, if the compound with the spectrum containing the shortest wavelengths, PPD (2,5-diphenyloxadiazole), is assumed to be the basic chromophore and  $\Delta\nu_s$  is computed from it, then  $k_x$  is also found to be inversely related to  $\Delta\nu_s$ .

The tetraphenylpyrene is an interesting compound because it is a derivative of pyrene, the compound that most readily forms excimers. This phenyl-substituted pyrene, within the limits of solubility, does not appear to form excimers. Steric hindrance plus a moderate spectral shift contribute to the small value of  $k_x$ . Pyrene itself was not measured because it forms excimers at a different rate in

TABLE II: Parameters of Compounds in Ethyl Bromide<sup>a</sup>

Compound	$\nu_{av}$	$k_x$ (BrB)	$k_x'$ (EBr)
Naphthalene	29,900	3.1	1.5
Acenaphthene	29,700	0.94	0.31
Fluorene	31,910	2.2	1.3
Chrysene	26,205	0.67	0.62
Fluoranthene	20,950	0.34	0.34
Anthracene	24,900	2.7	2.1

<sup>a</sup> The units of  $k_x$  and  $k_x'$  are  $10^9 \text{ sec}^{-1}$  and of  $\nu_{av}$ ,  $\text{cm}^{-1}$ .

different solvents, and the amount of excimers formed affects the value of the fluorescence decay time which in turn affects the values of the rate constants.

The last set of compounds are ring-chain compounds, and they probably have *trans*-stilbene as their basic chromophore. Since stilbene in liquids at room temperatures is susceptible to photoinduced *trans*-*cis* isomerization<sup>28</sup> no value of  $\nu_{av}$  for *trans*-stilbene is available. Here, too, as the chain becomes longer and the spectrum is shifted to the red,  $k_x$  becomes smaller because  $k_t$  becomes zero. As with stilbene, the larger chain compounds undergo conformational changes on becoming excited and these nonplanar forms appear to interfere with the quenching process. In fact, 1,8-diphenyloctatetraene has a slightly larger yield in BrB than in B. This may be an artifact, but in any case, the quenching is minimal.

It is the contention of some authors<sup>29,30</sup> that the red shift produced by substituents is related to the electron-donating properties of the substituents. Bromine, on the other hand, is an electron acceptor. Collisional quenching may therefore be interpreted by our results as follows. It is short range and a close encounter between the excited molecule and the high *Z* quencher is necessary so that the *p* orbital of the halogen atom can overlap with the  $\pi$  orbital of the chromophore.<sup>3</sup> At the time of this close collision, a transient charge-transfer state may be formed which, with the perturbation by the bromine, leads to a breakdown of the spin-selection rules. Steric hindrance and a conformational charge of excitation would be expected to interfere with collisional quenching.

Chlorine atoms are electronegative, yet in 9,10-dichloroanthracene, they produce a red shift in the fluorescence spectrum. Their electronegative character would prevent their forming a charge-transfer state with bromine, and would lead to very small values of  $k_1$  and  $k_x$ .

Ethyl bromide (EBr) was used as the quencher in a number of cases to verify our contention that the rate constant for quenching  $k_x$  is composed of two rate constants,  $k_T$  and  $k_1$ . Since EBr does not have low-lying triplet states, it follows that  $k_t = 0$  and  $k_x = k_1$ . Our results are tabulated in Table II. Compounds, such as fluoranthene, chrysene, and anthracene, which have singlet levels below those of BrB, have essentially equivalent values of  $k_x$  in both solvents because  $k_x$  equals  $k_1$  in both cases. On the other hand, components such as fluorene, acenaphthene, and naphthalene, whose singlet levels are above that of BrB, have much larger values of  $k_x$  in BrB.

(26) T. Medinger and F. Wilkinson, *Trans. Faraday Soc.*, **61**, 620 (1965).

(27) I. B. Berlman, H. O. Wirth, and O. J. Steingraber, *J. Phys. Chem.*, **75**, 318 (1971).

(28) E. Fischer, H. P. Lehmann, and G. Stein, *J. Chem. Phys.*, **45**, 3905 (1966).

(29) O. P. Shvaika and A. P. Grekov, *Opt. Spectrosc.*, **7**, 483 (1959).

(30) S. R. Sandler and S. Loshak, *J. Chem. Phys.*, **34**, 445 (1961).

A literature search was made to find values of the dipole moments of the compounds tested, and to look for a possible correlation with short-range order between solvent and solute molecules, but no such evidence was found. In many cases, an interesting correlation does appear to exist between values of  $k_x$  and a molecule's sensitivity to concentration quenching and/or excimer formation. Those compounds that have low values of  $k_x$  because of steric factors, *e.g.*, 9,10-diphenylanthracene, are also immune to concentration quenching and/or excimer formation for the very same reason. Some compounds that are planar in both their ground and excited states, and have large values of  $k_x$ , are also susceptible to concentration quenching, *e.g.*, anthracene, or to excimer formation, *e.g.*, naphthalene.

In an earlier experiment it was demonstrated that the quenching by oxygen was a diffusion-controlled process

and that its efficiency was directly related to the radiative lifetime of the fluorescence state.<sup>31</sup> The values of  $k_1$  in that work clustered around a value of  $5 \times 10^7 \text{ sec}^{-1}$ . As noted above, fluoranthene and its substituted derivatives have remained the sole exception, with values of  $k_1$  of about  $0.8 \times 10^7 \text{ sec}^{-1}$ . Since  $\text{O}_2$  is a smaller molecule than BrB, it is much less sensitive to molecular topology. Moreover, the breakdown in the spin-selection rules for the case of oxygen is for reasons other than that it is a high Z material. Oxygen has a triplet ground state and is therefore paramagnetic.

*Acknowledgment.* The author would like to thank Dr. Mitio Inokuti for several stimulating discussions.

(31) I. B. Beriman and T. A. Walter, *J. Chem. Phys.*, **37**, 1888 (1962).

## COMMUNICATIONS TO THE EDITOR

### Comment on the Paper "Application of Density Matrix Methods to the Study of Spin Exchange," by K.-I. Dahlqvist and S. Forsén

*Sir:* The above mentioned paper suffers from some errors.<sup>1</sup> First a careful study of the experimental curves indicates that the transverse relaxation time,  $T_2$ , is not 0.65 sec, as stated, but more nearly 4.0 sec. Also the parameters assigned to the curves in Figure 1 are not correct. Presumably the temperatures are correctly assigned but the values of  $\tau$  cannot be right. Each curve has been assigned a value of  $\tau$  about sixfold too low, *e.g.*, the second curve in Figure 1 has  $\tau = 0.125 \text{ sec}$ , this value should be about 0.8 sec. If the corrected value of  $\tau$  and  $T_2$  are used then the theoretical curves of Figure 1 may be obtained, however, they cannot be obtained if the incorrectly given values are used. One can only suggest that the authors have not converted angular frequencies to frequencies, or *vice versa* at some stage in their calculations, this could lead to an error of a factor of  $2\pi$  which would account for the discrepancy.

The errors in  $\tau$  mean that the Arrhenius plot displayed in Figure 3 will still be an approximately straight line with the same slope but with a different intercept. This in turn means that some of the values in Table II are wrong;  $T$ ,  $E_a$ , and  $\Delta H^\ddagger$  are unchanged, but  $\Delta S$  becomes  $-4.2 \pm 0.6 \text{ eu}$  and  $\Delta F$  becomes  $-13.4 \text{ kcal/mol}$ .

(1) K.-I. Dahlqvist and S. Forsén, *J. Phys. Chem.*, **73**, 4124 (1969).

Chemistry, Biochemistry, and  
Biophysics Department  
Mässon University  
Palmerston North, New Zealand

D. N. Pinder

Received April 24, 1972

### Comments on the Paper "Ionic Solvation Numbers from Compressibilities and Ionic Vibration Potentials Measurements," by J. O'M. Bockris and P. P. S. Saluja

*Publication costs assisted by the National Research Council of Canada*

*Sir:* Recently,<sup>1</sup> Bockris and Saluja have measured adiabatic compressibilities of electrolyte aqueous solutions and derived from them hydration numbers. I would like to comment on the interpretation of their data.

The authors have obtained hydration numbers from compressibilities using Passynski's equation.<sup>2</sup> An equivalent but more rigorous method is to use apparent molal compressibilities<sup>3</sup>  $\phi_K$  which are derived from the difference between the isothermal compressibilities of the solution and that of the solvent,  $\beta - \beta_0$ . These  $\phi_K$  can also be obtained from adiabatic compressibilities using known expansivities and heat capacities.<sup>3,4</sup> The advantage of this quantity is that it can be written as a function of concentration, *i.e.*

$$\phi_K = \phi_K^0 + A_K c^{1/2} + B_K c \quad (1)$$

where  $\phi_K^0$  is the standard apparent molal compressibility, equal to the standard partial molal compressibility  $\bar{K}^0$ ;  $A_K$  the Debye-Hückel limiting slope; and  $B_K$  an adjustable parameter related to all ion-ion interactions not accounted for by the limiting Debye-Hückel law. The parameter  $\phi_K^0$  is additive and independent of ion-ion interactions while  $B_K$  is nonadditive. The accuracy of experi-

(1) J. O'M. Bockris and P. P. S. Saluja, *J. Phys. Chem.*, **76**, 2140 (1972).

(2) A. Passynski, *Acta Physicochim.*, **8**, 385 (1938).

(3) H. S. Harned and B. B. Owen, "The Physical Chemistry of Electrolyte Solutions," Reinhold, New York, N. Y., 1958, Chapter 8.

(4) J. E. Desnoyers and P. R. Philip, *Can. J. Chem.*, **50**, 1094 (1972).



mental data can readily be checked by the additivity of  $\phi_K^0$  for different ion pairs or by comparison with some of the reliable literature values.

Ion-solvent interactions should be discussed whenever possible in terms of  $\phi_K^0$ . Passynski's method is equivalent to the use of  $\phi_K$  and the derived hydration numbers necessarily include ion-ion interactions. Since  $B_K$  is nonadditive the hydration numbers will also be nonadditive, as observed by Bockris and Saluja.

The standard apparent molal volume  $\phi_v^0$  of an ion can be related to the hydration number  $h$  by the relation<sup>5</sup>

$$\phi_v^0 = V_{in} + h(v_0^h - v_0) \quad (2)$$

where  $V_{in}$  is the intrinsic volume of the ion,  $v_0$  the molar volume of pure water, and  $v_0^h$  the molar volume of water in the hydration shell. Assuming that the ion and the water molecules in the hydration shell are incompressible and that  $h$  does not vary with pressure,  $\phi_K^0$  of an ion is then given by

$$\phi_K^0 = -(\partial\phi_v^0/\partial P)_T = h(\partial v_0/\partial P)_T = -h\nu_0\beta_0 \quad (3)$$

This relation can of course be refined by assuming, for example, that the water in the hydration shell is only partially compressed.

Hydration numbers<sup>5</sup> derived from eq 3 are comparable with those obtained by Bockris and Saluja. This is expected since both methods of treating compressibilities are equivalent in that they attribute all changes in  $\beta$  to ion-solvent interactions, which are usually larger than ion-ion interactions at low concentrations. The difficulty arises when these interactions are attributed to coulombic hydration (charge-dipole, charge-quadrupole type). The danger of this interpretation can best be shown by a comparison with other similar thermodynamic properties. The standard apparent molal expansivities  $\phi_E^0$  and heat capacities  $\phi_C^0$  are closely related to  $\phi_K^0$  since they are all proportional to the second differential of the standard chemical potential of the ions, and at ordinary pressures a variation in pressure usually affect water in the same general way as a change in temperature. Therefore, if eq 2 is differentiated with respect to  $T$ , assuming that  $h$ ,  $V_{in}$ , and  $v_0^h$  are all independent of temperature, then

$$\phi_E^0 = (\partial\phi_v^0/\partial T)_P = -h(\partial v_0/\partial T)_P = -h\nu_0\alpha_0 \quad (4)$$

where  $\alpha_0$  is the expansivity of pure water. Since  $h$  is by definition a positive number,  $\phi_E^0$  must be *negative*. Unfortunately with all alkali halides and tetraalkylammonium halides  $\phi_E^0$  of the pair of ions is *positive*. The assumptions leading to eq 3 and 4 are very similar; if they are correct for compressibilities, they would also be expected to be correct for expansivities. This is improbable since, to get the correct sign for  $h$ , one would have, for example, to assume that the expansivity of water in the

hydration shell is larger than that of pure water. Similarly, it can be shown that negative apparent molal heat capacities cannot readily be explained in term of strong coulombic hydration.<sup>6,7</sup>

On the other hand, it seems that structural hydration<sup>8</sup> (structure-making and -breaking effects) is the leading interaction causing changes in heat capacities and expansivities. The correction of Bockris and Saluja for the interaction between the ions and nonsolvated coordination water is not equivalent to a structural interaction since this interaction is assumed to take place essentially after the structure is broken down while structural hydration refers to the passage of water from the normally bonded state to the unbonded state in the presence of a structure-breaking ion.

The importance of these structural interactions can best be illustrated through transfer functions from H<sub>2</sub>O to D<sub>2</sub>O or urea-water mixtures. It is fairly well established that structural interactions are larger in D<sub>2</sub>O<sup>9,10</sup> and smaller in urea-water mixtures<sup>11,12</sup> while coulombic hydration effects are, as a first approximation, constant in these solvents. As an example, we can compare  $\phi_C$  (in J K<sup>-1</sup> mol<sup>-1</sup>) and  $\phi_E$  (cm<sup>3</sup> T<sup>-1</sup> mol<sup>-1</sup>) of a 0.1 aquamolal NaCl solution in these solvents.<sup>13</sup>

$$\begin{array}{ll} \phi_C(\text{H}_2\text{O}) & = -70.1 & \phi_E(\text{H}_2\text{O}) & = 0.079 \\ \phi_C(\text{D}_2\text{O}) & = -107.7 & \phi_E(8\text{ m urea}) & = 0.014 \\ \phi_C(8\text{ m urea}) & = +24.6 & & \end{array}$$

Unfortunately compressibilities are not available in D<sub>2</sub>O or urea-water mixtures. Still, by analogy with  $\phi_C$  and  $\phi_E$ , it is reasonable to expect that a large part of  $\phi_K$  is structural in origin and the reasonable order of magnitude of the hydration numbers may be somewhat of a coincidence.

- (5) J. E. Desnoyers and C. Jolicoeur, "Modern Aspects of Electrochemistry," Vol. V, B. E. Conway and J. O'M. Bockris, Ed., Plenum Press, New York, N. Y., 1969, Chapter I.
- (6) B. E. Conway, R. E. Verrall, and J. E. Desnoyers, *Z. Phys. Chem. (Leipzig)*, **230**, 157 (1965).
- (7) J. E. Desnoyers, "Electrostatic Interactions and the Structure of Water," XV<sup>e</sup> Conseil International de Chimie Solvay, Brussels, in press.
- (8) H. S. Frank and W.-Y. Wen, *Discuss. Faraday Soc.*, **24**, 133 (1957).
- (9) G. Némethy and H. A. Scheraga, *J. Chem. Phys.*, **41**, 680 (1964).
- (10) P. R. Philip and J. E. Desnoyers, *J. Solution Chem.*, **1**, 353 (1972).
- (11) T. S. Sarma and J. C. Ahluwalia, *J. Phys. Chem.*, **76**, 1366 (1972).
- (12) P. R. Philip, J. E. Desnoyers, and A. Hade, *Can. J. Chem.*, in press.
- (13) J. E. Desnoyers, N. Desrosiers, and G. Perron, manuscript in preparation.

Department of Chemistry  
Université de Sherbrooke  
Sherbrooke, P.Q. Canada

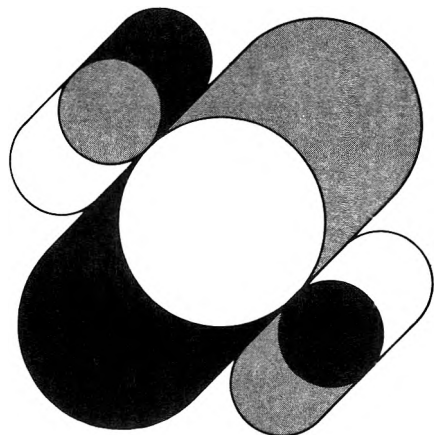
Jacques E. Desnoyers

Received September 18, 1972

# Nonequilibrium Systems In Natural Water Chemistry

ADVANCES IN CHEMISTRY  
SERIES No. 106

*Thirteen papers from a symposium by the Division of Water, Air, and Waste Chemistry of the American Chemical Society, chaired by J. D. Hem.*



Which is more important: efficient exploitation of our natural resources or a stable ecosystem? What is the relationship between a wide variety of life forms and a healthy environment? What do geology and groundwater flow patterns have to do with the chemical composition of water? How may one predict when a lake will reach equilibrium or tell how long it has supported life?

This volume features:

- principles of water pollution control
- methods of analysis for dissolved chemicals
- mathematical models
- discussion of stratified lakes
- chemical processes in a carbonate aquifer
- decomposition and racemization of amino acids

---

342 pages with index Cloth (1971) \$11.00  
Postpaid in U.S. and Canada; plus 40 cents elsewhere.  
Set of L.C. cards with library orders upon request.

---

Other books in the ADVANCES IN CHEMISTRY SERIES on water chemistry include:

**No. 105 Anaerobic Biological Treatment Processes**

Nine papers survey the state of the art of this natural process for waste treatment, with three papers on methane fermentation, others on process control and design. Considers volatile acid formation, toxicity, synergism, antagonism, pH control, heavy metals, light metal cations.  
196 pages with index Cloth (1971) \$9.00

**No. 79 Adsorption from Aqueous Solution**

Fifteen papers discuss thermodynamic and kinetic aspects of adsorption phenomena and the results of studies on a variety of adsorbate-adsorbent systems.  
212 pages with index Cloth (1968) \$10.00

**No. 73 Trace Inorganics in Water**

Research reports: analytical developments including atomic absorption, flame emission, and neutron activation; and broad reviews, such as effects of trace inorganics on the ice-water system and the role of hydrous manganese and iron oxides on fixing metals in soils and sediments.  
396 pages with index Cloth (1968) \$12.50

**No. 67 Equilibrium Concepts in Natural Water Systems**

Sixteen papers represent the collaboration of aquatic chemists, analytical chemists, geologists, oceanographers, limnologists, and sanitary engineers, working with simplified models to produce fruitful generalizations and valuable insights into the factors that control the chemistry of natural systems.  
344 pages with index Cloth (1967) \$11.00

**No. 38 Saline Water Conversion—II**

Fourteen papers from two symposia; includes recovery of minerals from sea water, minimizing scale formation, wiped thinfilm distillation, diffusion still, solar flash evaporation, osmosis, electrodialysis (3 paper), research in Israel, hydrate process.  
199 pages Paper (1963) \$8.00

**No. 27 Saline Water Conversion**

Thermodynamics of desalting, solvent extraction, freezing, centrifugal phase barrier recompression distillation, multi-stage flash evaporation, ion exchange, osmosis, and electrochemical demineralization.  
246 pages Paper (1960) \$9.00

Order from: **Special Issues Sales, American Chemical Society**  
1155 Sixteenth St., N.W., Washington, D.C. 20036

# Tape Cassettes From The American Chemical Society

# Famous Scientists

## ENERGY

- Energy: A Critique**  
Dr. Dean Abrahamson  
**Puzzles of Air Pollution** Arthur Levy
- Fusion: Prospects & Pitfalls—I**  
Dr. H. Furth & Dr. H. Forsen  
**Fusion: Prospects & Pitfalls—II**  
Dr. H. Furth & Dr. H. Forsen
- Antidote to the Energy Crisis**  
George Long  
**Chemicals in the Environment**  
Dr. Samuel Epstein
- Fusion and Fission: An Appraisal**  
Dr. James L. Tuck  
**The Prospects for Energy**  
Dr. M. King Hubert

## ENVIRONMENT

- Man & Nature in South Florida**  
Rose McCluney  
**The Slick Factor in Ocean Pollution**  
Dr. Eugene Corcoran
- The Damaged Air—I**  
**The Damaged Air—II**
- How Smells Shape Up**  
Dr. John Amooore  
**Urban Auto Design**
- Tough Filaments of Fragile Liquid**  
James Bacon  
**Electricity from Rooftops**  
Dr. Charles E. Backus
- The Struggle for Clean Water—I**  
**The Struggle for Clean Water—II**
- The Oil Mystery** Harold Bernard  
**The Language of Odors**  
Dr. Stanley Freeman
- The Muskegon County Experiment**  
Dr. W. Bauer & Dr. J. Sheaffer  
**The Sophisticated Dowser**  
Dr. Richard Parizek
- The Lonely Atom** Dr. Philip Skell  
**How Green the Revolution**  
Lester Brown
- Mercury: Another Look, Part I**  
Dr. John Wood  
**Mercury: Another Look, Part II**  
Dr. John Wood & D. G. Langley
- The Troubles with Water**  
Dr. Daniel Okun  
**Pure Oxygen for Polluted Water**  
Dr. Jack McWhirter
- Bubble Machines & Pollution Finders**  
Dr. K. Patel & Dr. L. Kreuzer  
**The Steam Engine: A Modern Approach**  
Dr. W. Doerner & Dr. M. Bechtold

- Insects: The Elements of Change—Parts I & II** Dr. Carroll M. Williams
- New Weapons Against Insects**  
Dr. G. Staal & Dr. J. Siddall  
**Moths, Drugs, & Pheromones**  
Dr. Wendell Roelofs
- The Lead Issue**  
H. Mayrhoth & M. H. Hyman  
**Smog: An Environmental Dilemma**  
Dr. James Pitts

- The Fusion Torch**  
Dr. B. Eastlund & Dr. W. Gough  
**The Impermanent Plastic**  
Dr. James Guillet

## CANCER RESEARCH

- Chemicals Combating Cancer**  
Dr. David Grasseti  
**Chemical Essence of Beer & Ale**  
Dr. Rao Palamand
- Cancer Research I—Perspective & Progress** Dr. Frank Rauscher  
**Cancer Research II—Viruses**  
Dr. R. Gallo & Dr. G. Todaro
- Cancer Research III—Chemotherapy**  
Dr. C. Gordon Zubrod  
**Cancer Research IV—Immunology**  
Dr. Paul Levine
- Cancer Research V—Environmental Agents** Dr. Umberto Saffiotti  
**Cancer Research VI—NCI Roundtable**

## SCIENCE

- Community Needs: New Emphasis in Research** Dr. H. Guyford Stever  
**Aspirin vs. Prostaglandins**  
Dr. John Vane
- A Breakdown in Plastics—I**  
Drs. J. Guillet & G. Scott  
**A Breakdown in Plastics—II**  
Drs. J. Guillet & G. Scott
- Protein: The Next Big Production?**  
Dr. Steven Tannenbaum  
**Clean Energy: A One-Way Dream**  
Dr. J. R. Eaton
- Science, Scientists, & the Public Interest—I**  
**Science, Scientists, & the Public Interest—II**
- Nitrosamines: A Reappraisal**  
Dr. Phillip Issenberg  
**The Emperor of Ice Cream**  
Dr. Wendell Arbuckle
- Ethics and Genetics**  
Dr. Robert F. Murray  
**The American Diet: A Critique**  
Dr. Arnold Schaefer

- Probing Creation** Dr. Myron A. Coler  
**New Directions in U.S. Science**  
Dr. William McElroy

- Aspirins, Enzymes, & Fragrant Redheads** An Essay Report  
**Vitamin D: A New Dimension**  
Dr. Hector DeLuca

- Pica** Dr. J. Julian Chisolm, Jr.  
**Technology in the Nursery**  
Dr. William J. Dorson

- Engineering Microbes**  
Dr. Elmer Gaden  
**Liquid Crystals: A Bright Promise**  
Dr. George Heilmeyer

- Hot Brines in the Red Sea**  
Dr. David Ross  
**Complete Corn** Dr. Edwin T. Mertz

- Lively Xenon** Dr. Neil Bartlett  
**The Repressor Hunt**  
Dr. Mark Ptashne

- The New Prospectors**  
Dr. William Prinz  
**A Sober Look at Alcoholism**  
Dr. Jack Mendelsohn

- Probing the Active Site**  
Dr. David Pressman  
**The Puzzle of Diversity**  
Dr. Oliver Smithies

- Help for the Have Nots**  
Dr. Harrison Brown  
**The Closing Circle** Dr. Preston Cloud

## BIO-MEDICAL

- Insulin & Diabetes—I**  
Dr. George Cahill  
**Insulin & Diabetes—II**  
Dr. George Cahill
- Stalking the Molecules of Memory**  
Dr. Leslie Iverson  
**Immunotherapy**  
Dr. Kenneth Bagshawe
- Engineering Enzymes**  
Dr. Victor Edwards  
**On Drugs, Plasticizers, & Mass Spec**  
Dr. G. W. A. Milne
- Body Metal** Dr. Thomas Clarkston  
**Judging Technology** Dr. E. G. Mesthene
- Prospects for the Living Filter**  
Dr. Richard Parizek  
**Coral Designs** Dr. Eugene White
- Bones, Teeth, & Ceramics**  
Thomas Driskell  
**PCBs: The Accidental Pollutants**  
Dr. Henry Enos
- Birth Control: Problems & Prospects**  
Dr. Carl Djerassi  
**Hormones, Terpenes, & the German Air Force** Dr. A. J. Birch

- Prospects for Implants**  
Dr. Donald Lyman  
**New Dimensions for Polymers**  
Dr. Alan Michaels

- Fabricating Life** An Essay Report  
**New Ways to Better Food**  
Dr. R. W. F. Hardy

- Chemistry of the Mind: Schizophrenia**  
Dr. Larry Stein  
**Chemistry of the Mind: Depression**  
Dr. Joel Elkes

- The Molecules of Memory**  
Dr. W. L. Byrne & Dr. A. M. Golub  
**The Matter with Memory**  
Dr. J. McCaugh

- Dissonant Harmony**  
Dr. Denham Harman  
**Why We Grow Old** Dr. Howard Curtis

- New Materials for Spare Parts**  
Dr. V. Gott & Dr. A. Rubin  
**Against Individuality**  
Dr. R. Reistfeld & Dr. B. Kahan

- A Richness of Lipids**  
Dr. Roscoe O. Brady  
**Life: Origins to Quality**  
Dr. Stanley Miller

- The Nitrogen Fixer**  
Dr. Eugene van Tamelen  
**Prostaglandins: A Potent Future**  
Dr. E. J. Corey & Dr. S. Bergstrom

- A Glass Revolution** Dr. S. D. Stookey  
**A View of Genes** Dr. Norman Davidson

- Chemical Evolution**  
Dr. Russell Doolittle  
**An Evolving Engine** Dr. R. E. Dickerson

## NOBEL PRIZE WINNERS

- Dr. Linus Pauling**  
The Committed Scientist  
**Dr. Jacob Bronowski**  
Science and Man
- Dr. Glenn Seaborg** The Atomic World of Glenn Seaborg  
**Dr. George Wald** Vision, Night Blindness, & Professor Wald
- Dr. Melvin Calvin** The Search for Significance—Parts I & II

## OUTER SPACE

- Molecules in Space**  
Dr. D. Buhl & Dr. I. Snyder  
**Chemistry Among the Stars**  
Dr. Bertram Donn
- Molecules Meeting Molecules**  
Dr. John Richards  
**The Neutrinos of the Sun**  
Dr. Raymond Davis

	ACS Members	Nonmembers
Single Cassette	\$4.49	\$5.49
Any Six Cassettes	\$3.95/cassette	\$4.95/cassette
Any 18 or more cassettes to one Address	\$3.75/cassette	

Please add 75 cents handling charge for all orders in U.S., \$1.00 for all orders outside U.S.

5% Discount if payment accompanies order

Order From: American Chemical Society, 1155 16th Street, N.W., Washington, D.C. 20036, ATTN: A. Poulos